Using 3D virtual plants to assess the control of splash dispersed diseases by wheat cultivar mixtures.

Christophe Gigot, Claude de Vallavieille-Pope, Marc M. Leconte, Claude Maumené, Laurent L. Huber, Sebastien Saint-Jean

FSPM 2013

7th International Conference on

FUNCTIONAL–STRUCTURAL PLANT MODELS

9–14 June 2013, Saariselkä, Finland

Proceedings

Editors

Risto Sievänen

Eero Nikinmaa

Christophe Godin

Anna Lintunen

Pekka Nygren

Proceedings of the 7th International Conference on Functional-Structural Plant Models, Saariselkä, Finland, 9 - 14 June 2013. Eds. Risto Sievänen, Eero Nikinmaa, Christophe Godin, Anna Lintunen & Pekka Nygren. http://www.metla.fi/fspm2013/proceedings. ISBN 978-951-651-408-9.

Publishers:
Finnish Society of Forest Science, Vantaa, Finland
Finnish Forest Research Institute, Vantaa, Finland
Department of Forest Sciences, University of Helsinki, Helsinki, Finland

Editorial office:
Finnish Society of Forest Science
PO Box 18
01301 Vantaa
Finland
tel: +358 40 801 5596
e-mail: sms@helsinki.fi

Foreword

These are the proceedings of the 7th event in a series of workshops on functional-structural plant models (FSPMs). Functional-structural plant models describe plants as entities consisting of individual elements, describe the characteristics and behaviour of these elements, and integrate the activities of the elements for modelling the functioning of a whole plant or a plant part.

As this is already the seventh in the series of FSPM meetings and there are a solid number of contributors and participants, we decided call this meeting a conference. The chain of the FSPM workshops is as follows:

- The first workshop in Helsinki in December 1996 focused on the modelling of the distribution of growth within an individual tree, and the mathematical description and measurement of three-dimensional tree structure. Selected papers were published in a special issue of Silva Fennica, Vol 31, No. 3.
- The second workshop, with the same scientific profile, was held in Clermont-Ferrand, France, in October 1998. Selected papers were published in a special issue of Annals of Forest Science, Vol. 57, No 5/6.
- The third workshop was held in Montreal, Canada, in September, 2001. It broadened the scope of the series to include models of tree stand structure and functions.
- The fourth workshop in Montpellier, France, in June 2004 broadened the scope further to include all types of plants (woody and herbaceous), and functional-structural plant models operating at the molecular and tissue levels. Selected papers were published in a special issue of New Phytologist, Vol 166, No 3.
- The fifth workshop took place in Napier, New Zealand, in November 2007. The scope of this workshop was similar to the previous workshop. Selected papers were published in special issue of Functional Plant Biology, Vol 35, No's 9&10.
- The format of the sixth workshop in Davis, California, USA, in September 2010 was similar to the previous two workshops. An increasing number of models were applied to study practical issues in crop and plant production. Selected papers were published in a special issue of Annals of Botany, Vol 108, No. 6.

We received 156 abstracts for oral and poster presentations. They fitted into the topic categories of the previous meetings. The automated reconstruction plant structure on the basis of LiDAR and other data is a popular topic and cellular level models get less attention than in the two previous meetings. Number of applications of FSPMs is increasing. This time we structured the programme following criteria based on the type of modelling effort, instead of the target (e.g. roots or nutrients). We applied a number of broad categories: Methods for FSPMs (session 3); modelling and measuring plant structures (sessions 1A and 1B); modelling processes from organ to plant community level (sessions 2A and 2B); growth and development of plants (session 4A) and plant communities (session 4B); and using models for problem solving (session 5). Papers of the presentations in this conference may be submitted for publication in a 2014 special issue of *Annals of Botany*.

Risto Sievänen
Finnish Forest Research Institute
Chair, International Programme Committee

Seventh International Conference on Functional-Structural Plant Models (FSPM2013), Saariselkä, Finland, 9-14 June 2013

Local organising committee

RISTO SIEVÄNEN (Chair), Finnish Forest Research Institute, E-mail: risto.sievanen@metla.fi
PEKKA NYGREN (Secretary), Finnish Society of Forest Science, E-mail: pekka.nygren@metla.fi
ANNA LINTUNEN (Editor) , University of Helsinki, E-mail: anna.lintunen@helsinki.fi
PEKKA KAITANIEMI, University of Helsinki
TUOMO KALLIOKOSKI, Finnish Forest Research Institute
EERO NIKINMAA, University of Helsinki
JARI PERTTUNEN, Finnish Forest Research Institute

Technical assistance

MIRJA VUOPIO, Finnish Forest Research Institute
JARI HIETANEN, Finnish Forest Research Institute

Sponsors

League of Finnish Learned Societies, Finland
Annals of Botany, United Kingdom
INRIA, France
Tree Physiology, United Kingdom

International programme committee

RISTO SIEVÄNEN (Chair), Finnish Forest Research Institute, Finland
EERO NIKINMAA (Co-chair), University of Helsinki, Finland
CHRISTOPHE GODIN (Co-chair), Institut national de recherche en informatique et en automatique (INRIA), France
BRUNO ANDRIEU, Institut national de la recherche agronomique (INRA), France
GERHARD BUCK-SORLIN, Institut de Recherche en Horticulture et Semences (IRHS), France
ERIC CASELLA, Forest Research, UK
MICHAËL CHELLE, INRA, France
KARINE CHENU, The University of Queensland, Australia
EVELYNE COSTES, INRA, France
PAUL-HENRY COURNÈDE, École Centrale Paris, France
THEODORE DEJONG, University of California - Davis, USA
YVES DUMONT, Centre international de la recherche agronomigue pour le développement (CIRAD), France
LIONEL DUPUY, The James Hutton Institute, UK
ABRAHAM ESCOBAR-GUTIÉRREZ, INRA, France

JOCHEM EVERS, Wageningen University and Research Centre, The Netherlands
PAULINA FERNÁNDEZ, Pontificia Universidad Católica de Chile, Chile
DAVID E. FORD, University of Washington, USA
THIERRY FOURCAUD, CIRAD, France
YANN GUÉDON, CIRAD, France
YAN GUO, China Agricultural University, China
JIM HANAN, The University of Queensland, Australia
TEEMU HÖLTTÄ, University of Helsinki, Finland
HENRIK JÖNSSON, Lund University, Sweden
MIKKO KAASALAINEN, Tampere University of Technology, Finland
KATRIN KAHLEN, Forschungsanstalt Geisenheim, Germany
PEKKA KAITANIEMI, University of Helsinki, Finland
TUOMO KALLIOKOSKI, University of Helsinki & Finnish Forest Research Institute, Finland
WINFRIED KURTH, University of Göttingen, Germany
ANDRÉ LACOINTE, INRA, France
CHRISTIAN MESSIER, Université de Québec à Montréal, Canada
PETER MINCHIN, The New Zealand Institute for Plant & Food Research Limited, New Zealand
PEKKA NYGREN, Finnish Society of Forest Science, Finland
HARRY OZIER-LAFONTAINE, INRA, Guadeloupe
LOÏC PAGÈS, INRA, France
MIKKO PELTONIEMI, Finnish Forest Research Institute, Finland
JARI PERTTUNEN, Finnish Forest Research Institute, Finland
PRZEMYSLAW PRUSINKIEWICZ, University of Calgary, Canada
MICHAEL RENTON, The University of Western Australia, Australia
ALLA SELEZNYOVA, Plant & Food Research, New Zealand
KATARINA SMOLENOVA, University of Göttingen, Germany
HARTMUT STÜTZEL, University of Hannover, Germany
KIYOSHI UMEKI, Chiba University, Japan
JAN VOS, Wageningen University and Research Centre, The Netherlands

Permanent FSPM board

THEODORE DEJONG, University of California - Davis, USA
CHRISTOPHE GODIN, INRIA, France
YAN GUO, China Agricultural University, China
KATRIN KAHLEN, Forschungsanstalt Geisenheim, Germany
RISTO SIEVÄNEN, Finnish Forest Research Institute, Finland
JAN VOS, Wageningen University and Research Centre, The Netherlands

Contents

Modelling Plant Structure

Reconstructing and observing plant structure

Oral presentations

Posters

Exchange and transport processes in plants

Distribution of resources and growth in plants

Oral presentations

Posters

Methods for functional-stuctural plant models

Oral presentations

Posters

Structural development of plants and light environment

Oral presentations

Posters

Growth and development of plant communities

Oral presentations

Posters

Functional-structural plant models for problem solving in vegetation management

Oral presentations

Posters

MODELLING PLANT STRUCTURE

Proceedings of the 7th International Conference on Functional-Structural Plant Models, Saariselkä, Finland, 9 - 14 June 2013. Eds. Risto Sievänen, Eero Nikinmaa, Christophe Godin, Anna Lintunen & Pekka Nygren. http://www.metla.fi/fspm2013/proceedings. ISBN 978-951-651-408-9.

KEYNOTE: Functional-structural modelling with L-systems: Where from and where to

Jim Hanan
The University of Queensland, Queensland Alliance for Agriculture & Food Innovation, St. Lucia, Queensland, Australia 4072
**correspondence:* j.hanan@uq.edu.au

Highlights: The L-systems formalism with turtle interpretation captures plant structural topology and geometry, signalling within the branching structure, and development over time, forming a basis for plant modelling languages. With the addition of environmental interfaces, they have been successfully used to model a variety of plants. Areas for future development include integration of different aspects of plant function, multi-scale modelling and development as a platform for further simulation.

Keywords: Lindenmayer-systems, plant modelling language

WHERE FROM

Since their inception by Aristid Lindenmayer (1968a&b), L-systems have provided an inspiration and formal foundation for a range of functional-structural plant modelling systems. The original formalism incorporated internal and environmental signalling and branching topology, aiming to capture elements of filamentous growth at a cellular level. Inspired by the ideas of Cohen (1967), Frijters and Lindenmayer (1974) moved from the cellular to the organ level of abstraction, developing an L-system model of aster incorporating signals for control of branching and "vigour" controlling flowering positions. This is the first example of L-systems capturing functional-structural aspects of plant growth and development.

In these early models, plant geometry was added in a post-processing phase. Hogeweg and Hesper (1974) explored patterns generated by a variety of such L-systems and found recurrence relations in line with higher plant growth. Following on from this work, Smith (1984) demonstrated the potential of L-systems for the synthesis of realistic images of plants, while Aono and Kunii (1984) explored modelling of trees. Szilard and Quinton (1979) proposed representation of geometry within the strings defining the plant structure based on a LOGO-style turtle (Abelson and diSessa 1982). This turtle interpretation scheme was further developed by Prusinkiewicz (1986, 1987) and is the standard approach used in L-systems-based systems today.

With a formalism that captures component topology and geometry, signalling within the branching structure, and development over time, the stage was set for development of plant modelling languages that could support functional-structural plant modelling of a broad range of phenotypes (Prusinkiewicz *et al.* 1988, Prusinkiewicz and Hanan 1989, Prusinkiewicz *et al.* 2000). With the addition of continuous parameters (Lindenmayer 1974; Prusinkiewicz and Hanan 1990, Hanan 1992), a greater variety of lineage and endogenous processes could be simulated (Prusinkiewicz and Lindenmayer 1996). Extension of this line of research continued with the inclusion of environmental effects in open L-systems (Mech and Prusinkiewicz 1996) through communication with an external program capturing environmental processes. Kurth (1994) developed a sensitive growth grammar approach representing an alternative line of development of the L-systems idea, initially aimed at eco-forestry applications. This work continued with transformation of the representation of the plant from strings to graphs (Kurth *et al.* 2005, Kniemeyer 2008), extending the possible range of applications. Other lines of L-system-inspired research (Lindenmayer 1987) moved away from the plant level to the tissue and cellular scale (Prusinkiewicz and Runions 2012).

L-system models of a variety of plants, from herbaceous to trees can be found, for example, in journal special issues (Godin and Sinoquet 2005, Hanan and Prusinkiewicz 2008, Fourcaud *et al.* 2008, Vos *et al.* 2010, de Jong *et al.* 2011, Guo *et al.* 2011), and are too many to list individually here. L-systems have also proved a useful reference for other plant modelling approaches, being compared with Greenlab (Loi and Cournede 2008) for example. They have also been incorporated into other plant modelling systems, such as Lignum (Perttunen and Sievänen 2005), and openALEA (Boudon et *al.* 2012).

WHERE TO

Many advances have been made in simulating individual processes in plants using L-systems-based approaches. Models of light interception (Chelle *et al.* 2004, Cieslak *et al.* 2008) allow local estimation of

leaf photosynthesis, while carbon allocation models (Allen *et al.* 2005) disburse photosynthate to drive vegetative and reproductive development. Biomechanics of bending of branches under fruit load (Costes *et al.* 2008) make feedback to the developmental processes possible. Some key future pathways for L-systems modelling will be development of methods to integrate these different aspects easily (Cieslak *et al.* 2011). Development of techniques supporting modelling of self-organisational processes (Palubiki *et al.* 2009) may play an important role, particularly for tree development, where what isn't there plays almost as important a role as what is.

Multi-scale modelling will also feature in L-systems models of the future. For example, current models of genetic and hormonal processes at a plant scale (Buck-Sorlin *et al.* 2005, Han *et al.* 2010) will need to become more localised to drive accurate modelling of genotype-environment-management scenarios. By combining with carbon allocation models, hypothesis-driven modelling of branching and flowering processes can then be explored.

In common with other FSPM systems, another key area of future application will be as a platform for further simulation. Examples include eco-physiological models, spray deposition (Dorr *et al.* 2008), insect-plant interactions (Hanan *et al.* 2002), and plant-pathogen interactions (Pangga *et al.* 2011).

L-systems have proved to be a robust formalism for describing growth and development, forming an integral part of many modern plant modelling languages and systems. As more detailed multi-scaled issues are tackled, both down to genetic scale and up to eco-scale, the challenge will be to extend the underlying formalism, to meet the needs of new scientific issues.

ACKNOWLEDGMENTS

I'd like to thank Gerhard Buck-Sorlin, Christophe Godin, Winfried Kurth, Przemek Prusinkiewicz, Philippe de Reffye, and Risto Sievanen for sharing their thoughts about the influence of L-systems on their work.

LITERATURE CITED

Abelson H, diSessa A. 1982. Turtle geometry. M.I.T. Press, Cambridge.

Allen M, Prusinkiewicz P, DeJong T. 2005. Using L-systems for modeling source-sink interactions, architecture and physiology of growing trees: the L-PEACH model. New Phytologist 166, 869-880.

Aono M, Kunii TL. 1984. Botanical tree image generation. IEEE Computer Graphics and Applications, 4(5):10-34

Boudon F, Pradal C, Cokelaer T, Prusinkiewicz P, Godin C. 2012. L-Py: an L-system simulation framework for modeling plant architecture development based on a dynamic language. Front. Plant Sci. 3:76. doi: 10.3389/fpls.2012.00076

Buck-Sorlin GH, Kniemeyer O, Kurth W. 2005. Barley morphology, genetics and hormonal regulation of internode elongation modelled by a relational growth grammar. New Phytologist 166: 859–867.

Chelle M, Hanan J, Autret H. 2004. Lighting virtual crops: the CARIBU solution for open L-Systems. In 'Proceedings of the 4th International workshop on functional–structural plant models'. p. 194. (UMR AMAP: Montpellier, France)

Cieslak M, Lemieux C, Hanan J, Prusinkiewicz P. 2008. Quasi-Monte Carlo simulation of the light environment of plants. Functional Plant Biology, **35**: 837-849.

Cieslak M, Seleznyova AN, Prusinkiewicz P, Hanan J. 2011. Towards aspect-oriented functional-structural plant modelling. Annals of Botany 108(6):1025-1041.

Cohen. 1967. Computer simulation of biological pattern generation processes. Nature, 216:246-248, 1967.

Costes E, Smith C, Renton M, Guédon Y, Prusinkiewicz P, Godin C. 2008 MAppleT: simulation of apple tree development using mixed stochastic and biomechanical models. Functional Plant Biology 35(10), pp. 936-950.

DeJong TM, Da Silva D, Vos J, Escobar-Gutiérrez AJ. 2011. Using functional–structural plant models to study, understand and integrate plant development and ecophysiology, Annals of Botany 108(6): 987-989

Dorr G, Hanan J, Adkins S, Hewitt A, O'Donnell CO, Noller B, 2008. Spray deposition on plant surfaces: a modelling approach., Functional Plant Biology 35:988–996

Fourcaud T, Zhang X, Stokes A, Lambers H, Körner C. 2008. Plant Growth Modelling and Applications: The Increasing Importance of Plant Architecture in Growth Models. Ann Bot 101(8): 1053-1063

Frijters D, Lindenmayer A. 1974. A model for the growth and flowering of Aster novae-angliae on the basis of table (l,O)Lsystems. In G. Rozenberg and A. Salomaa, editors, L Systems, Lecture Notes in Computer Science 15, pages 24-52. Springer-Verlag, Berlin.

Godin C, Sinoquet H, Costes E. 2005. Plant architecture modelling: virtual plants and complex systems. In: Turnbull C, ed. Plant architecture and its manipulation. Oxford, UK: Blackwell, 238–287.

Godin C, Sinoquet H. 2005. Functional–structural plant modelling. New Phytologist, 166: 705–708.

Guo Y, Fourcaud T, Jaeger M, Zhang X, Li B. 2011. Plant growth and architectural modelling and its applications. Ann Bot 107(5): 723-727

Han L, Gresshoff PM, Hanan J. 2010. A functional-structural modelling approach to autoregulation of nodulation. Annals of Botany 107(5): 855-863

Hanan J. 1992. Parametric L-systems and Their Application To the Modelling and Visualization of Plants. Ph.D. dissertation, University of Regina.

Hanan J, Prusinkiewicz P. 2008. Foreword: Studying plants with functional–structural models. Functional Plant Biology 35(10) vi – viii.

Hanan JS, Prusinkiewicz PW, Zalucki M, Skirvin D. 2002. Simulation of insect movement with respect to plant architecture and morphogenesis, Computers and Electronics in Agriculture, 35:255-269.

Hogeweg P, Hesper B. 1974. A model study on biomorphological description. Pattern Recognition, 6:165-179.

Kniemeyer O, 2008. Design and Implementation of a Graph Grammar Based Language for Functional-Structural Plant Modelling. PhD thesis, University of Cottbus.

Kurth W, 1994. Growth Grammar Interpreter GROGRA 2.4: a software tool for the 3-dimensional interpretation of stochastic, sensitive growth grammars in the context of plant modelling. Berichte des Forschungszentrums Waldökosysteme der Universität Göttingen, Ser. B (38).

Kurth W, Kniemeyer O, Buck-Sorlin G, 2005. Relational Growth Grammars - a graph rewriting approach to dynamical systems with a dynamical structure. Lecture Notes in Computer Science 3566, Springer, Berlin 2005, 56-72.

Lindenmayer A. 1968a. Mathematical models for cellular interactions in development I. Filaments with one-sided inputs. *Journal of Theoretical Biology* **18**: 280-299.

Lindenmayer A. 1968b. Mathematical models for cellular interactions in development II. Simple and branching filaments with two-sided inputs. *Journal of Theoretical Biology* **18**: 300-315.

Lindenmayer A. 1987. An introduction to parallel map generating systems. In H. Ehrig, M. Nagl, A. Rosenfeld, and G. Rozenberg, editors, Graph grammars and their application to computer science; Third International Workshop, Lecture Notes in Computer Science 291, pages 27-40. Springer-Verlag, Berlin.

Lindenmayer A. 1974 Adding continuous components to L-systems. In G. Rozenberg and A. Salomaa, editors, L Systems, Lecture Notes in Computer Science 15, pages 53-68. Springer-Verlag, Berlin.

Loi C, Cournede P-H. 2008. Description of the Greenlab development model with stochastic L-systems and monte-carlo simulations. Technical report, INRIA.

Mech R, Prusinkiewicz P. 1996. Visual Models of Plants Interacting with Their Environment. Proceedings of SIGGRAPH 96 (New Orleans, Louisiana, August 4-9, 1996). In Computer Graphics Proceedings, Annual Conference Series, 1996, ACM SIGGRAPH, pp. 397-410.

Palubicki W, Horel K, Longay S, Runions A, Lane B, Mech R, Prusinkiewicz P. 2009. Self-organizing tree models for image synthesis. ACM Transactions on Graphics 28(3), 58:1-10.

Pangga IB, Hanan J, Chakraborty S. 2011. Pathogen dynamics in a crop canopy and their evolution under changing climate. Plant Pathology 60:1, 70-81

Prusinkiewicz P. 1986. Graphical applications of L-systems. In Proceedings of Graphics Interface '86 -- Vision Interface '86, pages 247-253. CIPS.

Prusinkiewicz P. 1987. Applications of L-systems to computer imagery. In Ehrig, Nagl, Rosenfeld, and Rozenberg, eds, Graph grammars and their application to computer science; Third International Workshop, pages 534-548. Springer-Verlag, Berlin, 1987. Lecture Notes in Computer Science 291.

Prusinkiewicz P, Hanan J. 1989. Lindenmayer systems, fractals, and plants, volume 79 of Lecture Notes in Biomathematics. Springer-Verlag, Berlin.

Prusinkiewicz P, Hanan J. 1990. Visualization of botanical structures and processes using parametric L-systems. In Thalmann, ed., Scientific Visualization and Graphics Simulation, pp. 183-201. Wiley & Sons.

Prusinkiewicz P, Hanan J, Mech R. 2000. L-system-based plant modelling language. In: Nagl M, Schuerr A, Muench M. eds. *Applications of graph transformations with industrial relevance.* Lecture Notes in Computer Science. Berlin: Springer, 395–410.

Prusinkiewicz P, Lindenmayer A. 1996. The algorithmic beauty of plants. New York: Springer-Verlag.

Prusinkiewicz P, Lindenmayer A, Hanan J. 1988. Developmental models of herbaceous plants for computer imagery purposes. Proceedings of SIGGRAPH '88 (Atlanta, Georgia, August 1-5, 1988), in Computer Graphics 22,4 (August 1988):141-150, ACM SIGGRAPH, New York.

Prusinkiewicz P, Runions A. 2012. Computational models of plant development and form. New Phytologist 193, pp. 549-569.

Perttunen J, Sievänen R. 2005. Incorporating Lindenmayer systems for architectural development in a functional-structural tree model, Ecological Modelling, 181:479-491.

Room PM, Hanan J, Prusinkiewicz P. 1996. Virtual plants: new perspectives for ecologists, pathologists and agricultural scientists. Trends in Plant Science 1: 33-38.

Smith AR. 1984. Plants, fractals, and formal languages. Proceedings of SIGGRAPH '84 (Minneapolis, Minnesota, July 22-27, 1984) in Computer Graphics, 1,8, (July 1984), pages 1-10.

Szilard AL, Quinton RE. 1979. An interpretation for DOL systems by computer graphics. The Science Terrapin, 4:8-13.

Vos J, Evers JB, Buck-Sorlin GH, Andrieu B, Chelle M, de Visser PHB. 2010. Functional-structural plant modelling: a new versatile tool in crop science. J Exp Bot 61:2101–2115

Proceedings of the 7th International Conference on Functional-Structural Plant Models, Saariselkä, Finland, 9 - 14 June 2013. Eds. Risto Sievänen, Eero Nikinmaa, Christophe Godin, Anna Lintunen & Pekka Nygren.
http://www.metla.fi/fspm2013/proceedings. ISBN 978-951-651-408-9.

Biomechanics of Bark Patterning in Grasstree

Holly Dale*[1], **Adam Runions**[2], **David Hobill**[1] and **Przemyslaw Prusinkiewicz**[2]
[1]*Department of Physics and Astronomy and* [2]*Department of Computer Science,*
University of Calgary, AB T2N 1N4, Canada
**Correspondence:* hjdale@ucalgary.ca

Highlights: Bark patterns are a visually important characteristic of trees, attributed to fractures caused by secondary growth of the trunk and branches. A detailed understanding of bark patterns has been impeded by insufficient information regarding biomechanical properties of bark and the corresponding difficulties in faithfully modeling bark fractures using continuum mechanics. Here we focus on grasstrees, which have an unusual bark-like structure composed of distinct leaf bases connected by sticky resin. Due to its discrete character, this structure is exceptionally well suited for computational studies. We created a dynamic grasstree model, which captures both the phyllotactic patterning of the leaf bases during primary growth and the emergence of fractures due to secondary growth. The model reproduces key features of grasstree bark patterns, including inhomogeneities due to compression of leaf bases at the sites of inflorescences.

Keywords: Bark pattern, fracture mechanics, primary and secondary growth, biomechanical model.

INTRODUCTION

Grasstrees (*Xanthorrhoea*, Fig. 1) are a genus of monocots native to Australia with a morphology adapted to frequent fires. Their stems are pseudomonopodial. The straight course of the stem is disturbed when the terminal apex produces an inflorescence and an auxillary bud takes over further vegetative development (Borsboom 2005). Leaves are arranged into dense spiral phyllotactic patterns (Staff 1968). During fires, leaves are burnt back to their bases, which are cemented together by melting resin to form a type of bark that protects the tree from disease and future fires (Lamont et al. 2004). Over time, this resin fractures, partitioning interconnected leaf bases into separate regions. As a result, grasstree bark gradually progresses from a regular lattice of interconnected leaf bases near the top of the tree to a fractured pattern of patches similar to that observed in other tress near the base. Here we show that this progression, and its disturbances at the sites supporting past inflorescences, can be explained in mechanical terms. To this end, we have constructed a virtual grasstree that combines a descriptive model of primary growth and phyllotaxis with a mechanical model of fractures operating on the discrete lattice of parastichies induced by this phyllotaxis.

PREVIOUS WORK

Figure 1. Young and older grasstree.

Fractures have been simulated using both discrete and continuous models. Skjeltorp and Meakin (1988) introduced a mass-spring model to simulate fractures in an elastic layer under tension. Federl and Prusinkiewicz (1996) adopted this system to model fractures in tree bark. In contrast to the work presented here, they considered the mass-spring as an (imperfect) approxi-mation of bark thought of as a homogeneous material. Improving this approximation, Federl and Prusinkiewicz (2002) modified their previous model by replacing masses and springs with a finite-element method. The resulting model produced several plausible bark patterns, but the question of whether real bark is adequately approximated as a continuous, homogenous sheet was not addressed. The grasstree offers a unique opportunity to create a faithful bark model due to the macroscopic lattice structure induced by the underlying phyllotactic arrangement of leaf bases. This structure justifies the use of a discrete model.

SIMULATIONS

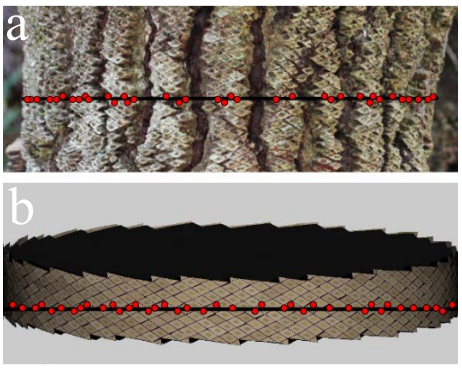

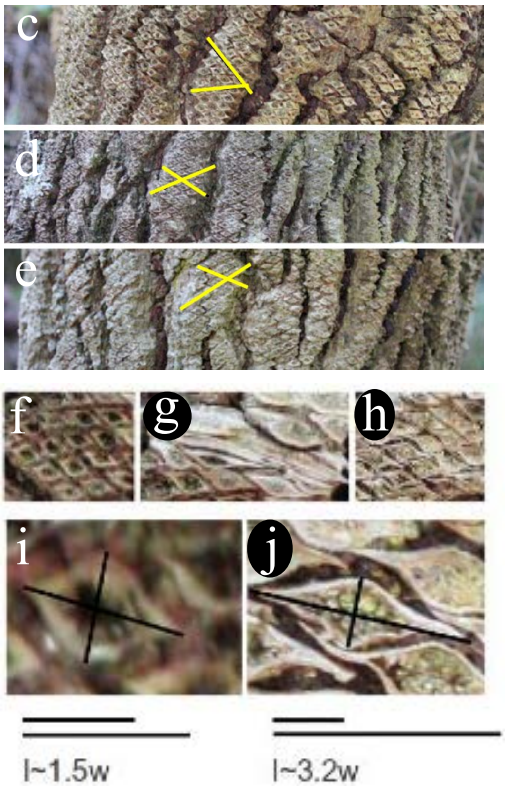

Figure 2. Estimating parameters of the phyllotactic pattern. (a,b) Number of bases that a horizontal line intersects in a real image (~37) and in the model (~40). (c-e) Estimation of the angle between parastichies (~56°). (f-j) The horizontal stretch of bases: (f,i) at the location between inflorescences, (g) at a bend of the stem where leaf bases are severely deformed, and (h,j) at the location of an inflorescence.

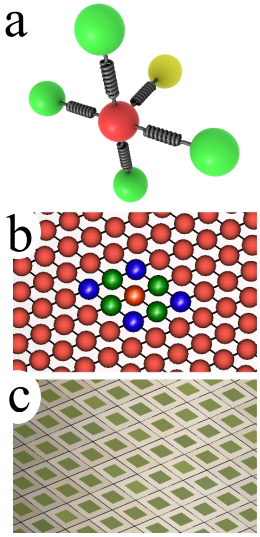

Figure 3. (a,b) Mesh of masses and springs. Yellow mass belongs to the inner layer that cau-ses growth in diameter. Blue masses complete leaf bases. (c) Resulting pattern of leaf bases.

The shoot apical meristem produces leaves sequentially in a phyllotactic pattern. Parameters of this pattern were inferred from photographs of real grasstrees (Fig. 2). In the model, we represented leaf bases as masses and their resin connections as (Hookean) springs, connecting each base to its four nearest neighbors (Fig. 3). The bark layer increased in radius, and thus in circumference, due to secondary growth. This was simulated by gradually pushing each mass outwards with springs that connected leaf bases to the inner core of the tree. Consequently, the spring forces between masses increased until a critical threshold value was reached and some springs broke (the threshold value was subject to small random variations, needed to break the symmetry of the system). The bark pattern was defined by the resulting fractures, which separated patches of bases connected by the remaining springs.

To simulate the influence of inflorescence sites, we have periodically shifted the growth axis and/or the radius of the bark layer. We used measurements of a real grasstree (Lamont et al. 1979) to calibrate proportions of this system. We also observed that leaf bases near the flowering sites have different aspect ratios, compared to the stem segments between flowering sites (Fig. 2c), and we incorporated these changes into the model by modifying parameters of the phyllotactic pattern.

RESULTS AND DISCUSSION

We have created a model of grasstree development (Fig. 4) as a basis for studying the emergence of grasstree bark patterns. These patterns are different near the sites of inflorescences and between these sites (Fig. 5). The areas near flowering sites are characterize by a network of diagonal fractures that run along the parastichies. Areas between flowering sites have long fractures running approximately parallel to the stem axis. Our biomechanical model emergently captures these differences. Although the generality of this result is qualified by the unusual structure of grasstree bark, it supports the hypothesis that bark pattern formation is primarily a biomechanical phenomenon. From a broader perspective, this result increases the spectrum of morphogenetic phenomena in which biomechanics and properties of space, rather than detailed genetic patterning, play a key role (Prusinkiewicz and de Reuille, 2010).

Figure 4. Simulation of grasstree development

ACKNOWLEDGMENTS

Thanks to Steven Longay for creating Fig. 3. Support of this work by Undergraduate Student Research Award and Discovery Grant from the National Sciences and Engineering Research Council of Canada is gratefully acknowledged.

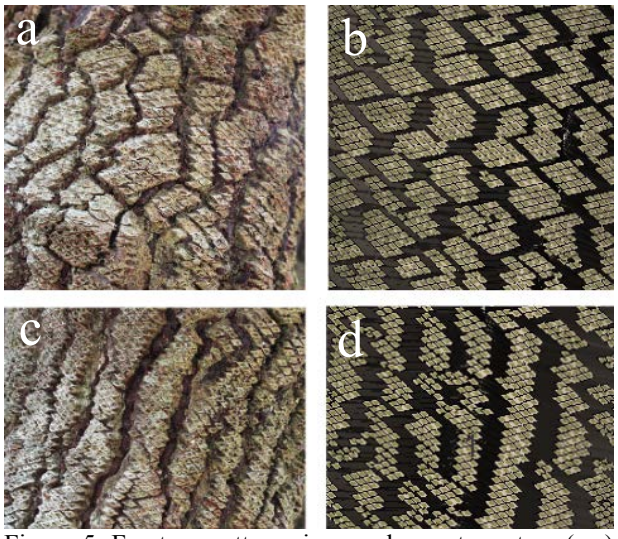

Figure 5. Fracture patterns in a real grasstree stem (a,c) and simulation (b,d). Areas near inflorescence sites have compressed bases with more diagonal fractures (a,b), regions without flowering have primarily vertical fractures (c,d).

LITERATURE CITED

Borsboom AC. 2005. *Xanthorrhoea:* A review of current knowledge with a focus on *X. johnsonii* and *X. latifolia*, two Queensland protected plants-in-trade. Environmental Protection Agency, Queensland, 87 pp.

Federl P, Prusinkiewicz P. 1996. A texture model for cracked surfaces. In *Proceedings of the Seventh Western Computer Graphics Symposium*, pp. 23-29.

Federl P, Prusinkiewicz P. 2002. Finite element model of fracture formation on growing surfaces. In *Proceedings of ICCS 2004*, Part II, *LNCS 3037*, pp. 138-145.

Lamont BB, Downes S. 1979. The longevity, flowering and fire history of the grasstrees *Xanthorrhoea preissii* and *Kingia Australis*. *Journal of Applied Ecology* **16**:893-899.

Lamont BB, Wittkuhn R, Korczynskyj D. 2004. Ecology and ecophysiology of grasstrees. *Australian Journal of Botany* **52**:561-582.

Prusinkiewicz, P, Barbier de Reuille, P. 2010. Constraints of space in plant development. *Journal of Experimental Botany* **61**:2117-2129.

Skjeltorp AT, Meakin P. 1988. Fracture in microsphere monolayers studied by experiment and computer simulation. *Nature* **335**:424-426.

Staff IA. 1968. A study of the apex and growth patterns in the shoot of *Xanthorrhoea media* R. Br. *Phytomorphology* **18**:153-165.

Proceedings of the 7th International Conference on Functional-Structural Plant Models, Saariselkä, Finland, 9 - 14 June 2013. Eds. Risto Sievänen, Eero Nikinmaa, Christophe Godin, Anna Lintunen & Pekka Nygren.
http://www.metla.fi/fspm2013/proceedings. ISBN 978-951-651-408-9.

Floral phyllotaxis of magnolia in computer simulations - towards understanding phyllotactic fingerprint

Beata Zagórska-Marek and **Marta Fijak**
Institute of Experimental Biology, University of Wroclaw,Kanonia Str.6/8, 50-328 Wroclaw, Poland
**correspondence:* beata@biol.uni.wroc.pl

Highlights: Magnolia's floral shoot, with its uniquely rich and diverse phyllotaxis, has been modeled with application of a special program based on geometric model of phyllotaxis. First survey of phyllotactic diversity obtained in the library of 1200 computer simulations proved that, besides the most common main Fibonacci, also other patterns, frequently encountered in nature, such as Lucas and bijugy, are readily formed. This is a part of extensive studies aimed to elucidate the mechanism of phyllotactic fingerprint – the species or genet specific pattern of phyllotactic diversity, first in magnolia flowers and then in other plant structures and taxa.

Keywords: phyllotaxis**,** *Magnolia*, floral parts, phyllotactic fingerprint, plant development, shoot apical meristem

INTRODUCTION

Double change in the identity of floral organ primordia, associated with the change in their sizes (Zagórska-Marek 1994, Xu 2006, Xu and Rudall 2006, Zagórska-Marek and Szpak 2008), creates the potential for extreme diversity of floral phyllotaxis in magnolia (Erbar and Leins 1982, Zagórska-Marek 1994). Yet different magnolia species or even genets execute this potential in different ways. Some have exceptionally rich, others rather limited spectrum of the diversity (Wiss and Zagórska-Marek 2012). The spectrum is so specific and persistent in consecutive blooming seasons that it can be treated as the individual tree's fingerprint (Zagórska-Marek 2011). Understanding this phenomenon seems to be a great challenge.

The aim of our work was to test, in computer simulations, how the changes in geometric parameters of primordia generated by apical meristem affect phyllotactic pattern formation in virtual magnolia flower. For that purpose we have used geometric model of phyllotaxis and special computer program Phyllotaxis ver. 0.3 (Zagórska-Marek and Szpak 2008).

RESULTS AND DISCUSSION

In the first step of testing we asked ourselves, is there a connection between evidently high and changing number of spirally arranged stamens and the number of patterns and phyllotactic transitions in magnolia gynoecium. We have noted in preliminary tests that the number indeed affects the quality of gynoecial phyllotaxis, defined (following Adler 1974) by modified contact parastichy pair formula (a_s:b_z), in which s and z indices stand for parastichy orientation (Fig.1).

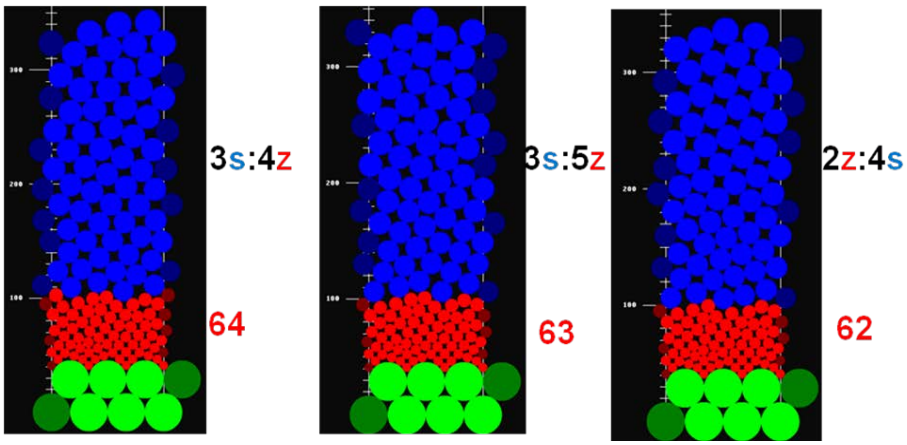

Fig. 1. Magnolia's virtual floral shoots. The parameters of all three simulations are the same except for the number of stamens (in red). Decreasing it by one in two consecutive steps, changes gynoecial phyllotaxis dramatically from Lucas (left), through main Fibonacci (middle) to bijugy (right); green, red and blue circles denote respectively the perianth elements, stamens and carpels. Gynoecial phyllotaxis is defined by contact parastichy pair formula.

Over 1200 pictures were created, divided into 3 groups. The only difference between them was the ratio between stable size of perianth elements and the size of the first stamen. The starting pattern of the perianth was always tricussate, with the 118° intersection angle between the 3s:3z connecting lines. In agreement with developmental changes observed in nature, we set the program to gradually increase the size of circles representing stamens and carpels. Speed of an increase was set to 1.001 for stamens and 1.004 for carpels, which means that every next stamen was bigger by 0.001 of the radius, and carpel was bigger by 0.004. To add a more realistic feel to the simulation we set a tolerance in radius change for 5%. The software allows setting a seed for the random number generator. The groups of simulations were created as follows: the small group (S), with the initial size of stamens set to 6.5 and of carpels to 8.0, the medium group (M) with the size of stamens set to 7 and of carpels to 8.5, and the large group (L) with the size of stamens set to 7.5 and of carpels to 9.0. We generated 400 pictures for each group, differing in a number of stamens from 60 to 100, having constant number of carpels set to 50, and differing in a seed for random factor from 1 to 10.

In every case, the initial phylotactic pattern, in the 3rd row, starting from the end of androecium zone, and the ultimate one, in the 3rd row down from the end of gynoecium, i.e. from the top of virtual floral shoot, have been determined. This way, apart from the initial gynoecial pattern we also acquired information on pattern rearrangements in given subgroups. Patterns were identified by counting contact parastichies and recorded in a form of contact parastichy pair formula (a_s:b_z). To process all these data we developed a small program (Counter ver. 0.1).

Qualities and frequencies of patterns have been summarized for all analyzed cases (Table 1), because there was no significant difference in these parameters among three groups. The most common was the main Fibonacci pattern. The Lucas pattern was the second and bijugy the third most frequent among the patterns. We have noted extreme asymmetry of pattern chiral configurations, which in nature occur in more similar frequencies. This effect of simulations is not yet fully understood.

Table 1. Quality and frequency of ultimate gynoecial patterns; F – main Fibonacci, L – Lucas, Bi – bijugy, T –tetrajugy, Tr- trijugy, P- pentajugy, irr.- irregular pattern

pattern expression	3s:5z	4s:5z	4s:6z	4s:4z	3s:4z	5s:5z	5s:6z	4s:7z	3s:3z	2s:4z	2s:5z	irr.
N° of cases	356	128	225	131	301	3	2	4	8	6	1	35
pattern type	F		F(Bi)	F(T)	L	F (P)		L	F(Tr)	F(Bi)		

In the next step, we analyzed the pattern rearrangements (phyllotactic transitions) in all 3 groups: S, M, L. The data for each group had been divided into 5 subgroups, according to the range of changes in the number of stamens: first one with 60 to 68 stamens, second with 69 to 76, third with 77 to 84, fourth with 85 to 92 and fifth with 93 to 100. The highest rate of phyllotactic transitions was recorded for each range in S group (Table 2).

Table 2. Number of rearrangements associated with changing number of stamens in 3 groups: S, M and L

range	60-68	69-76	77-84	85-92	93-100	Sum
S	58	40	47	39	40	224
M	26	14	17	22	29	108
L	31	24	13	13	7	88

From the same set of data it was possible to extract the information, which pattern is developmentally the most stable. Among the 5 most common patterns, surprisingly, the most stable was the Lucas pattern (Table 3).

Table 3. Gynoecial pattern stability. Most stable are those where an initial pattern frequency and the frequency of cases, in which the same pattern was stable, are similar. Their ratio is given at the bottom of the table.

Pattern	3s:5z	4s:5z	4s:6z	4s:4z	3s:4z
initial	493	119	255	58	104
ultimate	356	128	225	131	301
stable	342	60	190	33	103
%	69,37%	50,04%	74,50%	56,89%	99,00%

Finally we plotted the data about rearrangements in to a graph (Fig.2). To have a right scale we divided the number of rearrangements in each subgroup by the number of rearrangements in the whole group (S, M, L).

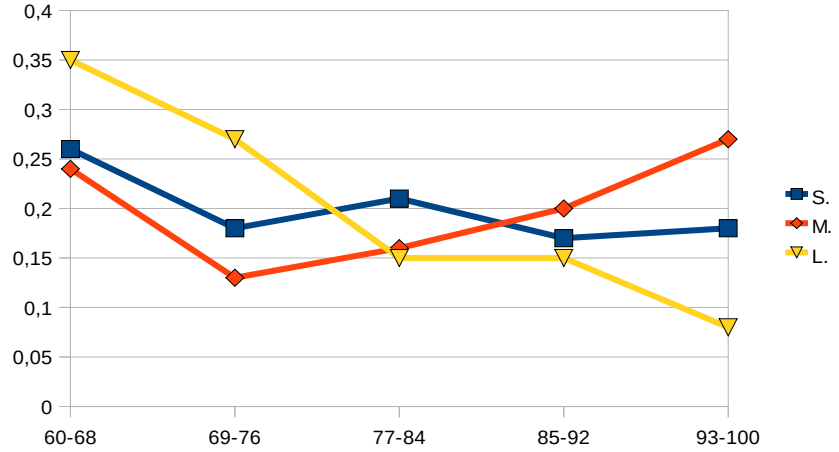

Fig. 2. Frequency of rearrangements depending upon the number of stamens in 3 groups: S, M and L. In the range between 77 and 92 stamens the pattern, regardless its quality, is the most stable.

It has been shown already, in similar simulations, that some phyllotactic patterns in their lowest expressions are more developmentally stable than others (Szpak and Zagórska-Marek 2011). In magnolia, however, pattern expressions in gynoecium are high. Shown here clear disproportion between the number of rearrangements in S and L group of magnolia virtual floral shoots as well as pattern stability, which depends upon the number of organs generated by floral meristem, are in fact the first hints of why some magnolias may have gynoecial phyllotaxis more diverse than others. More accurate empirical data should be collected, to create a collation with the data obtained from simulations. We also feel that developing a program for analyzing the quality of phyllotactic pattern should be considered to eliminate the human error in diagnosing the effects of simulations. More research is also needed to understand fully the phenomenon of phyllotactic fingerprint – our working hypothesis that changing number of stamens may favor selection of the specific patterns has been neither falsified nor verified, yet!

LITERATURE CITED

Adler I. 1974. A model of contact pressure in phyllotaxis. *J.Theor.Biol.***45**: 1-79.

Erbar C, Leins P. **1982**. Zur Spirale in Magnolien-Blüten. Beitr Biol Pflanzen.**56**:225–241.

Szpak M, Zagórska-Marek B. 2011. Phyllotaxis instability – exploring the depths of first available space. *Acta Soc. Bot. Pol*. **80**:279–284. http://dx.doi.org/10.5586/asbp.2011.043

Xu FX. 2006. Floral ontogeny of two species in *Magnolia* L. *J. Integr. Plant Biol.* **48**:1197–1203. http://dx.doi.org/10.1111/j.1744-7909.2006.00341.x

Xu FX, Rudall PJ. 2006. Comparative floral anatomy and ontogeny in Magnoliaceae. *Plant Syst Evol.* **258**:1–15. http://dx.doi.org/10.1007/s00606-005-0361-1

Wiss D, Zagórska-Marek B. 2012. Geometric parameters of the apical meristem and the quality of phyllotactic patterns in *Magnolia* flowers. *Acta Soc.Bot.Pol*. **81**:203-216. http://dx.doi.org/10.5586/asbp.2012.029

Zagórska-Marek B, Szpak M. 2008. Virtual phyllotaxis and real plant model cases. *Funct Plant Biol.* **35:**1025–1033. http://dx.doi.org/10.1071/FP08076

Zagórska-Marek B. 2011. Magnolia flower - the living crystal. *Magnolia. The Journal of the Magnolia Society International* **89**: 11-21.

Proceedings of the 7th International Conference on Functional-Structural Plant Models, Saariselkä, Finland, 9 - 14 June 2013. Eds. Risto Sievänen, Eero Nikinmaa, Christophe Godin, Anna Lintunen & Pekka Nygren.
http://www.metla.fi/fspm2013/proceedings. ISBN 978-951-651-408-9.

Modelling the spatial arrangement of vascular bundles in plants

Fabrizio Carteni[1]*, **Francesco Giannino**[1], **Gianni Boris Pezzatti**[2] and **Stefano Mazzoleni**[1]
[1]*Dipartimento di Agraria,University of Naples Federico II, via Università 100, 80055, Portici (Na), Italy,*
[2]*Swiss Federal Institute for Forest, Snow and Landscape Research, Ecosystem Boundaries Research Unit, Via Belsoggiorno 22, CH-6500 Bellinzona, Switzerland*
**correspondence:* fabrizio.carteni@unina.it

Highlights: The spatial arrangement of vascular bundles varies between plant species and organs. A novel reaction-diffusion 2D model is presented defining a set of logical and functional rules able to simulate the differentiation of procambium, phloem and xylem. The model shows that a common mechanism, lying behind the formation of vascular tissues, is able to qualitatively reproduce most stelar structures observed.

Keywords: PDE, reaction-diffusion, stele evolution, tissue differentiation

INTRODUCTION

Spontaneous spatial pattern formation as a result of the dynamic interactions of system components is common in nature at all scales. In plant development and morphogenesis, several regular patterns have been widely studied such as the establishment of the main axes, phyllotaxis, organ shape and venation. In the last decades, simulation models have proven to be useful tools for hypotheses testing on complex systems. Models have been often applied to unravel non-intuitive relations of local processes with the emergence of global forms and patterns. Several studies using computational modelling have been carried out on plant morphodynamics (Jönsson and Krupinski, 2010; Prusinkiewicz and Runions, 2012). Recent work (reviewed in: Jönsson et al., 2012) has focused on two topics: i) venation and phyllotaxis driven by auxin polar transport and ii) genetic regulation of stem cells in apical meristems. So far, no modeling effort has been done yet on the formation of primary vascular structures. We present a spatially explicit reaction-diffusion model defining a set of logical and functional rules able to simulate the differentiation of procambium, phloem and xylem. The model qualitatively reproduces most stelar structures observed in different plant taxa.

MODEL DESCRIPTION

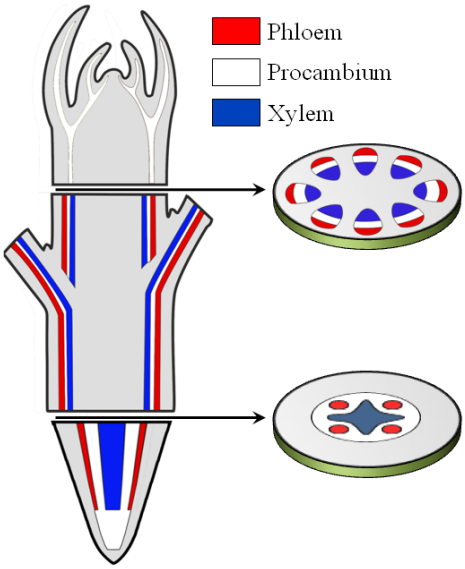

Fig. 1. Schematic representation of vascular patterns in plants.

We developed a mathematical model that simulates the development of a group of undifferentiated cells in a sub-apical transverse section of stems and roots (Fig. 1). We used the activator–inhibitor and activator-substrate modelling approaches introduced by Gierer & Meinhardt (1972), and fully developed by Meinhardt

(1982). The main assumptions of our model are the following:

- mitotic index strongly relates to cell position within the meristem, being significantly higher in the outer zone than in the inner zone (Laufs et al., 1998);
- sugar metabolism, particularly cellular sugar status (Koch, 2004; Eveland and Jackson, 2012), plays a fundamental role in plant development and definition of spatial domains within plant organs (Pien et al., 2001);
- the emergence of vascular tissues depends on the juxtaposition of adaxial/central and abaxial/peripheral spatial domains which sets a cascade of species-specific and organ-specific genetic and molecular dynamic processes.

We defined a system of 9 PDEs that describe the spatio-temporal dynamics of different compounds in a group of meristematic cells. A first equation describes the sugar status of the cells. A set of three equations describes the dynamics of an activator-substrate system which leads to the differentiation of procambium. Another set of 5 equations drives the emergence of phloem and xylem and describe the dynamics of two locally mutually exclusive compounds with lateral reciprocal facilitation (Meinhardt and Gierer, 1980). Meristematic cells are in a continuous state of division and the velocity of cellular division depends on their position within the organ. Sucrose cleavage to hexoses is positively correlated to the division rate, then fast dividing cells have higher hexoses concentrations. An hexose threshold value results in the activation of genes marking the cell as either adaxial or abaxial. The two newly defined cell domains start producing specific signals which are necessary to produce an autocatalytic activator responsible for the activation of procambium-fate genes. Once differentiated, provascular cells start the production of two other competing autocatalytic activators responsible for the activation of phloem-fate and xylem-fate genes respectively. According to the prevalence of either one or the other activator, procambial cells differentiate into either phloem or xylem.

RESULTS AND DISCUSSION

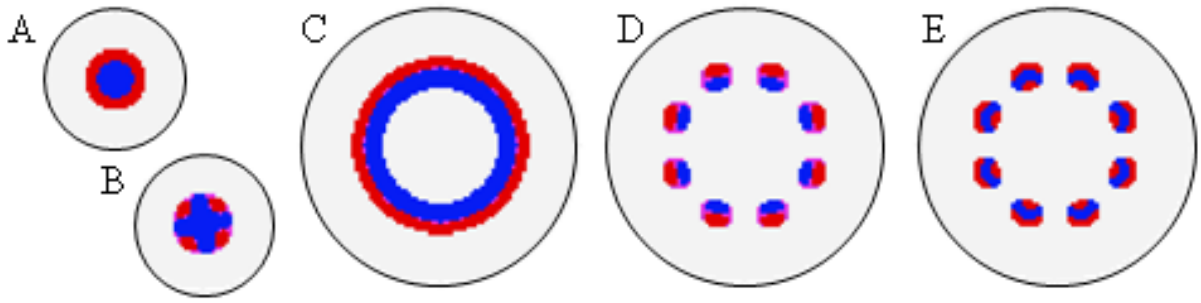

Fig. 2. Examples of simulated steles. Grey: ground tissue; Red: phloem; Blue: xylem. A) Protostele; B) Actinostele; C) Siphonostele; D) Eustele with collateral bundles; E) Eustele with bicollateral bundles.

The arrangement of vascular bundles observed in plant steles, can be summed up in three basic types: i) protostele presenting a solid column of vascular tissue (Fig. 2A); ii) siphonostele characterised by an hollow cylinder of vascular tissue (Fig. 2C); iii) eustele showing separated strands of vascular tissue, usually arranged as a discontinuous cylinder (Fig. 2D) (Beck et al., 1982).

Model simulations were able to effectively reproduce most stelar types observed in plants showing that different vascular patterns can be developed by similar molecular and genetic processes (Fig. 2). Model numerical analysis and simulation results of the first set of equations, show that the emergence of protostelic opposed to siphonostelic or eustelic patterns depends on domain dimension where the process occurs (Fig. 2 A,C). Varying only the domain diameter, a protostelic structure emerges in small domains, while either siphonostelic or eustelic structures are formed in larger domains. The formation of these latter spatial patterns mainly depends on the parameter controlling the autocatalytic reaction between procambium activator and its substrates. Moreover, the differentiation of both phloem and xylem occurs in consistent arrangements within the abovementioned vascular structures. The different spatial organization of phloem and xylem, e.g. collateral bundles (Fig. 2D) and bicollateral bundles (Fig. 2E), depends on levels of diffusion and reaction rates of respective activators.

Future work will be focused on a better definition of sugar metabolism and on the simulation of secondary growth.

LITERATURE CITED

Beck CB, Schmid R, Rothwell GW. 1982. Stelar morphology and the primary vascular system of seed plants. *Botanical Review* **48**:691-815.

Eveland AL, Jackson DP. 2012. Sugars, signalling, and plant development. *Journal of Experimental Botany* **63(9)**:3367-3377.

Gierer A, Meinhardt H. 1972. A theory of biological pattern formation. *Kybernetik* **12**:30-39.

Jönsson H, Gruel J, Krupinski P, Troein C. 2012. On evaluating models in computational morphodynamics. *Current Opinion in Plant Biology* **15**:103-110.

Jönsson H, Krupinski P. 2010. Modeling plant growth and pattern formation. *Current Opinion in Plant Biology* **13**:5-11.

Koch K. 2004. Sucrose metabolism: regulatory mechanisms and pivotal roles in sugar sensing and plant development. *Current Opinion in Plant Biology* **7**:235-246.

Laufs P, Grandjean O, Jonak C, Kieu K, Traas J. 1998. Cellular parameters of the shoot apical meristem in Arabidopsis. *Plant Cell* **10**:1375-1390.

Meinhardt H, Gierer A. 1980. Generation and regeneration of sequences of structures during morphogenesis. *Journal of theoretical Biology* **85**:429-450.

Meinhardt H. 1982. *Models of biological pattern formation*. London, UK: Academic Press.

Pien S, Wyrzykowska J, Fleming AJ. 2001. Novel marker genes for early leaf development indicate spatial regulation of carbohydrate metabolism within the apical meristem. *The Plant Journal* **25**:663-674.

Prusinkiewicz P, Runions A. 2012. Computational models of plant development and form. *New Phytologist* **193**:549-569.

Proceedings of the 7th International Conference on Functional-Structural Plant Models, Saariselkä, Finland, 9 - 14 June 2013. Eds. Risto Sievänen, Eero Nikinmaa, Christophe Godin, Anna Lintunen & Pekka Nygren. http://www.metla.fi/fspm2013/proceedings. ISBN 978-951-651-408-9.

Estimating the genetic value of F1 apple progenies for irregular bearing during first years of production

Jean-Baptiste Durand[1,2], **Baptiste Guitton**[3], **Jean Peyhardi**[2,4], **Yan Holtz**[5], **Yann Guédon**[2], **Catherine Trottier**[4] and **Evelyne Costes**[3]

[1]*Grenoble University, Laboratoire Jean Kuntzmann, BP53, F-38041 Grenoble Cedex 9, France,* [2]*CIRAD/Inria, Virtual Plants Team, UMR AGAP, F-34095 Montpellier, France,* [3]*CIRAD, UMR AGAP, F-34398 Montpellier, France,* [4]*Institut de Mathématiques et de Modélisation de Montpellier, Université Montpellier 2, F-34095 Montpellier, France,* [5]*INRA, AFEF Team, UMR AGAP, F-34398 Montpellier, France*

**correspondence:* jean-baptiste.durand@imag.fr

Highlights: Flowering regularity in apple trees during the beginning of their mature phase was assessed using new descriptors based on annual yields. These descriptors were approximated using subsamples of annual shoot sequences at axis scale to allow genotype evaluation at reasonable sampling costs. The approximation provided a good discrimination between regular and alternate bearing genotypes. QTLs were detected for some descriptors.

Keywords: alternation indices, biennial bearing, breeding, linear mixed model, *Malus x domestica*, QTL detection.

INTRODUCTION

Because irregular bearing generates major agronomic issues in fruit-tree species (Monselise and Goldschmidt, 1982), particularly in apple, the selection of regular cultivars is desirable. Here, we aimed at defining methods allowing an early diagnostic in populations segregating for bearing behaviour.

It was shown by Guitton *et al.* (2012) that biennial bearing is inheritable and segregates in an apple progeny ("Starkrimson"× "Granny Smith"), suggesting that selecting new varieties with intrinsic regular bearing is a possible strategy. However, breeding programs for fruit-tree species do not consider this trait yet, because it requires flowering observations over several years before its value for a given genotype can be assessed (and the first flowering occurs two to four years after grafting). Development of methods for a faster diagnostic of the bearing tendency of a genotype during its first years of production is thus highly desirable.

The Biennial Bearing Index (BBI) has been widely used to quantify biennial bearing at different scales (Wilcox, 1944): whole areas, individual trees or branches - on apple and other fruit trees. Huff (2001) highlighted that the distribution of BBI strongly depends on the mean and variance of yields, under the hypothesis that they are a random sample. Therefore, the accepted interpretation of BBI as a measure of the magnitude of irregular bearing is questionable. Moreover, it has been shown by Pearce and Dobersek-Urbane (1967) that using BBI on trended series may lead to confound alternation and trend. The observation that yield is subject to a progressive increase in the first years of tree production, motivated our research for new descriptors of alternation. With the aim to dissociate yield increase from bearing pattern, we investigated a new modelling approach incorporating a trend term for yearly yields, and terms representing dependencies and amplitudes of successive deviations from the trend. Our expectation was to distinguish the genotype bearing behaviour applying clustering methods on these new descriptors. To avoid measuring yearly numbers of flowers at tree scale, we also investigated the possibility of early discrimination between genotypes, based on the same descriptors, using samples of successive annual shoots (AS) at axis scale. Finally, from the analysis of correlations between descriptors at both tree and AS scales we explored how fruiting behaviour at tree scale may be obtained from that at axis scale.

MATERIALS AND METHODS

A segregating population obtained from a cross between 'Starkrimson' and 'Granny Smith' (Guitton *et al.*, 2012), was used. One or two tree replicates were available for each of the 120 genotypes composing the population. Flowering recurrence was measured at two scales: whole tree and AS scales. The total number of inflorescences per year and tree was observed from the 2nd to the 7th year after grafting. At AS scale, the

succession of vegetative v. floral AS over the same consecutive years were observed along different types of axes: trunk, long and short axillary shoots. Long axes were scaffolds chosen as similar as possible along the trunks. The data consisted of 2- to 6-year sequences of AS, with 4 to 45 sequences per genotype.

Let $T_{g,r}$ denote the number of years of growth of tree replicate r of genotype g and $Y_{g,r,t}$ its number of inflorescences at year t. A Gaussian linear mixed regression model with first-order autoregressive errors (to model the serial correlations between successive residuals) was used

$$Y_{g,r,t} = \beta + \beta_g + (\alpha + \alpha_g + \xi_{g,r})t + \varepsilon_{g,r,t} \quad (1), \quad \varepsilon_{g,r,t} = (\gamma_g + \gamma_{g,r})\varepsilon_{g,r,t-1} + u_{g,r,t} \quad (2).$$

Here, (1) is a trend sub-model, and the first-order autoregressive process (2) on the deviations $\varepsilon_{g,r,t}$ between $Y_{g,r,t}$ and the trend (Fig. 1) quantifies the alternation through the dependencies between successive residuals (measured by γ_g). Their amplitudes were quantified using a BBI-like index on $\varepsilon_{g,r,t}$, normalized by mean yields, defined as

$$\text{BBI\_res\_norm} = \frac{\left(\sum_r \sum_{t=2}^{T_{g,r}} \left|\hat{\varepsilon}_{g,r,t} - \hat{\varepsilon}_{g,r,t-1}\right|\right) / \sum_r (T_{g,r} - 1)}{\left(\sum_r \sum_{t=1}^{T_{g,r}} Y_{g,r,t}\right) / \sum_r T_{g,r}}.$$

A clustering of the genotypes based on BBI_res_norm and γ_g was obtained using a Gaussian mixture model and the Bayesian information criterion to select the number of clusters (Bishop 2006, Chap. 4 and 9). The ability to retrieve the genotype bearing behaviour (or *class*) from the subsample of AS sequences was assessed by approximating BBI_res_norm and γ_g by their values in the subsamples (leading to two indices referred to as BBI_res_norm_loc and γ_{loc}, respectively). Two other kinds of descriptors computed at AS scale were also used to predict the bearing behaviour: an index of synchronism in flowering based on entropy (Bishop, Chap. 1) and a 2nd-order Markov chain with memory × genotype and memory × year interactions.

Five descriptors, namely BBI_res_norm and γ_g at tree scale, and BBI_res_norm_loc, γ_{loc} and entropy at AS scale, were used for QTL detection which was performed using the STK×GS consensus genetic map (Guitton *et al.*, 2012) and MapQTL® 5.0. (Van Ooijen, 2004), with 4.0 as LOD score threshold for all traits.

RESULTS AND DISCUSSION

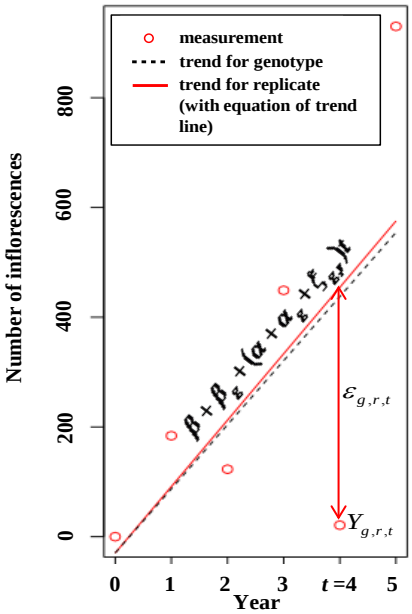

Fig. 1. Data, trend model and residuals for total yields at tree scale for a biennial bearing genotype (γ_g = -0.88, BBI_res_norm = 1.21)

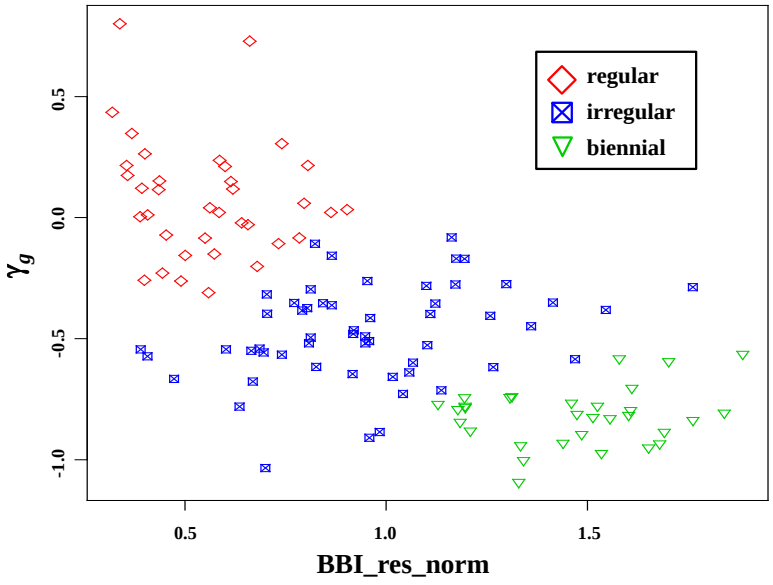

Fig. 2. Clustering obtained using a 3-component Gaussian mixture using BBI_res_norm (x-axis) and γ_g (y-axis). Cluster 1 can be interpreted as regular bearing genotypes, cluster 2 as biennial bearing genotypes and cluster 3 as irregular bearing genotypes.

The clustering obtained using the descriptors at tree scale BBI_res_norm and γ_g highlighted three clusters (Fig. 2). Cluster 1 is characterized by a low BBI_res_norm (low dispersion of yields around trend) and unstructured residuals ($\gamma_g \approx 0$ in (2)); thus, it is interpreted as regular genotypes. Cluster 2 is characterized by a high BBI_res_norm (high dispersion of yields around trend) and residuals with alternate signs (γ_g close to -1), and is interpreted as biennial bearing genotypes. The genotypes in cluster 3 have intermediate values and are interpreted as irregular.

The genotypes have the following behaviours at AS scale, depending on their cluster: genotypes in cluster 1 have high entropies (0.38 on average) (i.e. high uncertainty), which corresponds to asynchronous and irregular flowering at AS scale. The transition probabilities of the Markov chain highlight a higher probability of these genotypes to flower in year *t* after flowering in year $t-1$, and a higher probability to flower in 2009, which is an "off" year for the majority of biennial bearing genotypes (even years being "on" years, on the contrary). Genotypes in cluster 2 have low entropies (0.23 on average), which corresponds to synchronous and well-predictable flowering at AS scale. An AS preceded by a flowering AS in year $t-1$ and a vegetative AS in year $t-2$ has a lower probability to flower in year *t*, and any AS has a lower probability to flower in 2009. Genotypes in cluster 3 have high entropies (0.38 on average), and intermediate probabilities of AS to bear flowers during successive years or in 2009. Comparison of the genotype behaviours at AS and whole tree scales highlights that in the available progeny, regularity comes from the combination of irregular axes and asynchronism, whereas alternation comes from the combination of alternate axes and synchronism.

A clustering was also performed using the descriptors at AS scale, to assess whether the clusters approximate those obtained from descriptors at tree scale. Two confusions occurred between regular and alternate bearing genotypes, and 44 confusions occurred between irregular and both other clusters of genotypes. The other 69 genotypes were correctly classified. As a consequence, regular and biennial bearing genotypes are well discriminated from their behaviour at AS scale, whereas irregular genotypes are poorly discriminated. Thus, we can propose that breeders (i) progressively suppress biennial or irregular genotypes after the first observation of a large decrease in flowering during the beginning of the mature phase (ii) confirm the regular fruiting behaviour of the pre-selected genotypes during the stable mature phase.

Five QTLs altogether were identified in four separated genomic regions, and explained from 13.5 to 22.5% of the genetic variability. At tree scale, two QTLs were found for BBI_res_norm on LG1 and LG8 (LOD 6.69 and 5.82, respectively) and no significant QTL was detected for genotype AR coefficient γ_g. At AS scale, one QTL was mapped for BBI_res_norm_loc on LG8 in the same region (LOD 5.74) than the QTL mapped for BBI_res_norm at tree scale. Two QTL were also detected for γ_{loc} on LG11 and LG14 (LOD 7.24 and 4.55, respectively). By contrast, no QTL was detected for the entropy.

QTLs mapped on LG1 and LG8 corroborate zones that have been identified in a previous study (Guitton *et al.*, 2012). The QTL cluster on LG1 seems to be linked to the antagonist relationship between fruit production and inflorescence initiation in a same year, as reported by Bangerth (2009). The two QTL revealed on LG11 and LG14 for γ_{loc} are located on zones that were not previously associated to flowering or bearing traits in this progeny. Further exploration of these genomic regions is required to interpret precisely which mechanism could underlie these associations. The absence of QTL detection for other descriptors, especially γ_g at tree scale and entropy at AS scale, may be due to the population size. Indeed, 120 individuals can be limiting to detect QTL with small effects (Bernardo, 2004) and only major QTLs (explaining more than 13% of the trait variance) were confirmed in the present study. However, it may be noticed that the QTLs detected in the present study do not depend on year effects but rather are associated to genotype bearing behaviour over years.

LITERATURE CITED

Bangerth F. 2009. Floral induction in mature, perennial angiosperm fruit trees: Similarities and discrepancies with annual/biennial plants and the involvement of plant hormones. *Scientia Horticulturae* **122**: 153-163.

Bernardo R. 2004. What proportion of declared QTL in plants are false? *Theoretical and Applied Genetics* **109**: 419-424.

Bishop CM. 2006. Pattern Recognition and Machine Learning. Springer Verlag, 2006.

Guitton B, Kelner J-J, Velasco R, Gardiner SE, Chagné D, Costes E. **2012**. Genetic control of biennial bearing in apple. *Journal of Experimental Botany* **63**: 131-149.

Huff A. **2001**. A significance test for biennial bearing using data resampling. *Journal of Horticultural Science & Biotechnology* **76**: 534-535.

Monselise SP, Goldschmidt EE. **1982**. Alternate bearing in fruit trees. *Horticultural Reviews* **4**: 128-173.

Pearce SC, Dobersek-Urbane S. **1967**. The measurement of irregularity in growth and cropping. *Journal of Horticultural Science* **42**: 295-305.

Van Ooijen JW. **2004**. MapQTL® 5, Software for the mapping of quantitative trait loci in experimental populations. Wageningen, Netherlands: Kyazma B.V.

Wilcox J. 1944. Some factors affecting apple yields in the Okanagan Valley: tree size, tree vigor, biennial bearing, and distance of planting. *Scientific Agriculture* **25**: 189.

Proceedings of the 7th International Conference on Functional-Structural Plant Models, Saariselkä, Finland, 9 - 14 June 2013. Eds. Risto Sievänen, Eero Nikinmaa, Christophe Godin, Anna Lintunen & Pekka Nygren. http://www.metla.fi/fspm2013/proceedings. ISBN 978-951-651-408-9.

Biomechanical modelation of *Ravenala madagascariensis* petiole

Andrés Valencia-Escobar[1]*, M. Paulina Fernández[2] and Diego J. Celentano[3]
[1]*Industrial Design Faculty, Universidad Pontificia Bolivariana, Medellin, Colombia*
[2]*Faculty of Agronomy and Forest Engineering, Pontificia Universidad Católica de Chile, Santiago, Chile*
[3]*School of Engineering, Pontificia Universidad Católica de Chile, Santiago, Chile*
**correspondence: andres.valencia@upb.edu.co*

Highlights: The use of shape transformers methodology, local buckling Brazier model and finite elements analysisis to model the *Ravenala madagascariensis* petiole allows to discover how the relation between shape and mater gives to the plant a structural support to bear high bending and torsion loads without fail. The combination of an elliptical stiff perimeter (epidermis) reinforced with a highly ordered cellular core (aerenchyma) gives to Ravenala petiole two very efficient and secure stability mechanisms.

Keywords: *Ravenala madagascariensis*, Petiole, Structural efficiency, biomechanics modeling

INTRODUCTION

Modeling of structural behavior of plants is an important step in their biomechanical analysis. It allows identifying the relationships between the morphological and anatomical features and the mechanical behavior of the structure under analysis. The models obtained are useful for three purposes basically: to understand the physics behind biological processes (Niklas and Spatz, 2012), to support the behavior of natural materials with commercial interest like wood or bamboo (Mattheck, 1998; Niklas *et al.*, 2006; Vincent, 2012), and to bring the results of the model to the design table and translate them into objects or strategies (Vincent, 2006; Nychka and Chen, 2012).

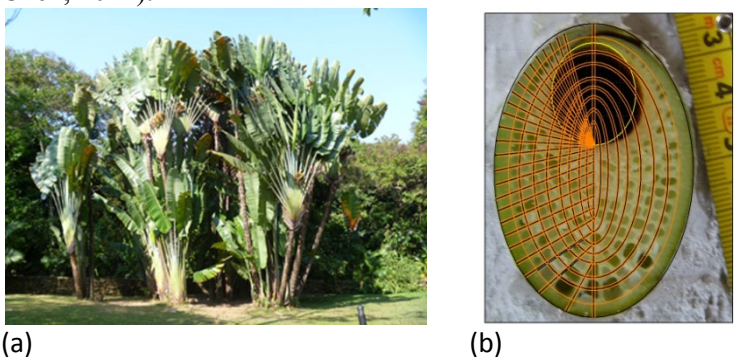

(a) (b)

Figure 1: (a) Ravenala madagascariensis exemplar in the Botanical Garden of Medellín, Colombia and (b) cross section of the petiole.

Nowadays, one of the most innovative work areas for plants biomechanical models is the design of structures based on the structural principles observed in them (Martone *et al.*, 2010; Shimomura, 2010) in order to optimize man-made structures (Vogel, 2000). This activity, called biomimicry, uses the structural models as its main tool to mimicry the natural behavior through the design process.

Petioles can be considered like cantilever beams subjected to bending and torsion (Niklas, 1992; Vogel, 1992). The combination of shape from its cross-section perimeter and the mechanical properties and distribution of tissues, are the main variables included in most of the models.

This work approximates the mechanical behavior of the *Ravenala madagascariensis* petiole (refered as *R. mad*). *R. mad* it's a monocotiledonean plant of the Zingiberales order and Strelizciaceae (Bird of Paradise) family, endemic of Madagascar island (Kress, Schatz, Andrianifahanana, & Morland, 1994) and is planted like ornamental tree throughout the tropics. The plant presents a set of long petioles and leaves arranged sideways in a bidimensional alternate pattern like a giant hand fan (Fig. 1a). The interest for this type of study about structural morphology lies on the remarkable formal mechanisms that this petiole presents to support all the loads imposed by self weight, wind, rain and animals, and the potential to use them like patterns for the mechanical design of artificial elements. In the modeling approach the contribution of the perimetral shape of the cross-section to the overall structural performance is considered. Moreover, we link the shape with the distribution and mechanical properties of the three main tissues present in the petiole (i.e. epidermis, the combination of parenchyma and aerenchyma and sclerenchyma) (Figure 1b), with the aim to model the efficiency of the real behavior.

MATERIALS AND METHODS

To model the structural behavior of *R. mad* petiole, 9 mature petioles were collected and analyzed microscopical and macroscopically. Cross-section cuts were prepared and microscopic images were obtained

with Computed Axial Tomography technique with a Toshiba Aquilion 64 CT Scanner, Motic SMZ 140 stereo zoom microscope and Jeol JSM-6490 SLV scanning electron microscope. From macroscopic images morphological and anatomical features were measure and described. Cantilever bending and torsion tests were developed to obtain the elastic load-displacement curves. To analyze and model the contribution of the perimetral shape in the overall behavior of the petiole, the shape transformers methodology -STM- was used. The STM proposes the mass minimization as optimization criteria in structural design (Pasini *et al.*, 2002). The modeling of the local buckling the cross-section under bending loads uses as reference the model proposed by Brazier (Brazier, 1927). To apply FEM, a 3-D digital model of the *R. mad* petiole cross-section was developed based on the real distribution of tissues, shapes and dimensions. Only peripheral sclerenchyma fiber bundles were taken into account, assuming that the fibers in other locations have only physiological and not a significant structural contribution to the overall petiole mechanical behavior. The model was meshed using 2D 4-node isoparametric cuadrilateral elements and 3D 8-node isoparametric hexahedrical elements with a special interpolation of the shear component for the bending test. The calculations were made by means of finite element-based code called VULCAN (Celentano, 1999).

RESULTS AND DISCUSSION

The average elliptical shape obtained from the sampled petioles has a width of 36.43mm ± 2.56mm and a height of 56.80mm ± 7.11mm with a thickness of 2.50mm ±0.16mm. This shape includes the epidermis and the first part of the parenchyma tissue which is reinforced with sclerenchyma fibers. Two models of cross-section were designed and analyzed with the STM to define comparatively its structural efficiency. Fig. 2 shows the results of the computation of structural efficiency parameters proposed by STM in bending and torsion: ψA, ψI and ψJ.

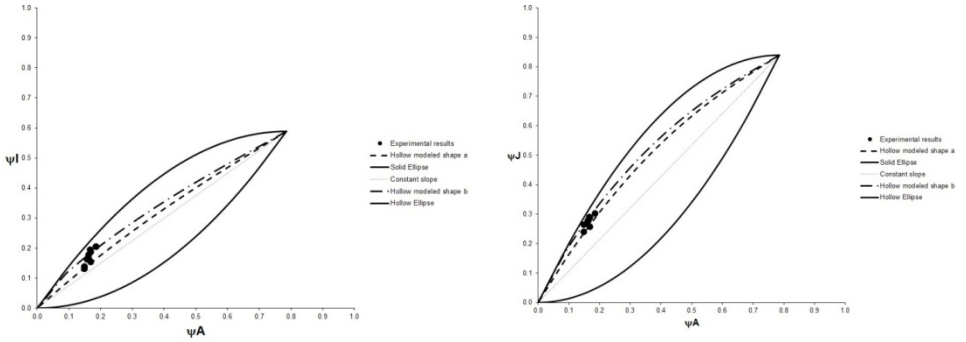

Fig. 2. a: structural efficiency maps for bending stiffness; b: structural efficiency maps for torsion stiffness.

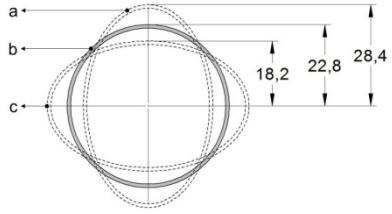

Fig. 3. Dimensional analysis of the local buckling ovalization process modeling. Dimensions in mm.

Closed elliptical shape allows the structural modeling of the open cross-section of *R. mad* petiole. The experimental calculations for the geometrical shape transformers ψA, ψI and ψJ lie over the modeled shapes curves. It means that the supposition of the closed section is valid to analyze the structural efficiency of *R. mad* petiole. The petiole cross-section behaves as less efficient compared to a perfect elliptical shape, at bending and torsion. Nevertheless, we have to consider that real shape is an open section probably responding to structural but also to physiological and morphological requirements. Analyzing real petioles cross-sections, it was found that the theoretical circumference of thickness of 1mm (shape marked with "b" in Figure 3) that would generate an elliptical ring with the same dimensions of those observed in the petioles (shape marked with "a" in Figure 3) would have an average radius of 22.8mm ± 2.1mm. Applying the Brazier model, the ovalized ellipse generated by local buckling process from this circular cross-section has the same dimensions of the original elliptical shape but rotated 90° (shape marked with "c" in Figure 3). If both elliptical sections, the original petiole cross-section shape and the ovalized elliptical shape, are compared with the theoretical circular shape that originate them, we see that the oval cross-sectional shape of the petiole acts as a structural security factor, with a second moment of inertia 44.8%± 9.7% higher than a circular cross-section with the same area. Besides, the ovalized elliptical shape generated from the theoretical circular cross-section modeled according to the Brazier model, has a second moment of inertia 27.8%±3.1% lower than circular section. If torsion constant of the sections are compared, the average loss of torsional stiffness of the elliptical shape with respect to the circular is just 15.8%±0.8%. Thus the use of elliptical shape with the major axis oriented with the vertical direction in cantilever beams subjected to bending and torsion

loads seems to be an evolutional structural advance of the *R. mad* petioles. The petiole rotates when the wind comes in, in order to reduce its projected area. The use of less-efficient shape in torsion, but stiffer in bending than circular section, helps the species adapting to extremely windy conditions.

FEM allows finding the normal and shear stress distribution over the cross-section. For this load the modeled petiole followed the behavior predicted for beam theory (Timoshenko and Goodier, 1969), where the maximum stresses are located on the points of the cross-section farther from the neutral axis. The shear stress distribution shows that modeled petiole exhibits a mechanical behavior which differs from the behavior predicted by elasticity theory. The values of stresses on the peripheral points over the minor axis of ellipse are very similar to the stresses on the peripheral points over the ellipse major axis, when the theory says that those values must differ proportionally to the ratio of the major and minor axis (Timoshenko and Goodier, 1969).

For bending, the Young modulus variation shows that parenchyma is the major stiffness-related tissue. A change of four orders of magnitude in the parenchyma Young modulus value, gives a bending load four orders of magnitude higher. While the same variation in the Young modulus of the epidermis and sclerenchyma fibers doesn´t respond similarly. For torsion, a variation in four orders of magnitude in the parenchyma Young modulus gives a torsional moment increase of the same magnitude order. While the same variation in the Young modulus of the other two tissues, doesn´t implies a similar magnitude variation in moment. For each load type, the level of contribution of each tissue is different. This could mean that the high level of anisotropy of each tissue affects its mechanical behavior. The change in the stiffness of the entire system is higher with the change of the Young modulus of the parenchyma for both bending and torsion, but not in same proportion. The contribution of epidermis differs in each load type. Sclerenchyma fibers appear as a tissue useful in bending but less important in torsion. FEA of modeled petiole shows that the peripheral points of the cross-section bear similar shear stresses. It could mean that the aerenchyma tissue not only helps to stabilization of the section to resist the compression stresses due bending, but redistribute the magnitude of shear stresses to decrease the warp of the elliptical section when rotation by wind, stabilizing the section to allow high angular deformations. The almost radial configuration of the aerenchyma chambers walls (Fig. 1b) suggests a mechanical based orientation. The aerenchyma anatomy shows a grid with non-circular spaces that generate almost straight lines through which the loads may be distributed. For that reason aerenchyma can be assumed as inner reinforcing mechanism.

Madagascar is an island located in the path of tropical cyclones and hurricanes with maximum wind velocity in normal weather conditions of 40km/h. This generates very complex and extreme environmental conditions to which *R. mad* seems to be properly adapted. A main conclusion is that the real contribution of each tissue to the mechanical resistance of the petiole depends more on form and organization than on individual mechanical properties.

LITERATURE CITED

Brazier LG. 1927. On the Flexure of Thin Cylindrical Shells and Other "Thin" Sections. *Proceedings of the Royal Society of London. Series A, Containing Papers of a Mathematical and Physical Character* **116**: 104-114.

Celentano D. 1999. Vulcan.

Martone PT, Boller M, Burgert I, Dumais J, Edwards J, Mach K, Rowe N, Rueggeberg M, Seidel R, Speck T. 2010. Mechanics without Muscle: *Biomechanical Inspiration from the Plant World. Integrative and Comparative Biology* **50:** 888-907.

Mattheck C. 1998. Design in nature: learning from tress. Springer, Berlin.

Niklas KJ. 1992. Plant biomechanics. The University of Chicago Press, Chicago.

Niklas KJ, Spatz HC. 2012. Plant physics. University Of Chicago Press

Niklas KJ, Spatz HC, Vincent JFV. 2006. Plant biomechanics: an overview and prospectus. *Am. J. Bot*. **93:** 1369-1378.

Nychka J, Chen PY. 2012. Nature as Inspiration in Materials Science and Engineering. *JOM Journal of the Minerals, Metals and Materials Society* **64:** 446-448.

P**asini D, Burgess SC, Smith DJ. 2002.** Performance indices for arbitrarily scaled rectangular cross-sections in bending stiffness design. *Proceedings of the Institution of Mechanical Engineers, Part L: Journal of Materials Design and Applications* **216:** 101-113.

Shimomura M. 2010. The New Trends in Next Generation Biomimetics Material Technology: Learning from Biodiversity. *Science and Technology Trends*. **Quarterly Review:** 53-75.

Timoshenko S, Goodier JN. 1969. Theory of elasticity. McGraw-Hill.

Vincent JFV. 2006. The Materials Revolution. *Journal of Bionic Engineering* **3:** 217-234.

Vincent, J.F.V., 2012. Structural Biomaterials. Princeton University Press.

Vogel S. 1992. Twist-to-Bend Ratios and Cross-Sectional Shapes of Petioles and Stems. *Journal of Experimental Botany* **43**: 1527-1532.

Vogel S. 2000. Ancas y palancas: mecánica natural y mecánica humana. Tusquets editores, Barcelona.

Proceedings of the 7th International Conference on Functional-Structural Plant Models, Saariselkä, Finland, 9 - 14 June 2013. Eds. Risto Sievänen, Eero Nikinmaa, Christophe Godin, Anna Lintunen & Pekka Nygren.
http://www.metla.fi/fspm2013/proceedings. ISBN 978-951-651-408-9.

Modeling and analyzing the topology development of young *Michelia chapensis*

Dong Li[1,2], **Mengzhen Kang**[3], **Philippe de Reffye**[4] and **Zhifu Xu**[1*]
[1] *Institute of Digital Agriculture, Zhejiang Academy of Agricultural Sciences, Hangzhou, Zhejiang Province,310021, P.R. China*
[2] *Zhejiang Tengtou Landscape CO.,LTD, Ningbo, Zhejiang Province,315100, P.R. China*
[3] *LIAMA&NLPR, Institute of Automation, Chinese Academy of Sciences, Beijing, 100190, China*
[4] *Cirad-Amis, UMR AMAP, TA 40/01 Ave Agropolis, F-34398 Montpellier cedex 5, France*
**correspondence:* zhifux868@163.com

Key words: *Michelia chapensis*, plant development, topology structure, GreenLab model

Highlights: *Michelia chapensis* is one of the most important landscape trees and it is important to study the plant topology structure. We measured the 2 years old michelia tree through one year, study the tree topology structure, well fit and simulate the tree with the new GreenLab version.

INTRODUCTION

Michelia chapensis is one of the most important landscape trees which are more and more broadly bred in the nursery garden in the South of China. When the plant topology structure is well studied and the dynamic plant structure model is used, the landscape designer can use the model to make the dynamic landscape design. It is important to study the plant topology structure.

For many studies about the plant structural model or functional-structural model, the plant was studied with one year as the time step, such as LIGNUM (Perttunen *et al.*, 1996, 1998) or GreenLab pine (Wang *et al*., 2012). It was enough to study the forestry trees, but it is not available to arrange the management strategies or landscape design for the garden trees.

In this study, we measured the 2 years old michelia trees, study the tree topology structure, fit and simulate the tree with the new GreenLab version.

MATERIAL AND METHODS

Field experiment

The field experiments were conducted in the nursery garden of Tengtou Landscape Company (29°42' N, 121°22' E) in Zhejiang province. The plant were sown in spring of 2010 by seeds and transplanted to the nursery garden in autumn. Plant grew at a spacing of 0.5 × 0.5 m. The branches which were below the 8th phytomer were pruned in the beginning of 2011. Fertilizer inputs and irrigation were conducted so as to avoid any mineral and water limitations to plant growth.

From 21 April,2011 to 13 March,almost every month, 20 plants were sampled and counted the phytomer number of the main stem. And at the same time 12 plants were sampled and the topology structure were recorded, as well as the branch level and position, the phytomer number of the branches, the blade living time and expansion time.

Brief description of GREENLAB model

Detailed descriptions of the model were presented in some previous studies (Yan *et al*., 2004; Guo *et al*., 2006) and we just recall its main principles and the new features. In the model, the plant architecture is described hierarchically according to their physiological age (PA), as presented in a review paper by Barthélémy and Caraglio (2007). The time step, called growth cycle (GC), is the time elapsed between emergences of two successive phytomers expressed in thermal time.

GL2 is a stochastic functional-structural model, where the plant topology development depends on probabilities related to bud functioning (e.g., branching probabilities, buds survival probabilities, rhythm ratio between different PAs). In the new version GL5, the topology and biomass production were fitted separately. We fitted the topology first and got the topology development for the plant. Then the biomass will be fitted for the total biomass and the allometry based on common pool and basic GreenLab principle.

In this study, we just considered the following probabilities , such as the growth probabilities of all the PAs, the delay growth cycle of the PA2 and PA3, the rhythm ratio between different Pas, the delay and growth in the winter, etc. The branch death was not considered in this study. All the probabilities were

described with the binomial distribution and fitted and simulated in Matlab software produced by the Mathworks Inc.

RESULTS

Descriptions on michelia structure

There was almost 1 branch, which were the 1st level branch (PA2), at each phytomer rank along the main stem (PA1). To these branches, there were about 4 growth cycles delay. The growth rate of PA2 is almost the same with PA1, sepecially for the new branches. At the beginning of the year 2011, there were about 14-19 phytomers in the michelia tree. Through the main stem there was no branch or there are little branches at the position from 15-23, maybecause the bud were dead in the winter.

There were the 2nd level branches (PA3) on the 1st level branch (PA2), but the PA3 didn't come out until the phytomer of PA2 is more than 6. And also there was 2 or 3 growth cycle delay in the PA3 compared to PA2.

The plant growth fast in the summer and early autumn, there was one new phytomer about three to five days from April to Octomer in 2011 (Fig.2a), but keep almost constantly from Octomer, 2011 to March, 2012. Almost all the plants grew in the same rate and the variability is small for the main stem of all the sampled trees.

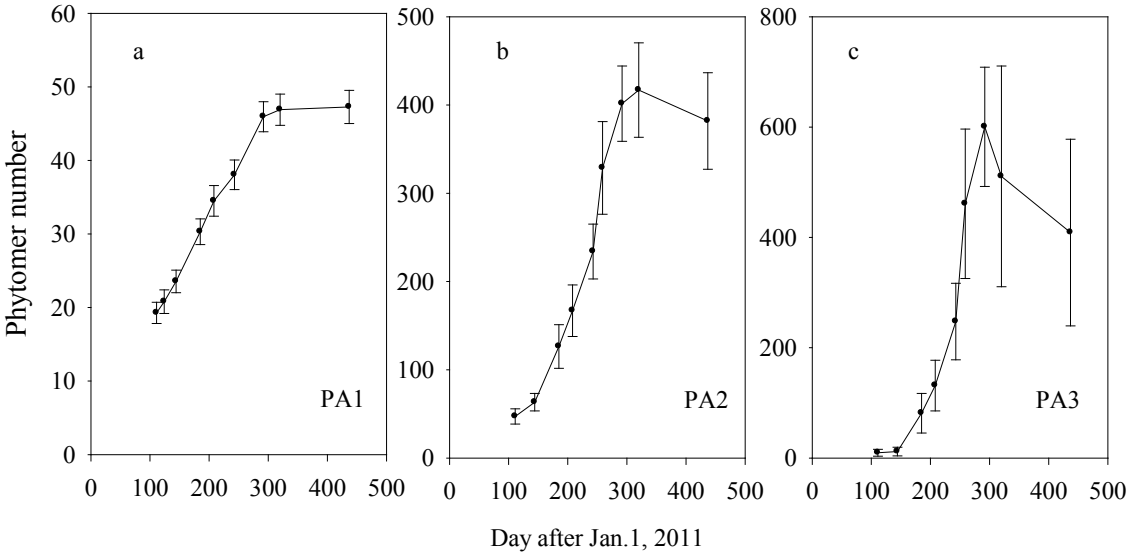

Fig. 2. Total phytomer number of the main stem and branches. Fig. 2a represents the phytomer number of the main stem (PA1) changing with time, Fig. 2b denotes the phytomer number of all the first level branches (PA2) varying with time and Fig. 2c represents the phytomer number of the total PA3s in one tree.

To PA2 and PA3, the total phytomer number decreased because some of the branches died in the autumn and winter. Also the variability is larger than PA1.

Fitting and simulating results

The phytomer number of different PAs was fitted separately and well simulated. The rhythm ratio was almost one for all PAs, that means the main stem grew one growth unit, the children branch could grew a growth unit, too. But the probability of growth for PA1 was larger than PA2 and probability of PA3 was the smallest. At the same time, the probability of branch death for PA1 was the smallest (nearly to zero) and probability of PA3 was biggest (data were not shown in this paper). The delay of year 2011 and the Inhibition control could also be modeled (Fig.3).

DISCUSSION

Trees can grow for many years, so many researchers study the tree growth using 1 year as the time step. Some information of the tree growth will be lost (Sievänen *et al*, 2000) and most of the information is very important especially for the young garden tree which grew in the nursery garden. In this study we observed, measured and simulated the young Michelia grown in one year, studied the growth rate of the main stem and

branches. The gardener can decide their irrigating, fertilizing strategies and also they can deciede when to prune and transplant the plant through the model.

We also found when the plants were pruned, the new branches grew in a very similar way as the young trees. And the model was also important to the big trees. So we can also use the model to show the influence of pruning and landscape design.

In the future, the climate factors, the biomass production and allocation will be considered in this model, which is then more useful in the management strategies.

ACKNOWLEDGEMENT

The research has been supported by Zhejiang Tengtou Landscape CO.,LTD. The authors are grateful to Mr. Feng Wang, Miss Xiujuan Wang, Ms Hong Guo and Miss Yue Li for their kind help on the experiment measurements.

REFERENCES

Cournède PH, Mathieu A, Houllier F, Barthelemy D, de Reffye P. 2008. Computing Competition for Light in the GREENLAB Model of Plant Growth: A Contribution to the Study of the Effects of Density on Resource Acquisition and Architectural Development. *Annals of Botany* **101**: 1207-1219.

Guo Y, Ma YT, Zhan ZG, Li BG, Dingkuhn M, Luquet D, de Reffye P. 2006. Parameter Optimization and Field Validation of the Functional-Structural Model GREENLAB for Maize. *Annals of Botany* **97**: 217-230.

Kang MZ, Cournède PH, de Reffye P, Auclair D, Hu BG. 2008. Analytical study of a stochastic plant growth model: Application to the GreenLab model. *Mathematics and Computers in Simulation* **78**: 57-75.

Perttunen J, Sievänen R, Nikinmaa E, Salminen H, Saarenmaa H, Väkevä J. 1996. LIGNUM: a tree model based on simple structural units. *Annals of botany* **77**: 87-98.

Perttunen J, Sievänen R, Nikinmaa E. 1998. LIGNUM: a model combining the structure and the functioning of trees. *Ecological Modelling* **108**: 189-198.

Sievänen R, Nikinmaa E, Nygren P, Ozier-Lafontaine H, Perttunen J, Hakula H. 2000. Components of functional-structural tree models. *Annals of forest science* **57**: 399-412.

Wang F, Letort V, Lu Q, Bai X, Guo Y, de Reffye P, Li B. 2012. A Functional and Structural Mongolian Scots Pine (Pinus sylvestris var. mongolica) Model Integrating Architecture, Biomass and Effects of Precipitation. PloS one, 7: e43531.

Yan HP, Kang MZ, de Reffye P, Dingkuhn M. 2004. A Dynamic, Architectural Plant Model Simulating Resource-dependent Growth. *Annals of Botany* **93**: 591-602.

Proceedings of the 7th International Conference on Functional-Structural Plant Models, Saariselkä, Finland, 9 - 14 June 2013. Eds. Risto Sievänen, Eero Nikinmaa, Christophe Godin, Anna Lintunen & Pekka Nygren. http://www.metla.fi/fspm2013/proceedings. ISBN 978-951-651-408-9.

Automated Parameter Estimation for a Plant Architecture Model

Florian Schöler*, Jenny Balfer and **Volker Steinhage**
Department of Computer Science III, University of Bonn, Römerstraße 164, 53117 Bonn, Germany
**correspondence:* schoele@iai.uni-bonn.de

Highlights: We present an automated procedure for the creation of architectural plant models. It uses an algorithm for the computation of skeletons from sensor data. The skeletons are annotated with semantic labels for the extraction of architectural parameters. The values of several samples are averaged and serve as the basis for the model, which is implemented as a Relational Growth Grammar.

Keywords: Architectural Modeling, Skeletonization, Relational Growth Grammar

INTRODUCTION

When creating a model for the architecture of a plant, questions arise, like what parameters describe the architecture, how they are captured, or how it is actually modeled. In one way or another many of those questions were already answered in previous works (Godin, 2000; Watanabe et al., 2005; Barthélémy and Caraglio, 2007; Dornbusch et al., 2007; Fourcaud et al., 2008). Almost always they contain a substantial amount of manual labor for determining parameter values, for example, for the length or the frequency of occurrence of a plant component. In this paper we show, using the example of berryless grape clusters of the grapevine plant (Vitis vinifera L.), how a large part of the process can be automated. To this end we make use of an algorithm that takes sensor data of the plant as input and computes a skeleton, which is a set of connected line segments that represents the structure of the original object. That skeleton is annotated with semantic labels like rachis or pedicel. Then, parameter values like lengths or frequency of occurrence of components are extracted from that skeleton. The values of several samples are averaged and serve as the basis for the actual model. We construct our architectural model as a Relational Growth Grammar (RGG) (Kurth et al. 2005). Figure 1 gives an overview of the process. In general, this procedure is also applicable to other plants or plant parts. To our best knowledge this is the first attempt of an automated parameter value extraction for the architectural plant modeling. Of course, the presented procedure still relies on a careful selection of plant samples and architectural parameters, but the process of extracting and averaging their values is greatly simplified.

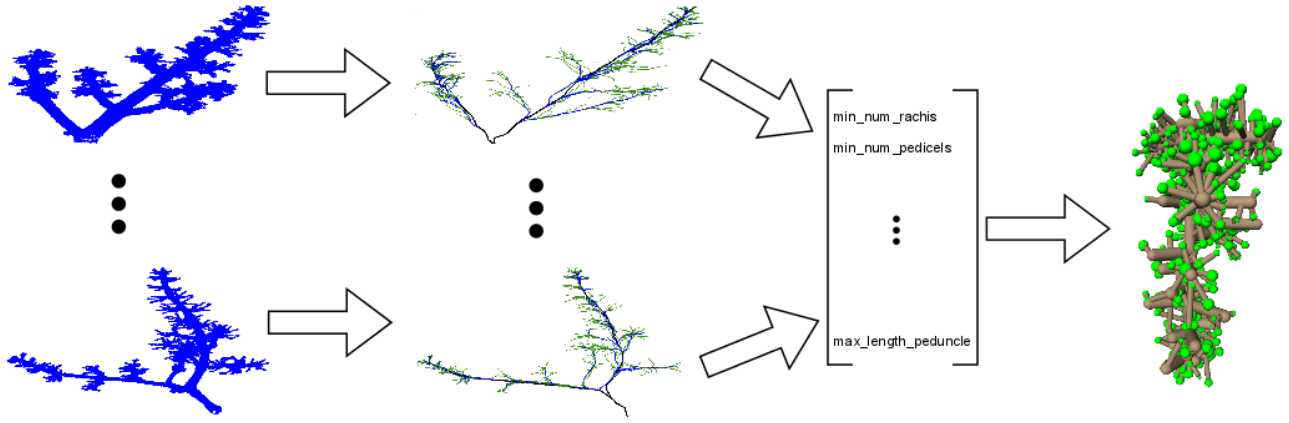

Figure 1: Overview of the procedure. From left to right: From every point cloud a skeleton is computed. The colors in the skeleton refer to the different semantic annotations (black: rachis, blue: lateral branch, green: pedicel). Based on the skeleton, values of architectural parameters are extracted and averaged. This is the basis for the RGG-model. See section MODEL CONSTRUCTION for an example of how the parameters are integrated into the model.

DATA AND PARAMETERS

For computing the skeletons we use the algorithm presented in (Balfer, 2012; Balfer et al., 2013). This algorithm not only computes the bare architecture but also adds semantic labels to the different parts: rachis,

lateral branch, and pedicel.

We have gathered 20 exemplars of grape clusters of the cultivar Riesling, an example of a very popular cultivar that usually produces very compact grape clusters. The clusters were cut off the trunks of ten grapevine plants and we always took the lowest two clusters. The plants were grown in the field, not in lab-conditions. According to the extended BBCH-scale from Lorenz et al. (1994) the clusters were taken at stage BBCH 65 "full flowering: 50% of flowerhoods fallen." (BBCH is short for *Biological Institute of Agriculture and Forestry, Federal Office for Plant Varieties and Chemical Industry* – in German: *Biologische **B**undesanstalt für Land- und Forstwirtschaft, **B**undessortenamt und **Ch**emische Industrie*). For each of the clusters we cut off the flowers (but not the pedicels), counted the flowers and scanned the clusters with a Perceptron ScanWorks V5 laser rangefinder, resulting in 20 dense point clouds with a minimum point-to-point resolution of 12 μm. These point clouds and their "starting points" were used as input to the skeletonization algorithm. The starting point is where the cluster was formerly connected to the plant.

The resulting semantic skeletons each produced one vector of parameter values. We then had to combine the single vectors into one vector representing the twenty clusters. For parameters with continuous values like the length of the rachis we could just compute the average and the standard deviation assuming a normal distribution. For other, non-continuous, parameters we had to do different calculations. For example, for the number of pedicels that branch from the same node we computed a relative histogram of the gathered values. In total we extracted 89 different parameters and, for now, assumed them to be independent. Some of the parameters are taken from the descriptor list of International Plant Genetic Resources Institute (IPGRI 1997), and the second edition of the descriptor list of the International Organization for Vine and Wine (OIV 2009). For example, for the number of rachises we found occurrences of 1, 2, 3, 4, 5 and corresponding occurrence probabilities of 0.05, 0.85, 0.05, 0.0, 0.05 respectively. This means that in 17 of the 20 cases we found exactly two rachises; one main rachis and one secondary rachis.

MODEL CONSTRUCTION

The thus gathered and averaged parameter values are the basis for the model construction. We demonstrate this by means of an example. We have several values concerning the main rachis of the grape cluster: Their lengths, number of lateral branches per node, number of secondary rachises, internode lengths, number of nodes, etc. These pieces of information are concentrated in a new module in our RGG, called *MainRachis*. For the main rachis module also a specific grammar rule exists. This rule demands that the first branching point on the main rachis can lead to a lateral branch or a secondary rachis. After that point only lateral branches or pedicels may emerge from nodes. In addition we know, for example, how long the rachis can be and how many nodes in what distances can be expected. Thereby we create only such rachises that are topologically and geometrically realistic, according to our model, which itself is based on real grape clusters. Likewise we create RGG-modules for secondary rachises, lateral branches and pedicels. Furthermore, this parameterized model allows setting the parameters to a different, consistent set of values to produce grape clusters of other cultivars or in other development stages.

DISCUSSION AND CONCLUSION

See Figure 2 for an overview of six example runs of the grape cluster model. As can be seen, lateral branches get shorter from base to tip, internode lengths vary, and sometimes there is a secondary rachis. As was shown in Steinhage et al. (2012) such a model can be used not only for virtualization or visualization purposes. Utilized for a reconstruction algorithm it helps vastly decreasing the space of possible reconstruction hypotheses. In this respect the term ‘possible’ is described in terms of the model since only such hypotheses are allowed that can be constructed by the model.

In conclusion we have shown (a) how the extraction of architectural parameter values of plants can be automated by use of a skeletonization algorithm, (b) how those values can be combined to gain averages for a specific cultivar, and (c) how such a model can be used for the purpose of reconstruction from sensor data. There are several possible paths to follow from here. One could make the skeletonization algorithm more adaptable to other plants, gather more parameter values and investigate possible dependencies, and optimize the algorithm for shorter runtimes.

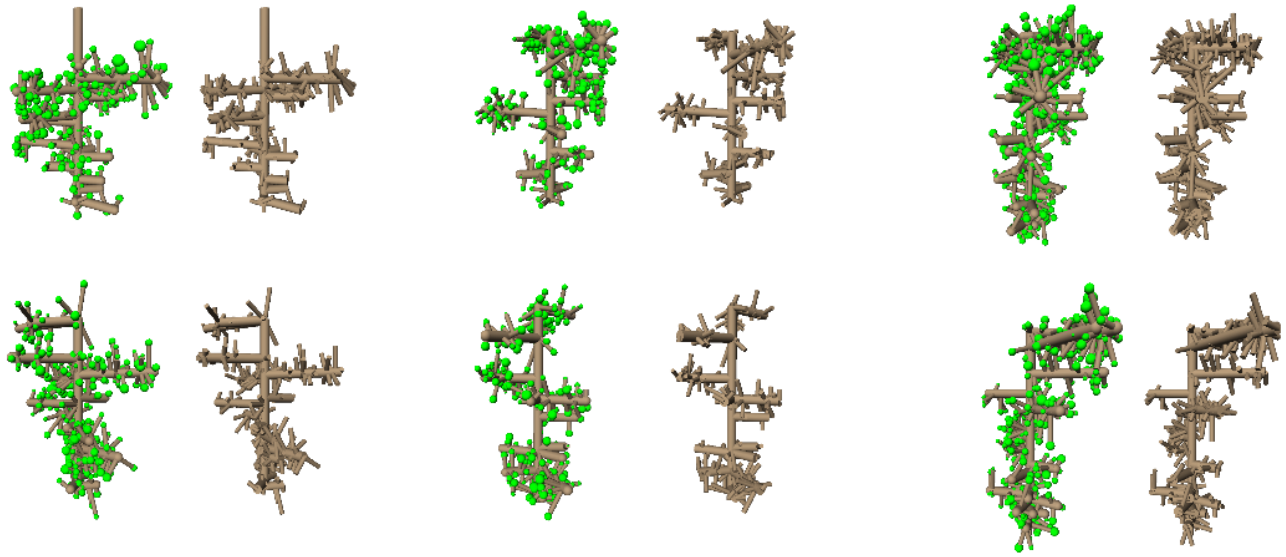

Figure 2: Six example runs of the RGG-model. For each run we show the generated grape cluster with and without flowers. One can see typical properties of grapevine grape clusters. For example, the lateral branches get shorter from base to tip, there can be secondary rachises, and from lateral branches pedicels emerge.

ACKNOWLEDGEMENTS

This work was supported by the Federal Ministry of Education and Research (BMBF). We thank all partners of sub-project D2 of CROP.SENSe.net for valuable discussions. Especially, we thank Reinhard Töpfer and Katja Herzog from the Julius-Kühn-Institute, Siebeldingen, Germany for providing the plant samples. We thank Heiner Kuhlmann and Stefan Paulus from the Department of Geodesy of the University of Bonn, Germany for generating the laser rangefinder measurements.

LITERATURE CITED

Balfer J. 2012. *3D Skeletonization for the Analysis of Grapevine Structure.* Master's Thesis, University of Bonn, Germany.

Balfer J, Schöler F, Steinhage V. 2013. *Semantic Skeletonization for Structural Plant Analysis.* Submitted to International Conference on Functional-Structural Plant Models.

Barthélémy D, Caraglio Y. 2007. Plant Architecture: A Dynamic, Multilevel and Comprehensive Approach to Plant Form, Structure and Ontogeny. *Annals of Botany* 99(3): 375–407.

Dornbusch T, Wernecke P, Diepenbrock W. 2007. A Method to Extract Morphological Traits of Plant Organs from 3D Point Clouds as a Database for an Architectural Plant Model. *Ecological Modelling* 200(1-2): 119–129.

Fourcaud T, Zhang X., Stokes A, Lambers H, Körner C. 2008. Plant growth modelling and applications: the increasing importance of plant architecture in growth models. *Annals of Botany* 101(8): 1053–1063.

Godin C. 2000. Representing and Encoding Plant Architecture: A Review. *Annals of Forest Science* 57(5–6): 413–438.

IPGRI, UPOV, and OIV. 1997. *Descriptors for Grapevine (Vitis ssp.).* International Union for the Protection of New Varieties of Plants, Geneva, Switzerland/Office Internationale de la Vigne et du Vin, Paris, France/International Plant Genetic Resources Institute, Rome, Italy.

Kurth W, Kniemeyer O, Buck-Sorlin G. 2005. Relational Growth Grammars – A Graph Rewriting Approach to Dynamical Systems with a Dynamical Structure. J.-P. Banâtre, P. Fradet, J.-L. Giavitto, O. Michel (eds.): *UPP 2004, LNCS 3566*, pp. 56 – 72, Springer.

Lorenz DH, Eichhorn KW, Bleiholder H, Klose R, Meier U, Weber E. 1994. Phänologische Entwicklungsstadien der Weinrebe (Vitis vinifera L. ssp. Vinifera). – Codierung und Beschreibung nach der erweiterten BBCH-Skala – Phenological growth stages of the grapevine (Vitis vinifery L. Ssp. Vinifera). *Vitic. Enol. Sci.* 49(2):66-70

Organisation Internationale de la Vigne et du Vin (OIV). 2009. *2nd Edition of the OIV Descriptor List for Grape Varieties and Vitis Species.* Organisation Intergouvernementale crée par l'Accord International du 3 Avril 2001.

Steinhage V, Schöler F, Balfer J. 2012. A Model-Based Approach to High Performance Phenotyping. *Proceedings of the International Conference on Informatics for Environmental Protection,* 303-310.

Watanabe T, Hanan JS, Room PM, Hasegawa T, Nakagawa H, Takahashi W. 2005., Rice Morphogenesis and Plant Architecture: Measurement, Specification and the Reconstruction of Structural Development by 3D Architectural Modelling. *Annals of Botany* 95(7): 1131–1143.

Proceedings of the 7th International Conference on Functional-Structural Plant Models, Saariselkä, Finland, 9 - 14 June 2013.
Eds. Risto Sievänen, Eero Nikinmaa, Christophe Godin, Anna Lintunen & Pekka Nygren.
http://www.metla.fi/fspm2013/proceedings. ISBN 978-951-651-408-9.

Modeling the blade shape of landscape trees

Fuping Lin[1], Xiujuan Wang[2], Haoyu Wang[2], Xueqiang Shi[3], Dong Li[1,4*]

[1] Zhejiang Tengtou Landscape Co., Ltd, Ningbo, Zhejiang Province,315100, P.R. China,[2] LIAMA&NLPR, Institute of Automation, Chinese Academy of Sciences, Beijing, 100190, China, [3] Northwest A & F University, Yangling, Shanxi Province, 712100, China, [4] Institute of Digital Agriculture, Zhejiang Academy of Agricultural Sciences, Hangzhou, Zhejiang Province,310021, P.R. China

**correspondence:* lidong808@163.com

Keywords: garden tree, blade modeling, 3D digitizing

Blade is very important organ which is not only for the physiology process but for the appearance structure of the plants, especially landscape plants. So it is necessary to make a library of blades for the plant 3D visualization. The 3D digitizing instruments were used in some researches to build the blade model (Loch, *et al.,* 2005). This blade model was made up of a lot of facets and it is time-consuming to visualize the plants using this model, especially for visualization of the dynamic growth of trees. In this study, a 3D blade library was built for more than twenty kinds of landscape trees, which were measured with 3D digitizing method. The data of these blades were transformed into horizontal coordinates and the leaf shapes of these plants were modeled by simple function models.

Blades from 22 kinds of plants were selected in the nursery garden of Tengtou Company (29°42' N, 121°22' E) in Zhejiang province. All the blades were either fusiform shape blade or lanceolate blade. 5 blades for each kind of tree were sampled and measured with a 3D digitizer (FastSCAN Scorpion, Polhemus, USA). The 3D blade models were built. A mouse interaction program was developed to obtain the coordinate data of blade margins by reading the scanned file, and then the coordinates were transformed into 2D data. These data was normalized to obtain the blade shape. Furthermore, the data of blade margins were computed with a quadratic function $y = a\,x^2 + b\,x + c$, which is often used to describe blade shape (Stewart and Dwyer, 1999), as well as the new composite function $y = \sin(\pi\, x^e)$. The parameters *a, b, c* and *e* of the two model were estimated with the Least Square methods and the similar and simple blade model was built.

All the sampled blades were measured and the blade models were built using the 3D digitizer (pictures not shown). The normalized blade shape was simulated using both quadratic function and the composite function. The parameters for 10 kinds of blades were given in Table1 (Others not shown here). For most of the blades, the results obtained with the composite function were better than the quadratic function. Moreover, only 1 parameter was used for the composite function. It was simple and useful for modeling the tree growth. By using these parameters, as well as the length and the largest width of blade, the simulated blade can be used to build the plant model.

The parameters for the blade shape were similar for some different kinds of plant. Thus, we can conclude that it is not enough to identify the tree only by using the parameters of leaf shape.

Table1. The parameters for the blade shape fitted by the two functions

Plant Names	*a*	*b*	*c*	*e*
Magnolia denudata	-4.048	3.987	0.017	0.994
Malus halliana	-3.748	3.482	0.216	0.723
Elaeocarpus decipiens	-4.105	4.143	-0.048	1.045
Michelia chapensis	-4.063	3.959	0.068	0.904
Cinnamomum camphora	-3.752	3.441	0.127	0.749
Myrica rubra	-3.523	3.916	-0.191	1.509
Prunus serrulata	-3.761	3.353	0.215	0.681
Koelreuteria paniculata	-3.846	3.478	0.178	0.729
Zelkova serrata	-3.526	3.048	0.252	0.626
Sapindus mukurossi	-3.814	3.574	0.148	0.765

Note: *a,b, c* were the parameters for the quadratic function model and *e* for the composite function

REFERENCES

Loch B, Belward JA, Hanan JS. 2005. Application of surface fitting techniques for the representation of leaf surfaces. MODSIM05: International Congress on Modelling and Simulation: Advances and Applications for Management and Decision Making. Melbourne, Australia, Modeling and Simulation Society of Australia and New Zealand Inc. 1272-1278.

Stewart D, Dwyer L. 1999. Mathematical characterization of leaf shape and area of maize hybrids. *Crop Science* **39**: 422-427.

Proceedings of the 7th International Conference on Functional-Structural Plant Models, Saariselkä, Finland, 9 - 14 June 2013. Eds. Risto Sievänen, Eero Nikinmaa, Christophe Godin, Anna Lintunen & Pekka Nygren. http://www.metla.fi/fspm2013/proceedings. ISBN 978-951-651-408-9.

Biomass-based rapeseed (*Brassica napus* L.) leaf geometric parameter model

Hongxin Cao [1], Wenyu Zhang [1], Weixing Zhang [1], Yan Liu [1], Yongxia Liu [1], Jim Hanan[2], Yuli Chen[1], Yanbin Yue[3], Zhiyou Zhang[4], Daokuo Ge[1]

[1] Institute of Agricultural Economics and Information ; Engineering Research Center for Digital Agriculture, Jiangsu Academy of Agricultural Sciences, Nanjing 210014, Jiangsu Province, P.R. China, [2]The University of Queensland, Centre for Biological Information Technology, Brisbane, Queensland 4068, Australia, [3]Institute of Agricultural Sci-tech Information, Guizhou Academy of Agricultural Sciences, Guiyang 550000, Guizhou, P.R. China, [4]Institute of Agricultural Sci-tech Information, Hunan Academy of Agricultural Sciences, Changsha 410000, Hunan, P.R. China

Highlights: A biomass-based model of leaf geometric parameters of rapeseed was developed, and the effects of cultivars and environmental conditions on rapeseed leaf morphogenesis were considered through the connection to rapeseed growth model via biomass.

Keywords: biomass, leaf geometric parameter, model, rapeseed (*Brassica napus* L.).

To quantify the relationships between rapeseed leaf geometric parameters and the corresponding leaf biomass, this paper presents a biomass-based model of leaf geometric parameters of rapeseed (Brassica napus L.) in the seedling stage, including Biomass-base leaf blade length model $LLj(i) = CPLBj(i) \cdot DWSP(i) \cdot RLWj(i)$, blade length-based leaf blade width model $LW_j(i) = e^{b_0 + b_1 LL_j(i)}$, leaf sheath length model $LS_j(i) = b_0 LL_j^{b_1}$, leaf blade bowstring length model $LBBL_j(i) = B_0 + B_1 LL_j(i)$, and leaf blade angle models $TA_j(i) = CPLB_j(i) \cdot DW_{SP}(i) \cdot RTW_j(i)$, $BA_j(i) = CPLB_j(i) \cdot DW_{SP}(i) \cdot RBW_j(i)$, designed to explain effects of genotypes and environmental conditions on rapeseed leaf morphogenesis at the individual leaf level. Various model variables, including biomass of blade, and blade length, were parameterized for rapeseed based on data derived from an outdoor experiment with rapeseed cv. Ningyou18, Ningyou16, and Ningza19. The leaf dimensions of rapeseed are modelled taking corresponding leaf biomass as an independent variable. Various variables in rapeseed showed marked consistency in observation and simulation, suggesting possibilities for a general rapeseed leaf geometric parameter model in the seedling stage. Our descriptive model is suitable for our objective. However, they can set the stage for connection to physiological model via biomass and development of Functional Structural Rapeseed Models (FSRM), and start with the localized production and partitioning of assimilates as affected by abiotic growth factors. The finding of biomass-based rapeseed leaf geometric parameter models also can be used in morphological models of internode, ramification, anthotaxy, and root of the other stages in rapeseed life.

Proceedings of the 7th International Conference on Functional-Structural Plant Models, Saariselkä, Finland, 9 - 14 June 2013. Eds. Risto Sievänen, Eero Nikinmaa, Christophe Godin, Anna Lintunen & Pekka Nygren.
http://www.metla.fi/fspm2013/proceedings. ISBN 978-951-651-408-9.

Optimize Tree Shape: Targeting for Best Light Interception

Jing Hua and **Mengzhen Kang**
State Key Laboratory of Management and Control for Complex Systems,
Institute of Automation, Chinese Academy of Sciences, China
**correspondence:* mengzhen.kang@ia.ac.cn

Highlights: It is assumed that plants have a certain kind of fitness so they can optimize their behaviors to maintain a specific target. Optimization algorithm is used to find tree shape that can maximize the light interception. The shape we got is reasonable and looks like a real tree, which proves partly the fitness of plants.

Keywords: Optimization, Tree Shape, GreenLab model, Fitness, Light interception

INTRODUCTION

It is observed that plants have some adaptively variable behaviors during their growth (Trewavas 2003), such as changing branch numbers and shape to intercept more light, transmitting biomass internally to guarantee growth of fruits, and reducing leaf area to preserve water in the arid environment, etc. From these phenomena, it is reasonable for us to assume that plants have a certain kind of fitness so they can change their behaviors in order to maintain a specific target. Trying to simulate and analyze this kind of fitness with virtual plants is an interesting and challenging work.

Functional-structural plant models (FSPMs), originated by combining Process-Based Models and plant structure, can be used to simulate plants fitness. In general, the simulation process in FSPM begins from a parametric setting, computes plant development (organ formation) and plant growth (biomass pruduction and partitioning) cycle by cycle, and finally gets some results such as organ biomass, organ number, 3D shape, etc. If this simulation process is regarded as a function whose inputs are model parameters and outputs are simulation results, it is possible for us to use some optimization algorithms to find parameters that can maximize or minimize some outputs. It is a feasible way to simulate the fitness of plants.

As light environment plays a key role for plant growth and development, light interception is a key topic in plant growth modeling. Tree shape, which is mainly decided by phyllotaxy, branching angle and bending, will greatly affect the light interception of a tree. Given the topological connections and organ sizes of a tree, there is an optimized tree shape that can maximize the light interception. In this work, we aimed to use some heuristic algorithms to find this optimized shape. Although it is just a simulation and needs further calibration, the result is interesting because the tree shape we got looks very similar to the real tree shape.

METHODS

We used GreenLab model to simulate growth of the tree. Detailed computation process can be referred to Yan HP et al. (2004) and Kang MZ et al. (2008). Once the simulation ended, we got topological connection of branches and size of all organs, based on which the 3D shape can be constructed. Our object is to find a tree shape that can maximize the light interception of this tree. Next we will describe briefly model parameters controlling tree shape, light distribution algorithm and optimization methods.

1. Parameters controlling tree shape

There are three important aspects that can affect tree shape: phyllotaxy, branching and bending. Firstly, phyllotaxy is the arrangement of leaves on a plant stem. As branches develop from axillary buds, phyllotaxy also decides the direction of branches. GreenLab model uses a parameter ϕ (ranging from 0 to 360 degree), which is defined as rotate angle between two adjacent internodes, to describe phyllotaxy, as shown in Fig.1. Secondly, branching angle is the angle between a branch and its mother stem. As it is assumed that branching angle increases along the main stem from top to bottom, GreenLab model uses a parameter θ (ranging from 0 to 180 degree) to describe the maximum branching angle, i.e., angle between the lowest branch and main stem, as shown in Fig.2. Other branching angles are calculated using linear interpolation. Finally, branches are seldom straight completely. They bend downward according to the gravity and upward according to the phototropism. As a result, branches are represented as many kinds of shapes. We use a method which originated from mechanical calculation to compute the branch bending. After simplification,

there are two parameters K (larger than zero) and p (ranging from 0.0 to 1.0) that control respectively the degree of bending and the position where the branch begins to fold upward. The effect of these two parameters is illustrated in Fig.3.

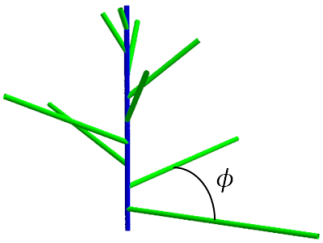

Fig. 1. Phyllotaxy angle ϕ, which is defined as rotate angle between two adjacent internodes

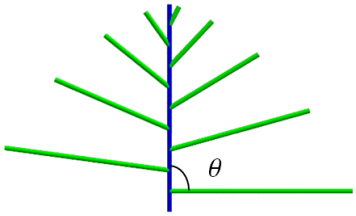

Fig. 2. Maximum branch angle θ

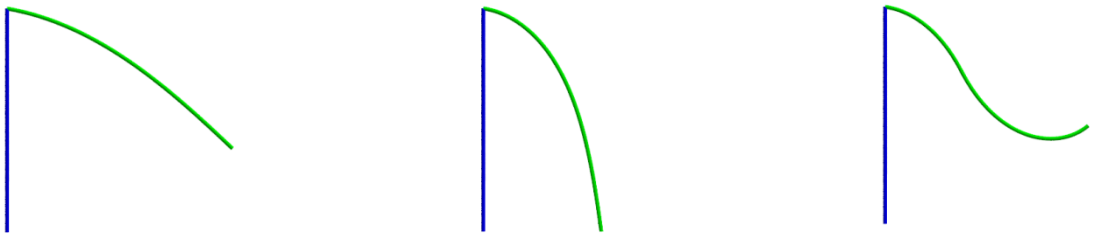

Fig.3. The effect of two parameters controlling the branch bending. Parameter values from left to right are: (1) $K = 0.02, p = 1.0$, (2) $K = 0.05, p = 1.0$ and (3) $K = 0.05, p = 0.4$

2. Light interception computation

In plant growth modeling, light interception is computed either by an empirical Beer-Law approach using leaf area index, or by summing up the light interception from individual organs. Since our object is to optimize the tree shape, we choose the latter method because it takes into account the detailed description of plant structure. There are several works concerning the light distribution in crop canopy (Wang XP et al. 2006, Zheng BY et al. 2011). Unfortunately, these methods can be hardly used in tree canopy because firstly there are more organs in trees than in a crop and secondly the ratio of single leaf size to the whole tree size is too small.

A simple light model is implemented in our system. Since leaf is represented as a mesh object in computer memory, several rays were emitted evenly into sky sphere from each point of the leaf mesh. For each ray, we counted leaves that this ray encounters (assuming n). The *visibility* of this ray is calculated as t^n, where t is the light transmittance of leaf. Finally, the *visibility* of a leaf is estimated using the mean value of *visibility* of all rays emitted from this leaf mesh. We use the sum of *visiblity* of all leaves (denoted by V) to measure the light interception of the tree.

3. Optimization algorithm

Given branch connections and sizes of all organs, the *visibility* V can be written as a function of four parameters described in part 1, $V = f(\phi, \theta, K, p)$. It is a typical optimization problem to find a set of parameters to maximize V. As the function is non-derivative or even discontinuous, heuristic algorithms are more suitable for this problem. We used PSO (Particle Swarm Optimization) algorithm (Shi et al. 1998).

As V has different sensitivities to different parameters, we used three steps to optimize. In each step, we fixed some parameters and optimize others. The order of optimized parameters is: firstly phyllotaxy, secondly branching angle and finally bending parameters.

RESULTS AND DISCUSSION

The simulation result is illustrated in Fig.4. All leaves are removed for showing more clearly the structure of the tree. We chose a relatively simple tree whose structure is shown in the left. The initial parameter values are: $\phi = 180, \theta = 25, K = 0.0, p = 1.0$, which means that all branches are straight and in a vertical plane, and all branching angle are the same. After optimization, we got the tree shape in the right, whose parameter values are $\phi = 48.52, \theta = 102, K = 0.0555, p = 0.21$. It is very intersting that the shape looks like a real tree. This result shows that it is possible to use optimization algorithm to get reasonable tree shape, and then proves partly the assumption that plants have a certain kind of fitness so they can optimize their behavior in a specific environment.

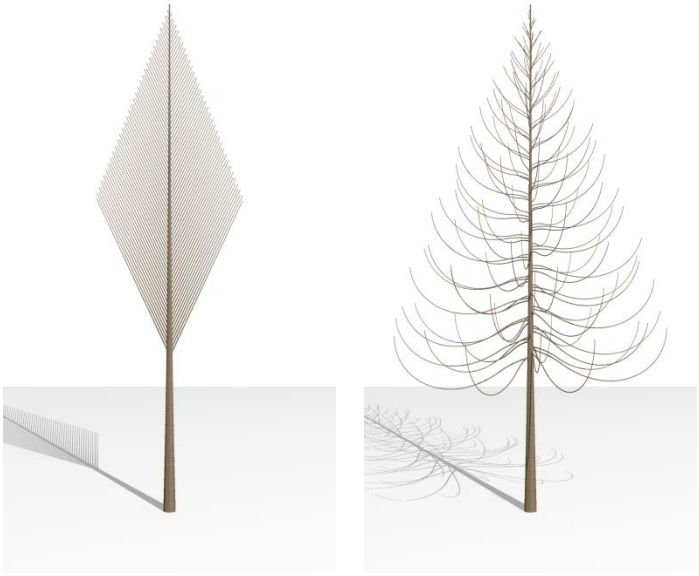

Fig. 4. Simulation result. Left is the topological structure of a tree and right is the optimized tree shape we got.

We choose a simple tree in this work just because of the computing efficiency, as both calculation of light distribution and the optimization algorithm are very time-consuming. There are no substantial difficulties to generalize this method to more complex trees because the computing time is proportional to the number of organs. What we need are just more powerful computers.

This method can also be used in crop fields to optimize phyllotaxy, leaf angle, and so on. It will be very useful if we could find the good crop shape in some conditions such as given planting density. It is challenging but deserves hard working.

LITERATURE CITED

Kang MZ, Cournede PH, de Reffye P, Auclair D, Hu BG. 2008. Analytical study of a stochastic plant growth model: Application to the GreenLab model. *Mathematics and Computers in Simulation* **78**:57-75..

Shi Y, Eberhart RC. 1998. A modified particle swarm optimizer. *Proceedings of IEEE International Conference on Evolutionary Computation* 69-73.

Trewavas A. 2003. Aspects of Plant Intelligence. *Annals of Botany* **92**:1-20.

Wang XP, Guo Y, Li BG, Wang XY, Ma YT. 2006. Evaluating a three dimensional model of diffuse photosynthetically active radiation in maize canopies. *International Journal of Biometeoroloy* **50**:349-357.

Yan HP, Kang MZ, de Reffye P, Dingkuhn M. 2004. A dynamic, architectural plant model simulating resource-dependent growth. *Annals of Botany* **93**:591-602.

Zheng BY, Ma YT, Li BG, Guo Y, Deng Q. 2011. Assessment of the influence of global dimming on the photosynthetic production of rice based on three-dimensional modeling. *Science China Earth Sciences* **54**:290-297.

Proceedings of the 7th International Conference on Functional-Structural Plant Models, Saariselkä, Finland, 9 - 14 June 2013. Eds. Risto Sievänen, Eero Nikinmaa, Christophe Godin, Anna Lintunen & Pekka Nygren.
http://www.metla.fi/fspm2013/proceedings. ISBN 978-951-651-408-9.

A novel plant cell division algorithm based on ellipse/ellipsoid fitting

Metadel K. Abera, Pieter Verboven, Thijs Defraeye, Maarten L.A.T.M. Hertog, Bart M. Nicolai
Flanders Centre of Postharvest Technology / BIOSYST-MeBios, University of Leuven, Willem de Croylaan 42, B-3001, Leuven, Belgium
**correspondence:* metadel.abera@biw.kuleuven.be

Highlights: A novel plant cell division algorithm is presented for both 2D and 3D representation of cells. The position and orientation of the dividing cell wall were determined by fitting ellipse/ellipsoid to the cell vertices. The new wall is then inserted along the minor diameter of the fitted ellipse/ellipsoid perpendicular to the major diameter of the fitted ellipse/ellipsoid.

Keywords: cell division, biomechanics, turgor pressure, thin-walled structure, Hooke's law, Newton's law, ellipse fitting, ellipsoid fitting

INTRODUCTION

Cellular pattern studies and simulation of higher level processes such as phyllotaxis and vascular patterning calls for models of the division and arrangement of cells into tissues (Smith *et al*., 2006). Many biophysiological processes in plant organs, such as gas transport, are strong functions of the microstructural geometry of the tissue (Ho et al., 2011) which is in turn dependent on the cell division and arrangement of cells.

In contrast to animal cells, plant cell walls are relatively rigid. The walls of the neighbouring cells are joined by the middle lamellas, which are composed mainly of pectins. Moreover, the walls are traversed by plasmodesmata (thin, intercellular, plasmic channels) (Romberger *et al.*, 1993). Unless the cell is in the division phase, or pores are generated by separation of cells or death of cells, the contiguous walls of the neighbouring cells do not slide or slip with respect to each other, thus the cell topology is maintained. These aspects should be taken into account when considering cell division and expansive growth. Cell division rules that were proposed by Hofmeister (1863), Sachs (1878) and Errera (1886) are still the most prominent works which are the basis for modern thoughts. According to Hofmeister, the dividing wall is inserted at right angle to the longitudinal axis of the mother cell; while Sachs suggested that the new wall intersects the side walls at right angles. Errera's rule states that the dividing wall should be the shortest wall that partitions the mother cell into two equal daughter cells (reviewed by Prusinkiewicz & Runions, 2012).

Besson and Dumais (2011) have developed a rule for symmetric division of plant cells based on probabilistic selection of division planes. According to their work, the Errera's rule of cell division failed to account for the variability observed in symmetric cell divisions, in particular, the fact that cells of identical shape do not necessarily adopt the same division plane. The variability in symmetric cell division is accounted for by introducing the concept of local minima rather than global minima. The division planes are then selected based on a probability which scales inversely to the difference between a candidate plane and a plane which is the global minima. In our model we have achieved this using the random selection of the minor diameter when the fitted ellipse/ellipsoid is a circle/sphere which will result in infinitely many possible candidates for the dividing wall. Robinson *et al*. (2011) introduced an asymmetric cell division algorithm in which the division wall is chosen as the shortest wall which passes through the nucleus of the mother cell. In their model, the asymmetric cell division is achieved by displacing the nucleus of the mother cell from the centroid of the cell in a random direction. In our model we have achieved this by randomly moving the position of dividing wall along the major diameter of the fitted ellipse/ellipsoid. The dynamic pattern of cell arrangement is a function of not only the position and orientation of division walls but also the timing of cell division and growth of the tissue. The early work of Korn (1969) reintroduced by Merks and Glazier (2005) represents cells as a set of points, and growth is achieved by the addition of new points to a cell. Cell division is carried out according to Errera's rule. Cell mechanics based models for 2D cell growth were developed by different researchers (Dupuy *et al*., 2010; Sahilin and Jönson, 2010 & Abera *et al*., 2012a 'in press'). The 2D cell growth model developed by Abera et al. (2012) has recently been extended to a 3D cell growth model (Abera et al. 2012b).

Based on the literatures detailed above, there is no single generic model. Some models are intended either for symmetric or asymmetric cell division. Some of them are focused merely on the division rules, without paying attention to the timing of cell division and the actual expansive growth and others are not accounting for cell mechanics when modeling cell growth. To our knowledge, 3D plant cell division models are scarce. Knowledge on the 3D arrangement of plant cells and their growth in tissues is however of high importance to our understanding of biophysiological processes. The objective of this paper is to develop both 2D and 3D plant cell division algorithms that are generic and based on cell growth mechanics.

METHODOLOGY

In our model, the cell is considered as a closed thin walled structure, maintained in tension by turgor pressure. The cell walls of adjacent cells are modeled as parallel, linear elastic elements which obey Hooke's law. Cell expansion then results from turgor pressure acting on the yielding cell wall material. To find the sequence of positions of each vertex and thus the shape of the tissue with time, a system of differential equations for the positions and velocities of each vertex is established and solved using a Matlab ordinary differential equation solver (For details, see Abera et al., 2012a 'in press'). The cell division algorithm calculates the area/volume of the cells and checks if there are cells which exceed a predefined cell area/volume. The readiness of the cell to divide was determined based on cell size which is a function of time. A dividing wall is inserted whenever a cell exceeds its predefined size. In order to determine the position and orientation of the new wall that divides the cell, an ellipse/ellipsoid fitting algorithm is implemented, based on the cell vertices. The new wall is then inserted along the shortest diameter of the fitted ellipse/ellipsoid perpendicular to the longest diameter of the fitted ellipse/ellipsoid (see Fig. 1). The cell vertices, walls and edges are then updated and the cell expansion resumes. By moving the position of the dividing wall in either direction along the major axis based on a random factor chosen between -1 and 1 a switch between symmetric and asymmetric division is possible.

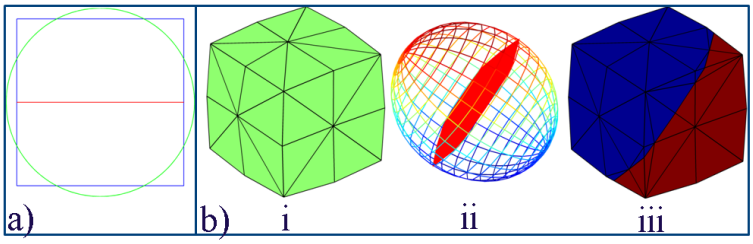

Fig. 1. Demonstration of the cell division algorithm: a) 2D cell division where blue lines are boundaries of the mother cell; green line is the fitted ellipse and red line is the new wall dividing the cell; b) 3D cell division where i) is the mother cell; ii) is the fitted ellipsoid (the red plane shows the orientation and position of the new wall); iii) shows the two daughter cells with distinct colors.

RESULTS AND DISCUSSION

We have developed a generic algorithm, based on cell wall mechanics, that is capable of producing variety of cell and tissue types. The algorithm can produce the variability observed in symmetric cell division without introducing the concept of local minima but sticking to the Errera's rule of global minima (Besson and Dumais, 2011). In our model, an ellipse/ellipsoid is fitted to the vertices of the mother cell. The position and orientation of the minor diameter of the ellipse/ellipsoid is used as the position and orientation of the dividing wall. If the fitted ellipse/ellipsoid is a circle/sphere, we have infinitely many possible orientations for the candidate dividing wall. The random selection of one of them made it possible to produce the variability observed in symmetric cell division (see Fig. 2).

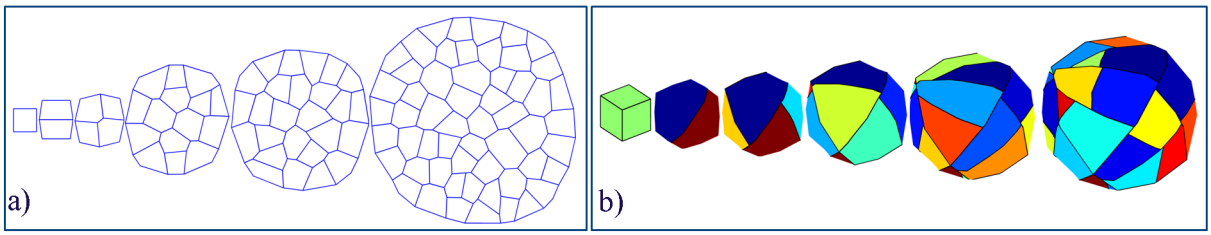

Fig. 2. Symmetric 2D cell division (a) and symmetric 3D cell division (b).

The asymmetric cell division (Robinson *et al*., 2011) is achieved by random displacement of the dividing wall along the major diameter of the fitted ellipse/ellipsoid. By making the mechanical properties and the maximum resting length of the walls/edges global direction dependent, the model allows both isotropic and anisotropic cell growth which leads to different tissue types. The cell division algorithms can be coupled to the 2D expansive plant cell growth model (Abera et al., 2012a, 'in press') and the 3D expansive plant cell growth model (Abera et al., 2012b) which were initiated from a 2D and 3D Voronoi tessellations respectively.

In conclusion, the main merits of the algorithm are: 1) both cell shape and topology are taken care of; 2) it is based on physics; 3) the equations for the actual growth of the cell walls (change in resting length of the walls) and cell division are solved continuously; 4) it is generic in that a switch between isotropic growth and anisotropic growth as well as between symmetric cell division and asymmetric cell division is automatic and easy; 5) there is no need for an iterative procedure to find the shortest wall for cell division. In our algorithm, the division wall is inserted along the minor diameter of the ellipse/ellipsoid. To our knowledge, the 3D cell division and cell growth algorithm presented here is the first one based on cell wall mechanics introduced to the literature.

LITERATURE CITED

Abera MK., Fanta SW, Verboven P, Ho QT, Carmeliet J, Nicolai BM. 2012a. Virtual Fruit Tissue Generation based on Cell Growth Modeling. *Journal of Food and Bioprocess Technology,* in press. DOI: 10.1007/s11947-011-0775-4.

Abera MK., Verboven P, Herremans E. *et al*. 2012b. 3D virtual pome fruit tissue generation based on cell growth modeling. Submitted.

Besson S, Dumais J. 2011. A universal rule for the symmetric division of plant cells. *Proceedings of the National Academy of Sciences*, USA, **108**: 6294–6299.

Dupuy L, Mackenzie J, Haseloff J. 2010. Coordination of plant cell division and expansion in a simple morphogenetic system. *Proceedings of the National Academy of Sciences*, USA, **107**: 2711–2716.

Errera L. 1886. Sur une condition fondamentale d'équilibre des cellules vivantes. *Comptes Rendus Hebdomadaires des Séances de l'Académie des Sciences***, 103**: 822–824.

Hofmeister W. 1863. Zusatze und berichtigungen zu den 1851 veröffentlichen untersuchungen der entwicklung höherer kryptogamen. *Jahrbucher für Wissenschaft und Botanik*, **3**: 259–293.

Ho Q, Verboven P, Verlinden B. *et al*. 2011. A 3-D multiscale model for gas exchange in fruit. *Plant Physiology*, **155** (3), 1158-1168.

Korn RW, 1969. A stochastic approach to the development of Coleocheate. *Journal of Theoretical Biology,* **24**:147–158.

Merks RMH, Glazier JA. 2005. A cell-centered approach to developmental biology. *Physica A*, **352**: 113–130.

Prusinkiewicz P, Runions A, 2012. Computational models of plant development and form. *New Phytologist*, **193**: 549-569.

Robinson S, Barbier de Reuille P, Chan J, Bergmann D, Prusinkiewicz P, Coen E. 2011. Generation of spatial patterns through cell polarity switching. *Science*, **333**: 1436–1440.

Romberger, JA., Hejnowicz, Z., Hill, J.F. 1993. *Plant Structure: Function and development*. Springer, Berlin Heidelberg.

Sachs J. 1878. Über die anordnung der zellen in jüngsten pflanzentheilen. *Arbeiten des botanischen Instituts in Würzburg*, **2**: 46–104.

Sahlin P, Jönsson H. 2010. A modeling study on how cell division affects properties of epithelial tissues under isotropic growth. *PLoS One*, **5**: e11750., doi:10.1371/journal.pone.0011750.

Smith RS, Guyomarc'h S, Mandel T, Reinhardt D, Kuhlemeier C, Prusinkiewicz P. 2006. A plausible model of phyllotaxis. *Proceedings of the National Academy of Sciences*, USA **103**: 1301–1306.

Proceedings of the 7th International Conference on Functional-Structural Plant Models, Saariselkä, Finland, 9 - 14 June 2013. Eds. Risto Sievänen, Eero Nikinmaa, Christophe Godin, Anna Lintunen & Pekka Nygren.
http://www.metla.fi/fspm2013/proceedings. ISBN 978-951-651-408-9.

Modeling Cucumber leaf orientation as growing in heterogeneous canopy

Tingting Qian[1,2], Chunjiang Zhao[1,2*], Xinyu Guo[1], Shenglian Lu[1]

[1]Beijing Research Center for Information Technology in Agriculture, Beijing 100097, China
[2]Shanghai Jiaotong University, Shanghai, 200240, China
**correspondence: zhaocj@nercita.org.cn*

Highlights: The change of leaf azimuth during cucumber growth was analyzed. Five plant density treatments were conducted to analyze the relationship between light environment and leaf azimuth. There is significant evidence shown in the results that leaf distribution frequency changed as the influence of heterogeneous light conditions.

Key words: LAI, Leaf azimuth, Sunlit greenhouse, Cucumber, Heterogeneity

INTRODUCTION

In cucumber canopy, it can be observed that cucumber leaves adjust the orientation into the direction of the incoming radiation to improve light interception (Kahlen *et al.* 2008). The study of Chen *et al.* (1994) shows that leaf orientation has much greater effects on canopy photosynthesis than spatial distribution of leaf area density. Leaf azimuth should be explicitly described as it has a big impact both on light distribution and photosynthesis (Sarlikioti 2011). Kahlen *et al.* (2008) have done some remarkable research on leaf phototropism in a cucumber canopy. A model was developed by considering leaf reorientation as triggered by the gradient in the R: FR ratio between left and right half of one leaf. Some of our early results show that cucumber leaves in a sunlit greenhouse usually reoriented their azimuth, especially, the leaves oriented to north as influenced by the north wall of the greenhouse which blocks most of the light. The leaf orientation was affected by not only the shade caused by leaf blocked but also the environment heterogeneous in sunlit greenhouse. The objective of this work is to analyze the changes of leaf azimuth during cucumber growth and describe the relationship between light environment and leaf azimuth character using a simplified model.

MATERIALS AND METHODS

Experiments

Four experiments were conducted in autumn 2012 in experimental sunlit greenhouse at Beijing Academy of Agriculture and Forestry Sciences (39º26′ N, 116 º 19′ E). The experiments had 5 density treatments, the planting spacing of treatments (row × plant) were: 30×40cm, 35×40cm, 40×40cm, 45×40cm, 50×40cm. Every two rows in one ridge, the distance between ridges was 70cm. Eight neighboring plants per treatment were selected to measure leaf azimuth, leaf length and leaf width at 2012-10-11, 2012-10-18, 2012-10-29 and 2012-11-8, respectively, as cucumber growing.

Leaf distribution statistics

Leaf distribution in canopy was separated into 8 orientation class. The frequency of leaf distribution in each class and in each canopy was counted. The data of leaf distribution frequency in 30×40cm, 40×40cm, 50×40cm canopies of four experiments were used to analyze the changes of leaf azimuth during cucumber growth and describe the relationship between light environment and leaf azimuth character. The data of 35×40cm and 45×40cm treatments were used to evaluate the accuracy of the model.

Due to the heterogeneous characteristics of light distribution in sunlit greenhouse, light environment is difficult to measure directly. Following the Beer-lambert law, light intensity in the canopy is directly impacted by LAI. Therefore, we use LAI to indicate the light condition in the canopy based on the theory that as LAI increased the light transmittance decreased. In order to study the leaf distribution in detailed, the leaf azimuth distribution range from 0º to 359º in a clockwise direction was separated into 8 orientation classes named in capital letters respectively (from I to VIII) and each class contains 45º angle ranges.

RESULTS

The data of leaf distribution frequency in each class as cucumber growing are shown in figure 1. Leaf distribution was uniform at an early stage in which the leaf number per plant was 8, but it became

non-uniform at late stage in which the leaf number per plant was more than 18. The azimuth of most leaves at late stage reoriented to south. Leaf frequency in class I and VIII decreased from nearly 12.5% to 5% while leaf frequency in leaf azimuth distribution classes IV and V increased from nearly 12.5% to 20%, and leaf frequency in II, III, VI and VII fluctuated during cucumber growing in different planting density treatments.

The LAI increased with the increase of leaf number and leaf area; at the same time, planting density also changes leaf area index. With the aim to simplify the relationship between leaf orientation and LAI, the orientation class was integrated into 4 classes which were north (316º-45º), east (46º-135º), south (136º-225º) and west (226º-315º). The leaf distribution frequency changing was different between 4 classes (Fig. 2). A linear function was used to describe the relationship between LAI and leaf distribution frequency in different classes. The regression function and determination coefficient are showed in table 1. The leaf distribution frequency in 316º-45º decreased as LAI increased while the opposite situation was found in the southern direction (136º-225º). There was no significant increase or decrease of frequency in east and west range. The regression functions also show that at the beginning of cucumber growth, the leaf distribution in 4 ranges is uniform (nearly 25%) which match the result in Fig. 1(A) very well.

The function accuracy was tested using data measured in 35×40cm and 45×40cm treatments. The data are shown in Fig. 3, and the RMSE is 6.46.

DISCUSSION

The aim of this study was to analyze the changes in leaf azimuth during cucumber growth and describe the relationship between the light environment and leaf azimuth character using the regression functions (Table 1). There was a significant change in leaf orientation distribution during cucumber growth. The results shown in Fig.1 B exhibited a great fluctuation between different orientation classes and we considered that it might be because of insufficient data. The determination coefficient for LAI dependent leaf distribution changes was low in the eastern and western azimuth classes. We considered that even the slope of the regression functions of this two distribution ranges was very small which means that the leaf distribution frequency changed little with LAI increased, but the frequency of leaf distribution was not constant, since the orientation of most leaves deviated from initial direction were restricted by maximum rotation angle, so some leaves re-orientated the direction from north to east or west. We considered that the frequency in eastern and western classes was affected by the two other ranges. The accuracy of the regression function of north and south distributions was higher than east and west. In the future we need more detailed experiments to refine the relationship between leaf distribution and LAI. The leaf distribution character will be used as parameter in cucumber canopy structural modeling which will be used in light interception calculation, so we also need to evaluate the accuracy of leaf distribution character using canopy light interception results.

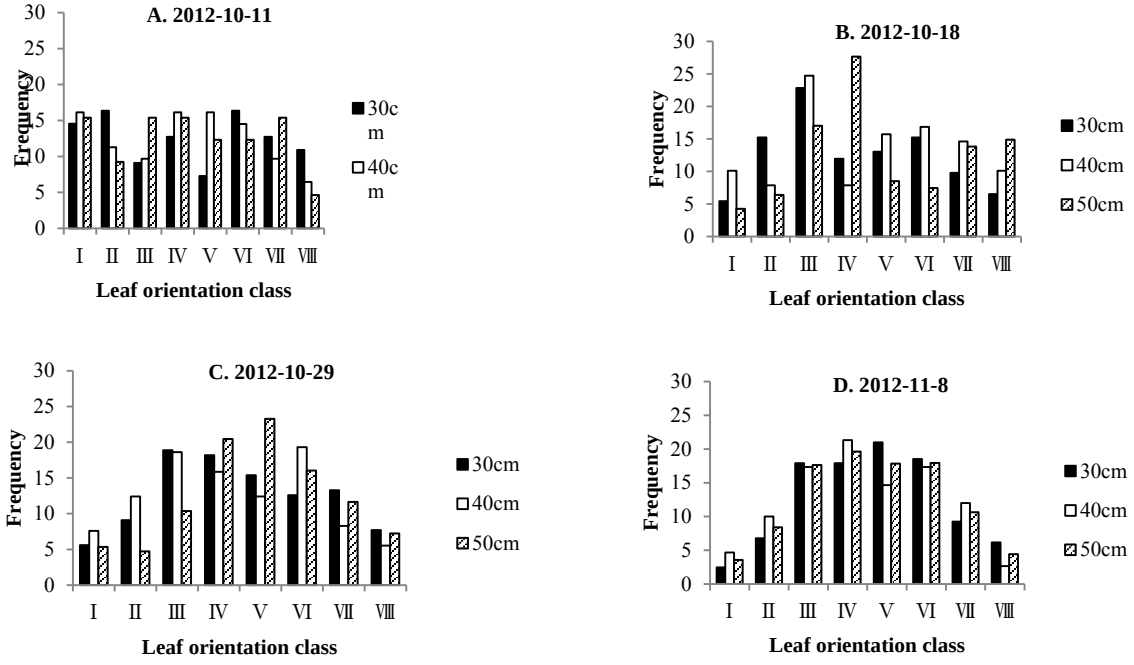

Fig. 1 leaf distribution frequency in each class of 3 treatments (30×40cm, 40×40cm, 50×40cm canopy density) at 4 times. Eight neighboring plants per treatment were selected and average leaf numbers per plant of 4 times were 8, 12,

18, 22, respectively.

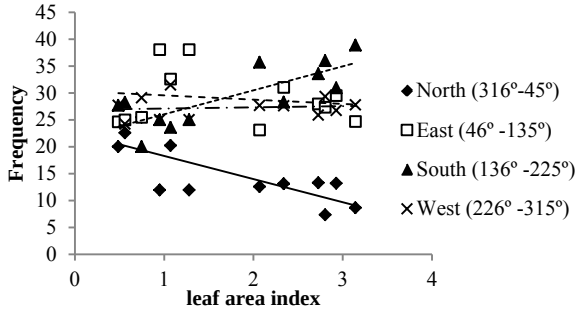

Fig. 2 Leaf distribution as LAI changes.

Table 1. Regression function and determination coefficient (R^2) for LAI dependent leaf distribution changes

Distribution	Regression function	R^2
316º-45º	y = -4.3061*L AI+ 22.598	0.5878
46º -135º	y = -0.7943*L AI + 30.341	0.0246
136º -225º	y = 4.461*L AI + 21.565	0.6187
226º -315º	y = 0.227*L AI + 26.885	0.012

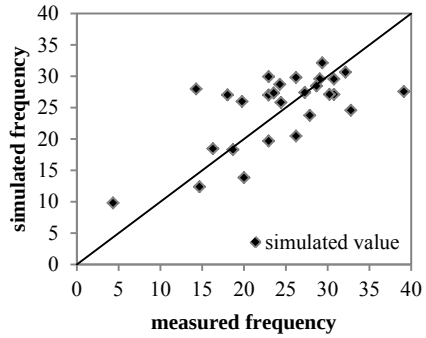

Fig. 3. Comparison between the simulated and measured leaf distribution frequency

LITERATURE CITED

Chen SG, Shao BY, Impens I, Ceulemans R. 1994. Effects of plant canopy structure on light interception and photosynthesis. *Journal of Quantitative Spectroscopy and Radiative Transfer* **52**: 115-123.

Kahlen K, Wiechers D, Stützel H. 2008. Modelling leaf phototropism in a cucumber canopy. *Funct Plant Biol* **35**: 876-884.

Sarlikioti V, de Visser PHB, Marcelis LFM. 2011. Exploring the spatial distribution of light interception and photosynthesis of canopies by means of a functional-structural plant model. *Ann Bot-London* **107**: 875-883.

RECONSTRUCTING AND OBSERVING PLANT STRUCTURE

Proceedings of the 7th International Conference on Functional-Structural Plant Models, Saariselkä, Finland, 9 - 14 June 2013. Eds. Risto Sievänen, Eero Nikinmaa, Christophe Godin, Anna Lintunen & Pekka Nygren.
http://www.metla.fi/fspm2013/proceedings. ISBN 978-951-651-408-9.

A combined method for quantifying 3D root architecture of field-grown maize

Jie Wu, Bo Yang and **Yan Guo***
Key Laboratory of Arable Land Conservation (North China), Ministry of Agriculture, College of Resources and Environment, China Agricultural University, Beijing 100193, China
**correspondence:* yan.guo@cau.edu.cn

Highlights: A new method for reconstructing 3D root architecture of field-grown maize was developed through integrating the spatial deployment of maize axile roots determined by digitizing *in situ* in the field with geometrical and topological information of scanned lateral roots. Spatial root length density and other root traits of maize can be estimated basing on this integrated method.

Keywords: root system architecture, topological structure, maize, root traits, model

INTRODUCTION

Root system architecture (RSA), refers to the topological arrangement of root segments and their geometrical characteristics (Fitter 1987; Danjon and Reubens 2008), has high capacity of plasticity responding to its rooting environment (Hodge 2004; Pagès et al. 2004). Camera and 3D laser scanner have been applied to non-invasively measure 3D dynamic RSA traits of young crop plants grown in transparent gel media (Fang et al. 2009; Clark et al. 2011). However, the root traits screens from non-soil media could be significantly different from or even reversed to those obtained from soil media (Gregory et al. 2009; Clark et al. 2011). To image and quantify 3D RSA in soil media, X-ray micro-computer tomography (CT) and neutron tomography have been utilized (Moradi et al. 2011; Mairhofer et al. 2012). However, high cost, restricted container size and limit of environmental factors restricts their applications in the field.

The objective of this study is to develop a combined method for quantifying 3D RSA of field-grown maize. We utilize digitizer to measure axile roots of individual plants *in situ* in the field, and develop a method to sample and collect topological and geometrical information of lateral roots using a software for root image analysis. We match the lateral root information with the axile roots to reconstruct and visualize the entire root system of individual plants. Different types of 2D and 3D root traits can be estimated based on the developed root model.

MATERIALS AND METHODS

Maize hybrids ZD958 (*Zea mays* L.) was seeded with row and plant spacing of 0.6 m and 0.3 m respectively on May 6, 2011 at the Shangzhuang experimental farm (40°08’ N, 116°10’ E) of the China Agricultural University.

For lateral roots measurement, three plants were selected at 75 days after sowing (10 days after silking). A self-made root auger (55 cm high, 50 cm diameter), composed by two half hollow cylinders, was put on soil surface with one sample plant at the center of the root auger. The root auger was hammered into the soil 50 cm in depth. A self-manufactured lift system was used to lift the root auger with sampled root system. Adjustable hydraulic nozzles were used to wash away soil with a disc kept at the base of the sampled root system to avoid root broken during washing. Then the root system was stored in a freezer with temperature kept 3 ℃. Two roots from the 4th to 8th nodal root whorls were selected for scanning. Branched zone of axile roots was cut into 5 cm segments from the base and first-order lateral roots along each axile root segment were cut. Axile root segment and its cut lateral roots were placed in a rectangular glass dish (25 cm × 20 cm) with water. Lateral roots were untangled carefully to minimize root overlap and then scanned using a scanner (ScanMaker i800 plus, Microtek, China). The eraser tool of WinRHIZO Pro 2009 software (Régent Instruments, Canada) was used to separate the overlapping of root segments in the images and remove noise. The developmental analysis function and Largard algorithm of the software were adopted to analyze the root developmental order, length and diameter of lateral roots while the former was also used to estimate the length and diameter of axile roots. Visual Basic Application embedded in Microsoft Excel 2007 was programmed to extract topological and geometrical information of lateral roots, length and diameter distribution of non-branched axile roots, and diameter of each 5 cm axile root segment.

Axile roots of two neighboring maize plants in a row were digitized *in situ* in the field using 3Space

Fastrak (Polhemus, USA) at 90 days after sowing (grain-filling stage). The axile roots were cut immediately after digitization and stored in a freezer for scanning to determine diameter and length of axile root segments.

3D RSA model of individual maize plant was built through matching measured lateral roots on the digitized axile roots using C++ language, boost library, SQLite and Visualization Toolkit. Model visualization was realized using ParaView software.

RESULTS AND DISCUSSION

The spatial deployment of axile roots of two neighboring maize plants at grain-filling stage was illustrated based on the dataset digitized *in situ* in the field (Fig.1A). Through matching measured lateral roots (Fig.1B) with digitized axile roots, the complete 3D RSA of an individual maize plant was reconstructed (Fig. 1C).

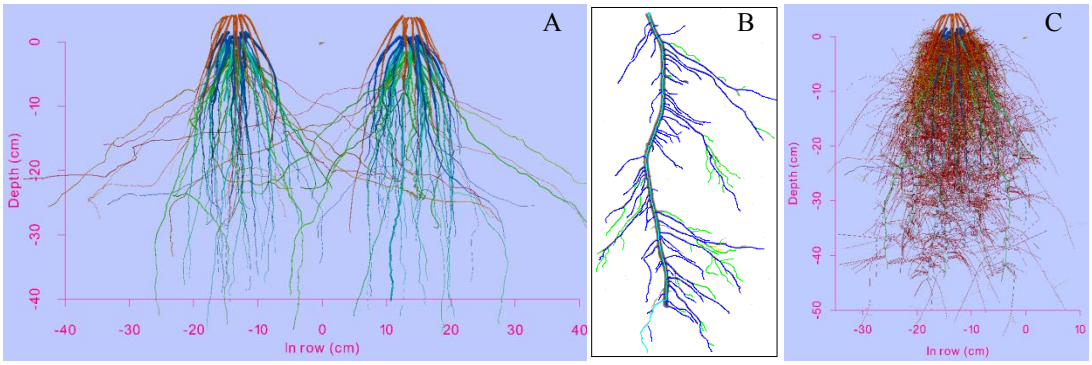

Fig. 1. A. 3D visualization of axile roots of two neighboring maize plants in a row, different colors indicate distinct root types. B. A sample of lateral root system output from WinRHIZO software, light blue, dark blue and green indicate first, secondary and tertiary order lateral roots. C. Visualization of the complete root architecture of an individual maize plant, red, yellow and green segments were first, secondary and tertiary order lateral roots, respectively.

Different root traits can be extracted based on the constructed RSA model. 2D root traits include the branching number and length density, the highest order of lateral roots, and the total length of each order lateral root on each 5 cm axile root segment of different root types. 3D RSA traits include angle and horizontal trajectory of different types of axile roots, and root length distribution of different orders of lateral roots and types of axile roots in each soil cell.

The distribution of lateral root length density of two neighboring maize plants at different soil depth was presented (Fig. 2). More than 70% of the lateral root length of the 0-40 cm soil profile was distributed in the 0-20 cm soil horizon. Significant variation of lateral root length density occurred in distinct soil horizons. For the top 10 cm soil horizon, most of root length concentrated around the plant base. In contrast, the distribution of root length density is much lower and more homogeneous at 20-40 cm soil horizon.

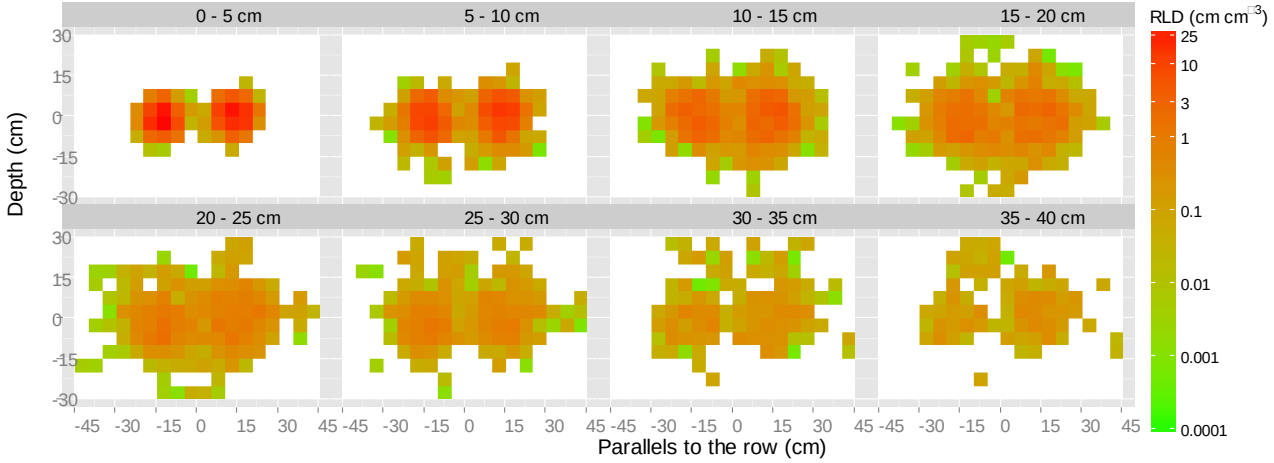

Fig. 2. The distribution of lateral root length density of maize at different soil horizons. The origin of the horizontal and vertical axis indicates the centre between two neighboring plants in a row and the vertical axis is perpendicular to

the row direction. The color mapping the values of root length density (RLD) in the legend is under logarithmic transformation.

ACKNOWLEDGEMENTS

This work was supported by the National Natural Science Foundation of China (41071205) and National Scientific and Technological Support Plan (2012BAD35B02).

LITERATURE CITED

Clark RT, MacCurdy RB, Jung JK, Shaff JE, McCouch SR, Aneshansley DJ, Kochian LV. **2011**. Three-dimensional root phenotyping with a novel Imaging and software platform. *Plant Physiology* **156**: 455 –465.

Danjon F, Reubens B. **2008**. Assessing and analyzing 3D architecture of woody root systems, a review of methods and applications in tree and soil stability, resource acquisition and allocation. *Plant and Soil* **303**: 1–34.

Fang S, Yan X, Liao H. **2009**. 3D reconstruction and dynamic modeling of root architecture in situ and its application to crop phosphorus research. *The Plant Journal* **60**: 1096–1108.

Fitter AH. **1987**. An architectural approach to the comparative ecology of plant root systems. *New Phytologist* **106**: 61–77.

Gregory PJ, Bengough AG, Grinev D, Schmidt S, Thomas WTB, Wojciechowski T, Young IM. **2009**. Root phenomics of crops: opportunities and challenges. *Functional Plant Biology* **36**: 922–929.

Hodge A. **2004**. The plastic plant: root responses to heterogeneous supplies of nutrients. *New Phytologist* **162**: 9–24.

Iyer-Pascuzzi AS, Symonova O, Mileyko Y, Hao Y, Belcher H, Harer J, Weitz JS, Benfey PN. **2010**. Imaging and Analysis Platform for Automatic Phenotyping and Trait Ranking of Plant Root Systems. *Plant Physiology* **152**: 1148 –1157.

Mairhofer S, Zappala S, Tracy SR, Sturrock C, Bennett M, Mooney SJ, Pridmore T. **2012**. RooTrak: Automated Recovery of Three-Dimensional Plant Root Architecture in Soil from X-Ray Microcomputed Tomography Images Using Visual Tracking. *Plant Physiology* **158**: 561 –569.

Moradi AB, Carminati A, Vetterlein D, Vontobel P, Lehmann E, Weller U, Hopmans JW, Vogel H-J, Oswald SE. **2011**. Three-dimensional visualization and quantification of water content in the rhizosphere. *New Phytologist* **192**: 653–663.

Pagès L, Vercambre G, Drouet J-L, Lecompte F, Collet C, Le Bot J. **2004**. Root Typ: a generic model to depict and analyse the root system architecture. *Plant and Soil* **258**: 103–119.

Proceedings of the 7th International Conference on Functional-Structural Plant Models, Saariselkä, Finland, 9 - 14 June 2013. Eds. Risto Sievänen, Eero Nikinmaa, Christophe Godin, Anna Lintunen & Pekka Nygren.
http://www.metla.fi/fspm2013/proceedings. ISBN 978-951-651-408-9.

Semantic Skeletonization for Structural Plant Analysis

Jenny Balfer, Florian Schöler* and **Volker Steinhage**
Department of Computer Science III, University of Bonn, Römerstraße 164, 53117 Bonn, Germany
**correspondence:* schoele@iai.uni-bonn.de

Highlights: Computational plant modeling from 3D sensor data is crucial for the early assessment of plant traits. Semantic modeling enables the incorporation of knowledge about the plant species, leading to an improvement of purely geometrical skeletonization approaches. Structural plant features can thereby robustly be extracted from the sensor data.

Keywords: Plant modeling, Structural plant analysis, 3D skeletonization, Feature extraction

INTRODUCTION

Structural plant analysis can help plant breeders to detect, e.g., a susceptibility of a new breed to a certain disease. Currently, the phenotyping bottleneck limits the throughput of automated plant trait assessment. In this work, we are interested in the automated extraction of structural features of plants, in particular grapevine, from 3D laser range data. We employ a skeletonization algorithm, which reduces the structure of an object represented by a point cloud to a vectorized representation in the form of a set of connected line segments, whilst preserving its topology and geometry. But for our purpose, structural preservation alone is not sufficient. We also need to know what part of the curve skeleton refers to what part of the original plant.

Therefore we propose to add a further layer to the skeletonization, namely semantics. Our goal is to automatically identify curve skeleton components as plant components. In order to achieve this we include a biological model into the skeletonization algorithm. This model enables a semantic annotation of the plant components, which in general allows us to extract the structural features.

RELATED WORK

Owing to an extensive survey by Cornea et al., it is widely accepted that curve skeletons should fulfill certain properties such as homotopy, thinness, centeredness, reliability, component-wise differentiation, smoothness, and hierarchy (Cornea et al., 2005; Cornea et al., 2007). Some of these properties may contradict each other, and especially for point cloud data with irregular sampling, some properties can be hard to achieve and evaluate. This is why many methods for the skeletonization of plants from 3D point clouds additionally incorporate model knowledge. One common prerequisite is to have the root point of the plant structure identified (Livny et al., 2010; Preuksakarn et al., 2010; Verroust and Lazarus, 2000; Xu et al., 2007). Other approaches try to fit cylindrical structures (Pfeifer et al., 2004; Runions et al., 2007) into the point cloud, thus implicitly simulating the geometric properties of branches.

Our work is based on a skeletonization method that follows a global optimization approach (Livny et al., 2010). This approach is specifically designed for the skeletonization and reconstruction of tree structures.

SEMANTIC MODELING, ANNOTATION, AND GEOMETRY CORRECTION

We exemplify our method on the berryless grape cluster, in the following termed grapevine stem system. This choice is motivated by two main reasons: First, stem systems determine the overall structure and geometry of the grape cluster. Second, they show typical characteristics that are generally challenging in plant analysis, namely self-occlusion, self-touching, and very fine structures.

The knowledge incorporated into the algorithm arises from a number of observations about the biological structure of the plant to model. To formalize these inherently informal observations, we utilize the implicit graph structure of the curve skeletons. We define the structural depth d of a vertex v in a curve skeleton as shown in equation 1, where p denotes the parent of vertex v, J denotes the set of junctions, i.e., vertices with more than one child, and l(v) the Euclidean length of the longest edge chain in v's subgraph. The proposed semantic annotation algorithm utilizes this definition of depth to annotate each vertex according to the structural plant part it belongs to. Figure 3 visualizes this semantic annotation with different colors, where each edge is assumed to have the label of its end vertex.

$$d(v) := \begin{cases} 0 & \text{if } p = \emptyset \\ d(p) & \text{if } p \notin J \vee l(v) = l(p) - \|v - p\| \\ d(p) + 1 & \text{otherwise} \end{cases} \quad (1)$$

The curve skeletons obtained by the method of Livny et al. (Livny et al., 2010) contain a number of erroneous edges for our data. Therefore, the approach presented herein aims at the automated identification and removal of these unnecessary edges. The semantic annotation described before is employed to assign each edge one of the labels ”rachis”, ”lateral branch”, ”pedicel”, or ”vascular remains of berries”. Edges that contradict biological constraints, e.g. by representing decreasingly long lateral branches in basipetal direction, are removed. Furthermore, all edge segments classified as vascular remains of berries are contracted. Figure 3 shows one remaining curve skeleton, which constitutes our final result.

Fig. 1: Point cloud of a stem system.

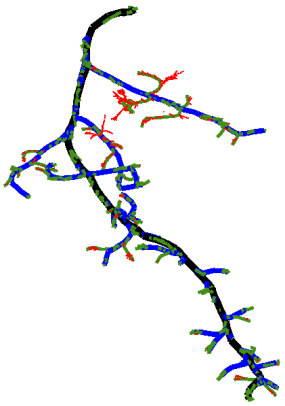

Fig. 2: Semantic annotation

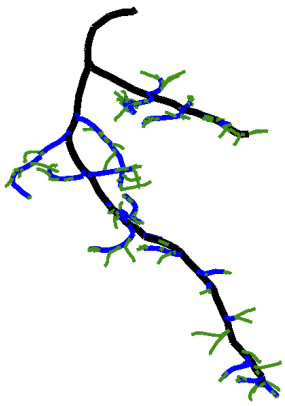

Fig. 3: Corrected curve skeleton.

FEATURE EXTRACTION

The semantic model and its implementation are designed to remove all edges from the curve skeleton that do not reflect branches in the grape cluster. This removal is crucial for the derivation of phenotypic characteristics for grapevine breeding. We will show how the semantically labeled and corrected curve skeletons can be used for the extraction of a formal grapevine descriptor from sensor data.

To identify possible features of grapevine, existing descriptor lists can be consulted. (IPGRI, 1997; OIV, 2009). The list of phenotypic features we compute include, amongst others, the existence of secondary bunches, the size of branching angles, or the length and thickness of branches and internodes.

Several of these features refer to the growth direction of the stem system or the number of internodes in one branch. In order to encode the growth direction and identify the number of vertices (and thus internodes) in one structural component, a unique numbering scheme for vertices is introduced. As a consequence, the formal features can be easily derived and used in a statistical analysis. The resulting statistical model can be used to infer knowledge about hidden object parts in the grape cluster including berries, and can furthermore serve as parameters for plant reconstruction (Schöler et al., 2013).

EXPERIMENTAL RESULTS

To quantitatively evaluate the obtained curve skeletons, we compare them to manually created reference skeletons. To operationalize the comparison of two curve skeletons, we formulate the given task as an assignment problem (Munkres, 1957) and match the number of skeletal junctions in both skeletons to each other. Then we compute precision and recall as performance measure for the number of skeletal junctions that are part of the assignment A (cf. Equation 2). Here, the precision P is given as the fraction of junctions J_S in the obtained curve skeleton that are part of the assignment, and therefore measures correctness of junctions. The recall R is the fraction of junctions in the reference skeleton J_R that are part of the assignment, and measures completeness of the obtained curve skeleton.

Our evaluations show that we are able to significantly improve the skeletons' precision by semantic geometry correction. Furthermore, we were able to keep high recall due to the deletion of erroneous edge segments, thus enabling a robust feature extraction. Figures 5 and 6 report the precision and recall values for a curve skeleton before and after semantic-driven geometry correction.

$$P := \frac{|J_R \cap A|}{|J_S|} \quad , \quad R := \frac{|J_R \cap A|}{|J_R|} \qquad (2)$$

For the evaluation of structural plant features, we compare the automatically computed values to those given by the manually created reference skeletons. We found that the errors of these feature values in the semantically corrected curve skeletons are significantly smaller than in the uncorrected ones. One example is the length of the peduncle, i.e., the "distance from insertion point on the shoot to the 1st ramification of primary bunch" (OIV, 2009). Due to erroneous edges in the curve skeletons before the semantic geometry correction, the first ramification of the primary bunch is detected too early, resulting in a very short peduncle. After semantic geometry correction, its length can be robustly measured (cf. figures 5 and 6).

CONCLUSION

In conclusion, we have shown how the skeletonization of 3D point clouds of grapevine stem systems can be enhanced by the introduction of a biological model. By means of this model, we can add semantic annotations to curve skeleton components. These annotations are used to correct the computed curve skeletons and to improve on the extraction of structural features. We performed an extensive evaluation of our approach and were able to show that both skeletonization and feature extraction could be significantly improved. Moreover, first investigations on whether the structural features can be used to distinguish different cultivars have shown to be beneficial for plant reconstruction results (Steinhage et al., 2012).

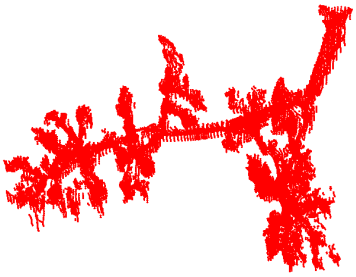

Fig. 4: Point cloud of a stem system (29,922 points).

Fig. 5: Curve skeleton before geometry correction (P = 0.29, R = 1.0).

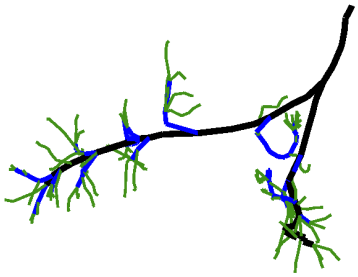

Fig. 6: Curve skeleton after geometry correction (P = 0.55, R = 1.0).

LITERATURE CITED

Cornea N, Silver D, Min P. 2005. Curve-Skeleton Applications. *Proceedings of the IEEE Visualization Conference* 2005:95-102.

Cornea N, Silver D, Min P. 2007. Curve-Skeleton Properties, Applications, and Algorithms. *IEEE Transactions on Visualization and Computer Graphics* 13:530-548.

IPGRI, UPOV, OIV. 1997. *Descriptors for Grapevine (Vitis spp.).* International Union for the Protection of New Varieties of Plants, Geneva, Switzerland/Office International de la Vigne et du Vin, Paris, France/International Plant Genetic Resources Institute, Rome, Italy.

Livny Y, Yan F, Olson M, Chen B, Zhang H, El-Sana J. 2010. Automatic Reconstruction of Tree Skeletal Structures from Point Clouds. *ACM Transactions on Graphics* 29:151:1-151:8.

Munkres J. 1957. Algorithms for the Assignment and Transportation Problems. *Journal of the Society for Industrial and Applied Mathematics* 5:32-38.

Organisation Internationale de la Vigne et du Vin. 2009. *2nd Edition of the OIV Descriptor List for Grape Varieties and* Vitis *Species.* Organisation Intergouvernementale crée par l'Accord International du 3 Avril 2001.

Pfeifer N, Gorte B, Winterhalder D. 2004. Automatic Reconstruction of Single Trees from Terrestrial Laser Scanner Data. *Proceedings of the 20th ISPRS Congress 114*-119.

Preuksakarn C, Boudon F, Ferraro P, Durand J-B, Nikinmaa E, Godin C. 2010. Reconstructing Plant Architecture from 3D Laser Scanner Data. *Proceedings of the 6th International Workshop on Functional-Structural Plant Models* 16-18.

Runions A, Lane B, Prusinkiewicz P. 2007. Modeling Trees with a Space Colonization Algorithm. *Proceedings of the Eurographics Workshop on Natural Phenomena 63*-70.

Schöler F, Balfer J, Steinhage V. 2013. Automated Parameter Estimation for a Plant Architecture Model. *Submitted to the International Conference on Functional-Structural Plant Models.*

Steinhage V, Schöler F, Balfer J. 2012. A Model-Based Approach to High Performance Phenotyping. *Proceedings of the 26th International Conference on Informatics for Environmental Protection* 1:303-310.

Verroust A, Lazarus F. 2000. Extracting Skeletal Curves from 3D Scattered Data. *The Visual Computer* 16:15-25.

Xu H, Gossett N, Chen B. 2007. Knowledge and Heuristic-based Modeling of Laser-Scanned Trees. *ACM Transactions on Graphics* 26:19:1-19:13.

Proceedings of the 7th International Conference on Functional-Structural Plant Models, Saariselkä, Finland, 9 - 14 June 2013. Eds. Risto Sievänen, Eero Nikinmaa, Christophe Godin, Anna Lintunen & Pekka Nygren. http://www.metla.fi/fspm2013/proceedings. ISBN 978-951-651-408-9.

PlantScan™: a three-dimensional phenotyping platform for capturing the structural dynamic of plant development and growth

Xavier Sirault[1], Jurgen Fripp[2], Anthony Paproki[2],Peter Kuffner[1], Chuong Nguyen[3], Rongxin Li[4], Helen Daily[1], Jianming Guo[1], Robert Furbank[1]

[1]*High Resolution Plant Phenomics Centre, CSIRO Plant Industry, Cnr Clunies Ross St and Barry dr, Canberra ACT 2601, Australia,* [2]*Australian e-Health Research Centre, CSIRO ICT Centre, Brisbane, Australia,* [3]*CSIRO CMIS, ANU,* [4]*CSIRO ICT Centre, Sydney*

**correspondence:* xavier.sirault@csiro.au

Highlights: PlantScan™ is an integrated analysis pipeline, seamlessly integrating hardware and software tools, to provide automated, non-invasive analyses of plant structure (topology, surface orientation, number of leaves, internode length...), morphology (leaf size, shape, area, volume...) and function (conductance,…). By utilising cutting edge information technology to automatically digitise plants in three-dimensions, it enables plant scientists to better understand the complex interactions involved in plant growth, i.e., the plant's genetic make-up, its physical characteristics and the environment in which it grows, thus, providing essential information to populate functional structural plant models.

Keywords: Plant architecture, transformational technology, automated feature extraction, quantification

INTRODUCTION

Plant architecture is of major importance for agricultural production. It is a major determining factor for yield potential as evidenced by the first green revolution, which resulted in a doubling of global cereal production worldwide. This was achieved by the breeding of high yielding cultivars with reduced plant stature (Hedden, 2003). Because plant architecture also determines the physical, chemical and biotic factors to which a plant is exposed (Wilson and Chakraborty, 1998), plant breeders and geneticists have been actively selecting for plant architecture and have been exploiting natural genetic variation in canopy architecture for centuries.

Nevertheless, the genetic control of plant architectural characteristics still remains today largely unknown due to the complexity and challenges in accurately and rapidly quantifying plant structure and geometry. This difficulty of measuring plant structure is compounded when studying plant architecture dynamically and its impact on physiological traits (conductance, light interception…) across a large number of genotypes. Indeed, not only does it require determination of plant topology and quantification of shape and size of each organ in high throughput but it also requires capturing and tracking organ expansion and growth over time under various environmental conditions. Despite the technological challenge, exploiting the dynamic nature of plant architecture and its influence on physiological traits within breeding programs represents a window of opportunities for improving yield potential in response to changing climatic conditions.

Analysis of digital representation of individual plants in three dimensions, in combination with proxy-sensing technologies (hyperspectral, infrared, visible imaging) is one way to determine plant topology, quantify plant geometry and assess simultaneously their impact on plant function. In this manuscript, we introduce an advanced automated phenotyping platform, PlantScan™, which combines the advantages of stereo-optical cameras and laser ranging sensors for faithfully digitising plants in three dimensions. Combining these two technologies is particularly valuable for digitising thin structures such as leaves and stems (Li *et al*, *in prep.*). To provide a link between plant structure and function, colour and thermal infrared images are projected onto these 3D structural representations. These digital objects are then fed to a generalised analysis processing pipeline that automatically derives structural (e.g. topology, surface orientation, number of leaves…), morphological (e.g. leaf size, shape, area, volume…) and functional information (conductance, photosynthesis...) at the whole organ or plant level (Paproki *et al*, 2012). Although the platform has been tested on a range of plant species (rice, wheat, canola, eucalyptus, tobacco, millet and tomato), we illustrate our results using mainly corn and cotton; nonetheless we will discuss the inherent difficulties at applying these *in-silico* methods to complex cereals such as rice or wheat.

THE DIGITISATION PLATFORM

PlantScan™ is a custom-built imaging chamber integrating multi-wavelength, optical-imaging sensors and Light Detection and Ranging (LiDAR) systems, which are arranged in a multi stereo configuration (Fig 1). Two microbolometer sensors (model A645, FLIR systems Inc, MA, USA) collect thermal information with temperature resolution of 0.045°K in the waveband 7.5 to 14 µm, while three JAI 3-CCD optical sensors (model AT-200GE) and one JAI 4-CCD RGB/NIR optical line scanner (model LQ-200 CL), equipped with Fujinon zoom lenses (model C22x17R2D-ZP1) collect information in the visible and near infrared spectra. In addition, two synchronised light detection and ranging (LiDAR) sensors (SICK LMS400) operating at a wavelength of 650nm with a 70° sweep collect time of flight data and reflectance data at a rate of 270Hz.

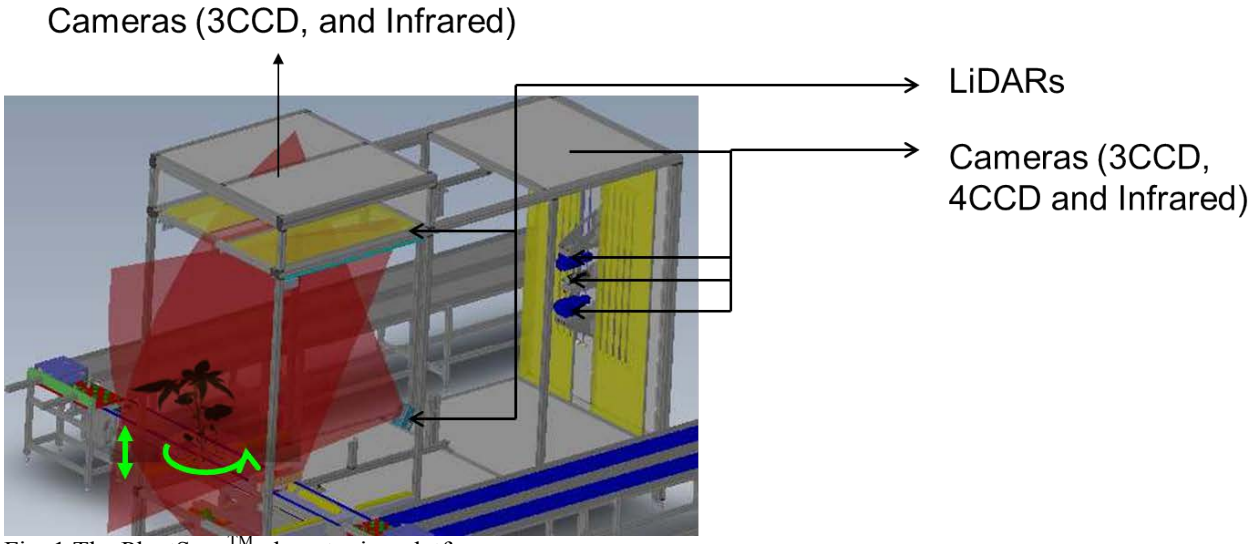

Fig. 1.The PlantScan™ phenotyping platform

The light spectrum in the chamber is generated by fluorescent light run on a 75 kHz electrical signal to avoid noise in the acquired images. The light is diffused to approximate Lambertian conditions using Y20 Miniprism diffuser panels within the imaging chamber (York precision panels, Sydney, Australia).

The platform is composed of a double conveyor belt, manually loaded, with plants held in position on pot carriers. Individual plants are identified by 2D bar codes. A first transfer station diverts the plant to a split conveyor belt which accurately positions the plant for imaging using laser proximity sensors. A rotating turntable, fitted with an incremental encoder with up to 2.5 million counts per revolution and mounted on a scissor-lift platform (10µm linear accuracy), ensures the plant is scanned from every angle in a 360° rotation. After imaging, the plant is conveyed to a second transfer station before being ejected by an actuator onto a double gravity belt. Plants are then manually unloaded and transported back to their growing environments.

All motion control and image acquisition was realised utilising the graphical programming environment LabVIEW (National Instrument).

The platform is able to scan very small seedlings or plants from a few centimetres to a couple of metres in height and up to a metre thick. Image and LiDAR data are captured simultaneously in 50 seconds (one image every 3° from all cameras, while LiDAR is continuously acquiring) with their contextual information and collated into one multi-layer data file before being stored in a purpose-built database.

THE SOFTWARE PIPELINE

To obtain 3D architectural representations of crops, trees and/or model species, overlayed with spectral information, a number of computer vision techniques have been simultaneously integrated in a reconstruction scheme running on a computer cluster, thus combining the respective advantage of each technique:

- Stereo-techniques using silhouette-based (Visual hull) and Embedded Voxel Colouring (Leung *et al*, 2012) (Fig 2A) and textural methods (Patch based Multi-view Stereo - PMVS) (Furukawa and Ponce, 2010)(Fig 2B);

- Fusion of LiDAR Point cloud to mesh results using Random sampling and Consensus (RANSAC) approaches associated with iterative closest point (ICP) algorithms (Fig 2C);
- Fusion of spectral signals onto 3D structural representations: only colour and thermal infrared images close to the surface normal (within 30°) of each mesh polygon are averaged and projected, thus taking into account the influence of plant geometry on data collected by proxi-sensing technologies (Guo *et al*, *in prep*) (Fig 2D).

To achieve higher reconstruction accuracy, we designed a new calibration algorithm, which estimates camera parameters (including geometric distortion) from all camera positions at once around a rotating axis (Chuong *et al*, *in prep.*). The results are high-resolution 3D plant meshes with sub-millimetre resolutions, which are then automatically segmented in order to semantically identify the different parts of the plants as detailed in Paproki *et al.* 2012. Figure 2E shows a maize mesh automatically segmented and Fig 2F shows the fitting of spline function to the midrib of two leaves from the corn plants in Fig 1E. A longitudinal 3D matching pipeline for plant mesh parts can also be used to evaluate temporal changes at the whole plant and/or organ level.

RESULTS AND DISCUSSION

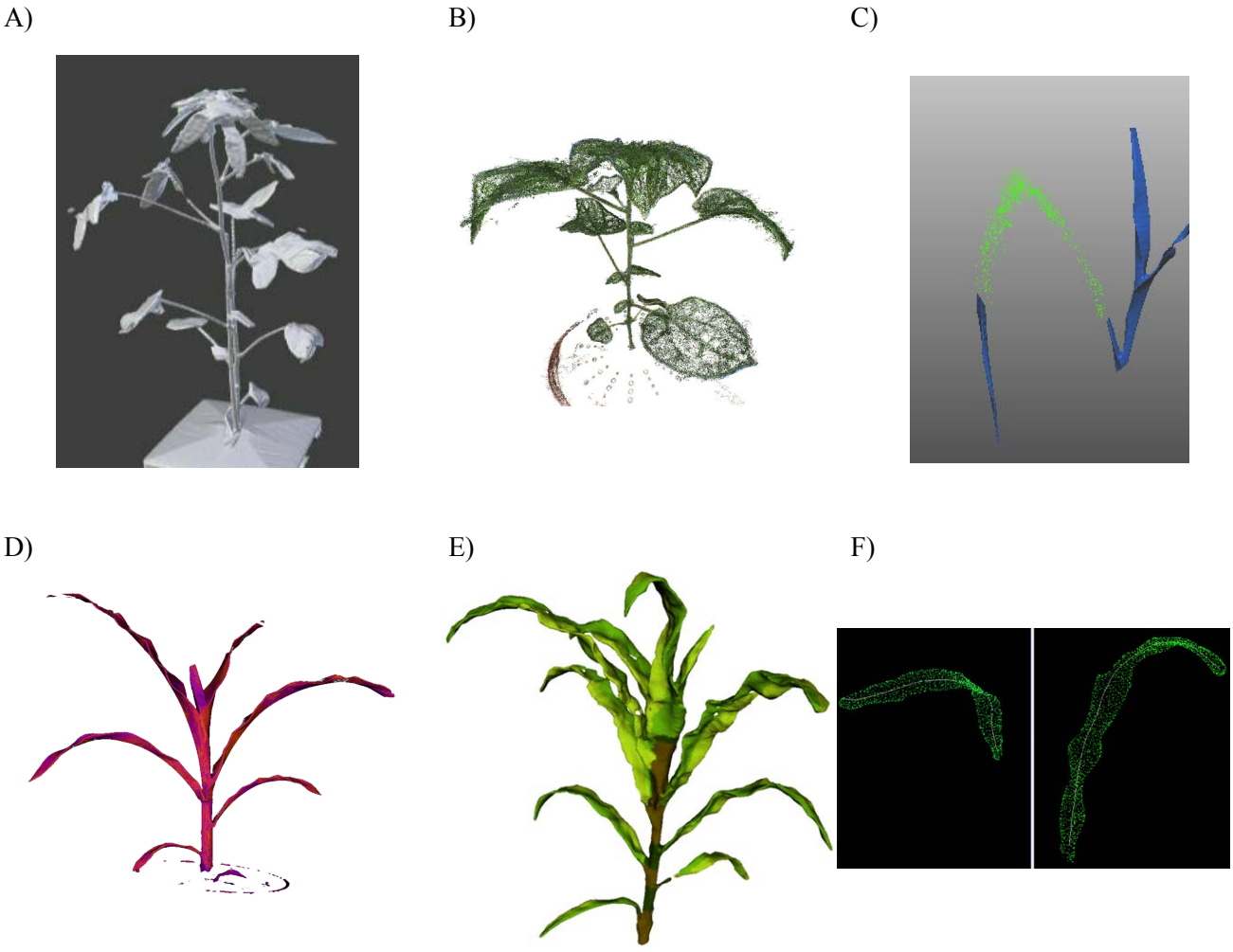

Fig. 2.Automated reconstruction of Gossypium species by A) Visual hull methods, and B) Patch-based Multi-view stereo. C) fusion of LiDAR and mesh information for wheat species (the mesh has been deleted to show the co-registration of LiDAR information), and D) 3D data fusion of Infrared information for Zea mays (false colour imaging of leaf temperature). E) False colour imaging of mesh segmentation for Zea mays: green identifying each leaf and brown identifying the stem, F) automated margin extraction and spline fitting of the midrib for two of the maize leaves in E)

Currently, there are a few limits to our methods, in particular when trying to reconstruct complex cereals like wheat or rice as our algorithms do not cope well with overlapping structures and concave surfaces when using visual hull-based methods alone. To address this issue, we are looking at integrating prior-knowledge of geometric structures by using x-ray geometric datasets, parametric models and statistical shape models as well as prior-knowledge of plant development in our reconstruction scheme. For PMVS methods, the accuracy relies on texture quality. Plants are known to lack surface texture. Improving results from PMVS can be addressed by using higher resolution images. Today, our system can resolve structures as small as 0.5mm. This is suitable for monitoring organ development or overall plant growth but not enough to resolve leaf thickness. Another area of improvement is on the calibration of our optical system. Currently our calibration algorithm does not work at sub-pixel resolution, thus limiting our ability to achieve higher accuracy.

By providing an integrated multi-sensing platform relying on a range of imaging sensors, PlantScan increases scientists' capacity to precisely and accurately quantify the biological processes involved in the development and functioning of plants and this with greater detail, frequency and objectivity than traditional methods. We point to the prospect that outputs from such a platform, which was developed for phenomics applications, i.e. measurement of correlated phenotypes in high-throughput, could provide a suite of new tools for populating functional structural plant models (FSPM) assuming that these outputs can be transformed into model parameters (Vos *et al*, 2010). These 3D models of plants with metadata will be made available via an on-line data repositories in self-contained collections (e.g. Data Access Portal - https://data.csiro.au/dap/), along with the means to handle, test, measure and interrogate them, allowing empirical research on these virtual models of crop plants. We are hoping that the information deposited on this repository will provide the necessary data for developing a predictive framework for enabling *in-silico* physiological breeding in the future.

LITERATURE CITED

Furukawa Y and Ponce J 2010 Accurate, dense and robust multiview stereopsis. IEEE Transaction on Pattern Analysis and Machine Intelligence, **32**(8): 1362-1376**.**

Hedden, P. 2003 The genes of the Green Revolution. Trends Genet. **19**: 5–9

Leung Carlos, Ben Appleton, Mitchell Buckley and Changming Sun 2012 Embedded Voxel Colouring with Adaptive Threshold Selection Using Globally Minimal Surfaces. International Journal of Computer Vision **99**(2): 215-231 (2012)

Paproki Anthony. Xavier Sirault, Scott Berry Robert Furbank and Jurgen Fripp 2012. A novel mesh processing based technique for 3D plant analysis.. *BMC Plant Biology* **12**(1): 63.

Peng SB, Laza R, Visperas RM, Khush GS, Virk PS, Zhu DF 2004. Rice: progress in breaking the yield ceiling. In "proceedings of the 4th international cro science congress" (eds T Fisher, N Turner, J Angus, L McIntyre, M Robertson, A Borrell, D Lloyd) (The regional institute Ltd: Brisbane).

Vos J, J. B. Evers, G. H. Buck-Sorlin, B. Andrieu, M. Chelle, and P. H. B. de Visser 2010 Functional–structural plant modelling: a new versatile tool in crop science J. Exp. Bot. **61**(8): 2101-2115

Wilson P and Chakraborty S 1998. The virtual plant: a new tool for the study and management of plant diseases. Crop Protection. **17**: 231–239.

Zheng Bangyou, Shi Lijuan, Ma Yuntao, Deng Qiyun, Li Baoguo and Guo Yan 2008. Comparison of architecture among different cultivars of hybrid rice using a spatial light model based on 3D digitising. Functional Plant Biology **35**: 900-910

Proceedings of the 7th International Conference on Functional-Structural Plant Models, Saariselkä, Finland, 9 - 14 June 2013. Eds. Risto Sievänen, Eero Nikinmaa, Christophe Godin, Anna Lintunen & Pekka Nygren.
http://www.metla.fi/fspm2013/proceedings. ISBN 978-951-651-408-9.

Improving branch distribution models in trees using X-ray computed tomography

Emmanuel Duchateau[1*], **David Auty**[1], **Frédéric Mothe**[2] and **Alexis Achim**[1]
[1]*Faculté de foresterie, géographie et géomatiques, Université Laval, 2405 rue de la Terrasse, Québec G1V 0A6, QC, Canada*
[2]*INRA, UMR1092 LERFoB, 54280 Champenoux, France*
**correspondence:* emmanuel.duchateau.1@ulaval.ca

Highlights: The use of external measurements to describe the distribution of branches on tree stems can induce imprecision and bias in estimates of both the number of annual growth units and the azimuthal distribution of branches. The scanning of logs using X-ray computed tomography yielded knot data that enabled more accurate identification of the limits of each growth unit. Such information, in conjunction with current models of tree architecture, can be incorporated into functional-structural models describing relationships between tree morphology and biological processes.

Keywords: X-ray computed tomography, tree architecture, black spruce, branch distribution

INTRODUCTION

Computer-based systems capable of simulating the 3D structure of plants, their metabolic processes and environmental interactions are increasingly being developed to increase our understanding of how plant architecture and biological processes interact (Fourcaud et al. 2008). In trees, such functional-structural models can be useful tools for understanding and predicting important wood quality attributes such as branch morphology and distribution. An underlying principle of these models is that plant structure can be described in terms of a hierarchical system of replicating 'architectural units' (Barthélémy et al. 1989). In temperate tree species, the 'growth unit' (GU) i.e. the annual elongation of the terminal shoot from the apical meristem (De Reffye et al. 1995), is the single most important component of existing branch distribution models (e.g. Colin and Houllier 1991).

Such models are normally parameterized using data from external measurements. This has the advantage that data collection is relatively straightforward and can be accomplished with limited equipment. However, this simplicity may come at the expense of accuracy for certain measurements, such as branch inclination and azimuthal orientation. More recently, X-ray computed tomography techniques have been developed that can generate high-precision internal information, which could lead to improved model accuracy.

Black spruce (*Picea mariana* (Mill.) BSP) is the dominant conifer in the North American boreal forest. It develops according to Rauh's model of monopodial, rhythmic growth and attains its final developmental stage after 10-15 years (Bégin and Filion, 1999). After this, the basic structure of first and second order axes (trunk and branches, respectively) and third and fourth order axes (twigs) is duplicated through a process known as reiteration. The high reiterative capacity of black spruce accounts for its characteristically high phenotypic plasticity. This leads to a complex and apparently disorganised branching structure that complicates the development of functional-structural models, since the precise delineation of annual growth units can be difficult. The objectives of this study were: 1) to develop a method based on selective filters to locate annual growth units on black spruce logs using data derived from X-ray computed tomography and 2) to examine the distribution of branches around black spruce stems at the stem and growth unit levels.

MATERIALS AND METHODS

Measurements were taken on 33 black spruce trees from unmanaged stands in Québec, Canada. First, branch and tree characteristics were recorded following the protocol established by Colin and Houllier (1991). Sample trees were then cut into successive 2.5 m logs for X-ray scanning. Each of the resulting 107 logs were scanned at 2 mm intervals along the longitudinal axis with a 2-mm-wide X-ray beam, so that the scanned segments were contiguous. This provided accurate internal profiles for 23,040 knots (Duchateau et al. 2013).

The total number of growth units in each 2.5-m section was determined from the difference in the number of annual growth rings between discs cut from each end of the log. However, the precise limits of each annual shoot were difficult to determine, even using the X-ray data (Fig. 1). We developed an empirical method based on two filters to select the most likely location of the limits of each GU, which should correspond to the location of nodal branches produced from subterminal buds. First, the basal area of each branch (i.e. cross-sectional surface at the bark) was calculated and summed when branches originated from the same point at the stem's pith. We then applied a series of thresholds to select basal area peaks along the main stem. Secondly, we tested thresholds of minimum GU lengths, as some of the identified peaks occurred in close proximity, presumably as a result of reiteration (Bégin and Filion, 1999). Once each GU was located, we analyzed the circular branch distribution at the scale of both the tree and the growth unit. This was carried out using circular statistics and a Rayleigh test (Jammalamadaka and Sengupta 2001).

RESULTS AND DISCUSSION

The number of GUs along the stem was significantly underestimated when only external branch measurements were used. On average, the underestimation was 2.4 GUs per 2.5-m log (SD=3.7), or around 15% of the total. For a mature tree, this would represent approximately 16 GUs, which is unsatisfactory for the development of accurate models. One possible explanation is that black spruce contains a relatively large number of branches along each growth unit, but the diameter ranges of nodal (terminal) and internodal (median) branches overlap, so the delineation of GUs based on branch basal area might be problematic.

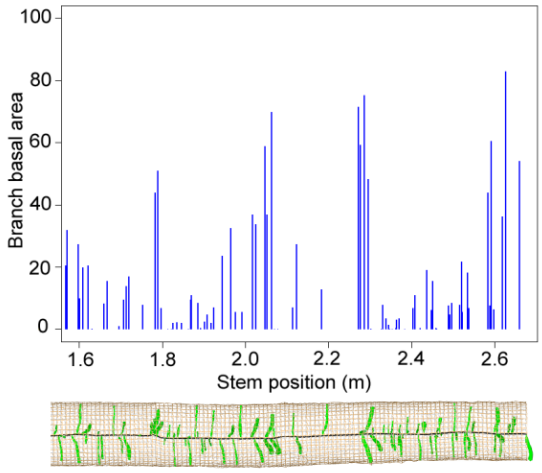

Fig. 1. Distribution of branch basal area along the stem from data extracted using the ImageJ Java plug-in 'Gourmand'.

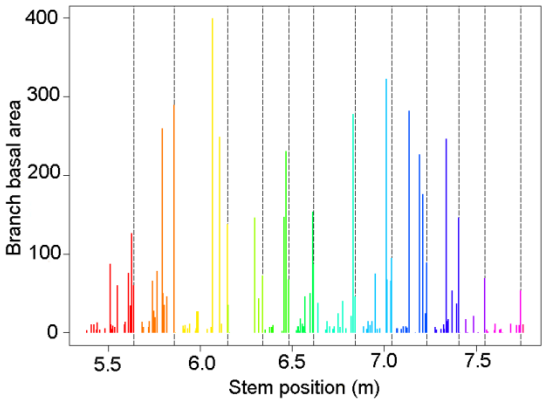

Fig. 2. Distribution of the branch basal areas along the stem and delineation of the separate growth units using our two-filter method.

For the identification of GUs using internal data, best results were obtained when 1) a GU limit was placed when the sum of branch basal areas initiating from the same point was above the 75th percentile for all branch initiation points within the log and 2) the next limit was located at a minimum distance of 7.5 cm along the main stem (Fig. 2). The utilization of the CT images coupled with this two-step method allowed us to significantly increase the accuracy of GU identification. The resulting mean bias in the number of GUs per log approached 0 (0.195). This represented a significant improvement compared to external assessment, although some variation remained (SD=2.8). The ability to identify branch initiation points at the pith of the main stem therefore allowed us to differentiate between nodal and internodal branches more accurately.

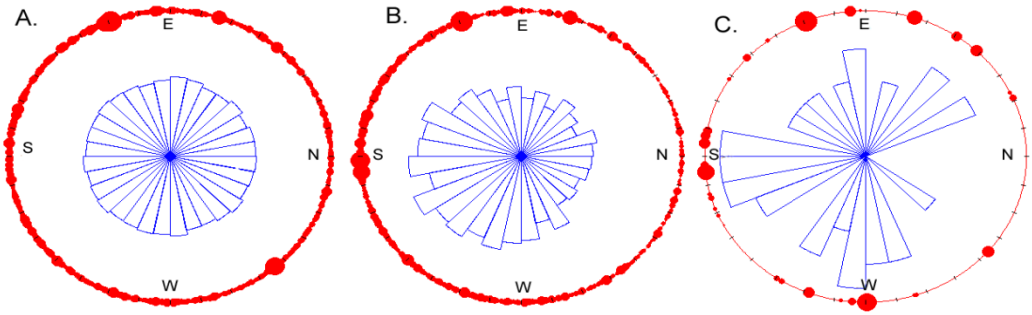

Fig.3. Distribution of branches around the stem by diameter (in red) and by number (in blue) for A) all branches, B) the largest diameter branch per GU and C) the largest diameter branch per tree.

Once we had obtained the best GU selection, we studied the circular distribution of the branches at the tree and the GU levels. For all branches on one tree, the distribution was uniform (Fig. 3A). However, the largest branch per GU had a preferential orientation of 194° (SD = 65°) and the distribution was non-uniform for 18 out of 33 sample trees (Fig 3B). The largest diameter branch in each tree had a similar mean orientation of 200° (Fig 3C). Future work will focus on 1) the influence of inter-tree competition on branch distribution around the stem, 2) testing the applicability of the two-filter method to other species and growing conditions, and 3) increasing data processing speed using automated knot detection and measurement algorithms (Longuetaud et al. 2012).

LITERATURE CITED

Barthélémy D, Édelin C, Hallé F. 1989. Architectural concepts for tropical trees. In Tropical forest. Botanical dynamics, speciation and diversity. Edited by L.B. Holm-Nielsen, I.C. Nielsen, and H. Balslev. Academic Press, London. pp. 89–100.

Bégin C, Filion L. 1999. Black spruce (*Picea mariana*) architecture. Botany 77: 664–672.

Colin F, Houllier F. 1991. Branchiness of Norway spruce in north-eastern France - Modeling vertical trends in maximum nodal branch size. Ann For Sci 48: 679–693.

De Reffye P, Houllier F, Blaise F, Barthelemy D, Dauzat J, Auclair D. 1995. A model simulating above-and below-ground tree architecture with agroforestry applications. Agroforest Syst 30: 175–197.

Duchateau E, Longuetaud F, Mothe F, Ung C-H, Auty D, Achim A. 2013. Modelling knot morphology as a function of external tree and branch attributes. Can J For Res 10.1139/cjfr-2012-0365.

Fourcaud T, Zhang X, Stokes A, Lambers H, Körner C. 2008. Plant growth modelling and applications: the increasing importance of plant architecture in growth models. Ann Bot-London 101: 1053-1063.

Jammalamadaka SR, Sengupta A 2001. *Topics in circular statistics*. World Scientific Pub Co Inc.

Longuetaud, F., Mothe, F., Kerautret, B., Krähenbühl, A., Hory, L., Leban, J.M., and Debled-Rennesson, I. 2012. Automatic knot detection and measurements from X-ray CT images of wood: A review and validation of an improved algorithm on softwood samples. Comput Electron Agr 85: 77-89.

Proceedings of the 7th International Conference on Functional-Structural Plant Models, Saariselkä, Finland, 9 - 14 June 2013. Eds. Risto Sievänen, Eero Nikinmaa, Christophe Godin, Anna Lintunen & Pekka Nygren. http://www.metla.fi/fspm2013/proceedings. ISBN 978-951-651-408-9.

tLiDAR methodologies can overcome limitations in estimating forest canopy LAI from conventional hemispherical photograph analyses

Eric Casella[1], Mat Disney[2], James Morison[1] & Helen McKay[1]
[1]*Centre for Sustainable Forestry and Climate Change, Forest Research, Farnham, Surrey, GU10 4LH, UK*
[2]*Department of Geography, University College London, London, WC1E 6BT, UK*
Correspondence: Eric.Casella@forestry.gsi.gov.uk

Highlights: The hemispherical photography technique has been widely used to assess the three-dimensional reconstruction quality of virtual plant canopy architectures (Casella & Sinoquet 2003). High-resolution terrestrial Light Detection And Ranging (tLiDAR) has recently been applied for measuring the 3-D characteristics of forest vegetation (Omasa et al. 2006.) and specifically the extraction of canopy directional gap fraction (Danson et al. 2007). In contrast with the digital hemispherical photography method, sky conditions appear to have little influence on the quality of the data collected by the tLiDAR technique. This study considers the resolution used during both point cloud data acquisition and the computation of equiangular hemispherical images, which may influence the resolving power of this technique in estimating gaps in a forest environment.

Keywords: TLS, laser, point cloud, gap fraction, equiangular projection, composite hemispherical picture, resolution

INTRODUCTION

Leaf area index (LAI) is defined as the one-sided leaf blade area per unit ground area. It is a key parameter in ecophysiology for scaling-up from leaf to canopy level gas exchange and energy fluxes between the vegetation and the atmosphere. LAI is one of the most difficult parameter to quantify *in situ* although many non-destructive methods have been proposed (Bréda 2003). The upward-looking hemispherical photography technique has been used extensively to map and quantify canopy gaps for LAI computation. However, photographs must be taken under uniform overcast sky conditions and image analyses involve complex and critical steps for pixel classification between sky and canopy components despite recent increases in the resolution of digital cameras.

Terrestrial laser scanners (TLS) have the potential to provide detailed information about forest canopy architecture by collecting 3-D point clouds of several million data points (Tab. 1) that can be transformed into hemispherical images by an equiangular projection procedure (Steyn 1980). However, the resolving power of this technique in estimating gaps in a forest environment may be affected by the resolution used during both point cloud data acquisition and the computation of hemispherical images as shown in Figure 1.

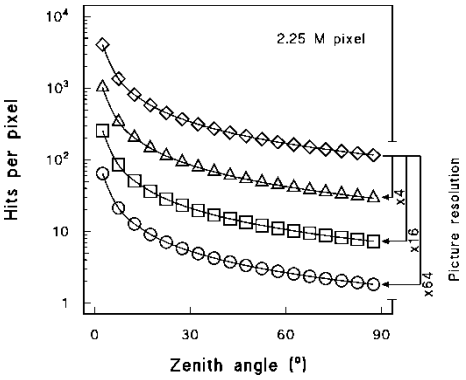

Fig. 1. Modelled mean number of laser return hits per pixel in each 5° zenith band from hemispherical images generated by an equiangular transform projection procedure (Fig. 2.) of a *x*, *y*, *z* coordinate data set computed from an opaque hemisphere for the Low (○), Medium (□), High (△) and Ultra-high (◇) TLS resolution levels (Tab.1).

METHODS

The TLS used was the pulsed time-of-flight HDS 6100 (Leica Geosystems Ltd.) which has a rotating mirror system that covers a 360º (horizontal) x 310º (vertical) field of view with a range of about 79 m at 90% albedo (Tab. 1). The laser beam wavelength is 670 nm with a 3 mm spot size at its source and a 0.22 mrad beam divergence. Hemispherical photographs were taken using a Nikon Coolpix 995 camera (2.25 M pixel) with the Nikon FC-E8 hemispherical lens.

Spatially and temporally coincident point-cloud data and digital hemispherical photographs were collected in a six-year-old stand of *Eucalyptus spp.* in southeast England. The stem density was 700 trees ha^{-1}, with an average tree height of 11±3 m. For each position (n=8) and for scan zenith angles of 0-90º, one point-cloud was recorded at each of the four predefined resolution levels of the TLS (Tab. 1).

Tab. 1. Characteristics of the Leica HDS-6100 TLS used in this study for point cloud acquisitions.

Pre-set scanner resolution levels	Low (L)	Medium (M)	High (H)	Ultra-high (U)
Angular sampling resolution (°)	0.072	0.036	0.018	0.009
Point spacing at 50 m (m)	0.063	0.032	0.016	0.008
Maximum point cloud size (M points)	6.255	25.01	100.02	400.04
Acquisition time (minute)	3.6	6.8	13.4	25.2

An equiangular projection procedure (Fig. 2) was used to transform each point cloud into 2.25, 9, 36 or 144 M pixel hemispherical images. Hemispherical photographs and images were processed with the HemiView program. Lens correction factors were applied after classifying the photographs using the CANEYE software. For each image, sky-maps were constructed by dividing the sky into an array of 18 annuli of equal zenith angle.

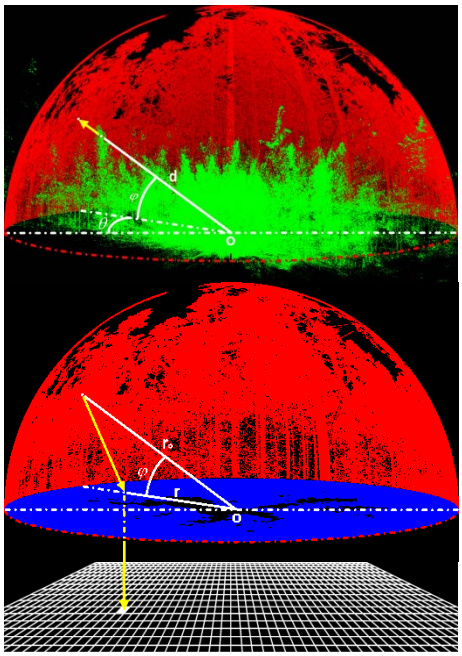

Fig. 2. Illustration of the Cartesian-spherical (top) and spherical-planar (bottom) equiangular transform projection procedures used to generate hemispherical images from the *x*, *y*, *z* coordinate TLS data. *O* is the TLS location and *d* is the distances from the laser beam source to a plant component hit. φ is the elevation angle and $r = 2r_o(90-\varphi)/\pi$.

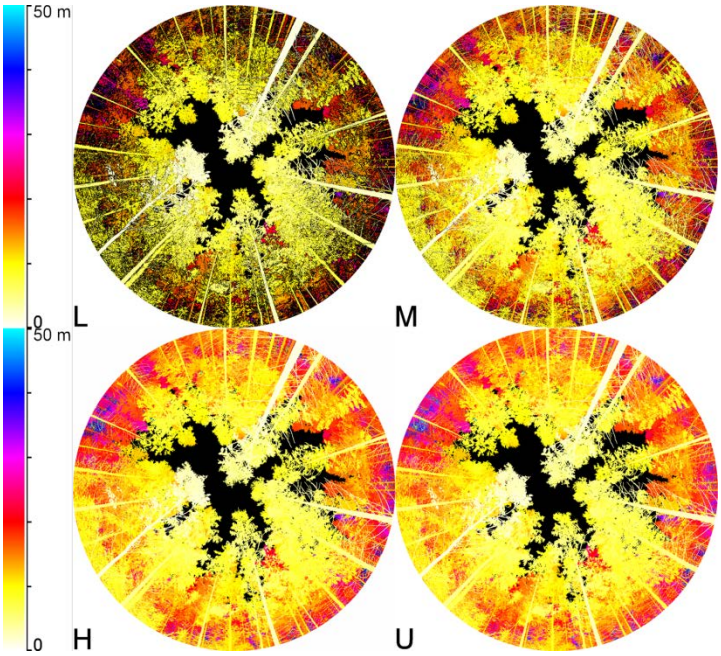

Fig. 3. Examples of computer-generated hemispherical images at 2.25 M pixel from the *x*, *y*, *z* coordinate TLS data (position #1) for the Low (L), Medium (M), High (H) and Ultra-high (U) TLS resolution levels. Colours represent the distance from the laser source to a plant component hit.

RESULTS AND DISCUSSION

Neither the range of the TLS, nor the sky conditions have any influence on the quality of the data collected (results not shown), but the quality of the reconstructed hemispherical images was gradually improved with: i) increasing levels in TLS resolution (Figs. 3 & 4); ii) increasing the resolution of the hemispherical image (Fig. 4). Alterations in the shape of the gap fraction distributions were explained by gradual increases in levels of non-return signal from the vegetation with increases in zenith angle values (Fig. 5). This loss of return signal was mainly explained by the effect of laser beam scattering around the edges of plant components (results not shown).

Therefore, the reconstruction method of the hemispherical images has been modified by taking into account this limitation in the resolving power of the technique as presented in Fig. 1. As a result, composite hemispherical images have been recomputed from the Ultra-high *x*, *y*, *z* coordinate data, showing gradual decreases in their resolution i.e., from 144 M pixel at the zenith to 2.25 M pixel at the horizon (Fig. 6).

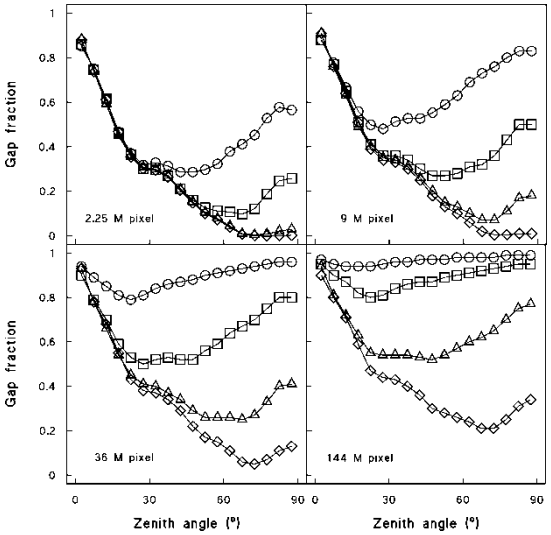

Fig. 4. Estimated gap fraction values in each 5° zenith band from hemispherical images (2.25, 9, 36 or 144 M pixel) generated by the equiangular transform projection procedures of the *x*, *y*, *z* coordinate TLS data for position #1. Same symbols as in Fig. 1.

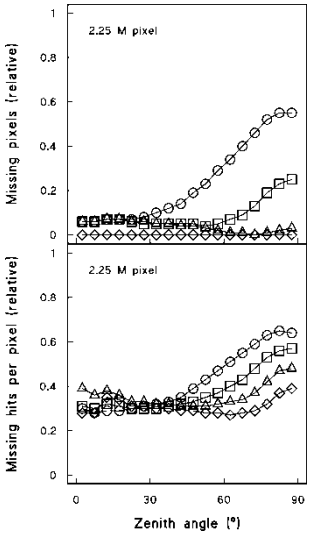

Fig. 5. Mean relative numbers of missing pixels per image and missing laser return hits per pixel in each 5° zenith band.

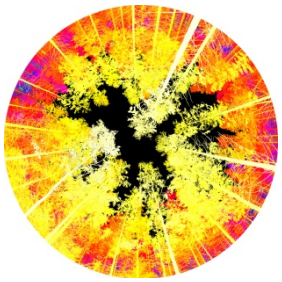

Fig. 6. Example of a composite hemispherical image computer-generated from the *x*, *y*, *z* coordinate TLS data for position #1.

Computed at the entire sky-map level, estimated gap fraction and plant area index (PAI) values from the hemispherical photographs were close to those estimated from the images (Fig. 7), especially when using the composite method (Fig. 6).

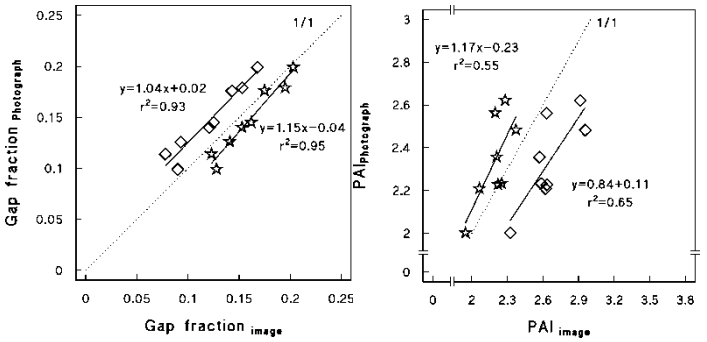

Fig. 7. Comparison between gap fraction values and plant area index (PAI) estimated from the hemispherical images (◇, 2.25 M pixel for the Ultra-high TLS resolution level; ✧, using the composite method) and the photographs over the entire sky-map. Each data point represents a different location within the stand.

CONCLUSION

The tLiDAR technique will be central to developments in acquiring canopy geometric characteristics in the future, especially for computations of solar radiation indices. Avoiding the problem of loss of return signal, the technique explained here shows promise in overcoming the discrepancies in cross-validation between direct and indirect methods for assessing canopy LAI (Bréda 2003). No effects of laser beam divergence on gap detection have been detected in this study, but further experimentation will be required to assess the influence of wind on the quality of the data collected as high scanning resolutions take longer.

Casella E, Sinoquet H. 2003. A method for describing the canopy architecture of coppice poplar with allometric relationships. *Tree Physiology* **23**:1153-1170.

Omasa K, Hosoi F, Konishi A. 2006. 3D lidar imaging for detecting and understanding plant responses and canopy structure. *Journal of Experimental Botany* **58**:881-898.

Danson FM, Hetherington D, Morsdorf F, Koetz B, Allgöwer B. 2007. Forest canopy gap fraction from terrestrial laser scanning. *IEEE Geosciences and Remote Sensing Letters* **4**.

Bréda NJJ. 2003. Ground-based measurements of leaf area index: a review of methods, instruments and current controversies. *Journal of Experimental Botany* **54**:2403-2417.

Steyn DG. 1980. The calculation of view factors from fisheye-lens photographs: Research note. *Atmosphere-Ocean* **18**:254-258.

Proceedings of the 7th International Conference on Functional-Structural Plant Models, Saariselkä, Finland, 9 - 14 June 2013. Eds. Risto Sievänen, Eero Nikinmaa, Christophe Godin, Anna Lintunen & Pekka Nygren.
http://www.metla.fi/fspm2013/proceedings. ISBN 978-951-651-408-9.

Shape reconstruction of fruit tree from colored 3D point cloud

Shenglian Lu, Xinyu Guo, Chunjiang Zhao, Weiliang Wen, Jianjun Du
Beijing Research Center for Information Technology in Agriculture, Beijing 100097, China
**correspondence:* lusl@nercita.org.cn

Highlights: An automatic and accurate method was presented for structure reconstruction of fruit tree from laser scanner measured colored point cloud. The color characteristics of different organs were selected as rules to segment point cloud into small point cloud. A skeleton of the tree was then extracted from some small point clouds, and final 3D reconstruction was achieved by combining some distribution model of leaf and shoot.

Key words: 3D Reconstruction, fruit tree, 3D point cloud, modeling plant structure

INTRODUCTION

Rapid and automatic reconstruction of plant structure is an interesting and challenging topic both in computer graphics and agronomic research. In most applications of 3D modeling for fruit tree, an entire and detailed mesh model is expected to enable potentially further application (e.g. calculating light intersection of canopy, demonstrating the difference between varieties and outside appearance). As such popular methods for modeling plant structure (e.g., L-systems, functional-structural model and interactive design method) will meet difficulties in reconstructing a 3D model of fruit tree with a satisfying accuracy for these kind applications, recently digitizing data from real objects have been used extensively for creating 3D models, and more methods reproduce virtual 3D plant models from real measured data. Electromagnetic digitizers were used earlier to measure the spatial position and orientation of stems and leaves for giving a quantitative assessment to the tree geometry (Sinoquet and Rivet, 1997; Sonohat et al., 2006) However, it is a tedious and time-consuming job in digitizing tree structure by using electromagnetic digitizers, and often not precise enough for accurately capture the detailed organ geometry. Recently non-contact laser scanners have been used for various plant measurement and reconstruction (Kaminuma, et al., 2004; Dornbusch, et al., 2007). Laser scanners enable us to rapidly quantify the surface of an object as a dense set of points. But if an organ or part of the plant is invisible to the scanner, its information will be missed in the captured point cloud. The missing information can be estimated by using existing or statistic knowledge about morphological structure of plants (Xu, et al., 2007). But this will lose accuracy for the measured plant. So these methods are more suitable for digital entertainment rather than agronomic research. In this paper, we aim to provide a method for automatic and accurate reconstructing the structure of fruit tree from laser scanner measured colored point cloud, and demonstrate some experimental results.

MATERIALS AND METHODS

A 10-year-old pear tree was chosen for data measurement at its fruiting stage. And a large range laser scanner (Focus3D 120, FARO Technologies, Inc.) was used to finish the measurement. Three stations scanning around the tree were made to obtain enough points for later reconstruction (see Fig. 1. left).

Fig. 1. Scanning pear tree by using FARO Laser Scanner Focus3D(left:); the measured colored point cloud(right).

Software FARO SCENE 5.0 (www.faro.com) was used to process the multi-station scanned data, which produce the 3D point cloud of the tree from these measured data. Each point also brings a RGB color as such we get a colored point cloud (see Fig. 1. right). We also use this software to remove noise points manually (coming from the ground and other trees) in the colored point cloud interactively.

SHAPE RECONSTRUCTION

The shape reconstruction process includes five steps. Firstly a pre-process was done to the point cloud because there are too many points in the origin scanned points (especially coming from leaves, see Fig.1 Right). A distance based noise points deleting method was used to remove noise points, and this could result in a simplified point cloud.

The second step was to segment the point cloud into several small organ point clouds. In other words we wish to separate different organs from the point cloud of the canned tree. We found that the color of each organ in pear tree is very different to other organs' , as such we can distinguish each organ from the point cloud by using its color feature. Firstly organs of pear tree were classified three categories (leaf, fruit, trunk and branch respectively). Then we calculated the color character of each category by selecting manually 20 points from the point cloud of this kind organ and computing average color value (RGB) of these selected points. The resulted average color value was used as the color character of this kind organ. After all color character of were calculated, a checking process was conducted to the simplified point cloud to check the nearest color character for each point basing on its color. The point cloud was then segment into three small organ point clouds. Fig.2 (left) shows the trunk and branch point cloud. A lot of data-missing could be found resulted from shelter of leaves.

In the next step we target to extract a skeleton of the tree directly from the trunk and branch point cloud. A constrained Laplacian smoothing method (Su et al., 2011) was used to extract the skeleton. Then we generated a skeleton model (see Fig.2 right) from the extracted . Some knowledge about the morphological structure of pear tree were used in this step to improve the skeleton because there are many discontinuous branches in the extracted skeleton. For example, some branches may be apart from the trunk, and one branch may be divided into several segments in the initial extracted skeleton, and these branches need to be connected to form a smooth skeleton of tree.

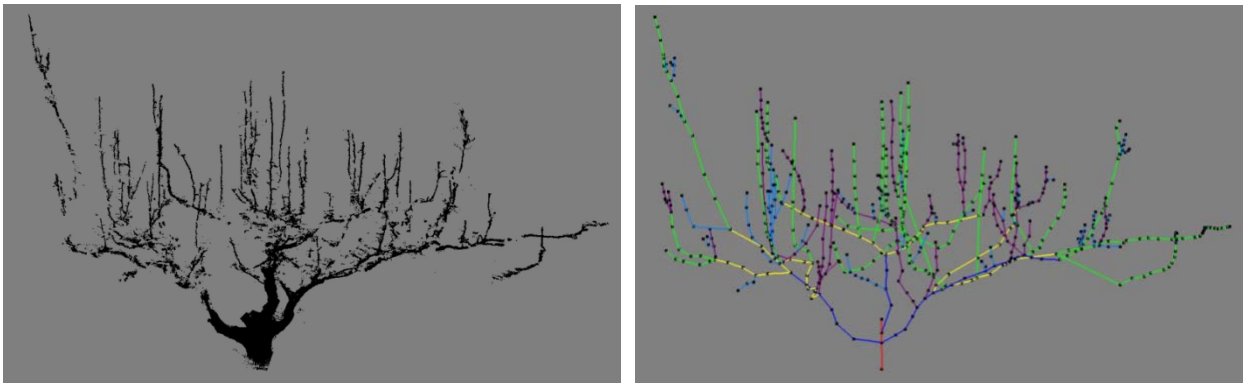

Fig. 2. The trunk and branch point cloud (left); projection vector of internodes (right).

The fourth step was to calculate the information of fruits from the fruit point cloud. A distance-based cluster algorithm was used to further divide the fruit point cloud into small point clouds. And each small point cloud represents a fruit and all points in this point cloud coming from the same fruit. Then the center coordinate of a fruit point cloud was calculated, which would be used as the position of the fruit in the final reconstruction step. The radius of a fruit was also calculated from its point cloud data.

Based on the extracted skeleton and fruit information, we finished the entire reconstruction of the scanned tree. But the little shoots and leaves were still missing in the extracted skeleton, which need to be restored for a complete reconstruction. Currently we addressed this problem by using a knowledge-driven strategy which could repair the missing little shoots and leaves. Concretely, we used distribution models about shoots and leaves based on how locating on different types of branches, which supplys little shoots and leaf model for the extracted skeleton model. In which a leaf model was a mesh surface measured from the real fruit tree by using a hand-held laser scanner.

RESULTS AND DISCUSSION

A pear tree has been reconstructed by proposed method, in which the number of fruit, the conposition and radius of each fruit all were calculated at the fourth step. Five leaf models (with texture mapping) were used in the reconstruction to achieve a more realistic results(see Fig.3).

The automatic 3D reconstruction of a whole plant from laser scanned data points is presently still an open problem.Currently we just use some knowledge about leaf distribution on the canopy to orient the reconstruction, instead of using the scanned leaf point cloud, since it is a very difficult task to restore the 3D surface of leaves directly from the scanned leaf point cloud. And our further study expect to remove errors which may be caused by knowledge-oriented method.

Fig. 3. The shape reconstructed result of the pear tree

Acknowledgments. This work is supported by China National Science and Technology Support Program (No. 2012BAD35B01) and Beijing Science and Technology Project of China (No. D111100001011002).

LITERATURE CITED

Sinoquet H, Rivet P. 1997. Measurement and visualisation of the architecture of an adult tree based on a three-dimensional digitising device, Trees: Structure and Function. 11,265-270.

Sonohat G, Sinoquet H, Kulandaivelu V, Combes D, Lescourret F. 2006. Three-dimensional reconstruction of partially 3D digitised peach tree canopies, Tree Physiology. 26:337-351.

Kaminuma E, Heida N, Tsumoto Y, Yamamoto N, Goto N. 2004. Automatic quantification of morphological traits via three-dimensional measurement of Arabidopsis. The Plant Journal. 38:358–365

Dornbusch T, Wernecke P, Diepenbrock W. 2007. A method to extract morphological traits of plant organs from 3D point clouds as a database for an architectural plant model. Ecological Modelling. 200: 119–129.

Xu H, Gossett N, Chen B. 2007. Knowledge and heuristic-based modeling of laser-scanned trees. ACM Transaction On Graphic. 26(4):19

Su Z, Zhao Y, Zhao C, Guo X, Li Z. 2011 Skeleton extraction for tree models. Mathematical and Computer Modelling，54: 1115－1120.

Proceedings of the 7th International Conference on Functional-Structural Plant Models, Saariselkä, Finland, 9 - 14 June 2013. Eds. Risto Sievänen, Eero Nikinmaa, Christophe Godin, Anna Lintunen & Pekka Nygren.
http://www.metla.fi/fspm2013/proceedings. ISBN 978-951-651-408-9.

Optimal 3D reconstruction of plants canopy from terrestrial laser scanner data by fusion of the 3D point information and the intensity value

Mathilde Balduzzi[1*], **Frédéric Boudon**[2] and **Christophe Godin**[1]
[1]INRIA/[2]CIRAD, Virtual Plants INRIA Team, UMR AGAP, 95 rue la Galéra, 34095 Montpellier, France
**correspondence: mathilde.balduzzi@inria.fr*

Highlights: We develop an algorithm to digitize *in situ* canopy and to tag automatically each of its leaves. This algorithm fuses the distance information and the intensity values of a terrestrial LiDAR scanner.

Keywords: Terrestrial LiDAR, leaves geometry, LiDAR intensity, shape-from-shading, Kalman filter

INTRODUCTION

Terrestrial LiDAR scanner (TLS) provides a novel tool for generating in a high measurement rate an accurate and comprehensive 3D geometrical description of the canopy. This device sends a laser beam and gives a precise estimation of the distance to the object surface with which it interacts. Combined with a zenithal and an azimuth rotation, it creates a virtual scene of its surrounding in the form of a TLS point cloud. It became a common metrology tool in several domains and draw itself plant scientists' attention. Despite the good accuracy of the measurement (estimation errors less than a few millimeters for most TLS in the measured range), only general indicators such as LAI, vertical plant profile and vegetative volume have been extracted (e.g. Rossel et al., 2009). These indicators are frequently used in physical models for canopy/environment interaction, such as light interception models (Sinoquet et al. 2005). However, these models rely on constraining hypothesis such as homogeneous distribution of leaves, infinitely small leaf elements, etc. In many applications, these assumptions simply do not hold and the condition of use of these models is therefore invalid. As an alternative, TLS can be used to reconstruct realistic foliage geometry that can be subsequently used in realistic physic-based models.

Several techniques based on surface fitting have been developed to digitized isolated leaves (Loch et al. 2005, Quan et al. 2006, Chambelland et al. 2008). They rely on user intervention and remain tedious for entire canopy reconstruction. In addition, they do not deal with *outliers points* present on leaves edges (Hebert & Krotkov 1992) and they suppose a high *signal-to-noise* ratio (i.e. variability due to the size of the object vs. variability of the noise), which is not always possible for field measurements.

The goal of this study is to digitize an entire canopy from laser TLS data so that the noise impact on the leaves reconstruction and segmentation is minimized. For this, we exploit the intensity information provided by the TLS. This information depends on the local inclination of the measured surface and thus provides complementary information to the distance measured by the scanner. Thanks to this information we could design a method for segmenting and reconstructing leaves geometry accurately from canopy scans. Leaf segmentation combines the intensity and distance information to detect outliers point, while leaf 3D reconstruction is made from intensity information using a propagation approach based on Shape-From-Shading (Durou et al. 2004). This reconstruction is progressively fused with the distance information using a Kalman filter to optimally merge both information from both sources (intensity and distance).

METHODS

In general, the intensity of pixels in an image is correlated to incidence angle of the light beam with the surface of the object at that point. Based on this information it is thus possible to design methods to reconstruct the local geometry of the scanned objects, i.e. the leaves. However, we have to face two main issues: i) the distance has an effect on the intensity amplitude and must be corrected; ii) The algorithm to reconstruct surfaces from the intensity must be able to integrate distance information.

To solve i), Balduzzi et al. (2011) have proven that the distance effect on intensity could be corrected and that a relationship between the incidence angle α and the intensity I can be built for a given leaf material. To

solve point ii), an algorithm of *shape-from-shading* (Durou et al. 2004) is developed. This algorithm proceeds by spatial *propagation* of an initial surface solution patch. Decisions to segment the reconstructed surface (here leaves) are taken during the reconstruction propagation.

To set it up, we proved several mathematical properties, in particular that: 1) the propagation can be done along the greatest slope direction on an iso-intensity region; 2) those directions can be computed from any 3D curves belonging on the surface when the incidence angle information is provided; and 3) the surfaces generated by those greatest slope line are specific surfaces called the *sand-pile surfaces.*

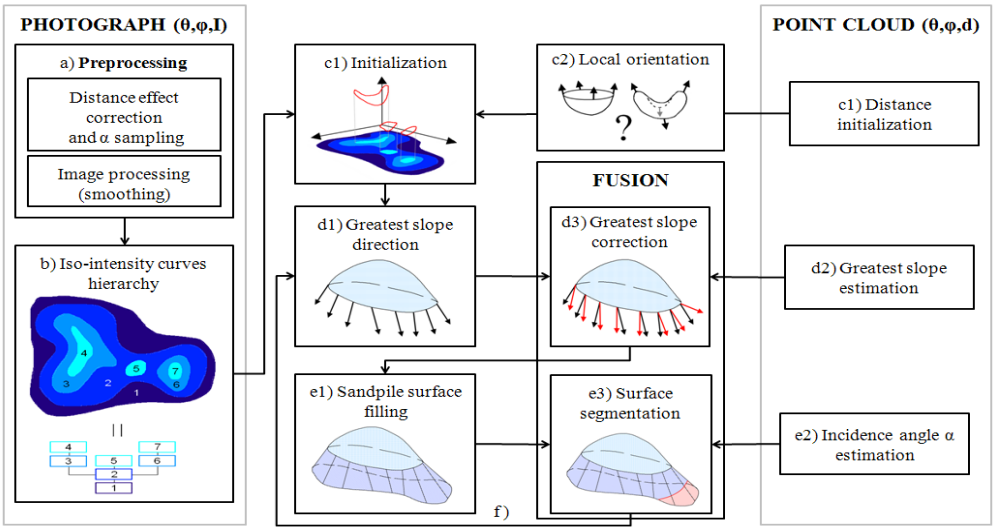

Fig 1. Algorithm flowchart for the surface reconstruction.

Thanks to those previous properties, the following pipeline has been set up (figure 1):

a) After the correction of the distance effect and the initialization of the I to α relationship, the intensity picture is smoothed out to make iso-intensity contours apparent.

b) Those contours are hierarchized to drive the propagation: the iso-intensity contours of highest value (maxima) will be the seeds of the propagation carried out along the iso-intensity contour hierarchy.

c) 1: The distance values of the seeds are initialized thanks to the point cloud. It is the initial boundary of the reconstructed surface.
2: At the same time, the analysis of these boundary geometries (e.g. sink or saddle case) makes it possible to disambiguate the positive (up) or negative (down) local orientation of the surface.

d) 1: The greatest slope directions are computed along the boundary of the reconstructed surface to start or to continue the propagation.
2: Simultaneously, we estimate the greatest slopes direction thanks to the point cloud.
3: The comparison of the two greatest slope calculations gives estimation on the confidence we can have on both. A Kalman filter is used to fuse them depending on this confidence.

e) 1: Sand-pile surfaces fill the space in between two isophotes, i.e. the surface portion that corresponds to iso-intensity region; and between two consecutive greatest slopes.
2: The incidence angle α is estimated on the corresponding point cloud portion.
3: As for d.2), we obtain an indication on the confidence we can have on both calculation. This indicator is used to make decision on the segmentation.

f) Finally, the propagation continues on the new reconstructed surface boundary (step d1) until the surface is entirely segmented.

Our algorithm is able to reconstruct and to segment step by step a surface from its intensity picture and its 3D point cloud. The uncertainties on distance and intensity are minimized using a Kalman filter.

PRELIMINARY RESULTS

To test the algorithm, we have generated several virtual surfaces. The greatest slope retrieving and the propagation are robust even if we can note that the accuracy of the reconstruction is a function of the

intensity and may be significant as the incidence angle approaches 90°. Figure 2 iii) shows the reconstruction of a virtual ellipsoid when both of its picture and point cloud are given (fig 2. i and ii).

In this talk, we will present leaves reconstruction and segmentation in the case of real scans (figure 3).

ACKNOWLEDGEMENT

This work is supported by the Labex NUMEV and the project Plantscan3D from the Agropolis Foundation.

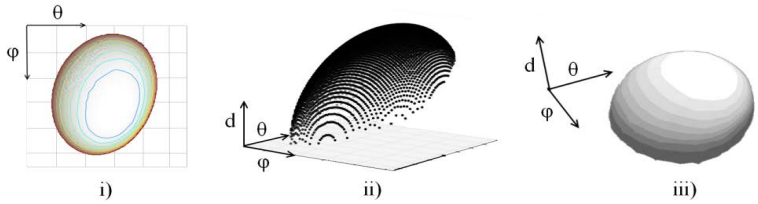

Fig 2. Reconstruction of a virtual ellipsoid. i) Its intensity picture and the iso-intensity curves (colored); ii) the initial 3D point cloud; iii) the reconstruction.

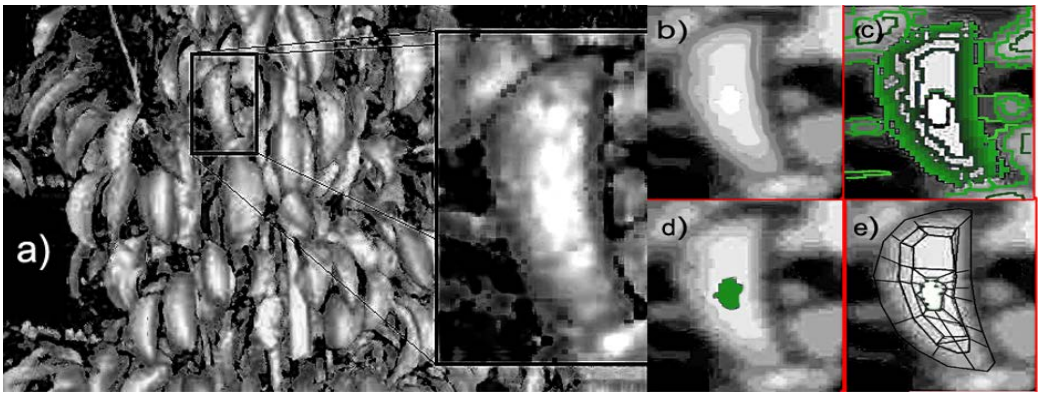

Fig 3. Illustration of the reconstruction algorithm. a) We focus on a single leaf of a pear tree canopy; b) the intensity picture is smoothed to make the iso-intensity region appearing; c) the iso-intensity contour are extracted and hierarchized; d) the iso-intensity region of maximal value is taken as the propagation seed; f) the greatest slope are propagated and the leaf is segmented.

LITERATURE CITED

Rossel JR, Sanz R, Llorenz J, Arno J, Escola A, Ribes-Dasi M, Masip J, Camp F, Gracia F, Solanelles F, Palleja T, Val L, Planas S, Gil E, Palacin J. 2009. A tractor-mounted scanning LiDAR for the non-destructive measurement of vegetative volume and surface area of tree-row plantations: A comparison with conventional destructive measurements. *Biosyst. Eng.***102**: 128-134.

Sinoquet H, Sonohat G, Phattaralerphong J, Godin C. 2005. Foliage randomness and light interception in 3D digitized trees: an analysis from multiscale discretization of the canopy. *Plant, Cell and Env.* **28**: 1158-1170

Chambelland JC, Dassot M, Adam B, Donès N, Balandier P, Marquier A, Saudreau M, Sonohat G, Sinoquet H. 2008. A double-digitizing method for building 3D virtual trees with non-planar leaves: Application to the morphology and light-capture properties of young beech trees (Fagus sylvatica). *Funct. Plant Biol.* **35**: 1059-1069.

Loch, B. I. and Belward, J. A. and Hanan, J. S. 2005. Application of surface fitting techniques for the representation of leaf surfaces. In: MODSIM05: International Congress on Modelling and Simulation: Advances and Applications for Management and Decision Making, 12-15 Dec 2005, Melbourne, Australia.

Quan, L., Tan, P., Zeng, G., Yuan, L., Wang, J., & Kang, S. B. 2006. Image-based plant modeling. *ACM Transactions on Graphics (TOG).* **25-3**: 599-604.

Hebert M, Krotkov E. 1992. 3D measurements from imaging laser radars: How good are they? *Image Vision Comput.* **10**: 170-178.

Balduzzi MAF, Van der Zande D, Stuckens J, Verstraeten WW, Coppin P. 2011. The properties of terrestrial laser system intensity for measuring leaf geometries: a case study with conference pear trees (Pyrus Communis). *Sensors* **11**: 1657-1681.

Durou JD, Falcone M, Sagona M. 2004. *A survey of numerical methods for shape from shading.* Rapport de recherche IRIT N°2004-2-R.

Proceedings of the 7th International Conference on Functional-Structural Plant Models, Saariselkä, Finland, 9 - 14 June 2013. Eds. Risto Sievänen, Eero Nikinmaa, Christophe Godin, Anna Lintunen & Pekka Nygren. http://www.metla.fi/fspm2013/proceedings. ISBN 978-951-651-408-9.

Bayes trees and forests: combining precise empirical and theoretical tree models

Mikko Kaasalainen[1*], Ilya Potapov[1], Pasi Raumonen[1], Markku Åkerblom[1], Risto Sievänen[2] and Sanna Kaasalainen[3]

[1]*Department of Mathematics, Tampere University of Technology, P.O. Box 553, 33101, Tampere, Finland*
[2]*Finnish Forest Research Institute, Vantaa Research Unit, PL 18, FI-01301, Vantaa, Finland*
[3]*Department of Remote Sensing and Photogrammetry, Finnish Geodetic Institute, Geodeetinrinne 2, FI-02431 Masala, Finland*
**correspondence:* mikko.kaasalainen [at] tut.fi

Highlights: With the new analysis methods for TLS scans, there will be a growing and improving database of 3D descriptions of trees and forest stands. The attributes determining these descriptions can be represented as Bayesian probability distributions, with functional-structural models providing the prior information. These distributions can then be used to create versions of new realistic *Bayes forests*, where none of the trees are copied from data, but the structure of each is drawn from the data-based distributions. Repeated TLS measurements add a fourth dimension, time, to the mathematical modelling; in this way, we can simulate functional *4D Bayes forests*. As in the modelling of the 3D structure, forest models and regularities of growth and mortality are used as prior information; conversely, the accumulating data and modelling results improve the theoretical models.

Keywords: Tree models: empirical, tree models: theoretical, TLS, Bayesian inference

INTRODUCTION

A general method, based on terrestrial laser scanning (TLS) data, has recently been developed for producing precise 3D tree surface models that are automatic and fast to compute and record the topological and geometric properties of the tree (Raumonen et al. 2013 and this meeting). One of the core ideas behind the method is that practically any external attribute of a tree can be approximated accurately at will from a compact surface model of this type.

Once we have determined the models of a representative number of trees at different sites, we can construct well-defined statistical attributes from these as functions of species, age, etc. On forest stand level, we record the typical distribution of trees. Once the distribution functions (DFs) of tapering, branching frequency, branching angles, branch curving, tree positions, etc. have been defined, we can carry out a reversed process. Now we can draw new samples from these DFs and use them to construct new trees and forests with similar statistics; i.e., *3D and 4D Bayes forests*. In this process, we can use our prior knowledge of functional-structural (FS) tree models to ensure biological consistency. This can be carried out via the Bayesian approach to obtain a posterior distribution. The process can also be used to improve the theoretical models by detailed, precise, and comprehensive measurements.

PROBABILISTIC TREE MODELS

In the broadest sense, a tree (or, ultimately, a forest) can be described as a probabilistic entity. Its form and structure, specified by some parameters $\boldsymbol{x}=(x_1,...,x_N)$, has a probability $p(\boldsymbol{x};\boldsymbol{u})$ in some measurement space spanned by $\boldsymbol{u}$. Some components of $\boldsymbol{u}$ might describe, e.g., the local width h of a branch and its 3D direction $\boldsymbol{d}$ along its length s, resulting in a four-dimensional subspace $(h,\boldsymbol{d},s)$ of the $\boldsymbol{u}$-space. From a large number of scanned and analyzed trees, we can determine an experimental $p_S(\boldsymbol{x})$ for a given species (possibly with different p-functions for different age groups or other identifiers, or by including them as components of $\boldsymbol{x}$). On the other hand, we can determine a theoretical $p_M(\boldsymbol{x})$ from a large ensemble of functional-structural models. In our representation, two trees that are not clones of each other but have the same p (i.e., $\boldsymbol{x}$) are identical in the mathematical sense. We note here that, formally, two isolated stochastic FS models that have the same initial parameters do not necessarily produce identical 3D DFs at later stages due to self-shadowing that takes different evolutionary routes depending on the random choices during growth. In practice, identical environmental factors mostly produce statistically similar trees of the same species.

The tree probability $p(\boldsymbol{x})$ can comprise a number of sub-probabilities. A probability may be a product of independent, lower-dimensional probability functions. These can be purely morphological; e.g., of the form $p(\{x_i\}; \boldsymbol{d}, h, s) = p[\{x_i\}; \{\boldsymbol{d}_i(s)\}, \{h_i(s)\}, s]$, where $\{\boldsymbol{d}_i(s)\}$ and $\{h_i(s)\}$ are sets of some basis functions modified by the set of parameters $\{x_i\}$. On the other hand, the sub-probabilities can describe stochastic processes, which is the natural way of describing the growth of a tree. The sub-probabilities are then Markovian in character, specifying the probability of a length element to differ from the previous one in various ways (with either independent or joint attributes; i.e., one- or multidimensional probabilities). The elements are similar in both the observational and theoretical models; e.g., cylindrical in our basic laser-scanning model and the LIGNUM FS model (Sievänen et al. 2008). For example, $\Delta\boldsymbol{d}$ can be taken to describe the difference between $\boldsymbol{d}$ of two adjacent elements. Then the probability distribution of this difference would be given by a $p(\Delta\boldsymbol{d})$. A model for p linear in some parameters $(x_i,...,x_j)$ is of the form

$$p(x_i, \dots, x_j; \Delta\boldsymbol{d}) = \sum_{k=i}^{j} x_k f_k(\Delta\boldsymbol{d}),$$

where $f_k(\Delta\boldsymbol{d})$ are some given basis functions. Another linear possibility is to discretize the $\Delta\boldsymbol{d}$-space into bins whose occupation probabilities are given by x_k.

The problem of determining the probabilities or statistical profiles $p(\boldsymbol{x})$ from either empirical data or synthetic models is that of determing the underlying distribution function from a set of samples (Kaasalainen 2008). This can be carried out, in the sense of the Radon transform, by least-squares fitting the parameters $\boldsymbol{x}$ such that the cumulative marginal distributions (CDFs) of $p(\boldsymbol{x};\boldsymbol{u})$ in various directions in the measurement space of $\boldsymbol{u}$ best match the corresponding CDF values $\boldsymbol{y}$ defined by the given set of sampled $\boldsymbol{u}$. In the case of linear models such as the $p(\Delta\boldsymbol{d})$ above, this is a linear least-squares problem of the matrix form $\boldsymbol{y}=A\boldsymbol{x}$.

Once we have determined a DF, we can resample it to create statistically equivalent new trees at will (Fig. 1). This is simple for the one-dimensional case via its cumulative DF; for multi-dimensional DFs we can use sprinkle algorithms (Kaasalainen 2008) or Markov Chain Monte Carlo methods.

BAYESIAN MODELS

Next, we introduce the concept of a Bayesian tree (or forest). To make the experimental and theoretical tree statistics p_S and p_M compatible in the Bayesian sense, we write a probability distribution that can smoothly incorporate any given degree of prior information from p_M. The desired posterior distribution can be obtained by a metaprobabilistic approach: we define the probability P of a tree to have a certain kind of statistical profile p represented by the parameters $\boldsymbol{x}$. Thus, the Bayesian principle yields

$$P(\boldsymbol{x}) \propto P_S(\boldsymbol{x}) P_M(\boldsymbol{x})$$

(without normalization as we are only interested in the shape of $P(\boldsymbol{x})$ in $\boldsymbol{x}$-space). The role of $P_M(\boldsymbol{x})$ is defined by some "tightening" or weight parameters that can be separate for each x_i. For zero weights, $P_M(\boldsymbol{x})$ is unity; i.e., a uniform distribution without any prior preferences for $\boldsymbol{x}$. For weights approaching infinity, $P_M(\boldsymbol{x})$ approaches the Dirac-delta distribution around its centre point $\boldsymbol{x}_0$.

If the models describing the DFs are linear in the parameters $\boldsymbol{x}$ in the form $\boldsymbol{y}=A\boldsymbol{x}$ above, we obtain a simple formula for the centre point or the maximum a posteriori estimate $\hat{\boldsymbol{x}}$ of the final distribution $P(\boldsymbol{x})$, if it as well as the distributions $P_M(\boldsymbol{x})$ and $P_S(\boldsymbol{x})$ are taken to be Gaussian:

$$\hat{\boldsymbol{x}} = Q^{-1}(E_0^{-1}\boldsymbol{x}_0 + A^T E_1^{-1}\boldsymbol{y}); \qquad Q = (E_0^{-1} + A^T E_1^{-1} A),$$

where E_0 and E_1 are, respectively, the covariance matrices of $P_M(\boldsymbol{x})$ and $P_S(\boldsymbol{x})$. The smaller their (diagonal) elements are, the more tightly the marginal probabilities of the components of $\boldsymbol{x}$ are constrained.

We can describe the probabilities in both 3D and 4D. In the 3D-case, we consider a snapshot of a tree, specifying its momentary form. The straightforward DF product approach above is then simplest to apply to essentially isolated trees. In the time-dependent 4D-case, we examine the history of trees; i.e., the shape probability as a function of time. The probabilities are then determined by a number of stochastic as well as deterministic processes. This is necessary especially for Bayes forests, where the collective history (competition etc.) should be taken into account. The growth rules of FS models, for example, are then rendered as prior DFs. The theoretical FS models not only serve as prior probabilities in the Bayesian sense; they also help to design the parameter space in which we describe the probabilities. To create prior DFs from

FS models, we can use stochastic FS processes and deterministic FS models with stochastic conditions initially and during the growth.

The Bayesian approach stabilizes the synthetic realizations of TLS-based DFs by, e.g., removing unrealistic outliers or biases due to selection effects in data. The FS models are also used to determine the best ways to select and express the actual tree attributes we should use in our virtual modelling. On the other hand, experimental data help to improve theoretical models.

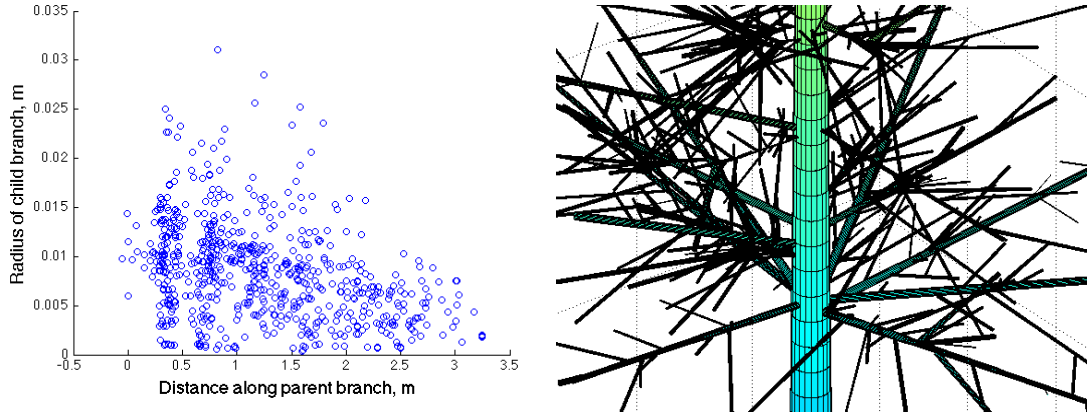

Figure 1. Left: a 2D-plot of the measured second-order branch statistics of one tree. Right: a closeup of the basic geometry (location, direction, and width) of synthetic branch generation by drawing samples from DFs corresponding to the data.

MEASUREMENTS

The development of a Bayes forest model requires continuous assimilation of measured data to the system. We measure and collect new TLS and other information from forests, including hyperspectral lidar (HSL) data for augmenting the structure data by information on source material and condition (Hakala et al. 2012). The sample sites and trees are chosen to acquire representative quantities, and to test a number of statistical hypotheses. For example, to which degree do the parameters $\boldsymbol{x}$ of presumably similar trees correlate? What are the typical deviations given by the experimental covariance matrix E_1? How much prior information needs to be introduced in practice? FS models and observations are used to determine the most appropriate parameter space for $\boldsymbol{x}$ and the measurement space for $\boldsymbol{u}$ best representing the various attributes of trees, including branch hierarchies. The preliminary results are reported in this meeting.

In 4D Bayes forest modelling, the DFs of the 3D Bayes forest have the additional dimension of time, based on the repeated observations of sample trees. Consequently, the realizations of these DFs for each Bayes forest include behaviour in time: litter production, growth, etc. As in the 3D Bayes forest, the prior constraints from the process-based studies (incorporated in LIGNUM) are important. A number of process descriptions are used as prior information sources taking into account the effects of, e.g., the competition for light, space, and resources. This information can be incorporated into the Bayes-forest model as, e.g., spatial competition indices and simple carbon-balance rules of foliage. With the biologically consistent prior components, the end product is a statistically and biologically realistic model of a forest and its processes in time.

LITERATURE CITED

Hakala T, Suomalainen J, Kaasalainen S, Chen Y. 2012. Full Waveform Hyperspectral LiDAR for Terrestrial Laser Scanning. *Optics Express.* **20:** 7119-7127.

Kaasalainen M. 2008. Dynamical tomography of gravitationally bound systems. *Inverse Problems and Imaging*. **2**: 527-549.

Raumonen P, Kaasalainen M, Åkerblom M, Kaasalainen S, Kaartinen H, Vastaranta M, Holopainen M, Disney M, Lewis P. 2013. Fast Automatic Precision Tree Models from Terrestrial Laser Scanner Data. *Remote Sensing*. **5**: 491-520.

Sievänen R, Perttunen J, Nikinmaa E, Kaitaniemi P. 2008. Toward extension of a single tree functional structural model of Scots pine to stand level: effect of the canopy of randomly distributed, identical trees on development of tree structure. *Functional Plant Biology*. **35**: 964-975.

Proceedings of the 7th International Conference on Functional-Structural Plant Models, Saariselkä, Finland, 9 - 14 June 2013. Eds. Risto Sievänen, Eero Nikinmaa, Christophe Godin, Anna Lintunen & Pekka Nygren. http://www.metla.fi/fspm2013/proceedings. ISBN 978-951-651-408-9.

Quantitative assessment of automatic reconstructions of branching systems

Frédéric Boudon[1], **Chakkrit Preuksakarn**[2,4], **Pascal Ferraro**[5], **Julien Diener**[3], **Eero Nikinmaa**[6] and **Christophe Godin**[2]

[1]*CIRAD/*[2]*INRIA/*[3]*INRA Virtual Plants Team, UMR AGAP, C.C. 06002, 95 rue de la Galera,34095 Montpellier, France,* [4]*Kasetsart University, Kamphaeng Saen Campus, Thailand,* [5]*CNRS LABRI, University of Bordeaux, France,* [6]*University of Helsinki, Finland*

**correspondence:* frederic.boudon@cirad.fr

Highlights: In this work, we propose a method to evaluate and compare different reconstruction methods from laser data using expert reconstruction and a new structural distance.

Keywords: Structural comparison, plant architecture, laser data

INTRODUCTION

In the context of biology and agronomy, acquisition of accurate models of real plants is still a tedious task and a major bottleneck for the construction of quantitative models of plant development. Recently, 3D laser scanners have made it possible to acquire 3D images representing a sampling of the surfaces of objects. To process such new type of data, dedicated reconstruction methods were developed. Although successful in most applications such as urban geometry, these methods fail on plants structures as they usually contain a complex set of irregular and branching surfaces distributed in space with varying orientations. A number of specific methods have been proposed to reconstruct plausible branching structures from laser data.

The first noticeable method was proposed by Xu *et al.* (2007) that extends the approach of Verroust and Lazarus (2000) to reconstruct branching structures. In their approach, points from the scans are first connected to their *k* closest neighbours to form a graph. The distance between any points can then be defined as the length of the shortest path between these points on the graph. The graph is then segmented into clusters of points according to the distance to a root point. The centres of clusters are then used to generate the skeleton of the tree. Alternatively, Livny *et al*. (2010) proposed to use a series of global optimisations to reconstruct major skeletal branches. Starting from the graph of shortest paths, long paths are favoured and used to align and prune the points. Remaining paths form the skeleton of the tree. Finally, the concept of space colonisation was introduced by Runions *et al*. (2007) and consists of guiding a simulated growing tree process with a set of points that represent the volume of the plant. It was first exploited by Coté *et al.* (2009) to generate realistic foliage of a tree from laser scans. Preuksakarn *et al*. (2010) extend this idea to follow precisely the point patterns of the scans to reconstruct the skeleton of trees.

While these methods produce realistic structures as shown by Fig. 1, no method to compare them quantitatively or evaluate their respective accuracy has been proposed so far. Such evaluation is of major importance for further exploitation of reconstructed models in biological applications. In this work, we address the problem of evaluating the accuracy of reconstructed structures from laser scanner data. For this, we first present a software tool that allows experts to define reconstruction from the point cloud. Using these expert-defined structures that will be considered as reference, we then propose different indices and algorithmic methods to quantify the similarities and differences between automatically reconstructed and reference structures. Such indices make it possible to compare the reconstructions made with the different methods proposed in the literature.

Fig. 1. Example of a lime tree reconstruction with the method of Preuksakarn et al. (2010). Left: an original picture of the tree. Right: the reconstructed virtual model inserted into same background.

MATERIALS

In this study, we use laser scans from city trees growing in the streets of Helsinki, Finland, which were scanned with a Leica Geosystems HDS 2500 laser scanner. We also use a scan of a Cherry tree near Clermont-Ferrand, France, which was scanned with a Leica Geosystems HDS 6200 laser scanner. Trees were scanned

from 3 to 4 positions to reduce occlusion. The scanner specification gives a range of accuracy of 4 mm for the position of a point in space. To assess more precisely the effect of the resolution and the quality of the scans on the accuracy of the reconstruction, we also use a virtual model of a Walnut tree (Sinoquet *et al*. 97), whose structure was first manually digitized from a real tree. This mock-up was virtually scanned and different levels of noise are introduced by removing a number of points.

On these data, reconstructions are performed using our implementation of methods of Xu *et al*. (2007), Preuksakan *et al*. (2010) and Livny *et al*. (2010). These procedures are now part of the PlantGL open source library (Pradal *et al*. 2009) of the OpenAlea platform.

For scanned trees, reference 3D models were built by editing the skeleton resulting from an automatic tree reconstruction. For this, we designed a visual tool and asked experts to correct the automatically reconstructed structure. Experts can edit the skeletal structure of each tree by adding, deleting, repositioning or reorganizing segments in the structure. Different visualisation tools of the software make it possible to focus display of the laser points on a specific location making it possible to identify clearly the local branching configuration. The results are tree-like structures, whose nodes are associated with branch segments, and that represent the skeleton of the tree branching structure. A database of such expert-defined structures has been established.

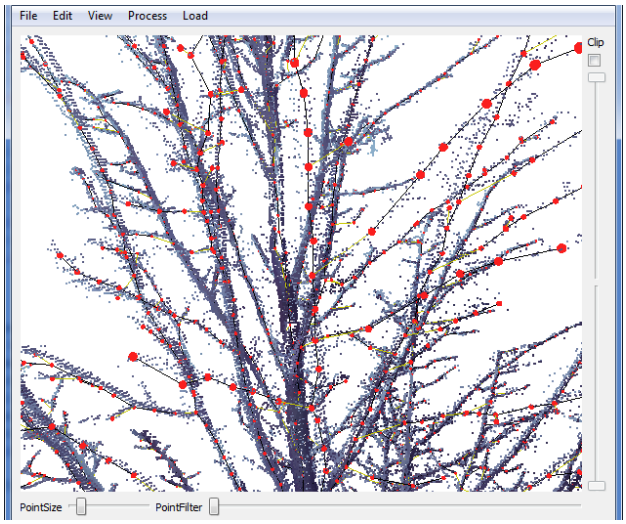

Fig. 2. The software tool used to create expert-defined structures from laser data. Red spheres represent nodes of the structure. Sliders make it possible to control the location and size of the laser points displayed. The user can edit the plant structure by adding, deleting, moving or changing properties of nodes.

METHODS

Two classes of quantitative evaluation tests can be made. The first one consists of summarizing an individual tree by a small number of global variables such as wood content, crown volume, amount of intercepted light from several directions, etc. The similarity of the models is then measured by the distance between these synthetic variables. As a first approach, the different reconstructions are compared to the reference trees with such global indices. We also compare the reconstructions with the original point sets by estimating the mean distance of the point set to the reconstructed models. While this gives a general assessment of the reconstruction quality, these indices give no information on the quality of the topology.

A second class of tests consists of comparing in more detail the three-dimensional structure of the models. For this, more structural comparison tools are required. As a first test, we experimented with the edit distance proposed by Ferraro and Godin (2000). The computation of this distance consists in determining a sequence of edit operations of minimum cost which transform an initial tree T_1 into a target tree T_2. Three edit operations are usually considered: substituting a vertex i of T_1 with a vertex j of T_1, deleting a vertex i in T_1 and inserting a vertex j in T_2. Each operation is associated with a cost that we parameterized according to geometrical similarities between nodes. As a side-product, the set of substitutions gives a mapping between elements of T_1 and T_2. However, only mappings that preserve the ancestor relationship between elements of the two trees are considered by the method. As a result, a simple inversion in the branching position of elements can create important differences with this comparison method.

To overcome the previous limitation, we designed a more flexible comparison pipeline that makes it possible to detect similarities between structures even in the case when connections mismatch. For this a number of algorithmic steps are performed to finally estimate two indices that reflect geometrical and structural similarities. Three main steps compose our pipeline: first, a homogenization of the scales of the tree T_1 and T_2 is made; second, a mapping of their nodes is determined, and finally a mapping of their edges. From these mappings, two indices are estimated. A more precise description of these different steps follows.

Before comparing a test reconstruction against the reference (expert) reconstruction, a homogenization procedure has to be carried out. Indeed, the two compared tree-like skeletal structures are in general composed of different types of segments with different sizes. To address this issue, we homogenized both skeletal

structures by re-segmenting both trees in terms of inter-ramification branch segments, *i.e*. one-piece segments connecting two branching points.

Based on the homogenized structures, the comparison of the test and reference structures could then be carried out. In 3D space, these two structures correspond to two sets of segments that may overlap partially making it difficult to find exact correspondence from the test reconstruction to the reference one. This association is often ambiguous and for each segment of the test (resp. reference) structure, one can associate a list of candidate segments in the reference (resp. test) structure. We formalize this matching as an optimization problem. Let us call T_1 and T_2 the reference and test tree skeletons respectively. For any two segments that can possibly be associated in T_1 and T_2, we quantify the distance between these two segments as the Hausdorff distance between their skeleton curves that intuitively represents the maximal deviation between the curves. During the mapping between the two structures, some element in the reference skeleton may have no counterpart in the test skeleton, and reciprocally. In this case, we say that we have respectively a deletion or an insertion with respect to the reference structure. A mapping has a cost that is defined as the sum of the costs of each individual mapping and of the deletions and insertions of nodes. The comparison of our two skeletal structures thus comes down to finding the mapping M that minimizes the cost of the mapping. To solve this assignment problem, we use an optimal flow formulation which is solved using Tarjan's (1983) extension of Edmonds and Karp's algorithm.

In the resulting optimal mapping M^*, some elements may be deleted or inserted. However, some of these insertions/deletions may simply result from the fact that several segments in one tree altogether cover a single segment in the other tree. To take this into account, a post processing step refines the mapping produced from the previous step by testing and adding mapping configurations that include multiple segments. As a result of this mapping procedure, a geometrical correspondence between elements is defined and can be quantified with the index $D_G = |M^*| / (|T_1|+|T_2|)$.

Finally, to evaluate the difference of topology between the two structures, we then inspect whether elements are connected in a similar way in their respective structures. We quantify the topological matching between the two structures with the index $D_T = 2^* |M^T| / (|E_1|+|E_2|)$, where M^T is the set of preserved relationships between T_1 and T_2, and E_1 and E_2 is the set of relationships of T_1 and T_2, respectively.

RESULTS AND DISCUSSION

A comparative evaluation of tree reconstruction using different methods from the literature was performed. An illustration of such an evaluation is given in Fig. 3. A more detailed comparison will be given in the presentation, such as the performance of each method with different levels of noise in the scan. Application of our method to the evaluation of automatic reconstruction of root architecture from images will also be presented.

Method	Mean Point Distance (mm)	Volume (Ref: 13.17m²)	D_G	D_T
Xu *et al*. (2007)	12.55	12.76	0.81	0.87
Livny *et al*. (2010)	6.49	12.7	0.69	0.65
Preuksakarn *et al*. (2010)	7.26	13.3	0.90	0.72

Fig. 3. Results of our comparison for lime tree reconstructions with different methods from the literature. Global indices and geometrical and structural accuracy indices are used.

LITERATURE CITED

Xu H., Gosset N., Chen B. 2007. Knowledge and heuristic-based modeling of laser-scanned trees. *ACM Transaction on Graphics* **26**(4) , 19.

Verroust A., Lazarus F., 2000. Extracting skeletal curves from 3d scattered data. *Visual Computer* **16**, 15–25.

Livny Y., Yan F., Olson M., Chen B., Zhang H., El-Sana J. 2010. Automatic reconstruction of tree skeletal structures from point clouds. *ACM Transaction on Graphics* **29**(6), 151.

Runions A., Lane B., Prusinkiewicz P., 2007. Modeling trees with a space colonization algorithm. *Proccedings of Eurographics Workshop on Natural Phenomena 2007.* 63–70.

Côté J.-F., Widlowski J.-L., Fournier R. A., Verstraete M. M., 2009. The structural and radiative consistency of three-dimensional tree reconstructions from terrestrial lidar. *Remote Sensing of Environment* **113**(5), 1067 – 1081.

Preuksakarn, C., Boudon, F., Ferraro, P., Durand, J.-B., Nikinmaa, E., Godin, C., 2010. Reconstructing plant architecture from 3D laser scanner data. *Proceedings of the 6th International Workshop on Functional-Structural Plant Models*,16-18.

Sinoquet H., Rivet P., Godin C., 1997. Assessment of the three-dimensional architecture of walnut trees using digitising. *Silva Fennica* **31**(3), 265–273.

Pradal C., Boudon F., Nouguier C., Chopard J., Godin C., 2009. PlantGL: a Python-based geometric library for 3D plant modelling at different scales. *Graphical Models*, 71(1), 1-21.

Ferraro P., Godin C., 2000. A distance measure between plant architectures. *Annals of Forest Science*, **57**, 445-461.

Proceedings of the 7th International Conference on Functional-Structural Plant Models, Saariselkä, Finland, 9 - 14 June 2013. Eds. Risto Sievänen, Eero Nikinmaa, Christophe Godin, Anna Lintunen & Pekka Nygren.
http://www.metla.fi/fspm2013/proceedings. ISBN 978-951-651-408-9.

Rank distributions and biomass partitioning of plants

Alexander Komarov[1], Elena Zubkova[1], Maija Salemaa[2] and Raisa Mäkipää[2]
[1]Institute of Physicochemical and Biological Problems in Soil Science, Russian Academy of Sciences, 142290, Pushchino, Moscow Region, Russian Federation; [2]Finnish Forest Research Institute, PO Box 18, 01301 Vantaa, Finland
**correspondence:* as_komarov@rambler.ru

Highlights: We study how well biomass partitioning patterns of plant compartments (organs) follow mathematical rank distributions using empirical data from the tree and dwarf shrub species in temperate-boreal zone as a test material. The simplest form of a rank distribution (Zipf's law) shows a good statistical fit to the data and its semi-empirical dependencies can successfully be applied also in a complex ecosystem models.

Keywords: Zipf's law, optimal plant organs partitioning, dwarf shrubs, trees, ranks and classification

INTRODUCTION

Certain statistical regularities as attributes of complex systems in the form of power laws are observed everywhere (Clause et al. 2009): these include many social and economic effects, and some applications in different branches of biology (Furusawa and Kaneko, 2003). One of the earliest applications of power laws are modelling the numbers of species in biological taxa (Willis and Jule, 1922).

These regularities have common mathematical structure and can be formulated as some properties of statistical rank distributions known as Zipf's, Pareto's, Heaps' and some other laws. Soukhovolsky (1996) applied Zipf-Pareto distribution for description of plant biomass partitioning. He used this distribution for evaluating the root biomass of trees.

Consider Zipf-Pareto law as the simplest example of a power rank distribution (Mandelbrot, 1969). It can be written for a ranked data in a form

$$x(i) = A/i^b,$$

where i denotes rank, A and b are parameters, maximal rank is set to 1, next ranks in size are increasing consequently. A and b can be easily evaluated after simple log-log transformation by least-squares method.

Main conditions for applying the rank distributions are as follows. Assume that available resource for total unit is distributed among its parts proportionally to its rank, i.e. to the ordered sequence of distributed resource, then distribution of resource parts has the form of Zipf's law. Accordingly, many mechanisms have been presented to explain the emergence of the Zipf's law (Newman 2005).

We analyzed partitioning of biomass to the main plant compartments of vascular plants (trees and dwarf shrub species in ground vegetation) using empirical data from the taiga zone in Russian North-West and Finland.

MATERIALS AND METHODS

We analyzed two data sets, one representing a deciduous tree (*Betula pendula*) and another deciduous dwarf shrub (*Vaccinium myrtillus)* biomass data, as a test material. The tree-wise data consists of measured biomass compartments (kg dry weight) of nine different-sized trees from a 38-years-old birch stand (*Oxalis* forest type) in Karelia (Kazimirov et al., 1978). For each tree we calculated the proportions (%) of the following biomass compartments: stem, (coarse) roots, branches, and leaves (Table 1).

The biomass data of *Vaccinium myrtillus* (kg dry weight/ha) is from 12 intensively monitored forest plots in Finland. Both in South and North Finland there were three Norway spruce and three Scots pine plots. The spruce plots represented mesic and moist site types whereas the pine plots represented poor and dry site types. The data of 28 small sample units (30x30 cm) have been joined for accurate description of the total biomass of *V. myrtillus* at each plot. We calculated the proportions (%) of the biomass compartments (rhizomes, living shoots and branches, fine roots, leaves and flowers) to normalize the heterogeneous data. The averages of the three plots in the same site type (separately in north and south) are given in Table 2.

Table 1. Proportion (%) of biomass compartments (out of the total biomass) for *Vaccinium myrtillus*. Averages and standard deviations (sd) for southern and northern pine and spruce plots (n=3 plots) given

		Rhizomes (diameter > 2 mm)	Living shoots and branches	Fine roots (diameter < 2 mm)	Leaves	Flowers and flower buds
South pine stand	Average	70.09	22.80	4.80	2.08	0.045
	sd.	6.31	4.81	0.9	0.69	0.016
South spruce stand	Average	55.87	31.89	6.77	5.37	0.1
	sd.	8.73	12.03	4.38	2.46	0.12
North pine stand	Average	67.22	22.92	7.79	2.03	0.47
	sd.	3.10	5.13	3.37	1.24	0.42
North spruce stand	Average	75.86	17.02	4.41	2.62	0.87
	sd.	4.80	4.12	0.65	1.32	0.88

Table 2. Proportions (%) of biomass compartments (out of the total biomass) for nine *Betula pendula* trees. Av. – averages, sd. – standard deviation.

	1	2	3	4	5	6	7	8	9	Av.	sd.
Stem	65.62	67.0	68.03	67.87	69.97	69.31	70.93	71.73	72.86	69.26	1.867
Roots	22.92	18.78	18.03	18.12	17.71	17.76	17.15	16.25	16.34	18.12	1.867
Branches	8.33	8.63	7.82	8.21	7.81	7.63	7.27	8.03	7.22	7.88	0.445
Leaves	3.12	5.58	6.12	5.80	4.51	5.29	4.65	3.99	3.58	4.74	0.979

RESULTS AND DISCUSSION

Biomass compartments (%) of *V. myrtillus* and *B. pendula* in relation to ranks with fitted power equations are presented in Figs. 1 and 2, respectively.

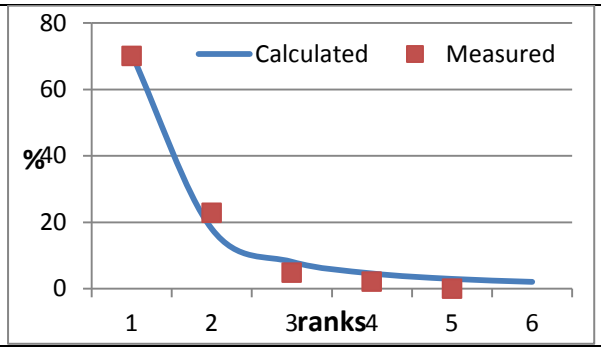

South pine stand. Power equation y=ax^b, coefficient data: a = 70.64; b = -1.97. R= 0.9929.

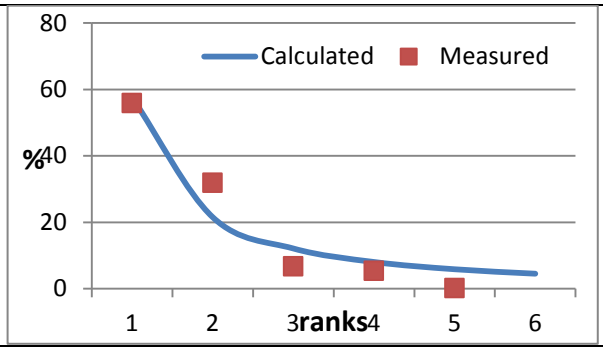

South spruce stand. Power equation y=ax^b, coefficient data: a = 57.66; b = -1.42. R= 0.9588.

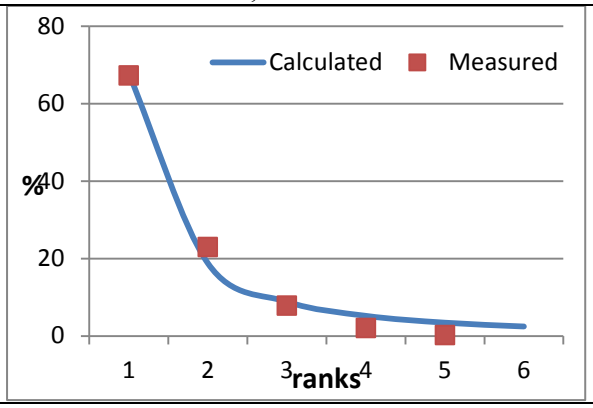

North pine stand. Power equation y=ax^b, coefficient data: a = 67.78; b = -1.85. R= 0.9935.

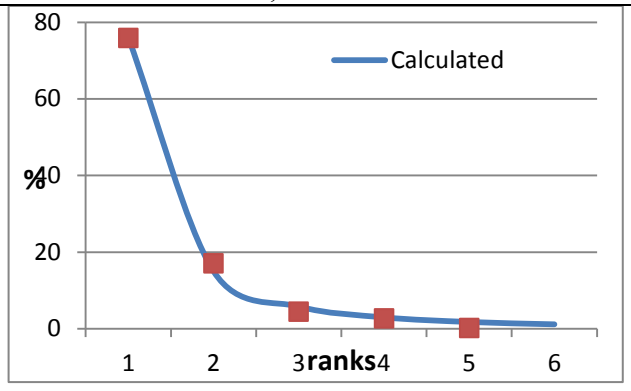

North spruce stand. Power equation y=ax^b, coefficient data: a = 76.04; b = -2.34. R= 0.9986.

Fig. 1. Dependency between ranks and corresponding averages of biomass compartments (%) of *Vaccinium myrtillus* in different sites (Table 1). Quadrats are empirical data

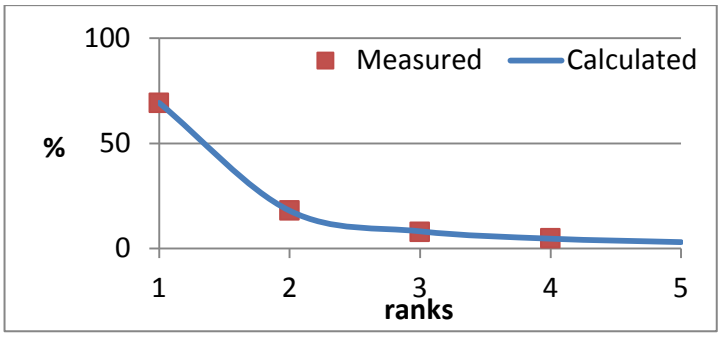

Fig. 2. Dependency between ranks and corresponding averages of biomass compartments (%) at a 38-year-old birch stand (Table 2). Line is power equation y=ax^b, coefficient data: a = 69.27; b = -1.95. R= 0.999980. Quadrats are empirical data.

Both *V. myrtillus* and *B. pendula* biomass data showed persistently good fit to power equations, which is equivalent to Zipf law. In all cases the shape of the power dependency stayed the same. We found that for the same species ranks correspond to the same biomass compartments in different climatic and edaphic conditions. However, coefficients of the power distributions can be different for the same species and reflect different response of the species to changed conditions. Thus, in Fig. 1 we clearly see that for *V. myrtillus* in spruce stands the portion of rhizomes (1st rank) is larger in northern conditions than in south.

An interesting question is whether ranks change along plant development stage and changing site conditions. In general, they can change as a result of long-term local unstable conditions (MacArthur, 1955). It seems that the populations of *V. myrtillus* in spruce stands with dense canopy (Fig.1, southern spruce stands) are more unstable. This question claims further studies for establishing of limits of applicability of the approach.

Our biomass distributions were close to the results of Enquist and Niklas (2002) on the log-log relationship between above- and belowground biomasses of tree stands. They averaged world wide dataset from stand characteristics and found pairwise linear allometric relationships among standing leaf, stem, and root biomass basing on general allometric model. Power-law rank distributions allow for obtaining more general relationships between plant organs linking all main biomass compartments together. Additionally, power-law dependencies can also be applied for descripting of organs' increment. Further, it would be interesting to compare the sequence of ranks between different functional plant groups for better understanding their role in carbon cycling in ground vegetation.

The study of power-law distributions is an area in which there is considerable current research interest. From a mathematical point of view, these dependencies are similar to first integral in complicated systems of differential equations. Usually knowledge of such links between variables helps to find solutions in these systems. Such dependencies will help to obtain rules needed for development of the forest simulation models. While the examples presented here certainly offer some insight, there is much work to be done both experimentally and theoretically before we can say we really understand the main processes driving these systems.

LITERATURE CITED

Clauset A,, Shalizi C,R,, Newman M.E.J. 2009. Power-law distributions in empirical data. *SIAM Rev* 51: 661–703.

Enquist B.J., Niklas K.J. 2002. Global Allocation Rules for Patterns of Biomass Partitioning in Seed Plants. *Scienc*295:1517-1520.

Furusawa C, Kaneko K. 2003. Zipf's Law in Gene Expression. *Phys Rev Lett* 90: 88-102.

Kazimirov, N.I., Morozova, R.M. and Kulikova, V.K. 1978. Organic Matter Pools and Flows in Pendula Birch stands of Middle Taiga. Nauka, Leningrad. 216 pp. (in Russian).

MacArthur R.H. 1955. Fluctuations of animal populations and measure of community stability // Ecology. V. 36. ¹7. Pp. 533-536.

Mandelbrot B. 1969. Final notes on a class of skew distribution function. Inform. and Contr. 36: 394-419.

Newman M.E.J. 2005. Power laws, Pareto distributions and Zipf's law. *Contemporary Physics* 46: 323–351.

Soukhovolsky V.G. 1996. Fractional structure and phytomass production in trees and stands, *Lesovedenie (Russian Forest Science)* 1: 30-40 (In Russian).

Willis J.C. Yule G.U. 1922..Some statistics of evolution and geographical distribution in plants and animals, and their significance. *Nature* 109: 177- 179.

Proceedings of the 7th International Conference on Functional-Structural Plant Models, Saariselkä, Finland, 9 - 14 June 2013. Eds. Risto Sievänen, Eero Nikinmaa, Christophe Godin, Anna Lintunen & Pekka Nygren. http://www.metla.fi/fspm2013/proceedings. ISBN 978-951-651-408-9.

Inference of structural plant growth from discrete samples

Christoph Stocker, Franz Uhrmann and **Oliver Scholz**
Fraunhofer Institute for Integrated Circuits, Department Contactless Test and Measuring Systems, Erlangen, Germany
**correspondence:* stockech@iis.fraunhofer.de, franz.uhrmann@iis.fraunhofer.de, oliver.scholz@iis.fraunhofer.de

Highlights: We present an approach for the rapid generation of plant growth models from a series of explicit growth stages. Multiple structural plant descriptions, which can be gained from 3D scans, are automatically inferred to an L-system grammar. Morphological leaf features are incorporated into this model by parameterization of the structural description.

Keywords: grammar inference, L-systems, plant growth modeling

Modern phenotyping systems like sheet-of-light scanners allow the accurate acquisition of plant geometry, from which a description of the branching structure can be extracted (see Bucksch et al. 2010). An explicit description of the structural development over time can be gained by measuring a plant at different growth stages. L-systems are commonly used to formally describe plant structure and its development during growth (Prusinkiewicz et al. 1990). However, the development of a growth model recreating specific plant structures requires expert knowledge and is often accomplished by time-consuming trial-and-error. We present an approach to computationally infer an L-system from feature vectors describing the structure of plants at successive growing stages. The aim of our approach is to close the gap between measured data and the plant growth model.

The approach consists of an inference step to model structural plant growth, which is amended by leaf morphology features in a parameterization step. The plant structure is derived from linear sequences of feature vectors (e.g. extracted from 3D scans) using a variation of the SEQUITUR-algorithm as introduced by Nevill-Manning (1996). In the course of this derivation, the inferred rules are unified to an L-System grammar with only a small set of rules. In order to incorporate leaves into the branching structure the L-system is parameterized with morphological leaf features, which can be imported from real measurement data. Intermediate plant growth stages can be created by parameter interpolation.

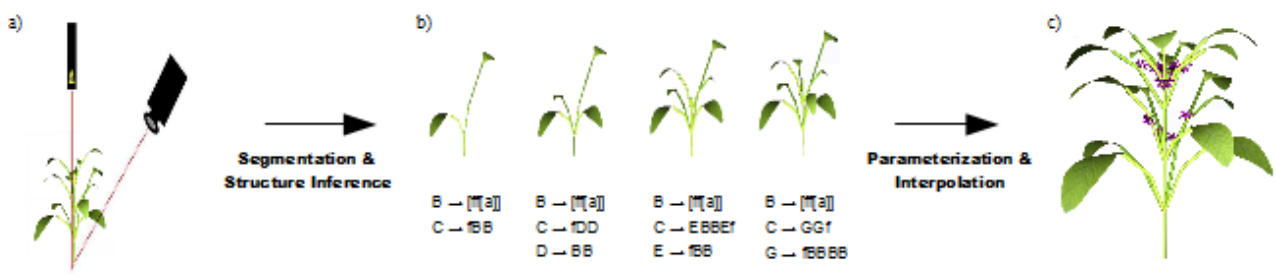

Fig. 1. Overview of the approach: a) Acquiring structual and morphological input e.g. by measurements. b) Result of the inference step (grammar and 3D-visualization). c) Final result: Parameterized plant model at one growth stage.

The generated parameterized L-system can be used as a basis for more sophisticated functional-structural plant models. Furthermore, the growth model can directly be used as input for system design tools in order to minimize occluded parts in the measurement data (Uhrmann et al. 2011).

LITERATURE CITED

Bucksch A, Lindenbergh R, Menenti M. 2010. SkelTre. *The Visual Computer* **26**: 1283-1300, *Springer*

Nevill-Manning, CG. 1996. Inferring Sequential Structure. *Ph.D. Thesis, University of Waikato, New Zealand.* 55 p.

Prusinkiewicz P, Lindenmayer A. 1990. The Algorithmic Beauty of Plants. *Springer* 40 p.

Uhrmann F, Seifert S, Scholz O, Schmitt P, Greiner G. 2011. Improving Sheet-of-Light Based Plant Phenotyping with Advanced 3-D Simulation, *Microelectronic Systems*, *Springer*. 247-258

Proceedings of the 7th International Conference on Functional-Structural Plant Models, Saariselkä, Finland, 9 - 14 June 2013. Eds. Risto Sievänen, Eero Nikinmaa, Christophe Godin, Anna Lintunen & Pekka Nygren.
http://www.metla.fi/fspm2013/proceedings. ISBN 978-951-651-408-9.

A spectral clustering approach of vegetation components for describing plant topology and geometry from terrestrial waveform LiDAR data

Dobrina Boltcheva[1], **Eric Casella**[2], **Rémy Cumont**[3] and **Franck Hétroy**[3]
[1]*Université de Nancy & Inria, LORIA, 54506 Nancy, France,* [2]*Forest Research, Centre for Forestry and Climate Change, Farnham, Surrey, GU10 4LH, UK,* [3]*Université de Grenoble & Inria, Laboratoire Jean Kuntzmann, 38334 Grenoble, France*
*Correspondence:*Franck.Hetroy@grenoble-inp.fr

Computer models that treat plant architectures as a collection of interconnected elementary units (internode, petiole, leaf lamina), which are spatially distributed within the above- and/or the below-ground space, have become increasingly popular in the FSPM scientific community (DeJong *et al*. 2011). The core of such 3-D plant architecture models deal with contrasting reconstruction methods generally based on stochastic, fractal or L-system approaches, or by describing accurately the geometry of each plant component *in situ* using 3-D digitizing technology. These methods can approximate the geometry of many species for understanding and integrating plant development and ecophysiology, but have generally been applied at a small scale.

High-resolution terrestrial Light Detection And Ranging (tLiDAR), a 3-D remote sensing technique, has recently been applied for measuring the 3-D characteristics of vegetation from grass to forest plant species (Dassot et al. 2011). The resulting data are known as a point cloud which shows the 3-D position of all the hits by the laser beam giving a raw sketch of the spatial distribution of plant elements in 3-D, but without explicit information on their geometry and connectivity.

In this study we propose a new approach based on a delineation algorithm (Fig. 1) that clusters a point cloud into elementary plant units. The algorithm creates a graph (points + edges) to recover plausible neighbouring relationships between the points and embed this graph in a spectral space in order to segment the point-cloud into meaningful elementary plant units (Fig. 2). Our approach is robust to inherent geometric outliers and/or noisy points and only considers the *x*, *y*, *z* coordinate tLiDAR data as an input.

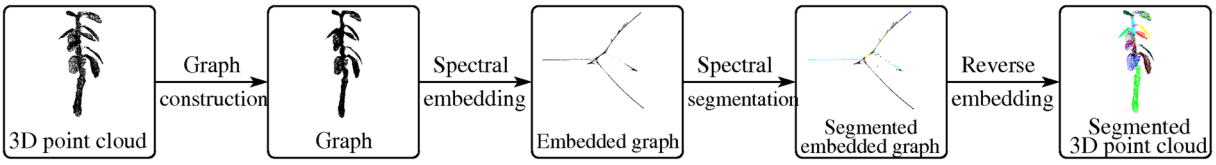

Fig. 1. Pipeline of the segmentation method proposed in this study.

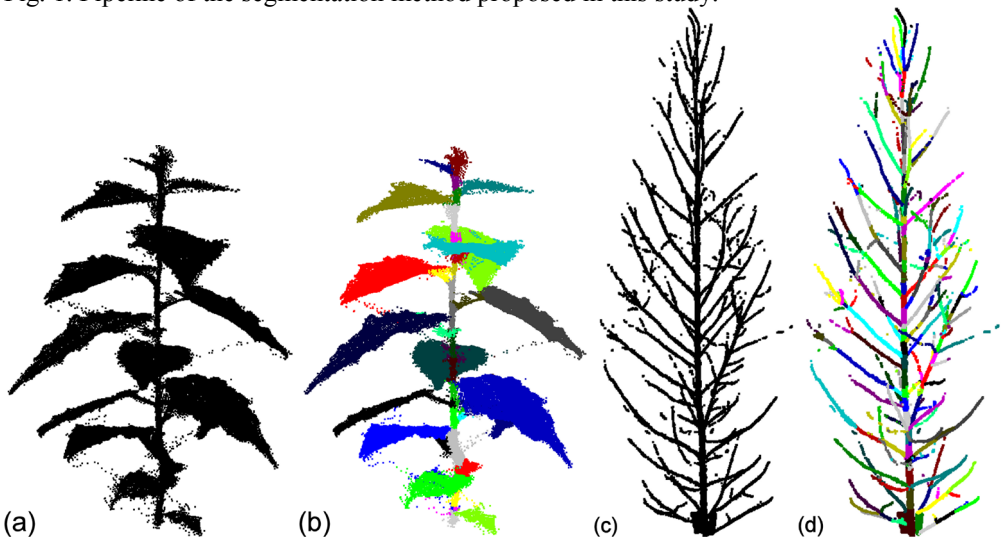

Fig. 2. Comparison of raw (a, c) and segmented (b, d) point clouds for a 0.4 m height poplar seedling (a, b) and a 3.7 m height eucalyptus tree.

Dassot M, Constant T, Fournier M. 2011. The use of terrestrial LiDAR technology in forest science: application fields, benefits and challenges. *Annals of Forest Science* **68**: 959-974.

DeJong TM, Da Silva D, Vos J, Escobar-Gutiérrez AJ. 2011. Using functional–structural plant models to study, understand and integrate plant development and ecophysiology. *Annals of Botany* **108**: 987-989.

Proceedings of the 7th International Conference on Functional-Structural Plant Models, Saariselkä, Finland, 9 - 14 June 2013. Eds. Risto Sievänen, Eero Nikinmaa, Christophe Godin, Anna Lintunen & Pekka Nygren.
http://www.metla.fi/fspm2013/proceedings. ISBN 978-951-651-408-9.

Modeling and analyzing rice canopies of different cultivars and densities by 3D digitizing method

Dong Li[1], **Zhifu Xu**[1], **Shihua Cheng**[2] and **Liyong Cao**[2,*]
[1] *Institute of Digital Agriculture, Zhejiang Academy of Agricultural Sciences, Hangzhou, Zhejiang Province,310021, P.R. China*
[2] *China National Rice Research Institute, Chinese National Center for Rice Improvement, Hangzhou, Zhejiang Province,310005 P.R. China*
**correspondence:* caolycgf@mail.hz.zj.cn

Key words: rice canopy, 3D digitizing, rice structural model, *Oryza sativa* L, model application, potential photosynthesis

INTRODUCTION

Rice is one of the most important crops in the world and it is the main crop in Zhejiang Province, China. It is important for breeding high yield cultivars and improving rice cultivation level to quantify rice spatial architecture. Studies on morphogenesis and development of rice plant structure have been carried out (Watanabe *et al*., 2005; Zheng *et al*., 2008, 2011). In the 3D model (Zheng *et al.*, 2008), rice canopies were measured in the field using a 3D digitizer and reconstructed. Light distribution in the canopy and the photosynthesis capacity could be computed. The model seemed useful to evaluate the rice cultivars and to design the cultivating strategies, but the measuring work was huge.

In this study, we did the experiments with different cultivars and densities, computed blade area and light distribution of rice canopies with the 3D model and analyzed the influence of cultivars and densities with the structural model. Also we wanted to study the advantages and disadvantages of the model if it was used to evaluate rice breeding and cultivation.

MATERIAL AND METHODS

Field experiment

Field experiment was conducted in 2012 at the experimental station of Xiaoshan Institute of Agricultural sciences in Hangzhou, Zhejiang province, southeast of China (30°19' N, 120°30' E). Three cultivars of hybrid rice (*Oryza sativa* L.) were planted. They were “Nei2You6”, “Nei5You8015”, “Liangyoupeijiu”, and we noted the cultivars as G6, G7 and LY for simple in this study. All these cultivars were newly-bred, high-yield and broadly planted in China for the recent years. For each cultivar, the rice was planted with three densities, which were high density (HD, the space was 16.7 × 14.3 cm), middle density (MD, 16.7 × 23.3 cm) and low density (LD, 30 × 23.3 cm), respectively. The experiment was determined by the randomized blocks design of three replications. The tiller number was dynamically recorded for each treatment through the growth period and the sampling number is 12 in each replication. The length and largest width of blade at different rank for each treatment were measured.

Nine plants (3 rows × 3 columns) for each treatment were chosen as the canopy at the dough stage (Oct.11-18). The plant organs, such as leaves, stems, and panicles, were measured by collecting their coordinates with a 3D digitizer (FastCAN Scorpion, Polhemus, USA). The blade length and width towards midrib were measured and the blade shape was modeled. The diameters of stems and the shape of rice spikes were measured after digitizing. With the data being checked, interpolated and modeled, the 3D canopies of these 5 treatments were reconstructed in Matlab software produced by the Mathworks Inc (Fig.1).

Each blade was divided into 200 triangles (see Wang *et al*., 2006; Zheng *et al*., 2008). The area of each triangle, as well as its inclination angle and azimuth angle, was calculated according to the 3D coordinates of the facet. Canopies were vertically divided into several layers with 5 cm interval. We calculated the leaf area distribution in the vertical profile. Also the leaf distribution in different inclination angle and azimuth angle was computed. In this study, the volume of stems and spikes were ignored.

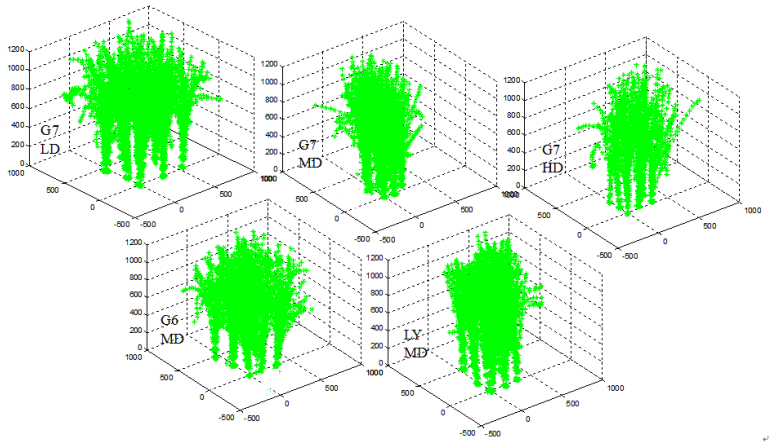

Fig 1. The visualization of the 5 treatments with blade midrib and stems and each organ were divided into 5 cm long sections. G6, G7, LY represented different cultivars and HD, MD and LD denoted different densities.

Before 3D digitizing measurement, light response curve (Pn-PFD) of different position leaves for all the treatments were measured using CIRAS-2 instrument (PP Systems, USA).

Results

During the late growth stages, the tiller number was great influenced by rice density. The density was higher, and the tillers for each plant were fewer. For all these cultivars, the difference between densities was significant (Fig.1). For the three cultivars, at the heading stage, the tiller number of LY cultivar was much larger than other cultivars, which has no significant difference from each other. However at the dough stage, there was no significant difference between the three cultivars (Fig.1).

There was no significant difference in the SPAD value for all the treatments. The net assimilation rate of LY at the measuring time was larger than the other cultivars for the flag leaf (Blade1 from up to bottom). The value was quite stable between densities with the same cultivars (Fig.2a). At the same time, the net rate was quite different for blades on different position in the same stem (Fig.2b). The difference between blades on different position was much larger than in different cultivars.

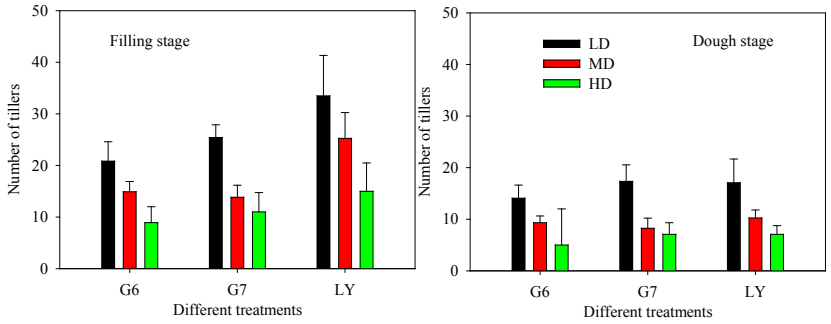

Fig. 2. Tiller number of the 3 cultivars and 3 densities of different stages.

The canopies for different treatments were reconstructed and visualize (Fig.1 show just stem and the midrib of blade). Based on the 3D model, the distributions of leaf inclination angle, azimuth angle and leaf area in the vertical profile were computed for different treatments. For the MD treatment, the blades of G6 were more concentrated and the total blade area was larger than the other cultivars. LY had a few more erect blades

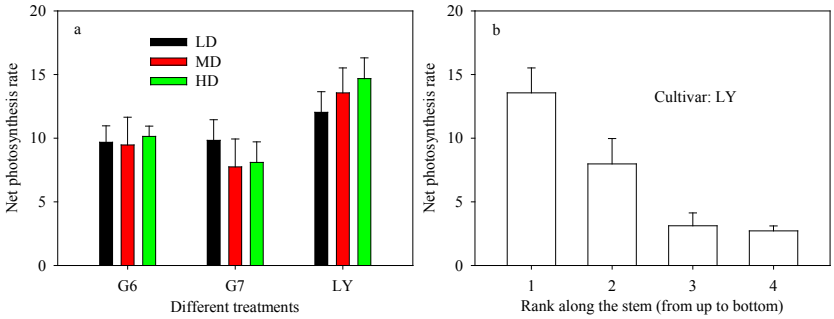

Fig. 3 Net assimilation rate for different treatments (a, blade1) and for blades on different positions (b).

DISCUSSION

Based on 3D digitizing, the rice canopies of different treatments were 3D visualized. And the vertical profile for leaf inclination angle, azimuth angle and leaf area distribution could be calculated and the difference between treatments could be analyzed by this model. Zheng compared the difference with three cultivars, one was bred 30 years before and the other two were bred recently. The light distribution was similar of the two modern high yield cultivars (Zheng *et al*., 2008). In this study, all the three cultivars were modern rice cultivars and the difference is not significant, just as the modern cultivars used in the previous study.

In this study the net assimilation rate of the canopy could not tell the difference of the plant yield because the light would distribute in a different way if the solar altitude (time) changed even if the canopies kept stable for all the time. Moreover, the canopies changed a lot irregularly for different cultivars because tillers changed in the different way between LY and G6/G7.

Also in the field experiment, the plant cannot be planted in a precise density and grow uniformly, especially for rice, whose tillers vary a lot between plants. And the total growth periods for the three cultivars were different (G6 138 days, G7 133 days and LY 145 days). They were not in the exactly the same stage. We also cannot make the statistical analysis of the potential photosynthesis because the measuring work is huge and there cannot be many replications of the digitizing plant canopies.

In the future, we will consider the diffuse radiation and improving the calculation of net assimilation by using the Farquhar model (Farquhar et al., 1980). But we think the 3D model will not be broadly used in rice breeding and cultivating until all these disadvantages were considered and solved.

Acknowledgments: This research has been supported by State Key Laboratory of Rice Biology. The authors are grateful to Yue Li, Qingsong Xu and Dinghua Mao for their kind help on the experiment measurements and to Dr. Bangyou Zheng and Dr. Zhigang Zhan for the help on the modeling and computer programming.

REFERENCES

Farquhar G, Caemmerer S, Berry J. 1980. A biochemical model of photosynthetic CO 2 assimilation in leaves of C 3 species. *Planta* **149**: 78-90.

Wang X, Guo Y, Li B, Ma Y. 2006. Evaluating a three dimensional model of diffuse photosynthetically active radiation in maize canopies. *International journal of biometeorology* **50**: 349-357.

Watanabe T, Hanan JS, Room PM, Hasegawa T, Nakagawa H, Takahashi W. 2005. Rice morphogenesis and plant architecture: measurement, specification and the reconstruction of structural development by 3D architectural modelling. *Annals of botany* **95**: 1131-1143.

Zheng B, Shi L, Ma Y, Deng Q, Li B, Guo Y. 2008. Comparison of architecture among different cultivars of hybrid rice using a spatial light model based on 3-D digitising. *Functional Plant Biology* **35**: 900-910.

Zheng BY, Ma YT, Li BG, Guo Y, Deng QY. 2011. Assessment of the influence of global dimming on the photosynthetic production of rice based on three-dimensional modeling. *Science China Earth Sciences* **54**: 290-297.

Proceedings of the 7th International Conference on Functional-Structural Plant Models, Saariselkä, Finland, 9 - 14 June 2013. Eds. Risto Sievänen, Eero Nikinmaa, Christophe Godin, Anna Lintunen & Pekka Nygren.
http://www.metla.fi/fspm2013/proceedings. ISBN 978-951-651-408-9.

The use of x-ray computed tomography for creating computational models of corn stalks and other plants: advantages, benefits, and common challenges.

Douglas Cook[1] and **Margaret Julias**[2]
[1]*Division of Engineering, PO Box 129188, New York University Abu Dhabi, Abu Dhabi, United Arab Emirates*
**correspondence:* douglascook@nyu.edu

Highlights: X-ray computed tomography (CT scanning) is a powerful tool for evaluating plant tissue, and is commonly applied in the field of biomechanics to obtain 3D representations of bone, arteries, and other anatomical data. We have applied this technique to the development of computational models of corn stalks and bamboo culms. While CT scanning has many advantages, the process of creating parsimonious models based on CT data is often challenging since this technique often produces several gigabytes of data for each scan. This paper provides an overview of the advantages, benefits, and common challenges associated with the use of computed tomography in plant modeling in the context of modeling corn stalks.

Keywords: computed tomography, CT, data, 3D modeling, corn

INTRODUCTION

Corn (Zea mays L., Figure 1) is the leading grain crop globally. In the US, over 300 million tons of corn are harvested annually from 80 million acres (135,000 mi2) (Hondroyianni et al. 2000). Only 4 US states (Alaska, Texas, Montana, and California), have a greater land area than that devoted to corn production. Corn is susceptible to late season crop failure (called stalk lodging), with yield losses due to stalk lodging range from 5 to 25% (Nielsen and Colville 1988). These losses affect the productivity of farms, negatively impact individual farmers, and may eventually affect the overall crop supply, thus affecting commodities trading and even the broader economy (Hagenbauch 2007). Reasons for crop failure have been challenging for plant geneticists to identify, measure, and control (Esechie et al. 1977, Loesch et al. 1963), largely because most plant research focuses on biology, not structural mechanics.

From an evolutionary perspective, the purpose of grain kernels is to propagate the species. The species known as Zea mays resulted from millions of years of optimization for this purpose. But humans have adopted corn for an entirely different purpose than nature intended. In the last 100 years, aggressive breeding programs have increased corn yields by over 400% (Gardunia, private communication). As a result, the highest-yield varieties currently suffer from persistent stalk failure, and further increases in crop yield are limited by the ability of the stalk structure to support such large kernels. This proposal is based on the concept that an understanding of the biomechanics of corn stalks can be used by plant breeders to develop breeding strategies that will produce stronger stalks, thus enabling further advances which would not otherwise be possible without the application of biomechanical principles. The objective of this research project is the identification of key geometric and material properties that influence structural attributes of corn stalk. Once these factors have been identified, plant breeders can use this information to develop varieties exhibiting stronger stalks. As a first step toward this long term objective, we require detailed 3D descriptions of corn stalk geometry. This paper desribes our efforts to develop a method for obtaining this information in an efficient manner using computed tomography to produce detailed digital models of corn stalks (see Figure 1).

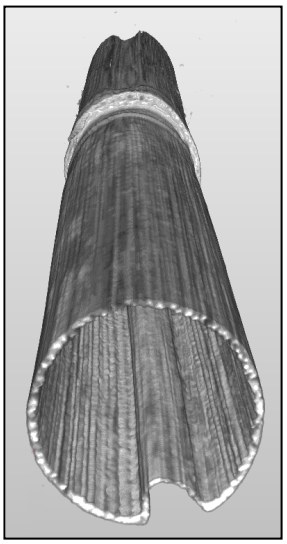

Figure 1: Digitized, three-dimentional corn stalk model.

SCAN METHODOLOGY

CT scanning was performed on multiple corn stalk samples using an X-5000 scanner from NorthStar Imaging (Rogers MN, USA). This scanner is capable of producing CT reconstructions ranging from 10µm

to 127µm. All CT scanners operate on a principle of combining a number of 2D x-ray to mathematically reconstruct a 3D representation of the scanned object. Typically, between one and two thousand images are required for an high quality scan.

The quality of CT reconstruction depends upon many factors, including x-ray intensity, frame-rate of data acquisition, rigidity of the holding fixture, the number of 2D radiographs, density variation within the object, and scan type (continuous or intermittent).

We constructed a holding fixture which consists of a central post, around which 5 corn stalks were arranged, attached by inserting the ends of each stalk into lightweight foam (first image in Figure 2). Scans were conducted using from 1000 to 2500 2D radiographs. To determine the effect that number of radiographs has on reconstruction quality, we have conducted an experiment involving 2400 scans. These scans were combined to create a 3D reconstruction. Half of the same set of radiographs were then used to create a second 3D reconstruction.

SEGMENTATION

While there are many software programs which utilize high-power computing resources to automatically generate 3D models based on CT data, there are several practical problems with this approach. First, these software are not affordable, especially for those just starting to explore this technology. Second, the models produced by such software are often highly complex, and require a great deal of computational resources (CAD, meshing, and finite element software) to fully utilize. Our institution recently purchased Simpleware, one of the leading software products in this category. This software cost approximately $20k. In using this software, we realized that it was not optimized for the extraction of the relatively simple shapes of corn stalks. Although the software is relatively easy to use, the models produced in this way required a great deal of computer memory to manipulate. Over the course of one week, we were able to develop a segmentation process based on freely available MATLAB routines. Our approach involved much less computational power and resources, and successfully extracted relevant data regarding the corn stalk geometry. This process is outlined below.

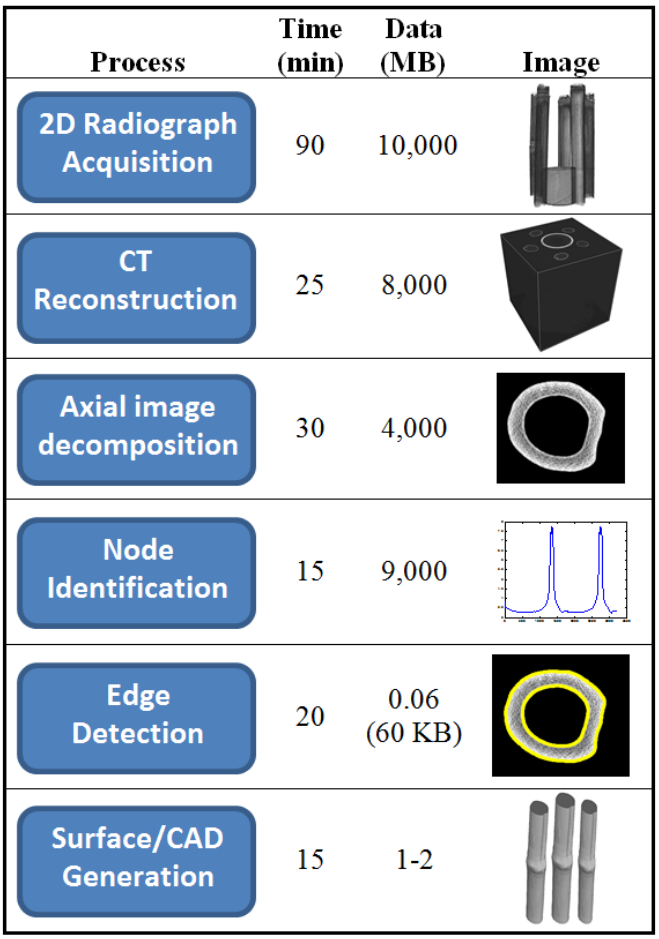

Figure 2: Process utilized in creating digital stalk models. Note that the relevant geometric data requires only 60KB of the original 10GB data set.

RESULTS AND DISCUSSION

One of the challenges associated with corn and other plant stalks is their inherent aspect ratio. The corn rind is approximately 1mm in thickness. Adequate resolution of the wall structure therefore requires a scan resolution of approximately 100µm, which provides approximately 10 pixels across the rind thickness. The stalk diameter is usually an order of magnitude larger, typically 15-23mm. Individual nodes are 10-20 cm in length and the entire stalk is around 1 meter in length. Thus, the data set required for CT reconstruction of a single stalk will consist of approximately 3.2 billion voxels. Of these 3.2 billion, perhaps 5%-10% are corn stalk, while the rest are background data. The first challenge is to segment the images, selecting only those portions that are relevant.

Of the many segmentation algorithms, we have found good success with a technique called the level set

method (Li et al. 2001). While many other methods will split each image into two regions (corn tissue and air), the level-set technique is particularly useful for identifying the boundary between regions, which is our primary interest. The drawback is that this method is computationally intensive, usually taking approximately 10 seconds per analyzed 2D image. However, because the corn stalk (and many other plants) have a relatively constant geometry and structure along the length of the stalk, we can attempt to reduce the number of 2D images that are analyzed. One nodal section of corn stalk may consist of around 1500 axial CT images, but not all need be analyzed. We developed an algorithm that uses a relatively crude thresholding measurement to estimate the number of pixels in each 2D image that represent corn tissue. Since the nodes contain more stalk tissue than the internode regions, this data allows us to infer the locations of the nodes. A sampling scheme is then derived which determines the number, spacing, and location of sample images.

This approach requires that edge detection be performed on a small subset of all axial CT images. In our experience, a set of 1500-1800 axial slices can be adequately approximated using 50-100 judiciously chosen images. This process results in a dramatic reduction in the amount of data (data reduced by a factor of 14,000), while successfully extracting the most important data (geometric boundaries), which can then be used independently, or as starting points for more advanced analysis.

Edge detection and surface generation images are shown in Figure 3. We are now proceeding to create finite element models based on the digitized models, as well as performing geometric analysis on various geometric features of the corn stalks that have been digitized. Finally, this information will be used to create virtual populations of corn stalk models for sensitivity analysis.

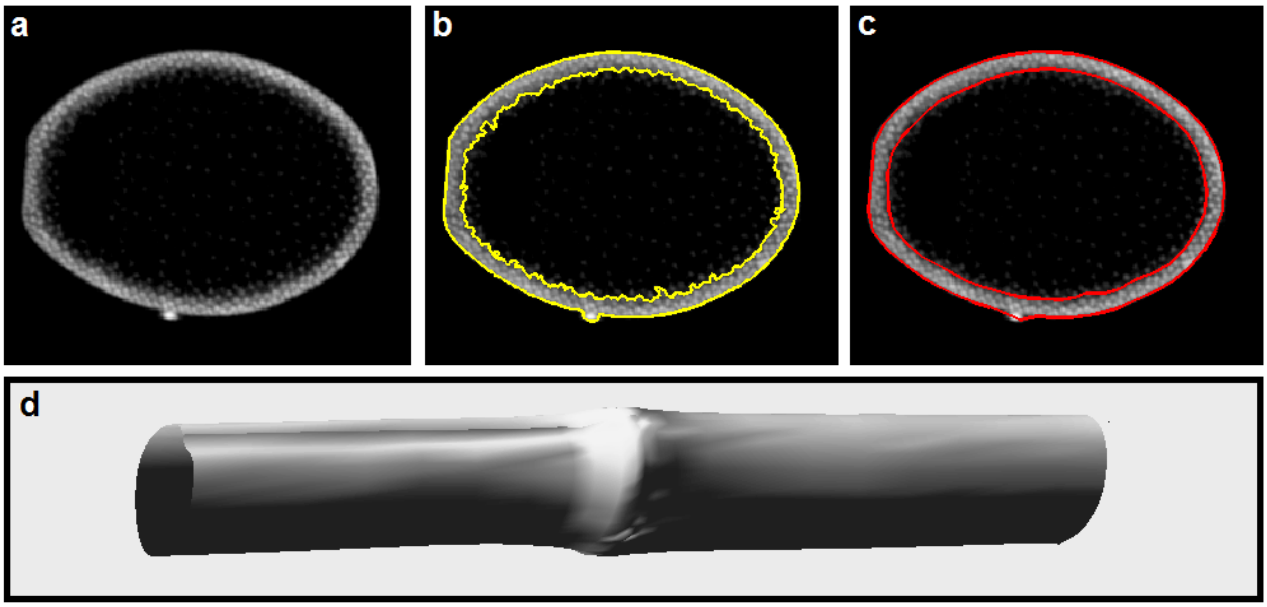

Figure 3: Representative corn stalk cross-sections: (a) axial CT image (179KB); (b) image overlayed with edges detected by level-set method (edges require 16KB); (c) smoothed & simplified edges contours (requiring less than 1KB total); (d) digitized surface model (15KB for shown geometry).

LITERATURE CITED

Esechie HA, Maranville JW, Ross WM. 1977. Resistance of stalk morphology and chemical composition to lodging resistance in sorghum. *Crop Science* **17**: 609-612.

Gardunia Brian (Dr.)**,** Monsanto Corporation., Private communication.

Hagenbauch B. 2007. Corn has deep economic roots as high prices create ripple effect, in USA Today.

Hondroyianni E et al. 2000. Corn stalk traits related to lodging resistance in two soils of differing salinity, ed, Vol. 45, Maydica, Bergamo, ITALIE.

Li C, Huang R, Ding Z, Gatenby C, Metaxas DN, Gore JC. 2001. A Level Set Method for Image Segmentation in the Presence of Intensity Inhomogeneities with Application to MRI, IEEE Trans. *Image Processing* **20** (7): 2007-2016.

Loesch PJ, Zuber MS, Grogan CO. 1963. Inheritance of crushing strength and rind thickness in several inbred lines of corn. *Crop. Sci.* **3**: 173-174.

Nielsen B, Colville D. 1988. Stalk Lodging in Corn: Guidelines for Preventive Management, Purdue University Cooperative Extension Service, 1988.

Proceedings of the 7th International Conference on Functional-Structural Plant Models, Saariselkä, Finland, 9 - 14 June 2013. Eds. Risto Sievänen, Eero Nikinmaa, Christophe Godin, Anna Lintunen & Pekka Nygren. http://www.metla.fi/fspm2013/proceedings. ISBN 978-951-651-408-9.

A Model-based Approach to Extract Leaf Features from 3D Scans

Franz Uhrmann[1], **Christian Hügel**[1] , **Sabine Paris**[1], **Oliver Scholz**[1], **Michael Zollhöfer**[2] and **Günther Greiner**[2]
[1]*Fraunhofer Institute for Integrated Circuits IIS, Am Wolfsmantel 33, 91058 Erlangen, Germany*
[2]*Computer Graphics Group, University Erlangen-Nuremberg, Germany*
**correspondence:* franz.uhrmann@iis.frauhnhofer.de

Highlights: We present a flexible and robust method for the extraction of leaf features from 3D point clouds. An adaptable leaf model is automatically fitted to the measured data in order to obtain a precise but compact parameterization of the leaf shape. As an application example the detection of stress using the fitted leaf parameters is demonstrated.

Keywords: Phenotyping, leaf model, vitality monitoring

INTRODUCTION

Modern computer vision technologies allow fast, detailed and yet affordable 3D acquisition of objects. Contactless acquisition methods like stereovision or laser scanning are increasingly used for plant phenotyping systems, as the surface of single plants can be measured at high resolution within seconds (see Seidel 2011, Biskup 2007 or Andersen 2005). The resulting datasets are usually very large containing millions of dense but independent point samples. As they cannot directly be used as interpretable features of the phenotype, a set of comprehensible geometric features e.g. leaf area or orientation has to be extracted from the point cloud. However, the relevant parameters depend on multiple aspects like the research subject or the investigated plant species. Thus the algorithms for feature extraction are highly adapted and customized to the specific problem.

In this paper a flexible method for the extraction of leaf features is presented: We introduce a geometric model, which allows the description of a leaf shape with a small set of parameters corresponding to physical properties. The model can easily be adapted to various plant species. Furthermore, we present a method to automatically match the model with a point cloud of a real leaf. As the model parameters provide a compact but detailed description of the leaf geometry, they can directly be used as features for further analysis of the plant phenotype.

PARAMETRIC LEAF MODEL

The basis of the geometric leaf model is a 2D image of a single leaf of the respective plant species, which is created using a custom flatbed scanner. After separating leaf pixels from the background, a mesh representation of the leaf shape is generated by triangulation of the leaf pixels. To emulate natural leaf deformations in 3D space a series of geometric transformations is defined, which are applied to the initially flat leaf template: Besides a rigid transformation currently 9 leaf-specific transformations are implemented like rolling or bending along the main axis. All transformations are parameterized by a set of currently 26 parameters.

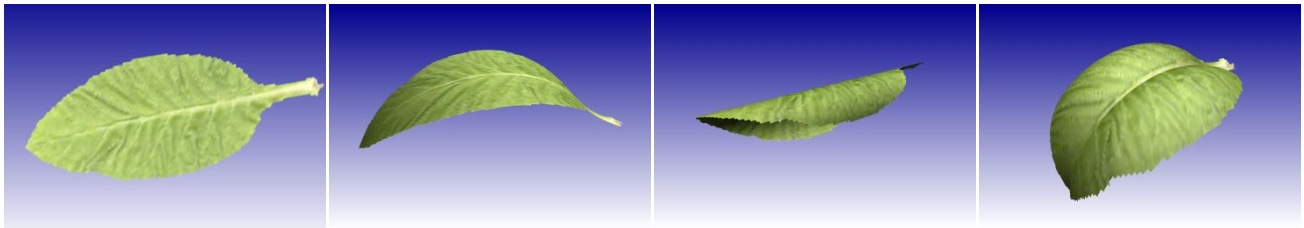

Fig. 1. Examples for different leaf model transformations (from left to right): Flat leaf template, bending along leaf axis, rolling along leaf axis and a combination of multiple transformations.

MODEL FITTING

In order to determine the geometric parameters of the measured leaf, the parametric model representation is fitted to the data. For a set of measured points $\boldsymbol{p} = \{p_1, p_2, \dots, p_n\}$ the model parameters $\boldsymbol{\alpha}$ are determined, such that the distance between the points of the transformed leaf model $\boldsymbol{m}(\boldsymbol{\alpha}) = \{m(\boldsymbol{\alpha})_1, m(\boldsymbol{\alpha})_2, \dots, m(\boldsymbol{\alpha})_n\}$ and the measured points $\boldsymbol{p}$ is minimized. This can be formulated as an optimization problem minimizing

$$d(\alpha) = \sum_{i}^{n} |p_i - m(\boldsymbol{\alpha})_j|$$

with $m(\boldsymbol{\alpha})_j$ being the nearest neighbor to measurement point p_i and $|\dots|$ being the Euclidian distance between two points. As the model transformations contain multiple trigonometric functions and the neighbor relationships change during optimization, $d(\boldsymbol{\alpha})$ is nonlinear. Thus the Levenberg-Marquardt optimization algorithm (see e.g. Madsen 2004) was chosen as a numerical solver and applied iteratively.

EXPERIMENTS

We verified the model-based feature extraction approach with data of a phenotyping system for tobacco plants. The scanning unit covers a maximum size of 1 m³ and uses multiple sheet-of-light units to acquire the surface of the plant with high coverage at a lateral resolution of approx. 0.5 mm (see Fig. 2). Thereafter the resulting point could is segmented into single leaves. For certain types of plants separation of the measured point cloud into single leaves works nicely using a standard point cloud segmentation algorithm (Rabbani 2006, see Fig 3). Finally a leaf model is fitted to each segmented leaf, which can be seen in Fig. 4 for the example of a *N. tabacum* plant.

The monitoring of a plant during application of stress was chosen as an example to show the potential of our approach. In order to cause a quick stress reaction, a single *N. tabacum* plant was cut at the stem and fixed in a container with saline solution. An initial measurement of the plant was performed immediately after stress induction, a second measurement 35 minutes later. Additionally pictures were taken before each measurement, which are shown in Fig. 5 and Fig. 6.

Fig. 2. Phenotyping hardware setup.

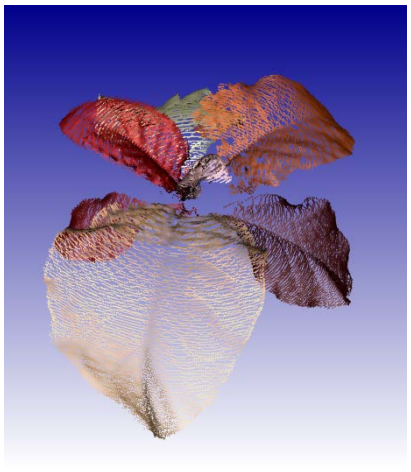

Fig. 3. Point cloud of measured plant with segmented leaves shown in different colors.

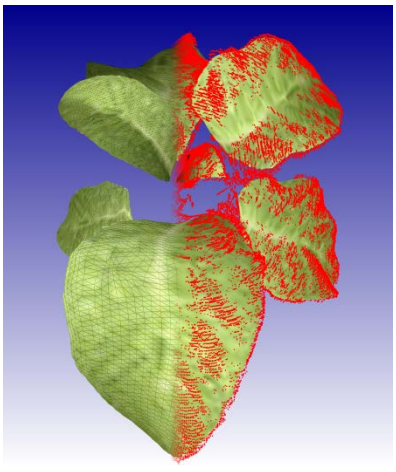

Fig. 4. Leaf model fitted to each segmented leaf. In the right half the measurement points are visible as a red dot overlay.

Fig. 5. *N. tabacum* immediately after stress induction

Fig. 6. *N. tabacum,* 35 minutes under stress

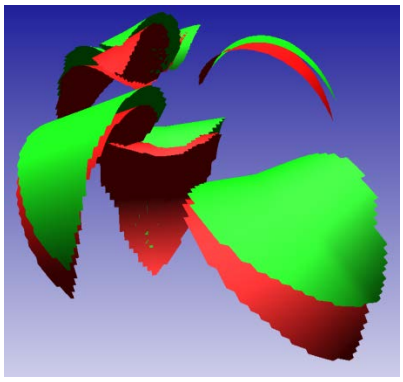

Fig. 7. Leaf models of both measurements. Green: immediately after stress induction. Red: after 35 minutes under stress

RESULTS

Comparing the photographs it is difficult to quantify the differences caused by the stress induction. When the fitted model representations are visualized in a common view as can be seen in Fig. 7, the downward bending of the leaves are already clearly visible. The decline is represented by two parameters in our leaf model: The first parameter indicates bending of the lamina defined as the slope of the straight line between lamina base and leaf apex. The second parameter is the absolute height from the top edge of the pot to the base of the leaf lamina. The difference in this parameter of both measurements represents the decline of the lamina caused by the bending of the petiole. Values of this parameter for each leaf are shown in Table 1, with the bases of all leaf laminas being lower in the second measurement with the exception of leaf #6. This leaf is the youngest and has an almost upright petiole, which tilts inwards under stress resulting in a slightly greater height of the leaf base.

Leaf Index	Absolute height of lamina base [mm]		Height difference [mm]
	t = 0 min	t = 35 min	
1	28	10	17
2	52	45	7
3	77	70	7
4	145	135	10
5	151	144	6
6	153	156	-3
7	156	142	15

Table 1: Comparison of parameter absolute height of lamina base.

CONCLUSION AND OUTLOOK

We presented a leaf model that is adaptable to different plant species simply by exchanging the leaf template. Along with the fitting algorithm a universal approach was presented that has proven to be robust delivering a compact set of parameters representing a plant's phenotype in great detail. The ability to derive information about a plant's state of health simply by reading the appropriate parameters opens up numerous applications, starting with the detection of stress symptoms as shown. By exploring the detailed parametric descriptions of large plant populations during growth, a standard growth behavior and furthermore deviations from this standard growth can be detected. Therefore, this approach is generally suitable for vitality assessment of plants.

LITERATURE CITED

Andersen HJ, Reng L, Kirk K. 2005. Geometric plant properties by relaxed stereo vision using simulated annealing. *Computers and Electronics in Agriculture*. **49**:219-232

Biskup B, Scharr H, Schurr U, Rascher U. 2007. A stereo imaging system for measuring structural parameters of plant canopies. Plant, Cell and Environment **30**:1299-1308.

Madsen K, Nielsen HB, Tingleff O. 2004. Methods for Non-Linear Least Squares Problems. *Informatics and* Mathematical *Modelling, Technical University of Denmark,* 60p.

Rabbani T, van den Heuvel FA, Vosselmann G. 2006 Segmentation of point clouds using smoothness constraint. *Proceedings* of ISPRS, **36**: 248-253

Seidel D, Beyer F, Dietrich H, Fleck, Leuschner C. 2011. 3D-laser scanning: A non-destructive method for studying above- ground biomass and growth of juvenile trees. *Agricultural and Forest Meteorology* **151:**1305–1311.

Proceedings of the 7th International Conference on Functional-Structural Plant Models, Saariselkä, Finland, 9 - 14 June 2013. Eds. Risto Sievänen, Eero Nikinmaa, Christophe Godin, Anna Lintunen & Pekka Nygren. http://www.metla.fi/fspm2013/proceedings. ISBN 978-951-651-408-9.

Root growth and distribution of gooseberry (*Physalis peruviana*) under field conditions in the Andean soil

Roveda-Hoyos Gabriel[1] and **Moreno-Fonseca L.P.**[1]
[1]*Department of Agronomy, PO Box 14490, National University of Colombia, Bogotá*
**correspondence:* groveda@gmail.com

Highlights: A field technology with the computer model called "RACINE" was used to estimate root-length density (RLD) and the root exploration from root count on soil profiles. The results indicated a drastic reduction on root development due to restrictions as low phosphorous and decreasing organic matter. However, *Glomus mosse* can promote the root system, on RLD and root front.

Keywords: root model, *Physalis peruviana*, *Glomus mosse*.

A field technology was used to estimated root-length density (RLD) and the root exploration from root count (grid method) on soil profiles. This method includes a computer model, developed by Chopart and Siband (1999), and called "RACINE"**,** that was calibrated and validated in volcanic soils of South America (Roveda-Hoyos *et al*., 2001). This research was focused on determining the effect of symbiotic association between arbuscular mycorrhizal fungi (AMF) and gooseberry crops on the root-length density and the root exploration under field conditions (Van der Heijden, 2003). The experiments were done in two localities of Boyacá and Cundinamarca departments of Colombia at 2900 and 2050 meter over sea level, respectively. Both soils were classified as Typic Dystrandepts, with low phosphorous available (< 10 mg Kg^{-1}), low macronutrients saturation (N, K, Ca, Mg y S), and acid pH < 5. Both calibration and validation methods carried out using two experimental designs of random complete blocks were used with 3 treatments and 4 repetitions as follows; with two control treatments without inoculation of AMF, without fertilizing (T_0), and 100% of fertilizing (T_{100}) with application of triple superphosphate (TSF), a treatment with 50% fertilizing of TSF and inoculated with AMF, *Glomus mosse* (T_{50+G}), all treatments were fertilized with N (149.5 Kg Ha^{-1}), K (196.9 Kg Ha^{-1}), Ca (46.9 Kg Ha^{-1}), Mg (14.1 Kg Ha^{-1}), S (21.1 Kg Ha^{-1}), and micronutrients (B, Cu). The experimental results demonstrated that all the treatments had a shallow root system (> 90%) of the total root length, after the top soil deep (15 cm), the RLD showed a drastic reduction of *P. peruviana* roots, the soil profiles were evaluated at vegetative and flowering stages (2 and 6 month after planting). This shallow root system of gooseberry plants suggested a chemical restrictions, as low availability phosphorous in the soil profile (<5 mg Kg^{-1}), and decreasing organic matter in a deep soil profile, those proprieties are typical in volcanic ash soils. The principal differences in RLD among treatments in the top soil were due to the effect produced by the application of phosphorous fertilizer (TSF) and the inoculation with *G. mosse*, as follows: The highest values of RLD (14.9 cm cm-3) were found in the inoculated treatment (T50+G) to compare to no inoculated treatments, T100 (12.1 cm cm-3), and T0 (8.0 cm cm-3). There were also differences among these treatments with the maximum rooting deep (root front). The highest root front (35 cm) was observed in inoculated treatment with *G. mosse* (T50+G) to compare with the no inoculated treatments, T100 (30 cm), and T0 (25 cm). The experimental results indicated a drastic reduction on root development on gooseberry plants as limiting factors, such as low available phosphorous (Vance, 2003) and decreasing organic matter in deep soil profile. Nevertheless, the inoculation of AMF (*G. mosse*) can promote the root system of gooseberry, on both RLD and root front.

LITERATURE CITED

Chopart JL, Siband P. 1999. Development and validation of a model to describe root length density of maize form root counts on soil profiles. *Plant and Soil* **214**: 141-157.

Roveda-Hoyos G, Chopart JL, Baquero JE, et al. 2001. Modelling growth and distribution of maize (*Zea mays* L.) roots under field conditions in the eastern plains of Colombia. XIV International Plant Nutrition Colloquium "Food security and sustainability of agro-ecosystems Kluwer Academic Publishers. Hannover, Germany. 576-578.

Vance CP, Uhde-Stone C, Allan DL. 2003. Phosphorus acquisition and use: critical adaptations by plants securing a nonrenewable resource. *New Phytol.* **157**: 423-447.

Van der Heijden MGA, Sander IR. 2003. *Mycorrhizal Ecology*. Ed. 2nd Springer-Verlag Berlin Heidelberg, New York. Pg. 234-261.

Smith SE, Read DJ. 2008. *Mycorrhizal Symbiosis*. New York, Academic Press, Third Edition.

Proceedings of the 7th International Conference on Functional-Structural Plant Models, Saariselkä, Finland, 9 - 14 June 2013. Eds. Risto Sievänen, Eero Nikinmaa, Christophe Godin, Anna Lintunen & Pekka Nygren. http://www.metla.fi/fspm2013/proceedings. ISBN 978-951-651-408-9.

Defining reliability coefficients in an automated radial file identification and characterization method in microscopic images of gymnosperms

Guilhem Brunel[1,2], **Philippe Borianne**[2], **Gérard Subsol**[3], **Marc Jaeger**[2] and **Yves Caraglio**[2]
[1]*CIRAD - UMR AMAP, France.* [2]*Université Montpellier 2, France.* [3]*CNRS – LIRMM, France.*
guilhem.brunel@cirad.fr

Highlights: The analysis of wood anatomical sections is of great interest for understanding the growth and development of plants. We propose a novel method for automatically identifying and characterizing radial files in wood microscopic images of gymnosperms. A key point is to be able to assign *a priori* reliability coefficient to the results, particularly for statistical processing in large-scale analyses. We describe in this paper the principle used to establish reliability coefficients to evaluate the radial file identification process and the geometrical measurements of cells and their components.

Keywords: image processing, wood microscopic images, radial file identification, *a priori* reliability.

INTRODUCTION

Wood structure reflects the physiological and molecular regulation of cambium activity (Cato et al. 2006) and also registers environmental conditions (Barlow et al. 2005). Understanding cambium growth mechanisms calls for a study of cell pattern regularity, and of cell disruption or modification in space and time (Liang et al. 1997). Two types of organizations are considered: the growth ring representing cell production at a given time, and the radial file representing the activity of an initial cell over time (Rozenberg et al. 2004); radial files help in understanding the development, differentiation and temporal changes of cells.

Morphological fluctuations of successive cells along a radial file and the influence of external factors have been investigated for a long time (Ford et al. 1978), but those investigations were greatly restricted by a limited number of radial file comparisons and a restrictive number of successive cell descriptions. Those studies, concerning secondary growth and its relationships with primary growth, were based on fragmentary studies, due to high acquisition and processing costs. Large-scale studies for understanding wood growth and disturbance are available nowadays thanks to automated radial file identification and cell characterization (Brunel et al. 2012, Kennel et al. 2011). In fact, wood continuously records changes in the development of the tree. Such new methodologies and approaches offer real new opportunities for more in-depth investigations of tree biology and climate change (Fonti et al. 2010). The size and shape fluctuations observed along radial files are usually considered to be the result of external constraints (Frankenstein et al. 2005). This is a restrictive and simplified viewpoint: these fluctuations are probably due to a combination of external and internal factors. We aim to promote an objective quantification of these measurements, on the basis of statistics based on numerous image datasets.

This paper focuses on the reliability of such data from statistical studies, i.e. produced by automated radial file identification (Brunel et al. 2012). For large-scale data analyses, it is necessary to ensure *a posteriori* that the measurements are valid in order to find invariants or validate hypotheses. This is a classic line taken in statistics (Bruton et al. 2000) and experimental approaches.

MATERIALS

We processed histological sections of several gymnosperm species: *Pinus caramanica*, *Pinus nigra* and *Abies alba*. Wood cross-sections with a thickness of 20 µm were produced with a vibratome. The sections were stained to increase the contrast between the lumen and cell walls. They were then digitized with an Olympus DP71 LCD camera on an Olympus BX51 microscope. The square color images produced had a resolution of 4 million pixels.

OVERVIEW OF THE METHOD

Radial files are alignments of substantially similar cells in terms of color dynamics, shapes and sizes. Intuitively, the notion of cell alignment implies the existence of cellular organization based on the neighborhood relationships between cells. Those properties are used to identify radial files.

Our approach, described in (Brunel et al. 2012) was divided into three steps: cell identification which specified single cells, cell organization which detected radial files, and cell classification which gave the biological and qualitative typing of cells and radial files.

The incremental construction of radial files was based on two assumptions: (i) such a file is independent from image orientation; (ii) two consecutive cells of a file are very similar. From a methodological point of view, cell individualization was derived from a watershed algorithm (Vincent et al. 1991), and the cell pattern was described by an adjacency graph created from the watershed crest lines. Radial files were then built by finding a reversible path in the graph under spatial constraints (maintaining a specific direction) and similarity constraints (two consecutive cells should show close geometric characteristics). Our method produced several layers of results, respectively corresponding to different observation levels: (i) radial files were classified according to their length, their fractionation and their cell self-similarity, (ii) cells were characterized by geometric parameters (such as size, diameter, shape, etc.) and topological parameters (number of neighbors), (iii) cell component elements (wall, lumen) were characterized by geometric parameters (size, thickness, diameter, etc.).

DEFINITION OF *A PRIORI* RELIABILITY COEFFICIENTS

Quality assessment of these results depends on many factors. It concerns the data set itself (image noise, biological configuration complexity, etc.), the process (algorithm approximations, computation costs, stability, etc.), and the geometrical scale (related to the observation level). Each result should be qualified using different indicators, notably to keep the significant outcome while processing high volume data. It is thus relevant to assign an estimated reliability coefficient to each result. We illustrate cases on file and cell scales.

Radial file construction reliability. We propose defining this radial file reliability coefficient R_f from three criteria: length, fractionation and similarity. The first criterion derives from the file length, L_f, compared to the threshold value T. T is set by 2means and defines the minimum significant length. Fractionation is evaluated from the file construction algorithmic cost. It involves the total number of cells L_{fm} stacked to build the file, the length L_f of the file, and the number of sections N_f. The similarity criterion is built from the product of the *n-1* consecutive cell surface variations. The final reliability coefficient R_f of the file *f* is then defined by a product of normalized terms ranging between 0 and 1. When this coefficient tends to 1, the reliability of the radial file increases.

$$R_f = \left(1 - max\left(\frac{T - L_f}{T}, 0\right)\right)\left(1 - \frac{L_{fm} - L_f}{N_f * L_{fm}}\right)\prod_{j=0}^{n-1}\left(1 - \frac{|Sf_j - Sf_{j+1}|}{Sf_j + Sf_{j+1}}\right)$$

Lumen area estimation reliability. The reliability coefficient of the lumen surface is defined on a similar principle, by a product of two normalized terms, based on the cell size and an image local blur estimation. In fact, the watershed algorithm is known as a robust method for extracting cell boundaries, since it is based on intensity discontinuities which are less sensitive to blurring, whereas the lumen area shows high sensitivity to local blur. The cell area definition involves a two-class clustering split, corresponding to the lower and the higher intensity classes. The local blur estimator is derived from (Ladjal 2006), based on the relationship between local dynamics and intensity differences.

EXPERIMENTS, CONLUSION AND WORK IN PROGRESS

Experiments were performed on ten colored sections of different species of gymnosperms, representative of biological variability. The color quantifies the reliability results, both on a global (Fig. 1) and local (Fig. 2) scale. On a global scale, we can see in Fig. 1 that the reliability estimator properly qualifies the cell files: green colors are assigned to straight and regular cell lines whereas red colors correspond to incomplete cells on the side of the image or incrusted cells. Such a color map alerts the expert to potential unsure classifications and emphasizes the ambiguous biological status of a file or cells. On a local scale, for lumen area computation, the estimator also retrieves obvious cases. The reliability factor also ensures areas showing lower intensity variations (areas in green in Fig. 2, right).

Several points were studied. (i) in angiosperms, the vessel morphology is different and calls for a different evaluation of cell similarity *which defines the third term of the file reliability coefficient*, by taking into account the larger diameter instead of its surface. (ii) other blur estimators were studied, such as estimators based on multi-scale filtering in order to assess the independence of the reliability coefficient with

respect to the blur estimation method. (iii) how the local reliability coefficient could be used to correct the measured values according to the local blur estimator relationship (Fig 2. Left).

To conclude, we introduced some reliability coefficients for image processing related to cell organization identification and illustrated the cases of radial file detection and of lumen area computation. The reliability coefficients were essentielly used to filter the input data of statistical studies conducted by botanists or to draw attention to special biological configurations.

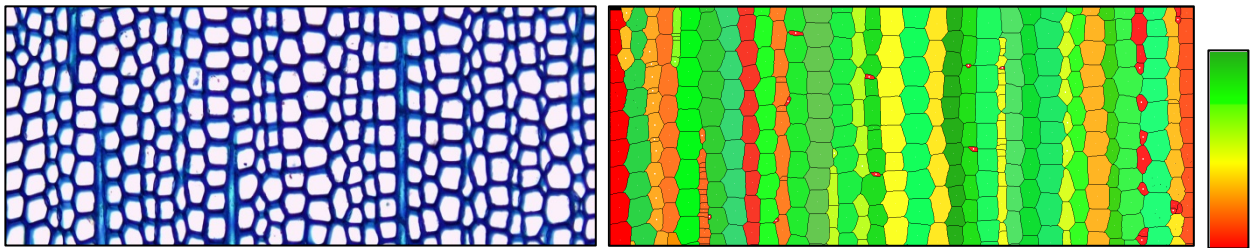

Fig. 1. Left: cross-section of *Abies alba*. Right: automated identification of radial files. Color value qualifies the reliability coefficient: weakly reliable files appear in red tones and highly reliable files are in green tones.

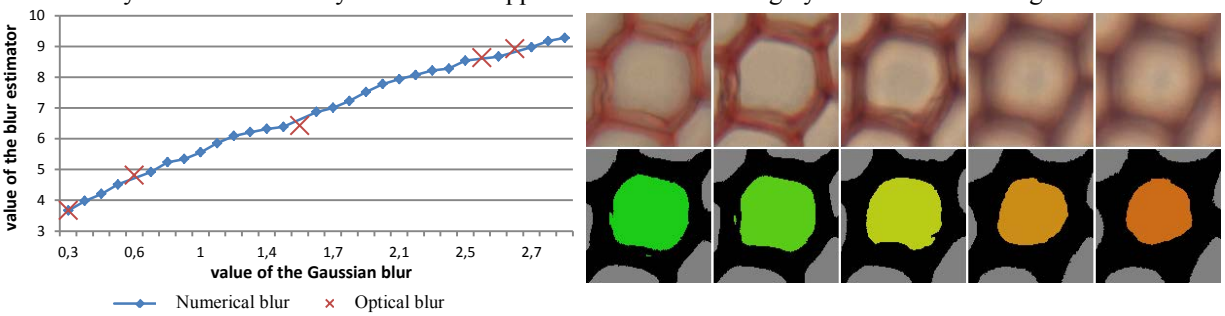

Fig. 2. Left: relationship between a Gaussian blur applied to a cell image and the local blur estimator. The estimator emphasizes the blur tendency; red crosses stand for five microscopic optical blurs, matched from their area variance. Right: the five corresponding lumen areas from the optical blurs: the color qualifies the reliability coefficient, from green for the real lumen area to orange for the reduced lumen area.

The authors acknowledge NUMEV Labex and SIBAGHE Graduate School of the University of Montpellier 2 for their support.

LITERATURE CITED

Barlow PW, Powers SJ. 2005. Predicting the environmental thresholds for cambial and secondary vascular tissue development in stems of hybrid aspen**.** *Annals of Forest Science* **65**: 565-573.

Brunel G, Borianne P, Subsol G, Jaeger M, Caraglio Y. 2012. Automatic characterization of the cell organization in light microscopic images of wood: application to the identification of the cell files, *Plant Growth Modeling, Simulation, Visualization and Applications, IEEE press, ISBN 978-1-4673-0070-4*, 58-65.

Bruton A, Conway JH, Holgate ST. 2000. Reliability: What is it, and how is it measured?, *Physiotherap* **86**:94-100

Cato S, McMillan L, Donaldson L, Richardson T, Echt C, Gardner R. 2006. Wood formation from the base to the crown in *Pinus radiata*: gradients of tracheid wall thickness, wood density, radial growth rate and gene expression. *Plant Molecular Biology* **60**:565–581.

Fonti P, von Arx G, Garcia-Gonzalez I, Eilmann B, Gärtner H, Eckstein D. 2010. Studying global change through investigation of the plastic responses of xylem anatomy in tree rings. *New Phytologist* **185**: 42–53.

Ford ED, Robards A, Piney MD. 1978. Influence of environmental factors on cell production and differentiation in the early wood of *Picea sitchensis*. *Annals of Botany* **42** *(3): 683-692.*

Frankenstein C, Eckstein D, Schmitt U. 2005. The onset of cambium activity – A matter of agreement? Dendrochronologia **23**: 57-62.

Kennel P, Subsol G, Guéroult M, Borianne P. 2010. Automatic identification of cell files in light microscopic images of conifer wood. *2nd International Conference on Image Processing Theory Tools and Applications* 98–103.

Ladjal S. 2006. Blur estimation in Natural Images, *15^{e} congrès francophone AFRIF-AFIA Reconnaissance des Formes et Intelligence Artificielle* 112-124.

Liang C, Filion L, Cournoyer L. 1997. Wood structure of biotically and climatically induced light rings in eastern larch (*Larix laricina*). *Canadian Journal of Forest Research* **27**: 1538.1547.

Rozenberg P, Schüte G, Ivkovitch M, Bastien C, Bastien JC. 2004. Clonal variation of indirect cambium reaction to within-growing season temperature changes in Douglas-fir. *Forestry* **77**:257-268.

Vincent L, Soille P. 1991. Watersheds in Digital Spaces: An Efficient Algorithm Based on Immersion Simulations, *IEE Transactions on Pattern Analysis and Machine Intelligence* **13-6**:583–598.

Proceedings of the 7th International Conference on Functional-Structural Plant Models, Saariselkä, Finland, 9 - 14 June 2013. Eds. Risto Sievänen, Eero Nikinmaa, Christophe Godin, Anna Lintunen & Pekka Nygren. http://www.metla.fi/fspm2013/proceedings. ISBN 978-951-651-408-9.

An automated image-processing pipeline for high-throughput analysis of root architecture in OpenAlea

J. Diener[1]*, **P. Nacry**[2], **C. Périn**[3], **A. Dievart**[3], **X. Draye**[4], **F. Boudon**[1], **A. Gaujon**[2], **C. Godin**[1]
[1]*Virtual Plants, INRIA, CIRAD, INRA, 34095 Montpellier France,* [2] *Biochimie et Physiologie Moléculaire des Plantes, INRA, CNRS, UM2, 34060 Montpellier, France,* [3] *UMR DAP, CIRAD, 34398 Montpellier, France,* [4] *Unité d'Ecophysiologie et d'Amélioration végétale, Université catholique de Louvain, B-1348 Louvain la Neuve, Belgium.*
**correspondence:* julien.diener@inria.fr

Highlights: FSPM analysis of root systems requires structural data obtained on large data set. This paper describes a processing pipeline developed to extract automatically the architecture of root system from images databases.

Keywords: Root architecture, Image processing, Analysis pipeline, High-throughput, OpenAlea

INTRODUCTION

Automated acquisition systems of Root System Architecture (RSA) are now readily available for developmental research and provide high-throughput image data of roots. Existing acquisition systems provide many types of data, from images of dispersed root pieces to full 3d scans of underground root systems. Here we consider RSA grown in Petri plates. This is a traditional experimental protocol for which image data can be acquired easily and in large amount. Their analysis is thus a major challenge for researches on root development.

Existing tools range from the automatic estimation of global traits distribution to details extraction of the root architectures through tedious manual work. Software such as Rootreader2d (Clark et al., 2012), EZ-Rhizo (Armengaud et al., 2009), Rootfly (Zeng et al., 2008) and RootTrace (Naeem et al., 2011) extract in a single image a limited part of the architecture data such as the main axes length and the number of lateral roots. Similarly, programs such as WinRhizo (Arsenault et al., 1995) or GiaRoot (Galkovskyi et al., 2012) extract representative value of the whole RSA such as total root length, area, or branching number. These are suitable for processing high-throughput data but do not provide architectural data, as they do not order the detected root segments in an arborescent structure.

To extract the full root system architecture, the available software are either entirely manual such as DART (Le Bot et al., 2010), or semi-automated such as SmartRoot (Lobet et al., 2011) or a high-end version of WinRhizo (WinRhizo Pro, 2012b). Those are suitable for detail inspection of architectural trait of a few root systems. But because of the time required by user interaction they cannot be used for high-throughput analysis.

In this study, we present a solution for extracting the full root architecture automatically and on a large-scale data set. Because our framework is included in the OpenAlea platform, in addition to traditional data analysis such as the ones provided by existing software, the extracted data can also be used seamlessly as input of all the architectural analysis packages already contained in OpenAlea.

MATERIAL AND METHOD

For the purpose of development and validation, two data sets have been used. The first set studies the growth of nine genotypes of *Arabidopsis thaliana* in three different nitrate concentrations (see fig. 2). For each of these experimental modalities, four Petri boxes containing each five root systems are daily imaged during six days. The second data set contains images of rice (*Oryza sativa* of the nipponbarre genotype) of eight Petri boxes, each containing five root systems, which were scanned once per day avec a 6 days period (see fig. 3). In total both data sets represent 688 images and 3440 root systems in total. Comparisons with expert measurements have been done for around 300 plants.

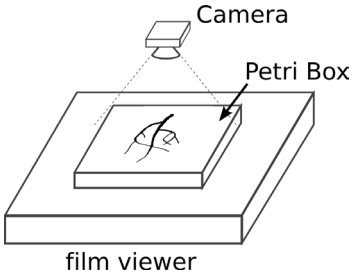

Fig. 1. Schema of the acquisition setup

Image acquisition is done either using a high-resolution scanner (~100Mp) with back-lighting for the rice data, or with a camera setup associated with a x-ray film viewer that provide back-lighting (see fig. 1)

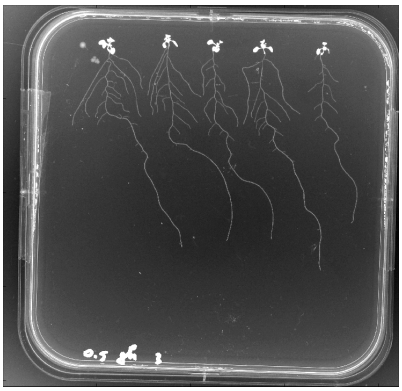

Fig. 2. One image of the Arabidopsis data set

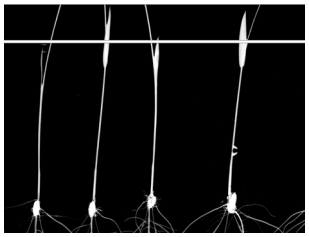

Fig. 3. One image of the Rice data set

To allow processing and analysis of large experimental data, the proposed framework organises images data sets in a two level structure. At the bottom, *root sequences* contain a time sequence of images where each image contains several root systems for a specific experimental modality (e.g. one genotype in one environment condition). On top, root sequences are organized in *projects* that first automate common processing of image sequences, and second allow comparative analysis of different experimental modalities.

All images of the project are processed through a three steps pipeline (see fig 4):

1. Image segmentation

Initial root images have to be segmented, i.e. each pixel should be classified as either background or root objects. This is done in two passes. First the smooth but non-uniform background lighting is estimated based on minimum pixel intensity with large-scale distribution. It is then removed from the original images. Second, the pixels are classified by fitting a gaussian mixture model of the remaining background noise and of the root pixels intensity.

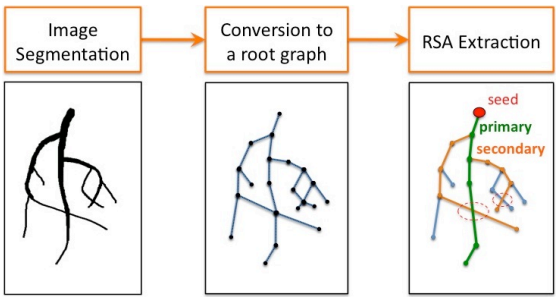

Fig. 4. Image processing pipeline

In addition to this binary classification, seeds and leaves areas are detected using specific characteristics of the observed plants. In the case of Arabidopsis, leaves are difficult to describe by their shape and they are segmented as pixels with higher intensity. Arabidopsis roots being more transparent than leaves, these last one appear whiter (see fig. 2). For rice, it is the seeds that are detected based on their radius, which is much larger than for the roots (see fig. 3).

2. Extraction of a graph representing of the observed root systems

In this step, the segmented image pixels are clustered in root *segments*, i.e. root pieces of linear shape, which contains no branching or crossing. This is done by first applying a thinning algorithm (skeletonization) to the binary images. Then each linear curve of the obtained skeleton is further divided in a set of line segment by fitting a 1st order spline on the curve pixels. A graph is then created containing the set of extracted segments as vertices, and the set of all pairs of segments that are contiguous as edges. At this stage, the constructed graph is not necessarily a tree structure as it usually contains loops.

3. Estimation of a root architecture

The root architecture is obtained by converting the root graph to an *axial tree* structure (Godin et al., 1998). This is done in two passes. First the graph is converted to a tree rooted at the detected seeds or leaves. The tree is computed using the shortest path algorithm that select the parent of each segment such that the sum of the edge cost along the path from the segment to the seed is minimal. The edge cost (i.e. the distance between two segments of the graph) is defined as the turning angle. The algorithm thus generates a tree structure with the straighter possible paths. This conversion breaks graph loops, meaning that it solves the axe crossing ambiguities (as shown by orange circles in the right image of fig. 4). The second pass then identifies branching relationship by selecting for each parent segment its direct child, i.e. that belongs to the same root axe. Again, the selection is done in order to minimize the axes curvature.

RESULTS

After the image-processing step, the project contains the sequences of the extracted arborescent structure (see fig 5).

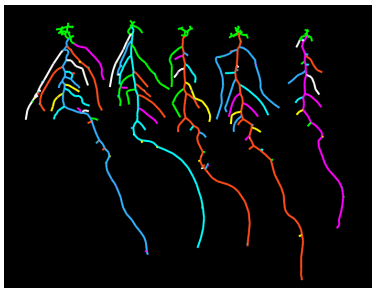

Fig. 5. Extracted RSA from the image in figure 2. Each root axe is drawn with a random colour.

In order to quantify the accuracy of our reconstruction, reference data were obtained by manual annotation of the analysed root systems. Experts manually specified the root architectures on a series of images. We then compared these reference data with the structures automatically reconstructed with our pipeline. A comparison has been done on a first data set for different RSA scales. Selected results are shown in figure 6.

We also have used the structural validation method of (Boudon et al., 2013). Two indices are provided by this method. For the first one, the reference and tested structured are mapped one onto each other to find similarities and differences. This gives the percentage of correctly identified elements. The second characterises the similarity of organisation of these elements in the two structures i.e. the percentage of correct connections between elements. This validation procedure has given promising results on an initial data set (between 80 and 90% correspondence). Results showing more complete analysis and over the whole data sets will be presented and discussed at the conference.

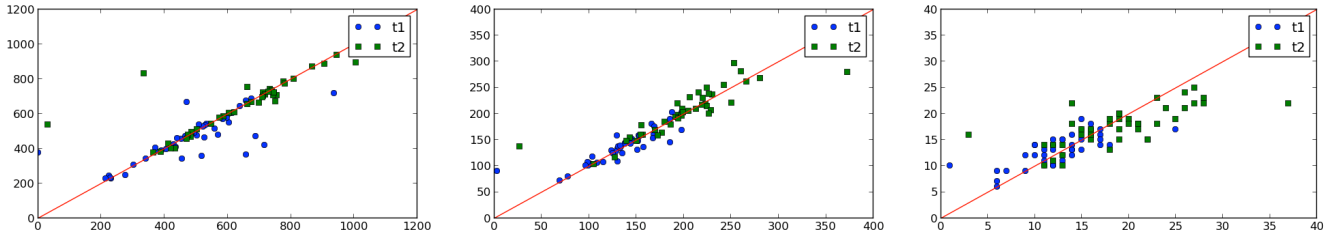

a) Smallest convex hull area containing each root system

b) Total root length

c) Number of secondary root axes per plant

Fig. 6: selected comparison with ground truth data. For all subfigures, the y-axis is the ground truth and x-axis the measures obtained with our method. The red line indicates exact match. The compared data are from 40 plants of *Arabidopsis thaliana* over 2 time steps.

LITERATURE CITED

Armengaud P, Zambaux K, Hills A, Sulpice R, Pattison RJ, Blatt MR, Amtmann A. 2009. EZ-Rhizo: integrated software for the fast and accurate measurement of root system architecture. *The Plant Journal* **57**:945–956

Arsenault JL, Pouleur S, Messier C, Guay R. 1995. WinRHIZO™, a root-measuring system with a unique overlap correction method. *HortScience* **30**: 906

Boudon F, Preuksakarn C, Ferraro P, Diener J, Nikinma E, Godin C. 2013. Quantitative assessement of automatic reconstructions of branching systems. *Submitted*

Clark R T, Famoso A N, Zhao K, et al. 2012. High-throughput 2D root system phenotyping platform facilitates genetic analysis of root growth and development. *Plant Cell & Environment* **36**:454-466

Galkovskyi T, Mileyko Y, Bucksch A, et al. 2012. GiA Roots: software for the high throughput analysis of plant root system architecture. *BMC Plant Biology* **12**:116

Godin C, Caraglio Y. 1998. A multiscale model of plant topological structures. *Journal of Theoretical Biology* **191**

Le Bot J, Serra V, Fabre J, Draye X, Adamowicz S, Pagès L. 2010. DART: a software to analyse root system architecture and development from captured images. *Plant and Soil* **326**:261-273

Lobet G, Pagès L, Draye X. 2011. A Novel Image Analysis Toolbox Enabling Quantitative Analysis of System Architecture. *Plant Physiology* **157**:29-39

Naeem A, French AP, Wells DM, Pridmore TP. 2011. High-throughput feature counting and measurement of roots. *Bioinformatics* **27**:1337-1338

Preuksakarn C. 2012. *Reconstructing plant architecture from 3D laser scanner data*. Ph.D. thesis, University of Montpellier 2, France, 126 p.

WinRhizo, Pro, 2012b. http://www.regent.qc.ca/assets/winrhizo_software.html *Regent Instruments Inc., Canada*.

Zeng, G., Birchfield, S.T., Wells, C.E. 2008. Rapid automated detection of roots in minirhizotron images. *Machine Vision and Applications* **21:**309–317.

Proceedings of the 7th International Conference on Functional-Structural Plant Models, Saariselkä, Finland, 9 - 14 June 2013. Eds. Risto Sievänen, Eero Nikinmaa, Christophe Godin, Anna Lintunen & Pekka Nygren. http://www.metla.fi/fspm2013/proceedings. ISBN 978-951-651-408-9.

Terrestrial LiDAR-based tree/stand model that can simulate light interception and photosynthesis of branches, individuals, and a stand

Kiyoshi Umeki* and Akira Kato
Graduate School of Horticulture, Chiba University, 648 Matsudo, Matsudo city, Chiba, Japan 271-8510
**correspondence*: umeki@faculty.chiba-u.jp

Highlights: We developed a tree/stand model that simulates light interception and photosynthesis of first-order branches individuals, and a stand. The architecture of modelled trees was generated using tree skeletons (a main trunk and basal part of first-order branches) extracted from terrestrial LiDAR data and some architectural rules to add foliage to branches.

Keywords: first-order branch, light interception, photosynthesis, terrestrial LiDAR, tree architecture

Although terrestrial LiDAR has been used to extract architectural information of trees (e.g. Kato et al. 2011), the obtained architectural information has been rarely used in functional-structural plant models. In this study, we developed a tree/stand model by combining the tree skeletons extracted from terrestrial LiDAR data and some architectural rules describing extension of foliage of branches (Delagrange and Rochon 2011) in order to simulate light interception and photosynthesis of branches, individuals, and a stand.

We obtained 3D point cloud data for eight *Betula platyphylla* trees (14.6 – 18.3 m in height) using a terrestrial LiDAR, and extracted architectural information of main trunk (3D position of stem base and tip of main trunk) and first-order branches (position, diameter, and direction of branch). We also measured length, width, and thickness of foliage of 129 first-order branches and obtained architectural rules to predict the expansion of branch foliage from the basal branch diameter that was extracted from LiDAR measurements. We added the predicted foliage to extracted tree skeletons to obtain tree mock-ups (Fig. 1), and voxelized them (Fig. 2). The hourly amount of light intercepted by voxels was determined by a ray tracing method, and converted to hourly photosynthetic gain. The Hourly photosynthetic gains of voxels were summed up to obtain values for branches, individuals, and a stand.

The developed model calculated diurnal changes in photosynthetic gains of branches realistically including the effect of mutual shading among branches belonging to the same and neighbouring individuals (Fig. 3).

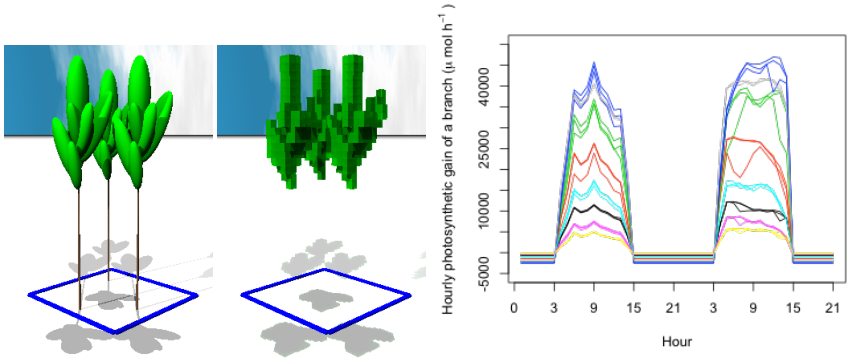

Fig. 1 (left). Modelled trees.
Fig. 2 (center). Voxelized foliage.
Fig. 3 (right). Predicted hourly photosynthetic gain of branches.

LITERATURE CITED

Delagrange S, Rochon P. 2011. Reconstruction and analysis of a deciduous sapling using digital photographs or terrestrial-LiDAR technology. Annals of Botany108: 991–1000.

Kato A, Moskal LM, Kobayashi T. 2011. Effect of scan coverage on stem diameter measurement using terrestrial lidar. Proceedings of Silvilaser, Hobart, Australia.

Proceedings of the 7th International Conference on Functional-Structural Plant Models, Saariselkä, Finland, 9 - 14 June 2013. Eds. Risto Sievänen, Eero Nikinmaa, Christophe Godin, Anna Lintunen & Pekka Nygren. http://www.metla.fi/fspm2013/proceedings. ISBN 978-951-651-408-9.

Fast automatic method for constructing topologically and geometrically precise tree models from TLS Data

Pasi Raumonen[1*], Eric Casella[2], Mathias Disney[3], Markku Åkerblom[1] and Mikko Kaasalainen[1]
[1]*Department of Mathematics, Tampere University of Technology, P.O. Box 553, 33101, Tampere, Finland*
[2]*Sustainable Forestry and Climate Change, Forest Research Agency, Surrey GU10 4LH – UK*
[3]*Department of Geography, University College London, London WC1E 6BT, United Kingdom*
**correspondence:* pasi.raumonen@tut.fi

Highlights: We present a computational method that produces automatically precision models of trees from terrestrial laser scanning (TLS) data. The method is fast, typically few minutes per tree, and the resulting model contains both the topological and geometrical information of the tree. The method is validated using artificial and real TLS data. The results show that TLS together with computational reconstruction method provides fast and nondestructive means to collect structural information of trees.

Keywords: Tree models, TLS, topological branching structure, branch size distribution

INTRODUCTION

Scanning the surface of a tree with terrestrial laser scanning (TLS) produces easily and quickly a point cloud with millions of measurements, which form a dense and comprehensive sample of the tree surface. The sample contains information of the topological and geometrical structure of the measured tree. Retrieving this information requires computational methods to process the data (van Leeuwen et al.).

We have presented a fast and automatic method producing a tree model containing practically any external structural information of woody parts of the tree (Raumonen et al., Åkerblom et al.). In the method the point cloud is segmented into trunk and branches and then the segments are approximated flexibly with multiple cylinders or their generalizations such as cones. From the resulting tree model one can approximate e.g. the volumes, lengths, and taper of trunk and branches, branch size distribution, branching angles and frequency, branching structure, etc. The method works even when there are some small gaps in the measurement cover and the trunk and branches are not measured all around.

THE METHOD

In the method the point cloud is first partitioned into small subsets corresponding to connected patches on the tree surface. These subsets form easy-to-handle sample of the tree surface and their size needs to be small enough to capture all the details. Geometrical and topological properties of the sets, such as the neighbor-relation and underlying branch direction, are easy to determine. With these known local details the unknown global tree structure can be reconstructed. First, possible points not part of the tree, such as the measurements from the ground, are automatically removed and the base of the trunk is determined. Because some branches will often shadow other parts of the tree, there are often lots of gaps in the measurement cover and thus the subsets are in multiple connected components. To get the subsets into one component, connections between close by components are formed by updating the neighbor-relation. Then using the neighbor-relation, one can locally expand along the tree surface and recognize bifurcations. This way the subsets are automatically partitioned into segments corresponding to pieces of the trunk and branches: each segment is connected and has no bifurcations, ideally corresponding to a real branch (see Figs. 1 and 2). The segmentation starts from the base of the trunk and proceeds hierarchically separating each branch from its sub-branches. Next the surface of every segment is reconstructed with cylinders using least squares fitting. Also generalized cylinders such as cones and deformed cylinders can be used for the surface reconstruction. Finally, possible gaps between cylinders can be filled with new cylinders and the branching structure can be updated.

VALIDATION

For validation and controlled testing of the reconstruction method we will use an artificial tree model with simulated scanning to produce point clouds. We also use a real eucalyptus tree (see Fig. 2) and laser scanning in a laboratory. The 3D structural tree model used here represents a 30 yr old Scots pine tree (see

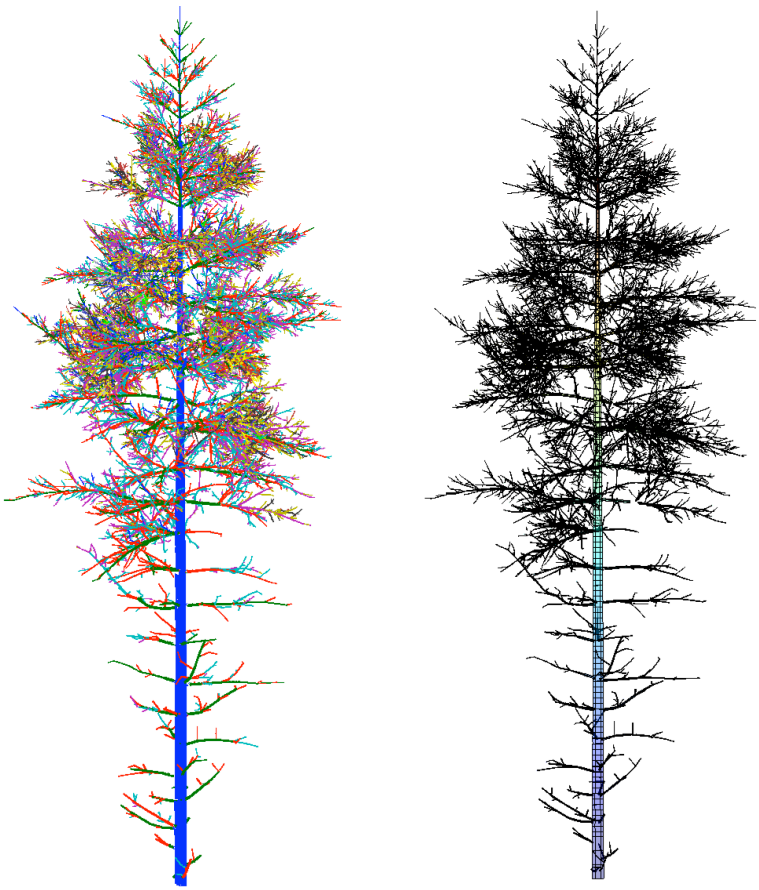

Fig. 1. Segmented point cloud (left) and the reconstructed cylinder model (right) of the artificial Scots pine. The point cloud contains measurements from tree scanning positions. Model reconstruction time: 8 min.

Fig. 1). The model is generated using an empirical growth model parameterized by species-dependent branching statistics in conjunction with specified external environmental conditions (Leersnijder). TLS point clouds were simulated using the librat Monte Carlo ray tracing code (Disney et al.). For the artificial tree model we know the cylinders defining it, thus we know all the same attributes as in our reconstructed models. In the eucalyptus the mass (corresponds to volume) of the branches and the trunk is measured. We will test how well the reconstructions correspond to original tree attributes (geometrical and topological) and how the reconstructions depend on the number of scanning positions and density. For the eucalyptus we have used 1 to 4 scanning positions and three different scanning resolutions with angular sampling resolutions of 0.036 (low), 0.018 (mid) and 0.009 (high) degrees.

RESULTS AND DISCUSSION

Figs. 1 and 2, showing the segmented point clouds and the reconstructed models, show that most of the tree structures are reconstructed faithfully. Particularly for the pine the reconstruction and original model have 100 and 99 first order branches, respectively. The reconstructions of the trunk and large branches are nearly perfect. For the smallest pine branches the measurement cover is too sparse to get meaningful reconstructions (cf. branch lengths and number of branches in Table 1). For the eucalyptus the results (see Table 1) show that the more scanning positions the better the cover is and more branches are revealed. Similarly for the scanning density: higher density reveals more branches. The volume and length of the trunk are quite well reconstructed in all cases. For branches the reconstructed volume is much larger compared to the measured one, but the situation is more complex. Most of the branches in this case are smaller or comparable with the size of the laser spot, which is about few millimeters in size. Also there is few millimeters error when different scans are registered into one coordinate system. Thus in this case the reconstruction of the radius and thus the volume is not accurate for branches. However, the branching structure and the lengths of the branches can be still reconstructed with much less error.

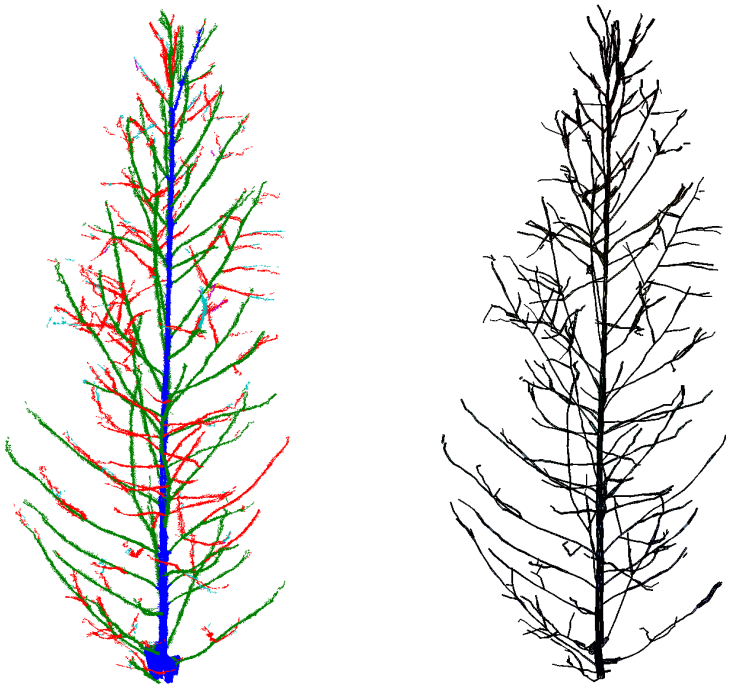

Fig. 2. Segmented point cloud (left) and the reconstructed cylinder model (right) of the eucalyptus fixed in a stand. The point cloud contains measurements from three high-resolution scans. Model reconstruction time: 30 sec.

Table 1. Some tree attributes for the pine and eucalyptus. For the eucalyptus there is measured values and reconstructed values with 1, 2, 3, and 4 scanning positions with "high" resolution and also for 2 scanning positions there are reconstructed values for "low" and "mid" resolutions.

	tot. vol. (dm^3)	trunk vol. (dm^3)	branch vol. (dm^3)	trunk length (m)	branch length (m)	Number of branches
Pine original	651	348	303	17.2	2623	13607
Pine reconstructed	758	349	409	17.2	2109	7799
Euca measured	3.7	3.2	0.5	4.5		
Euca 1 pos. high res.	6.6	3.6	3.0	4.5	62	137
Euca 2 pos. high res.	7.1	3.0	4.1	4.5	77	209
Euca 3 pos. high res.	6.7	2.8	3.9	4.5	82	255
Euca 4 pos. high res.	9.5	2.8	6.7	4.5	87	317
Euca 2 pos. mid res	7.4	2.8	4.6	4.5	48	94
Euca 2 pos. low res.	8.6	2.6	6.0	4.4	26	41

ACKNOWLEDGEMENT

We thank Sanna Kaasalainen and Harri Kaartinen for providing measured TLS data from trees for development and validation of the method.

LITERATURE CITED

Disney M, Lewis P, Saich P. 2006. 3D modelling of forest canopy structure for remote sensing simulations in the optical and microwave domains. *Remote Sensing of Environment*. **100**: 114-132.

Leersnijder R.P. 1992. *PINOGRAM: A pine growth area model*. WAU dissertation 1499, Wageningen Agricultural University, The Netherlands.

van Leeuwen M, Nieuwenhuis M. 2010. Retrieval of forest structural parameters using lidar remote sensing. *European Journal of Forest Research*. **129**: 749-770.

Raumonen P, Kaasalainen M, Åkerblom M, Kaasalainen S, Kaartinen H, Vastaranta M, Holopainen M, Disney M, Lewis P. 2013. Fast Automatic Precision Tree Models from Terrestrial Laser Scanner Data. *Remote Sensing*.

Åkerblom M, Raumonen P, Kaasalainen M, Kaasalainen S, Kaartinen H. 2012. Comprehensive quantitative tree models from TLS data. *Geoscience and Remote Sensing Symposium (IGARSS) 2012*, 6507-6510.

Proceedings of the 7th International Conference on Functional-Structural Plant Models, Saariselkä, Finland, 9 - 14 June 2013. Eds. Risto Sievänen, Eero Nikinmaa, Christophe Godin, Anna Lintunen & Pekka Nygren.
http://www.metla.fi/fspm2013/proceedings. ISBN 978-951-651-408-9.

A geometrical model generator for quasi-axisymmetric fruit

Seppe Rogge*, Shiferaw Beyene, Els Herremans, Thijs Defraeye, Pieter Verboven, Bart Nicolai
Flanders Centre of Postharvest Technology / BIOSYST-MeBioS, University of Leuven, Willem de Croylaan 42, B-3001, Leuven, Belgium
**correspondence:* seppe.rogge@biw.kuleuven.be

Highlights: A geometrical model generator for fruit is presented. The generator uses X-ray tomography images of quasi-axisymmetric fruit as input, describes the shape of the fruit with elliptical Fourier descriptors, and uses statistical analysis to randomly generate new representative fruit shapes from this dataset, which can be directly used as CAD models for CFD or FEM analysis.

Keywords: elliptic Fourier descriptors, shape description, shape generation, biological variability

INTRODUCTION

Structure, shape and size are significant features of plant organs for gas and water exchange in relation to physiological processes such as growth (Abera et al., 2012), respiration (Ho et al., 2011) and photosynthesis (Ho et al., 2012), as well as to postharvest quality of plant products such as fruit (Jancsók et al., 2001; Nguyen et al., 2006; Veraverbeke et al., 2006; Delele et al., 2008, 2009; Ambaw et al., 2012). However, realistic descriptors and models of the geometry of biological products are not always available, and complex shapes are often replaced by basic geometries, like ellipsoids (Rashidi & Gholami, 2008) or spheres (Delele et al., 2008, 2009; Ambaw et al., 2012).

2D shape description and representation of complex shapes has recently been achieved (Costa et al., 2011; Moreda et al., 2012). A popular way to describe the contour of a 2D image are Fourier descriptors (FD). FD have some advantages compared with other methods: the descriptors are simple to compute, they have a physical meaning, and they capture both global and local features (Zhang & Lu, 2004). Mebatsion et al. (2011) described the contour of sections of plant organs with these descriptors, and interpolated different contours to construct 3D models of the plant organs. The more complex the shape, the higher the number of contours used for one image. A drawback of this method is its destructive nature. New techniques, such as MRI (magnetic resonance imaging) and X-ray tomography reveal the inner and outer structure of biological material in a non-destructive way (Lammertyn et al., 2003; Herremans et al., 2013). Furthermore, shape description analysis on a set of products opens perspectives to automatic generation of random shapes, based on statistical analysis of the dataset, but has not been explored yet. The resulting database of biological products could introduce biological shape variability, as present in reality, into numerical simulations.

Here, we present a geometrical model generator for apple fruit based on X-ray tomography of whole apples; once a limited number of fruit shapes is analysed by means of FD, an unlimited amount of new shapes, representing the variability of a certain species or even cultivar, can be generated. The procedure was entirely coded in Matlab (The MathWorks Inc., Natick, MA), and the amount of necessary manual intervention was reduced to a minimum.

METHODOLOGY

The geometrical model generator consists of two parts: in the first part, shapes are analysed by means of FD, and in the second part, new models are generated based on the FD statistics. The input dataset consists of X-ray computed tomography (CT) scans of 73 Braeburn apples. For each apple, a cross section image was constructed. This section was chosen manually in such a way that it always contains the centre of the apple, and that the stem appears as little as possible in the image. Large stems cannot appear in the image, because they are curved and disrupt the (quasi-)symmetry of the apple that results in 3D shape artefacts, when generating a new fruit shape. The contour of the section was extracted by Matlab's built-in edge detection and boundary tracing routines.

Fourier descriptors were calculated from the contours. In this study, elliptic Fourier descriptors (EFD) introduced by Kuhl and Giardina (1982), were applied. The important advantage of this type of FD is that they can deal with outlines that curve back on themselves. The number of computed EFD is a multiple of four: a sine and a cosine term both in the r and z-direction (cylindrical coordinates). From sensitivity

analysis, 25x4 descriptors were found to be sufficient; higher order descriptors represented unnecessary details in the contour. In the resulting 3D model, fluctuations in the r and z-direction should not be too prominent compared with those in the θ-direction. From the 73 sets of FD, a new set of FD with the average value of each descriptor, and the covariance matrix of all descriptors, was calculated.

With the covariance decomposition method described in Alabert (1987), new 2D geometrical contours were generated, using the descriptor averages and the covariance matrix. The first step towards making a 3D model of the new set of descriptors was calculating the EFD of its mirror image along the axis of (quasi)symmetry. Subsequently, a number of new FD sets was generated by interpolating between these two sets of descriptors. Each set is then converted to a contour (see Figure 1). Next, the contours are rotated around the axis of symmetry at an angle between 0 and π. An example with only 20 (for clarity) half-contours can be seen in Figure 2a. This way, a smooth 3D shape is created by interpolation. The final step was creating a NURBS surface, that fits to the set of datapoints, and exporting this surface as an IGES file, a file format which can be directly used as a CAD input in numerical software for modelling transport and physiological processes.

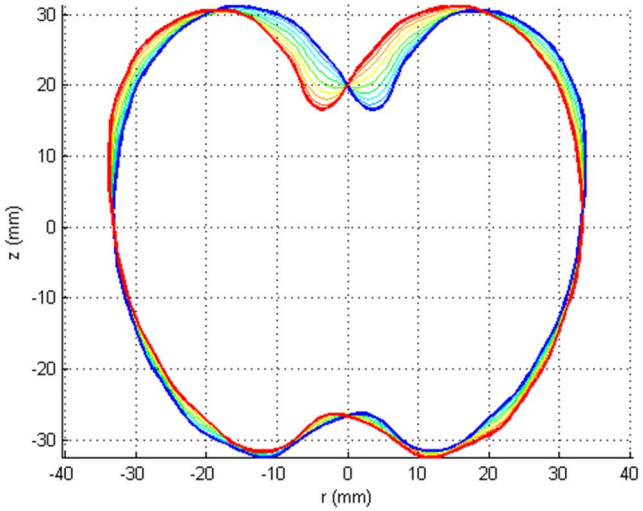

Fig. 1. A newly generated contour (thick blue line), the mirror image of this contour (thick red line), and contours created by interpolating between the two sets of EFD of these contours (small lines). Only 10 contours are shown for clarity.

RESULTS AND DISCUSSION

A resulting apple shape can be seen in Figure 2b. The quality of the generated shapes was tested by comparing the volumes of the original 73 Braeburn apples with the volumes of the generated shapes. For this purpose, 1000 new shapes were generated. They had an average volume of 208 cm³, with a standard deviation of 36 cm³, while the original apples had an average volume of 208 cm³, with a standard deviation of 31 cm³.

The perfect agreement of the average volume of the generated shapes with that of the real fruit indicates that the shape generator is a stable algorithm. The slightly higher spread in volumes, on the other hand, can be explained by the fact that only one section is used to generate a new shape. In real apples, cross-sections with a small or large surface will be somewhat averaged out by the other cross-sections.

It should be noted that some of the generated shapes do not represent realistic apple shapes with smooth axisymmetric features. These shapes originate particularly when asymmetric contours are revolved. Nevertheless, the majority of the shapes (roughly 80%) are good-quality (both shape and size) apple-like shapes; bad shapes can easily be excluded by the user.

In conclusion, a geometrical model generator for quasi-axisymmetric shapes is presented. The method is found to be fast and requires little human intervention. The resulting output are generally realistic apple shapes, which are exported in the form of CAD models, that can easily be used for numerical simulations.

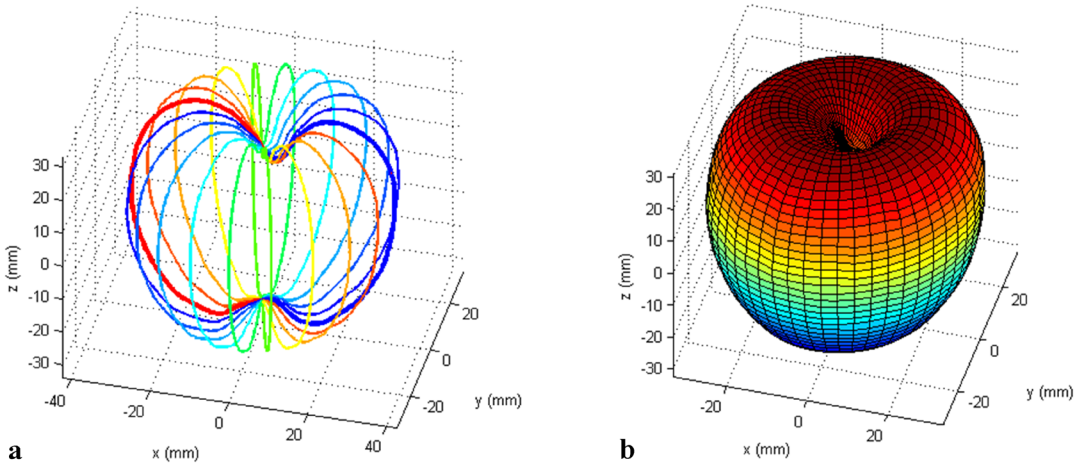

Fig. 2. New 3D generated shape of an apple. a) Contours revolved around the rotation axis. The thick blue line at the right and the thick red line at the left describe the original contour. Only 20 half-contours are shown for clarity. b) NURBS surface fitted to the revolved contours.

LITERATURE CITED

Abera MK, Fanta SW, Verboven P, Ho QT, Carmeliet J, Nicolai BM. 2012. Virtual Fruit Tissue Generation Based on Cell Growth Modelling. *Food and Bioprocess Technology* in press DOI: 10.1007/s11947-011-0775-4.

Alabert F. 1987. The practice of fast conditional simulations through the LU decomposition of the covariance matrix. *Mathematical Geology* **19**:369-386.

Ambaw A, Verboven P, Delele MA, et al. 2012. CFD Modelling of the 3D Spatial and Temporal Distribution of 1-methylcyclopropene in a Fruit Storage Container. *Food and Bioprocess Technology* in press DOI: 10.1007/s11947-012-0913-7.

Costa C, Antonucci F, Pallottino F, Aguzzi J, Sun DW, Menesatti P. 2011. Shape analysis of agricultural products: A review of recent research advances and potential application to computer vision. *Food and Bioprocess Technology* **4**:673-692.

Delele MA, Tijskens E, Atalay YT, et al. 2008. Combined discrete element and CFD modelling of airflow through random stacking of horticultural products in vented boxes. *Journal of food engineering* **89**:33-41.

Delele MA, Schenk A, Tijskens E, Ramon H, Nicolai BM, Verboven P. 2009. Optimization of the humidification of cold stores by pressurized water atomizers based on a multiscale CFD model. *Journal of food engineering* **91**:228-239.

Herremans E, Verboven P, Bongaers E, et al. 2013. Characterisation of 'Braeburn' browning disorder by means of X-ray micro-CT. *Postharvest Biology and Technology* **75**:114-124.

Ho QT, Verboven P, Verlinden BE, et al. 2011. A three-dimensional multiscale model for gas exchange in fruit. *Plant physiology* **155**:1158-1168.

Ho QT, Verboven P, Yin X, Struik PC, Nicolai BM. 2012. A microscale model for combined CO2 diffusion and photosynthesis in leaves. *PloS one* **7**:e48376. doi:10.1371/journal.pone.0048376

Jancsók PT, Clijmans L, Nicolai BM, De Baerdemaeker J. 2001. Investigation of the effect of shape on the acoustic response of 'conference'pears by finite element modelling. *Postharvest biology and technology* **23**:1-12.

Kuhl FP, Giardina CR. 1982. Elliptic Fourier features of a closed contour. *Computer graphics and image processing* **18**:236-258.

Lammertyn J, Dresselaers T, Van Hecke P, Jancsók P, Wevers M, Nicolai BM. 2003. Analysis of the time course of core breakdown in 'Conference' pears by means of MRI and X-ray CT. *Postharvest biology and technology* **29**:19-28.

Mebatsion H K, Boudon F, Godin C, et al. 2011. A novel profile based model for virtual representation of quasi-symmetric plant organs. *Computers and Electronics in Agriculture* **75**:113-124.

Moreda GP, Muñoz MA, Ruiz-Altisent M, Perdigones A. 2012. Shape determination of horticultural produce using two-dimensional computer vision–A review. *Journal of Food Engineering* **108**:245-261.

Nguyen TA, Dresselaers T, Verboven P, et al. 2006. Finite element modelling and MRI validation of 3D transient water profiles in pears during postharvest storage. *Journal of the Science of Food and Agriculture* **86**:745-756.

Rashidi M, Gholami M. 2008. Determination of kiwifruit volume using ellipsoid approximation and image-processing methods. *International Journal of Agriculture & Biology* **10**:375–380

Veraverbeke EA, Verboven P, Lammertyn J, Cronje P, De Baerdemaeker J, Nicolai BM. 2006. Thermographic surface quality evaluation of apple. *Journal of food engineering* **77**:162-168.

Zhang D, Lu G. 2004. Review of shape representation and description techniques. *Pattern recognition* **37**:1-19.

Proceedings of the 7th International Conference on Functional-Structural Plant Models, Saariselkä, Finland, 9 - 14 June 2013. Eds. Risto Sievänen, Eero Nikinmaa, Christophe Godin, Anna Lintunen & Pekka Nygren.
http://www.metla.fi/fspm2013/proceedings. ISBN 978-951-651-408-9.

Automatic 3D plant reconstruction from photographies, segmentation and classification of leaves and internodes using clustering

Thiago Santos[1] and **Julio Ueda**[1]
[1]*Embrapa Agricultural Informatics, PO Box 6041, 13083-886 Campinas, Brazil*
**correspondence:* thiago.santos@embrapa.br

Highlights: A stereo approach for 3D plant modelling is presented. Using only a set of photographies, the method produces a dense 3D point cloud that samples the plant surface. Clustering automatically segments the plant structure into meaningful parts, which are classified as leaves or internodes. Measurements can be computed for each element, as area or surface normals.

Keywords: 3d plant models, image-based reconstruction, multiple view stereo, structure segmentation

INTRODUCTION

Non-invasive imaging and image analysis are novel technologies that have been employed to narrow the "phenotyping bottleneck". Three-dimensional plant models are traditionally acquired by invasive, slow and tedious manual measurements, aided by electromagnetic 3D tracking devices. Laser scanning figures as an alternative (Preuksakarn *et al.*, 2010; Delagrance and Rochon, 2011), but it presents some drawbacks as sensitivity to occlusion, lack of color and texture information and the high price of the laser scanning devices. A generated 3D point cloud must be properly segmented and classified for automatic measurement and characterization of the plant structure. Stereo-based techniques are emerging as a cheap and non-invasive alternative for 3D modelling of plants (Quan *et al.*, 2006; Biskup *et al.*, 2007; Santos and Oliveira, 2012). The present work extends our previous work (Santos and Oliveira, 2012) by (a) segmenting the plant models in significant structures using clustering in 3D space, (b) classifying the recovered segments into meaningful classes (leaves and internodes) and (c) performing area measurements in the model and comparing them against ground-truth data, validating the framework as an effective metrology tool.

MATERIAL

A set of 387 pictures of a mint specimen (*Mentha*) was acquired by a Canon Powershot G11 camera placed in different positions (see Fig. 1A and Fig. 1B). The potted specimen was photographed indoors, avoiding movements caused by wind. After the image acquisition step, the leaves were removed and placed in a table scanner to acquire the area measurements used as ground-truth.

METHOD

The proposed technique is composed by the following steps:

Multiple view stereo plant reconstruction – The method input is a set of several high-resolution photographies for each specimen. Camera position is automatically recovered by *structure from motion*. First, the SIFT algorithm (Lowe, 2004) is employed to detect and describe *image features* in each photography. The feature descriptors are used to find matches between features in different images. Projective reconstruction and robust estimation techniques (Hartley and Zisserman, 2003) are employed to define the relative position between images, i.e., the position of the camera at each image acquisition (Fig. 1B). Once each camera pose is defined, a *sparse* 3D point cloud for the plant surface is produced based on feature matching. Finally, a region growing multiple view stereo technique is employed to produce a *dense* 3D point cloud (Fig. 1C). Santos and Oliveira (2012) present a more detailed description of this 3D reconstruction step.

Segmentation by clustering of surface normals – The dense point cloud is segmented using a smoothness constraint, as proposed by Rabbani *et al.* (2006). First, the surface normals are estimated at each point p_i. This estimation is performed by finding a plane tangent to the surface by least-squares plane fitting, using the points in the neighbourhood of p_i. Then a region growing algorithm is applied: for a point p_i in a segment R, each neigh point p_j is added to R if the angle between the normal vectors of p_i and p_j is inferior to a

threshold θ. This process is repeated until every point is assigned to a region. The detailed algorithm can be found in Rabbani *et al.* (2006).

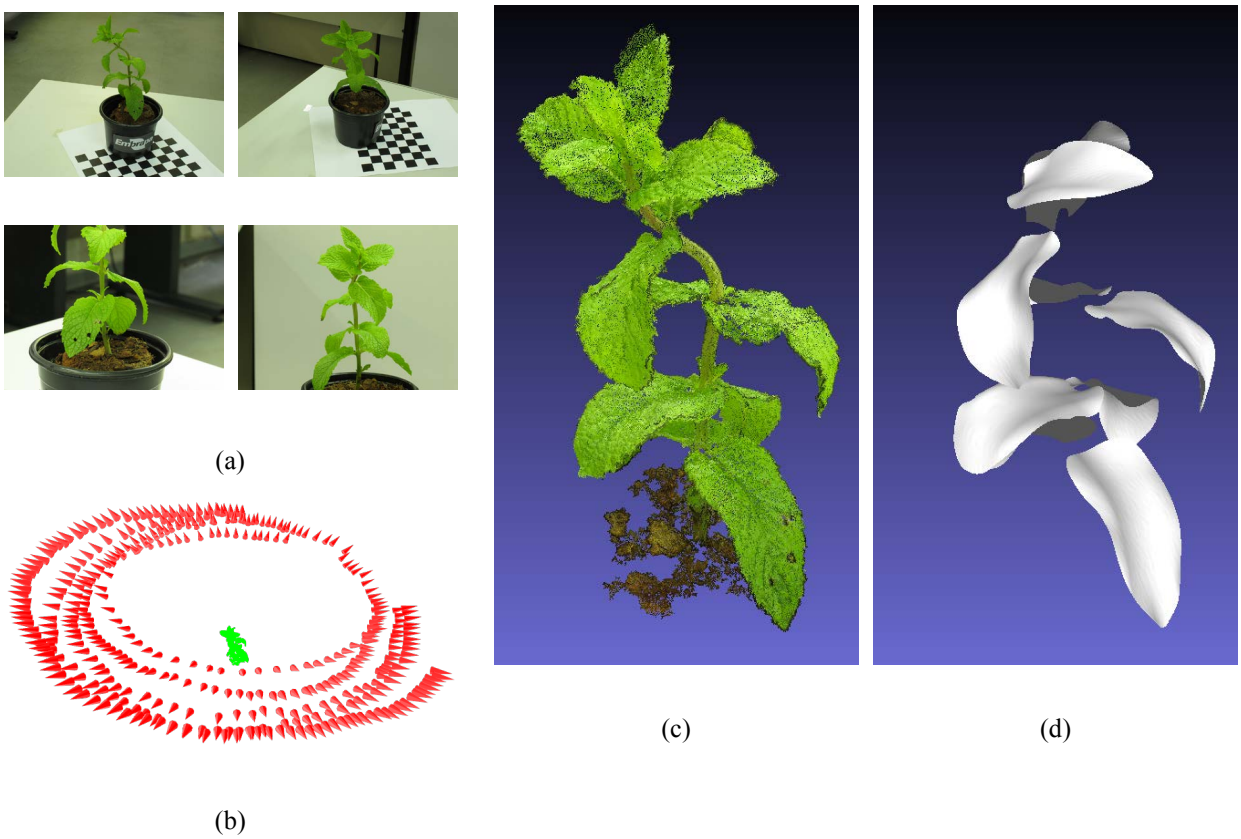

Fig. 1. Results for the *mint* dataset. (a) Input images acquired from different angles. (b) Result from the structure from motion step: camera poses (red cones) and a sparse point cloud for the plant (green). (c) Result from the multiple view stereo step, a dense point cloud sampling of the plant surface. (d) Smooth surfaces for the largest leaves, computed using the NURBS fitting procedure, after leaf segmentation and classification.

Classification using width/length ratio – Each segment is composed by a set of 3D points. Features can be computed from this set for segment characterization and further classification. For the specimen used in this work, the recovered segments correspond to leaves, internodes or spurious structures, as fragments from soil. These classes can be easily discriminated using their size and dimensions. Taking each point in the segment as a three-dimensional vector $p_i = (x_i, y_i, z_i)$, principal component analysis (PCA) was applied. In the transformed space, the ordered variances were used to describe the segments' dimensions in their main axes. A simple linear classifier was able to classify the leaves, if properly segmented.

Leaf surface fitting using NURBS – Leaves surfaces were approximated by NURBS fitting (Piegl, 1991), getting a smooth and regularized 3D mesh representing the surface (Fig. 1D).

RESULTS

Fig. 1B shows the recovered camera poses and sparse 3D model produced by structure from motion. The chessboard observed in Fig. 1A is generally used in computer vision for camera calibration, but in the present experiment it is employed just to define the scale factor for the final model – the leaves' textures and edges provide all the image features needed for the camera pose estimation. Fig. 1C shows the 3D dense point cloud produced by the multiple view stereo step. After cloud segmentation and classification, the largest leaves were successfully identified. Small leaves were sub-sampled in the point cloud, resulting in over-segmentation and misclassification. A smoothed surface was produced for each one of the correct leaves by NURBS fitting. Table 1 shows the estimated area vs. the ground-truth data.

Table 1. The 3D model as a measurement tool. Individual leaf area computed on the the smooth NURBS surfaces vs. ground-truth produced using a common scanner.

Leaf/Area (mm²)	Ground-truth	Computed on the 3D model	Difference
1	1434.48	1510.60	5.31%
2	1464.68	1500.91	2.47%
3	1144.59	1167.69	2.02%
4	1157.50	1177.38	1.72%
5	1007.02	1005.48	-0.15%
6	791.39	735.33	-7.08%
7	899.51	956.64	6.35%
8	954.69	1079.98	13.12%
9	660.58	660.68	0.02%

CONCLUSION

In the proposed methodology, a free moving camera is able to capture the plant structure from different views, differently of Biskup *et al.* (2007) fixed-camera approach. The structure is recovered only from image data, without human intervention as the branches sketches employed by Quan *et al.* (2006). The large number of input images should not be a problem because video acquisition is able to provide thousands of video frames that could be automatically selected. Further steps under development are (i) more extensive tests on different species, (ii) an interactive tool to help human operators to perform computer-aided video acquisition with feedback and (iii) an egomotion system based on structure from motion for robot path planning in automatized platforms.

FUNDING

This work was supported by Brazilian Agricultural Research Corporation (Embrapa) under grant [03.11.07. 007.00.00].

LITERATURE CITED

Biskup B, Scharr H, Schurr U, Rascher U. 2007. A stereo imaging system for measuring structural parameters of plant canopies. *Plant, Cell & Environment*, **30**:1299–1308.

Delagrange S, Rochon P. 2011. Reconstruction and analysis of a deciduous sapling using digital photographs or terrestrial-LiDAR technology. *Annals of botany*, **108**:991–1000.

Hartley R, Zisserman A. 2003. *Multiple View Geometry in Computer Vision*, 2th edn. Cambridge: Cambridge University Press.

Lowe DG. 2004. Distinctive Image Features from Scale-Invariant Keypoints. *International Journal of Computer Vision*, **60:**91-110.

Piegl L. 1991. On NURBS: a survey. *IEEE Computer Graphics and Applications*, **11**(1):55-71.

Preuksakarn C, Boudon F, Ferraro P, Durand J-B, Nikinmaa E, Godin, C. 2010. Reconstructing plant architecture from 3D laser scanner data . In *Proc. of the 6th Intl. Workshop on Functional-Structural Plant Models*, 14-16.

Quan L, Tan P, Zeng G, Yuan L, Wang J, Kang SB. 2006. Image-based plant modelling. *ACM Transactions on Graphics*, **25**: 599–604.

Rabbani T, van den Heuvel F, Vosselmann G. 2006. Segmentation of point clouds using smoothness constraint, In *International Archives of Photogrammetry, Remote Sensing and Spatial Information Sciences*, **36**(5):248–253.

Santos TT, Oliveira AA. 2012. Image-based 3D digitizing for plant architecture analysis and phenotyping. In *Workshop on Industry Applications (WGARI) in SIBGRAPI 2012 (XXV Conference on Graphics, Patterns and Images)*, 21-28. http://www.decom.ufop.br/sibgrapi2012/index.php/call/wgari.

Proceedings of the 7th International Conference on Functional-Structural Plant Models, Saariselkä, Finland, 9 - 14 June 2013. Eds. Risto Sievänen, Eero Nikinmaa, Christophe Godin, Anna Lintunen & Pekka Nygren. http://www.metla.fi/fspm2013/proceedings. ISBN 978-951-651-408-9.

Monitoring the diel growth of individual *Arabidopsis* leaves using a laser scanning approach

Tino Dornbusch*, **Olivier Michaud** and **Christian Fankhauser**
[1]*Center for Integrative Genomics, Faculty of Biology and Medicine, University of Lausanne, 1015 Lausanne, Switzerland*
**correspondence:* tino.dornbusch@unil.ch

Highlights: A novel phenotyping approach is presented to monitor diel variation in elongation and elevation angle of individual leaves with high precision and throughput. Leaf elongation and changes in leaf elevation angle follow characteristic diel rhythms and show an overall decrease with increasing leaf age.

Keywords: Arabidopsis, phenotyping, leaf growth, laser scanning

INTRODUCTION

During their life cycle, flowering plants are frequently facing fluctuating environmental conditions, which are often sub-optimal for growth. To cope with that, plants possess a range of adaptive growth responses and protection mechanisms.

The model plant *Arabidopsis thaliana* provides a good platform to link phenotypic plasticity to the function of specific genes, proteins or protein complexes. Indeed genetic resources are well explored and available tools are extremely well developed. On the other hand, phenotyping of leaf growth have largely depended on semi-automated two-dimensional (2D) image processing (Millenaar *et al.* 2005; Wiese *et al.* 2007; De Vylder *et al.* 2012). These methods are of limited throughput and usually restricted to analyze few time-points, since imaging (in particular at night) interferes with growth processes.

We have applied a laser scanning technique using the Scanalyzer HTS (Lemnatec GmbH, Würselen, Germany) to monitor the diel growth pattern of individual leaves. Laser scanner images of growing *Arabidopsis* plants were recorded at intervals of 10 to 60 minutes. Images, containing the 3D information of individual plants were processed. As principal output, length and elevation angle of individual leaves were computed.

MATERIAL AND METHODS

Plants were grown in pots filled with a mixture of peat-rich soil and vermiculite. Before their transfer to the Scanning device ScanAlyzer HTS (Lemnatec GmbH, Würselen, Germany) they were kept 10 days in a Percival CU-36 L4 incubator (Percival Scientific Inc., Perry, IA, USA). The photoperiod was 16 h. Relative humidity inside the Percival incubator was between 80-85% and temperature was maintained at 21°C. More detailed information on growth conditions and laser scanning protocol are given by Dornbusch et al. (2012). Plants were imaged over a period of 9 days. Images were taken each 60 min. The image-processing pipeline to extract geometric features of individual leaves is illustrated in Figure 1. As a result, length l and elevation angle φ are displayed as function of time t.

RESULTS AND DISCUSSION

As an example, we present here the growth pattern of the first four leaves (two cotyledons not counted) by looking at the diel pattern of leaf elongation (l_{tip}, Fig. 2a) and leaf elevation angle (φ_{tip}, Fig. 2b) for the first four leaves (leaf 4 being the youngest). Leaf 1,2 developed at the same time and grew at similar rates. At day 4, the younger leaves 3 and 4 were shorter than leaf and 2, but they were expanding at a higher rate during this specific period and became longer starting from day 6. Leaf elongation was reduced during night periods and increased shortly after dawn (Fig. 2a) and generally decreased with increasing leaf age.

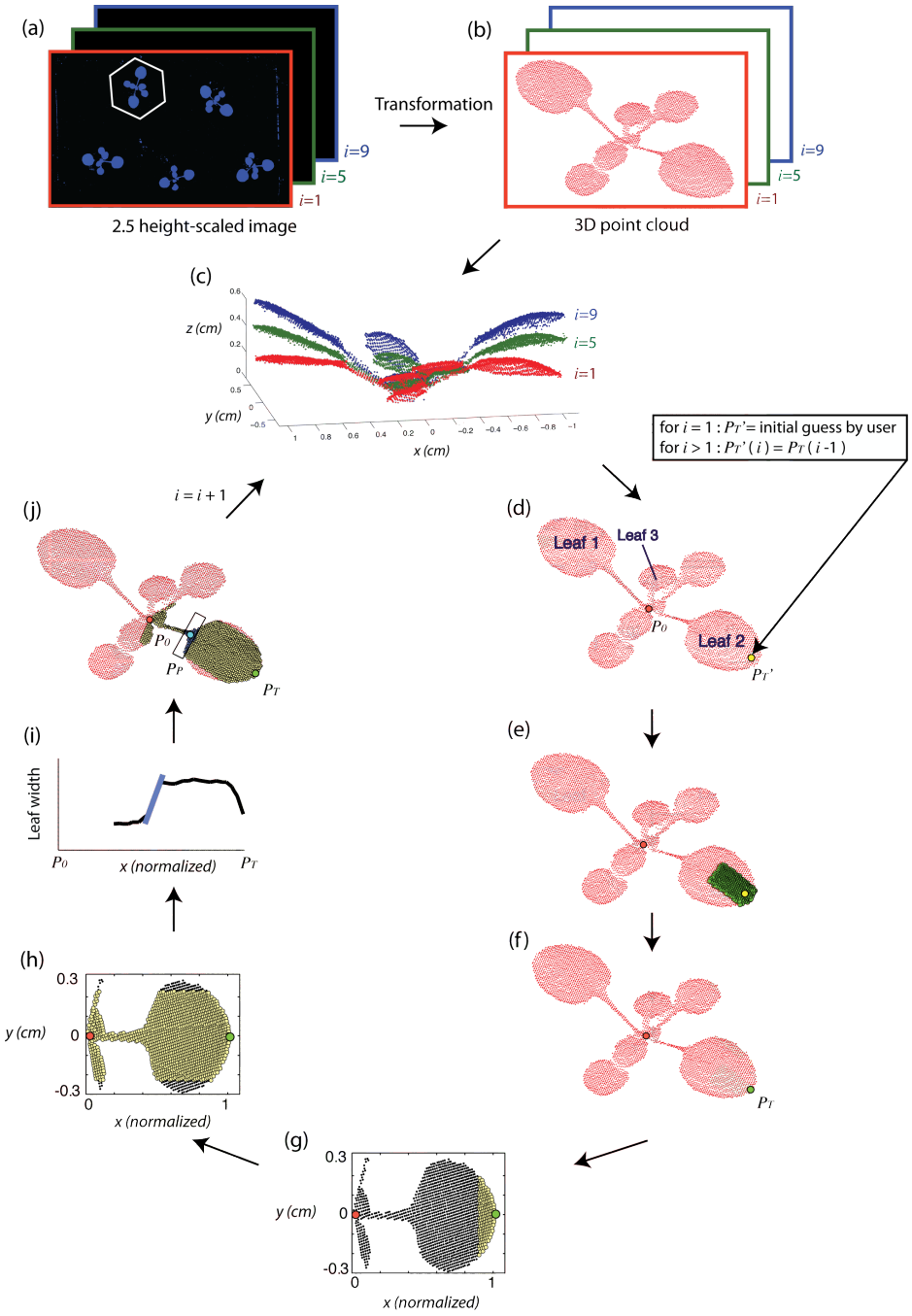

Fig. 1. Flow chart representing the different steps of the developed image processing algorithm: **(a)** 2.5D height-scaled images of plants, which are transformed into 3D point clouds, recorded at different scanning or iteration steps *i*. 3D point clouds of individual plants are obtained by segmentation, **(b)** 3D point cloud of the plant circled in Fig. 2a (example here for illustrating the following algorithm), **(c)** superimposition of point clouds of the plant in (b) at different iteration steps *i*, **(d)** As first step of the iterative loop: P_T' is determined by the user if i =1 or P_T'=P_T (i -1) if i > 1, **(e)** result of the filtering with the selection of points (in green) that are in a defined area around P_T', **(f)** computation of $P_T(i)$ from filtered points, **(g)** Point cloud in (f) rotated and normalized such that $P_T(i)$ = [1,0,0]. The considered leaf is hence in the *x*-*y* plane. In yellow, points nearby the tip of the leaf, **(h)** same projection than in (g). In yellow, points resulting from an additional filtering, which should cover most of the leaf surface (leaf 2 here), **(i)** Computing the maximum of the first derivative of the 'width' of the leaf, **(j)** Obtaining $P_P(i)$, which is the centroid of the set of points close to the computed max. derivative (highlighted by the black box); Having computed $P_T(i)$ and $P_P(i)$, the point cloud of the next time step *i+1* is processed, initiating the same loop (d) to (i) using P_T (i -1) as input for (d). Note that apart from the first iteration step i=1, the algorithm is fully automated.

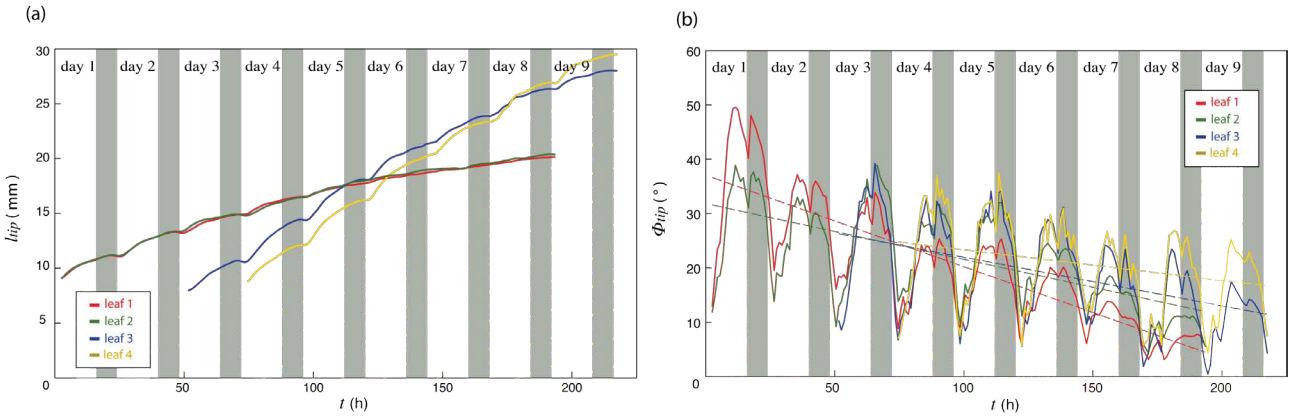

Fig. 2. **(a)** Mean leaf length l_{tip} and **(b)** leaf elevation angle Φ_{tip} for leaves 1 to 4 plotted against time (t). Grey bands represent night periods**.** One curve represents the mean value computed from 5 individual leaves, which were tracked over the whole period. The dashed lines in (b) represent the trend lines to illustrate the decreasing leaf angle.

In general, leaves followed a sinusoidal diel pattern of leaf elevation angle (φ_{tip}), being most horizontal in the early morning and most vertical in the evening (Fig. 2b). An abrupt upward movement of leaves (increase in φ_{tip}) was measured at day-night transitions for all four leaves throughout the whole period. There was a clear trend of decreasing φ_{tip} with increasing leaf age (dashed lines in Fig 2b). At the same time the maximal difference in elevation angle (amplitude during 24 h) was also reduced with leaf age (Fig. 2b) in the same fashion as leaf elongation (Fig. 2a).

This leads to the interesting question to what extent leaf elongation and concomitant changes in leaf angle of *Arabidopsis* leaves are linked and rely on the same growth mechanisms. For instance, Schuster and Engelmann (1997) have shown that circumnutations in hypocotyls (similar to changes in elevation angle in leaves) were more prominent for young hypocotyls growing at faster rates. To the best of our knowledge, no comparable study has been done for *Arabidopsis* leaves.

To conclude, we have presented a non-invasive methodology that allows phenotyping of individual *Arabidopsis* leaves at high temporal and spatial resolution. The throughput is compatible with genetic screens and, in combination, both would allow to unravel molecular mechanisms behind the dynamic aspects of leaf growth.

LITERATURE CITED

De Vylder J, Vandenbussche F, Hu Y, Philips W, VanDerStraeten D. 2012. Rosette Tracker: an open source image analysis tool for automatic quantification of genotype effects. *Plant Physiology* **160**:1149-1159.

Dornbusch T, Lorrain S, Kuznetsov D, Fortier A, Liechti R, Xenarios I, Fankhauser C. 2012. Measuring the diurnal pattern of leaf hyponasty and growth in Arabidopsis–a novel phenotyping approach using laser scanning. *Functional Plant Biology* **39**:860-869.

Millenaar F, Cox M, van Berkel Y. 2005. Ethylene-induced differential growth of petioles in Arabidopsis. Analyzing natural variation, response kinetics, and regulation. *Plant Physiology* **137**:998-1008.

Schuster J, Engelmann W. 1997. Circumnutations of Arabidopsis thaliana seedlings. *Biological Rhythm Research* **28**: 422-440.

Wiese A, Christ MM, Virnich O, Schurr U, Walter A. 2007. Spatio-temporal leaf growth patterns of Arabidopsis thaliana and evidence for sugar control of the diel leaf growth cycle. *New Phytologist* **174**:752-761.

Proceedings of the 7th International Conference on Functional-Structural Plant Models, Saariselkä, Finland, 9 - 14 June 2013. Eds. Risto Sievänen, Eero Nikinmaa, Christophe Godin, Anna Lintunen & Pekka Nygren. http://www.metla.fi/fspm2013/proceedings. ISBN 978-951-651-408-9.

A Blender addon for the 3-d digitizer FASTRAK for plant structure acquisition

Katarzyna Wasilczuk,[1] **Michael Henke,**[1] **Katarína Smoleňová,**[1] **Yongzhi Ong**[1] and **Winfried Kurth**[1]*
[1]*Department Ecoinformatics, Biometrics and Forest Growth, Georg-August University of Göttingen, Büsgenweg 4, 37077 Göttingen, Germany*
**correspondence:* wk@informatik.uni-goettingen.de

Highlights: An addon for the open-source 3-d graphical modelling software Blender was implemented. It enables communication with the electromagnetic 3-d digitizer FASTRAK via a serial interface. Discrete and continuous point acquisition mode, immediate visualization in Blender's 3-d view, acoustic feedback, creation of standard geometry (e.g., cylindrical internodes) and of free-form volumetric shapes (for fruits, tree trunks etc.), calibration and rectification in case of field disturbances, and MTG export are supported. Tests confirmed that the addon has some advantages against previous software for the FASTRAK digitizer.

Keywords: electromagnetic digitizer, 3-d data, position tracking, Blender, FASTRAK, Polhemus

Blender (Blender Foundation 2012) is a multi-purpose, open-source 3-d modelling tool providing various interactive navigation, editing and animation functions. We implemented an addon which can be activated within the GUI of Blender and which communicates with the Polhemus FASTRAK digitizer. Our addon provides some extensions compared to existing software (e.g., Donès et al. 2006), namely, the option to switch between discrete and continuous position acquisition mode, improved calibration and rectification facilities (using linear transformations) and sound feedback during the tracking process. Export of the resulting 3-d virtual plants in simple tables and in a subset of the MTG data format (Cokelaer & Pradal 2009), which can be processed by GroIMP (Kniemeyer & Kurth 2008) and by OpenAlea (Pradal et al. 2008), are supported. Future improvements will include extensions to the MTG export and enhancement of the triangulation method which we currently use for free-form shapes (leaves, fruits, flowers). – This research was partially funded by DFG under project identifier Ku 847/8-1. All support is gratefully acknowledged.

Fig. 1 (from left to right): Screenshot of Blender, photograph of a strawberry plant and virtual reconstruction as result of using the FASTRAK 3-d digitizer with the new Blender addon (from Wasilczuk 2012).

LITERATURE CITED

Blender Foundation. 2012. *Blender Documentation Contents – Blender 2.62.2 – API documentation.* http://www.blender.org/documentation/blender_python_api_2_62_2/ (last access: Sept. 10, 2012).

Cokelaer T, Pradal C. 2009. *MTG User Guide.* http://openalea.gforge.inria.fr/doc/vplants/mtg/doc/html/user/ (last access June 11, 2012).

Donès N, Adam B, Sinoquet H. 2006. PiafDigit – software to drive a Polhemus Fastrak 3 SPACE 3D digitiser and for the acquisition of plant architecture. Version 1.0. UMR PIAF INRA-UBP: Clermont-Ferrand.

Kniemeyer O, Kurth W. 2008. The modelling platform GroIMP and the programming language XL. In: Schürr A, Nagl M, Zündorf A (eds.): *AGTIVE '07*. **LNCS** 5088, Springer, Berlin, 570-572.

Pradal C, Dufour-Kowalski S, Boudon F, Fournier C, Godin C. 2008. OpenAlea: A visual programming and component-based software platform for plant modeling. *Functional Plant Biology* **35**:751-760.

Wasilczuk, K. 2012. Implementation, Test und Dokumentation einer nutzerfreundlichen Schnittstellensoftware für den 3D-Scanner FASTRAK. B.Sc. thesis, Department of Computer Science, University of Göttingen.

EXCHANGE AND TRANSPORT PROCESSES IN PLANTS

Proceedings of the 7th International Conference on Functional-Structural Plant Models, Saariselkä, Finland, 9 - 14 June 2013. Eds. Risto Sievänen, Eero Nikinmaa, Christophe Godin, Anna Lintunen & Pekka Nygren.
http://www.metla.fi/fspm2013/proceedings. ISBN 978-951-651-408-9.

KEYNOTE: Interplay between material flows and structural properties in dynamics of tree

Teemu Hölttä and **Eero Nikinmaa**
Department of Forest Sciences, PO Box 27, 00014 University of Helsinki, Finland
**correspondence:* teemu.holtta@helsinki.fi

Highlights: A whole tree level theoretical framework on the linkage between leaf gas exchange, long distance xylem and phloem transport and tree growth is presented.

Keywords: cambial growth, cavitation, hydraulic architecture, phloem transport, stomatal control, xylem transport

INTRODUCTION

Pressure driven transport in the xylem and phloem of trees means that leaf gas exchange, long distance material transport, growth and structural development are linked processes with feedbacks. However, the time constants of these different processes are very different which makes integrating studies of these phenomena a challenging task. Proper matching of the gas exchange, current structural growth and accumulated structure with the environmental conditions is crucial to the success and survival of trees (Brodridd 2009), particularly in the rapidly changing climate. This determines both the competitive capacity and resistivity to extreme conditions of trees.

The efficiency xylem transport is crucial for tree productivity, growth and overall performance (Bond and Kavanagh 1997). Water in the xylem is in a metastable state under negative hydrostatic pressure and thus vulnerable to phase transition by cavitation, which threatens xylem transport capacity (Tyree and Sperry 1989, Choat et al. 2012). Excessive cavitation during drought has been suggested to be main reason for tree mortality during drought (McDowell 2011). The requirements for xylem efficiency (i.e. hydraulic conductance) and safety (ability to withstand negative pressure without cavitation) are in conflict with each other; more conductive tissue tends to be more vulnerable to cavitation (e.g. Martinez-Vilalta et al. 2002). Xylem conductance increases, and vulnerability to cavitation decreases, with increasing xylem conduit size and increasing porosity of the pit membrane found between neighbouring conduits (Sperry and Hacke 2004).

Osmotic matching of the negative xylem hydrostatic pressure is involved in a number of central plant processes such as in leaf gas exchange, phloem transport and cambial growth. In phloem transport the positive turgor pressure required to drive the flow is obtained by active loading of osmotic substances, mainly sugars, to the phloem at the sources. Phloem transport and utilization of photosynthates in sinks have to maintain the rate of carbon assimilation in photosynthesis, or carbohydrate accumulation will force stomatal closure and down-regulation of photosynthesis (Paul and Foyer, 2001). The functioning of the phloem tissue in relation to environmental and structural factors is not well understood, although some theoretical predictions (e.g. Hölttä et al. 2009) and laboratory measurements (Mullendore et al. 2012) relating phloem structure to flow rate have been made. Adjustment of the stomatal opening controls leaf gas exchange in response to various environmental and internal signals. This topic has long been under rigorous study, but is still far from being understood (Buckely 2005). One obstacle is that our present understanding is based mainly on leaf level relations (Ball et al. 1987) without much consideration having been paid to whole tree level interactions and constraints.

As in the case of leaf gas exchange and phloem transport, the growth of new tissues also requires high carbohydrate availability and high turgor pressure in the different phases of growth including cell division, enlargement, and cell wall synthesis. The positive turgor pressure results from the interplay between the negative water pressure in xylem and sufficient sugar concentration in the living cambium to maintain positive pressure osmotically. In addition, carbon assimilates have a dual role in growth as apart from providing the sufficient enlarging pressure, they provide the raw material for cell wall thickening (e.g. DeSchepper and Steppe 2010, Hölttä et al. 2010, Pantin 2012). Maintenance of the balance between hydrostatic and osmotic pressures set strong boundary conditions for leaf gas exchange, within tree transport, storage, structure and growth and help to reveal how biological regulation needs to work to maintain measurable attributes, such as pressure and sugar concentration, within observed range. Resource wise, the construction and maintenance of the xylem and phloem tissue require a major proportion of the trees carbon

and nitrogen. With growth in tree height, the transport distance within the tree increases, and the transport of water (e.g. Koch et al. 2004), and perhaps even that of the assimilate products (e.g. Thompson 2006), become increasingly limiting for tree performance and growth. At the same time, the proportion of resource allocation to both of these tissues must increase.

Here we present a whole tree level theoretical framework on the linkage between leaf gas exchange, long distance xylem and phloem transport, and sink relations such as growth. Using this theoretical framework we demonstrate how xylem and phloem transport constrain whole tree level water and carbon exchange and growth in varying environmental conditions.

WHOLE TREE LEVEL LINKAGE OF LEAF GAS EXCHANGE, XYLEM AND PHLOEM TRANSPORT AND SINK RELATIONS

The interconnections and the underlying mathematical formulation amongst transpiration, photosynthesis, xylem and phloem transport, soil water status, and sink sugar status are depicted in Fig. 1. At leaf level, water is lost and carbon assimilated to and from atmosphere through stomatal openings (*). The driving forces for these fluxes are saturation pressure deficit ($C_{H2O,i}$-$C_{H2O,a}$) of water vapor in the atmosphere, and the difference in CO_2 concentration between the ambient air and the internal CO_2 concentration in the gas phase in the leaf ($C_{CO2,a}$-$C_{CO2,i}$). The utilization of CO_2 in photosynthesis (**, inside the dotted box) creates and maintains the difference in the CO_2 concentration required for assimilation. Accumulation of assimilated sugars and/or decrease in water potential in the leaf may decrease photosynthesis (**) due to stomatal and non-stomatal factors, e.g. due to down-regulation of photosynthetic machinery and decreases in mesophyll conductance (e.g. Chaves et al. 2003). The sugars assimilated by photosynthesis are passed mostly passively along the concentration gradient in trees (Turgeon 2010) from the mesophyll cells (where photosynthesis occurs) to the phloem. The photosynthesis box (**) contains many processes including the solution of CO_2 to the liquid phase and its diffusion in it, light and dark reactions of photosynthesis, and phloem loading which are not depicted in the figure.

Water loss at the transpiring surfaces in the leaves lowers the leaf xylem water potential which creates a force to draw water to the leaves though the xylem tissue from all the way from the roots and soil in the direction of the xylem water potential gradient (†). The assimilated sugars loaded to the leaf phloem draw osmotically water from the adjacent xylem tissue to maintain water potential equilibrium (††) and increase phloem hydrostatic (turgor) pressure. This positive pressure in the leaf phloem pushes water and dissolved sugars in the direction of the pressure gradient (†††) towards locations where the sugars are used in carbon sinks. Sugar utilization in the sink (***) lowers the osmotic concentration of the sap and keeps the turgor pressure low. In the absence of sugar utilization in the sink, the information of increase in sugar concentration at the sink is transmitted rapidly though the phloem to the source (leaves) due to pressure changes. Water potential equilibrium between the xylem and phloem is maintained at all locations in the tree (††). Cambial growth (‡) occurs as sugars are unloaded from phloem to cambium and this draws water osmotically from the xylem to the cambium to create pressure for cell expansion.

All these processes are coupled and constrained by one another. In steady state, the transpiration rate (E) must equal xylem sap flow rate (J_x), CO_2 assimilation rate (A) must equal the phloem sap flow rate (J_p), which in turn must equal the rate of sugar utilization at sink. The xylem and phloem are hydraulically coupled so that phloem turgor pressure plus osmotic pressure must equal the xylem water potential in all parts of the tree (††). Xylem conductance (k_x) is dependent on xylem water potential due to embolism formation by cavitation (Tyree and Sperry 1989), and phloem conductance (k_p) is dependent on phloem sugar concentration due to viscosity, which increase highly non-linearly with sugar concentration (Hölttä et al. 2009). Conductances also depend on temperature due to the temperature dependency of viscosity. Furthermore, there seems to be a connection between phloem transport and recovery of xylem from embolism (Nardini et al. 2011). Transpiration, soil water availability, photosynthesis and sugar utilization at the sinks set the pressure gradients for xylem and phloem transport. In addition, photosynthesis is directly coupled to leaf xylem water potential and osmotic concentration, which, in turn are closely linked to avoid loss of turgor pressure and leaf dehydration. Finally, the rate of cambial growth at each height is dependent on pressure in the cambium, which is tightly linked to local phloem sugar concentration and xylem pressure. The formation of new xylem and phloem tissue in cambial growth affects the xylem water pressure and phloem turgor pressure after growth has been completed.

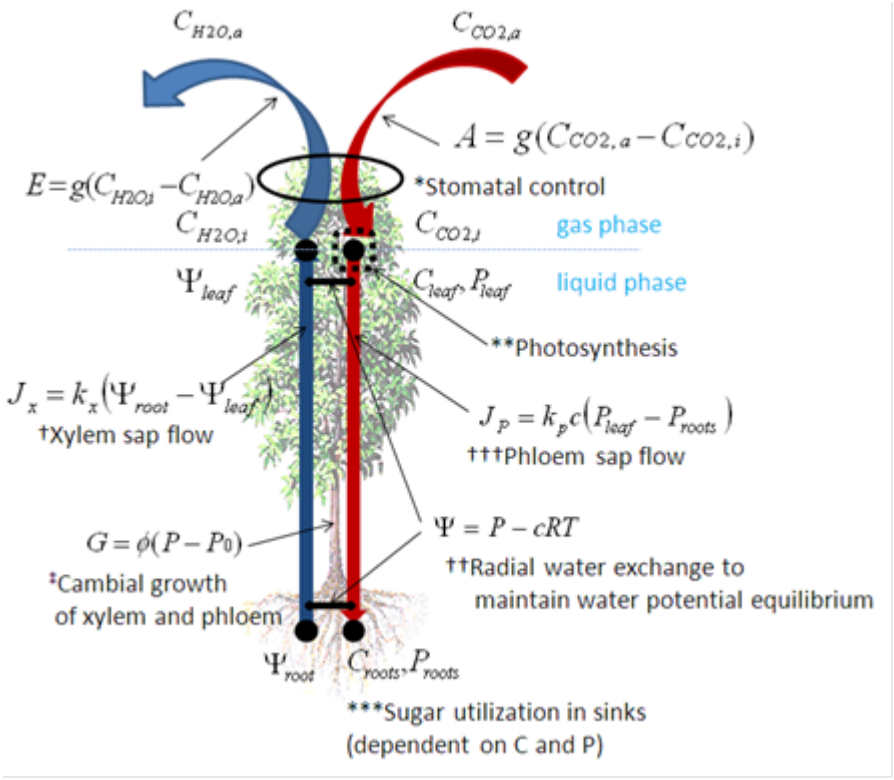

Fig. 1. Xylem and phloem transport, stomatal conductance and photosynthesis, and sink relations are interrelated. E is transpiration rate, J_x xylem sap flow rate, k_x xylem conductance, ψ_{leaf} leaf xylem water potential, ψ_{soil} root xylem water potential, g stomatal conductance, $C_{H2O,a}$ ambient H2O concentration, $C_{H2O,i}$ leaf internal H2O concentration, A photosynthesis rate, c "average" sugar concentration in phloem, k_p phloem conductance, P_{leaf} turgor pressure in leaf, P_{root} turgor pressure in root, J_p phloem sap flow rate, $C_{CO2,a}$ ambient CO_2 concentration, $C_{CO2,i}$ leaf internal CO_2 concentration, R a physical constant, T temperature, G is growth rate, Φ is cell wall (irreversible) extensibility, and P_0 is threshold pressure for cell wall extensibility.

The structure of the xylem, i.e. mainly conduit size and number and pit pore size and density, will determine vulnerability to cavitation and the specific xylem conductivity which together with xylem cross-sectional determines xylem conductive capacity (k_x). Similarly, the structure of the phloem, i.e. sieve tube size and number, and sieve plate or pore size and number, will determine the conductive capacity of phloem which together with phloem cross-sectional area determines phloem conductivity (k_p). Phloem osmotic pressure and turgor depend, in addition, on the phloem loading and unloading dynamics as they determine the sugar concentration (c) in phloem. The former is linked to photosynthesis especially tightly in trees where the sugars diffuse from the mesophyll cells to phloem sieve tubes passively along a concentration gradient (e.g. Turgeon 2010), and the latter is linked to sugar utilization for growth, respiration and root exudates. Structural development of tree is an outcome of resource capture, allocation and turnover of structures. The rate of resource capture and allocation between productive (capturing) and non-productive organs determine the long term growth rate. Size increase will change the balance between productive and non-productive tissue. The change depends on the scaling of the xylem and phloem tissue properties but the size also influences the flow rates and the specific capacities of the active tissue. Dynamics of tissue specific activities, allocation between productive and non-productive tissue and organ turnover rate influence the rate of development and attainable final size of trees.

LITERATURE CITED

Ball JT, Woodrow IE, Berry JA. 1987. A model predicting stomatal conductance and its contribution to the control of photosynthesis under different environmental conditions. *Progress in Photosynthesis Research, Vol. IV (ed. I. Biggins), pp. 221–224.*

Bond B, Kavanagh K. 1997. Stomatal behavior of four woody species in relation to leaf-specific hydraulic conductance and threshold water potential. *Tree Physiology* **19**: 503-510.

Brodribb TJ. 2009. Xylem hydraulic physiology: the functional backbone of terrestrial plant productivity. *Plant Science* **177**: 245-251.
Buckley TN. 2005. The control of stomata by water balance. *New Phytologist* **168**: 275–292.
Chaves MM, Maroco JP, Pereira JS. 2003. Understanding plant response to drought: from genes to the whole plant. *Functional Plant Biology* **30**: 239–264.
Choat B, Jansen S, Brodribb TJ, et al. 2012. Global convergence in the vulnerability of forests to drought. *Nature* **491:**752-756**.**
DeSchepper V, Steppe K. 2010. Development and verification of a water and sugar transport model using measured stem diameter variations. *Journal of Experimental Botany* **61:** 2083-2099.
Hölttä T, Mencuccini M, Nikinmaa E. 2009. Linking phloem function to structure: Analysis with a coupled xylem–phloem transport model. *Journal of Theoretical Biology* **259**: 325-337.
Hölttä T, Mäkinen H, Nöjd P, Mäkelä A, Nikinmaa E. 2010. A physiological model of softwood cambial growth. Tree Physiology 30: 1235-1252.
Hölttä T, Mencuccini M, Nikinmaa E. 2011. A carbon cost–gain model explains the observed patterns of xylem safety and efficiency. *Plant, Cell and Environment* **34**: 1819–1834.
Hölttä T, Nikinmaa E. 2013. Modelling the Effect of Xylem and Phloem Transport on Leaf Gas Exchange. ***accepted to*** *Acta Horticulturae***.**
Koch GW, Sillett SC, Jennings GM, Davis SD. 2004. The limits to tree height. *Nature* **428**: 851–854.
McDowell N. 2011. Mechanisms linking drought, hydraulics, carbon metabolism, and vegetation mortality. *Plant Physiology* **155**:1051–1059.
Martinez-Vilalta J, Prat E, Oliveras I, Pinol J. 2002. Xylem hydraulic properties of roots and stems of nine Mediterranean woody species. *Oecologia* **133**: 19–29.
Mullendore DL, Windt CW, Van As H, Knoblauch M. 2010. Sieve tube geometry in relation to phloem flow. *Plant Cell* **22**: 579–593.
Nardini A, Lo Gullo M, Salleo S. 2011. Refilling embolized xylem conduits: is it a matter of phloem unloading? *Plant Science* **180:** 604-611.
Nikinmaa E, Hölttä T, Hari P, Kolari P, Mäkelä A, Sevanto S, Vesala T. 2013. Assimilate transport in phloem sets conditions for leaf gas exchange. *Plant Cell Environ*. **36**: 655-669.
Pantin F, Simonneau T, Muller B. 2012. Coming of leaf age: control of growth by hydraulics and metabolics during leaf ontogeny. *New Phytologist* **196**: 349–366.
Paul MJ, Foyer CH. 2001. Sink regulation of photosynthesis. *Journal of Experimental Botany* **52**:1383–1400.
Sperry JS, Hacke UG. 2004. Analysis of circular bordered pit function. I. Angiosperm vessels with homogenous pit membranes. *American Journal of Botany* **91**: 369–385.
Thompson MV. 2006. Phloem: the long and the short of it. *Trends in Plant Science* **11**: 26–32.
Turgeon R. 2010. The role of phloem loading reconsidered. *Plant Physiology* **152**: 1817-1823.
Tyree MT, Sperry JS. 1989. Vulnerability of xylem to cavitation and embolism. *Annu. Rev. Plant Physiol. Plant Mol. Biol.* **40**: 19-38.

Proceedings of the 7th International Conference on Functional-Structural Plant Models, Saariselkä, Finland, 9 - 14 June 2013. Eds. Risto Sievänen, Eero Nikinmaa, Christophe Godin, Anna Lintunen & Pekka Nygren. http://www.metla.fi/fspm2013/proceedings. ISBN 978-951-651-408-9.

Transpiration from stomata via the leaf boundary layer: a microscale modelling approach

Thijs Defraeye[1*], **Pieter Verboven**[1], **Jan Carmeliet**[3,4], **Dominique Derome**[3] and **Bart Nicolai**[1,2]
[1] *MeBioS, Department of Biosystems, University of Leuven, Willem de Croylaan 42, 3001 Heverlee, Belgium,*
[2] *VCBT, Flanders Centre of Postharvest Technology, Willem de Croylaan 42, 3001 Heverlee, Belgium,*
[3] *Laboratory for Building Science and Technology, Swiss Federal Laboratories for Materials Testing and Research (Empa), Überlandstrasse 129, 8600 Dübendorf, Switzerland,* [4] *Chair of Building Physics, Swiss Federal Institute of Technology Zurich (ETHZ), Wolfgang-Pauli-Strasse 15, 8093 Zürich, Switzerland*
**correspondence:* thijs.defraeye@biw.kuleuven.be

Highlights: Convective mass transport from entire leaf surfaces was investigated with computational fluid dynamics. A novel aspect is that the stomata were modelled discretely. The convective exchange rate was relatively large, even for the limited surface coverage by stomata, and had a complex dependency on surface coverage and air speed. In addition, insight into the boundary-layer transfer at microscale level was obtained.

Keywords: convective transfer, transpiration, leaf, computational fluid dynamics, stomata

INTRODUCTION

Stomata are local elliptical perforations in the leaf's epidermis which have sizes of a few tens of micron and which occupy one to a few percent of the leaf surface. As the cuticle is quasi impermeable, leaf transpiration occurs predominantly via stomata. Hence, they play an important role in the plant hydrological cycle (Berry et al., 2010) and influence plant water uptake and water stress. Apart from the stomatal aperture and density, the transpiration rate is also dependent on the air flow in the boundary layer on the leaf surface, and the exchange processes therein (Nobel, 2005). This convective exchange between stomata and the environment is a subject of active research (Roth-Nebelsick et al., 2009).

As stomata are distributed discretely over the leaf surface, they lead to a very heterogeneous (non-uniform) mass exchange over the leaf surface, at a microscale level (10^{-5} m). The impact of these small mass sources on the convective exchange is usually not considered by conventional convective transfer studies on leaves: for real leaves, measurements of individual stomatal transpiration rate are not straightforward, and therefore only bulk transpiration of leaves is assessed; for numerical studies or experimental studies using artificial leaves, homogeneous mass boundary conditions are usually imposed at the leaf surface, such as a uniform distribution of water vapour pressure over the entire surface.

Only a few researchers have investigated in detail the effect of discretely-distributed moisture sources on mass transfer, but mainly for applications related to droplet evaporation (Cannon et al., 1979; Leclerc et al., 1986). The aforementioned experimental studies often considered macroscale moisture sources (> 10^{-3} m) and only the total convective transfer rate was determined. An assessment of the local exchange processes in the boundary layer was not performed as this is very challenging at the microscale. Some of these limitations could be alleviated by numerical modelling, which is the perspective of the present study. To the knowledge of the authors, the only numerical study undertaken to quantify transpiration via microscopic sources (Roth-Nebelsick et al., 2009) considered stomata arranged in a single stomatal crypt and investigated their effect on the crypt conductance. In the present study, the convective exchange in the boundary layer is modelled with computational fluid dynamics (CFD, both 2D and 3D) from leaf level (10^{-1}-10^{-2} m) down to the stomatal scale (10^{-5} m), thus covering a very large spatial range for a numerical study. This is particularly challenging with respect to numerical grid generation, which is required to accurately solve the governing equations in the boundary layer. A systematic study is undertaken to identify the effect of the stomatal surface coverage and the air speed on the convective exchange.

SIMULATIONS

A 2D and 3D model of a leaf were constructed to study convective transfer from microscopic scalar sources, such as stomata. Both models represent a flat leaf, which was placed in low turbulent air flow with a free-stream speed U_b. The length of the leaf was 100 mm in 2D and 25 mm in 3D. The computational grids contained 0.226 x 10^6 cells and 5.88 x 10^6 cells, for 2D and 3D, respectively. In order to model the microscopic stomata discretely, very small computational cells (~ 50 μm) were required on the leaf surface.

Instead of modelling mass transfer from these sources, heat transfer (i.e., a passive scalar) was modelled since this led to a significant decrease of the computational cost: in this case, the flow field had to be solved only once at each air speed, since the air properties (e.g., density) could be taken constant. As such, only the scalar (heat) transfer, and not the flow field, had to be recalculated for the different imposed boundary conditions, i.e., stomatal coverage ratios. The resulting heat transfer data can easily be converted to mass transfer by means of the heat and mass transfer analogy, and is presented in dimensionless form anyway in the present study. The boundary-layer development is also similar since the Lewis number is almost equal to one (≈ 0.8). As such, heat (or mass) will be referred to as a scalar from now on. Only air-side transfer was modelled. A constant scalar value (temperature) was imposed at the stomata and a no-flux condition was used on the rest of the leaf surface. Different coverage ratios (CR) were evaluated, representative for those of real stomata, which vary roughly between 0.2% and 5%. The coverage ratio is defined as the ratio of the area occupied by the stomata (A_{eff} [m²]), to the total leaf area (A [m²]), i.e., CR = A_{eff}/A. The CFD simulations were performed with the commercial code ANSYS Fluent 13. Steady Reynolds-averaged Navier-Stokes (RANS) was used in combination with the shear stress transport (SST) k-ω model (Menter, 1994). Low-Reynolds number modelling (LRNM) was applied to resolve the transport in the boundary-layer region. This RANS turbulence model, in combination with LRNM, has already been shown to be very accurate for similar complex flow problems (e.g., Defraeye et al., 2012).

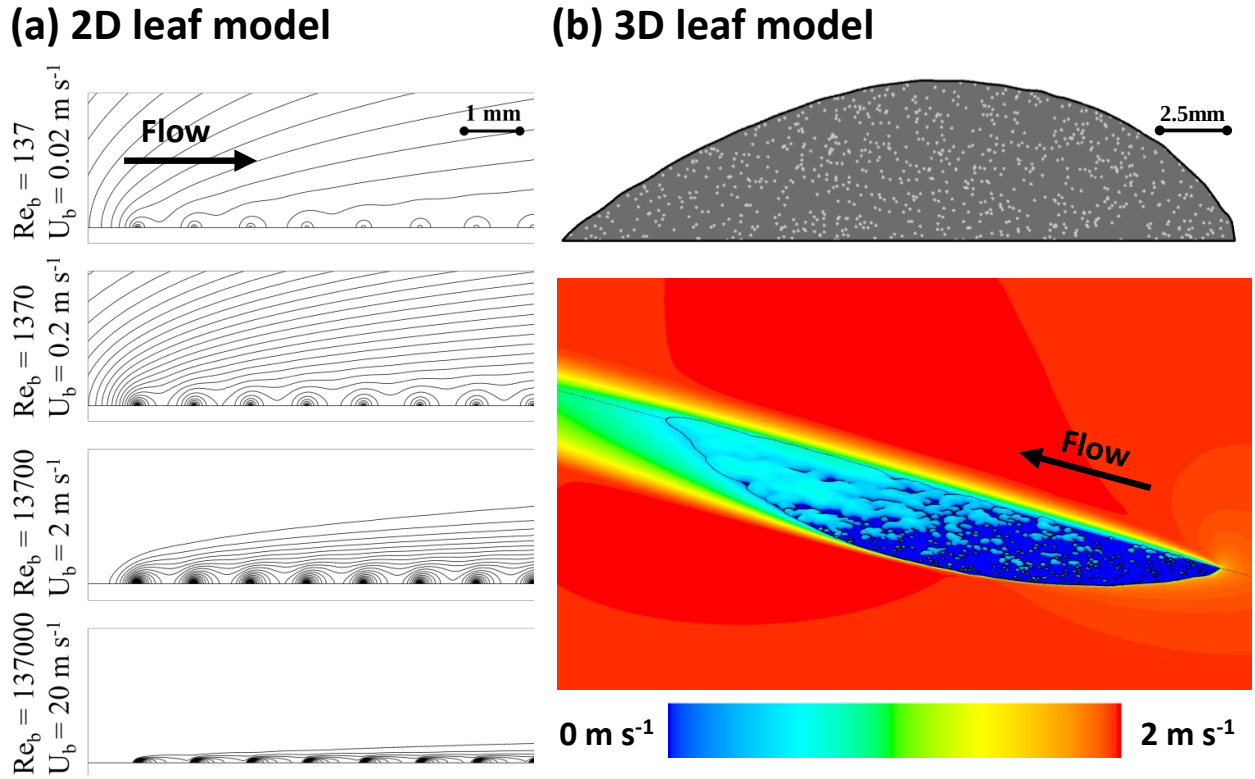

Fig. 1. (a) Scalar concentration contours (isocontours) in the boundary layer at the leading edge of the 2D leaf for a coverage ratio of 5% for different air speeds. (b) Top: distribution of stomata on 3D leaf surface (only one half shown) for a coverage ratio of 1%; Bottom: air speed on a scalar isosurface (i.e., a surface which represents a constant scalar concentration in the computational domain) in the boundary layer of the 3D leaf and on both vertical and horizontal symmetry planes for a coverage ratio of 1% for U_b = 2 m s^{-1}.

RESULTS AND DISCUSSION

In Fig. 1a, the scalar concentration contours are shown at the leading edge of the 2D leaf for different air speeds (Reynolds numbers) for a coverage ratio of 5%. The scalar boundary-layer thickness decreases with increasing air speed. At low speeds, the contours look more symmetrical on both sides of the sources, but at higher speeds, the scalar is convected more downstream and a wake zone is observed. In Fig. 1b, the air speed on a scalar isosurface in the boundary layer of the 3D leaf, and on both vertical and horizontal symmetry planes is shown for a coverage ratio of 1%. The boundary layer clearly becomes more saturated downstream of the leading edge, as the size of the volume occupied by the isocontour clearly increases.

The surface-averaged convective scalar flows ($Q_{c,w,avg}$) from the 2D leaf are shown in Fig. 2a as a function

of the coverage ratio. The results at different air speeds (U_b), thus d/δ_{VSL} ratios, are presented. Here d is the size of the scalar sources (50 µm) and δ_{VSL} is the average thickness of the viscous sublayer, i.e., the lower part of the boundary layer where laminar transport occurs and where large velocity and scalar gradients are found. These scalar flows are scaled with the surface-averaged scalar flow for a coverage ratio of 100% ($Q_{c,w,avg,100\%}$). Note that these scalar flows are directly proportional to the leaf's convective transfer coefficient. Similar results are shown in Fig. 2b for the 3D leaf, but only for a single air speed (U_b = 2 m s^{-1}).

From Fig. 2, relatively high scalar flows at the surface are found at low coverage ratios (for all d/δ_{VSL} ratios), thus they clearly do not vary linearly with the coverage ratio. This trend is predicted by both 2D and 3D modelling. This effect is more pronounced at low d/δ_{VSL} (Fig. 2a), implying low air speeds (or small source sizes). These findings however also indicate that well-established convective transfer coefficients from plates or leaf models, obtained for a coverage ratio of 100%, can result in a significant overprediction of the convective exchange, compared to a more realistic, lower, stomatal coverage ratio, due to the discrete distribution of these microscopic sources. Furthermore, the largest decrease in scalar flows with coverage ratio was found at low coverage ratios (CR < 10%, i.e., the range shown in Fig. 2), which implies that small variations in the leaf's stomatal density (CR), e.g., due to biological variability, or a temporal variation of stomatal aperture have a large impact on the convective exchange as well.

In conclusion, the convective exchange from stomata was shown to be strongly dependent on surface coverage and air speed. The applied microscale modelling aproach provided more insight in convective exchange processes at the stomatal level. Such a numerical modelling framework seems promising in contributing to the understanding of leaf transpiration, but also of microclimatic conditions in the boundary layer and the transport therein.

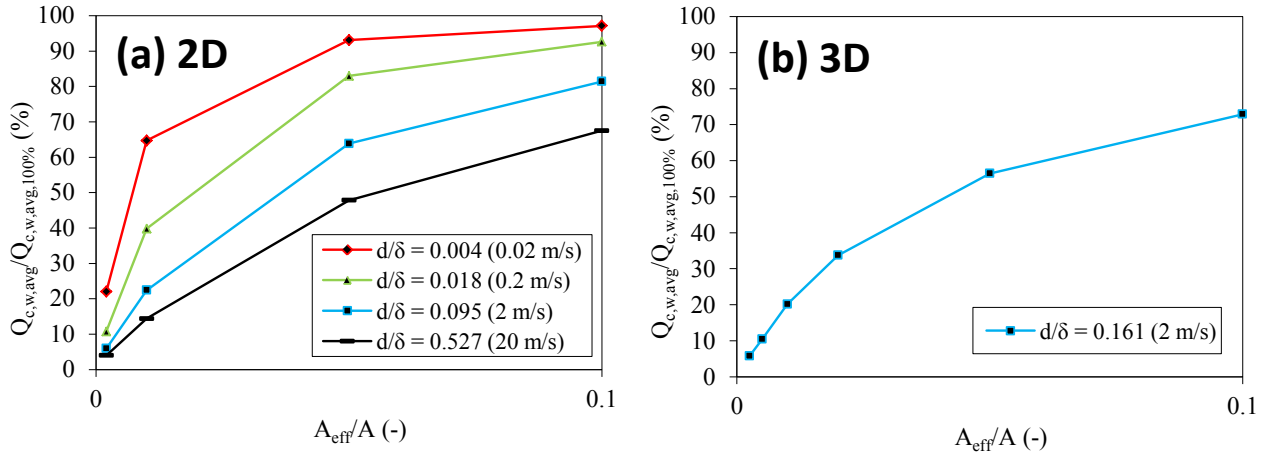

Fig. 2. Surface-averaged convective scalar flows at the leaf surface as a function of the coverage ratio, for CR up to 10%. The flows are scaled with the surface-averaged scalar flow for a coverage ratio of 100% ($Q_{c,w,avg,100\%}$): (a) 2D model at different air speeds (U_b, i.e., d/δ_{VSL} ratios); (b) 3D model at a single air speed.

LITERATURE CITED

Berry JA, Beerling DJ, Franks PJ. 2010. Stomata: key players in the earth system, past and present. *Current Opinion in Plant Biology* **13**:233-240.

Cannon JN, Krantz WB, Kreith F, Naot D. 1979. A study of transpiration from porous flat plates simulating plant leaves. *International Journal of Heat and Mass Transfer* **22**:469-483.

Defraeye T, Herremans E, Verboven P, Carmeliet J, Nicolai B. 2012. Convective heat and mass exchange at surfaces of horticultural products: a microscale CFD modelling approach. *Agricultural and Forest Meteorology* **162-163**:71-84.

Leclerc MY, Schuepp PH, Thurtell GW. 1986. Electrochemical simulations of mass transfer from isolated wet spots and droplets on realistic fluttering leaves. *Boundary-Layer Meteorology* **34**:399-410.

Menter FR. 1994. Two-equation eddy-viscosity turbulence models for engineering applications. *AIAA Journal* **32**:1598-1605.

Nobel PS. 2005. *Physicochemical and Environmental Plant Physiology*. 3rd Edition, Elsevier Academic Press, London.

Roth-Nebelsick A, Hassiotou F, Veneklaas EJ. 2009. Stomatal crypts have small effects on transpiration: a numerical model analysis. *Plant Physiology* **151**:2018-2027.

Proceedings of the 7th International Conference on Functional-Structural Plant Models, Saariselkä, Finland, 9 - 14 June 2013. Eds. Risto Sievänen, Eero Nikinmaa, Christophe Godin, Anna Lintunen & Pekka Nygren. http://www.metla.fi/fspm2013/proceedings. ISBN 978-951-651-408-9.

LEAFC3-N: Modeling Effects of Drought Stress on Photosynthesis, Stomatal Conductance and Transpiration

Jens Bastet*, Johannes Müller and Olaf Christen
Institute of Agricultural and Nutritional Sciences, University of Halle-Wittenberg, D-06900 Halle, Germany
**correspondence:* jens.bastet@landw.uni-halle.de

Highlights: LEAFC3-N combines photosynthesis, stomatal conductance, transpiration, leaf energy balance, and leaf nitrogen content. The response to drought is simulated accounting for the effect of leaf water potential on stomatal conductance and of a finite mesophyll conductance on intracellular CO_2 concentration.

Keywords: Photosynthesis, drought stress, water potential, model.

INTRODUCTION

A previous version of LEAFC3-N (Braune et al., 2009) accounts for drought stress based on effects of leaf water potential (Ψ_l) on stomatal conductance (g_{sv}), carboxylation, and electron transport. Mesophyll conductance (g_m) was assumed infinite. However, a finite g_m may significantly affect photosynthesis under drought (Niinemets et al., 2009). Here we re-analyse these patterns by including a finite g_m into LEAFC3-N.

MODEL DESCRIPTION

LEAFC3-N (Müller et al., 2005) extends the LEAFC3 model (Nikolov et al., 1995) of the coupled processes of photosynthesis, stomatal action, transpiration, and leaf energy balance by relating the characteristics V_m, J_m, T_p, φ_a, m, θ, and R_d in the equations below to leaf nitrogen content per leaf area, N_a. For the N_a–dependencies currently used see Braune et al. (2009). Below we list only main model equations related to this study. For further explanation see the references above, and for a complete description of the model and for improvements recently introduced (accounting for different stomata frequencies at each leaf side, dynamic model of plant water transport, advanced solution algorithms, user interface and simulation tools, model extension for a finite g_m) consult documentation and code which are available by request.

$$A_n = A_g\,(1-\Gamma^*/C_c) - R_d, \tag{1}$$

if $C_c > (1+3\alpha_p)\,\Gamma^*$:

$$\beta A_g^2 - (A_{g,e}+A_{g,p})\,A_g + A_{g,e}\,A_{g,p} = 0, \qquad 0 \le \beta \le 1, \tag{2}$$

$$\alpha A_{g,e}^2 - (A_{g,c}+A_{g,j})\,A_{g,e} + A_{g,c}\,A_{g,j} = 0, \qquad 0 \le \alpha \le 1, \tag{3}$$

elseif $C_c \le (1+3\alpha_p)\,\Gamma^*$:

$$\alpha A_g^2 - (A_{g,c}+A_{g,j})\,A_g + A_{g,c}\,A_{g,j} = 0, \qquad 0 \le \alpha \le 1. \tag{4}$$

$$A_{g,c} = \frac{V_m\,C_c}{C_c + K_c(1+O/K_o)}, \quad A_{g,j} = \frac{J\,C_c}{\mu_1 C_c + \mu_2\,\Gamma^*}, \quad A_{g,p} = \frac{3T_p\,C_c}{C_c - (1+3\alpha_p)\,\Gamma^*}, \tag{5), (6), (7}$$

$$J = \left[(J_m+\varphi_a Q_a) - \sqrt{(J_m+\varphi_a Q_a)^2 - 4\theta\varphi_a Q_a J_m}\right]/2\theta, \tag{8}$$

A_n: net photosynthesis rate; A_g: CO_2 exchange rate defined as the minimum of $A_{g,c}$, $A_{g,j}$, and $A_{g,p}$; $A_{g,c}$, $A_{g,j}$, and $A_{g,p}$: see eqs. (5), (6), (7); C_c: intracellular CO_2 concentration; f_Ψ: function defining a sigmoid response to Ψ_{leaf} (eq.(13)); K_c and K_o: Michaelis-Menten parameters of Rubisco for carboxylation and oxygenation of RuBP, respectively; J: electron transport rate; J_m: light saturated J; O: concentration of O_2; Q_a: absorbed photosynthetic photon flux density; R_d: mitochondrial respiration rate at given incident photosynthetic photon flux density ('day respiration'); T_p: potential rate of triose phosphate utilisation; V_m: maximum carboxylation rate; α: coefficient defining the smoothness of the transition between $A_{g,c}$ and $A_{g,j}$; α_p: fraction of glycolate carbon not returned to chloroplast; β: coefficient defining the smoothness of the transition between $A_{g,p}$ and $A_{g,e}$; Γ^*: CO_2 compensation point in the absence of R_d; φ_a: quantum yield of electron transport based on Q_a; μ_1 and μ_2: coefficients quantifying the electron requirement for the formation of $NADPH^+$ and ATP in terms of mol electrons per mol CO_2 fixed; θ: curvature coefficient.

$$C_c = C_a - A_n / g_t, \tag{9}$$

C_c, C_a: concentration of CO_2 at the reaction site in the chloroplast, in the ambient air; g_t: total conductance for CO_2 transport.

$$g_t = \frac{M_{bv}\, g_{bv}\, g_{sv}\, g_m}{M_{bv}\, g_{bv}\, g_{sv} + 1.6\, M_{bv}\, g_{bv}\, g_m + 1.37\, g_{sv}\, g_m}, \tag{10}$$

g_{bv} and g_{sv}: two-sided leaf boundary layer and leaf stomatal conductance, respectively, M_{bv}: function accounting for the effective portion of g_{bv} arranged in series with g_{sv} depending on the ratio of the numbers of stomata on each leaf side.

The stomatal part g_{sv} of g_t is calculated by a modified Ball et al. (1987) model:

$$g_{sv} = m\, f_\Psi\, (A_n + R_d)\, h_b / C_b + g_{sv0}, \qquad if\ C_b \geq 200\ \mu mol\ mol^{-1} \tag{11}$$
$$g_{sv} = g_{sv}(C_b = 200\ \mu mol\ mol^{-1}) \qquad else,$$

$$m = k_{0,m}\, N_a^{\,k_{1,m}}, \tag{12}$$

$$f_\Psi = 1 / \left[1 + (\Psi_l / \Psi_c)^{k_\Psi} \right], \qquad 0 \leq f_\Psi \leq 1, \tag{13}$$

g_{sv0}: minimum g_{sv}; m: coefficient (dimensionless) that defines the combined sensitivity of g_s to A_n, h_b, and C_b; h_b, C_b: relative humidity (decimal fraction) and CO_2 concentration (µmol mol^{-1}) of the air at the leaf surface within the leaf boundary layer, respectively; f_Ψ defines a sigmoid response to Ψ_l; Ψ_c: critical leaf water potential [Pa]; k_Ψ: curvature parameter [dimensionless].

The mesophyll part g_m of g_t is calculated according to Yin et al. (2009):

$$g_m = g_{m0} + \delta\, (A_n + R_d) / (C_c - \Gamma^*), \qquad if\ C_c > \Gamma^*, \tag{14}$$

g_{m0}: minimum g_m; δ: proportionality factor that defines the combined sensitivity of g_m to $A_n + R_d$ and C_c.

EXPERIMENTAL DESIGN

Spring barley (*Hordeum vulgare* L., cv. 'Scarlett') was grown in a climate chamber in pots containing sandy loam soil at different treatments of water supply (W1, W2). Wc1 was maintained at optimum soil water content, which corresponds to 60 % of soil water capacity (W_c) or a water content of 23.1 vol. %. Wc2 was dried to 35 % of W_c (or 13.5 vol. %) and then kept on this level. The drought stress period of nine days was started when the visible part of leaf number four of the main tiller had reached a length of 10 cm. Further growth conditions were: incident photon flux density Q_i = 310 µmol m^{-2} s^{-1}, $C_a \approx$ 360 µmol mol^{-1}, and ambient air humidity $h_a \approx$ 60 %. On leaves of rank four, the following characteristics required for analyzing the data with the LEAFC3-N model were measured: area, contents of chlorophyll and total nitrogen (N), water potential (Ψ_l), light and CO_2 response curves of net photosynthesis rate. After gas exchange measurements, the leaf blades were quickly covered by plastic sheaths made of thin foil and then cut off at the proximal emersion point at the measurement chamber. The water potential of these leaf parts was then measured using a scholander pressure bomb.

RESULTS AND DISCUSSION

In the present simulation study, the basic parameterization of LEAFC3-N was adopted from Braune et al. (2009). However, the parameters K_c, K_o, V_m, and J_m (respectively the slopes s_v and s_j of the linear relations of V_m and J_m to N_a) were revised as required in case of introducing a finite g_m. Considering corresponding results of Bernacci et al. (2002) and Yin et al. (2009), we re-analyzed the diurnal time course measurements of A_n, Tr, and g_{sv} given by Braune et al. (2009). The revised parameters introduced on this basis were K_c = 272 µmol mol^{-1}, K_o = 166 mmol mol^{-1} (Bernacci et al., 2002), s_v = 91.62 µmol CO_2 (g N)$^{-1}$, and s_j = 158.6 µmol e^- (g N)$^{-1}$. Further, we derived from that parameterization study with respect to the N_a–dependency of m (eq. (12)): $k_{0,m}$ = 20.58 m^2 g^{-1} and $k_{1,m}$ = -0.45, with respect to f_Ψ (eq. (13)): Ψ_c = -1.7 MPa and k_Ψ = 3, and with respect to g_m (eq. (14)): δ = 1.1 and g_{m0} = 0.1 mol m^{-2} s^{-1}. Based on this parameterization, the diurnal time courses of A_n, Tr, and g_{sv}, including the midday depression, could be reproduced well by the new model version that was extended by introducing a finite g_m (eqs. (10) and (14)). No additional effects of Ψ_l on V_m and J_m were assumed as in Braune et al. (2009). This result here was confirmed based on data obtained by the special experimental design described above. With the same parameter values as before, except setting Ψ_c = -1.2 MPa, A_n, Tr, and g_{sv} simulated for a range of incident photon flux density (Q_i) and Ψ_l agreed quite well with the corresponding measurements (Fig.1, Table 1).

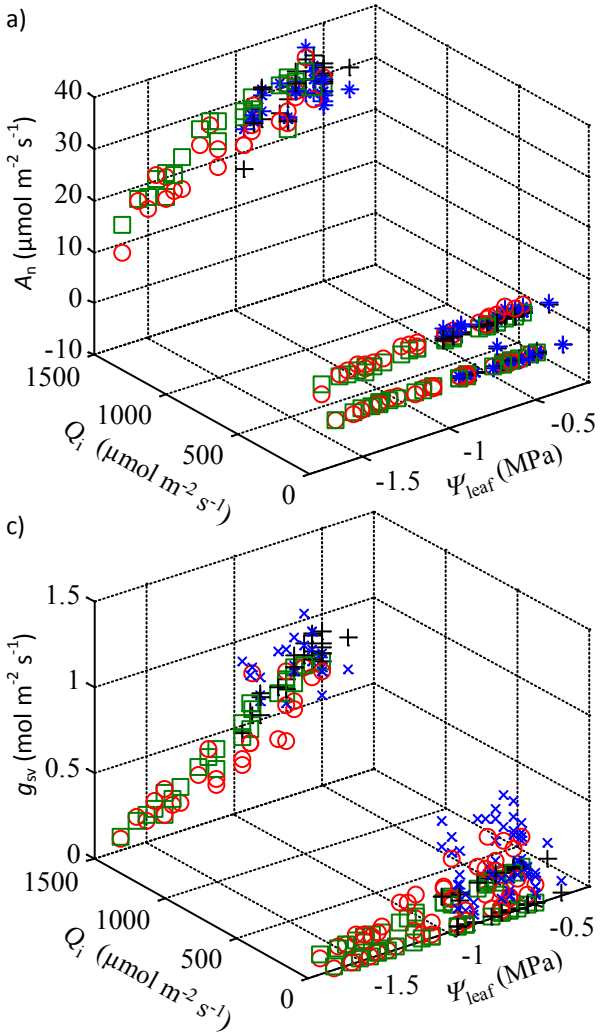

Table 1. Linear regression of simulated vs. measured values: $\mathbf{r^2}$= coefficient of determination $\mathbf{a_1}$= slope of regression $\mathbf{a_0}$= absolute term of regression

	W	r^2	a_1	a_0
A_n	1	0.97	1.04	-0.390
Tr		0.89	1.09	-1.822
g_{sv}		0.79	1.03	-0.151
A_n	2	0.96	1.09	-0.295
Tr		0.82	1.06	-0.397
g_{sv}		0.78	1.05	-0.023

Fig. 1. Simulation results for a) A_n, b) Tr, and c) g_{sv} for a range of Ψ_{leaf} and Q_i; measurements W1 (x), W2 (○) and simulations W1 (+), W2 (□).

ACKNOWLEDGEMENT

This research was supported by the Deutsche Forschungsgemeinschaft (DFG, contract No. DFG 1379/2-1).

LITERATURE CITED

Braune, H., Müller, J., Diepenbrock, W. 2009. Integrating effects of leaf nitrogen, age, rank, and growth temperature into the photosynthesis-stomatal conductance model LEAFC3-N parameterised for barley (Hordeum vulgare L.). *Ecol. Model*. **220**:1599–1612.

Ball, J.T., Woodrow, I.E., Berry, J.A. 1987. A model predicting stomatal conductance and its contribution to the control of photosynthesis under different environmental conditions. In: Biggins J (ed.), *Progress in Photosynthesis Research. Proceedings of the VII. International Congress on Photosynthesis*. Martinus Nijhoff Publishers, Dordrecht-Boston-Lancaster, **4**:221–224.

Bernacchi, C.J., Portis, A.R., Nakano, H., von Caemmerer, S., Long, S.P. 2002. Temperature response of mesophyll conductance. Implications for the determination of Rubisco enzyme kinetics and for limitations to photosynthesis in vivo. *Plant Physiology* **130**:1992–1998.

Niinemets, Ü., Díaz-Espejo, A., Flexas, J., Galmés, J., Warren, C.R. 2009. Importance of mesophyll diffusion conductance in estimation of plant photosynthesis in the field. Journal of Experimental Botany **60**:2271–2282.

Müller, J., Wernecke, P., Diepenbrock, W. 2005. LEAFC3-N: a nitrogen-sensitive extension of the CO_2 and H_2O gas exchange model LEAFC3 parameterised and tested for winter wheat (Triticum aestivum L.). *Ecol. Model*. **183**:183-210.

Nikolov, N.T., Massman, W.J., Schoettle, A.W. 1995. Coupling biochemical and biophysical processes at the leaf level: An equilibrium photosynthesis model for leaves of C-3 plants. Ecol. Model. 80:205-235.

Yin X., Struik P.C., Romero P., Harbinson J., Evers J.B. 2009. Using combined measurements of gas exchange and chlorophyll fluorescence to estimate parameters of a biochemical C_3 photosynthesis model: a critical appraisal and a new integrated approach applied to leaves in a wheat (*Triticum aestivum*) canopy. *Plant, Cell Environ*. **32**:448–464.

Proceedings of the 7th International Conference on Functional-Structural Plant Models, Saariselkä, Finland, 9 - 14 June 2013. Eds. Risto Sievänen, Eero Nikinmaa, Christophe Godin, Anna Lintunen & Pekka Nygren. http://www.metla.fi/fspm2013/proceedings. ISBN 978-951-651-408-9.

Modelling transport processes in tissues and organs at a mesoscopic scale

Ansgar Bohmann[1], **Juliane Claus**[1] and **Andrés Chavarría-Krauser**[1,*]
[1]*Interdisciplinary Center for Scientific Computing & Center for Modelling and Simulation in the Biosciences, Universität Heidelberg, Im Neuenheimer Feld 368, 69120 Heidelberg, Germany*
**correspondence:* andres.chavarria@bioquant.uni-heidelberg.de

Highlights: Three mesoscopic models of transport processes in plants are presented: water fluxes in tissues, zinc uptake in roots, and gas fluxes in leaves. The models aim at increasing our understanding of the interaction between physical and biological processes in plants. Besides giving ideas for derivation of other mesoscopic models, the presented results can be of use in functional-structural plant models.

Keywords: transport, uptake, transpiration, metals, zinc, nutrients, water, roots, leaves, genetic regulation

INTRODUCTION

Transport of water, nutrients and gases in tissues and organs takes place in highly structured domains with multifaceted paths: symplastic, apoplastic and transcellular (Steudle, 2000). While the apoplast is a porous medium in which Darcy's law applies, fluid movement in the symplast follows a viscous flow law (e.g. Stokes). In general, different physical processes have to be considered, in particular when these are coupled. To obtain mesoscopic mathematical models of sufficient physiological background, it is necessary to pose microscopic models, valid at e.g. the cell scale, to couple the microscopic domains by transmission conditions, and to derive mesoscopic/macroscopic models by "upscaling" for simulation and analysis. This approach is used widely in engineering (Hornung, 1997), but much less in biology (e.g. Marciniak-Czochra and Ptashnyk, 2008; Chavarría-Krauser and Ptashnyk, 2010). Regardless of the mathematical technicality, the ideas and steps carried out are intuitive: modelling of microscopic processes, determination of macroscopic models and simulation. Depending on the problem's scale, upscaling might be senseless as in discrete or semi-discrete models of auxin transport and morphogenesis (e.g. Goldsmith et al., 1981; Kramer, 2004; Chavarría-Krauser et al., 2005; Jönsson et al., 2012). Transport, deformation, flow, etc. are physical processes occurring in general independently of organisms yet tamed by cells to accomplish a specific function. For example, zinc uptake and transport in roots follow diffusion-advection-reaction laws modulated by expression of ZIP-transporters (Krämer and Sinclair, 2012; Claus et al., 2012). Regarding transport processes in plants, a duality between physical and biological processes is found. Understanding this duality is important to establishing functional-structural plant models (FSPM) and to plant physiology in general. We present three models to exemplify how mesoscopic integrative plant models can be obtained and elucidate further the interaction between physical and biological processes in plants. We focus on: water fluxes in tissues, regulated zinc uptake in roots, and gas fluxes in leaves.

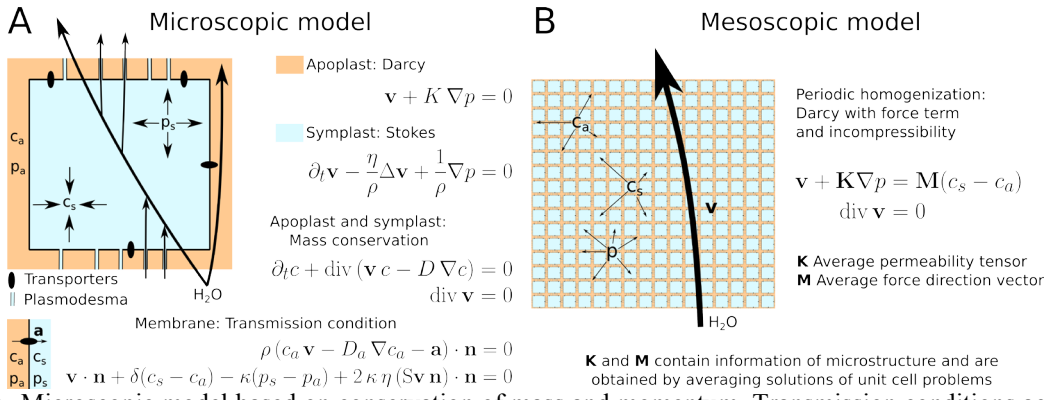

Fig. 1. A, Microscopic model based on conservation of mass and momentum. Transmission conditions account for transport over the membrane. B, Mesoscopic model obtained using periodic homogenization. The model is based on one pressure p, one velocity **v** and two concentrations: c_a and c_s.

WATER FLUXES IN TISSUES

The existence of the apoplast and symplast in plant tissues opens diverse paths to water (Steudle, 2000). The contribution of the symplastic, apoplastic and transcellular paths is still unknown. We derive a model to analyse further these contributions by assuming an ideal tissue of perfect periodicity. The cells are assumed to have cell walls, plasma membranes and cytoplasm; plasmodesmata join their cytoplasms (Fig. 1A). The microscopic model consists of flow and transport equations for water and osmotic solutes. The flow is assumed to follow Darcy in the apoplast and plasmodesmata and Stokes in the symplast (Fig. 1A). We derive transmission conditions connecting the symplast and apoplast by balancing the fluxes at the interface. A regulation of transport is considered via ordinary differential equations describing the amount of free and bound transporters. Although the microscopic model is continuous, it could be reformulated as a discrete cellular model. Using homogenization techniques (Hornung, 1997), we obtain an average "upscaled" mesoscopic model (Fig. 1B). It is a Darcy law with a force term proportional to the local difference in solute concentration. Representations of the average transport coefficients are obtained from solutions of unit cell problems, which are posed for one cell and account for the microscopic structure. The mesoscopic model obtained is simple in structure, straightforward to solve numerically and can be applied in FSPM to describe water fluxes in tissues and organs.

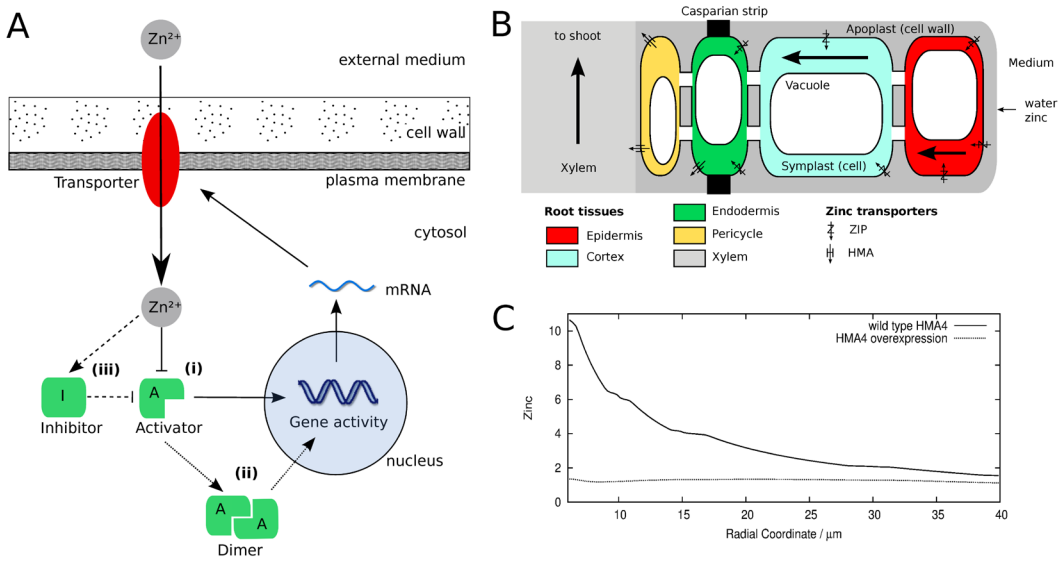

Fig. 2. Zinc and water uptake in roots. A, Schematic description of feasible zinc regulation models: (i) activator only, (ii) activator with dimerization, (iii) activator-inhibitor. B, Schematic description of radial transport of zinc. C, Simulation result showing zinc distributions under different levels of HMA4 (lower panel).

REGULATED ZINC UPTAKE IN ROOTS

The heavy metal zinc is an essential micronutrient yet potentially toxic for plants. Its uptake in roots needs to include mechanisms for the quick adaptation to a varying environment. Transport of zinc from the root epidermis to the central cylinder depends on three main processes: diffusion in the medium, advection with water, and cross-membrane transport. Modelling these processes allows analysing their relative impact and question biological hypotheses. Strict regulation of zinc uptake is presumably accomplished by modulation of zinc transporters in the membrane in response to changes of the cells' internal zinc concentration. Experimental measurements showed that the number of transporters is adjusted according to external concentrations by a still unknown system of transcription factors and activating and inhibiting agents (Talke et al., 2006; Assunção et al., 2010). We analysed the biological relevance of different simple scenarios comprising a simple activator, a dimerizing activator, and an additional inhibitor in an ordinary differential equations model (Fig. 2A). Our simulations suggest the existence of a dimerising activator and an inhibitor due to advantages in stability and robustness (Claus and Chavarría-Krauser, 2012a). Zinc uptake in roots depends also on passive diffusion and radial flow of water towards the xylem. To analyse the relative significance of these processes and the effect of geometry and microstructure, we posed a spatio-temporal transport model of the root of *Arabidopsis thaliana* (Fig. 2B; Claus et al., 2012b). The simulations show an inverse relation between accumulation and the level of the efflux transporter HMA4 (Fig. 2C), which is in accordance with measurements of HMA4 over expression (Hanikenne et al., 2008).

GAS FLUXES IN LEAVES

To gain insight in the physics and regulation of gas exchange (water vapour, carbon dioxide, and oxygen) in plant leaves we propose a dynamical first-principle model for a small disc-shaped section of a leaf around a single stoma (see Fig. 3). We focus on the mechanical interaction between epidermis cells and guard cells, coupled to water and solvent transport in the epidermis (symplastic and apoplastic compartments), as well as evaporation into and diffusion within the interstitial air space. Vapour exchange to the ambient air is controlled by the stomatal aperture which in turn is determined by the mechanics and the guard cell solute content. The underlying physical processes along with typical parameter values are described in standard literature (e.g. Nobel, 2005). The structure of the resulting model is a coupled system of ordinary and partial differential equations providing a more detailed description as compared to resistor network models. It also captures dynamic effects, and links microscopic physical properties to observable variables such as stomatal aperture and water loss. The model provides a physically accurate explanation to the inverse behaviour of stomatal aperture after sudden changes in ambient parameters, such as ambient moisture (Mott et al., 1997). This model is intended to serve as one building block for a future more comprehensive model of the leaf.

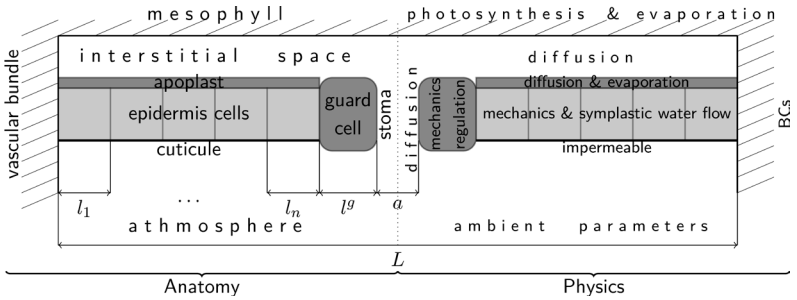

Fig. 3. Section through leaf epidermis centered around a single stoma.

LITERATURE CITED

Assunção AGL, Schat H, Aarts MGM. 2010. Regulation of the adaptation to zinc deficiency in plants. *Plant Signaling & Behavior* **5**:1553-1555.

Chavarría-Krauser A, Jäger W, Schur U. 2005. Primary root growth: a biophysical model of auxin-related control. *Func. Plant Physiol.* **32:** 849-862.

Chavarría-Krauser A, Ptashnyk M. 2010. Homogenization of long-range auxin transport in plant tissues. *Nonlinear Anal.-Real.* **11:** 4524-4532.

Claus J, Chavarría-Krauser A. 2012a. Modeling Regulation of Zinc Uptake via ZIP Transporters in Yeast and Plant Roots. *PloS ONE* **7(6)**:e37193.

Claus J, Bohmann A, Chavarría-Krauser A. 2012b. Zinc uptake and radial transport in roots of *Arabidopsis thaliana*: a modelling approach to understand accumulation. *Annals of Botany*, doi: 10.1093/aob/mcs263

Marciniak-Czochra A, Ptashnyk M. 2008. Derivation of a macroscopic receptor-based model using homogenisation techniques. *SIAM J. Math. Anal.* **40:** 215-237.

Goldsmith MHM, Goldsmith TH, Martin MH. 1981. Mathematical analysis of the chemiosmoticpolar diffusion of auxin through plant tissues. *Proc. Natl. Acad. Sci. USA* **78:** 976-980.

Hanikenne M, Talke IN, Haydon MJ, et al. 2008. Evolution of metal hyperaccumulation required *cis*-regulatory changes and triplication of HMA4. *Nature* **453**:391-395.

Hornung U. 1997. *Homogenization and porous media.* Springer-Verlag.

Jönsson H, Gruel J, Krupinski P, Troein C. 2012. On evaluating models in Computational Morphodynamics. *Curr. Op. Plant. Biol.* **15:** 103-110.

Kramer EM. 2004. PIN and AUX/LAX proteins: their role in auxin accumulation. *TRENDS in Plant Sci.* **9:** 1360-1385.

Krämer U, Sinclair SA. 2012. The zinc homeostasis network of land plants. *BBA Molecular Cell Research* **1823:** 1553-67.

Mott KA, Denne F, Powell J. 1997. *Interactions among stomata in response to perturbations in humidity.* Plant, Cell & Environment, **20:** 1098–1107, 1997.

Nobel, PS. 2005. *Physicochemical and environmental plant physiology.* Elsevier, 3rd edition.

Steudle E. 2000. Water uptake by plant roots: an integration of views. *Plant Soil* **226:** 45-56.

Talke IN, Hanikenne M, Krämer U. 2006. Zinc-dependent global transcriptional control, transcriptional deregulation, and higher gene copy number for genes in metal homeostasis of the hyperaccumulator *Arabidopsis halleri*. *Plant Physiology* **142**:148-167.

Proceedings of the 7th International Conference on Functional-Structural Plant Models, Saariselkä, Finland, 9 - 14 June 2013. Eds. Risto Sievänen, Eero Nikinmaa, Christophe Godin, Anna Lintunen & Pekka Nygren. http://www.metla.fi/fspm2013/proceedings. ISBN 978-951-651-408-9.

Spatial and temporal variability of leaf gas exchange and temperature responses of apple trees to drought assessed by a 3D turbid medium model

Jérôme Ngao[1,2], **Boris Adam**[1,2], **Marie Charreyron** [1,2] and **Marc Saudreau**[1,2]
[1]*INRA, UMR 547 PIAF, F-63100 Clermont-Ferrand, France,* [2]*UBP, UMR547 PIAF, F- 63000 Aubière, France*
**correspondence:* jerome.ngao@clermont.inra.fr

Highlights: Drought stress alters tree carbon and water balance, and it could affect pest and disease development as affected by changes in microclimate. Spatial and temporal variability of leaf gas exchange and microclimate (through leaf temperature) were assessed by adapting a 3D turbid medium model to drought stress and comparing model outputs to drought experiments.

Keywords: canopy microclimate, drought, leaf nitrogen, RATP model, stomatal conductance, transpiration

INTRODUCTION

Tree 3D-structure induces environmental and physiological gradients, which have to be taken into account for understanding the acclimation of various plant processes such as photosynthetic assimilation (A_{net}), stomatal conductance (g_S) and leaf transpiration (TR) to the main driving factors, particularly intra-canopy microclimate. Modelling such variability is also a prerequisite for upscaling to the whole plant or population. Numerous studies have investigated the acclimation of g_S and A_{net} to local light interception (Hollinger1996; Leuning et al. 1991). Spatial variability of A_{net} has been shown to be tightly related to that of light interception *via* leaf nitrogen distribution expressed per surface area (N_a, Thornley 2004). Characterization of the spatial distribution of g_S within the canopy has been done generally to relate it with hydraulic traits (Sperry et al., 2008), or to A_{net} (Prieto et al. 2012). Another consequence of the canopy light gradient is the spatial variability of the energy balance, particularly that of the latent heat (determined by g_S) and the sensible heat (leaf temperature, T_{leaf}) terms (Monteith and Unsworth 1990). Thus g_S may allow assessing and modelling spatial variability of T_{leaf}, which is an agronomic challenge in fruit tree species as the development of numerous pests are temperature-dependent.

The effects of summer drought on A_{net}, TR and g_S have been widely studied, and various models have been proposed (Damour et al. 2010). However, intra-canopy variability of such responses has received much less attention than temporal dynamics. One major difficulty lies on the tools available for assessing both the processes of interest (light interception, carbon assimilation, etc.) and their spatial distribution in a realistic way (Niinemets, 2012). Moreover, there are still very few models able to simulate T_{leaf} spatially distributed, and include leaf functions together with A_{net} and g_S.

The RATP model (Sinoquet et al., 2001) allows simulating (i) the radiation intercepted by the crown foliage, (ii) leaf temperature (T_{leaf}) and g_S as outputs of the energy balance, and (iii) A_{net} and TR (Fig. 1). It considers the canopy 3D structure by discretizing the crown foliage into voxels as turbid media, and thus allowing simulation of A_{net} and TR at both canopy level and voxel levels. This model has been applied for various aims, for example assessing the foliage randomness (Sinoquet et al., 2005), simulating the thermal microclimate and its effect on leaf miner development (Pincebourde et al., 2007), and disentangling structural and functional effects on TR and A_{net} (Massonnet et al., 2008). But until now, the RATP model relied on optimal water conditions, as the Jarvis g_S submodel (Jarvis, 1976) did not simulate the response to water potential, thus the model was not adapted to drought conditions.

Our aim was to assess spatial variability, and its temporal evolution, of transpiration, stomatal conductance and temperature responses of young apple trees to drought (*Malus pumila* Mill., var. Delbard Jubilé®). We adapted the RATP model to drought by adding a response function to soil water content in the Jarvis sub-model. We tested the TR outputs (TR_{RATP}) against xylem sapflow measurements as proxi values of total tree canopy transpiration (TR_{sap}) during drought experiments.

MODEL DEVELOPMENT AND PARAMETRIZATION

The g_S submodel as formulated by Jarvis (1976) was first parameterized for the photosynthetically active radiation (PAR), T_{leaf}, and vapour pressure deficit (VPD) response functions in optimal irrigation conditions.

Then during a two-week-long drought period, g_S was measured at different dates during which the *PAR*, T_{leaf} and VPD values were concurrently measured. The residuals between g_S simulated with the measured microclimatic variables and actual g_S, were linearly related to normalized soil water content. This linear relationship was added in the Jarvis subroutine.

For the foliage structure, only leafy shoots were digitized, and individual leaves were reconstructed by allometric relationships (Sonohat et al., 2006). Computations of transpiration and leaf temperature were performed at a 30-min time step according to the meteorological dataset. The model has been implemented in RATP and integrated into the OpenAlea plant modelling platform (Pradal et al., 2008)

RESULTS AND DISCUSSION

The temporal evolution of TR_{sap} prior the drought was mostly well reproduced by the model. TR_{sap} decreased dramatically eight days after the start of the water shortage and remained very low for several days after the end of the drought (Fig. 2). Driven by soil water content input data, simulated TR_{RATP} decreased dramatically six days after the start of the water shortage. The temporal shift between the TR_{sap} measurements and TR_{RATP} simulations may be attributed to the buffering effect of tree hydraulic capacitance (Sperry et al., 2008), which should be included in the response function, but not represented as input or intermediate data. Furthermore, while TR_{RATP} increased rapidly after irrigation restart, TR_{sap} for unharmed trees remained at very low level, and increased regularly up to five days after restarting irrigation, despite a very fast recovery of g_S. This could be explained by xylem embolism which may have developed during the drought period and decreased the sap flow rate (Cruiziat et al., 2002). Even if g_S recovered quickly to pre-drought levels, xylem vessels have to be refilled by water, but the involved mechanisms are still discussed (Nardini et al., 2011).

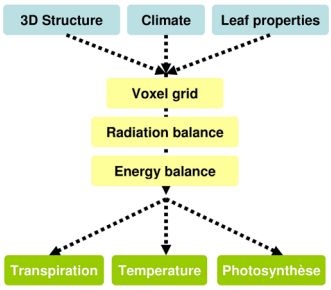

Fig. 1. Main features of the RATP model. The blue boxes are the input data, the main computation processes are in the yellow boxes and the outputs are in the green boxes. Each calculation step is done for each voxel at a 30-min time-step.

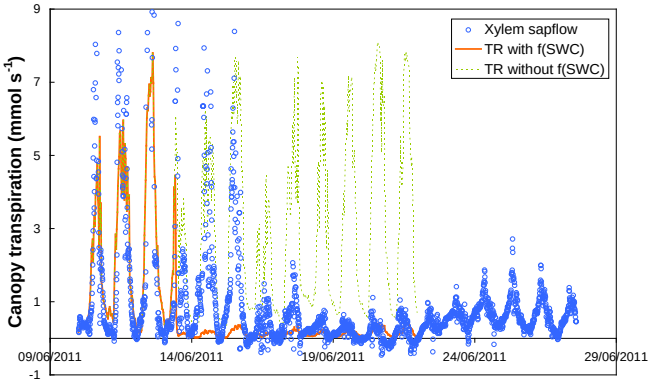

Fig. 2. Temporal course of canopy transpiration (i) as measured by xylem sapflow measurements (blue circles), (ii) as simulated by taking into account soil water shortage (orange lines) or not (green broken lines). The water shortage started on June 7, 2011. The simulations were stopped after June 22 as visible damages on the leaf crown were observed.

As expected, there was a large variability in TR_{RATP} values (Fig. 3a) when the trees experienced optimal irrigation conditions. At the end of the drought experiment, TR_{RATP} values were very low and varied in a very narrow range (Fig. 3b). Further simulations will allow determining the degree of heterogeneity of *TR* decrease during drought.

On the other hand, the mean T_{leaf} varied temporally according to the air temperature. Moreover, the T_{leaf} range under optimal water conditions varied at the diel scale up to 4°C (Fig. 4a), and according to air temperature. But when both simulations and measurements values of *TR* were very low, typically at the end of the drought period, the diel range of T_{leaf} decreased, averaging ≈ 2.5°C, even if the mean air temperature increased (Fig. 4b). This is in good agreement with measurements done on almond trees under drought by Gonzalez-Dugo et al. (2012).

Among the model parameters, the leaf nitrogen content expressed per area unit (N_a) had an important influence in the simulation outputs. In RATP, N_a drives the maximal g_S (g_{Smax}) which is degraded by the response functions of the Jarvis submodel. Leroux et al (1999) found a linear relationship between the daily cumulated PAR averaged over several days and N_a, allowing a fixed distribution of N_a within the canopy

Prieto et al. (2012) showed that N_a varied over the growing seasons in grapevines. This implies that seasonal changes in N_a distribution within the canopy have to be taken into account, as well its relationship with g_{Smax} for which Leroux et al. (1999) showed seasonal differences.

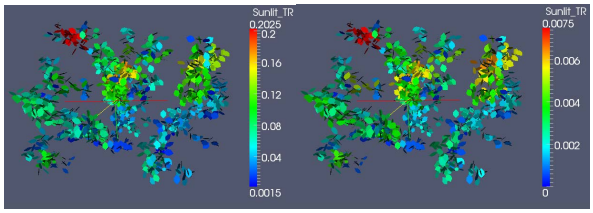

Fig. 3. Example of spatial distribution of sunlit leaf transpiration (a) on June 5th (optimal soil water content) and (b) on June 21st (end of the drought period). Both pictures display transpiration values at 12:00.

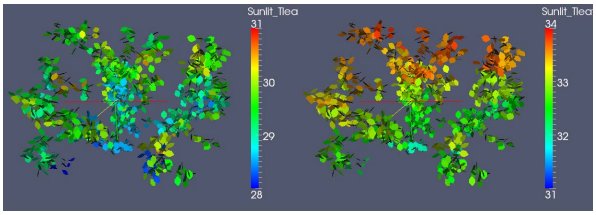

Fig. 4. Example of spatial distribution of sunlit leaf temperature (a) on June 5th (optimal soil water content) and (b) on June 21st (end of the drought period). Both pictures display transpiration values at 12:00.

LITERATURE CITED

Cruiziat P, Cochard H, Ameglio T. 2002. Hydraulic architecture of trees: main concepts and results. *Annals of Forest Science* **59**:723-752.

Damour G, Simonneau T, Cochard H, Urban L.2010. An overview of models of stomatal conductance at the leaf level. *Plant, Cell & Environment* **33**:1419–1438.

Gonzalez-Dugo V, Zarco-Tejada P, Berni JAJ, Suarez L, Goldhamer D, Fereres E. 2012. Almond tree canopy temperature reveals intra-crown variability that is water stress-dependent. *Agricultural and Forest Meteorology* **154**:156-165.

Hollinger DY. 1996. Optimality and nitrogen allocation in a tree canopy. *Tree Physiology* **16**:627-634.

Jarvis PG. 1976. The interpretation of the variations in leaf water potential and stomatal conductance found in canopies in the field. *Philosophical Transactions of the Royal Society B* **273**:593–610.

Le Roux X, Sinoquet H, Vandame M. 1999. Spatial distribution of leaf dry weight per area and leaf nitrogen concentration in relation to local radiation regime within an isolated tree crown. *Tree Physiology* **19**: 181-188.

Leuning R, Wang YP, Cromer RN. 1991. Model simulations of spatial distributions and daily totals of photosynthesis in *eucalyptus-grandis* canopies. *Oecologia* **88**:494-503.

Massonnet C, Regnard JL, Lauri PE, Costes E, Sinoquet H. 2008. Contributions of foliage distribution and leaf functions to light interception, transpiration and photosynthetic capacities in two apple cultivars at branch and tree scales. *Tree Physiology* **28**:665–678.

Monteith JL, Unsworth MH. 1990. Principles of Environmental Physics. Edward Arnold, London, p.291.

Nardini A, Lo Gullo MA, Salleo S. 2011. Refilling embolized xylem conduits: Is it a matter of phloem unloading? *Plant Science* **180**:604-611.

Niinemets Ü. 2012. Optimization of foliage photosynthetic capacity in tree canopies: towards identifying missing constraints. *Tree physiology* **32**:505-509.

Pincebourde S, Sinoquet H, Combes D, Casas J. 2007. Regional climate modulates the canopy mosaic of favourable and risky microclimates for insects. *Journal of Animal Ecology* **76**:424-438.

Pradal C, Dufour-Kowalski S, Boudon F, Fournier C, Godin C. 2008. OpenAlea: a visual programming and component-based software platform for plant modelling. *Functional Plant Biology* **35**:751-760.

Prieto JA, Louarn G, Pena JP, Ojeda H, Simonneau T, Lebon E. 2012. A leaf gas exchange model that accounts for intra-canopy variability by considering leaf nitrogen content and local acclimation to radiation in grapevine (*Vitis vinifera* L.). *Plant Cell & Environment* **35**:1313-1328.

Sinoquet H, Le Roux X, Adam B, Ameglio T, Daudet FA. 2001. RATP: a model for simulating the spatial distribution of radiation absorption, transpiration and photosynthesis within canopies: application to an isolated tree crown. *Plant Cell & Environment* **24**:395-406.

Sinoquet H, Sonohat G, Phattaralerphong J, Godin C. 2005. Foliage randomness and light interception in 3-D digitized trees: an analysis from multiscale discretization of the canopy. *Plant Cell & Environment* **28**:1158-1170.

Sonohat G, Sinoquet H, Kulandaivelu V, Combes D, Lescourret F. 2006. Three-dimensional reconstruction of partially 3D-digitized peach tree canopies. *Tree physiology* **26**:337-351.

Sperry JS, Meinzer FC, McCulloh KA. 2008. Safety and efficiency conflicts in hydraulic architecture: scaling from tissues to trees. *Plant Cell & Environment* **31**:632-645.

Thornley JHM. 2004. Acclimation of photosynthesis to light and canopy nitrogen distribution: an interpretation. *Annals of Botany* **93**:473-475.

Proceedings of the 7th International Conference on Functional-Structural Plant Models, Saariselkä, Finland, 9 - 14 June 2013. Eds. Risto Sievänen, Eero Nikinmaa, Christophe Godin, Anna Lintunen & Pekka Nygren.
http://www.metla.fi/fspm2013/proceedings. ISBN 978-951-651-408-9.

Dynamic properties of foliage photosynthesis

E. David Ford* and **Shawn Behling**
School of Environmental and Forest Science, University of Washington, Box 352100, Seattle, WA 98195, United States.
**correspondence: edford@u.washington.edu*

Highlights: Increasing results illustrate the importance of modelling photosynthesis as a dynamic process where the parameters of the standard photosynthesis curve vary in response to fluctuations in environmental conditions and developmental status of the plant. We describe how engineering approaches to the analysis of dynamic systems can be used and provide information for incorporating the dynamics of photosynthesis into large scale FSPMs.

Keywords: Photosynthesis, stomatal conductance, time constant, dynamic properties.

INTRODUCTION

An achievement of Functional-Structural Plant Modelling (FSPM) has been development of techniques for measurement and representation of the spatial distribution of plant organs and their connections. This in turn has led to a standpoint, expressed by Godin and Sinoquet (2005), that "the growth of the plant continuously modifies the network of components and space occupation, which in turn changes the general balance between organ demand and production." They refer to this as representing dynamic feedback between structure and function and suggest that its study requires integrating various sources of knowledge into a consistent modelling framework. Photosynthesis is the essential pre-requisite of plant growth and an important question is how to define its dynamics and potentially integrate that understanding in FSPMs. This is a challenge because models for leaf photosynthesis are most frequently designed to simulate instantaneous or short term changes of environmental conditions whereas many FSPMs are designed for longer terms when additional influences must be considered, e.g., sink control (Paul and Foyer 2001).

We consider two related problems. First: How can we measure and model the dynamics of photosynthesis? Increasingly research is showing variation in parameters of standard light saturation and A/C_i curves over daily and seasonal periods. We introduce some techniques used in the analysis of control systems that can aid in understanding such variation. We consider the types of question that may be asked using these techniques, the experiments and measurements that might be made and models that can be used to understand variation found in dynamic responses.

Second: What type of feedback might be expected in the control of photosynthesis? When we say a system is "dynamic" we frequently imply that it responds to change in some form of self-correcting way, which implies some form of "feedback". Engineers have developed theories of the control of dynamic systems and we examine how they may be applied to study of photosynthesis dynamics.

THE DYNAMICS OF PHOTOSYNTHESIS

Photosynthesis can be defined by its dependence on light and carbon dioxide concentration. There is well established theory that explains these relationships (Taiz and Zeiger 2010): production of ATP and NADPH by light reactions and their utilization in the Calvin-Benson cycle by which carbon from CO_2 is incorporated into organic compounds. The response of foliage photosynthesis to light can be fitted with the non-rectangular hyperbola model (Lambers *et al.* 1998, p27):

$$A = \frac{\phi \cdot Q + A_{\max} - \sqrt{(\phi \cdot Q + A_{\max})^2 - 4 \cdot \phi \cdot Q \cdot \theta \cdot A_{\max}}}{2\theta} - R_d \qquad (1)$$

in which Q is the available incident PPFD, A is the CO_2 assimilation rate, A_{max} is the assimilation rate at saturating light, ϕ is the apparent quantum efficiency (the initial slope of the linear part of the curve), θ is the convexity of the curve, and R_d is the dark respiration.

Equation 1 represents photosynthesis as an *instantaneous* system—the output of the process, A, the photosynthesis rate, depends upon light. The equation does not take into account whether prior conditions

may affect current photosynthesis rate. More complete analyses incorporating the components of gaseous diffusion through stomata, mesophyll and cell have been developed (e.g., Farquhar et al. 2001) but these too consider photosynthesis as a more complex but still an instantaneous system.

Studies of the effects of sunflecks on photosynthesis rate illustrate it does not respond instantaneously to increase in light but that there is an induction period (Way and Pearcy 2012). For example, when sunflecks are simulated experimentally as a step increase in light there is a generally curvilinear increase in photosynthesis rate. Investigators (see Way and Pearcy 2012) have described this rate of increase by calculating a time constant of response. The time constant equation for increase of photosynthesis from base value of zero is:

$$A = A_{max} * (1 - e^{(-t/\tau)}) \qquad (2)$$

where A_{max} is an estimated asymptotic value for maximum photosynthesis rate attained following the step increase in light, *t* is time, usually measured in seconds, and τ is the time constant and which represents the time it takes for the step response to reach 63.2% of the asymptotic maximum.

We present results and analyses showing that the response described by Eqn 2 is just one example of change in response to changing conditions. Different patterns of increasing photosynthesis in response to step functions of light for shade grown *Abies amabilis* and *Tsuga heterophylla* show leaves to be in different dynamic states associated with the ambient light they are receiving before the step increase. A frequently encountered pattern is represented by addition of two time constant equations one with τ in the range of 8 to 20 seconds and the other with τ in the range of 80 to 150 seconds. Another pattern is overshoot, where A increases to a maximum before settling to a lower value. These are well known response types found in engineering analyses of dynamic systems. For these species control of photosynthesis through variation in stomatal conductance, g_s, tends to occur over considerably longer time intervals with $\tau \sim 600$ s.

DYNAMIC SYSTEMS AND FEEDBACK

Porcar-Castell and Palmroth (2012) draw attention to the requirement for models that take account of the dynamic response of photosynthesis to changing conditions. However, they draw attention to an important problem: "While dynamic models present a substantial improvement compared to steady state models, their parameterization remains a challenge … because parameters change across time and space …"

Dynamic models of leaf photosynthesis are based on theories of chloroplast and leaf function and define pool sizes and conductance of precursors, enzyme characteristics and how these change in response to changes in the environment, particularly light. While recognizing the heuristic value of such models we present a complementary approach with two components: (a) examining the plant through different conditions of its growth and exposing it to changes in weather; while (b) applying step functions and other patterns of changing conditions used in the analysis of dynamic systems (e.g., Franklin et al. 2009). The purpose of this approach is to define variation in the photosynthesis system directly in systems terms i.e., using properties such as time constants of response to changes of different types and estimates of capacitance and resistance to flows of basic components.

Models representing photosynthesis as a series of metabolic pools and processes can make *a priori* assumptions about the type of control system that exists. These are typically open-loop control systems in which control action is dependent on fluctuations in resources and removal of products. This can be contrasted with active control systems such as controlled by transcription processes or removal of enzyme inhibitors which may be analogous to closed-loop control systems in which the control action is dependent on the output. For engineers: **"***Feedback* is a property of closed-loop systems which permits the output to be compared with the input to the system so that appropriate control action may be formed as some function of output and input" (Distefano et al. 2011).

An interesting question for study of dynamics of FSPMs in general and photosynthesis in particular is the extent to which the system can be represented as either a linked collection of open-loop systems with no active control or an active control system, e.g., through sink regulation (Paul and Foyer 2001). We will discuss over what time scales and conditions control of photosynthesis may be considered active or passive.

REFERENCES

Bauerle WL, Oren R, Way DA, Qian SS, Stoy PC, Thornton PE, Bowden JD, Hoffman FM, Reynolds RF. 2012. Photoperiodic regulation of the seasonal pattern of photosynthetic capacity and the implications for carbon cycling. *Proceedings of the National Academy of Sciences USA* **109**: 8612-8617.

Distefano J, Stubberud A, Williams I. 2011. *Schaum's Outline of Feedback and Control Systems.* Second edition. Ohio, McGraw-Hill.

Farquhar GD, voin Caemmerer S, Berry JA. 2001. Models of photosynthesis. *Plant Physiology* **125**: 42-45.

Franklin GF, Powell JD, Emami-Naeini A. 2009. *Feedback Control of Dynamic Systems.* Sixth edition. New York, Pearson.

Godin C, Sinoquet H. 2005. Functional-structural plant modelling. *New Phytologist* **166**: 705-708.

Mäkelä A, Hari P, Berninger F, Hänninen H, Nikinmaa E. 2004. Acclimation of photosynthetic capacity in Scots pine to the annual cycle of temperature. *Tree Physiology* **24**: 369-376.

Paul MJ, Foyer CH. 2001. Sink regulation of photosynthesis. *Journal of Experimental Botany* **52**: 1383-1400.

Pearcy RW, Gross LJ, He D. 1997. An improved dynamic model of photosynthesis for estimation of carbon gain in sunfleck light regimes. *Plant, Cell and Environment* **20**: 411-424.

Porcar-Castell A, Palmroth S. 2012. Modelling photosynthesis in highly dynamic environments: the case of sunflecks. *Tree Physiology* **32**: 1062-1065.

Taiz L, Zeiger E. 2010. *Plant Physiology.* Fifth Edition. Sunderland MA, Sinauer.

Way DA, Pearcy RW. 2012. Sunflecks in trees and forests: from photosynthetic physiology to global change biology. *Tree Physiology* **32**: 1066-1081.

Proceedings of the 7th International Conference on Functional-Structural Plant Models, Saariselkä, Finland, 9 - 14 June 2013. Eds. Risto Sievänen, Eero Nikinmaa, Christophe Godin, Anna Lintunen & Pekka Nygren. http://www.metla.fi/fspm2013/proceedings. ISBN 978-951-651-408-9.

Revealing the relative importance of photosynthetic limitations in cucumber canopy

Tsu-Wei Chen[1*], Michael Henke[2], Katrin Kahlen[3], Pieter H.B. de Visser[4], Gerhard Buck-Sorlin[5], and Hartmut Stützel[1]

[1]Institute of Biological Production Systems, Leibniz Universität Hannover, Herrenhäuser Straße 2, 30419 Hannover, Germany, [2]Department Ecoinformatics, Biometrics and Forest Growth, Georg-August University of Göttingen, Göttingen, Germany, [3]Geisenheim University, Von-Lade-Straße 1, 65366 Geisenheim, Germany, [4]Greenhouse Horticulture, Wageningen UR, Droevendaalsesteeg 1, 6708 PB Wageningen, the Netherlands and [5]UMR 1345 Institut de Recherche en Horticulture et Semences (IRHS), AGROCAMPUS OUEST Centre d'Angers, 2 rue André le Nôtre, 49045 Angers Cedex 01, France

[*]correspondence: chen@gem.uni-hannover.de

Highlights: We identified that in a two meter high greenhouse grown cucumber canopy, photosynthesis is mostly light-limited, and light interception and biochemical capacity are the major factors limiting photosynthesis. The diffusion pathways, stomatal and mesophyll conductance, are minor restrictions.

Keywords: Digitizing, photosynthesis, photosynthetic limitations, FvCB model, *Cucumis sativus*, *GroIMP*

INTRODUCTION

Improving the crop photosynthesis is important for increasing yield. To achieve this goal, methods to identify and to quantify the factors restricting photosynthesis are required. Several approaches to analyse the relative or quantitative magnitude of diffusional (stomatal and mesophyll resistance to CO_2) and non-diffusional (biochemical and light) limitations of photosynthesis are proposed in the literature (Jones, 1985; Wilson *et al.*, 2000; Grassi and Magnani, 2005; Grassi *et al.*, 2009). The method proposed by Grassi and Magnani (2005), by which the restriction of photosynthesis (% of maximum photosynthesis) can be quantitatively partitioned to the stomatal, mesophyll and biochemical components of limitations, is based on the Farquhar von Caemmerer and Berry model (FvCB model, Farquhar *et al.*, 1980) and considered to be a '*more complex*' but '*more realistic*' approach (Grassi *et al.*, 2009). However, Grassi´s approach can only be applied at light-saturated conditions (Rubisco-limited), and plants in nature, especially at canopy level, should be more often grown under non-saturated light conditions (RuBP-limited). Therefore, modification of Grassi´s approach is required if the limitation analysis should be conducted at canopy level. The objective of this work is to quantify the relative importance of the photosynthetic limitations. We used digitized data to reconstruct a static 3D greenhouse cucumber canopy using the interactive modelling platform *GroIMP*. A modified version of the limitation analysis of Grassi and Magnani (2005) was conducted. This modification allows the limitation analysis to be conducted at non-saturated light conditions, which correspond to the plant conditions in greenhouse.

MATERIALS AND METHODS

Reconstructing a 3D cucumber canopy using GroIMP

Whole plant architecture of cucumbers with 21 mature leaves grown in a greenhouse experiment was digitized as described by Wiechers *et al.* (2011b). Each leaf was represented by a predefined set of triangles and it was reconstructed using the commands *FloatList* and *PolygonMesh* in *GroIMP* (Kniemeyer, 2008). For reconstructing the virtual canopy structure, 18 cucumber plants with density 1.33 (plants per m^2) were distributed in 3 rows. Distance between plants in one row and distance between rows were 0.5 m and 1.5 respectively. The corresponding set-up was used in the virtual reconstruction.

Model description and limitation analysis

The light environment was simulated based on the approach of Buck-Sorlin *et al.* (2010) assuming the photosynthetic photon flux density (PPFD) above the virtual canopy is 600 µmol photon $m^{-2}s^{-1}$, diffuse/direct light ratio is 1:4 and sun position is on 1 July at 12:00. For computing the light distribution an advanced GPU-based ray-tracer, integrated into *GroIMP*, was used, with 10 million rays and a recursion depth of 10 reflections (Buck-Sorlin *et al.*, 2010). A modified version of limitation analysis according to Grassi and Magnani (2005) was used to identify and quantify the stomatal (S_{Lj}), mesophyll (MC_{Lj}), biochemical (JB_L) and light (JL_L) limitation of to photosynthesis (Chen *et al.*, in preparation):

$$\frac{A_{max}^{ref}-A}{A_{max}^{ref}} \cong S_{Lj} + MC_{Lj} + JB_L + JL_L = l_{sj} \cdot \frac{dg_{cs}}{g_{cs}^{ref}} + l_{mcj} \cdot \frac{dg_m}{g_m^{ref}} + l_j \cdot \frac{dJ_b}{J_{cmax}^{ref}} + l_j \cdot \frac{dJ_{light}}{J_{cmax}^{ref}} \quad (1)$$

where l_{sj}, l_{mcj} and l_j, are the relative limitations of stomatal and mesophyll conductance and the electron transport rate, g_{cs}^{ref}, g_m^{ref} and J_{cmax}^{ref} are their maximum values. The limitations are expressed in percentages of the potential photosynthesis (A_{max}^{ref}) . For this analysis, the intercepted light intensity at leaf level and the parameters of FvCB model and stomatal conductance for cucumber (Wiechers *et al.* 2011a) are used. Here, temperature is assumed to be 25°C.

RESULTS AND DISCUSSION

Photosynthesis is RuBP-regeneration limited

If the chloroplastic CO_2 concentration (C_c) was larger than the intersection point of FvCB model (C_{ctr}), photosynthesis was limited by RuBP-regeneration. Under light-saturated conditions, at which $C_c < C_{ctr}$, limitations were from CO_2-diffusion. In cucumber, C_c remained constantly around 200 µmol mol^{-1} (Fig. 1A and 1B) and at 600 PPFD C_{ctr} was below 150 µmol mol^{-1} (Fig. 1C). This indicated that under the simulated conditions the photosynthesis of the whole canopy was light-limited.

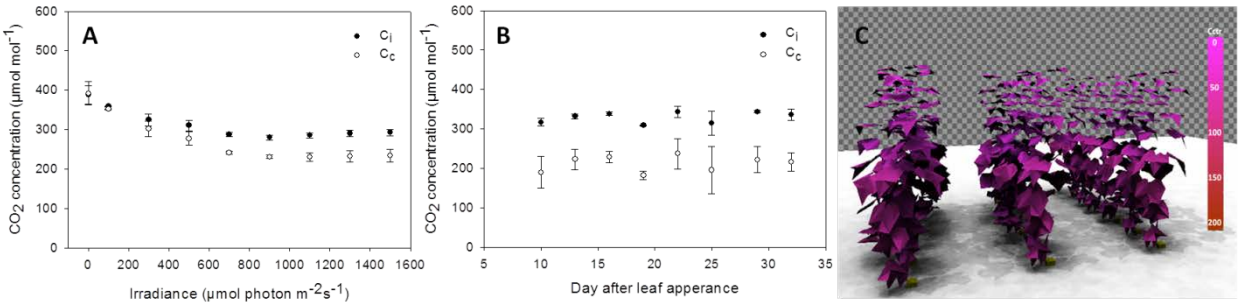

Fig. 1. (A) Influence of irradiance on the intercellular (C_i) and chloroplastic (C_c) CO_2 concentrations of cucumber leaves. (B) Under light saturated condition (1500 PPFD), C_i ranged between 300-320 µmol mol^{-1} and C_c were (n=3). (C) Simulated values of the intersection point of FvCB model (C_{ctr}) in cucumber canopy are between 0-150 µmol mol^{-1}, which is lower than C_i and C_c.

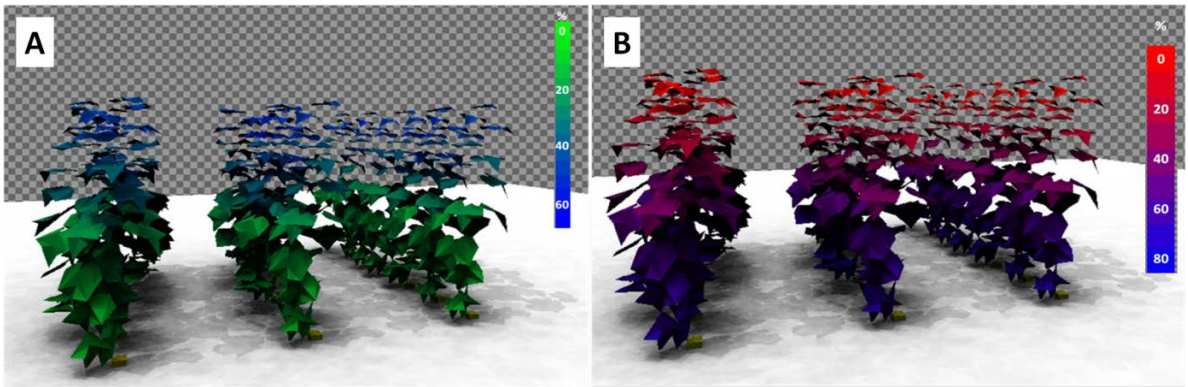

Fig. 2. Visualization of the light limitation (A) and biochemical limitation (B) within a 2 m high cucumber canopy. Light intensity above the canopy is assumed to be 600 µmol photon $m^{-2}s^{-1}$.

Sources of photosynthetic limitation

The sources of photosynthetic limitation changed dramatically with the canopy depth (Fig. 2A, 2B). The CO_2-diffusion pathways only restrict about 3-7 % of photosynthesis (Fig. 3A). The stomatal restriction increased with the leaf rank and mesophyll resistance only reduced less than 2% of the

photosynthesis capacity. Light interception and biochemical capacity were the most important factors reducing photosynthesis (Fig. 3B). At the lower canopy, about 68% of photosynthesis was limited by the biochemical capacity and 12% was limited by the light. At the upper canopy, 47% of the photosynthesis was restricted by light, without any biochemical limitation. Interestingly, although older leaves receive less light than the younger leaves, whereas older leaves are less light-limited than the youger leaves. This can be explained by the fact that the decrease in electron transport rate of the older leaves is mainly due to the reduction of biochemical capacity and improving the light interception of the leaves below rank 10 may only increase their photosynthesis rate up to 20%.

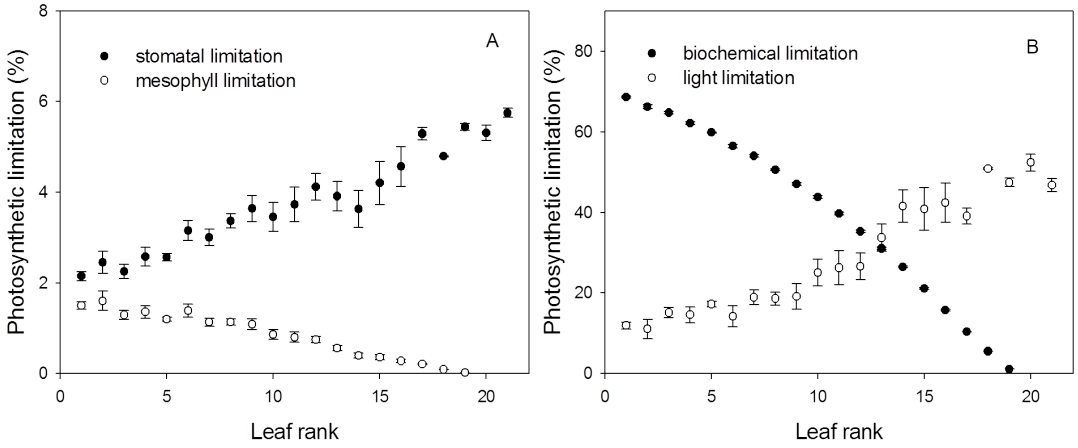

Fig. 3. Photosynthetic limitation. (A) The diffusion pathways of CO_2 restrict 4-6% of photosynthesis. Stomata limitation is 4% higher at upper part (higher leaf rank) than the lower part of the canopy. Above the rank 19, mesophyll limitation drops to zero. (B) Biochemical limitation of older leaves is about 70% and drops to zero at rank 20. Light limitation increases with leaf rank (n = 5).

Here we only demonstrate the simulation assuming that the PPFD above the canopy is 600 µmol photon $m^{-2}s^{-1}$. It will be fruitful to apply this analysis with different light intensities. Further simulations with different canopy structures (e.g. isometric or V-shape training system) and plant densities would also be helpful in discovering the influence of these factors on the photosynthetic limitation. Furthermore, it is known that temperature influences stomatal, mesophyll and electron transport rate. Therefore, a more complex description of the temperature response to these physiological processes would aid in revealing the interaction of temperature and photosynthetic limitation. Using a dynamic structural model (Kahlen and Stützel, 2011; Wiechers *et al.* 2011a) would enable us to explore the effect of developmental stage on photosynthetic limitation at canopy level. These analyses could help greenhouse farmers to determine the strategy for supplemental light.

LITERATURE CITED

Buck-Sorlin GH, Hemmerling R, Vos J, de Visser PHB. 2010. Modelling of spatial light distribution in the greenhouse: description of the model. In: Li B, Jaeger M, Guo Y, eds. Plant growth modeling, simulation, visualization and applications, Proceedings – PMA09. IEEE Computer Society Conference Publishing Services, 79–86.

Farquhar G, Caemmerer S von, Berry J. 1980. A biochemical model of photosynthetic CO_2 assimilation in leaves of C_3 species. *Planta* **149**: 78–90.

Grassi G, Magnani F. 2005. Stomatal, mesophyll conductance and biochemical limitations to photosynthesis as affected by drought and leaf ontogeny in ash and oak trees. *Plant Cell & Environ* **28**: 834–849.

Grassi G, Ripullone F, Borghetti M, Raddi S, Magnani F. 2009. Contribution of diffusional and non-diffusional limitations to midday depression of photosynthesis in Arbutus unedo L. *Trees* **23**: 1149–1161.

Jones HG. 1985. Partitioning stomatal and non-stomatal limitations to photosynthesis. *Plant Cell & Environ* **8**: 95–104.

Kahlen K, Stützel H. 2011. Modelling photo-modulated internode elongation in growing glasshouse cucumber canopies. *New Phytologist* **190**: 697–708.

Wiechers D, Kahlen K, Hartmut Stützel. 2011a. Dry matter partitioning models for the simulation of individual fruit growth in greenhouse cucumber canopies. *Ann. Bot.* **108**: 1075–1084.

Wiechers D, Kahlen K, Stützel H. 2011b. Evaluation of a radiosity based light model for greenhouse cucumber canopies. *Agricultural and Forest Meteorology* **151**: 906–915.

Wilson K, Baldocchi D, Hanson P. 2000. Spatial and seasonal variability of photosynthetic parameters and their relationship to leaf nitrogen in a deciduous forest. *Tree Physiol* **20**: 565–578.

Proceedings of the 7th International Conference on Functional-Structural Plant Models, Saariselkä, Finland, 9 - 14 June 2013. Eds. Risto Sievänen, Eero Nikinmaa, Christophe Godin, Anna Lintunen & Pekka Nygren. http://www.metla.fi/fspm2013/proceedings. ISBN 978-951-651-408-9.

Integrating architecture and physiological perspectives in fruit development

Mikolaj Cieslak[1^*], **Michel Génard**[2], **Frédéric Boudon**[3], **Valentina Baldazzi**[2], **Christophe Godin**[3], and **Nadia Bertin**[2]

[1]*Department of Computer Science, University of Calgary,* [2]*INRA, UR 1115 Plantes Systèmes de Culture Horticoles,* [3]*INRIA project-team Virtual Plants, with CIRAD and INRA, UMR AGAP*

^*The presented work was done as part of a postdoctoral fellowship with INRA*[2] *and INRIA*[3]

**correspondence:* msciesla@ucalgary.ca

Highlights: Architectural properties of a fruit, such as its shape, vascular patterns, and skin morphology, play a significant role in determining the distributions of water, carbohydrates, and nutrients inside the fruit. Understanding the impact of these properties on fruit quality is difficult, because they develop over time and are highly dependent on both genetic and environmental controls. We developed a 3D fruit model that can be used to investigate effects of the principle architectural properties on fruit quality.

Keywords: Fruit quality, water and carbon transport, fruit vasculature, skin microcracking, *Prunus persica*

INTRODUCTION

Fruit size, shape, composition and texture are all major qualities that determine consumer preference. Understanding the factors that regulate the development of these qualities is challenging, because they result from the interplay between physical and physiological processes that are under the control of both genetic and environmental factors. In the last 15 years, fruit quality has been largely investigated by using process-based models that treat the fruit as one large, homogeneous compartment, neglecting the fruit's internal structure (Bertin et al., 2006).

The architectural properties of a fruit, such as its size, shape, internal structure (number of carpels) and pattern of vasculature, however, can be remarkably diverse among varieties (Rodriquez et al., 2011). Since water and carbon are delivered to fruit tissues through a complex vasculature system, these architectural properties may have a significant impact on the distribution of water and carbon inside the fruit. For example, vascular patterns may account for the preferential supply of metabolites to specific tissues, and for causing physiological disorders such as blossom-end-rot (apical tissue necrosis) and shrivelling of the fruit's skin. Also, there is a positive relationship between the distribution of sugars inside the fruit and the morphology of its skin. Water loss due to transpiration depends on both the pattern and density of cuticular cracks (Gibert et al., 2007, 2010) and the microclimate surrounding the fruit (Li et al., 2001), which increases the soluble solids content (sugar level) inside the fruit.

The aim of this work was to investigate effects of fruit architectural properties on fruit quality by means of a 3D functional-structural fruit model that integrates architectural and physiological perspectives in fruit quality development, under the control of the environment. Existing 3D fruit models focus on the external shape of the fruit and treat its interior as homogeneous, without differentiation into tissue types (Saudreau et al., 2007, Mebatsion et al., 2011). Additionally, these fruit models do not consider the vascular tissue that supplies the fruit with resources and how the supply and other physiological processes affect fruit growth. In the following, we describe our generic 3D fruit model, which accounts for fruit shape, tissue compartmentalization, and vascular patterns, and use it to investigate the impact of fruit structure on sugar composition and distribution within a nectarine fruit.

RESULTS AND DICUSSION

We present a generic 3D fruit model that integrates architectural features and physiological processes of fruit development, with effects of the environment. For the fruit architecture, the geometry of the various fruit tissues is represented using 3D geometric shapes and the topological connections between them. For the physiological processes, we consider only those that are involved in the balance of water and carbon flows between the fruit, plant, and environment, as these drive fruit growth. In addition, we consider how this balance is modulated by exogenous factors like the availability of resources from the plant and the environmental conditions, such as temperature and humidity, and by endogenous factors that control the transport and accumulation of water and carbon to various fruit tissues via the xylem vessels and phloem

sieve tubes. The challenge is to represent the different fruit architectures as seen in nature, and to integrate the physiological processes that modulate fruit quality development.

A generic 3D model of fruit development

To construct a generic functional-structural fruit model, we developed a modelling pipeline in the OpenAlea platform (Pradal et al., 2009) that involves three steps: (a) creating a 3D volumetric mesh representation of the internal and external fruit structure, (b) generating a complex network of vasculature that is embedded within this mesh, and (c) integrating aspects of the fruit's function, such as water and carbon transport, with the fruit's structure. The model describes the late phase of fruit development when fruit growth is mostly due to cell expansion, once cell division has stopped.

Most methods for generating 3D fruit geometry represent the external shape of the fruit using equation-based techniques (Saudreau et al., 2007), or using reconstructions from images (Mebastion et al., 2011), and assume the fruit has a homogeneous internal structure. For that reason, in a previous work (Cieslak et al. 2012), we developed a procedure for generating a 3D volumetric representation of fruit architecture, including the external shape and internal structure. To generate the geometry of the large tissues, such as the pericarp, the reconstruction algorithm uses Delaunay refinement that produces high quality tetrahedral meshes from 3D image data (Alliez et al., 2011), where each tetrahedron is labelled according to the part of the fruit tissue it represents. To generate the geometry of the vascular tissue, we used an algorithmic approach based on the assumption that vascular bundles are competing for space within the fruit, which was originally proposed for synthesizing leaf venation patterns (Runions et al., 2005). Figure 1 shows architectural models of nectarine and peach fruit that were constructed using this procedure.

Based on this procedure, we made a generic model of fruit development by incorporating a model of water and carbon transport, which includes the flow of water and carbon in the fruit's vasculature. This was achieved by extending a previously developed process-based model of fruit growth (Fishman and Génard, 1998) with features of recently developed phloem-xylem transport models that can handle branched architectures (Lacointe and Minchin, 2007). In this approach, the tetrahedral elements of the mesh are treated as compartments that represent a collection of cells within the fruit, and the model captures the aggregated response of those cells to changes in water and carbon content. The transport of water and carbon through the vasculature is based on the hypothesis of osmotically driven bulk flow, where a hydrostatic pressure gradient (due to differences in local sugar concentrations) drives the flow of water and carbon between regions of sugar loading and unloading. In our model, we assume loading of sugar occurs outside of the fruit's vasculature so that sugar concentration in the pedicel is taken as input, whereas unloading may occur at any point inside the fruit that is linked by vasculature.

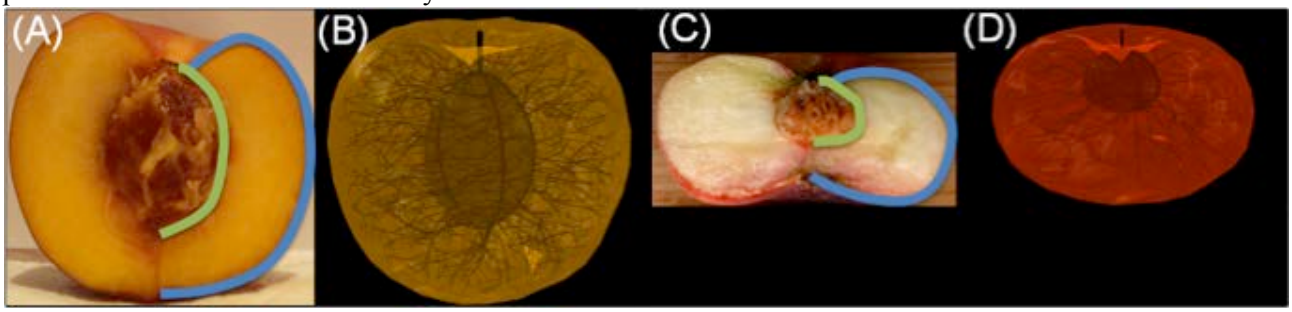

Fig 1. Architectural model of nectarine and peach fruit. The images (A,C) show a photograph of a longitudinal section of a nectarine and peach fruit, respectively, that were used to generate 3D volumetric meshes (B,D). The user-defined blue and green lines highlight the exocarp and endocarp, respectively, which are used to define two polyhedral surfaces (one for the stone and another for the fruit's surface) that serve as input into the mesh generation procedure. The green-line defines the main ventral and dorsal vascular bundles on the endocarp, whereas the branching secondary bundles are generated algorithmically according to the competition for space (Runions et al., 2005).

Application to modelling sugar distribution inside nectarine fruit

In nectarine fruit (*Prunus persica*), the spatial pattern of cuticular cracks on the fruit skin varies between the polar regions (stylar and peduncle ends) and equatorial regions (Gibert et al., 2007). This pattern changes the rate of water loss due to transpiration on different parts of the skin (Gibert et al., 2010), which may have an effect on the sugar concentrations inside the fruit. To analyse how such a pattern can cause a heterogeneous distribution of sugar inside a nectarine fruit, we used our functional-structural fruit model to perform simulations on the basis of our own experiments and on the work of Gibert et al. (2007, 2010).

The percentage of microcracks on 32 regions (four transversal and eight longitudinal sections) of the

fruit's skin has been measured by image analysis using a similar procedure as Gibert et al. (2007). For each of the 32 regions, the sugar content (degrees Brix) in the internal and external section of the fruit's mesocarp (for a total of 64 measurements) was assessed. A linear relationship was found between the percentage of microcracks and sugar content (degrees Brix) for both the external and internal regions of the fruit (Fig. 2A,B). A 3D visualization of the results shows a gradient of sugar concentration from the fruit interior towards the fruit surface (Fig. 3A).

We then created a functional-structural nectarine model using our modelling pipeline (Fig. 1B) and used it to simulate nectarine growth from 60 to 140 days after full bloom (dafb), because the heterogeneity in sugar distribution arises over time as the microcracks appear during the last 20 days of growth. During this time, the increase in fresh weight may be as much as 125 g (Gibert et al., 2007). The initial fresh mass was set to 25 g (Gibert et al., 2007) whereas the values of input variables (including temperature and humidity) and parameters were taken from a model of peach fruit growth (Fishman and Génard, 1998). However, the stomatal, cuticular, and crack components of conductance were modelled according to equations and parameters developed by Gibert et al., (2010). The percentages of cuticular cracks on the 32 regions of the fruit surface were taken from our own experiments, but the total cuticular crack surface area per fruit surface area was modelled as a function of the fruit fresh weight (g) according to data from Gibert et al., (2007).

At the end of the simulation (140 dafb), the sugar concentrations of the 64 exterior and interior regions of the fruit were compared with sugar content (degrees Brix) data from our own measurements. In qualitative agreement, the model output showed a direct linear relationship between sugar content and the percentage of microcracks (Fig. 2C,D). A 3D visualization of the model output also shows a gradient of sugar concentration from the interior to the exterior of the fruit (Fig. 3B). Furthermore, simulations with no microcracking (not shown) resulted in a decrease in sugar content for the whole fruit, which is in agreement with the observed outcome of covering fruit with clear plastic film (Li et al., 2001). Although the parameter values have not yet been fitted to data, these results show that our model is capable of simulating the observed effects of architectural features, like skin microcracking, on the quality of the fruit.

CONCLUSIONS

We integrated architectural and physiological perspective in fruit development to construct an integrative computational model of fruit. The result was a dynamic system that gives us the ability to model fruit growth driven by resource availability and exogenous factors like temperature and humidity. With this type of functional-structural model, it is possible to investigate the important architectural features that affect fruit quality. We demonstrated this by examining the role of skin microcracking on determining the distribution of sugar content in nectarine fruit. This model will lead to more work on quantifying the effects of architectural features on fruit quality, such as examining effects of asymmetric vascular structure on nutrient distribution in tomato fruit.

LITERATURE CITED

Alliez P, Rineau L, Tayeb S, Tournois J, Yvinec M (2011) 3D Mesh Generation. In CGAL User and Reference Manual. 3.8 ed: CGAL Editorial Board.

Bertin N, Bussières P, Génard M (2006) Ecophysiological models of fruit quality: a challenge for peach and tomato. *Acta Horticulturae* **718**: 633-645.

Cieslak M, Boudon F, Kenouche S, Zanca M, Goze-Bac C, et al. (2012) Generating 3D volumetric meshes of internal and external fruit structure. *Acta Horticulturae* **957**: 239-245.

Fishman S, Génard M (1998) A biophysical model of fruit growth: simulation of seasonal and diurnal dynamics of mass. *Plant, Cell and Environment* **21**: 739-752.

Gibert C, Chadœuf J, Vercambre G, Génard M, Lescourret F (2007) Cuticular Cracking on Nectarine Fruit Surface: Spatial Distribution and Development in Relation to Irrigation and Thinning. *Journal of the American Society for Horticultural Science* **132**: 583-591.

Gibert C, Génard M, Vercambre G, Lescourret F (2010) Quantification and modelling of the stomatal, cuticular and crack components of peach fruit surface conductance. *Functional Plant Biology* **37**: 264-274.

Lacointe A, Minchin PEH (2008) Modelling phloem and xylem transport within a complex architecture. *Functional Plant Biology* **35**: 772-780.

Li SH, Génard M, Bussi C, Huguet JG, Habib R, et al. (2001) Fruit quality and leaf photosynthesis in response to microenvironment modification around individual fruit by covering the fruit with plastic in nectarine and peach trees. *Journal of Horticultural Science & Biotechnology* **76**: 61-69.

Pradal C, Dufour-Kowalski S, Boudon F, Fournier C, Godin C (2008) OpenAlea: a visual programming and

component-based software platform for plant modelling. *Functional Plant Biology* **35**: 751-760.

Rodriguez GR, Munos S, Anderson C, Sim SC, Michel A, et al. (2011) Distribution of SUN, OVATE, LC, and FAS in the Tomato Germplasm and the Relationship to Fruit Shape Diversity. *Plant Physiology* **156**: 275-285.

Runions A, Fuhrer M, Lane B, Federl P, Rolland-Lagan AG, et al. (2005) Modeling and visualization of leaf venation patterns. *ACM Transactions on Graphics* **24**: 702-711.

Saudreau M, Sinoquet H, Santin O, Marquier A, Adam B, et al. (2007) A 3D model for simulating the spatial and temporal distribution of temperature within ellipsoidal fruit. *Agricultural and Forest Meteorology* **147**: 1-15.

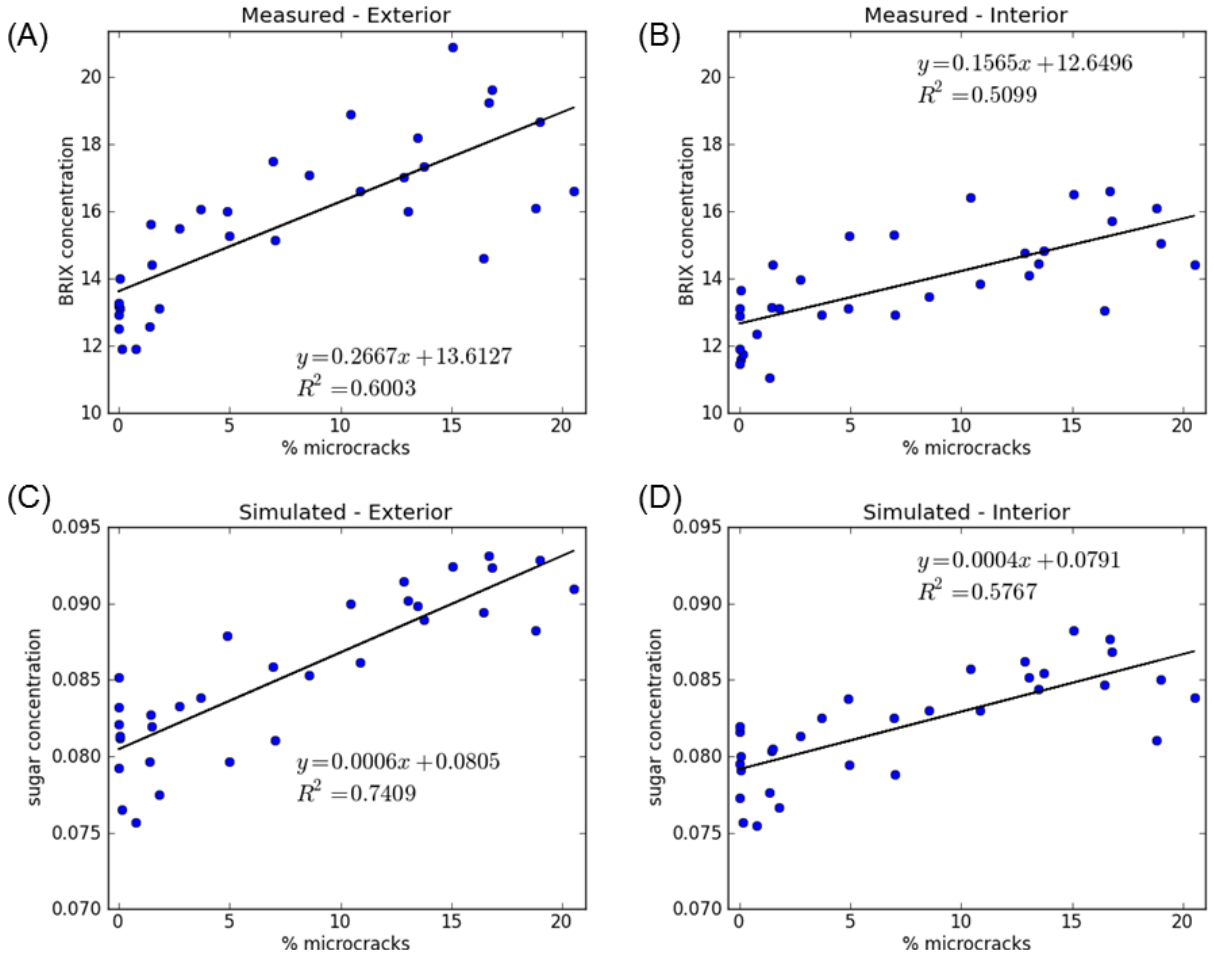

Fig. 2. Sugar content in nectarine fruit as a function of the percentage of microcracks at 140 dafb. The two graphs on the top show the results of measurements on the percentage of microcracks and sugar content (degrees Brix) in the exterior region (A) and interior region (B) of a nectarine fruit. The two graphs on the bottom show the simulations results of sugar content (g soluble sugars / g FW) in the exterior region (C) and interior region (D) obtained by modelling increased surface conductance due to microcracks.

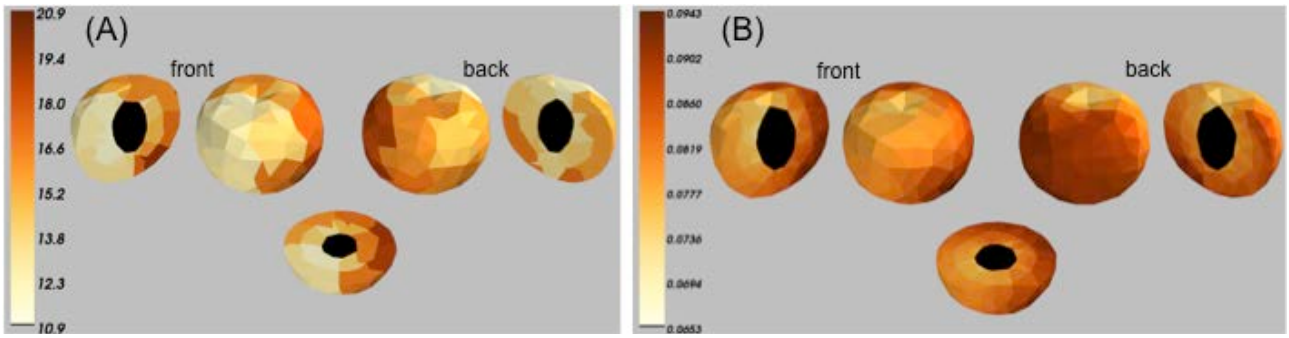

Fig. 3. A 3D visualization of sugar content in a nectarine fruit at 140 dafb. Each tetrahedron is coloured according to measured sugar content in degrees Brix (A), or to the model output in g soluble sugars / g FW (B). The visualization shows the whole fruit from the front and back, with corresponding longitudinal sections, and a transversal section. Dark brown indicates high sugar content while light yellow indicates low sugar content. The tetrahedra representing the stone are coloured black, as the sugar content is assumed not to change.

Proceedings of the 7th International Conference on Functional-Structural Plant Models, Saariselkä, Finland, 9 - 14 June 2013. Eds. Risto Sievänen, Eero Nikinmaa, Christophe Godin, Anna Lintunen & Pekka Nygren. http://www.metla.fi/fspm2013/proceedings. ISBN 978-951-651-408-9.

Up-scaling salt effects in cucumber: trade-off between photosynthesis and toxic ion accumulation

Tsu-Wei Chen[1*], Katrin Kahlen[2] and **Hartmut Stützel[1]**
[1]*Institute of Biological Production Systems, Leibniz Universität, Herrenhäuser Straße 2, 30419 Hannover, Germany,* [2]*Geisenheim University, Von-Lade-Straße 1, 65366 Geisenheim, Germany*
[*]*correspondence:* chen@gem.uni-hannover.de

Highlights: A dynamic cucumber FSPM, describing the effects of salinity on the plant morphology and the pattern of sodium accumulation in leaves, is parameterized and evaluated. This model is a first step in exploring mechanisms which improve plant tolerance and WUE at canopy level under salinity stress.

Keywords: Salinity stress, Na^+ accumulation, toxic effect, L-Cucumber, photosynthesis, transpiration

INTRODUCTION

Under salinity stress, concentrations of Na^+ and Cl^- ions in the xylem sap increase significantly (Wolf and Jeschke, 1987) and these two ions accumulate excessively in mature leaves (Munns and Tester, 2008). Once the cells in leaves become incapable of compartmentalising those ions in the vacuole, chlorosis or even necrosis appears (Stępień and Kłobus, 2006). Plants attempt to maximize carbon assimilation and minimize water loss, but there is a trade-off between transpiration and carbon assimilation. Optimization of this trade-off can be interpreted mathematically as the maximization of water use efficiency (WUE, assimilation per unit of water loss). Since the toxic ions are transported by the transpiration stream, an increase in WUE indicates a lower uptake of toxic ions per unit of carbon assimilated under salinity. This means that plants with higher WUE may delay the accumulation of ions to a toxic level which is in line with experimental results showing an inverse relation between Na^+ accumulation and WUE in a comparison of tomato cultivars (Al-Karaki, 2000). Moreover, inhibition of photosynthetic ability caused by accumulated toxic ions diminishes WUE further (Stępień and Kłobus, 2006). Therefore, a low WUE under salinity stress may even result in a negative feedback on plant growth. Since WUE and transpiration is closely related to leaf morphology and leaf distribution within canopy, functional-structural plant models (FSPM) should be a proper tool to study how WUE can be improved under salinity stress. The aim of this work is to construct and to parameterize the first FSPM describing Na^+ accumulation and its toxic effect on physiological functions.

MATERIALS AND METHODS

Experiments and measurements

Cucumber (*Cucumis sativus* L.), a salt sensitive crop, was chosen. Cucumber seedlings (‘Aramon’ Rijk Zwaan, De Lier, the Netherlands) were grown in three growth chambers in the Institute of Biological Production Systems, Leibniz Universität, Hannover, Germany. Cucumber plants were grown hydroponically under a 12-h photoperiod of 350 µmol $m^{-2}s^{-1}$ PPFD (photosynthetic photon flux density) with 24/20°C day-night temperature and 380 ppm CO_2 concentration with four salinity levels, 0, 28, 56 and 84 mM NaCl in solution. In experiment 1, light response curves of gas-exchange parameters (photosynthesis, stomatal conductance and transpiration) were measured between days 8-10 after salinity start using a Li-6400 gas analyzer (LI-COR Inc., Lincoln, NE, USA). Final organ size (leaf, petiole and internode) was measured and dry masses of plant materials were weighed after drying at 70°C for 72 hours. Thereafter, plant samples were ground for Na^+ analysis. Sodium concentration in the transpirational stream was estimated by total Na^+ accumulated in the shoot over total transpiration. These data were used for model parameterization. In the experiment 2, cucumber plants were grown at the same environmental condition and data were used to evaluate the model.

Model description

Cucumber architecture model is based on *L-Cucumber* (Kahlen and Stützel, 2011). Influences of salinity stress on plant morphology and physiology are sketched in Fig. 1. Final internode length (*FIL*) is reduced proportionally with salinity level S_s:

$$FIL(S_s) = FIL(1-0.0017S_s) \quad (1)$$

Stomatal conductance (g_s) is a function of PPFD (I_{Inc}) with additional influence by S_s and ion concentration in leaves (S_{leaf}):

$$g_s = f(S_{leaf})(g_{s\_min} + b\, I_{Inc})(1-\alpha S_s) \quad (2)$$

where minimum g_s (g_{s_min}) is 0.26, b and α are 0.0001 and 0.0065 respectively. $f(S_{leaf})$ is the function described in Fig.2. Light conversion efficiency (*LCE*) is influenced by I_{Inc}, osmotic restriction and S_{leaf}

$$LCE = f(S_{leaf})f(I_{Inc})(1-\beta S_s) \quad (3)$$

where $f(S_{leaf})$ is the function described in Fig. 2, $f(I_{Inc})$ is described in Wilson *et al.* (1992) and β (0.0047) is the osmotic effect on *LCE* derived from measured data. Transpiration (E) is linearly related to g_s ($E = 8.93g_s + 0.08$), and ion accumulation (S_{acc}) is the product of the ion concentration in the xylem sap (S_{xy}) and E. S_{xy} is calculated by S_s:

$$S_{xy} = 0.51e^{(0.05\,Ss)} \quad (4)$$

and 38% of S_{acc} was partitioned to the supporting tissues. The relationship between the Na^+ concentration and gas-exchange parameters was derived by normalizing and refitting corresponding published data (James *et al.*, 2002, Fig. 2). The reduction of leaf area due to salinity is determined by the dry weight partitioned to the leaves and specific area (290 $cm^2\ g^{-1}$, not influenced by salinity).

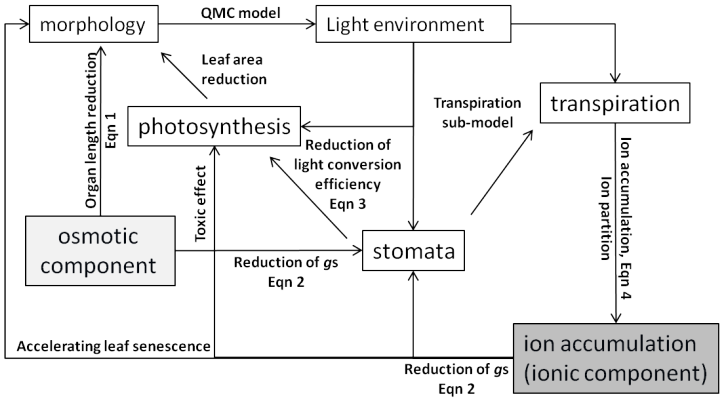

Fig. 1 Model structure representing effects of different components of salinity on morphology and function.

RESULTS AND DISCUSSION

In this model, a reduction of leaf area under salinity stress is due to the decrease of light conversion efficiency and then the dry mass partitioned to the leaves. In comparison with the control plants, leaf area at slight and high salinity stress (28 and 56 mM NaCl) was reduced about 15-20% and 50-60% respectively. The simulated results are quite in agreement with the measurements (Fig. 3).

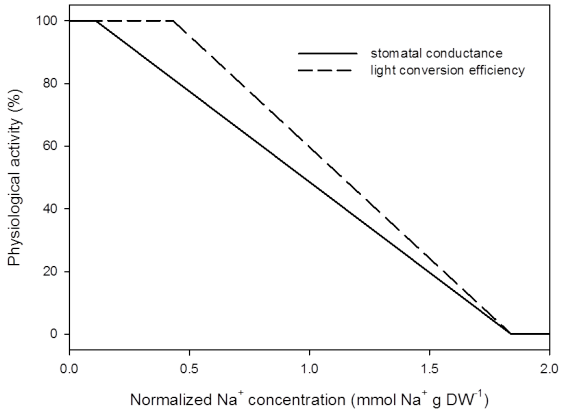

Fig. 2 Effects of Na^+ concentration on stomatal conductance and light conversion efficiency. The equations are obtained by refitting the data from James et al. (2002), which are normalized by the threshold Na^+ concentration of cucumber (1.84 mmol Na^+ g DW^{-1}).

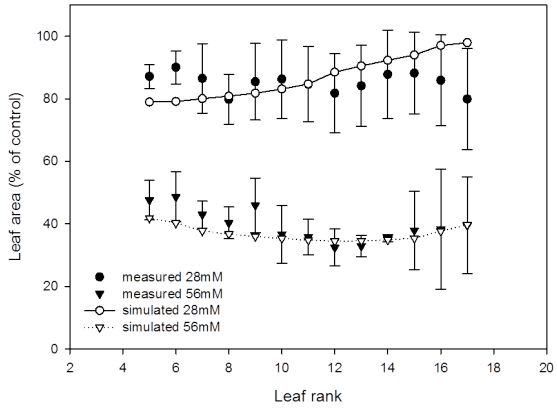

Fig. 3 Measured and simulated reduction of leaf area at 28 and 56 mM NaCl (n=3).

The patterns of Na^+ accumulation in the 6th leaves after leaf appearance (Fig. 4A) and the patterns of Na^+ concentration along the leaf rank after exposing to salinity for 28 days (Fig. 4B) can be simulated, but not very accurately, especially at high salinity level. Interestingly, the Na^+ concentration was overestimated at higher leaf rank but underestimated at lower leaf rank in both salinity levels (4B). Two arguments stated in

the literature could explain this model error: 1) S_{xy} should not be constant but decrease along the leaf rank, as described in the literature (Wolf and Jeschke, 1987) or 2) Na^+ reaching young leaves could be transported to old leaves via the phloem (Wolf *et al.*, 1991). However, the changes of S_{xy} along the stem are difficult to estimate accurately and could be influenced by the plant age and the length of stem (Wolf *et al.*, 1991). To estimate the re-translocation of Na^+ from young leaves to old leaves experimentally is even more difficult. Munns and Tester (2008) stated that this re-translocation is an important mechanism to avoid the damage of young leaves, but some authors suggest that Na^+ export has no significant contribution to the reduction of leaf Na^+ (Wolf *et al.*, 1991, Watson *et al.*, 2001). Our model framework could allow us to answer the following questions: 1) what are important mechanisms of Na^+ transport in plant? 2) How important is the Na^+ re-translocation to salt tolerance? 3) How to improve WUE by plant management strategies to avoid the toxic ion accumulation in leaves. To our knowledge, this is the first model up-scaling the Na^+ accumulation from leaf level to whole plant level and we expect that model improvement could provide insight to the and plant tolerance to ionic stress.

ACKNOWLEDGEMENTS

This work is supported by the German Research Foundation (DFG).

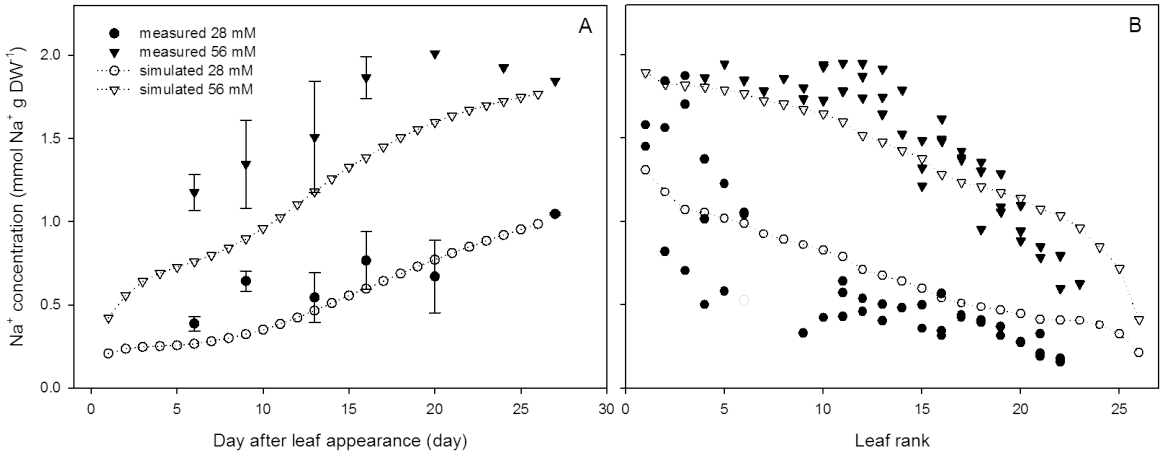

Fig. 4 Measured and simulated Na^+ concentration in the cucumber leaves at 28 and 56 mM NaCl. (A) Increase of the Na^+ concentration in the 6th leaves with days after leaf appearance and (B) the Na^+ concentration along the leaf rank after exposing to salinity for 28 days.

LITERATURE CITED

Al-Karaki GN. 2000. Growth, water use efficiency, and sodium and potassium acquisition by tomato cultivars grown under salt stress. *J. Plant Nutri.* **23**: 1–8.

James RA, Rivelli AR, Munns R, Caemmerer S von. 2002. Factors affecting CO_2 assimilation, leaf injury and growth in salt-stressed durum wheat. *Functional Plant Biol.* **29**: 1393.

Kahlen K, Stützel H. 2011. Modelling photo-modulated internode elongation in growing glasshouse cucumber canopies. *New Phytologist* **190**: 697–708.

Munns R, Tester M. 2008. Mechanisms of salinity tolerance. *Annu. Rev. Plant Biol.* **59**: 651–681..

Stępień P, Kłobus G. 2006. Water relations and photosynthesis in *Cucumis sativus* L. leaves under salt stress. *Bio. Plant.* **50**: 610–616.

Wilson J, Hand D, Hannah M. 1992. Light interception and photosynthetic efficiency in some glasshouse crops. *J. Exp. Bot.* **43**: 363–378.

Watson R, Pritchard J, Malone M. 2001. Direct measurement of sodium and potassium in the transpiration stream of salt-excluding and non-excluding varieties of wheat. *J Exp Bot* **52**: 1873–1881.

Wolf O, Munns R, Tonnet ML, Jeschke W. 1991. The role of the stem in the partitioning of Na^+ and K^+ in salt-treated barley. *J Exp Bot* **42**: 697–704.

Wolf O, Jeschke W. 1987. Modelling of sodium and potassium flows via phloem and xylem in the shoot of salt-stressed barley. *J. Exp. Bot.* **128**: 371–386.

Proceedings of the 7th International Conference on Functional-Structural Plant Models, Saariselkä, Finland, 9 - 14 June 2013. Eds. Risto Sievänen, Eero Nikinmaa, Christophe Godin, Anna Lintunen & Pekka Nygren. http://www.metla.fi/fspm2013/proceedings. ISBN 978-951-651-408-9.

A model of mechanics and gas exchange in a neighborhood of a single stoma

Ansgar Bohmann[1,*] and **Andrés Chavarría Krauser**[1]
[1]*Interdisciplinary Center for Scientific Computing & Center for Modelling and Simulation in the Biosciences, Universität Heidelberg, Im Neuenheimer Feld 368, 69120 Heidelberg, Germany*
**correspondence:* ansgar.bohmann@uni-hd.de

Highlights: The interplay of stomatal behaviour, epidermis mechanics, water flow, and diffusion is modeled dynamically with a system of ordinary and partial differential equations based on mechanical and thermodynamic principles. Simulation results of the discretised equations are shown.

Keywords: Stomata, mechanics, turgor, diffusion, model, simulation.

To gain insight in the physics and regulation of gas exchange (water vapour, carbon dioxide, and oxygen) in plant leaves we propose a dynamical first-principle model for a small disc-shaped section of a leaf around a single stoma (see Fig. 1). We consider different layers of tissues starting from the lower surface: the lower epidermis with a perfectly impermeaple cuticule and stomata controlled by guard cells, the interstitial air space, and the photosynthetically most active tissues (spongy and palisade parenchyma cells lumped together). The upper epidermis with its cuticule is assumed to contain no stomata and is treated as impermeable. We focus on the mechanical interaction between epidermis cells and guard cells, coupled to water transport driven by water potential gradients and diffusion of solvents in the symplastic and apoplastic compartments of the epidermis, as well as evaporation into and diffusion within the interstitial air space. Vapour exchange with the ambient air is controlled by stomatal aperture which in turn is determined by the mechanics and the guard cell solute content. During opening and closing of stomata solvents are pumped between the guard cell symplast and apoplast. The underlying physical processes, along with typical parameter values are described in standard literature (e.g. Nobel, 2005).

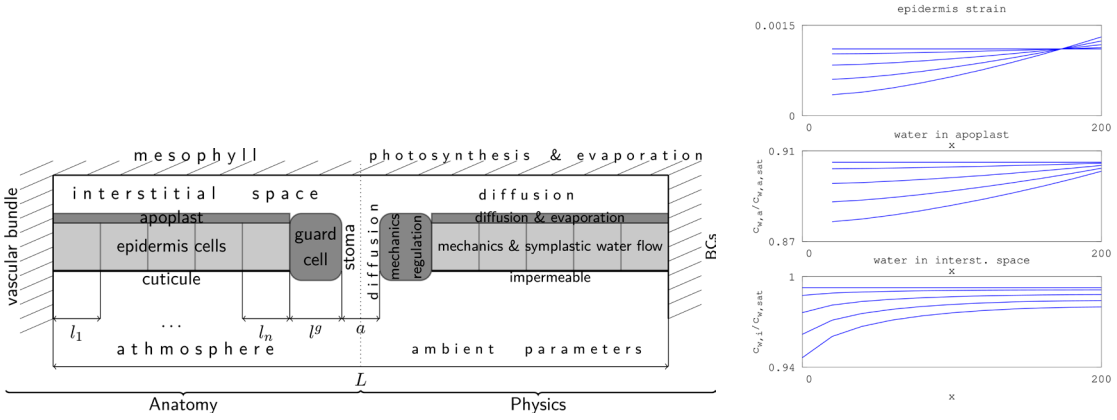

Fig. 1.a) Section through leaf centered around a single stoma b) Steady state profiles for apertures 0 – 10 µm

The structure of the resulting model is a coupled system of ordinary and parabolic partial differential equations (reaction diffusion equations). This provides a more detailed description in particular with respect to spatial resolution as compared to resistor network models. It also captures dynamic effects and links microscopic physical properties, such as known diffusion constants, to observable quanities such as stomatal aperture and net transpiration rates. It provides a physically accurate explanation to the inverse behaviour of stomatal aperture after sudden changes in ambient parameters such as ambient moisture (see Mott et al., 1997). A finite volume approach was applied for space discretisation and computational results are shown. This model is intended to serve as a building block for a more comprehensive model of the leaf.

LITERATURE CITED

Mott KA, Denne F, Powell J. 1997. *Interactions among stomata in response to perturbations in humidity.* Plant, Cell & Environment, **20:** 1098–1107, 1997.

Nobel, PS. 2005. *Physicochemical and environmental plant physiology.* Elsevier, 3rd edition.

Proceedings of the 7th International Conference on Functional-Structural Plant Models, Saariselkä, Finland, 9 - 14 June 2013. Eds. Risto Sievänen, Eero Nikinmaa, Christophe Godin, Anna Lintunen & Pekka Nygren. http://www.metla.fi/fspm2013/proceedings. ISBN 978-951-651-408-9.

A mechanistic model for the estimation of the quantum yield of photochemistry based on light, temperature, and chlorophyll a fluorescence

Beñat Olascoaga and **Albert Porcar-Castell**
Department of Forest Sciences, PO Box 27, 00014 University of Helsinki, Finland
**correspondence:* benat.olascoagagracia@helsinki.fi

Highlights: By studying chlorophyll a fluorescence emissions from a range of light intensities in Scots pine saplings acclimated to different temperatures, we aim to build a model to interpret chlorophyll a fluorescence capable of estimating the quantum yield of photochemistry (ϕ_P).

Keywords: chlorophyll a, fluorescence, Scots pine, *Pinus sylvestris* L.

INTRODUCTION

The analysis of the chlorophyll a fluorescence emitted from vegetation is an approach to estimate the light use efficiency (LUE), a term used for the estimation of gross primary productivity (GPP) by remote sensing, and the measurement of changes in fluorescence can be used to infer information about changes in ϕ_P, which is a good proxy of LUE.

Nevertheless, fluorescence is only one of the possible pathways in which the absorbed excitation energy can be used, and it competes with two other pathways: photochemistry, and thermal energy dissipation. The link between photochemistry and fluorescence is not trivial, and variations in fluorescence can be caused by both changes in photochemical or in non-photochemical energy utilization. This difficulty can be solved by studying chlorophyll a fluorescence by a saturating light pulse technique, which momentarily saturates the photochemical pathway and allows ϕ_P estimation from fluorescence parameters.

But this active technique cannot be implemented from large distances as those of remote sensing, where the sun-induced passive fluorescence is used instead. Thus, linking fluorescence to LUE in the absence of saturating pulse technique still remains to be improved.

The aim of this study is to develop a mechanistic model capable of bypassing the lack of saturating pulse capabilities in sun-induced fluorescence measurements by estimating the status of the reactions centres and quinone pools, the dynamics of photochemical capacity and non-photochemical quenching (NPQ), and energy fluxes from variations in fluorescence and using light and temperature to constrain photoinhibition and NPQ.

MATERIAL AND METHODS

In summer 2011, a total of 17 Scots pine (*Pinus sylvestris* L.) saplings growing in the field were transferred to a weather chamber and acclimated to different temperatures ranging from -5 to 40 °C. For each temperature, current-year needles were exposed to different light treatments ranging from 50 to 1500 μmol photons m^{-2} s^{-1} during an hour, and fluorescence emissions were recorded every second by a monitoring-PAM system (Heinz Walz GmbH, Germany). Fluorescence emissions were also recorded during sapling recovery in the darkness after the light treatments. During the whole process, a series of saturating light pulses (1s, 4000 μmol photons m^{-2} s^{-1} actinic light) were also given in order to get fluorescence parameters necessary to estimate ϕ_P.

RESULTS AND DISCUSSION

The maximum quantum yield of the photosystem II (Fv/Fm) was highest around 20 °C, and decreased gradually towards cooler temperatures. Fv/Fm decreased drastically towards warmer temperatures.

NPQ building under light reached higher values towards the highest light treatments, and reached faster a constant value under warm conditions, except in the coldest temperatures studied. NPQ relaxation in the darkness reached faster its initial values under warmer conditions except under -5 °C, where it was kept steady or even increased slightly.

The results concerning parameterization and model development are being developed and will be presented in the 7th International Conference on Functional-Structural Plant Models.

Proceedings of the 7th International Conference on Functional-Structural Plant Models, Saariselkä, Finland, 9 - 14 June 2013. Eds. Risto Sievänen, Eero Nikinmaa, Christophe Godin, Anna Lintunen & Pekka Nygren. http://www.metla.fi/fspm2013/proceedings. ISBN 978-951-651-408-9.

Simulated interaction between tree structure and xylem and phloem transport in 3D tree crowns using model LIGNUM

Eero Nikinmaa[1,*], Risto Sievänen[2], Jari Perttunen[2], and Teemu Hölttä[1]
[1]Department of Forest Sciences, PO Box 27, 00014 University of Helsinki, Finland, [2]Vantaa Res. Ctr, Finnish Forest Research Institute, PO Box 18, 01301 Vantaa, Finland
**correspondence*: eero.nikinmaa@helsinki.fi

Highlights: We have implemented xylem and phloem transport model (Hölttä et al. 2006) with 3D tree model LIGNUM to study how structural traits in tree crown influence the transport in branched architecture with observed transpiration and photosynthetic response to driving environmental variables. We study how structural traits in tree crown influence the xylem and phloem transport and associated pressure gradients when observed transpiration and photosynthetic response to driving environmental variables are applied in branched architecture.

Keywords: phloem translocation, sap flow, photosynthesis, transpiration, tree architecture

Transpiration of tree crowns is directly connected to xylem pathway conductivity from soil to transpiring leaves. Assimilate transport in phloem is closely connected to xylem transport (Hölttä et al. 2006). Low water potential in leaves will slow down phloem transport or cause even reversal of flow (Hölttä et al. 2006). The environmental variables that drive photosynthesis and transpiration vary a lot within tree crowns and canopies influencing the attainable photosynthetic and transpiration rates. The hydraulic architecture of a tree crown along with the environmental conditions at each site within the canopy will influence local (and thus global) assimilation and transpiration rates (Nikinmaa et al. 2012).

We combined the assimilation and transpiration model (Mäkelä et al. 2006), xylem and phloem transport model (Hölttä et al. 2006) with 3D tree model LIGNUM (Sievänen et al. 2008) for Scots pine trees. The xylem and phloem transport model deals with water pressure in xylem (P_x) and phloem (P_p) and the amount of sugar solute in phloem (N_p). In LIGNUM, the woody parts of trees consist of internodes. We formulate the transport model as differential equations for each internode as

$$\frac{dP_i}{dt} = a_i\left(Q_{i,ax,in} - Q_{i,ax,out}\right) + E_{xp} - S_i \;\; (i = x,p) \qquad \frac{dN_p}{dt} = a_n\left(Q_{i,ax,in} - Q_{i,ax,out}\right)N_p + L - U$$

where $Q_{i,ax,in}$ and $Q_{i,ax,out}$ are axial inflow and outflow of water, E_{xp} is accounting for flow of water between xylem and phloem in the internode, S_i is sink of water depending on transpiration rate of the internode, a_i and a_n are coefficients depending on physical conditions and the properties of the internodes (including volume and elastic modulus), and L and U are rates of loading and uploading of sugars. L is proportional to photosynthetic rate and U is proportional to growth and respiration rates of the internode. We solve the equations using fourth order Runge-Kutta method with time step of order of seconds and follow daily patterns of environmental drivers (radiation, temperature and water vapor deficit).

We study how vertical variation in xylem conductivity, variation in leaf-area vs. sapwood area relation in different branching orders and variation in phloem cross-sectional area reflect to diurnal within crown water and assimilate transport rates and water potentials and discuss the results against know features of tree transport. We use the results to evaluate feasible crown structure and its ecological significance.

LITERATURE CITED

Hölttä T, Vesala T, Sevanto S, Perämäki M, Nikinmaa E. 2006. Modeling xylem and phloem water flows in trees according to cohesion theory and Münch hypothesis. *Trees* **20**, 67–78.

Mäkelä A, Kolari P, Karimäki J, Nikinmaa E, Perämäki M, Hari P. 2006. Modelling five years of weather-driven variation of GPP in a boreal forest. *Agricultural and Forest Meteorology* **139**, 382-398.

Nikinmaa E, Hölttä T, Hari P, Kolari P, Mäkelä A, Sevanto S, Vesala T. 2012. Assimilate transport in phloem sets conditions for leaf gas exchange. *Plant Cell and Environment* First published online : 11 OCT 2012, DOI: 10.1111/pce

Sievänen R, Perttunen J, Nikinmaa E, Kaitaniemi P. 2008. Toward extension of a single tree functional structural model of Scots pine to stand level: effect of the canopy of randomly distributed, identical trees on development of tree structure. *Functional Plant Biology* **35**(9/10): 964-975.

Proceedings of the 7th International Conference on Functional-Structural Plant Models, Saariselkä, Finland, 9 - 14 June 2013. Eds. Risto Sievänen, Eero Nikinmaa, Christophe Godin, Anna Lintunen & Pekka Nygren. http://www.metla.fi/fspm2013/proceedings. ISBN 978-951-651-408-9.

Integrating water transport into L-kiwi using an aspect-oriented approach

Helge Dzierzon and **Alla N. Seleznyova**
The New Zealand Institute for Plant &Food Research Limited, Palmerston North 4442, New Zealand
**correspondence:* Helge.Dzierzon@plantandfood.co.nz

Highlights: A simple as well as transparent soil-vine water transport model was created and integrated into the functional model L-kiwi using L-Systems and the aspect-oriented approach. The model will play an important part in modelling variability of the fruit quality within the vine canopy.

Keywords: Water transport, *Actinidia deliciosa*, kiwifruit, plant model, aspect-oriented approach

Water transport from the soil into the plant canopy plays an essential role in plant growth and development; it brings nutrients from the soil and root-produced hormones from the roots and influences many physiological processes. In kiwifruit, effects of manipulations such as use of rootstocks and root pruning on water potential and water transport are of considerable interest. Hence, our aim was to integrate the water transport into an existing model of a kiwifruit vine, L-kiwi (Cieslak et al. 2011a). We chose a version of L-kiwi (Cieslak et al. 2011b) which uses an aspect-oriented approach based on multi-modules. Namely, each element of the plant structure is represented by a sequence of L-system modules with each module representing an aspect of the element's function. Separate sets of productions are used for modelling each aspect, with context-sensitive rules facilitated by local lists of modules to consider/ignore.

The biological system comprised a kiwifruit vine grafted on a rootstock. The initial model (Cieslak et al. 2011b) included sub-models for architecture, carbon transport, auxin transport and biomechanics. In the water transport sub-model, we used transpiration fluxes from the leaves as boundary conditions for the water transport system. We used an empirical model of daily variation of leaf transpiration rate and included a feedback of leaf water potential on transpiration as suggested by Jarvis (1976). Another boundary condition for the vine transport system was set by the soil water potential based on the soil relative water content (Thornley et al. 1990). The root/soil space was represented by a two dimensional finite element system (Blendinger 1996). Effect of soil water content on the soil conductivity was implemented as suggested by Thornley & Jonson (Thornley et al. 1990). At each derivation step of the model, the computation of water transport included three phases: calculating the water flux in the plant structure based on the transpiration fluxes from the leaves, calculating water potentials of the plant modules, and adjusting the values of the water fluxes to take into account feedback impacting water content in the soil and evaluating errors.

The resulting model is simple and transparent. The aspect-oriented approach allowed the addition of the water transport sub-model without changes to other aspects of the system. Compared to L-peach (Allen et al. 2005), which uses an electric circuit analogy for implementation of water transport, the current model is more straightforward and each of its variables has a direct physiological interpretation. In particular, we do not use a notion of electromotive force to represent transpiration of leaves, but rather use the transpiration directly as boundary conditions. Further, the soil component of the model is more comprehensive as it allows adding variation of the soil water potential on the root soil boundary. The model is able to represent the patterns of water potential distribution within the plant and responses to irrigation and soil drying. In the future, the model will include a sub-model of fruit fresh weight and dry weight which requires carbon concentration and water potential as boundary conditions at the point of fruit attachment. This will allow to model variability of the fruit quality within the vine canopy.

LITERATURE CITED

Cieslak M, Seleznyova AN, et al. 2011. A functional-structural kiwifruit vine model integrating architecture, carbon dynamics and the effects of the environment. *Annals of Botany 107*: 1025-1041.

Cieslak, M, Seleznyova AN, et al. 2011. Towards aspect-oriented functional-structural plant modelling. *Annals of Botany 108*: 1025-1041

Allen MT, Prusinkiewicz P, et al. 2005. Using L-systems for modeling source-sink interactions, architecture and physiology of growing trees: the L-PEACH model. *New Phytologist 166(3):* 869-880.

Jarvis PG 1976. The interpretation of the variations in leaf water potential and stomatal conductance found in canopies in the field. *Philosophical Transactions of The Royal Society of London, B 273(927):* 593-610.

Thornley JHM, Johnson IR. 1990. Plant and crop modelling: a mathematical approach to plant and crop physiology. Caldwell, NJ: The Blackburn Press.

Blendinger, Ch. 1996. Eine Approximation des gesättigt-ungesättigten Darcy-Flusses in dünnen Gebieten. Dissertation, Rheinische Friedrich-Wilhems-Universität zu Bonn.

Proceedings of the 7th International Conference on Functional-Structural Plant Models, Saariselkä, Finland, 9 - 14 June 2013. Eds. Risto Sievänen, Eero Nikinmaa, Christophe Godin, Anna Lintunen & Pekka Nygren. http://www.metla.fi/fspm2013/proceedings. ISBN 978-951-651-408-9.

Integration of a mechanistic biochemical and biophysical leaf gas exchange model in L-PEACH

Inigo Auzmendi[1,*], Romeo Favreau[2], David Da Silva[2] and **Theodore DeJong[2]**
[1]National Wine and Grape Industry Centre, Charles Sturt University, Locked Bag 588, Wagga Wagga, NSW 2678, Australia and [2]Department of Plant Sciences, University of California Davis, Davis, CA 95616, USA
[*]correspondence: iauzmendi@csu.edu.au

Keywords: Photosynthesis, transpiration, L-PEACH, plant growth simulation

L-PEACH is a functional structural model that simulates the growth of peach trees based on carbon partitioning between organs. Further development incorporated water transport, through transpiration and water potential, allowing studies of the effect of water stress on carbon partitioning (Da Silva *et al.* 2011). Our first approach to model leaf photosynthesis and transpiration with environmental sensitivity at an hourly time step, based on Kim and Lieth (2003), was not validated or computationally optimised. To overcome these issues we used the LEAFC3 model published by Nikolov *et al.* (1995). This model was computationally optimised and validated for forest trees and annual crops and it has been included in functional structural barley models. Even though LEAFC3 has been validated at the leaf level, this was done using an enclosed chamber, hence avoiding issues corresponding to whole plant estimations. Nikolov's model assumed that the leaf temperature was an input of the model or it was estimated from the bi-directional short and long-wave radiation absorbed by the leaf, which can be easily determined in an enclosed leaf chamber but is complex to determine in an open canopy. Instead, we employed an empirical function obtained from measurements of canopy temperature in peach trees growing in a well irrigated orchard (Glenn *et al.* 1989). This function connected the difference between leaf and air temperature to vapour pressure deficit, which can be estimated from air temperature and relative humidity. Hence, using this function is simpler and more computationally efficient than the energy balance previously used (Nikolov *et al.* 1995).

The leaf sub-model was developed as a stand-alone module that was integrated into L-PEACH as shown in Figure 1. The model was successfully used to simulate the effects of relative humidity on peach growth. This model integration is an important step for using functional-structural plant models in further studies to investigate long term effects of different environmental variables on canopy photosynthesis, transpiration, structure and yield characteristics, thus improving our understanding on the interactions of perennial plants with the environment.

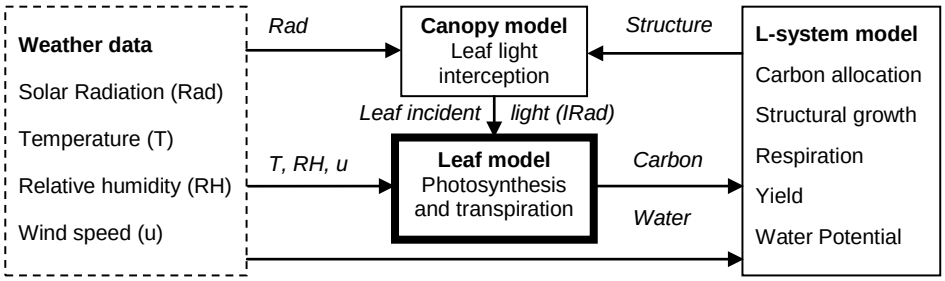

Fig. 1. Schematic representation of the integration of the mechanistic biochemical and biophysical leaf gas exchange model (leaf model) and the interactions with other sub-models in L-PEACH.

LITERATURE CITED

Da Silva D., Favreau R., Auzmendi I. and DeJong T.M. 2011. Linking water stress effects on carbon partitioning by introducing a xylem circuit into L-PEACH. *Annals of Botany* **108**: 1135-1145.

Glenn D.M., Worthington J.W., Welker W.V. and McFarland M.J. 1989. Estimation of peach tree water use using infrared thermometry. *Journal of the American Society for Horticultural Science* **114**: 737-741.

Kim S.H. and Lieth H.J. 2003. A coupled model of photosynthesis, stomatal conductance and transpiration for a rose leaf (*Rosa hybrida* L.). *Annals of Botany* **91**: 771-781.

Nikolov N.T., Massman W.J. and Schoettle A.W. 1995. Coupling biochemical and biophysical processes at the leaf level: an equilibrium photosynthesis model for leaves of C_3 plants. *Ecological Modelling* **80**: 205-235.

Proceedings of the 7th International Conference on Functional-Structural Plant Models, Saariselkä, Finland, 9 - 14 June 2013. Eds. Risto Sievänen, Eero Nikinmaa, Christophe Godin, Anna Lintunen & Pekka Nygren. http://www.metla.fi/fspm2013/proceedings. ISBN 978-951-651-408-9.

Towards integrating primary C-N metabolism and physiology of crop growth across different plant scales: the ProNet-CN model – a multiscale approach for functional-structural plant modeling

Johannes Müller*, **André Eschenröder, and Olaf Christen**
Institute of Agricultural and Nutritional Sciences, University of Halle-Wittenberg, D-06900 Halle, Germany
**correspondence:* johannes.mueller@landw.uni-halle.de

Highlights: ProNet-CN is a new multiscale process network integrating biophysical, metabolic, and physiological processes of biomass formation across plant scales. It combines the LEAFC3-N model describing the exchange of CO_2, water vapor, and energy with a new model of the dynamics of mass balances of main carbon and nitrogen metabolites and its allocation between interacting compartments or organs.

Keywords: Model, multiscale, photosynthesis, carbon, nitrogen, biomass

INTRODUCTION

The understanding of biological systems may be greatly enhanced by multiscale modeling approaches that span several structural and temporal scales and enable predicting emergent properties of the system using information from – respectively models of – more basic levels (Dada and Mendes 2011; Weinan, 2011). During last years, functional structural plant models were refined by integrating classical process-based plant models (review: de Reffye et al. 2009). On the other hand, current efforts in systems biology have triggered the development of detailed kinetic models of carbon and nitrogen metabolism (e.g., Poolman et al. 2004, Foyer et al. 2006; Rasse and Tocquin 2006; Uys et al. 2007; Nägele et al. 2010). Bridging the gap between these modeling domains could facilitate integrating the knowledge on plant processes across different scales. Here we present a first version of such a multiscale modeling framework.

MODEL

ProNet-CN calculates the dynamics of mass balances of main carbon (C) and nitrogen (N) metabolites, accounting for major biochemical conversions, allocation, and biomass formation. These processes are coupled across four nested scales: (i) metabolic scale, (ii) reaction compartments, (iii) organs, and (iv) plant (Fig. 1). To keep the complexity of the model manageable and consistent with the analytical capabilities, for the present we consider plants represented by only one shoot. Photosynthetic C input and transpiration (*Tr*) are calculated by the LEAFC3-N model (Müller et al. 2005; Braune et al. 2009). The water uptake and flux through the plant is assumed equal to *Tr*. Limiting soil water availability and plant water storage are not considered. N uptake is reduced to a passive influx of nitrate with the water stream. Mass balance and rate equations are formulated in terms of moles C and N associated with the considered metabolites. Concentrations are defined per projected organ area. Both individual steps and lumped sequences of biochemical reactions or transport are modeled phenomenologically in terms of Michaelis-Menten kinetics or as driven by a concentration gradient, respectively. If appropriate, extensions were introduced to account for control by concentrations of C or N metabolites. The formation of organic N-compounds is condensed to the stoichiometry of proteins and formally included into the C and N balances of the cytosol. The calculation of respiratory C losses relies on the concept of growth and maintenance respiration (McCree 1970). Leaf area growth is assumed proportional to the rate of synthesis of cellulose and hemicelluloses in leaves.

MATERIAL AND METHODS

Data were gathered on spring barley (*Hordeum vulgare* L.) grown in partially (glasshouse, exp. 1) or fully climatized (climate chamber, exp. 2) conditions at different levels of N supply (Müller et al. 2009). In exp. 1, lateral shoots were cut immediately after emergence to get a simplified plant structure. This enables to measure twice a week the CO_2 exchange and transpiration rates on all leaves and the characteristics listed below on all 'organs' comprising visible parts of the individual leaf blades, pseudo-stem (pooled nodes, internodes, leaf sheaths, enclosed parts of leaf blades, and ear before heading), ear after heading, and roots of the entire plant. The analyses involved dry mass, leaf area, chlorophyll (leaf blades), total C, C bound to soluble carbohydrates and to fiber substances, total N, N bound to nitrate, amino acids and amids, and to proteins. In exp.

2, main shoots were analyzed in similar way, whereas lateral shoots were pooled and analyzed for overall dry mass, total C, and total N. For parameterizing the LEAFC3-N photosynthesis model, light and CO_2 response curves of net photosynthesis rate were recorded in exp. 1 on all leaves and in exp. 2 on leaves of rank 4 and the leaf below the flag leaf (Braune et al. 2009; Müller et al. 2009). As additional information, data were available on the content of glucose, fructose, sucrose, starch, fructans (M.-R. Hajirezaei, IPK Gatersleben, Germany), and cell wall compounds (B. Usadel, MPI Potsdam-Golm, Germany) in barley leaves, as well as on the diurnal dynamics of main carbon metabolites in grasses grown under different N supply and CO_2 concentration (Isopp et al. 2000). Matlab-Simulink (The Mathworks®) was used as simulation environment. Simulation studies covered the development of barley plants from leaf emergence until ripeness. The environmental data recorded at plant height in exp. 1 were used in the simulation studies (time step 5 min).

RESULTS AND DISCUSSION

Generally, the simulated dynamics of the conversion and transport rates of the considered metabolites and of the related mass balances were in good agreement with both the expected response and the experimental data. As an example of the simulations, the net rate of the interconversion of two central metabolites of the carbon metabolism, namely of cytosolic hexose (Hex) and sucrose (Suc) for leaves 1 to 10 during plant ontogenesis are shown in Fig. 2 (in terms of mol C). This simulation output reflects that leaves 2 to 10 during their early phase of development are sinks for C (import of Suc and thus Suc → Hex dominates) and thereafter act as a source of C (export of Suc and thus Hex → Suc dominates). This is mirrored by similar patterns of the net transport rate of Suc into/out of the phloem (simulation not shown). Skipping a large number of analogous simulation results for other C and N metabolites, the growth patterns are shown in Fig. 3. Again, the simulation results were generally in good agreement with the data. A more detailed comparison with data is planned after further refinement of the model and improved calibration. Simulink was proved to represent a powerful tool for developing a multiscale dynamic systems model that integrates C and N metabolism, organ based C and N mass balances, and process up-scaling to biomass formation.

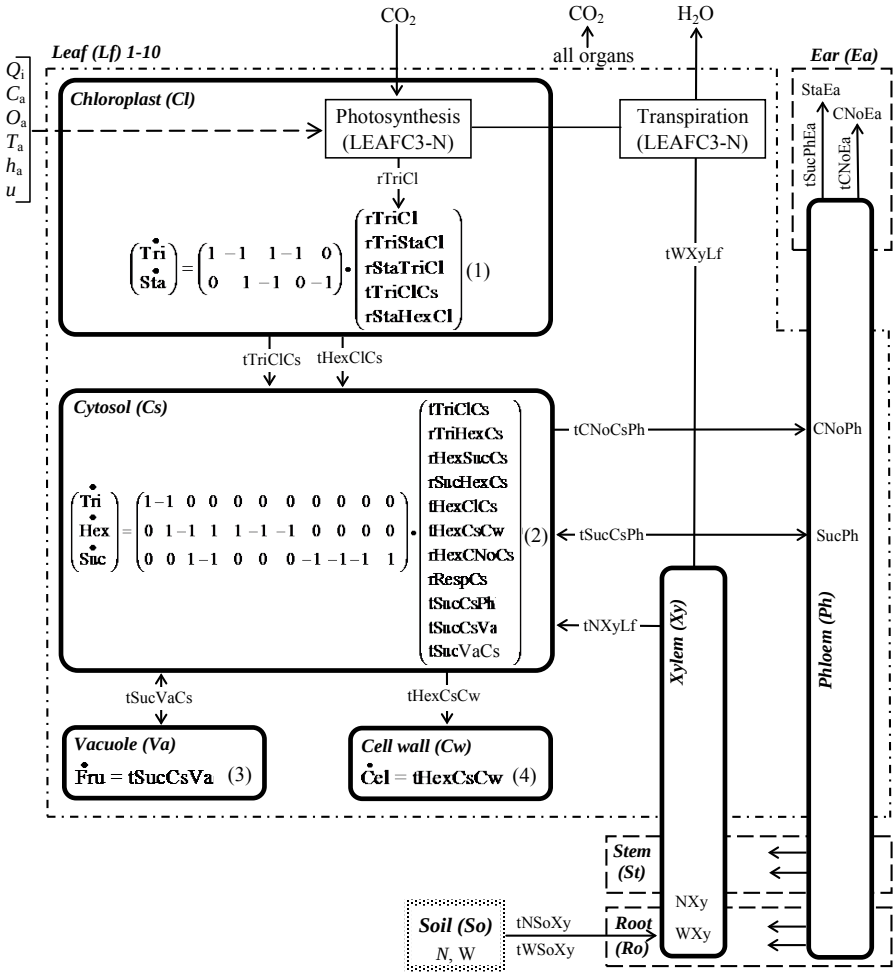

Fig. 1. Model scheme.

Model inputs: C_a – ambient CO_2 concentration, h_a – air humidity, N – nitrogen bound to nitrate in soil water, O_a – ambient oxygen concentration, T_a – air temperature, Q_i – incident irradiance, u – wind speed, W – water.

Carbon entities: Cel – C in cellulose and hemicelluloses, CNo – C in organic N compounds (mol), Fru – C in fructans (mol), Hex – C in hexoses (mol), Sta – C in starch (mol), Suc – C in sucrose (mol), Tri – C in trioses (mol).

Organs and compartments: see figure.

Composite symbols as in the following examples: HexCs – C in hexoses in the cytosol (mol), rTriHexCs – rate of C flux from triose phosphate to hexoses due to transformation of triose phosphate to hexoses in the cytosol (mol s^{-1}), tTriClCs – rate of C flux due to transport of trioses from chloroplast into the cytosol (mol s^{-1}).

Other symbols: rRespCs: rate of release of C from the sucrose pool in leaf cytosol due to growth and maintenance respiration.

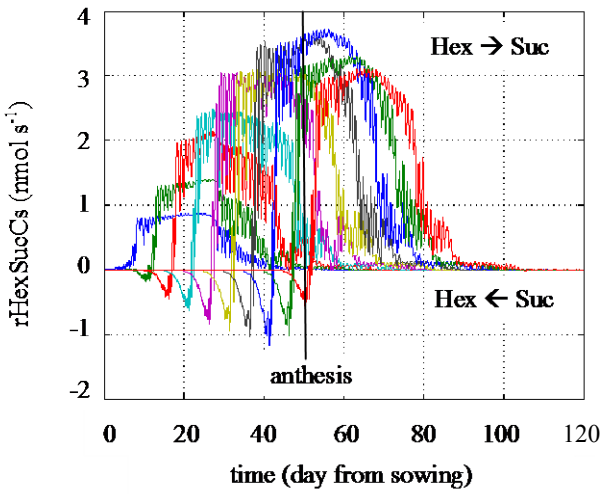

Fig. 2. Simulated ontogenetic courses of the rate of conversion hexose ↔ sucrose (rHexSucCs) in the cytosol of leaves of rank 1 to 10 (in terms of mol C s^{-1}). The fluctuations represent the diurnal cycles.

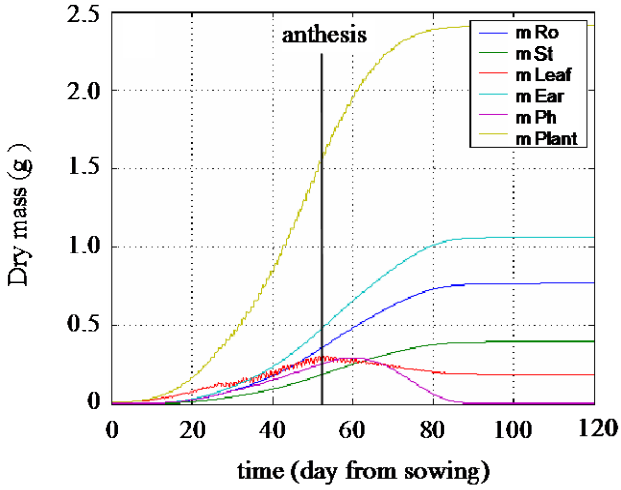

Fig. 3. Ontogenetic courses of dry mass of the whole plant (m Plant) and plant organs (Ro: root, St: fiber substances of the stem, m Ph: substances transported via phloem).

ACKNOWLEDGEMENT

This research was supported by the Federal Ministry for Education and Research (contract No. 0315426B). The authors thank two unknown reviewers for critics and helpful comments.

LITERATURE CITED

Braune H, Müller J, Diepenbrock W. 2009. Integrating effects of leaf nitrogen, age, rank, and growth temperature into the photosynthesis-stomatal conductance model LEAFC3-N parameterised for barley (*Hordeum vulgare* L.). *Ecological Modelling* **220**:1599-1612.

Dada JO, Mendes P. 2011. Multi-scale modelling and simulation in systems biology. *Integrative Biology* **3**:86-96.

De Reffye P, Heuvelink E, Guo Y, Hu B-G, Zhang B-G. 2009. Coupling process-based models and plant architectural models: a key issue for simulating crop prodiction. In: Cao W, White JW, Wang E (Eds.): *Crop Modeling and Decision Support.* Berlin Heidelberg/Beijing: Springer/Tsinghua University Press, 130-146.

Foyer CH, Noctor G, Verrier P. 2006. Photosynthetic carbon-nitrogen interactions: modellinfg inter-pathway control and signalling. In: Plaxton WC, McManus MT. 2006. Control of Primary Metabolism in Plants. Annual Plant Reviews **22**:325-347.

McCree KJ. 1970. An equation for the rate of respiration of white clover plants grown under controlled conditions. In: Setlik, I (Ed.): *Prediction and Measurement of Photosynthetic Productivity*. Pudoc, the Netherlands, pp. 221-229.

Isopp H, Frehner M, Almeida JFP, et al. 2000. Nitrogen plays a major role in leaves when source-sink relations change: C and N metabolism in *Lolium perenne* growing under free air CO_2 enrichment. *Australian Journal of Plant Physiology.* **27**:851-858.

Müller J, Wernecke P, Diepenbrock W. 2005. LEAFC3-N: a nitrogen-sensitive extension of the CO_2 and H_2O gas exchange model LEAFC3 parameterised and tested for winter wheat (*Triticum aestivum* L.). *Ecological Modelling* **183**:183-210.

Müller J, Braune H, Diepenbrock W. 2009. Complete parameterisation of photosynthesis models – an example for barley. In: Cao W, White JW, Wang E, eds. *Crop Modeling and Decision Support*. Berlin Heidelberg/Beijing: Springer/Tsinghua University Press, 12-23.

Nägele T, Henkel S, Hörmiller I, Sauter T, Sawodny O, Ederer M, Heyer AG. 2010. Mathematical modeling of the central carbohydrate metabolism in arabidopsis reveals a substantial regulatory influence of vacuolar invertase on whole plant carbon metabolism. *Plant Physiology* **153**:260–272.

Poolman MG, Assmus HE, Fell DA. 2004. Applications of metabolic modelling to plant metabolism. *Journal of Experimental Botany* **55**:1177-1186.

Rasse DP, Tocquin P. 2006. Leaf carbohydrate controls over *Arabidopsis* growth and response to elevated CO_2: an experimentally based model. *New Phytologist* **172**:500–513.

Uys L, Botha FC, Hofmeyr J-HS, Rohwer JM. 2007. Kinetic model of sucrose accumulation in maturing sugarcane culm tissue. *Phytochemistry* **68**:2375–2392.

Weinan E. 2011. Principles of Multiscale Modeling. Cambridge University press, 488 p.

Proceedings of the 7th International Conference on Functional-Structural Plant Models, Saariselkä, Finland, 9 - 14 June 2013. Eds. Risto Sievänen, Eero Nikinmaa, Christophe Godin, Anna Lintunen & Pekka Nygren. http://www.metla.fi/fspm2013/proceedings. ISBN 978-951-651-408-9.

Modelling zinc uptake and radial transport in roots

Juliane Claus[1*], Ansgar Bohmann[1] and **Andrés Chavarría-Krauser**[1]
[1]*Interdisciplinary Center for Scientific Computing & Center for Modelling and Simulation in the Biosciences, Im Neuenheimer Feld 368, 69120 Heidelberg, Germany*
**correspondence:* juliane.claus@bioquant.uni-heidelberg.de

Highlights: Modelling of zinc radial transport in roots was undertaken to understand the experimentally observed pattern of zinc accumulation near the central cylinder of the root. The model confirms the hypothesis that low abundance of the efflux transporter HMA4 produces this radial gradient in zinc concentration, but surprisingly, transpiration was found also to be a key parameter.

Keywords: zinc, radial transport, regulation, diffusion, root

Zinc is an essential micronutrient in green plants, yet toxic at high concentrations. Only specialized hyperaccumulator plants can tolerate high zinc doses and are therefore of special interest for their potential application in phytoremediation and crop development (Clemens et al., 2002). Zinc ions are taken up from the soil along with water and are transported radially towards the root's vascular bundle in two parallel pathways: the cell wall (apoplast) and the cytoplasm (symplast). Cross-membrane transport into and out of the cytoplasm is mediated by ZIP and HMA transporter proteins, respectively (Fig. 1). Experimental results show a pattern of zinc accumulation close to the centre of the root, which disappears at high levels of HMA (Hanikenne et al., 2008). Using a computational model, we study the roles of ZIP regulation, HMA level and water flow velocity in creation of this radial pattern.

A comprehensive one-dimensional dynamical model of radial zinc transport is developed to conduct simulations (Claus et al., 2012). This model accounts for the structure of the root consisting of symplast and apoplast and includes effects of water flow, diffusion, and cross-membrane transport via transporters. It also incorporates the radial geometry and varying porosity of root tissues, as well as regulation of ZIP transporters. We use existing biological data to estimate parameters and analyze the properties of the model in numerical simulations.

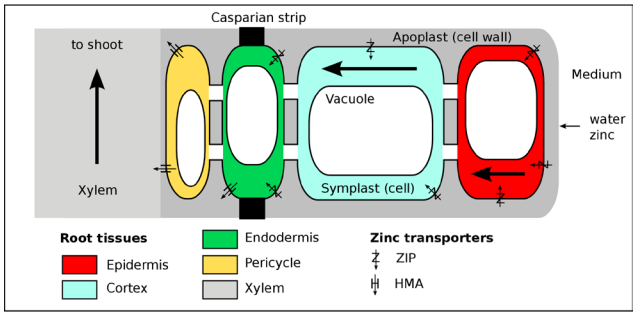

Apoplast:

$$\partial_t(\Psi\, rZ) + \partial_r\big((D/r)\,\Psi\, rZ - \Psi\, D\,\partial_r(rZ)\big) = r\,Q_{apo}$$

Symplast:

$$\partial_t(\Phi\, rZ) + \partial_r\big((v + D/r)\,\Phi\, rZ - \Phi\, D\,\partial_r(rZ)\big) = r\,Q_{sym}$$

Ψ, Φ	volume fraction in apoplast/symplast
r	radial coordinate
Z	zinc concentration
D	diffusion coefficient
v	water flow velocity
$Q_{apo,sym}$	membrane fluxes into apoplast, symplast

Fig. 1. Schematic description of zinc transport in roots from the medium towards the xylem. Arrows indicate the direction of transport. Equations on the right describe the radial transport of zinc in symplastic and apoplastic compartments (see Claus et al., 2012 for details).

In the steady state, the model reproduces the zinc gradient found in experiments as well as its loss at increased levels of HMA. Surprisingly, water flow velocity is found to be also a key parameter for producing this gradient. Simulations in time and space show short adaptation times to changes in external conditions. Since a slow ZIP regulation lead in these scenarios to high-amplitude oscillations, our results suggest that the time scales of regulation and transport need to be similar in the order of seconds to minutes.

LITERATURE CITED

Claus J, Bohmann A, Chavarría-Krauser A. 2012. Zinc uptake and radial transport in roots of *Arabidopsis thaliana*: a modelling approach to understand accumulation. *Annals of Botany*, doi: 10.1093/aob/mcs263

Clemens S, Palmgren MG, Krämer U. 2002. A long way ahead: understanding and engineering plant metal accumulation. *TRENDS Plant Sci.* **7**:309-315s.

Hanikenne M, Talke IN, Haydon MJ, et al. 2008. Evolution of metal hyperaccumulation required *cis*-regulatory changes and triplication of HMA4. *Nature* **453**:391-395.

Proceedings of the 7th International Conference on Functional-Structural Plant Models, Saariselkä, Finland, 9 - 14 June 2013. Eds. Risto Sievänen, Eero Nikinmaa, Christophe Godin, Anna Lintunen & Pekka Nygren. http://www.metla.fi/fspm2013/proceedings. ISBN 978-951-651-408-9.

Simulating the impact of ("long-distance" or "root-to-shoot") hormonal signaling and non-uniform soil water distribution on plant transpiration

K. Huber[1,*], J. Vanderborght[1], M. Javaux[1,2], N. Schroeder[1,3], I. Dodd[4], H. Vereecken[1]
[1]Agrosphere (IBG-3), Forschungszentrum Juelich GmbH, Germany; [2]Earth and Life Institute, Université Catholique de Louvain, Belgium; [3]Juelich Supercomputing Centre, Forschungszentrum Juelich GmbH, Germany; [4]The Lancaster Environment Centre, Lancaster University, UK
**correspondence:* k.huber@fz-juelich.de

Highlights: In response to non-uniformly distributed soil water, root water uptake and actual (whole plant) transpiration was simulated using R-SWMS as part of the soil dried. These variables varied widely (reduction between 10 and 55 percent) between plants with different controls of stomatal conductance, i.e. controlled by leaf pressure and/or by the concentration of a hormonal signal triggered by low root water potentials in dry soil regions. Hormonal regulation of transpiration was effective only for a limited time, when water flow out of drying soil regions was sufficient to transport hormones to the shoot.

Keywords: R-SWMS, hormonal signaling, transpiration reduction, stomatal conductance

THEORY

Low soil water availability causes most plants to reduce their actual transpiration, T_{act}, via stomatal closure. Tardieu and Simmoneau [1998] classified stomatal adjustments for several different species and distinguished between isohydric and anisohydric plant types, the first type keeping leaf water pressure h_{leaf} constant via stomatal closure during drying and the latter type showing decreasing h_{leaf} for higher transpiration rates and lower soil water contents.

The triggers for stomatal closure that reduceT_{act} compared with the potential transpiration, T_{pot} can be driven either by plant hydraulics, hormonal signaling or a combination of both (Equation 1) [*Tardieu and Davies*, 1993].

$$\alpha = \left(g_{s,min} + \left(g_{s,max} - g_{s,min}\right) e^{\beta[signal]e^{\delta h_{Leaf}}} \right) \frac{1}{g_{s,max}} \quad \textbf{(1)}$$

where $g_{s,min}$ and $g_{s,max}$ are minimal and maximal stomatal conductances [µmol cm^{-2} d^{-1}], [signal] is the hormone concentration in the leaf [µmol cm^{-3}], h_{Leaf} [cm] is the pressure head in the leaves, and β [cm^3 $µmol^{-1}$] and δ [cm^{-1}] are empirical parameters. The reduction factor α [-] is the ratio between T_{act} and T_{pot} and takes values between 0 and 1.

The most common studied plant hormone that is responsible for stomatal closure is abscicid acid (ABA) [*Davies et al.*, 2005]. As the soil dries, the rate of ABA produced by the roots increases and is proportional to the root water pressure [*Simonneau et al.*, 1998]. It is assumed that the ABA is transported with the xylem water flow towards the leaves to trigger stomatal closure.

SIMULATIONS

Virtual experiments were simulated using R-SWMS, which describes the water flow in the soil, towards, and in the 3-D network of roots mechanistically and based on basic laws of fluid dynamics [*Javaux et al.*, 2008]. This model simulates the soil, root, and leaf water pressure heads. To model the hormonal signal concentrations in the leaf, [signal], a transport equation in the root network with signal mass production rate at the root tips, M_{signal} [µmol d^{-1}], and advection terms in the root xylem segments that are derived from the flow equation was solved using a particle tracking algorithm. M_{Signal} is a function of the pressure head at the root tips, h_{root} (Eq. 2).

$$M_{signal} = \begin{cases} 0 & for\ |h_{Root}| < |h_0| \\ a\ h_{Root} - b & for\ |h_{Root}| \geq |h_0| \end{cases} \quad \textbf{(2)}$$

where a [µmol cm^{-1} d^{-1}] and b [µmol d^{-1}] are production factors and h_0 is a threshold potential that triggers the signal production. The particle tracking algorithm simulates the mass flux of the signal at the root collar

which is divided by the transpiration stream to obtain the signal concentration in the leaf. The signal concentration may also be calculated by assuming that all produced signal arrives instantaneously at the root collar by dividing the sum of the signal production rates at the root tips by the transpiration stream (Eq. 3)

$$[signal] = \frac{\sum M_{signal}}{T_{act}} \quad \textbf{(3)}$$

Stomatal conductance is not modeled explicitely but as a reduction factor (varying between 0 and 1) for T_{pot} using Equation 1.

Simulations were conducted in a virtual split root setup in a soil domain of 15.5 cm depth and 21 cm² soil surface with a top soil boundary condition (irrigation) of 10 $cm^3 d^{-1}$ and an upper root boundary condition (T_{pot}) of 9.9 $cm^3 d^{-1}$. Initial soil water content was uniformy distributed over depth. The irrigation was uniform over the total soil domain for the first 5 days. Then the same irrigation rate was applied only to one side of the soil domain. Hence only the water distribution changed; the plants had always sufficient water to maintain T_{pot}.

Five different cases were compared (Table 1). For the first case, denoted as **'PH (pressure head)'**, the upper root boundary condition (h_{leaf}) cannot be lower than a critical water potential h_{crit}. If h_{leaf} reaches h_{crit} the type of the upper boundary condition is switched from flow to constant water potential. For **'Signal'**, T_{act} is calculated with Equation 1 and δ zero so that the leaf water pressure has no influence on stomatal closure. For **'PH+Signal'** also the influence of of h_{leaf} on stomatal conductance is considered. To compare the impact of signal transport towards the leaf 'PH+Signal' is also calculated assuming an instantaneous signal without simulating transport (**'PH+Sign inst.'**). Those four cases are compared with **'No Regulation'**, where stomata remain fully open.

Table 1. Model parameters*

	PH	**Signal**	**PH+Signal**
$\|\psi_{Crit}\|$	*-7100*	-	-
β	-	$1*10^{-3}$	$1*10^{-3}$
δ	-	*0*	$1*10^{-5}$
a	-	$1.5*10^{-4}$	$1.5*10^{-4}$
b	-	*1.065*	*1.065*
$\|\psi_0\|$	-	*-7100*	*-7100*

* Orders of magnitude from *Tardieu and Davies* [1993]

RESULTS AND DISCUSSION

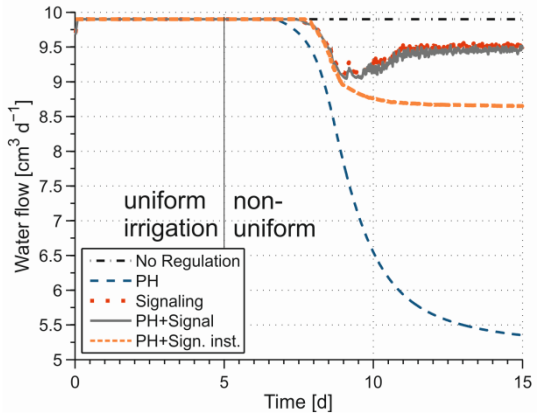

Fig. 1. Comparison of actual (whole plant) transpiration rate for the five different cases

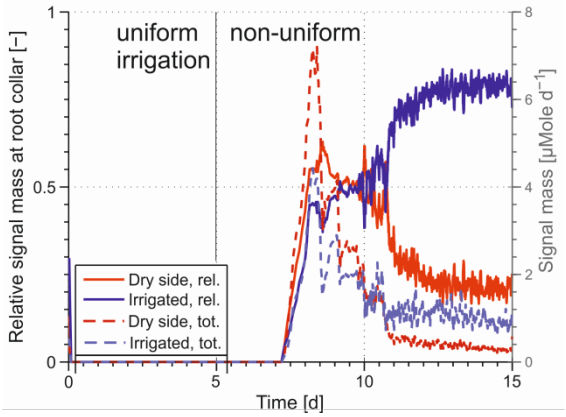

Fig. 2. Rates of signal mass arriving at the root collar and originating from the dry and irrigated side for PH+Signal case: left axis; relative signal mass rates normalized by the total signal mass rates, right axis: absolute signal mass rates.

Figure 1 shows that the onset of transpiration reduction is earlier for the purely hydraulic regulation ('PH'). Transpiration for the signaling cases with transport first decreases but start to increase around day 9. This seems counter-intuitive as the stress for the drying part of the soil system is still increasing. Through comparison with the'PH+Sign.inst.' case, this effect can be related to particle transport. Initially the relative signal mass (solid lines in Figure 2) arriving at the root collar from the dry side is higher than that arriving from the wet side. But around day 9 the ratios change and about 75% of the signal arriving at the leaves originates from the irrigated part of the root system. After four days of drying there is no more water uptake from the dry soil part. Therefore the water velocity inside the dry roots is close to zero so that produced signal is not transported anymore. This leads to a distinct maximum in the signal concentration when plotted versus water content in the dry soil compartment (Figure 3). This behavior was reported previously in plants exposed to partial [*Dodd et al.*, 2008, Figure 5] or alternated root zone soil drying [*Stoll et al.*, 2000].

However, the relation between leaf signal concentration and root zone water content is expected to depend on the soil water distribution. Due to internal water redistribution within the plant from deeper roots located in wet soil, flow velocities might not reach zero even in some very dry parts of the root system. Also the diurnal dynamics of the transpiration rates were not considered in the simulation. During the night when transpiration is diminished, water can redistribute within the root system (according to plant water potential gradients), increasing signal transport in the morning when stomata re-open and the redistributed water is transported from dry root zones to the shoot. Simulations using R-SWMS to evaluate these effects are currently being carried out.

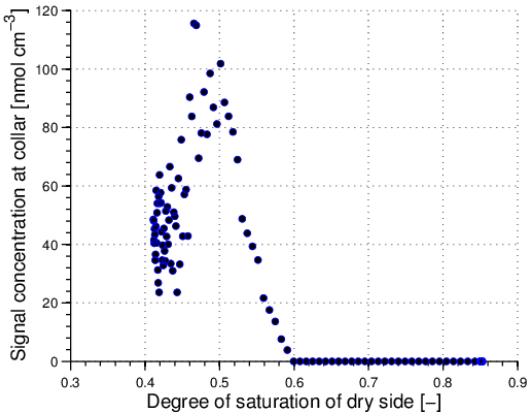

Fig. 3. Relationship between hormone concentration arriving in the leaves and soil water content of the drying part of the soil domain

LITERATURE CITED

Davies, W. J., G. Kudoyarova, and W. Hartung 2005. Long-distance ABA signaling and its relation to other signaling pathways in the detection of soil drying and the mediation of the plant's response to drought, *Journal of Plant Growth Regulation*, **24(4)**, 285-295.

Dodd, I. C., G. Egea, and W. J. Davies 2008, Abscisic acid signalling when soil moisture is heterogeneous: decreased photoperiod sap flow from drying roots limits abscisic acid export to the shoots, *Plant Cell Environ.*, *31*(9), 1263-1274.

Javaux, M., T. Schröder, J. Vanderborght, and H. Vereecken 2008. Use of a Three-Dimensional Detailed Modeling Approach for Predicting Root Water Uptake, *Vadose Zone Journal*, **7(3)**, 1079-1079.

Simonneau, T., P. Barrieu, and F. Tardieu 1998, Accumulation rate of ABA in detached maize roots correlates with root water potential regardless of age and branching order, *Plant Cell Environ.*, **21(11)**, 1113-1122.

Stoll, M., B. Loveys, and P. Dry (2000), Hormonal changes induced by partial rootzone drying of irrigated grapevine, *Journal of Experimental Botany*, **51(350)**, 1627-1634.

Tardieu, F., and W. J. Davies 1993., Integration of Hydraulic and Chemical Signaling in the Control of Stomatal Conductance and Water Status of Droughted Plants, *Plant Cell Environ.*, **16(4)**, 341-349.

Tardieu, F., and T. Simonneau 1998, Variability among species of stomatal control under fluctuating soil water status and evaporative demand: modelling isohydric and anisohydric behaviours, *Journal of Experimental Botany*, **49**, 419-432.

ACKNOWLEDGMENTS

K.H. is funded by the SFB TR32: Transregional Collaborative Research Center 32 (*www.tr32.de*).

Proceedings of the 7th International Conference on Functional-Structural Plant Models, Saariselkä, Finland, 9 - 14 June 2013. Eds. Risto Sievänen, Eero Nikinmaa, Christophe Godin, Anna Lintunen & Pekka Nygren. http://www.metla.fi/fspm2013/proceedings. ISBN 978-951-651-408-9.

Modelling Spatial and Temporal Leaf Temperature Dynamics A focus on the leaf boundary layer

Marc Saudreau [1,2,*], Boris Adam [1,2], Amélie Ezanic [3] and Sylvain Pincebourde [3]
[1]*INRA, UMR547 PIAF, F-63100 Clermont-Ferrand, France,* [2]*UBP, UMR547 PIAF, F- 63000 Aubière, France,* [3]*IRBI, IRBI UMR CNRS 7261, Université de Tours, Tours, France*
**correspondence:* marc.saudreau@clermont.inra.fr

Highlights: A 3D leaf temperature model is proposed to estimate dynamics of temperature gradients at leaf surface. The 3D leaf shape, the leaf physiology, and the microclimate are accounted for. Computational Fluid Dynamics was used to simulate realistic spatial evolution of the sensible heat flux at the leaf surface.

Keywords: 3D Leaf Model, Heat balance, Nusselt Number, Free Convection, Boundary Layer

INTRODUCTION

Leaf temperature is an important factor involved in many biological processes such as leaf transpiration and photosynthesis (Gates 1968), leaf – pathogen interactions (Bernard et al. 2013) or insect development rates (Beck 1983). Within a plant canopy, leaves can exhibit a wide variety of temperature dynamics (frequency, amplitude, spatial gradients) related to the leaf position within the canopy (sunlit vs shaded leaf), the leaf shape and orientation (small vs large, downward vs upward), the leaf physiology (stomatal regulation), and the variability in microclimatic conditions (wind, light, air temperature and air relative humidity). Such variability in leaf temperature dynamics result from changes in heat energy exchanges between the leaf and its local environment. The underlying physics is well known and the temperature dynamics can be inferred by solving a heat balance equation where microclimate and leaf physiology are taken into account through radiation (R), convection (C), evapotranspiration (λE) and diffusion (G) terms: $R + C + \lambda E + G = 0$ (Monteith and Unsworth 1990). Among these terms, the convective term (C) is definitively the more difficult to estimate because it describes the heat transfer process due to the leaf boundary layer.

Many leaf energy models have been developped so far and have been integrated in crop and plant canopy models (Sinoquet et al. 2001; Brisson et al. 2003) but they only simulate the dynamics of the spatially average leaf temperature. Our aim was to build up a flexible and fast 3D leaf temperature model to predict main trends of spatial temperature patterns dynamics at leaf surface. Both leaf geometry, leaf physiology and microclimate were accounted for (Fig. 1). Based on theoretical and Computational Fluid Dynamics (CFD) results, forced and free laminar boundary layers were implemented for the convective term. The free convective boundary layer implementation and the 3D model are presented and discussed.

THE 3D LEAF TEMPERATURE MODEL

Among the different terms of the heat balance equation presented above, the diffusion term and the leaf thickness are neglected ($G \approx 0$), based upon values of the leaf thickness (~10^{-4} m) and the leaf thermal conductivity (0.4 $W.m^{-1}.K^{-1}$ (Vogel 1983)), and the time step used (from 30 minutes to one hour). Thus, the leaf volume is assumed to be zero and the surface is decomposed into n triangles.

On each triangle, the heat balance equation is solved following Monteith and Unsworth (1990): $R + C + \lambda E = 0$. The radiation heat flux is split into a direct and a diffuse component, and PAR and NIR wavebands are considered. The convective and evapotranspirative heat fluxes are modelled using classical relationships (Monteith and Unsworth 1990). The Jarvis model is used for the leaf stomatal conductance (Damour et al. 2010).

The entire leaf temperature model is written in Python. Numerical integrations and the iterative procedure used to solve the heat balance equation are based upon numpy and scipy libraries (Jones et al. 2001).

Both theoretical (plates) and real (3D scanned apple leaves) surfaces were used to assess the model and to perform temperature computations.

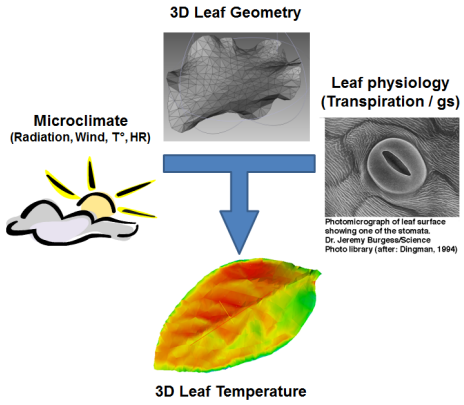

Fig. 1. Schematic view of the main features of the 3D leaf model

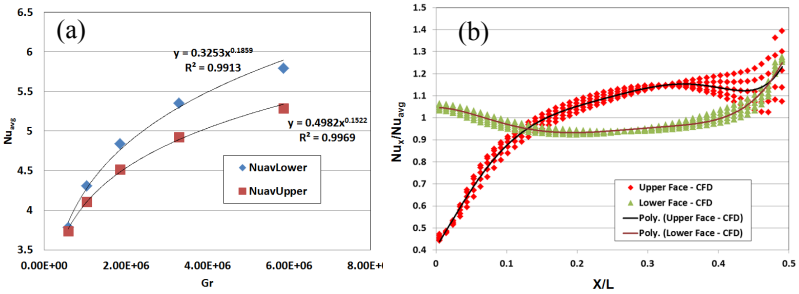

Fig. 2. Free convection – CFD results: (a) Average Nusselt number function of the buoyancy force intensity: $Nu_{avg} = 1/L \int_L Nu_x dx$, and (b) Local Nusselt number Nu_x/Nu_{avg} along the main axis for several Grashof numbers ($X/L = 0$ corresponds to the plate center and $X/L = 0.5$ to the edge of the plate).

THE BOUNDARY LAYER

Loss of energy by the leaf boundary layer is highly dependent on the main force driving the flow (Schuepp 1993). For a leaf, two forces could induce a movement of the air at its surface: the inertial force due to the main outer flow (i.e. the wind speed U), and the buoyancy force due to temperature gradient between the leaf surface (*Tleaf*) and the air (*Tair*). If the flow imposed by the external wind is weaker than the flow induced by the temperature difference between the leaf and the surrounding air, the convection is defined as "free". On the contrary if the boundary layer is driven by the external wind flow the convection is defined as "forced". The flow pattern and thus the heat exchange coefficient pattern dramatically change from a "free" to a "forced" convection The convective heat transfer per unit of surface is defined by $h(Tleaf - Tair)$ where h is the heat transfer coefficient ($W.m^{-2}.K^{-1}$). For convenience of scaling, the Nusselt number (Nu) defined as $Nu = \frac{h.L}{k}$, where L is a characteristic length scale (m), and k is the thermal conductivity of air ($W.m^{-1}.K^{-1}$), is used instead of h (Monteith and Unsworth 1990).

The intensity of free and forced convection can be estimated with the Grashof number (the ratio of buoyancy force to viscous force - $Gr = \beta g L^3 (T_{leaf} - T_{air})/\nu^2$) and the Reynolds number (the ratio of inertial force to viscous force - $Re = UL/\nu$) (Monteith and Unsworth 1990) where β (K^{-1}) is the thermal expansion coefficient of the air, g ($m.s^{-2}$) is the acceleration of the gravity, and ν ($m^2.s^{-1}$) the kinematic viscosity of the air. Theoretical and experimental results have shown that the Nusselt numbers for free and forced convections are proportional to Gr^a and Re^b respectively (Schuepp 1993). The use of CFD (Comsol Multiphysics v4.3a) enables us to estimate the exponent coefficients a and b for a wide variety of driving force intensity and surface geometry.

Based on simple geomerical considerations (distance from the leaf leading edge according to the wind direction, distance from the leaf edge, main surface inclination angle) and estimates of Nusselt numbers from CFD, both kind of convection type were implemented in the 3D Leaf model.

RESULTS AND DISCUSSION

Figure 2a shows the effect of Grashof number on average Nusselt numbers for a horizontal thin plate. For both faces the Nusselt number exibits an exponential relationship with the Grashof number: $Nu \sim m.Gr^a$ with $a \approx 0.186$,$m \approx 0.325$ for the lower face, and $a \approx 0.152$, $m \approx 0.498$ for the lower faces. These values are in agreement with the study of Wei et al. (2002) who performed numerical simulations of the natural convection heat transfer for an uniformly heated plate with metallic physical properties: $a \approx 0.2$, $m \approx 0.317$ and $a \approx 0.16$, $m \approx 0.675$ for the lower and upper faces respectively. Some heat transfer observations from uniformly heated metallic leaf models are available from early studies of Knoerr and Gay (1965) and Dixon and Grace (1983). They reported values of a between 0.1 and 0.2.

For several Grashof numbers i.e. free convection intensities, the ratio between the local Nusselt number Nu_x and the average Nusselt number Nu_{avg} (see figure 2a) along the main axis of the plate is plotted in figure 2b. For the range of Grashof numbers investigated, the ratio Nu_x/Nu_{avg} do not change with Gr except at the edge of the upper face. The Nusselt number presents different patterns between faces with a quasi flat curve at the lower face except at the edge, and with increasing values from the plate center to the edge for the

upper face. The ratio Nu_x/Nu_{avg} can be fitted with 5th and 6th order polynomial functions with R^2 coefficient up to 0.94 for lower and upper faces respectively.

The above CFD results show that some simple and robust relationships of heat transfer coefficients can be found for a free laminar convective boundary layer. Of course leaf boundary layers could exhibit local and sudden patterns for high inclination angle of the surface or when high wind velocity promotes the transition to turbulence of the leaf boundary layer, and the creation of large energetic structures in the trailing edge of the leaf. Such situations cannot be handled with the above relationships.

Above relationships of local and average heat transfer coefficients $Nu_x\ (x/L)$ and $Nu_{avg}(Gr)$ of free laminar convective boundary layer for both lower face and upper face were implemented in the 3D leaf model (figure 3a). Based upon such results and when all features of the 3D leaf model are used together, leaf temperature heterogeneity can be revealed (Figure 3b). In the future, a sensitivity analysis of the main parameters of the model and a model assessment based on IR infra-red camera measurements will be performed.

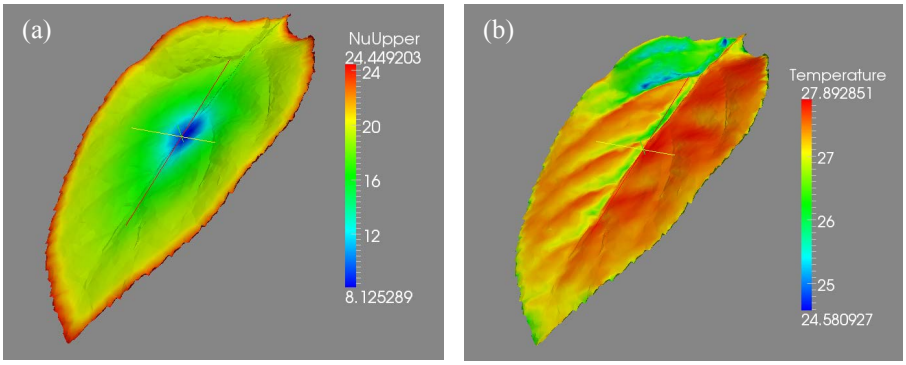

Fig. 3. Illustrations of (i) the Nusselt number implementation for a free convection for an horizontal 3D leaf model (a), and of (ii) a simulated temperature pattern according to given microclimate characteristics (b).

LITERATURE CITED

Beck SD. 1983. Insect Thermoperiodism *Annual Review of Entomology* **28**:91-108

Brisson NC, Gary et al. 2003. An overview of the crop model stics. *European Journal of Agronomy* **18(3–4)**: 309-332.

Bernard F, Sache I, Suffert F and Chelle M. 2013. The development of a foliar fungal pathogen does react to leaf temperature! *New Phytologist*, **198**: 232–240

Damour G, Simonneau T, Cochard H, Urban L. 2010. An overview of models of stomatal conductance at the leaf level, *Plant Cell and Environment*, **33(9):**1419-38

Dixon M and Grace J. 1983. Natural convection from leaves at realistic Grashof numbers. *Plant, Cell & Environment* **6(8)**: 665-670.

Gates D. M. 1968. "Transpiration and Leaf Temperature." *Annual Review of Plant Physiology* **19(1)**: 211-238

Jones E, Oliphant T., Peterson P et al. 2001. SciPy: Open Source Scientific Tools for Python, http://www.scipy.org

Knoerr KR and Gay LW. 1965. Tree Leaf Energy Balance, *Ecology* **46**: 17-24

Monteith J and Unsworth MH. **1990**. *Principles of environmental physics*, 2nd edn. Edward Arnold, London, pp. 291.

Schuepp PH. 1993. Tansley review no. 59: Leaf boundary-layers. *New Phytologist* **125(3):** 477-507.

Sinoquet H, Le Roux X, Adam B, Ameglio T, Daudet FA. 2001. RATP: a model for simulating the spatial distribution of radiation absorption, transpiration and photosynthesis within canopies: application to an isolated tree crown. *Plant, Cell and Environment* **24:** 395–406.

Vogel S. 1983. The lateral thermal conductivity of leaves, *Canadian. Journal of Botany*, **62**:741-744

Wei JJ, Yu B, et al. 2002. Numerical study of simultaneous natural convection heat transfer from both surfaces of a uniformly heated thin plate with arbitrary inclination. *Heat and Mass Transfer* **38(4):** 309-317.

ACKWNOLEDGEMENT

This work was funded by the French National Research Agency project MicroCliMite No ANR-10-BLAN-01706-02

Proceedings of the 7th International Conference on Functional-Structural Plant Models, Saariselkä, Finland, 9 - 14 June 2013. Eds. Risto Sievänen, Eero Nikinmaa, Christophe Godin, Anna Lintunen & Pekka Nygren. http://www.metla.fi/fspm2013/proceedings. ISBN 978-951-651-408-9.

Hydraulic constraints influence the distribution of canopy photosynthetic properties

Mikko Peltoniemi[1,2,3,*], **Remko Duursma**[4] and **Belinda Medlyn**[3]

[1]*Finnish Forest Research Institute (METLA), Vantaa, Finland.*[2]*Department of Forest Sciences, University of Helsinki, Helsinki, Finland.*[3]*Department of Biological Sciences, Macquarie University, North Ryde, NSW, Australia.*[4]*Hawkesbury Institute for the Environment, University of Western Sydney, Penrith, NSW, Australia*.

**correspondence:*mikko.peltoniemi@metla.fi

Highlights: We showed that limited water transport capacity to upper canopy leaves leads to sub-optimal photosynthetic performance of a tree. In these cases, the widely applied assumption of optimal N distribution that follows irradiance distribution does not hold. Hydraulically constrained optimum N distribution would be flatter than the distribution of irradiance. We further showed that in order to maximize canopy photosynthesis, trees should allocate water transport capacity and N co-optimally, which means allocating both of them according to irradiance distribution.

Keywords: Canopy, Hydraulic conductance, Nitrogen, Optimal, Photosynthesis, Resource allocation

Leaf properties vary significantly within plant canopies, due to the strong gradient in light availability through the canopy. Leaves near the canopy top have high nitrogen (N) and phosphorus content per unit leaf area, high leaf mass per area, and high photosynthetic capacity, compared to leaves deeper in the canopy. Variation of leaf properties has been explained by the optimal distribution of resources, particularly nitrogen, throughout the canopy. Studies of the optimal distribution of leaf nitrogen (N) within canopies have shown that, in the absence of other constraints, the optimal distribution of N is proportional to light. This is an important assumption in the big-leaf models of canopy photosynthesis and widely applied in current land-surface models. However, measurements have shown that the gradient of N in real canopies is shallower than the optimal distribution. One thing that has not yet been considered is how the constraints on water supply to leaves influence leaf properties in the canopy. Leaves with high stomatal conductance tend to have high transpiration rate, which suggests that for the efficient operation of canopy, high light leaves should be serviced by more water. The rate of water transport depends on the hydraulic conductance of the soil-leaf pathway. We extend the work on optimal nitrogen gradients by considering the optimal co-allocation of nitrogen and water supply within plant canopies. We developed a simple "toy" two-leaf canopy model and optimised the distribution of N and hydraulic conductance (K) between the two leaves. We asked whether the hydraulic constraints to water supply can explain shallow N gradients in canopies. We found that the optimal N distribution within plant canopies is proportional to the light distribution only if hydraulic conductance is also optimally distributed. The optimal distribution of K is that where K and N are both proportional to incident light, such that optimal K is highest to the upper canopy. If the plant is constrained in its ability to construct higher K to sun exposed leaves, the optimal N distribution does not follow the gradient in light within canopies, but instead follows a shallower gradient. We therefore hypothesize that measured deviations from the predicted optimal distribution of N could be explained by constraints and costs on the distribution of K within canopies. Distribution of N in tall canopies would be particularly constrained unless these trees were unable to invest in the construction and maintenance of high hydraulic conductance to peripheral leaves. Further empirical research is required to the extent to which plants can construct optimal K distributions, and whether shallow within-canopy N distributions can be explained by sub-optimal K distributions. Future development of ecosystem carbon and water exchange models could benefit from integration of water supply and other constraints influencing canopy N distribution.

LITERATURE CITED

Peltoniemi MS, Duursma RA, Medlyn BE. 2012. Co-optimal distribution of leaf nitrogen and hydraulic conductance in plant canopies. Tree Physiology **32**: 510-519

Proceedings of the 7th International Conference on Functional-Structural Plant Models, Saariselkä, Finland, 9 - 14 June 2013. Eds. Risto Sievänen, Eero Nikinmaa, Christophe Godin, Anna Lintunen & Pekka Nygren. http://www.metla.fi/fspm2013/proceedings. ISBN 978-951-651-408-9.

Reliable estimation of parameters of the Farquhar-Von Caemmer-Berry Biochemical model cannot be obtained by fitting A_n/C_i curves

Qingguo Wang[1,3], David H. Fleisher[2], Jong Ahn Chun[3], Jonathan Resop[2], Dennis Timlin[2] and **V.R. Reddy[2]**

[1]Wye Research and Education Center, University of Maryland, Queenstown, MD 21658 USA; [2]USDA-ARS System Crops and Global Change Lab, Beltsville, MD 20705 USA, [3]APEC Climate Center, 12 Centun 7 ro, Haeundae-gu, Busan 612 020, Republic of Korea.

**correspondence:* qingguo.wang@apcc21.org

Highlights: Because of the limited accuracy and limited number of data points of an A_n/C_i curve, the parameters of the Farquhar-von Caemmerer-Berry photosynthesis model cannot be reliably estimated by analysis of A_n/C_i datasets with the data measured from currently available commercial gas exhange device. However , the fitted parameters remains useful to predict photosynthesis.

Keywords: FvCB model, prameters, fitting, A_n/C_i curve,

The Farquhar-von Caemmerer-Berry (FvCB) leaf photosynthesis model for C_3 plants (Farquhar et al, 1980) has been widely used to simulate CO_2 assimilation and the response of plant to climate change from leaf to canopy scales due to its solid theoretical basis and simplicity. The fitting methods can be divided into two types: type I method fits parameters with the original FvCB model (Sharkey et al. 2007). Type II fits parameters with the quadratic equation (Gu et al., 2010). Each method relies on different assumptions and has technical limitations. Depending on the methods used, the estimated parameters can be substantially different. To the best of our knowledge, there is no publication on testing the fitting methods with generated ideal data sets and data sets superimposed by possible measurement errors, an essential step for fully evaluating the fitting methods because the true parameter values are known and the A_n/C_i curves can be stimulated under all possible conditions. The objectives are to verify the reliability of parameterization approaches for fitting A_n/C_i curves by three approaches. One was from type I, a commonly used method of Sharkey et al. (2007); the second is from type II methods, which have been stated to overcome some major issues of extant methods (Gu et al., 2010); and the third is the analytical method that assumes the errors in A_n/C_i data are negligible.

Two groups of data sets with different accuracies are generated for examining the reliability of three different methods. One group of datasets are generated with 15 data points with three different fixed accuracies: (1) data with high accuracy of 9 decimal places (DSH-15); (2) data with the same accuracy of the currently available commercial gas exchange device (DSL-15) without measurement error; (3) data with the same accuracy of the currently available commercial gas exchange device and with measurement error imposed (DSE-15). Another group of datasets are generated with either varied accuracy or varied number of data points.

All three methods cannot estimate reliable parameters of the FvCB model by analyzing A_n/C_i curves with the same accuracy of the measured data produced from the currently available commercial gas exchange device. The method of Sharkey et al. (2007) cannot obtain accurate parameters even with highly accurate datasets because one equation used is theoretically incorrect and has unrealistic assumptions. Analytical methods and the method of Gu et al. (2010) can estimate reliable parameters from highly accurate datasets with enough data points. However, the resulting fitted parameter set by methods of Sharkey et al. (2007) and Gu et al. (2010) remains useful to predict A_n under the same conditions under which the A_n/C_i curves were derived.

LITERATURE CITED

Farquhar GD, Von Caemmerer S, Berry JA. 1980. A biochemical model of photosynthetic CO2 assimilation in leaves of C3 species. *Planta* **149**, 78–90.

Gu L, Pallardy SG, Tu K, Law BE, Wullschleger SD. 2010. Reliable estimation of biochemical parameters from C_3 leaf photosynthesis–intercellular carbon dioxide response curves. *Plant, Cell & Environment* **33**:1852-1874.

Sharkey TD, Bernacchi CJ, Farquhar GD, Singsaas EL. 2007. Fitting photosynthetic carbon dioxide response curves for C-3 leaves. *Plant, Cell & Environment* **30**, 1035–1040.

DISTRIBUTION OF RESOURCES AND GROWTH IN PLANTS

Proceedings of the 7th International Conference on Functional-Structural Plant Models, Saariselkä, Finland, 9 - 14 June 2013. Eds. Risto Sievänen, Eero Nikinmaa, Christophe Godin, Anna Lintunen & Pekka Nygren. http://www.metla.fi/fspm2013/proceedings. ISBN 978-951-651-408-9.

Stem diameter variation: endogenous regulation versus environmental dynamics and its implication for functional modelling

Maurits Vandegehuchte[1], Adrien Guyot[2], David Lockington[2] and Kathy Steppe[1]
[1]Laboratory of Plant Ecology, Faculty of Bioscience Engineering, Ghent University, Coupure links 653, 9000 Gent, Belgium, [2]National Centre for Groundwater Research and Training- School of Civil Engineering, The University of Queensland, 4072 Brisbane, Australia
**correspondence:* maurits.vandegehuchte@ugent.be

Highlights: Stem diameter variations are generally modelled based on the time lag between transpiration and root water uptake. However, small differences in endogenous osmotic regulation of the storage tissue can result in significant changes in stem diameter variation. This endogenous control needs to be taken into account in functional-structural plant models to accurately predict growth.

Keywords: stem diameter variation, *Rhizophora*, *Avicennia*, growth, osmotic regulation

INTRODUCTION

When interpreting and modelling the plant water status, radial transport between xylem and surrounding storage tissues is of crucial importance as it allows turgor to build up which ultimately leads to plastic growth, providing a specific threshold pressure is overcome (Lockhart, 1965). Moreover, water in the storage tissue buffers discrepancies between water demand and supply, avoiding hydraulic failure in the xylem. As such, it has been commonly accepted that a clear time lag exists between the transpiration at leaf level and the water uptake at root level, caused by the hydraulic resistance between the two (e.g. Zweifel et al., 2000, Peramaki et al., 2001, Sevanto et al., 2002, Steppe et al., 2006). This time lag causes a decrease in stem diameter in the morning as then the water supply from the roots lags behind the transpiration at leaf level, necessitating water flow from the storage compartments (Hinckley and Bruckerhoff, 1975). In the afternoon, when xylem water potential rises because of a decreased atmospheric water demand, water again flows back to the storage tissues, resulting in a diameter increase (Molz and Klepper, 1973).

In functional plant models, diameter changes are modelled based on the in- and outflow of water in the storage tissues from and to the xylem. In these models, the single cell approach is often applied, considering the stem storage as a single volume separated from the xylem by a water permeable membrane with a specific resistance (e.g. Génard et al., 2001, Steppe et al., 2006). Water transport to this storage compartment then increases turgor, resulting in dynamic diameter changes or plastic growth if a threshold value is exceeded. In these models, however, endogenous osmotic activity is not taken into account.

Our aim was to assess possible differences in diameter variations and coupled endogenous osmotic regulation between two representatives of the two most dominant mangrove genera, *Avicennia marina* (Forssk.) Vierh. and *Rhizophora stylosa* Griff. These species are known to thrive in saline, and, hence, drought inducing conditions, requiring specific water use strategies.

MATERIALS AND METHODS

Measurements were conducted at the west coast of North Stradbroke Island, Queensland, Australia (S27°27.061' E135°25.806'), a vegetated sand dune island. The island is characterized by sandy soils and acidic waterbodies intertwined by a complex mix of groundwater-fed lakes, swamps and creeks (Page *et al.*, 2012). On this field site, three full grown trees of both *Avicennia marina* (Forssk.) Vierh. and *Rhizophora stylosa* Griff. were chosen, located in proximity of each other to avoid tidal effects and spatial salinity gradients. The field site was subjected to tidal movement, flooding the site approximately twice every 24 hours. Air temperature, relative humidity, solar radiation, rainfall and windspeed were measured and recorded every ten minutes at 2 m above soil surface (HOBO weather station, Onset, Cape Cod, Massachusetts, USA). Vapour pressure deficit (*VPD*, kPa) was inferred from measured air temperature (T_{air}) and relative humidity (*RH*) according to Buck (1981). Soil salinity and water table depth were determined with in situ pressure sensors (Aqua Troll 200, In-Situ Inc., Fort Collins, CO, USA) installed in piezometers, located close to the measured trees at depths of 25 and 180 cm. All trees were equipped with a dendroband

(DRL26 – Logging Band Dendrometer, ICT international, Armidale, NSW, Australia), continuously recording stem diameter variations, and Sapflow+ sensors, registering sap flux density (Vandegehuchte and Steppe, 2012). Stem water potentials were recorded with stem psychrometers (PSY-1 Stem Psychrometer, ICT International, Armidale, NSW, Australia). Besides these continuous measurements, stomatal resistance was measured for four days (DOY 241, 247, 251 and 254) throughout the measurement period, applying a dynamic porometer (AP4 dynamic porometer, Delta-T Devices Ltd, Cambridge, UK).

By slightly modifying the mathematical flow and storage model of Steppe et al. (2006) based on the work of De Swaef et al. (2012), a mechanistic model was obtained to assess dynamics in xylem and storage water potentials based on stem sap flux density and stem diameter variations. This model was applied as a tool to synthesise the conducted measurements and derive trends in osmotic potential of the stem storage tissue. Modelled xylem water potentials were compared with psychrometric measurements.

RESULTS AND DISCUSSION

Contrary to what is expected from literature, stem diameter of *Rhizophora* increased during the morning and decreased in the afternoon. Even though a similar pattern has been shown for CAM plants (Gouws et al., 2005, Matimati et al., 2012), stomatal closure was measured during the night, indicating that the CAM mechanism was not applicable for *Rhizophora*. As sap flux density and stem water potential showed similar patterns for *Avicennia* and *Rhizophora* and these trees were subjected to the same environmental conditions, the differences in diameter variations patterns are likely due to endogenous osmotic regulation. Our model outputs based on stem diameter input suggest that, unlike what is generally expected, xylem water potential lags behind the storage water potential for *Rhizophora* (Figure 1b), due to an earlier decline in storage osmotic potential compared to *Avicennia* (Figure 2a). When decoupling the volumetric effect and the presence of osmotic active compounds on storage osmotic water potential, it is clear that, while both species seem to endogenously regulate the amount of osmotic compounds present in the storage tissues, *Rhizophora* manages to increase this amount earlier during the day than *Avicennia* (Figure 2b).

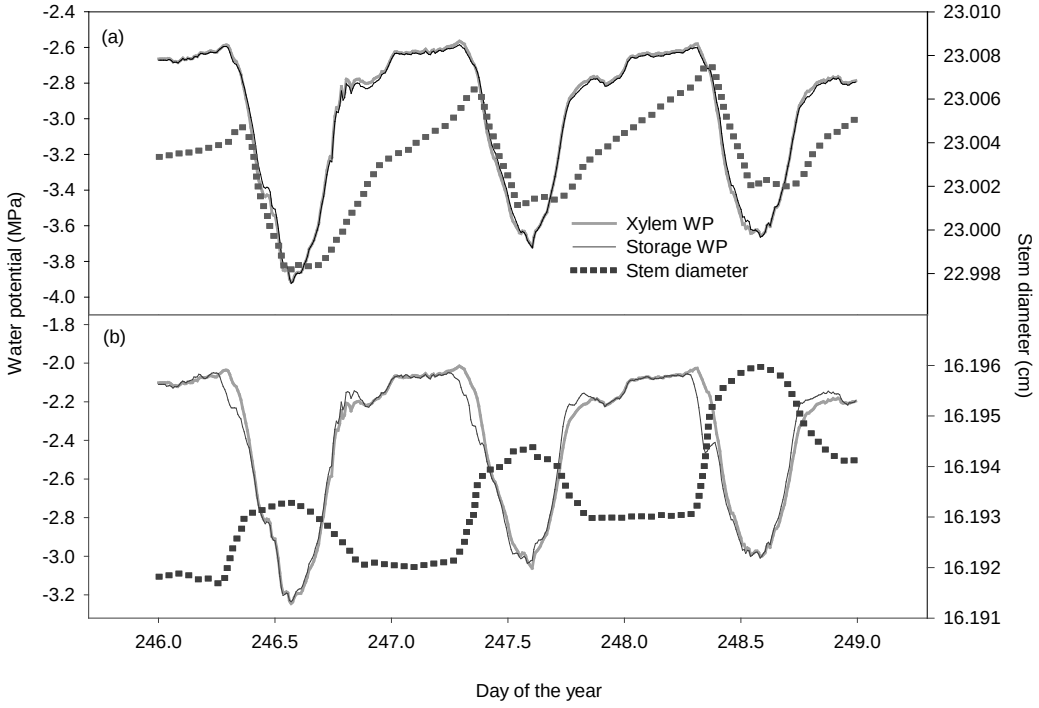

Figure 1 Model results showing the diameter input and xylem and storage water potential output for both *Avicennia* (a) and *Rhizophora* (b).

These results indicate that stem diameter variations, and, hence, growth, may not only be determined by environmental dynamics but may also be strongly influenced by endogenous control. This implies that also these endogenous adaptations need to be included in functional-structural plant models to allow correct predictions of plant behaviour. Our results indeed show that very small differences in osmotic active compound regulation may have drastic influences on important plant physiological variables such as stem diameter. A more thorough knowledge on how these features influence stem diameter variations will result

in new insights into why species differ in growth patterns and, hence, which strategies are more beneficial, depending on the environmental conditions. Moreover, it will allow to assess the relative importance of endogenous regulation and environmental dynamics to long-term growth.

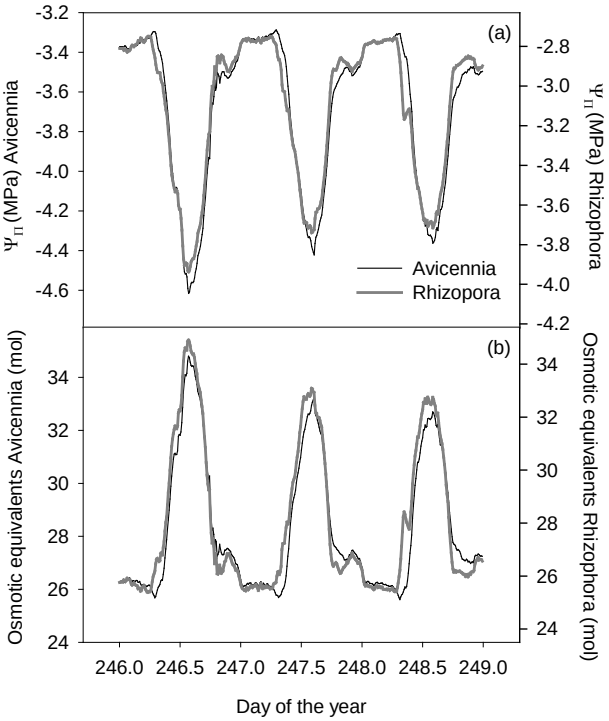

Figure 2 Osmotic potential of the storage tissue (a) and derived osmotic equivalents of the entire storage volume (b) for *Avicennia* and *Rhizophora*

LITERATURE CITED

Buck AL. 1981. New Equations for Computing Vapor Pressure and Enhancement Factor. *Journal of Applied Meteorology*, **20**: 1527-1532.

De Swaef T, Hanssens J, Cornelis A, Steppe K. 2012. Non-destructive estimation of root pressure using sap flow, stem diameter measurements and mechanistic modelling. *Annals of Botany*.

Génard M, Fishman S, Vercambre G, Huguet JG, Bussi C, Besset J, Habib R. 2001. A biophysical analysis of stem and root diameter variations in woody plants. *Plant Physiology*, **126**: 188-202.

Gouws LM, Osmond CB, Schurr U, Walter A. 2005. Distinctive diel growth cycles in leaves and cladodes of CAM plants: differences from C(3) plants and putative interactions with substrate availability, turgor and cytoplasmic pH. *Functional Plant Biology*, **32**: 421-428.

Hinckley TM, Bruckerhoff DN. 1975. The effects of drought on water relations and stem shrinkage of Quercus alba. *Canadian Journal of Botany*, **53**: 62-72.

Lockhart JA. 1965. An analysis of irreversible plant cell elongation. *Journal of Theoretical Biology*, **8**: 264-275.

Matimati I, Musil CF, Raitt L, February EC. 2012. Diurnal stem diameter variations show CAM and C-3 photosynthetic modes and CAM-C-3 switches in arid South African succulent shrubs. *Agricultural and Forest Meteorology*, **161**: 72-79.

Molz FJ, Klepper B. 1973. On the Mechanism of Water-Stress-Induced Stem Deformation1. *Agronomy Journal*, **65**: 304-306.

Page TJ, Marshall JC, Hughes JM. 2012. The world in a grain of sand: evolutionarily relevant, small-scale freshwater bioregions on subtropical dune islands. *Freshwater Biology*, **57**: 612-627.

Peramaki M, Nikinmaa E, Sevanto S, Ilvesniemi H, Siivola E, Hari P, Vesala T. 2001. Tree stem diameter variations and transpiration in Scots pine: an analysis using a dynamic sap flow model. *Tree Physiology*, **21**: 889-897.

Sevanto S, Vesala T, Peramaki M, Nikinmaa E. 2002. Time lags for xylem and stem diameter variations in a Scots pine tree. *Plant Cell and Environment*, **25**: 1071-1077.

Steppe K, De Pauw DJW, Lemeur R, Vanrolleghem PA. 2006. A mathematical model linking tree sap flow dynamics to daily stem diameter fluctuations and radial stem growth. *Tree Physiology*, **26**: 257-273.

Vandegehuchte MW, Steppe K. 2012. Sapflow+: a four-needle heat-pulse sap flow sensor enabling nonempirical sap flux density and water content measurements. *New Phytologist*, **196**: 306-317.

Zweifel R, Item H, Hasler R. 2000. Stem radius changes and their relation to stored water in stems of young Norway spruce trees. *Trees-Structure and Function*, **15**: 50-57.

Proceedings of the 7th International Conference on Functional-Structural Plant Models, Saariselkä, Finland, 9 - 14 June 2013. Eds. Risto Sievänen, Eero Nikinmaa, Christophe Godin, Anna Lintunen & Pekka Nygren.
http://www.metla.fi/fspm2013/proceedings. ISBN 978-951-651-408-9.

Crop load effects on stem diameter variations in peach evaluated with an integrated plant and fruit model

Tom De Swaef[1*], **Carmen D. Mellisho**[2], **Annelies Baert**[1], **Veerle De Schepper**[1], **Wenceslao Conejero**[2] and **Kathy Steppe**[1]
[1]*Laboratory of Plant Ecology, Ghent University, Ghent, Belgium,* [2] *Dpto. Riego. Centro de Edafología y Biología Aplicada del Segura (CSIC). Murcia, Spain*
**correspondence:* tom.deswaef@ugent.be

Highlights: Integrating a mechanistic carbon and water flow model with a model of peach fruit water and carbon accumulation enabled to quantify plant carbon relations with varying crop load. Physiological processes at the plant level could as such be related to effects on fruit growth.

Keywords: water relations, carbon relations, stem diameter, fruit growth

INTRODUCTION

Peach fruit production and quality (*Prunus persica* (L.) Batsch.) are substantially affected by physiological processes related to whole-plant water and carbon relations (e.g. Fishman and Génard, 1998; Conejero et al., 2010). To enhance the understanding of water and dry matter accumulation in peach fruit, it is therefore essential to assess the link with plant water and carbon status. In recent years, some effort has already been done to unravel and interpret variations in stem diameter (D_{stem}) with respect to the plant water and carbon status (e.g. Sevanto et al., 2003; Daudet et al., 2005; De Schepper and Steppe, 2011; De Swaef et al., 2012). Recorded variations in D_{stem} are an overall result of several distinct mechanisms which are (in)directly related to water and carbon status: irreversible radial growth, reversible shrinking and swelling (in relation to varying levels of hydration) of living cells and expansion or contraction of dead conducting xylem elements due to the increase or relaxation of internal tensions (Daudet et al., 2005).

The present study aims at unravelling the quantitative effects of crop load on D_{stem}, the plant carbon status and fruit growth. Therefore, the dynamic water and carbon flow and storage model of De Schepper and Steppe (2010) was coupled to the fruit water and carbon accumulation model of Fishman and Génard (1998) and was used to describe D_{stem} for three different crop loads.

MATERIALS AND METHODS

The experiment was performed in 2008, in a seven-year-old early maturing peach orchard (*Prunus persica* (L.) Batsch, cv. Flordastar grafted on GF-677 peach rootstock) at the CEBAS-CSIC experimental station in Santomera (Murcia, Spain) (38°06'N, 1°02'W, elevation 110 m). Trees were irrigated daily above the estimated crop evapotranspiration (156% ET_c) to assure non-limiting soil water availability. On 10 March (DOY 70) the peach trees were thinned to obtain three different crop load treatments. In a control treatment (*Commercial crop load*) fruits were hand-thinned to leave 25 cm between the fruits to obtain a commercial crop load. In a second treatment, fruits were not thinned, leaving all fruits on the tree (*High crop load*). In a third treatment, all fruits were removed by hand (*Zero crop load*). Three trees were monitored per treatment. On 30 April (DOY 121) fruits of the *Commercial* and *High crop load* treatments were harvested.

Solar radiation, air temperature, relative humidity and wind speed at 2 m above the soil surface were measured by an automatic weather station located near the experimental site and stored every 30 min.

In addition, stem diameter (D_{stem}) variations were measured throughout the experimental period on three trees per treatment. Therefore, a set of linear variable displacement transducers (LVDT) (Model DF 2.5, accuracy 10 µm, Solartron Metrology, Bognor Regis, UK) was used.

MODEL DESCRIPTION

We extended the tree model of De Schepper and Steppe (2010) with a fruit model (Fishman and Génard, 1998) as demonstrated in Fig. 1. Climatic data were used as input variables to estimate transpiration rate

based on Penman-Monteith (Allen et al., 1998). In the model, vertical water transport within the conductive xylem (X) or phloem (Pc) is driven by pressure potential gradients, because such transport does not require membranes to be crossed. In the case of radial flow or flow to the fruits, membranes need to be crossed and, consequently, flows were described based on total water potential gradients. Within the phloem, dissolved sugars were assumed to be transported by the flowing water according to the principle of mass flow. Unloading at the root level (U) was defined to be dependent on the sucrose concentration. Loading in the crown (L) was simplified to a single parameter which was calibrated using D_{stem} data. Transport of carbon and water from the xylem and phloem compartment in the crown towards the fruits was calculated using the model of Fishman and Génard (1998). The number of fruits varied between the different treatments and this was included in the model by multiplying the fruit carbon and water accumulation by the number of fruits.

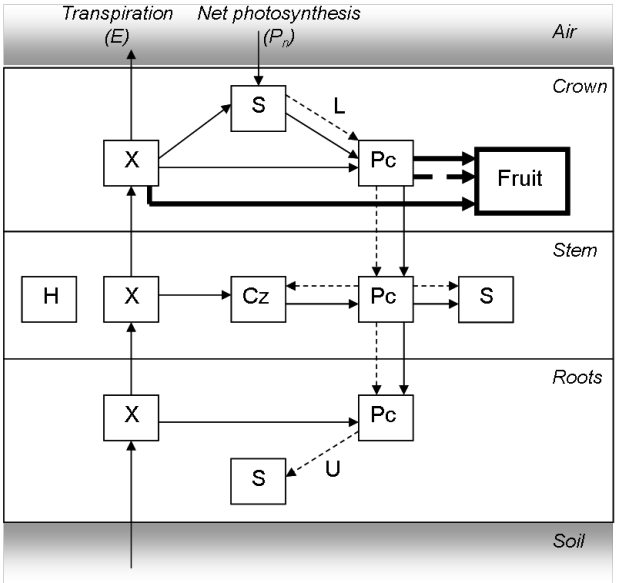

Fig. 1. Diagram with model compartments (H, heartwood; X, conductive xylem; Pc, conductive phloem; S, storage cells; Cz, cambial zone; Fruit) and water (full line) and sugar (dashed line) transport. This transport can occur in both directions: the flow is positive when it is in the direction of the arrow and negative when it is in the opposite direction. L represents loading of sugar in the phloem, U represents unloading of sugar in the storage cells. Thick lines represent flows calculated with the Fishman and Génard model (1998).

The concurrent water and carbon transport causes changes in water content in the different tissues. In the stem and fruit compartment these were converted to volume and corresponding stem and fruit diameter changes (Steppe et al., 2006). Finally, respiration and starch conversion are taken into account in order to close the carbon balance. More details on the model description and equations can be found in De Schepper and Steppe (2010).

The model, consisting of a set of algebraic and differential equations, was implemented and solved numerically using the modelling and simulation software package PhytoSim (Phyto-IT BVBA, Mariakerke, Belgium). This environment allows model implementation, simulation, calibration, sensitivity analysis, identifiability analysis and data acquisition.

RESULTS AND DISCUSSION

The three treatments (*zero, commercial* and *maximum crop load*), varied in the number of fruits at the start of the simulation (DOY 70): on average 0, 547, 3114 fruits per tree, respectively. From harvest on (DOY 121), the number of fruits was zero for all treatments. Apart from the number of fruits, model parameters for all treatments were equal. A set of parameters was optimised using measured data on three treatments, with three trees per treatment. Model simulations and measurements of stem diameter are presented in Fig. 2. Simulations of diurnal variations and overall growth rate of D_{stem} corresponded very well with measurements on all three treatments.

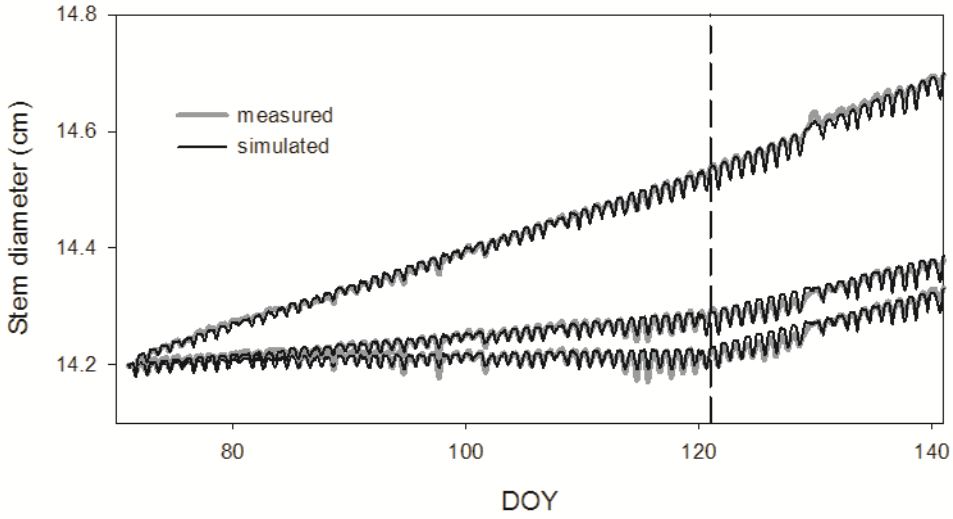

Fig. 2. Measured and simulated stem diameter for the three treatments: *zero cop load* (top), *commercial crop load* (middle) and *maximum crop load* (low). Measured and simulated data are the mean of three trees per treatment. The vertical dashed line indicates harvest of the fruits.

Before harvest, D_{stem} growth rate of the *zero crop load* treatment exceeded the growth rate in other treatments because of a relatively higher availability of sugars in the phloem tissue, which were laterally used for growth in the cambial zone of the stem (Fig. 2). D_{stem} growth rate increased after harvest for the *commercial* and *maximum crop load* treatments, as a result of an increased amount of sugars available in the phloem tissue after fruit removal.

During the fruit growth period, the enhanced fruit number in the *maximum crop load* treatment increased the competition for sugars between different individual fruits. Consequently, the amount of sugars in the phloem decreased, causing a reduced growth of individual fruits. As such, the average fruit weight in the *commercial crop load* was 123.5 g, whereas for the *maximum crop load* the average was 30.23 g (Conejero et al., 2010).

LITERATURE CITED

Allen RG, Pereira LS, Raes D, Smith M. 1998. Crop evapotranspiration: guidelines for computing crop water requirements. *Irrigation and Drainage* **56,** FAO, Roma.

Conejero W, Ortuño MF, Mellisho CD, Torrecillas A. 2010. Influence of crop load on maximum daily trunk shrinkage reference equations for irrigation scheduling of early maturing peach trees. *Agricultural Water Management* **97**: 333-338.

Daudet FA, Améglio T, Cochard H, Archilla O, Lacointe A. 2005. Experimental analysis of the role of water and carbon in tree stem diameter variations. *Journal of Experimental Botany* **56:** 135–144.

De Schepper V, Steppe K. 2010. Development and verification of a water and sugar transport model using measured stem diameter variations. *Journal of Experimental Botany* **61**: 2083-2099.

De Schepper V, Steppe K. 2011. Tree girdling responses simulated by a water and carbon transport model. *Annals of Botany* **108:** 1147-1154.

De Schepper V, van Dusschoten D, Copini P, Jahnke S, Steppe K. 2012. MRI links stem water content to stem diameter variations in transpiring trees. *Journal of Experimental Botany* **63:** 2645–2653.

De Swaef T, Driever SM, Van Meulebroek L, Vahaecke L, Marcelis LFM, Steppe K. 2012. Understanding the effect of carbon status on stem diameter variations. *Annals of Botany* doi: 10.1093/aob/mcs233

Fishman S, Génard M. 1998.) A biophysical model of fruit growth: simulation of seasonal and diurnal dynamics of mass. *Plant, Cell and Environment* **21**: 739–752.

Sevanto S, Vesala T, Peramaki M, Nikinmaa E. 2003. Sugar transport together with environmental conditions controls time lags between xylem and stem diameter changes. *Plant, Cell and Environment* **26**: 1257–1265.

Steppe K, De Pauw DJW, Lemeur R, Vanrolleghem PA. 2006. A mathematical model linking tree sap flow dynamics to daily stem diameter fluctuations and radial stem growth. *Tree Physiology* **26:** 257–273.

Proceedings of the 7th International Conference on Functional-Structural Plant Models, Saariselkä, Finland, 9 - 14 June 2013. Eds. Risto Sievänen, Eero Nikinmaa, Christophe Godin, Anna Lintunen & Pekka Nygren. http://www.metla.fi/fspm2013/proceedings. ISBN 978-951-651-408-9.

Physiological growth model CASSIA predicts carbon allocation and wood formation of Scots pine

Pauliina Schiestl-Aalto[1], **Liisa Kulmala**[2*], **Harri Mäkinen**[2], **Tuomo Kalliokoski**[1,2] and **Annikki Mäkelä**[1]
[1]*Department of Forest Sciences, PO Box 27, 00014 University of Helsinki, Finland,* [2]*Vantaa Res. Ctr, Finnish Forest Research Institute, PO Box 18, 01301 Vantaa, Finland*
**correspondence:* liisa.kulmala@metla.fi

Highlights: The dynamic, intra-annual model CASSIA combines detailed models of wood formation and properties with a process-based growth simulation system. It predicts the daily growth of wood, needles, shoots and roots of Scots pine based on weather variation and photosynthetic production.

Keywords: dynamic modeling, *Pinus sylvestris* L, sink, source, xylogenesis

INTRODUCTION

The growth of trees varies according to genetic origin, tree age and environmental drivers like tree position in the stand, the weather conditions of the current and previous years, and soil characteristics (Oleksyn et al. 2001, Salminen and Jalkanen 2005, Chuine et al. 2006, Pinto et al. 2011). Mechanistic understanding of the external and internal control of growth is needed to understand the effects of changing environment on tree growth and wood formation. Drew et al. (2010), for example, has developed a process-based approach to model wood property variation but dynamic model CASSIA (Carbon Allocation Sink-Source Interaction Analysis) is one of the first attempts to combine detailed models of intra-annual wood formation (xylogenesis) with a process-based growth simulation system in a whole-tree carbon balance framework. It predicts the daily growth of wood, needles, shoots and roots of Scots pine (*Pinus sylvestris* L.) based on weather variation and photosynthetic production. It also includes a description of wood formation at time scales ranging from days to several years, in a whole-tree carbon balance framework. Especially, the model is able to describe how the sink and source relationships interact through various time scales in tree growth.

THE MODEL

In the model, the state variables are the storages of short chain sugars (sucrose), long chain sugars (starch), and the biomasses of needles, primary wood, secondary wood and fine root (Fig. 1). The model further divides the cambial growth to enlarging, wall forming and mature tracheids. The model projects the states of growth at any point in time with a time step of one day.

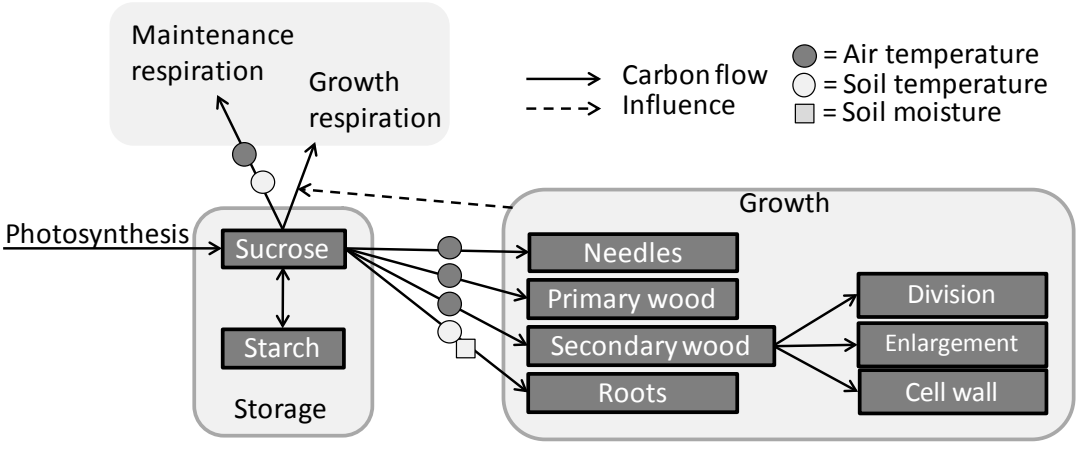

Fig. 1. A schematic presentation of the model. The photosynthesis is the source of carbon whereas the growth of needles, wood and roots and respiration act as carbon sinks. The arrows represent flows of carbon and the shapes stand for the environmental effects of factors.

The daily change in the pool of sugars without the exchange between sucrose and starch storages (d*S*/d*t*, g C day^{-1}) depends on photosynthesis, $P(t)$, and maintenance respiration, $R^M(t)$, growth, $G^{tot}(t)$, and growth respiration, $R^G(t)$:

$$\frac{dS}{dt} = P(t) - R^M(t) - G^{tot}(t) - R^G(t), \quad (1)$$

The photosynthesis, $P(t)$, is calculated according to Mäkelä et al. (2008). The maintenance respiration, $R^M(t)$, depends on the biomass and ambient temperature that is the air temperature for the aboveground parts and soil temperature for the roots. The empirical temperature dependence of each part is obtained from continuous measurements at the SMEARII station. The growth respiration, $R^G(t)$, is linearly dependent on growth according to Running and Coughlan (1988).

The potential growth i.e. growth sink is based on external environment. The most important environmental factor for the above ground growth is the air temperature whereas soil temperature and moisture determine the potential growth of roots. The potential growth follows the annual cycle of tree activity in terms of thermal time, which is assumed to progress with daily mean temperature (Hänninen and Kramer 2007). In the model, the thermal time is an accumulation of a sigmoid function of temperature (Hänninen 1990). The active growth period begins and ends when the accumulation of thermal time reaches threshold values. The level of growth proceeds with the accumulated thermal time as a sine function for shoots, needles and roots whereas the cambial growth follows a square root function of the accumulated thermal time.

The potential growth occurs when carbon is not a limiting factor, i.e., sink strength regulates the growth. If photosynthetic input exceeds the sinks, the sugars are converted and stored as starch. The carbon storages are used to supplement the growth, if the carbon bound in photosynthesis is insufficient to cover the need of the sinks entirely. If the carbon storage is low, the growth becomes source-limited and it is lower than the potential growth.

MEASUREMENTS

We measured the tree growth in middle-aged Scots pine stands in Norhern Finland at SMEARI (67°46′N, 29°35′E) and in Southern Finland at SMEARII (61°52′N, 24°17′E) and in Ruotsinkylä (60°21′N, 25°00′E). We took microcore samples at SMEARI and SMEARII during 2007–2009 and in Ruotsinkyla during 2002–2010 for the timing of tracheid formation and differentiation.

The length growth of needles and branches in different parts of the canopy were measured 2–3 times in a week during the growing seasons. Because measurements were not made every day, an average daily growth of the measuring days was calculated. The shoot growth was measured in SMEARI during 2007–2009 and in SMEARII in 2003–2009. Needle growth was measured at SMEARII in 2003–2009.

We estimated the model parameters using the measurements in SMEARII in 2008 and used them for the model runs of the other sites and years.

PRELIMINARY RESULTS

The model runs for SMEARII during 2002–2009 reveal that the growth was mainly sink-driven, except for the late growing season in 2006 and the early season in 2007. The growth was suppressed by a prolonged drought in August 2006 that decreased the photosynthetic input.

The model succeeded to predict the growth of shoots (Fig. 2A) in years 2006, 2008 and 2009, whereas in years 2005 and 2007, the onset and cessation were consistent with the measurements but the final shoot length was overestimated. In general, the model succeeded to predict the timing of growth (Fig. 2B) and average final length of needles, apart from years 2005–2007 when the model accurately estimated onset and growth cessation but overestimated the final needle length. Moreover, the model succeeded to predict the dynamics of cambial growth (Fig. 2C), except for the year 2009, when the estimated number of cells was lower and the onset of cambial growth later than the observed ones.

With the parameters estimated for SMEARII stand in year 2008, the model succeeded to predict the timing of cambial growth in Värriö and in Ruotsinkylä in years 2007–2008 but in year 2009, the model resulted in an underestimation similar to Hyytiälä in 2009. The model accomplished to predict the final ring

width in Värriö, but in Ruotsinkylä that is a more fertile site, the model underestimated the final ring width indicating a need to tune the fertility-specific parameters.

In future, we will develop the model by refining the description of uptake, allocation, and transport processes of sugars and water within trees to improve understanding of stress responses, especially the effects of prolonged drought on tree growth.

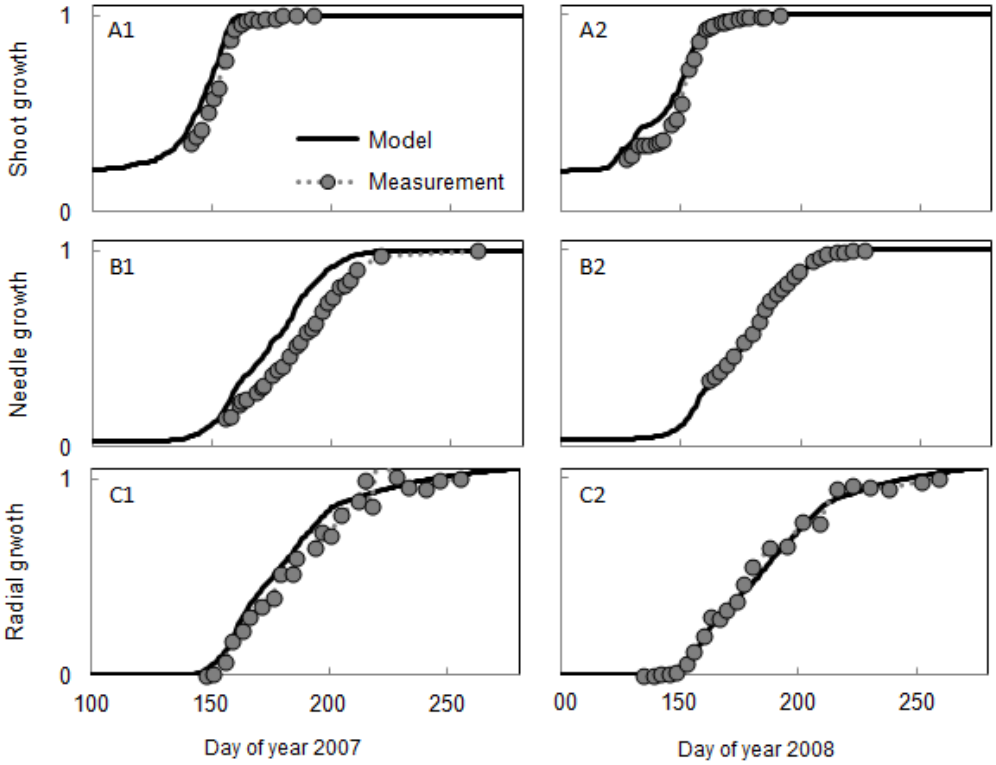

Fig. 2: The modeled (lines) and measured (circles) daily average relative growth of shoots (A1-A2), needles (B1-B2) and the stem radius (C1-C2) at SMEARII in 2007 (left panels) and in 2008 (right panels).

LITERATURE CITED

Chuine I, Rehfeldt GE, Aitken SN. 2006. Height growth determinants and adaptation to temperature in pines: a case study of Pinus contorta and Pinus monticola. *Canadian Journal of Forest Research* **36**: 1059-1066. doi:10.1139/X06-005

Drew DM, Downes GM, Battaglia M. 2010. CAMBIUM, a process-based model of daily xylem development in Eucalyptus. Journal of Theoretical Biology 264: 395–406

Hänninen H. 1990. Modeling dormancy release in trees from cool and temperate regions. In: Dixon, R.K.,Meldahl, R.S., Ruark, G.A. & Warren, W.G. (eds.). *Process modeling of forest growth responses to environmental stress*. Timber Press, Portland p. 159-165.

Hänninen H, Kramer K. 2007. A framework for modelling the annual cycle of trees in boreal and temperate regions. Silva fennica 41(1): 167-205.

Mäkelä A, Pulkkinen M, Kolari P, Lagergren F, Berbigier P, Lindroth A, Loustau D, Nikinmaa E, Vesala T, Hari P. 2008. Developing an empirical model of stand GPP with the LUE approach: analysis of eddy covariance data at five contrasting conifer sites in Europe. Global Change Biology 14: 92-108. DOI: 10.1111/j.1365-2486.2007.01463.x

Pinto CA, Henriques MO, Figueiredo JP, David JS, Abreu FG, Pereira JS, Correia I. 2011. Phenology and growth dynamics in Mediterranean evergreen oaks: Effects of environmental conditions and water relations. *Forest Ecology and Management* **262**: 500–508. doi:10.1016/j.foreco.2011.04.018

Oleksyn J, Reich PB, Tjoelker MG, Chalupka W. 2001. Biogeographic differences in shoot elongation pattern among European Scots pine populations. *Forest Ecology and Management* 148:207-220. DOI: http://dx.doi.org/10.1016/S0378-1127(00)00537-5

Running SW, Coughlan JC. 1988. A general model of forest ecosystem processes for regional applications I. Hydrologic balance, canopy gas exchange and primary production processes. *Ecological Modelling* **42**: 125-154.

Salminen H, Jalkanen R. 2005. Modelling the effect of temperature on height increment of scots pine at high latitudes. *Silva Fennica* **39**(4): 497-508.

Proceedings of the 7th International Conference on Functional-Structural Plant Models, Saariselkä, Finland, 9 - 14 June 2013. Eds. Risto Sievänen, Eero Nikinmaa, Christophe Godin, Anna Lintunen & Pekka Nygren. http://www.metla.fi/fspm2013/proceedings. ISBN 978-951-651-408-9.

Understanding and evaluating some allometric relationships useful for functional-structural plant modeling

M. Paulina Fernández[1]

[1]*Faculty of Agronomy and Forest Engineering, Pontificia Universidad Católica de Chile, Santiago, Chile*

**Correspondence: pfernan@uc.cl*

Highlights: The dynamic process of development and growth of *Pinus radiata* trees was studied during an entire growing season and the allometric relationship between foliage biomass and the supporting conductive area of tissues analyzed. Changes in the stem through time of this relationship suggest that the use of a constant and fixed value for modeling purposes leads to wrong results. This subject is discussed and illustrated by means of simulations.

Keywords: Plant allometry; pipe model; foliage development; wood formation.

INTRODUCTION

When new structures are formed two important principles seem to operate: economy and optimization. Economy in the sense of minimal use of energy or material to obtain the goal; optimization, in the sense of optimal configuration in order to achieve multiple goals or attain a balance between physiological and structural demands. As a result we observe an harmonic structure so designed as to maintain those principles throughout the lifespan of the individual. We perceive an optimal equilibrium, even if we do not fully understand the commanding forces behind it, as allometric relationships between organs, tissues, between structure and function, as studied by Niklas (1994) among others.

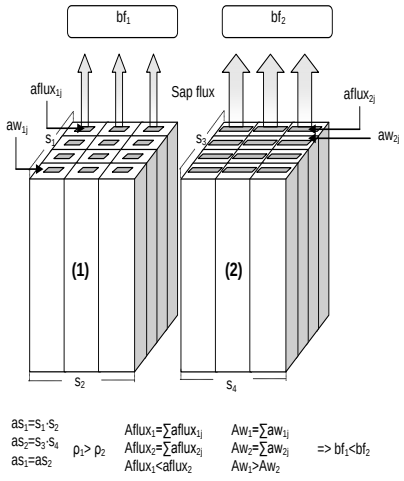

$$Aflux_t = A_t - Aw_t = \omega_1 Bf_t^{\omega_2} \qquad \rho_t = \frac{Bw_t}{\Delta V_t}$$

Figure 1: Sketch showing the assumption of proportionality between the demanding foliar biomass (bf1 and bf2) and the cross section area characteristics. Aflux corresponds to the truly conductive cross section area (summ of all cell lumens or $aflux_i$). With A_t total area and A_w area of cell wall. We assume that $Aflux_t$ is proportional to foliar biomass ($\omega_1 Bf_t^{\omega 2}$) in a power relation. Therefore it will influence the value of B_w (wood biomass that will be assign to wood cell), and the associated wood density ρ.

If these rules apply to stem building during tree growth it should conduct water and metabolic products as a pipe system but at the same time it will have to withstand the increasing weight and mechanical forces acting on the crown and bole. These goals are to be achieved at a minimal cost and as an optimized solution. Already Shinozaki (1964) and later many other authors like Mäkelä (2002) have analyzed the allometry involved in this pipe system, and Matheck and Kluber (1997), Niklas (1992) among others, the bio-mechanical balance of these at times huge structures.

In functional-structural modeling one of the key factors that concerns us is the way in which growth is allocated. After photosythesis and respiration have been taken care of, surplus material may be sent to new organs or to enlarge existing ones. Particularly, when modeling the stem growth of the trees, key questions are the amount of material that is used to build the new mantle of wood and the kind of structure derived therefrom. Leaves require a continuous supply of water from roots to replace that lost in transpiration. So, a relationship should exist between the amount of foliage (leaf biomass) and the cross section of the trunk or branches that support it in order to satisfy the required flow of water. To solve this matter a common solution in various models is to use an allometric relation between the mass of transpiring foliage and the pipe system that has to be constructed to supply it. Such a relationship has actually been documented for different species (Mäkelä, 2002) and has been used in structural-functioning models. Obviously, it is not only the area of cross sections that are involved in the flow, but also the inherent conducting capacity, which in turn depends on the density of the wood (Santiago

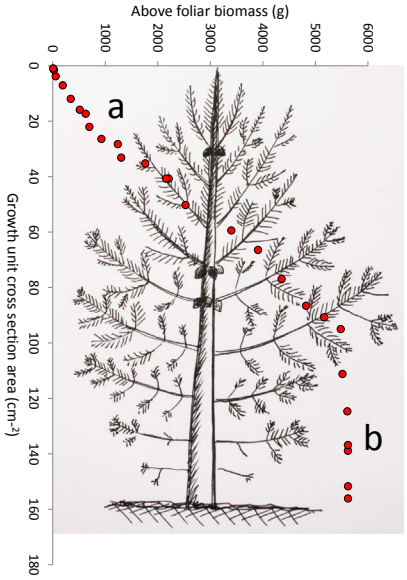

Figure 2: Sketch of a pine tree crown indicating the relationship between the upper foliar biomass and the corresponding supporting cross section area. Section (a) shows a linear relation between both variables in the living crown. Section (b) shows an increase of the cross section area while foliar biomass remains rather constant.

et al., 2004; Bucci *et al*., 2004). In addition, as shown by Santiago *et al.* (2004) and Bucci *et al.* (2004) density is negatively correlated with the water saturation capacity of tissues, with the specific hydraulic conductivity of leaves, with the net assimilation rate of CO_2 , stomatal conductance, specific leaf area and the leaf water potential. It may then be inferred that wood of high density would restrict the productive activity of leaves by reducing flow of water and nutrients in the sapwood. Therefore, we expect that the effective area of water conduction (Aflux, Figure 1) in the xylem should be proportional to the foliar biomass (Mäkela, 2002; Fernández 2008).

MATERIALS AND METHODS

During a growing season (June 2009–August 2010) the development of foliage, main apex, and wood of 38 nine years old *Pinus radiata* trees in an unmanaged stand (Mediterranean Central region of Chile) were monitored. Every 15 days at the beginning of the growing season and every 30 days later on, the development of wood was traced by means of microcores. Simultaneously, we measured the development of the main apex and foliage. In each occasion 3 trees were felled, their whole tree architecture measured and described, and discs from each growth unit collected for further analysis. The discs where stained with a solution of benzidine (Koch and Krieg 1938) in order to detect heartwood. No heartwood was observed in the majority of the discs. The whole foliar biomass was classified according to position and age, collected and weighed. Two pieces of the stem, at the base of the living crown and at the middle of the crown, were analyzed by Magnetic Resonance Imaging that showed the distribution or concentration of water in the wood. Also, an X-ray transversal profile was obtained at the same level the microcores were sampled to analize the wood density. Hourly environmental data (temperature, rainfall, wind speed, solar radiation) were recorded on a nearby automatic weather station . Pertinent soil data was obtained to compute water balance and thermal accumulation (Fernández et al. 2011).

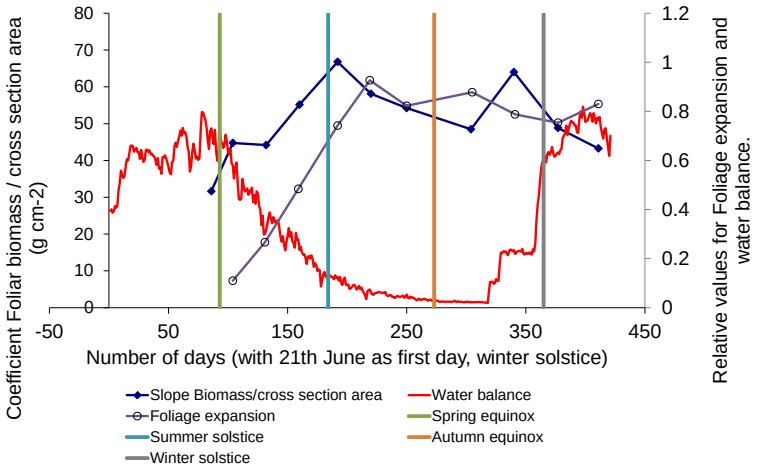

Fgure 3: Evolution of the ratio foliar biomass / cross section area during the growing season, showing marked changes as foliage expands. Water balance is also shown.

RESULTS AND DISCUSSION

For each tree, the relationship between the total cross section area of the growth units and the total leaf biomass over them was analyzed. Figure 2 shows a typical profile. As can be seen foliar biomass is linearly related to the cross section area in the zone of the active crown (Figure 2a). In contrast, in the lower part of the crown (Figure 2, b) the foliar biomass shows a rather constant value while the cross section area steadily increases. These trends are a clear indication that the value of the allometric relation of these parameters depends on what part of the crown we are dealing with. In most trees there were no evidence of heartwood as shown by benzidine staining, but the fact is that the cross section area in the lower part of the crown appears to be active no more.

Figure 3 shows the slope of the relation Y=a*X with Y foliar biomass and X the cross section area of the supporting section. Each dot corresponds to the slope found on the three trees sampled at each date. Time is

indicated in days with number 1 as June 21th (winter solstice in the southern hemisphere). The water balance is given as the ratio ET/ET_{max}, with ET as the real evapotranspiration and ET_{max} maximum atmospheric water demand. The close relationship between the slope values and the extent of the foliage is clear. Also, the seasonal pattern of the allometric relation is evident. Both matters have important implications in sampling and modeling.

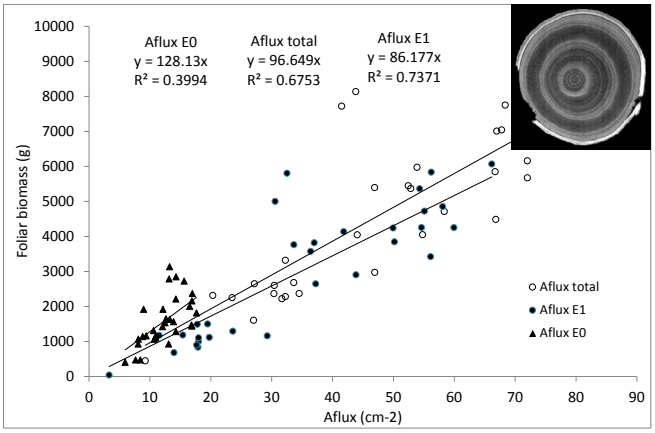

Figure 4: (a) Relationship between real conductive area (Aflux) of the total cross section area, of the developing ring (Aflux E0) and of the previously formed rings (Alfux E1) with the respective foliar biomass (Etotal, E0 and E1). (b) Cross section proton image obtained with Magnetic Resonance Imaging. The different gray values indicate higher or lower concentrations of water in the tissues.

Figure 4 shows the relationship between the leaf biomass and the real or effective conductive cross section area obtained by analysis of MRI images. The data have been divided into (a) the foliar biomass developed during the sampling season (E0) and the corresponding conductive area formed in the new ring (Aflux E0) and (b) the foliar biomass and conductive tissue of the previous years (E1 and Aflux E1). The value of slopes changes in every case showing a larger amount of foliar biomass in relation to cross section in the new ring, in comparison to the previous one. Probably the steady development of wood after the foliage expansion ends (observed also in Figure 3) triggers this change of proportions. Usually, samples are taken at predetermined times, not necessarily in tune with dynamic events of development and growth. In addition, we investigated the strategy of wood deposition along the stem. Results (not shown here) indicated a variable distribution of the wood mantle during the year. These results and the consequences of not taking them into account in the modeling process will be presented and discussed.

Aknowledgment. Research financed by Chilean Research Grants FONDECYT project number 11085008.

LITERATURE CITED

Bucci SJ, Goldstein G, Meinzer FC, Scholz FG, Franco AC, and Bustamante M. 2004. Functional convergence in hydraulic architecture and water relations of tropical savanna trees : from leaf to whole plant. Tree Physiology, **24**, 891-899.

Fernández MP. 2008 Functional-structural model for radiata pine (Pinus radiata D. Don). Tesis para optar al título de Doctor en Ciencias de la Ingeniería, Pontificia Universidad Católica de Chile, Santiago, Chile.

Fernández MP, Norero A, Vera J, Pérez E. 2011. A functional-structural model for radiata pine (*Pinus radiata*) focusing on tree architecture and wood quality. *Annals of Botany **108**: 1155-1178*

Koch JE, Krieg W. 1938. New method for distinguishing between the heart wood and sap wood of Pinus. Chem. –Ztg. **62**, 140-141.

Mattheck C, Kluber H. 1997. *The internal optimization of wood.* Springer-Verlag, Berlin.127 pp.

Mäkelä A. 2002. Derivation of stem taper from the pipe theory in carbon balance framework. *Tree Physiol.*, **22**, 891-905.

Niklas KJ. 1994. *Plant allometry: The scaling of form and process.* The University of Chicago Press, London. 412 pp.

Niklas KJ. 1992. Plant Biomechanics: An Engineering Approach to Plant Form and Function. The University of Chicago Press, London.

Santiago LS, Goldstein G, Meinzer FC, Fisher JB, Machado K, Woodruff D. and Jones T. 2004. Leaf photosynthetic traits scale with hydraulic conductivity and wood density in Panamanian forest canopy trees. Oecologia, **140**, 543-550.

Shinozaki K, Yoda K, Hozumi K, Kira T. 1964. A quantitative analysis of plant form-the pipe model theory. I. Basic analyses. *Jap. J. Ecol.* **14**,97-105

Proceedings of the 7th International Conference on Functional-Structural Plant Models, Saariselkä, Finland, 9 - 14 June 2013. Eds. Risto Sievänen, Eero Nikinmaa, Christophe Godin, Anna Lintunen & Pekka Nygren. http://www.metla.fi/fspm2013/proceedings. ISBN 978-951-651-408-9.

What are the processes driving carbon allocation to stem and fine roots in a mature coppice of *Quercus ilex* in the Mediterranean? A data model analysis

Nicolas K. Martin-StPaul [*1], Morine Lempereur [2], Nicolas Delpierre[1], Jean-Marc Ourcival[2], Hendrik Davi[3] Francois Christophe, Leadley Paul, Eric Dufrene[1] and Serge Rambal[2]

[1]*ESE Lab (UMR 8079), CNRS, Orsay FRANCE;* [2]*CEFE (UMR 5175), CNRS, Montpellier, FRANCE;* [3]*URFM, Avignon, France*

** correspondence:* nico09.martin@gmail.com

Highlights: Improving carbon allocation in process based model is a challenging issue. A process model was prescribed using an extensive data set of growth and carbon fluxes (11 years) at the stand scale in order to draw new carbon allocation scheme in *Q. ilex*. Our results suggest that a part of summer photosynthesis is used for the renewal of fine roots.

Keywords: Carbon partitioning, sink source limitations, growth, drought, phenology, hydraulic

INTRODUCTION

Anticipating the fate of trees and forest ecosystems under the threats of climate changes involve numerical models. Process based models (PBMs) are predominantly used for this purpose because they were well-parameterized and able to run over spread out area (e.g. regional or continental scale). Despite such models have often been validated on the short term (from hour to year) through extensive comparisons with eddy covariance fluxes (water and carbon fluxes), they often fail to accurately represent the longer term processes that determine the growth of the different tree compartments. This is because processes related to carbon allocation inherently rely on multiple and complex interactions involving the source activities of photosynthesis, the sink activity of the different organs as well as the plant hydraulic and allometric structure.

In PBMs, carbon allocation is often computed using empirical coefficients that set which proportion of the current NPP (*i.e.* photosynthesis – autotrophic respiration) is used for the growth of the plant compartments (*e.g.* stem, roots, fine roots, leaves, storage). Such coefficients may be set empirically or may vary according to structural and biological rules (*e.g.* allometry, phenology or hydraulic constraints). Identifying the most important rules of carbon allocation for a given species in a given ecosystem is fundamental to improve the simulations of forest growth productivity and tree species persistence in a changing future (Leuzinger and Thomas 2011).

The Mediterranean climate is seasonal, winters are cool and wet whereas summers are dry and hot. The growth activity of stems of the evergreen *Quercus ilex* matches this climatic pattern as it takes place principally during the short favorable season of spring whereas little activity are observed during the rest of the year. Because the climate seasonality affects simultaneously most functions of trees, it is often difficult to figure out which of the source (Photosynthesis) or the sink (tissues development) activity are limited first and exerts the strongest influence on growth. An ongoing study using automatic dendrometers on a Mediterranean *Q. ilex* site (Lempereur *et al*., in prep) suggests that the decrease of plant water potential that occurred during early summer is likely to preclude the development of tissue well before gross photosynthesis reaches zero. In such a situation a surplus of carbon substrate might be available for the growth of reproductive tissue, fine roots, or non structural carbohydrate (NSC) storage. Using a data-model approach, we first tested whether the decrease of stem growth of *Q. ilex* during summer was source or sink driven. Further, we attempted to identify the most likely sink for a surplus of carbon available. The implications our findings are discussed in terms of plant hydraulic architecture, structure and functioning in order to draw new carbon allocation rules.

MATERIALS, METHODS & SIMULATIONS

All simulations were performed for the period 2000-2010, using the PBM CASTANEA (Dufrene *et al*., 2005), on a mature Mediterranean coppice largely dominated by *Q. ilex* and located in southern France on the experimental site of Puéchabon (hereafter PSite, see Rambal *et al*., 2003, 2004, http://puechabon.cefe.cnrs.fr/ for details). CASTANEA is a forest soil-vegetation-atmosphere model coupled with a growth module. It simulates carbon (photosynthesis and respiration) and water fluxes (transpiration

soil water content, soil water potential) at a half hourly to daily time step for an average tree in a homogeneous stand of forest. A carbon allocation module that uses empirical coefficients assign a proportion of the daily NPP toward the different plant compartment considered (stem, roots, fine roots, flowers, acorn, leaves and storage). Carbon and water fluxes, including gross and net ecosystem photosynthesis, respiration, transpiration, latent heat fluxes, soil water content and plant water potential were previously validated on the site (Davi *et al*., 2005; Delpierre *et al*., 2012; Martin-StPaul 2012). Discrete measurements of biomass and productivity (annual forest inventories, monthly litter collection) combined with allometric relationships established on the PSite as well as leaves, flowers and radial growth phenologies were used to constrain the carbon allocation module of CASTANEA. Carbon allocation to leaves, flowers, acorn, stem and coarse roots, was prescribed seasonally using phenological models for each compartment. Conversely, allocation toward storage and fine roots occurred all over the year.

In order to explain the decreased carbon allocation toward woody tissue during the summer drought period and to understand the fate of carbon allocation in summer we tested **three alternative assumptions**. The source limitation hypothesis (hereafter **SL**) states that the decrease C allocation to woody tissue during the summer is caused by a decreased source activity (drought induces stomatal closure and a decrease of the photosynthetic activity). The sink limitation hypothesis in favor of fine roots (**SkFr**), states that the decrease C allocation to woody tissue during summer is caused by a decreased sink activity (*e.g.* decreased growth due to turgor losses of woody tissue) and that carbon allocation is prioritize toward the renewal of the water acquisition tissue (*i.e.* fine roots). The sink limitation hypothesis in favor of storage (**SkSt**) is similar to the latter hypothesis with the exception that the carbon allocation during summer is prioritized to storage. The simulated seasonal pattern of C allocation under the 3 hypotheses is depicted on Fig. 1a. The likelihood of each hypothesis was assessed based on the temporal behavior of i) the storage concentration and, ii) the ratio of fine roots biomass over foliar biomass. We assumed that to be likely, the simulations of both the storage concentration and the fine root to leaf biomass ratio (BFR/BL) should remain stable over the simulation period.

RESULTS AND DISCUSSION

Simulations performed under **SkFr** and **SkSt** hypothesis yielded better predictions of the inter-annual variations of growth than using the **SL** (Fig 1b). This result confirms the general assumption that in drought prone ecosystems growth is mostly sink-driven (Korner 2003). Simulations using the **SkSt** hypothesis showed stable BFR/BL ratio over the study period but, NSC contents of the sapwood increased dramatically; from the 10% prescribed at the beginning of the simulations, NSC reached up to 60% in 2010 (Fig 1c). Such an increase seems very unlikely. It indicates that the surplus of carbon accumulated during the growth interruption in summer, could not be consumed neither by the maintenance respiration nor by the growth of the different tissues. Conversely, assuming that the carbon sequestered during the summer is allocated in priority to the fine roots renewal - as set in the **SkFr** hypothesis - lead to both, stable BFR/BL and stable storage content (Fig 1c). Whereas the BFR/BL was close 1.5 using the former hypothesis, it was close to 2 when simulations were performed using the **SkFr**. We do not have direct estimation of fine roots biomass and production on our experimental site, but measurements performed on a similar *Q. ilex* coppice (same age, climate and management) on a nearby site indicate that BFR/BL should be close to unity (Lopez et al., 2001). The difference between our simulations and the data reported by Lopez *et al*., (2001) suggests that we probably underestimated fine roots turnover. As fine roots are known to be highly sensitive to water-stress-induced cavitation, and are often considered as the bottleneck of the soil plant hydraulic systems, it is therefore possible that the surplus of carbon sequestered during summer was used to repair the hydraulic systems by building new roots in deeper and wetter soil horizons. Ongoing developments of a hydraulic and allometric model of carbon allocation will be used to test the latter hypothesis.

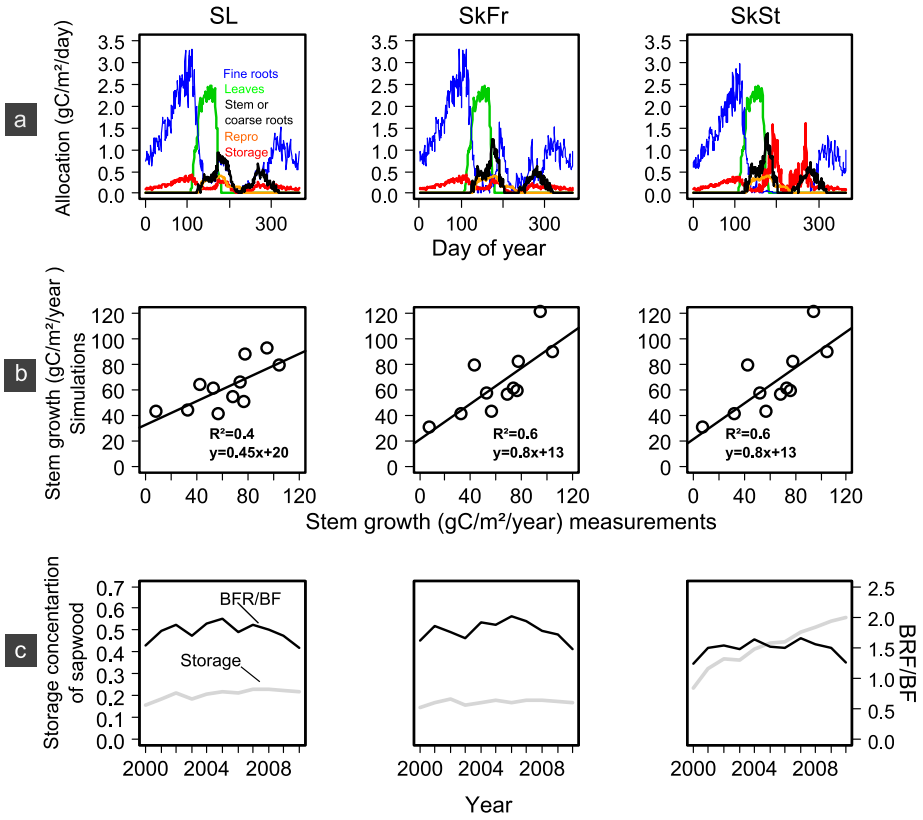

Figure 1 Results of simulations under the 3 hypotheses tested (SL, SkFr, SkSt, see text). (a) Simulations of the seasonal pattern of carbon allocation towards different tree compartments. (b) Yearly stem growth simulated *vs.* yearly stem growth measured on a *Q. ilex* stand over the study period (2000-2010), the R^2 and the fitted relationships are shown. (c) Yearly temporal dynamic of sapwood storage content and of the ratio of fine root biomass over leaf biomass.

LITERATURE CITED

Davi H, Dufrêne E, Granier A, *et al.* 2005. Modelling carbon and water cycles in a beech forest Part II: Validation of the main processes from organ to stand scale. *Ecological Modelling* **185**:387-405.

Delpierre N, Soudani K, François C, *et al.* 2012. Quantifying the influence of climate and biological drivers on the interannual variability of carbon exchanges in European forests through process-based modelling. *Agricultural and Forest Meteorology* **154**, 99-112.

Dufrêne E, Davi H, Francois C, Le Maire G, Le Dantec V, Granier A. 2005. Modelling carbon and water cycles in a beech forest Part I: Model description and uncertainty analysis on modelled NEE. *Ecological Modelling* **185**:407-436.

Korner C. 2003. Carbon limitation in trees. *Journal of Ecology* **91**: 4-17.

Lempereur M, Martin-StPaul NK, Damesin C, Ourcival JM, Rambal S. *in prep*. What limits the radial growth of *Quercus ilex* in a Mediterranean coppice?

Leuzinger S, Thomas R. Q. 2011, 'How do we improve Earth system models? Integrating Earth system models, ecosystem models, experiments and long-term data', *New Phytologist* **191**(1), 15--18.

Lopez B, Sabate S, Gracia CA. 2001, 'Annual and seasonal changes in fine root biomass of a Quercus ilex L. forest', *Plant and Soil* **230**(1), 125-134.

Martin N. 2012. Ajustements fonctionnels du chêne vert (*Quercus ilex* L.) à la sécheresse à différentes échelles temporelles : Incidences sur la modélisation des processus. PhD thesis, Université Montpellier 2, France.

Rambal S, Joffre R, Ourcival JM, Cavender-Bares J, Rocheteau A. 2004. The growth respiration component in eddy CO2 flux from a Quercus ilex mediterranean forest. *Global Change Biology* **10**: 460-1469.

Rambal S, Ourcival J, Joffre R, *et al.* 2003. Drought controls over conductance and assimilation of a Mediterranean evergreen ecosytem: scaling from leaf to canopy. *Global Change Biology* **9**: 1813-1824.

Proceedings of the 7th International Conference on Functional-Structural Plant Models, Saariselkä, Finland, 9 - 14 June 2013. Eds. Risto Sievänen, Eero Nikinmaa, Christophe Godin, Anna Lintunen & Pekka Nygren. http://www.metla.fi/fspm2013/proceedings. ISBN 978-951-651-408-9.

Modelling temperature-modulated internode elongation in greenhouse grown cucumber canopies

Katrin Kahlen[1*], **Tsu-Wei Chen**[2], **Jana Zinkernagel**[1] and **Hartmut Stützel**[2]
[1]*Department of Vegetable Sciences, Geisenheim University, von-Lade-Str. 1, 65366 Geisenheim, Germany*
[2]*Institute of Biological Production Systems, Leibniz Universität, Herrenhäuser Str. 2, 30419 Hannover, Germany*
**correspondence:* katrin.kahlen@hs-gm.de

Highlights: This study highlights the significance of temperature signals for predicting final internode length: Growth and appearance rates need to be adapted to the prevailing temperature conditions. Variations in the light environment additionally alter the pattern of final internode length along the main stem and thus indicate the importance of considering simultaneously acting factors.

Keywords: Temperature, *L-Cucumber*, Arrhenius function, organ growth, light, functional-structural plant model

INTRODUCTION

Plant architecture is significantly influenced by the temperature conditions during plant growth and development (e.g. de Koning 1992, Schouten et al. 2002, Siebert and Ewert 2012). However, in a natural environment, plants are faced with various changing environmental factors acting simultaneously (e.g. Tardieu et al 2012). Models may serve as a tool for a systematic system's analysis (Vos et al. 2010). E.g., concerning the pattern of internode growth along the main stem of greenhouse grown cucumber plants, light-modulated final internode length of each rank can be estimated accurately under a variety of light conditions resulting from independently changing light quality and light quantity signals using the functional-structural model *L-Cucumber* (Kahlen and Stützel 2011a, b). Here, a light response curve for final internode length was parameterized which is valid for temperature conditions optimal for cucumber plant growth. However, even under controlled greenhouse production systems, temperature conditions are rarely constant. High light conditions may increase the temperature inside the greenhouse. In addition, temperatures might be adapted to control plant growth (Kahlen et al. 2012).

A recent study of Kahlen et al. (2012) indicated that temperature conditions during cucumber plant growth affect both, final internode lengths and internode appearance rates. Thus, the light response curve of *L-Cucumber* was extended by a multiplicative factor derived from average internode lengths and the appearance rates were adapted to the measured rates (Kahlen et al. 2012, their Eq. (1) and Fig. 2). Using this adaptations, simulations resulted in accurate final internode lengths on the level of the individual internode and reproduced pattern of FIL along the main stem similar to the measured data. However, the analysis lacked a proper evaluation. Moreover, the derived temperature response curves might have been "experiment"-dependent and lacked universal validity. Interestingly, a recent meta-analysis (Parent and Tardieu 2012) showed that the temperature responses of developmental processes such as organ elongation or the duration of a plant cycle follow an Arrhenius-type response curve after normalization by their rates at 20°C. Maximal normalized developmental rates and their corresponding temperatures vary between species, but not between the above mentioned developmental processes. According to Parent and Tardieu (2012, their Tab. S2) any temperature-modulated elongation rate can be estimated by its value at 20°C multiplied by the value of the species-specific Arrhenius value for the considered temperature, whereas a temperature-modulated duration of a phase at a given T equals its value at 20°C divided by the value for the considered temperature.

The aim of this work was to analyse effects of temperature on internode growth and development of cucumber plants under naturally fluctuating light conditions in a greenhouse production system. We extended the functional-structural plant model of cucumber, *L-Cucumber* (Kahlen and Stützel 2011a) using the proposed approach of Parent and Tardieu (2012) to implement the temperature responsiveness of internode elongation rates and organ appearance rates. For an initial model evaluation, we used data of a greenhouse experiment with three temperature levels.

MODEL

To the knowledge of the authors, at present, there is no cucumber specific parameterisation of the Arrhenius function of the meta-analysis of Parent and Tardieu (2012) available. Thus, we used the average input data of the 17 crop species and Arabidopsis, i.e. the activation enthalpy ΔH_A (69350 J mol^{-1}) and the temperature at which the rate is maximum (305 K), to estimate an average temperature response function for all 18 species, $F_{av}(T)$. The model extension of *L-Cucumber* was done by implementing $F_{av}(T)$ into the light response curve for FIL (cm):

$$FIL_T(T, PAR, R:FR) = F_{av}(T) \cdot FIL(PAR,R:FR) \quad (1)$$

where the function for FIL equals Eq. (MA2) in (Kahlen and Stützel 2011a):

$$FIL(PAR,R:FR)= 13.4–0.14 \cdot PAR + f(R:FR) \quad (2)$$

and *f*(R:FR) represents a stepwise linear response of the final internode to local light quality. PAR corresponds to the mean PAR (µmol m^{-2} s^{-1}) above the canopy of four days starting six days before the internode has reached its maximum growth rate and R:FR equals the mean value of the R:FR ratio at the whole stem at the same timing and the R:FR at the internode at its maximum growth rate. Moreover, the appearance rate was adapted via its reciprocal value, the duration between the appearance of successive organs (d). The duration at 20° was divided by $F_{av}(T)$.

SIMULATIONS

To analyse the interplay of temperature x light on FIL along the main stem simulation runs with the extended *L-Cucumber* model were done. In the virtual scene, a corresponding canopy set-up as in the experiment (number of plants, distances between plants, training and pruning system) was created. As model input the data sets of measured daily PAR data of the above described experiment were used in the simulations. The coupled light model simulated a hemispherical approximation of the sky at the location of the experiments, Hannover, Germany, and was set up for the path of the sun on day 200 of the year. In contrast to these input data, the local light quality conditions (R:FR) emerged from the interaction of canopy architecture and optical light properties of the virtual canopy. For each temperature level of the experiment, individual simulations were run for five slightly different initial leaf orientations with five replications for 24 days. Further details on the virtual canopy can be found in (Kahlen et al. 2012, Kahlen and Stützel 2011a).

RESULTS AND DISCUSSION

Simulations mimicked both, the average numbers and lengths of internodes above rank 8 which reached their final length within the time span of 24 days. Average numbers were ca. 14, 9 and 7 and average lengths were 11.0 cm, 10.5 cm and 9.3 cm for 24°C, 20°C and 16°C, respectively. We excluded internodes below rank 8 from the analysis, because it could be assumed that they were initiated before the different temperature regimes were applied and, so far, it is not clear, during which phase temperature conditions most significantly effect on the internode growth and development. It is also important to reveal the role of temperature on the duration of internode extension. This aspect is missing in this study. A second step of this analysis will include hypotheses on the timing and duration of the temperature signal. However, for the different constant temperature conditions as in our evaluation experiment, simulated data agreed well with measured data and showed similar pattern of FIL along the main stem (Fig. 1).

Even the different patterns in final internode lengths along the main stem observed in our experiment already indicated that for a precise estimation of FIL of cucumber plants grown under different temperature regimes both characteristics, growth and appearance rates, need to be adapted to the actual temperature condition. Altered light conditions during the light-sensitive phase of internode growth might additionally affect on growth and thus result in significantly different internode patterns along the main stem. This can be nicely visualized by simulations with temperature responsiveness of either the internode elongation rate (Fig. 2A) or its appearance rate (Fig. 2B). However, there is still a need for further research to predict FIL under varying temperature and light conditions. It would also be fruitful to analyse the impact of these simultaneously acting factors on time of harvest and yield. Here, the study of Wiechers et al. (2011) could be a good starting point.

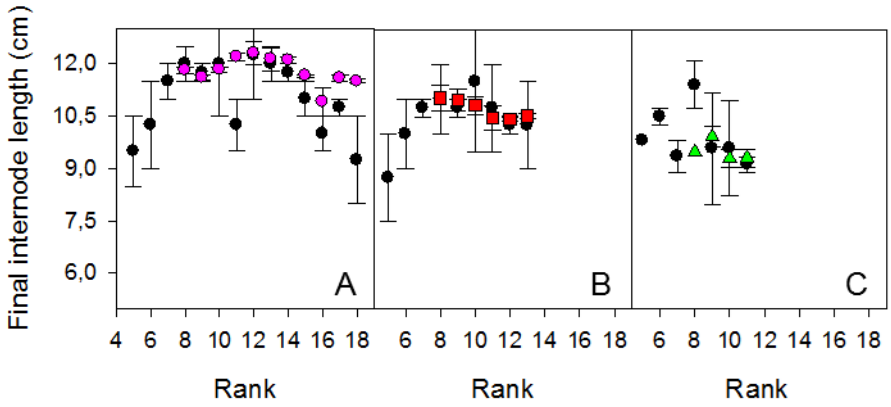

Fig. 1. Final internode length along the main axis of cucumber plants 24 days after treatment start for 24 °C (A), 20°C (B) and 16°C (C) day temperature in the greenhouse. Black circles represent measured data, whereas the coloured symbols represent simulated data for the corresponding temperature conditions.

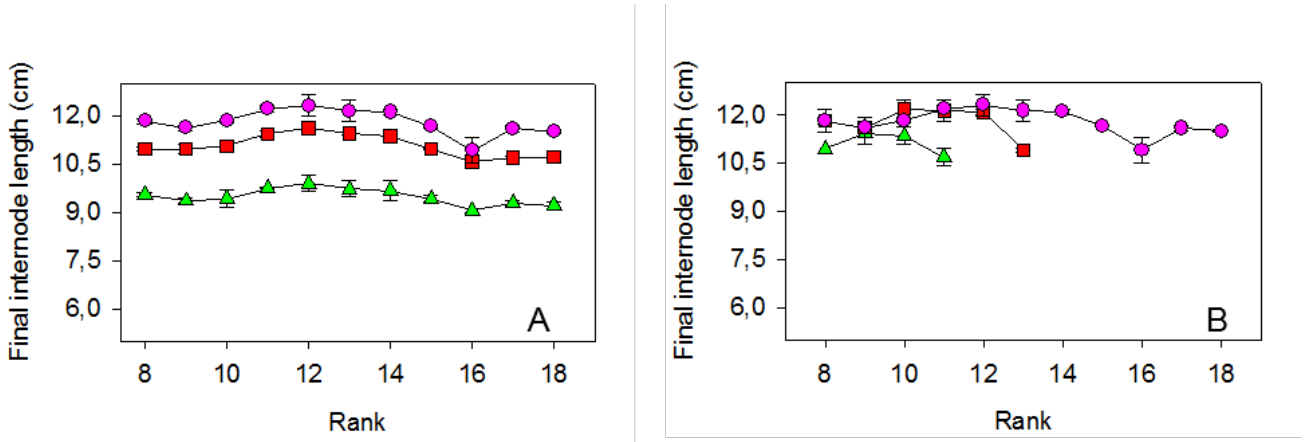

Fig. 2. Simulated final internode length along the main axis of cucumber plants 24 days after treatment start for scenarios of 24°C (pink circles), 20°C (red squares) and 16°C (green triangles) day temperature, where the temperature responsiveness of (A) the elongation rate or (B) the appearance rate were used in the model.

LITERATURE CITED

de Koning ANM. 1992. Effect of temperature on development rate and length increase of tomato, cucumber and sweet pepper. *Acta Horticulturae* **305**: 51–55.

Kahlen K, Stützel H. 2011. Modelling photo-modulated internode elongation in growing glasshouse cucumber canopies. *New Phytologist* **190**: 697-708.

Kahlen K, Stützel H. 2011. Simplification of a light-based model for estimating final internode length in greenhouse cucumber canopies. *Annals of Botany* **108**: 1055-1063.

Kahlen K, Chen T-W Stützel H, Zinkernagel J. 2012. Modeling temperature-modulated stem growth of cucumber plants (*Cucumis sativus* L.). In Kang, MZ, Dumont Y: *IEEE Proceedings of 4th International Symposium on Plant Growth Modeling, Simulation, Visualization and Applications*. ShangHai, China, 31 October -3 November. 1-4.

Parent B, Tardieu F. 2012. Temperature responses of developmental processes have not been affected by breeding in different ecological areas for 17 crop species. *New Phytologist* **194**: 760–774.

Schouten RE, Carvalho SMP, Heuvelink E, van Kooten O. 2002. Modelling of temperature-controlled internode elongation applied to Chrysanthemum. *Annals of Botany* **90**: 353–359.

Siebert W, Ewert F. 2012. Spatio-temporal patterns of phenological development in Germany in relation to temperature and day length. *Agricultural and Forest Meteorology* **152:** 44-57.

Tardieu F, Reymond M, Hamard P, Granier C, Muller B. 2000. Spatial distributions of expansion rate, cell division rate and cell size in maize leaves: a synthesis of the effects of soil water status, evaporative demand and temperature. *Journal of Experimental Botany* **51**: 1505-1514.

Vos J, Evers JB, Buck-Sorlin GH, Andrieu B, Chelle M, de Visser PHB. 2010. Functional–structural plant modelling: a new versatile tool in crop science. *Journal of Experimental Botany* **61**: 2101–2115.

Wiechers D, Kahlen K, Stützel H. 2011. Modelling individual fruit growth in cucumber under different canopy architectures. *Annals of Botany* 108: 1075-1084.

Proceedings of the 7th International Conference on Functional-Structural Plant Models, Saariselkä, Finland, 9 - 14 June 2013. Eds. Risto Sievänen, Eero Nikinmaa, Christophe Godin, Anna Lintunen & Pekka Nygren.
http://www.metla.fi/fspm2013/proceedings. ISBN 978-951-651-408-9.

Height increment formation of hybrid aspen: empirical model

Aris Jansons, Juris Rieksts-Riekstins, Martins Zeps, Oskars Krisans
Latvian State Forest Research Institute "Silava", Rigas 111, Salaspils, LV-2169
**correspondence:* aris.jansons@silava.lv

Highlights: Model predicting height growth rate based on mean daily temperature was statistically significant ($p < 0.01$), both intercept and slope coefficient were significantly different from zero ($p < 0.01$) and determination coefficient high $R^2=0.83$. Model predictions for height increment in next season did not differ significantly from the measurements. It can be used as part of the system for predictions of effect of global climatic changes on height growth in hybrid aspen plantations.

Keywords: Height increment, shoot elongation, temperature, *Populus tremuloides* x *Populus tremula*

INTRODUCTION

Hybrid aspen (*Populus tremuloides* x *Populus tremula*) is one of the most promising alternatives for the establishment of plantations on abandoned agricultural lands in the Baltic Sea region countries (Tullus et al., 2011). Its growth rate notably (2-6 times) exceeds that of any of the parent species (Li and Wu, 1996), and biomass production can reach as much as 8 t of dry matter per hectare and year in the second rotation (Rytter, Stener, 2005). Notable differences among clones within family and among families in traits characterising stem wood density, fibres, productivity as well as leaf area, number, size, intensity of photosynthesis, water use efficiency and others were found (Beuker, 2000; Yu, 2001). Therefore rather intensive breeding has been carried out for this hybrid in Latvia, starting in 1960th with the aim to create a basis for supply of raw material for matches' production and continued from late 1990th with a target to develop suitable clones for cellulose and biomass production. Notable increase in productivity has been achieved, similar to that reported in Sweden: starting from 16 $m^3h^{-1}y^{-1}$ on average in first stands established during 1960th and reaching 20-25 $m^3h^{-1}y^{-1}$ in current stands and selections of the best clones (Stener, 2001).

Superior productivity of hybrid aspen clones has been attributed both to longer growth period and higher growth intensity (Li et al., 1998). Length of the growing (shoot elongation) period is related to adaptation to climatic conditions of particular area: genotypes starting the bud burst too early in spring have a high risk of being affected by spring frosts, but those genotypes that continue the growth for too long before dormancy – by autumn frosts or cold temperatures of winter. Exact fit of growth period to environmental conditions ensures possibilities to maximize photosynthetic productions (Kolari et al., 2007) and therefore provides competitive advantage for particular genotypes. Long time series of observations demonstrate the effect of rising temperature on data of bud-burst. For example, Linkosalo et al. (2009) found the advancements of 7.6 days per century in the bud burst of European aspen in Finland. Thermal time models, describing the start of the bud development – formation of components for new cells (Sarvas, 1972) – from a fixed calendar date in spring and using temperature sum (above certain threshold) accumulation to predict bud burst, was found to be accurate (Linkosalo et al., 2008). Bud set time of *Populus* species has been found to depend on both photoperiod and temperature (Jonsson and Óskarsson, 2007; Rohde et al., 2011). Using these models changes in length of growth period due to climatic changes can be predicted, but not the second parameters with equal importance to determine total length of height increment: growth intensity. Therefore aim of our study was to develop mathematical model linking meteorological conditions and shoot elongation rate of hybrid aspen that could serve as initial information for development of process-based model for predictions of height growth in future environmental conditions.

MATERIAL

Development of model was based on data on shoot growth rates, collected in hybrid aspen trial. Trial was established in central part of Latvia (latitude 56°26' longitude 22°52'), on former agricultural land in year 2007 using one year old containerized plants obtained via microclonal propagation. Initial spacing 3x3m, no thinning carried out prior to measurements. Ramets of 15 clones were randomly distributed in 25 replications. Mainly due to browsing damages some trees had not survived and the growth of others was severely hampered, therefore only trees higher than 1 m were included in analysis and each clone was represented by 18 ramets on average (ranging from 12 to 23 ramets).

Height measurements were carried out during the 5th and 6th growth periods with frequency once per week on average from May until October.

Pearson's correlation coefficient was used as a measure of linear dependency between the intensity of height increment and climatic factors. Multiple linear regression analysis with forward selection criteria was performed using mean daily temperature, mean daily rainfall and sum of rainfall as independent variables and height increment per day as the dependent variable. Model indicated that only mean daily temperature had a significant (α=0.05) effect on the height increment and the other variables did not improve the model.

RESULTS AND DISCUSSION

Model best describing height growth rate based on measurements at 5th growing season was:

$$Hi=7.3934+0.9939*t \quad (1),$$

where:

- Hi – height growth rate, mm per day;
- t – mean daily temperature, °C.

Obtained model was statistically significant ($p < 0.01$), both intercept and slope coefficients were significantly different from zero ($p < 0.01$) and R^2=0.83, which indicates a very strong linear relationship between the temperature and height increment. Using the model it was possible to predict the height growth rate for the next season and the obtained results were not statistically significantly different from the actual measurements.

The regression model was used to estimate formation of height increment in the end of the century, year 2099, using simulated temperatures for the territory of Latvia (Cepīte-Frišfelde et al., 2012). Beginning of the growth period was estimated based on the temperature sum for bud burst data from 5th and 6th growth period and the same temperature sum requirement were assumed to remain in year 2099, resulting in prediction of one-week earlier bud-burst. Ending of the vegetation period was assumed to be dependent on the mean daily temperature, and in 2099 it was two weeks later than in 2010.

Estimated values of height increment in 2099 were tested against the real values in 2010 using two-sided t-test assuming equal variances. Results did not indicate statistically significant differences which means that the average growth intensity would not change in the future, but as the vegetation period would become longer, the total increment might increase by 11 % (Fig. 1). If the vegetation period in 2099 was assumed to be exactly the same as in 2010, the increase in height increment was only 5 %, which is due to slight increase in the mean temperature. Rather small (and insignificant) increase in daily mean temperature in specific year (2099) in comparison to year of measurements (2010) can be the main cause of detected minor differences in annual height increment among the years. Further study will address the impact of predicted climatic (30 year average) differences in temperature on length of height increment.

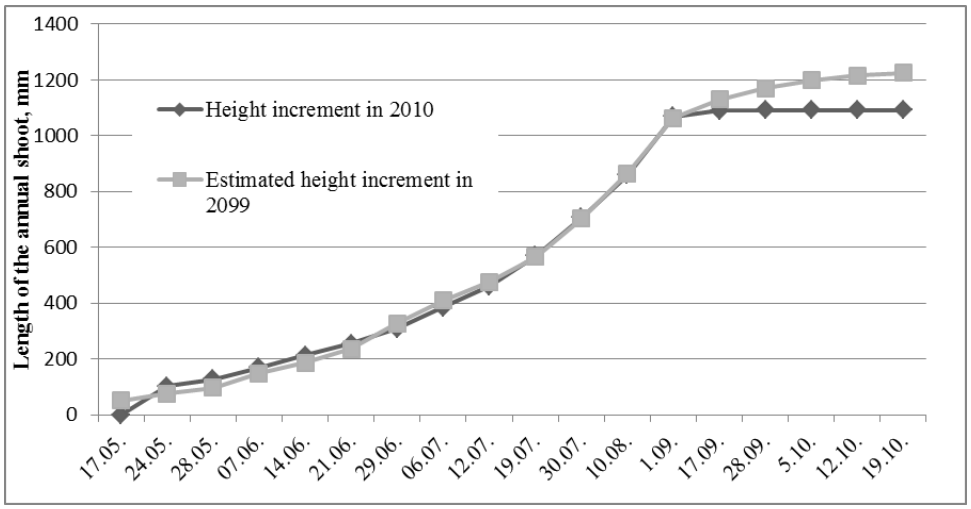

Fig.1. Development of height increment in year 2010 and year 2099 (estimated)

Model can serve as initial basis for development of prediction of height growth in hybrid aspen plantation in future climatic conditions. Study is limited by only one soil type and relative small number of clones, creating difficulties in the extrapolation of results. Data for height growth development have been obtained from young trees, however, comprehensive study of hybrid aspen height growth in Sweden (10 sites, 38-107

clones per site) demonstrates no age-related trends in mean annual height increment for trees from age 2-4 years to age 15-18 yeas (Rytter and Stener, 2005), that is close to the optimal rotation length of hybrid aspen (around 20 years). Also predicted increase in CO_2 level might not have a direct influence on the predictions – it was found that European aspen relative quickly adapts to elevated levels of carbon dioxide no permanent effect on growth can be detected (Tjoelker et al., 1998). Accuracy of predictions can be affected by changes in soil temperature (Landhäusser et al., 2001) and predicted changes in rate of precipitation and higher evapotranspiration that might reduce the growth and change biomass allocation (Liu and Dickmann, 1992). Predicted increase of temperature might also cause differences in growth period: increase the relative importance of chilling in determination of time of bud-burst (Linkosalo, 2000) and change the bud set time as response to photoperiodic conditions (Welling, 2002). Responses to climatic conditions are affected by genetic factors, further decreasing the possibilities for accurate general predictions.

AKNOWLEDGEMENTS

Financial support of European Regional Development Fund project No 2DP/2.1.1.2.0/10/APIA/VIAA/ 021 is aknowledged.

LITERATURE CITED

Beuker E. 2000. Aspen breeding in Finland, new challenges. *Baltic Forestry* **6**:81-84.

Cepīte-Frišfelde D, Bethers U, Seņņikovs J, Timuhins A. 2012. Penalty function for identification of regions with similar climatic conditions. In: M. Kļaviņš, A. Briede (eds.) Climate change in Latvia and adaptation to it. LU, Riga, pp. 8-16.

Jonsson TH, Óskarsson Ú. 2007. Shoot growth strategy of 29 black cottonwood (*Populus trichocarpa)* clones. *Iceland Agricultural sciences* **20**: 25-36.

Kolari P, Lappalainen H, Hänninen H, Hari P. 2007. Relationship between temperature and the seasonal course of photosynthesis in Scots pine at nothern timberline and in southern boreal zone. *Tellus* **59B**:542–552.

Landhäusser SM, DesRochers A, Lieffers VJ. 2001. A comparison of growth and physiology in *Picea glauca* and *Populus tremuloides* at different soil temperatures. *Canadian Journal of Forest Research* **31**: 1922-1929.

Li B, Howe GT, Wu R. 1998. Developmental factors responsible for heterosis in aspen hybrids (*Populus tremoloides x P. tremula*). *Tree Physiology* **18**:29-36.

Li B, Wu R. 1996. Genetics cause of heterosis in juvenile aspen: a quantitative comparison across intra- and inter-specific hybrids, *Theoretical and Applied Genetics* **93**:380-391.

Linkosalo T, Häkkinen R, Terhivuo J, Tuomenvirta H, Hari P. 2009. The time series of flowering and leaf bud burst of boreal trees (1846–2005) support the direct temperature observations of climatic warming. *Agricultural and forest meteorology* **149**:453-461.

Linkosalo T, Lappalainen H, Hari P. 2008. A comparison of phonological models of leaf bud burst and flowering of boreal trees using independent observations. Tree Physiology **28**:1873–1882.

Linkosalo T. 2000. *Analyses of the spring phenology of boreal trees and its response to climate change*. Ph.D. thesis, University of Helsinki, Finland, 55p.

Liu Z, Dickmann DI. 1992. Responses of two hybrid *Populus* clones to flooding, drought, and nitrogen availability. I. Morphology and growth. *Canadian Journal of Botany* **70**: 2265-2270.

Rohde A, Bastien C, Boerjan W. 2011. Temperature signals contribute to the timing of photoperiodic growth cessation and bud set in poplar. *Tree Physiology* **31**: 472-482.

Rytter L, Stener L-G. 2005. Productivity and thinning effects in hybrid aspen (*Populus tremula* L. × *P. Tremuloides* Michx.) stands in southern Sweden, *Forestry* **78**:285-295.

Sarvas R. 1972. Investigations on the annual cycle of development of forest trees. Active period. *Communicationes Instituti Forestalis Fenniae* **76**.3:1–110.

Stener LG. 2001. Broad-leaved breeding in Sweden. In: *Management and utilization of broadleaved tree species in Nordic and Baltic countries birch, aspen, and alder*: proceedings of the workshop Vantaa, Finland, pp. 45-47.

Tjoelker MG, Oleksyn J, Reich PB. 1998. Temperature and ontogeny mediate growth response to elevated CO_2 in seedlings of five boreal tree species. *New Phytologist* **140**: 197-210.

Tullus A, Rytter L, Tullus T, Weih M, Tullus H. 2011. Short-rotation forestry with hybrid aspen (*Populus tremula* L. X *P. tremuloides* Michx.) in Northern Europe. *Scandinavian Journal of Forest Research* **27**:10-29.

Welling A, Moritz T, Palva ET, Junttila O. 2002. Independent activation of cold acclimation by low temperature and short photoperiod in hybrid aspen. *Plant Physiology* **129**: 1633-1644.

Yu Q. 2001. *Selection and propagation of hybrid aspen clones for growth and fiber quality*. Ph.D. thesis, University of Helsinki, Finland, 41p.

Proceedings of the 7th International Conference on Functional-Structural Plant Models, Saariselkä, Finland, 9 - 14 June 2013. Eds. Risto Sievänen, Eero Nikinmaa, Christophe Godin, Anna Lintunen & Pekka Nygren. http://www.metla.fi/fspm2013/proceedings. ISBN 978-951-651-408-9.

Masting changes canopy structure, light interception, and photosynthesis in *Fagus crenata*

Atsuhiro Iio
National institute of environmental studies, 16-2 Onogawa Tsukuba 305-8562 Japan,
**correspondence* aaiio@ipc.shizuoka.ac.jp

Highlights: Masting-dependent changes in canopy structure, light interception, and photosynthesis in natural *Fagus crenata* forests were examined with field-research and light transfer model. Masting significantly decreased canopy leaf area, especially in the upper layer, but increased whole canopy photosynthesis because of increased light interception in the lower layer. These masting-dependent changes are important for precise carbon budget estimation in forest ecosystems.

Keywords: Masting, canopy, structure, light interception, photosynthesis, Fagus crenata Blume

Synchronous intermittent production of large seed crops in perennial plant populations is called masting. Several studies have shown that masting reduces shoot length and leaf area, most likely because of the high resource demands of fruit production. Although structural changes in shoots can affect canopy light interception and photosynthesis, no studies have been carried out to quantify such impacts. Because fruit production in *Fagus* trees relies on current photoassimilation rather than internal storage of carbohydrates (Hoch 2005, Hoch et al. 2013), precise prediction of canopy structure, light interception, and photosynthesis in mast years is essential for understanding eco-physiological mechanisms of masting. Consequently, the primary objective of this study was to examine the impact of masting on canopy structure and photosynthesis in *F. crenata* forests.

The study was conducted in natural *F. crenata* forests on Naeba Mountain in Japan (36°51'N, 138°40'E). A total of 40 branches, 40–60 cm long, were collected from sunlit portions of the canopy during summer (July–August) in mast (2009, 2011) and non-mast (2010, 2012) years. Fruit mass, current-year shoot length, leaf number, total leaf area, and light interception efficiency (silhouette to projected area ratio, SPAR) was measured for each branch. Three-dimensional (3D) distribution of branch leaf area was measured in non-mast years (2008, 2010) using the vertical point quadrat method (Iio et al. 2011), and that in mast-years was estimated from spatial distribution of branch fruit mass measured for heavy mast trees in 2009 and from the dependence of branch leaf area on the fruit mass. Light response curves of leaf and fruit gas exchange rates were also measured at sunlit portions of canopy across growing season (May to October) in mast and non-mast years (leaves only). Canopy photosynthesis under heavy mast and non-mast conditions was calculated for 11 mature trees using the light response curves, 3D distribution of leaf area and SPAR, and a light transfer model based on a Monte-Carlo ray tracing approach (Iio et al. 2011).

Although various branch structural parameters were measured, significant impact of masting was found only for leaf area; leaf area decreased with increasing fruit mass. As a consequence, total leaf area of heavy mast canopy was 15% lower than that of non-mast canopy. Canopy photosynthesis in summer, however, was 11% higher under heavy mast conditions than under non-mast conditions. Fruit photosynthetic rate was always lower than the respration rate, and there were no clear differences in leaf photosynthetic capacity between mast and non-mast years. The increase in canopy photosynthesis is thus because the reduction in leaf area occurred primarily in the upper layer, the site of heaviest fruit production, with the resulting increased light interception in the lower layer exceeding the reduction in photosynthesis in the upper layer. My study showed that canopy photosynthesis in *F. crenata* increases in mast year due to release from significant leaf self-shading within the canopy.

LITERATURE CITED

Hoch G. 2005. Fruit-bearing branchlets are carbon autonomous in mature broad-leaved temperate forest trees. *Plant, Cell & Environment* **28**: 651-659. DOI.10.1111/j.1365-3040.2004.01311.x

Hoch G, Siegwolf RTW, Keel SG, Korner C, Han Q. 2013. Fruit production in three masting tree species does not rely on stored carbon reserves. *Oecologia in press*. DOI 10.1007/s00442-012-2579-2

Iio A, Kakubari Y, Mizunaga H. 2011. A three-dimensional light transfer model based on the vertical point-quadrant method and Monte-Carlo simulation in a Fagus crenata forest canopy on Mount Naeba in Japan. *Agricultural and Forest Meteorology* **151**: 461-479. DOI:10.1016/j.agrformet.2010.12.003.

Proceedings of the 7th International Conference on Functional-Structural Plant Models, Saariselkä, Finland, 9 - 14 June 2013. Eds. Risto Sievänen, Eero Nikinmaa, Christophe Godin, Anna Lintunen & Pekka Nygren. http://www.metla.fi/fspm2013/proceedings. ISBN 978-951-651-408-9.

The effect of low phosphorus on morphological and physiological characters of gooseberry plants (*Physalis peruviana*)

Roveda-Hoyos Gabriel[1] and **Moreno-Fonseca L.P.**[1]
[1]*Department of Agronomy, PO Box 14490, National University of Colombia, Bogotá*
**correspondence:* groveda@gmail.com

Highlights: P-deficiency decreased total biomass and changed the dry matter distribution, the leaf numbers, the total leaf area, and the root length density, as consequence of the photosynthesis rate reduction. In addition, P-deficiency induced enhancement of antioxidant activity, catalase, peroxidase, with a reduction of the total protein. There are evidences related to the damage of cell membranes by reactive oxygen species (ROS).

Keywords: Phosphorus stress, *Physalis peruviana*, plant adaptation.

Physalis peruviana is a tropical fruit (gooseberry) native to South America, used by Precolombian cultures. This plant is well adapted to Andean mountain conditions, including low phosphorous available which is a characteristic from volcanic soils of South America (Herrera *et al*., 2011). This research was focused on determining the stress effect by phosphorus deficiency on some morphological and physiological characteristics of P. *peruviana*. The experiments were performed under greenhouse conditions of the National University, Colombia. The experimental design of random complete blocks was used with 5 treatments, 4 repetitions as follows; two control treatments with 0 and 6 mg P_2O_5 kg^{-1} substrate (P0 and P6), and three treatments with increasing levels of P in soil solution, 12, 25 and 50 mg P_2O_5 kg^{-1} substrate (P12, P25 and P50).

The main results showed that P-deficiency significantly decreased the accumulation of total biomass (leaf, steam and root), changes the dry matter distribution in plant, increasing the Root: Shoot ratio under stress treatments (P0 and P6). The leaf numbers, the total leaf area, and root length density also decreased under stress treatments, as consequence the reduction rate of photosynthetic and transpiration. In addition, P-deficiency induced the significant enhancement of antioxidant activity (Ruiz-Sánchez *et al*., 2010**)**, in term of catalase from P0 to P50 (392 to 163 CAT mg g^{-1} leaf tissue, respectively), peroxidase from P0 to P50 (0.78 to 0.16 POD mg g^{-1} leaf tissue, respectively), in 30 days old seedlings, and the remarkable enhance of the prolina synthesis was observed, from P0 to P50 (771 to 161 mg g^{-1} leaf tissue, respectively), in 60 days old seedlings. On the other hand, it was showed increasing levels of the soluble protein, from the stress treatment P0 (0.109 mg g-1 leaf tissue) to the other treatments P6, P12, P25 and P50, form 0.535, 0.569, 1.086 and 1.277 mg g-1 leaf tissue, respectively), in 30 days old seedlings. Two evidences were found related to the damage or alteration of cell membranes configuration by ROS activity. First, it was observed an increase of electrolytes leakage under stress treatments (P0 and P6) in contrast with P25 and the positive control treatment (P50); second, it was observed a remarkable change between phosphorous (P) and sulphur (S) concentration in the leaf tissue. The experimental results showed the lowest P concentrations in leaf tissue under the stress treatment, P6 (1.4 g K^{-1}), with respect the other treatments P12 (1.5 g K^{-1}), P25 (1.9 g K^{-1}) and P50 (2.9 g K^{-1}), and *vice versa* the highest S concentration in leaf tissue, under the stress treatment (3.55 g K^{-1}), with the other treatments, P12 (1.42 g K^{-1}), P25 (2.02 g K^{-1}) and P50 (2.43 g K^{-1}). Those results suggested the composition of cell membranes could change from phospholipids by sulpholipids, with a change in the cell membrane configuration; this variation could facilitate the electrolytes leakage, which can be detected with increasing levels of conductivity in distilled water solution with leaf tissue. Finally, the results have been used to design a functional model related to the interaction between morphological and physiological characters.

LITERATURE CITED

Herrera AM, Ortiz JD, Fischer G, *et al.* 2011. Behavior in yield and quality of 54 cape gooseberry (*Physalis peruviana* L.) accessions form north-eastern Colombia. Agronomy Colombiana **29**(2): 189-196.

Ruiz-Sánchez M, et al. 2010. The arbuscular mycorrhizal symbiosis enhances the photosynthetic efficiency and the antioxidative response of rice plants subjected to drought stress Journal of Plant Physiology **167**: 862-869.

Porcel R, Ruiz-Lozano JM 2004. Arbuscular mycorrhizal influence on leaf water potential, solute accumulation, and oxidative stress in soybean plants subjected to drought stress. Journal of Experimental Botany **55**: 1743-1750.

Proceedings of the 7th International Conference on Functional-Structural Plant Models, Saariselkä, Finland, 9 - 14 June 2013. Eds. Risto Sievänen, Eero Nikinmaa, Christophe Godin, Anna Lintunen & Pekka Nygren.
http://www.metla.fi/fspm2013/proceedings. ISBN 978-951-651-408-9.

A fifty-year-old conceptual plant dormancy model provides new insights into dynamic phenology modelling

Heikki Hänninen[1]***, Robin Lundell**[1] and **Olavi Junttila**[2]
[1]*Plant Ecophysiology and Climate Change Group (PECC), Department of Biosciences, PO Box 65, 00014 University of Helsinki, Finland*
[2]*Department of Arctic and Marine Biology, University of Tromsø, Norway*
** correspondence:* heikki.hanninen@helsinki.fi

Highlights: Vegis' (1964) conceptual plant dormancy model has been largely ignored in dynamic models of growth onset phenology. We formulate a dynamic model including the phenomenon assumed in the conceptual model and show that the phenomenon 1) potentially explains previous contradictory results of model testing and 2) is crucial with respect to the effects of climate warming on boreal trees.

Keywords: Bud burst, chilling, climate warming, dormancy, frost damage, growth onset

Air temperature has in boreal and temperate trees two major effects regulating the timing of growth onset. Firstly, prolonged exposure to chilling temperatures is required for removing the growth arresting physiological conditions in the buds. Secondly, exposure to high forcing temperatures causes microscopic ontogenetic development in the buds so that a prolonged exposure causes visible growth onset. Since the 1970s both the chilling and the forcing effect have been addressed in dynamic models of growth onset. In these models chilling changes the dormancy status of the bud and the changing dormancy status in turn changes the air temperature response of ontogenetic development. Before the chilling requirement is met either no ontogenetic development takes place, or more realistically the ontogenetic development takes place at a reduced rate. No interaction of the dormancy status and the prevailing forcing temperature is included so that accumulation of chilling affects the rate of ontogenetic development similarly regardless of the forcing temperature. In other words, chilling affects the level of the air temperature response curve of ontogenetic development, but not its location on the air temperature axis. Based on the ideas included in Vegis' (1964) conceptual model we introduce a novel model including such interaction. According to the original conceptual model the growth promoting temperature range changes as a result of the changing dormancy status so that as a result of chilling growth is possible in gradually lower temperatures. The conceptual model found support in a recent experimental study with two *Betula* species (Junttila and Hänninen 2012). We extend the original model to cover also the rate of ontogenetic development and formulate a dynamic model based on this extension. In our model the air temperature response curve moves towards lower temperatures as a result of chilling accumulation. Using simulations with air temperature data from both experimental and natural conditions we show that the phenomenon assumed in the extended model is potentially able to explain earlier contradictory results where the current models have found support in experimental tests but not in tests carried out with long-term phenological records from natural conditions. Using simulations with scenario air temperature data we further show that the phenomenon reduces the risk of frost damage caused by a premature growth onset under climatic warming. Based on these findings from simulation studies we conclude that the phenomenon described in the extended model should be tested experimentally with a wide variety of tree and other plant species.

LITERATURE CITED

Junttila O, Hänninen, H. 2012. The minimum temperature for budburst in *Betula* depends on the state of dormancy. *Tree Physiology* **32**: 337-345.
Vegis, A. 1964. Dormancy in higher plants. *Annual Review of Plant Physiology* **15**:185-224.

Proceedings of the 7th International Conference on Functional-Structural Plant Models, Saariselkä, Finland, 9 - 14 June 2013. Eds. Risto Sievänen, Eero Nikinmaa, Christophe Godin, Anna Lintunen & Pekka Nygren. http://www.metla.fi/fspm2013/proceedings. ISBN 978-951-651-408-9.

A single tree basal area growth model

Jan Hoogesteger
Dept of Forest Sciences, PO Box 27, 00014 University of Helsinki, Finland
**correspondence:* jan.hoogesteger@helsinki.fi

Highlights: What is the role of the structural and circular constraints on tree growth dynamics? Simple rules about growth and self-pruning result in a 2-dimensional dynamic growth model in a framework of structural and circular constraints. The results suggest that onset and rate of self-pruning are key factors in the partitioning of dry matter between foliage and wood.

Keywords: tree rings, heartwood, sapwood, self-pruning, partitioning

INTRODUCTION

Tree ring series are effective tools to study the impact of the environment on tree growth (Speer 2010). External factors influencing ring width often work on tree growth indirectly through their effect on the amount of foliage (Long et al. 2004). The amount of foliage is, according to the pipe model theory (Shinozaki et al. 1964), proportional to the sapwood cross section area. Because of the structural relationships between foliage, sapwood and heartwood, the pipe model sets constraints on tree growth and allocation (Mäkelä and Valentine 2006).

In this context it would be useful to know the role of the structural and circular constraints on the growth dynamics visible in tree ring series. Here I present a growth model based on the 2-dimensional cross section of the stem. Simple rules about growth and self-pruning result in a dynamic growth model. The aim is to get insight in the influence of structural and circular constraints on tree ring series and on tree growth in general.

THE MODEL

Self-pruning is the death of branches because of shading. Self-shading is biggest near the stem, creating a cavity inside the crown without foliage (Mäkelä and Valentine 2006). With an expanding crown, also this cavity becomes bigger. This suggests that the tree adjusts its amount of foliage according to the amount of light, and that there is a maximum thickness of the foliage layer (distance from surface to inner leaves).

The 2-dimensional model assumes that there are two forces causing structural changes: growth and self-pruning. Growth is a function of the sapwood area which results in a new growth ring, giving increase in basal area. At the same time the border between heartwood and sapwood shifts outward because of self-pruning, which will add a ring of transition wood to the heartwood. The growth rate of the sapwood area is calculated through the component of growth minus the component of transition from sapwood to heartwood. In the present model, the growth component is represented by the circumference of the basal area, and the transition component by the circumference of the heartwood area. If growth ring and transition ring have the same thickness, then the new growth ring becomes:

$$G_A(k+1) = x\, S_A(k) \frac{R_{CIRC}(k)}{R_{CIRC}(k) + H_{CIRC}(k)} \qquad (1)$$

where G_A is the growth ring area, k is current year, S_A is sapwood area, R_{CIRC} is circumference of the basal area, H_{CIRC} is circumference of the heartwood area, x is growth rate parameter, which depends on the nutrient status of the site; and the new transition ring becomes:

$$T_A(k+1) = x\, S_A(k) \frac{H_{CIRC}(k)}{R_{CIRC}(k) + H_{CIRC}(k)} \qquad (2)$$

where T_A is the area of transition from sapwood to heartwood. To account for a different width of the transition ring, a parameter of self-pruning q is added, which depends on the amount of shading. Equation (1) then remains the same, but equation (2) becomes:

$$T_A(k+1) = q \times S_A(k) \frac{H_{CIRC}(k)}{R_{CIRC}(k) + H_{CIRC}(k)} \quad (3)$$

The circumference of the basal area is proportional to the stem radius, and the circumference of the heartwood area is proportional to the heartwood area radius, so the equations can be simplified by:

$$G_A(k+1) = x \, S_A(k) \frac{R(k)}{R(k) + H(k)} \quad (4)$$

and

$$T_A(k+1) = q \times S_A(k) \frac{H(k)}{R(k) + H(k)} \quad (5)$$

When the tree ages, the non green parts become larger in relation to the leaf area, which reduces the growth efficiency and causes an age related growth decline (e.g. Hubbard et al.1999). Comparing simulations with real growth data is justified only when taking into account this growth decline. In the model the dependency of leaf area on tree dimension is expressed as S/R, where sapwood layer thickness (S) reflects the dimension of the leaf area, and stem radius (R) the dimension of the whole tree. This is also in agreement with recent studies indicating a strong dependency of metabolic processes on the amount of phloem, which causes a bottle neck for tree growth (Nikinmaa et al. 2013). The relationship is included in both equations by multiplying with S and dividing by R. Equation (4) can then be reduced to:

$$G_A(k+1) = pi \times S^2 \quad (6)$$

and equation (5) can be reduced to:

$$T_A(k+1) = \frac{pi \, q \times S^2 H}{R} \quad (7)$$

In a free standing tree the foliage expands outward also horizontally. This causes more shading inside the crown, so foliage is lost by self-pruning at the same rate. Thus in a free standing healthy tree the thickness of the foliage layer will tend to fluctuate around the same value. This will be reflected in the stem cross section as a tendency of constant width of the sapwood layer, while the area of sapwood increases. However, in a young vigorous tree the sapwood width may still increase because the crown also expands in upward direction, but when height growth slows down, sapwood width will fluctuate more and more around the same value.

The tendency of a constant sapwood layer makes that the transition ring between heartwood and sapwood is about as thick as the growth ring. In this case the parameter of self-pruning gets the value 1.

Growth of a tree in a stand depends on the level of competition. According to the level of competition we can divide trees in a closed stand roughly into two classes: dominant and suppressed. In dominant trees the self-pruning is less than growth, in suppressed trees the self-pruning is the same as or bigger than growth.

The parameter of self-pruning is easiest to calculate for suppressed trees where self-pruning is equal to growth, because the area of the transition ring is as big as the area of the growth ring. The equation for the transition ring is then the same as for the growth ring, equation (6), from which follows that the parameter of self-pruning has the value of R/H. In seriously suppressed trees, so where self-pruning is bigger than growth, this parameter is even bigger than R/H, and the crown will become smaller. In dominant trees the parameter has a value higher than in suppressed trees but lower than in free standing trees, so between R/H and 1. In trees released from suppression, the value will be less than 1.

RESULTS

Preliminary results show that

- growth simulations are conform general trends of growth and yield tables.
- simulations of suppression and release are in close accordance with tree ring data from Scots pine (see fig. 1a and b).

This suggests that the assumptions in the model are realistic. Model simulations further suggest that onset and rate of self-pruning are key factors in the partitioning of dry matter between foliage and wood.

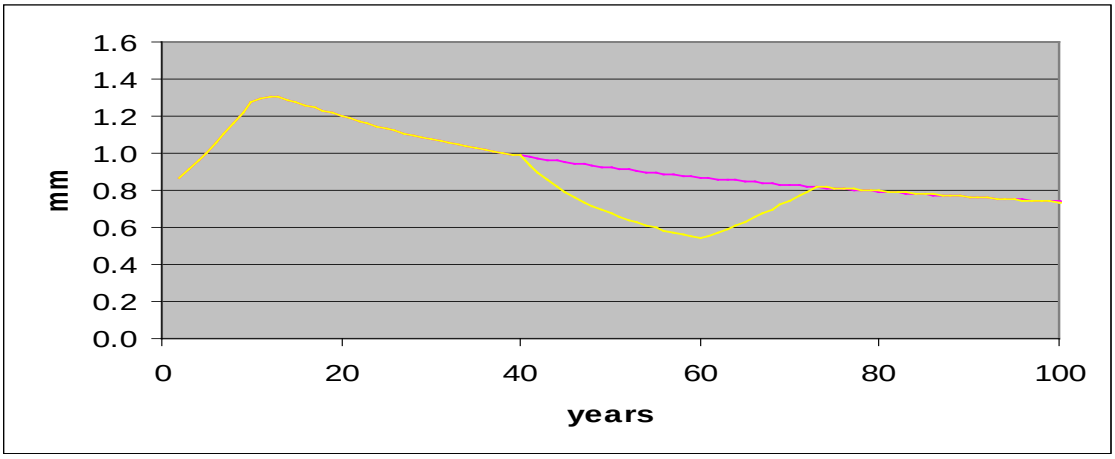

Fig.1a. Simulation: stand closure and suppression at age 40, release at age 60. The self-pruning parameter q is 1 until age 40, q =R/H between age 40 and 60, q = <1 after age 60 until sapwood thickness reaches the same value as before suppression.

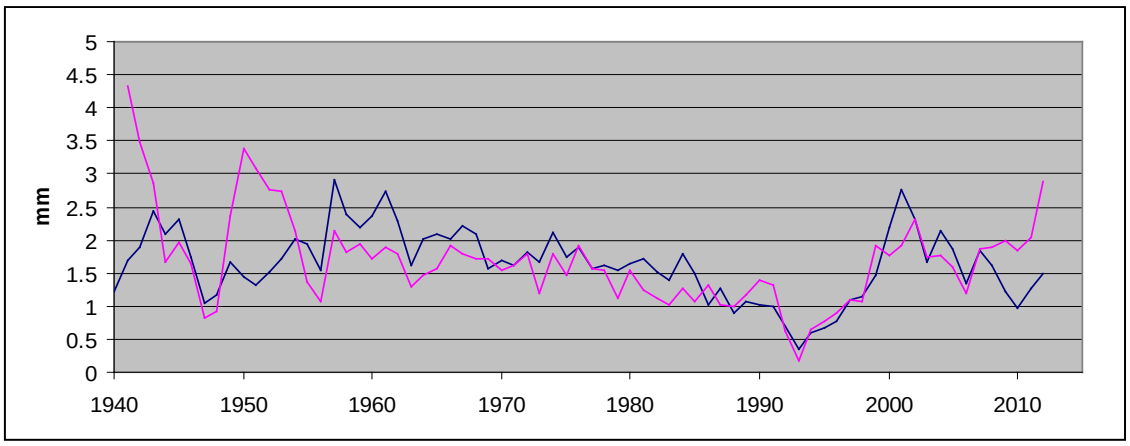

Fig. 1b. Ring width curves of two suppressed Scots pines in a stand, released by thinning in 1994.

LITERATURE CITED

Hubbard RM, Bond BJ, Ryan MG. 1999. Evidence that hydraulic conductance limits photosynthesis in old Pinus ponderosa trees. *Tree Physiology* **19**: 165-172.

Long JN, Dean TJ, Roberts SD. 2004. Linkages between silviculture and ecology: examination of several important conceptual models. *Forest Ecology and Management* **200**: 249-261.

Mäkelä A, Valentine HT. 2006. Crown ratio influences allometric scaling in trees. *Ecology* **87(12)**: 2967-2972.

Nikinmaa E, Hölttä T, Hari P, Kolari P, Mäkelä A, Sevanto S, Vesala T. 2013. Assimilate transport in phloem sets conditions for leaf gas exchange. *Plant, Cell & Environment* **36(3)**, 655-669.

Shinozaki K, Yoda K, Hozumi K, Kira T. 1964. A quantitative analysis of plant form – the pipe model theory. I. Basic analyses. *Japanese Journal of Ecology* **14(3)**, 97-105.

Speer JH. 2010. *Fundamentals of tree-ring research.* The University of Arizona Press, Tucson. 333pp.

Proceedings of the 7th International Conference on Functional-Structural Plant Models, Saariselkä, Finland, 9 - 14 June 2013. Eds. Risto Sievänen, Eero Nikinmaa, Christophe Godin, Anna Lintunen & Pekka Nygren.
http://www.metla.fi/fspm2013/proceedings. ISBN 978-951-651-408-9.

Towards a FSPM of bud outgrowth for rosebush: experimental analysis of sugar effect.

Jessica Bertheloot[1], François Barbier[2], Yves Gibon[3], Rachid Boumaza[2], Soulaiman Sakr[2], Sabine Demotes[1]
[1]INRA, UMR IRHS, SFR QUASAV, F-49071 Beaucouzé. [2]Agrocampus-Ouest, UMR IRHS, SFR QUASAV, F-49071 Beaucouzé. [3]INRA, UMR BFP, F-33883 Villenave d'Ornon
**correspondence: jessica.bertheloot@angers.inra.fr*

Highlights: This study provides experimental data on rosebush to extend the auxin-based FSPM model of bud outgrowth to account for sugar roles. The analysis of the relationship between sugar availability and bud outgrowth at both plant and bud scales showed that sugar availability is able to decrease apical dominance by reducing the lag time before bud outgrowth.

Keywords: bud, light, sugar, apical dominance, Rosa hybrida

Outgrowth of axillary buds is a critical process of plant architectural plasticity, by which plants adapt to environment and growing constraints. FSPM based on experimental data is a potential powerful tool to understand bud outgrowth regulation at the plant scale, which involves several internal and external factors (Evers et al., 2011). By including in a FSPM experimentally-described molecular processes, Prusinkiewicz et al. (2009) have demonstrated the role of auxin canalization in regulating bud outgrowth at plant scale. To complete this model, accounting for sugar role is required, since they are critical for bud outgrowth and their availability within plants is sensitive to environment (Henry et al., 2011). Such development requires a preliminary experimental quantification of sugar effect on bud outgrowth.

This study assesses the relationship between bud outgrowth and sugar availability for rosebush primary shoots by experiments at plant and bud scales. In a first experiment, a branching-responsive cultivar was grown in growth chamber under three PAR treatments known to induce contrasted final outgrowth percentage (Demotes-Mainard et al., 2013). Spatio-temporal patterns of different sugar types and of bud outgrowth were quantified. In a second experiment, single-node cuttings were grown *in vitro* to quantify the response of single buds to various sugar supply levels.

In experiment 1, PAR treatments resulted in contrasted sugar spatio-temporal patterns within primary shoots. In particular, the abrupt transfer of plants to high PAR after temporary low PAR resulted in a doubling in total sugar amount available for buds compared to continuous low or high PAR. In all treatments, buds grew out sequentially in the basipetal direction due to apical dominance; but, while the lag time between two successive outgrowths along the shoot was high under both continuous low and high PAR, it was drastically reduced when plants were transferred from low to high PAR. There was thus a positive relationship between sugar availability and the basipetal propagation rate of bud outgrowth along the shoots. In experiment 2, high sugar feeding of single buds was able to alleviate auxin inhibitory effect by increasing outgrowth percentage and/or reducing the lag time before bud outgrowth, depending on sucrose:auxin ratio.

By quantifying that sugar availability is able to decrease apical dominance by reducing the lag time before bud outgrowth, this study provides valuable information to extend the auxin canalization model of Prusinkiewicz et al. (2009) and to build a comprehensive FSPM of branching.

LITERATURE CITED

Demotes-Mainard S, Huché-Thélier L, Morel P, Boumaza R, Guérin V, Sakr S. 2013. Temporary water restriction or light intensity limitation promotes branching in rosebush. *Scientia Horticulturae*, **150**: 432-440.

Evers JB, van der Krol AR, Vos J, Struik PC. 2011. Understanding shoot branching by modelling form and function. *Trends in Plant Science*.

Henry C, Rabot A, Laloi M, Mortreau E, Sigogne M, Leduc N, Lemoine R, Sakr S, Vian A, Pelleschi-Travier S. 2011. Regulation of RhSUC2, a sucrose transporter, is correlated with the light control of bud burst in Rosa sp. *Plant Cell and Environment*, **34**: 1776-1789.

Prusinkiewicz P, Crawford S, Smith RS, Ljung K, Bennett T, Ongaro V, Leyser O. 2009. Control of bud activation by an auxin transport switch. *Proceedings of the National Academy of Sciences of the United States of America*, **106**: 17431-17436.

Proceedings of the 7th International Conference on Functional-Structural Plant Models, Saariselkä, Finland, 9 - 14 June 2013. Eds. Risto Sievänen, Eero Nikinmaa, Christophe Godin, Anna Lintunen & Pekka Nygren. http://www.metla.fi/fspm2013/proceedings. ISBN 978-951-651-408-9.

Geometrically saturated growth and the pipe model of tree form

Lars Hellström[1], **Linus Carlsson**[1] and **Åke Brännström**[1,2]
[1]*Department of Mathematics and Mathematical Statistics, Umeå University, 90187 Umeå, Sweden*
[2]*Evolution and Ecology Program, International Institute for Applied Systems Analysis, 2361 Laxenburg, Austria*
**correspondence:* lars.hellstrom@residenset.net

Highlights: We combine our self-thinning model of geometrically saturated growth with the pipe model of Shinozaki et al. to yield a composite model that can be used to make predictions about quantities traditionally found in functional models of tree growth.

Keywords: self-thinning, pipe model of tree form, self-similarity, geometric saturation, trunk geometry

Functional-structural plant models traditionally focus on resource production and allocation, which means plant growth is viewed as primarily limited by the amount of available carbon and other nutrients. However, for sufficiently large plants the geometry of space itself may become a more important limitation, in that the resources the plant has available to grow new branches and leaves exceed what it can usefully benefit from growing; at some point, more leaves would only mean higher leaf density and cannot increase the amount of absorbed sunlight enough to raise the net energy production. When this happens, we say that the growth has reached geometric saturation, and one would expect that the surplus production is instead directed towards activities other than growth, such as reproduction.

Previously (not yet in press), we have combined the idea of geometric saturation with (i) the architectural (Barthélémy–Caraglio 2007) view of plant structure and (ii) the self-similarity observation that branches of a given size tend to look pretty much the same regardless of the size of the full plant, to produce the self-thinning model of tree growth: trees discard branches (and a branch may discard subbranches) as they grow, because if they did not then they would quickly exceed the geometric saturation density. This model predicts how the number of metamers of a certain age changes over time, therefore how many must be lost as dead wood, and it also gives many details on what the expected branching structure in a tree should look like. However, to extract from it data on quantities more traditionally considered in functional models, such as total biomass or biomass turnover, one must complement it with a rather extensive table of expected sizes of plant organs of all kinds and ages.

In this follow-up on that earlier work, we combine our self-thinning model with the pipe model of Shinozaki et al. (1964a, 1964b). From a purely mathematical perspective, the two models make a good fit in that there is much overlap regarding the quantities they make claims about, while at the same time approaching them from very different starting points and thus setting up quite independent equations relating these quantities. The net outcome is then that the number of free variables is reduced considerably, and we are therefore able to extract far more functional-style data on the growth of plants from the combined model than from either model by itself, while at the same time reducing the number of parameters to the order of magnitude that would be usual for a functional-structural model.

It should also be pointed out that the model is not primarily a simulation of a process, but rather a system of equalities and inequalities that a plant would have to satisfy. The fastest growth geometrically permitted is then the maximal solution to this system.

LITERATURE CITED

Barthélémy D, Caraglio Y. 2007. Plant Architecture: A Dynamic, Multilevel and Comprehensive Approach to Plant Form, Structure and Ontogeny. *Annals of Botany* **99**: 375–407.

Shinozaki K, Yoda K, Hozumi K, Kira T. 1964a. A quantitative analysis of plant form — the pipe model theory, I: Basic Analyses. *Japanese Journal of Ecology* **14**: 97–105.

Shinozaki K, Yoda K, Hozumi K, Kira T. 1964b. A quantitative analysis of plant form — the pipe model theory, II: Further Evidence of the Theory and its Application in Forest Ecology. *Japanese Journal of Ecology* **14**: 133–139.

Proceedings of the 7th International Conference on Functional-Structural Plant Models, Saariselkä, Finland, 9 - 14 June 2013. Eds. Risto Sievänen, Eero Nikinmaa, Christophe Godin, Anna Lintunen & Pekka Nygren. http://www.metla.fi/fspm2013/proceedings. ISBN 978-951-651-408-9.

Functional-structural modelling of tree and wood formation: new parameters and relations.

M. Paulina Fernández[1] and **Iván Lillo**[2]
[1]*Faculty of Agronomy and Forest Engineering, Pontificia Universidad Católica de Chile, Santiago, Chile*
[2]*School of Engineering, Pontificia Universidad Católica de Chile, Santiago, Chile*
**Correspondence: pfernan@uc.cl*

Highlights: Foliage development and growth of *Pinus radiata* are modulated by temperature, water balance, and probably also by photoperiod, with marked tendency changes associated to solstices and equinoxes or at times close to them. Being a highly coordinated process, wood density of growing rings also vary, increasing or decreasing, according to current crown developmental trends. In addition, it appears that a constant thermal accumulation value triggers the formation of a new wood cell. A functional-structural model combines these phenomena and links new foliage development and expansion to wood formation and density.

Keywords: Photoperiod; crown development; thermal accumulation; foliage development; wood ring formation; wood density.

INTRODUCTION

The relationship between crown development and growth and wood ring formation is relevant to the understanding of the whole tree ontogeny, carbon allocation and structural design. Fernández et al. (2011) presented the first functional-structural model for *Pinus species*, and specifically calibrated for *Pinus radiata.*

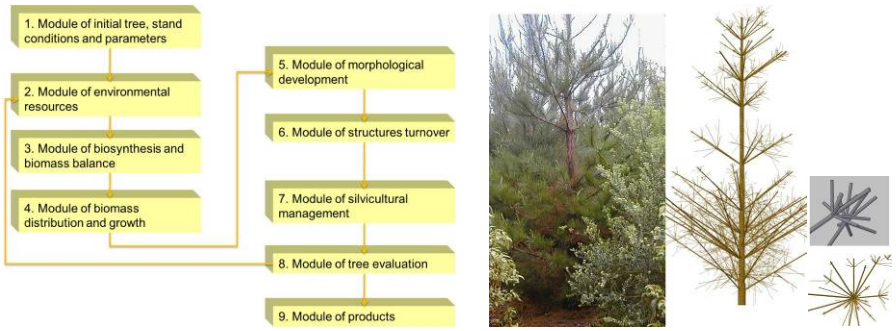

Figure 1: (a) General modular flowchart of the functional-structural model; (b) Some outputs of trees and structures.

It models the development and growth of individual trees under different soil, climate and stand conditions. The model integrates physiological processes following morphological development rules based on thermal and photoperiod control signals. Allometric relationships between demanding foliage and the conductive structure of wood are satisfied. A biomass balance is established and photosynthates allocation hierarchies are assigned that lead to a stochastic production of new organs and structures turnover, to heartwood formation and self-pruning (Figure 1a). The model and sub-models were based on previous research work of several authors on *Pinus radiata* other *Pinus* species (Bollman and Sweet, 1976; Madwick, 1994; Ryan et al. 1996; Kozlowski and Pallardy, 1997; Mäkelä 2002; Rodríguez *et al.* 2003; Pilatti and Norero, 2004, among many others) as well as on personal research (Fernández and Norero 2006; Fernández *et al.* 2007; Fernández et al. 2011). The model has been written in the Lindenmayer Systems language (Prusinkiewicz and Lindenmayer 1990) that generates a 3D tree at monthly time steps. The results are expressed in terms of biometric variables (height, diameter, volume); biomass outputs and by wood characteristics, such as knots size and position in wood, width of growth ring and wood density (Figure 1b). The model yields satisfactory results except for wood density values and efforts to improve this subject were therefore undertaken. To this end, a better understanding of the close relationship between development and growth processes of the crown and of wood formation appears to be the key issue, as indicated by several authors (Richardson 1964; Larson 1969; Downes et al. 2002; Drew et al. 2012 among others). Thus, we began a new project to get answers concerning (a) the allometric relation between newly formed foliage and the new lumen area, the true or effective conductive area of the developing wood ring; (b) the relation between sexual maturation and external and internal

characteristics of the tree; (c) the combined phenology of shoot, foliage and wood production, and (d) the relation between wood density and water conductivity.

The prospective presentation will show main results and how these results are to be incorporated into the structure of the above mentioned model.

MATERIALS AND METHODS

The development of foliage, main apex, and wood of 38 nine years old *Pinus radiata* trees of an unmanaged stand in the Mediterranean Central region of Chile were measured during the June 2009–August 2010 growing season. Every 15 days at the beginning of the season and every 30 days later on, microcores, 2 mm diameter x 12 mm length, were drilled out from each tree with a Trephor instrument, 40 cm above the ground surface. Simultaneously, the development of the main apex and of foliage was measured. In each occasion three trees were felled; their whole tree architecture measured and described, and discs from every growth unit cut and collected for further analysis. The entire biomass was weighed and classified according to position and age. Hourly temperature, rainfall, wind speed and solar radiation were recorded on a nearby weather station. These data were combined with pertinent soil conditions to compute changes in water balance and thermal accumulation according to the procedure of Fernández et al. (2011).

Microcores were sliced in a microtome and photographed in a microscope. By means of image processing techniques, cells and lumen size, wall thickness and number of cells were computed. Wood density was estimated considering 1.410 kg m^{-3} the cell wall density. When trees were felled, an X-ray transversal profile of wood was obtained at the same level the microcores were sampled. As these measurements accumulated a correlation was apparent between both parameters. It was thus possible to define the consecutive limits of annual growth rings at a given date, and investigate relationships among ring characteristics, such as cell size, lumen size, wall thickness and X-ray wood density values. Each piece of the growth ring was dated. With this information it was possible to analyze, relate and model the connection between ring development, foliage and apex development and environmental variables.

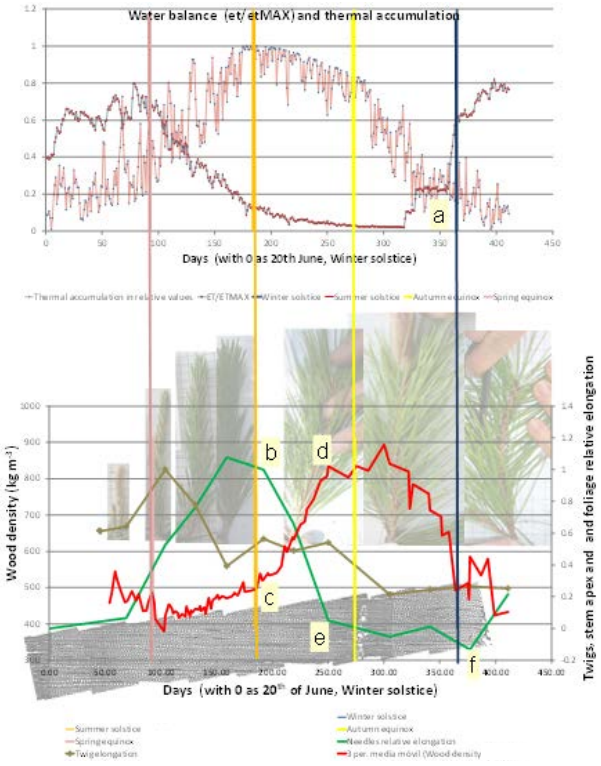

Figure 2: Upper image shows water balance (as et/etMAX) and thermal accumulation (in relative values). Lower image shows the simultaneous evolution of wood density, stem and twigs elongation, and foliage growth. Vertical lines connect both graphs at solstices and equinoxes.

RESULTS AND DISCUSSION

The upper part of Figure 2 shows the water balance of the sampling year, expressed as the ratio between Real Evapotranspiration (et) and Maximum Evapotranspiration (etMAX), and the thermal accumulation as a function of temperature (modified by water balance when too low). Solstices and equinoxes are indicated; time (x-axis) is given in days from June 21 as day = 1, the first day of the growing period (winter solstice in the southern hemisphere). Earlywood formation coincides with the period when needle elongation rate was steadily increasing. When this tendency changed (close to summer solstice) (Figure 2b) needles continued to enlarge but at lower rate the wood ring density changed sharply from a low to a high value (Figure 2c). Needles ceased to enlarge near the autumn equinox (Figure 2e) At this time (Figure 2d) wood density attained its highest values.

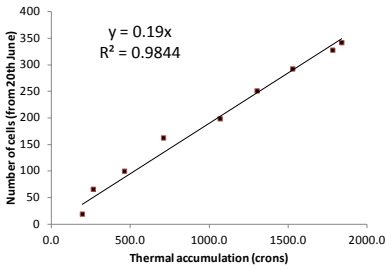

Figure 3: Relationship between thermal accumulation (in chron units, Fernández et al. 2011) and the accumulated number of new cells forming the wood ring.

Temperature has been recognized as a commanding factor on cambial activation and cambial rate of activity (Gricar et al, 2007; Begum et al., 2008). Figure 3 shows the relationship of thermal accumulation and number of cell produced during the sampling period. The linear relation indicates that it is necessary 5.26 thermal units or *chrons* (=1/0.19) for the production of one new cell. Wood density depends on wood cell size, cell wall thickness and lumen size. Cell wall thickness, in turn, depends on the rate of wood generation at the cambial zone, the permanence of the cell in the formation and enlarging area and the availability of material for cell wall build up (Taiz and Zeiger 2010). In increasingly warm periods (spring) with good water balance the thermal accumulation rises and the production of cells is accelerated. But as new foliage is at an early stage of development, the total amount of photosynthates is low compared to periods in full foliage display. As a result, there is a shorter time for enlargement and a lower availability of material leading to cell of large lumens and thin cell walls (= low wood density = earlywood type). During autumn, temperature and heat accumulation decrease, rate of new cell production slows down, but the period of enlargement increases. With all the new foliage fully displayed, *Pinus* photosynthesis continues to provide ample material to developing cells. As a result, larger amount of mass directed to fewer cells contribute to larger wall thickness. These findings will be incorporated into the above mentioned functional-structural model of *Pinus radiata* (Fernández et al. 2011) How this is to be achieved and what kind of results are to be expected of future simulations will be the subject and discuss during the presentation. We plan to extend the research to more sites conditions in order to confirm the generality of the relation of cells formation with thermal accumulations.

Aknowledgment. Research financed by Chilean Research Grants FONDECYT project number 11085008.

LITERATURE CITED

Begum S, Nakaba S,Oribe Y, Kubo T & Funada R. 2007 Induction of cambial reactivation by localized heating in a deciduous hardwood hybrid poplar (Populus sieboldii x P. grandidentata). Annals of Botany **100**, 439–447.

Bollmann MP and Sweet GB. 1976. Bud morphogenesis of Pinus radiata in New Zealand. 1: The initiation and extension of the leading shoot of one clone at two sites. *New Zealand Journal of Forest Science* **6**, 376-392.

Drew DM, Downes GM, Battaglia M. 2012. A new process-based model of wood formation in Pinus. In: Proceedings of the 2012 IUFRO Conference Division 5 Forest Products. 8-13 de Julio 2012, Estoril Congress Centre, Lisboa, Portugal.

Fernández, MP and Norero A. 2006. Relation between length and diameter of Pinus radiata branches. *Scandinavian Journal of Forest Research* **21**, 124-129.

Fernández MP, Norero A, Barthélémy D. and Vera J. 2007. Morphological trends in main stem of *Pinus radiata* D. Don: transition between vegetative and reproductive phase. *Scandinavian Journal of Forest Research* **22**, 398-406.

Fernández MP, Norero A, Vera J, Pérez E. 2011. A functional-structural model for radiata pine (*Pinus radiata*) focusing on tree architecture and wood quality. *Annals of Botany **108**: 1155-1178*

Gricˇar J., Zupancˇicˇ M., Cufar K., Koch G., Schmitt U. & Oven P. 2006. Effect of local heating and cooling on cambial activity and cell differentiation in the stem of Norway spruce (Picea abies). Annals of Botany **97**, 943–951.

Kozlowski, T. T. And Pallardy, S. G. 1997. Growth control in woody plants. San Diego: Academic Press.

Larson PR. 1969. Wood formation and the concept of wood quality. Bulletin No 74, Yale University, School of Forestry.

Madgwick HAI 1994. *Pinus radiata: Biomass, growth and form.* Rotorua, New Zealand: Ed. Madgwick, 428.

Mäkelä A. 2002. Derivation of stem taper from the pipe theory in carbon balance framework. *Tree Physiol.*, **22**, 891-905.

Pilatti MA, Norero A. 2004. Simulación de cultivos anuales. Formulaciones básicas del desenvolvimiento normal. Ediciones UNL. Universidad Nacional del Litoral, Santa Fé, Argentina.

Prusinkiewicz P, Lindenmayer A. 1990. The algorithmic beauty of plants. New York: Springer Verlag. pp. 228.

Richardson SD. 1964. The external environment and tracheid size of conifers, In Zimmermann M.H. (Ed). *The formation of wood in forest trees.* Academic Press, New York, London.

Rodríguez R, Hofmann G, Espinosa M, and Ríos D. 2003. Biomass partitioning and leaf area of Pinus radiata trees subjected to silvopastoral and conventional forestry in the VI Region, Chile. *Revista Chilena de Historia Natural*. **76**, 437-449.

Ryan MG, Hubbard RM, Pongracic S, Raison RJ and McMurtrie RE. (1996). Foliage, fine root, woody-tissue and stand respiration in Pinus radiata in relation to nitrogen status. *Tree Physiology*, 16, 333-343.

Taiz L, Zeiger E. 2010. Plant physiology. Sinauer Associated Inc., Sunderland. 782 pp.

Proceedings of the 7th International Conference on Functional-Structural Plant Models, Saariselkä, Finland, 9 - 14 June 2013. Eds. Risto Sievänen, Eero Nikinmaa, Christophe Godin, Anna Lintunen & Pekka Nygren.
http://www.metla.fi/fspm2013/proceedings. ISBN 978-951-651-408-9.

Functional overwintering types as basis for modelling the overwintering of northern field layer plants under climate warming

Robin Lundell*, **Heikki Hänninen**, **Timo Saarinen** and **Helena Åström**
Plant Ecophysiology and Climate Change Group (PECC), Department of Biosciences, PO Box 65, 00014 University of Helsinki, Finland
** correspondence:* robin.lundell@helsinki.fi

Highlights: Three overwintering types were identified among boreal field layer plants by using growth chamber experiments in combination with phenological dynamic models of the annual cycle. These types form the basis for modelling the responses of overwintering plants to climate change.

Keywords: Climate warming, chilling, dormancy, dynamic models, functional types, growth onset.

The environmental conditions of plants are projected to change globally during the coming decades due to climate change. The changes are predicted to be especially pronounced in the north during the winter. This will bring about novel combinations of environmental factors not experienced by contemporary plants. Experimental determination of the effect of various climate change scenarios on plants are often limited by the resources and effort needed to carry out multiple treatments. This shortcoming can, in part, be overcome by the use of ecophysiological process-based dynamic models. The successful use of dynamic models in climate change research requires that the models are properly tested and parameterised by experimental data.

Towards winter, many plants enter a state of rest, or endodormancy, which is maintained physiologically, and gradually released by the effect of chilling. Endodormancy is followed by ecodormancy, during which microscopic ontogenetic development towards growth onset is taking place in the buds in response to temperature. Growth onset results in physiological changes in the plant, such as loss of freezing tolerance, which can be detrimental if the plants start growing prematurely during warm spells in winter.

By modifying phenological dynamic models of the annual cycle of forest trees (Hänninen 1990, Hänninen and Kramer 2007), we developed dynamic models for the overwintering of perennial field layer plants in the boreal zone with the purpose of identifying functional overwintering types among these in order to create tools to study the effects of wintertime climate change on field layer plants in the boreal zone. The models were parameterised by using data from a series of growth chamber experiments with plants representing different functional groups from dwarf shrubs, hemicryptophytes, overwintering rosette plants, and grasses. The plants were allowed to overwinter in constant conditions in freezer storage at -2.5 °C. At various times in winter, plants were transferred to growth chambers to constant or fluctuating temperatures, and the onset of growth was monitored. Based on these results, we identified overwintering types that form the basis of both modelling and experimental work.

Our results show that there are differences among both plant species and functional groups in the timing of growth onset following warm periods in the winter. Several responses regarding timing of growth onset could be seen. Three overwintering types could be identified based mainly on the amount of chilling required to break endodormancy, determined by using dynamic models of overwintering. These overwintering types are characterized by having shallow, moderate or deep endodormancy, respectively. The identified types agree with types previously defined in the literature (Yoshie and Yoshida 1989). Considerable variation can, however, be found among species within the types, e.g. with respect to the rate of ontogenetic development.

Premature growth onset during winter affects other physiological traits such as plant cold hardiness and carbon metabolism. Differential responses among species may result in changes in species composition. Dynamic process-based models of the overwintering responses of plants can also be incorporated in larger scale models and thus used to refine predictions of the consequences of climate change on the vegetation.

LITERATURE CITED

Hänninen H. 1990. Modelling bud dormancy release in trees from cool and temperate regions. *Acta Forestalia Fennica* **213**: 1-47.

Hänninen H, Kramer K. 2007. A framework for modelling the annual cycle of trees in boreal and temperate regions. *Silva Fennica* **41**: 167-205.

Yoshie F, Yoshida, S. 1989. Wintering forms of perennial herbs in the cool temperate regions of Japan. *Canadian Journal of Botany* **67:** 3563-3569.

Proceedings of the 7th International Conference on Functional-Structural Plant Models, Saariselkä, Finland, 9 - 14 June 2013. Eds. Risto Sievänen, Eero Nikinmaa, Christophe Godin, Anna Lintunen & Pekka Nygren. http://www.metla.fi/fspm2013/proceedings. ISBN 978-951-651-408-9.

Patterns of carbon and nitrogen allocation in trees predicted by a model of optimal plant function

Ross E. McMurtrie[1] and **Roderick C. Dewar**[2]

[1]*School of Biological, Earth and Environmental Sciences, The University of New South Wales, Sydney, NSW 2052, Australia;* [2]*Research School of Biology, The Australian National University, Canberra, ACT 2600, Australia*

**correspondence:* r.mcmurtrie@unsw.edu.au

Highlights: Annual carbon allocation to leaves, stems and roots of trees is predicted by a model that simulates canopy photosynthesis and root nitrogen uptake with the overlying hypothesis that annual wood production is maximised.

Keywords: Carbon and nitrogen allocation, forest growth model, Norway spruce, optimisation model, photosynthesis, root nitrogen uptake

Annual carbon (C) allocation belowground in forests can range from 40 % of annual C allocation to wood at fertile, productive sites to 300 % under infertile conditions (Litton et al. 2007; Dybzinski et al. 2011). C allocation is therefore an important determinant of terrestrial C sequestration. However, because the C allocation process is inadequately understood (Franklin et al. 2012), it is a weakness in current ecosystem and earth-system modelling. This paper presents a new theoretical perspective on forest C allocation derived from a model that incorporates the hypothesis that annual wood growth is maximised (Valentine and Mäkelä 2012). The model simulates photosynthesis by a vertically-distributed leaf canopy and nitrogen (N) uptake by a vertically-distributed root system, but does not include a specific C allocation mechanism. It makes predictions of optimal vertical profiles of photosynthetic N-use efficiency *PNUE* of leaves and N-uptake efficiency *NUpE* of roots. Leaf *PNUE* decreases with canopy depth because of light attenuation, and root *NUpE* decreases with soil depth as a consequence of reduced soil N availability at depth. At steady state the model predicts a relationship between *PNUE* of basal leaves and *NUpE* of basal roots that depends on leaf and root longevities and N concentrations. This relationship will be used to determine optimal patterns of annual C and N allocation to leaves, roots and stems in stands of Norway spruce growing at sites with contrasting N fertility (Dewar et al. 2009; McMurtrie and Dewar 2011; Dewar et al. 2012; McMurtrie et al. 2012).

LITERATURE CITED

Dewar RC, Franklin O, Mäkelä A, McMurtrie RE, Valentine HT. 2009. Optimal function explains plant responses to global change. *Bioscience* **59**:127-139.

Dewar RC, Tarvainen L, Parker K, Wallin G, McMurtrie RE. 2012. Why does leaf nitrogen decline within tree canopies less rapidly than light? An explanation from optimization subject to a lower bound on leaf mass per area. *Tree Physiol*ogy **32**:520–534.

Dybzinski R, Farrior C, Wolf A, Reich PB, Pacala SW. 2011. Evolutionarily stable strategy carbon allocation to foliage, wood, and fine roots in trees competing for light and nitrogen: an analytically tractable, individual-based model and quantitative comparisons to data. *American Naturalist*, **177**:153–166.

Franklin O, Johansson J, Dewar RC, Dieckmann U, McMurtrie RE, Brännström Å, Dybzinski R. 2012. Modelling carbon allocation in trees: a search for principles. *Tree Physiology* **32**:648-666.

Litton CM, Raich JW, Ryan MG. 2007. Carbon allocation in forest ecosystems. *Global Change Biol.* **13**:2089-2109.

McMurtrie RE, Dewar RC. 2011. Leaf-trait variation explained by the hypothesis that plants maximize their canopy carbon export over the lifespan of leaves. *Tree Physiology* **31**:1007–1023.

McMurtrie RE, Iversen CM, Dewar RC, Medlyn BE, Näsholm T, Pepper DA, Norby RJ. 2012. Plant root distributions and nitrogen uptake predicted by a hypothesis of optimal root foraging. *Ecology and Evolution* **2**:1235–1250.

Valentine HT, Mäkelä A. 2012. Modeling forest stand dynamics from optimal balances of carbon and nitrogen. *New Phytologist* **194**:961-971.

Proceedings of the 7th International Conference on Functional-Structural Plant Models, Saariselkä, Finland, 9 - 14 June 2013. Eds. Risto Sievänen, Eero Nikinmaa, Christophe Godin, Anna Lintunen & Pekka Nygren. http://www.metla.fi/fspm2013/proceedings. ISBN 978-951-651-408-9.

L-Rose: a model simulating organ expansion of individual plants within a bush rose crop

Sabine Demotes-Mainard[1*], Jessica Bertheloot[1], Bruno Andrieu[2], Gaelle Guéritaine[1], Lydie Huché-Thélier[1], Vincent Guérin[1], Rachid Boumaza[3]

[1]INRA, UMR 1345 IRHS (INRA, Agrocampus-Ouest, Université d'Angers), SFR 4207 QUASAV, F-49071 Beaucouzé, France. [2]INRA, UMR 1091 EGC (INRA, AgroParisTech), F-78850 Thiverval-Grignon, France. [3]Agrocampus-Ouest, UMR 1345 IRHS (INRA, Agrocampus-Ouest, Université d'Angers), SFR 4207 QUASAV, F-49045Angers, France

**correspondence: sabine.demotes@angers.inra.fr*

Highlights: A model has been developed to simulate the dynamics of expansion of the individual organs of bush rose primary shoots. This model is designed to provide a tool calibrated on experimental data to investigate plant response to phylloclimate, especially light.

Keywords: architectural modeling, expansion, FSPM, L-systems, *Rosa hybrida* L., bushrose

Three-D empirical models that mimic accurately the dynamics of plant architecture can be used, together with physical models, to investigate the climate perceived at the level of individual organs. In bush rose the commercial product is the individual plant and its architecture determines its visual quality. It is thus important to explain not only mean plant architecture but also interplant architectural variability, which can be high in bush rose canopies. The aim of this work was to develop a model that reproduces the expansion of primary shoots within bush rose canopies accounting for interplant variability. Our model is designed to be calibrated on a minimal amount of non-destructive and easy-to-measure experimental data.

An analysis of organ expansion dynamics using datasets obtained in three different growing conditions (different years and densities) was undertaken to find out stable relationships at the individual plant scale that coordinate the expansion along time of the individual organs. A first set of relationships relates the rates of expansion of individual leaves or internodes to their relative position along the shoot and their final length. A second set of relationships coordinates the timing of organ expansion. We showed that leaf and internode of a same phytomer expand almost simultaneously and that expansion periods of successive leaves and internodes overlap. The time of maximal expansion rate for leaves and internodes is related to the time of leaf appearance. A third set of relationships deals with leaf allometry, relating length and width of all leaflets to a unique dimension that is terminal leaflet length. These relationships were used to build a model that was implemented in L-Py (Boudon et al. 2012) under the OpenAlea platform (Pradal et al. 2008). The model was tested using cross-validation, it correctly reproduced the dynamics of expansion of leaflets and internodes of individual primary shoots (RMSEP of 7.3% and 10.2% of final length, respectively, when the analysis was conducted at individual plant scale), using solely measurements of organ numbers and sizes at the end of primary shoot growth and of phyllochron. This first version focused on the phase preceding branching since it will first be used to investigate budbreak regulation.

The originality of the model is to account for inter-plant variability in expansion within a crop. In a next step this model will be coupled with a light model to explore the relationships between local light environment and bud break in bush rose, aiming to explain both mean crop behavior and interplant variability.

LITERATURE CITED

Boudon F, Pradal C, CokelaerT, Prusinkiewicz P, Godin C. 2012. L-Py: an L-system simulation framework for modeling plant architecture development based on a dynamic language. Frontiers in Plant Science 3: 76. doi: 10.3389 /fpls.2012.00076.

Pradal C., Dufour-Kowalski S., Boudon F., Fournier C., Godin C.2008. OpenAlea: a visual programming and component-based software platform for plant modelling. *Functional Plant Biology* **35**: 751-760.

METHODS FOR FUNCTIONAL-STRUCTURAL PLANT MODELS

Proceedings of the 7th International Conference on Functional-Structural Plant Models, Saariselkä, Finland, 9 - 14 June 2013. Eds. Risto Sievänen, Eero Nikinmaa, Christophe Godin, Anna Lintunen & Pekka Nygren. http://www.metla.fi/fspm2013/proceedings. ISBN 978-951-651-408-9.

KEYNOTE: Biotic systems as multilevel dynamic information processing systems

Paulien Hogeweg[1]

[1]*Theoretical Biology and Biolinformatic Group, University of Utrecht, Padualaan 8 3584CH Utrecht, Netherlands*

**correspondence:* P.Hogeweg@uu.nl

Highlights: Multilevel Modeling may simplyfy the modeling of complex biological processes

Keywords: Multilevel modeling, gene regulation, whole genome duplication, multilevel evolution, development

Most studies of (information processing in) biological systems, focus on one level of organization, e.g. gene regulation, or ecosystem interactions. Such single level biological systems are already very complex, and even relatively simple models of them are hard to study, for example because of the large number of unknown or only partially known parameters.

In this talk I will argue that, extending such models to multiple levels can, paradoxically, make things simpler. Mutual interaction among levels may constrain the dynamics, tune parameters and/or make the dynamics more dependent on structure and less sensitive to parameters. Such extensions can be either by explicitly defining multiple levels in the model or allowing new levels of organization to emerge.

The argument will be illustrated in a number of case studies, focusing on gene regulation (adaptation to a varying environment at regulatory and evolutionary timescales; the role of bi-stability(van Hoek and Hogeweg 2006,2007)), genome evolution (the role of whole genome duplication, homeostasis (van Hoek and Hogeweg 2009, Cuypers and Hogeweg 2012, and in prep), development (the role of size and shape of cells and tissues in cell fate specification (Grieneisen et al 2007, 2012) and ecosystems (higher levels of organization and the role of mutualism and cheaters (Takeuchi and Hogeweg).

In these multilevel models counter-intuitive results are obtained, which often challenge conventional 'wisdom' and yet reflect observed but unexplained patterns in 'real' biological systems

LITERATURE CITED

Cuypers TD, Hogeweg P. 2012. Virtual genomes in flux: an interplay of neutrality and adaptability explains genome expansion and streamlining***. Genome Biol Evol. 2012;4(3):212-29***

Grieneisen VA, Xu J, Marée AF, Hogeweg P, Scheres 2007. Auxin transport is sufficient to generate a maximum and gradient guiding root growth. *Nature. 2007 Oct 25;449(7165)1008-1013*

Grieneisen VA, Scheres B, Hogeweg P, M Marée AF. 2012. Morphogengineering roots: comparing mechanisms of morphogen gradient formation. *BMC Syst Biol. 2012 May 14;6:37. doi: 10.1186/1752-0509-6-37.*

van Hoek MJ, Hogeweg P. 2006. In silico evolved lac operons exhibit bistability for artificial inducers, but not for lactose. *Biophys J. 91(8):2833-43. Epub 2006 Jul 28*

van Hoek MJ, Hogeweg P. 2007. The effect of stochasticity on the lac operon: an evolutionary perspective.. ***PLoS Comput Biol. 2007 Jun;3(6):e111.***

van Hoek MJ, Hogeweg P. 2009. Metabolic adaptation after whole genome duplication. M*ol Biol Evol. (11) 2441-53*

Takeuchi N, Hogeweg P. 2009. Multilevel selection in models of prebiotic evolution II: a direct comparison of compartmentalization and spatial self-organization. *PLoS Comput Biol. 2011 Mar;7(3):e1002024*

Proceedings of the 7th International Conference on Functional-Structural Plant Models, Saariselkä, Finland, 9 - 14 June 2013. Eds. Risto Sievänen, Eero Nikinmaa, Christophe Godin, Anna Lintunen & Pekka Nygren.
http://www.metla.fi/fspm2013/proceedings. ISBN 978-951-651-408-9.

Integrating multiple scale dynamics: Application to *Fagus sylvatica* under ozone exposure

Yongzhi Ong*, Katarína Smoleňová, Michael Henke and **Winfried Kurth**
Department of Ecoinformatics, Biometrics and Forest Growth, Georg-August University of Göttingen, Büsgenweg 4, 37077 Göttingen, Germany
**correspondence:* yong@gwdg.de

Highlights: An integrated dynamic model of ozone concentration trends, stand dynamics, radiation interception, structural growth, functional systems and molecular pathways is constructed for beech trees. The model composes incomparable spatial decompositions and functional processes in a single graph-based framework. Extensions to the programming language XL for multi-scale rule-based modeling are applied in order to gain insights into the challenges that scale integration poses on language formalisms.

Keywords: XL language, GroIMP platform, multi-scale, up-scaling, down-scaling, *Fagus sylvatica*, ozone

INTRODUCTION

European beech (*Fagus sylvatica*) is one of the most important tree species in central Europe (Scalfi et al. 2004). Models and observations indicate increasing concentrations of tropospheric ozone in Europe since 1996 (Denby et al. 2010). The trends, however, are not consistent throughout Europe. A general north to south gradient in accumulated ozone exposure over a threshold of 40 parts per billion (AOT40) can be seen. Tropospheric ozone triggers oxidative stress responses in the enzymes of the Shikimate pathway (Betz et al. 2009) as well as in protein levels related to the Calvin cycle (Kerner et al. 2011) in beech trees. These responses lead to structural (e.g. leaf lesions) and functional (e.g. photosynthetic capacity) depreciations.

In previous studies, relationships between the environment (in terms of radiation, precipitation and temperature) and trees or stands have been represented in functional-structural models (Sinoquet and Le Roux 2000) mostly at a single spatial and temporal scale level. At the scale of stands, models have been created for the dynamics of competition and dispersion (Kurth et al. 2012). Within the scale of individual trees, structural topology has been decomposed into various scales of representation (Godin and Caraglio 1998), whereas functional models have been re-arranged into multiple aspects (Cieslak et al. 2011). Carbon partitioning and morphological plasticity in beech trees were addressed by a model in Letort et al. (2008). At an even finer scale, studies at the transcript and protein levels of trees have been conducted (Abril et al. 2011). In this study, the dynamics expressed by selected models from different scales are integrated and implemented using the programming language XL with extensions for multi-scale modeling (Ong 2012). The objectives are to gain insights into the non-linear causalities experienced by ozone-exposed beech trees and to address practical challenges and performance issues posed by scale integration.

MODEL DESCRIPTION AND SIMULATION

A partially ordered set, a so-called structure of scales (Fig. 1) is used to represent the inter-scale relationships. The coarsest scale consists of geographical data, light sources and climatic conditions. The second scale describes a stand and includes positional information of trees. A rule-based stand structure model works at this scale. Individual beech trees with aggregated information also reside here. The stand scale is refined into two incomparable scales: the growth unit scale and the crown scale. The crown scale contains collective information of tree crowns and crown layers. The layers contain unique vertical height sections that divide the tree crown one-dimensionally. The crown scale is further refined into an internode scale. The internode scale is adjointly a refinement of the growth unit scale. The crown scale also refines to the metabolic network scale. For reasons of efficiency, we simulate the ozone modulated metabolisms not for each entity in the internode scale separately, but collectively for plant organs in a layer. The model segregates spatial scales but uses a single temporal scale.

A type graph is specified after the structure of scales. The type graph consists of nodes representing the modules (in the sense of the language XL (Kniemeyer 2008)), i.e. the types of objects of each scale in the structure of scales and the allowed relationships between them. More specifically, a unique directed edge type representing a ”refinement” relationship is adopted to relate modules from coarser scales to finer scales. Graph matching and re-writing rules depend on these relationships during intepretation.

The annual mean AOT40 values (in µg m^{-3}.h) of selected locations ranging between northern Europe and southern Europe from the computation results of Denby et al. (2010) are used to initiate separate plots at the environment scale (Fig. 2). Annual sunlight exposure hours and changes to AOT40 are computed in individual plots using rules during simulation.

An irregular and dynamic forest stand structure in the bounded environment is simulated with crown radius dynamics under competition similar to that proposed by Kurth et al. (2012). However, the stand structure model is modified such that individual trees are represented using only singular nodes. The individual trees are further refined into their complete topological structures and crown structures (Fig. 2).

The structural growth of individual beech trees at two scales is simulated. The finer internode scale consists of buds, leaves and internodes while the coarser scale consists of annual growth units (Godin and Caraglio 1998). Photon tracing technique (Hemmerling et al. 2008) is employed to determine the photon flux for each leaf. For each tree, the photon flux per crown layer is computed as the mean photon flux of leaves in the layer. As sun leaves are less responsive to oxidative stress as compared to shade leaves (Olbrich et al. 2010), metabolic processes in crown layers are modulated using the layer's photon flux. Photosynthetic output for each leaf is computed as a result of photon flux on the leaf and a factor of the metabolic state at its residing crown layer and plot node. A transport system based on the implementation by Hemmerling et al. (2008) allows basi-petal transport with allocation and export of carbon assimilates from leaves to organs (buds and internodes). The exported carbon assimilate is redistributed in the tree structure from a common pool using a weighted system (Kang and de Reffye 2007). Secondary growth is modeled based on a pre-allocated percentage for maintenance respiration as well as organ volume (Strobel 2004). The radii of internodes at the base of buds are used to determine the number of primordial leaves formed in the buds (Cochard et al. 2005). Thereafter, the type of growth units (long or short) and number of internodes are determined based on the number of primordial leaves in the buds.

The crown layers are connected to the metabolic network instance via a refinement relationship. The Shikimate pathway is modeled using a multi-scale graph-based representation similar to the implementation in Ong and Kurth (2012) and based on Maus et al. (2011). Four of the seven enzymes in the pathway are induced in response to ozone concentrations (Betz et al. 2009) in the connected macro-scale.

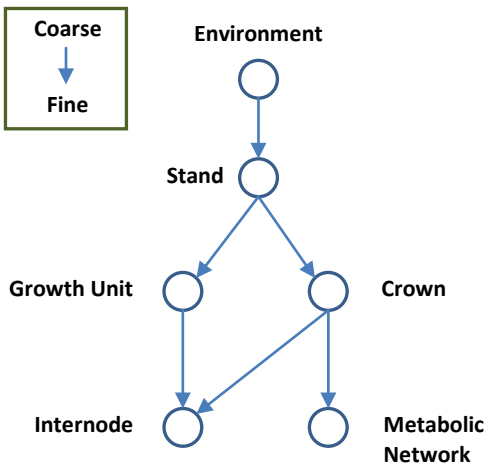

Fig. 1. Structure of scales depicting inter-scale relationships. The circles are abstract representations of the scales in the model.

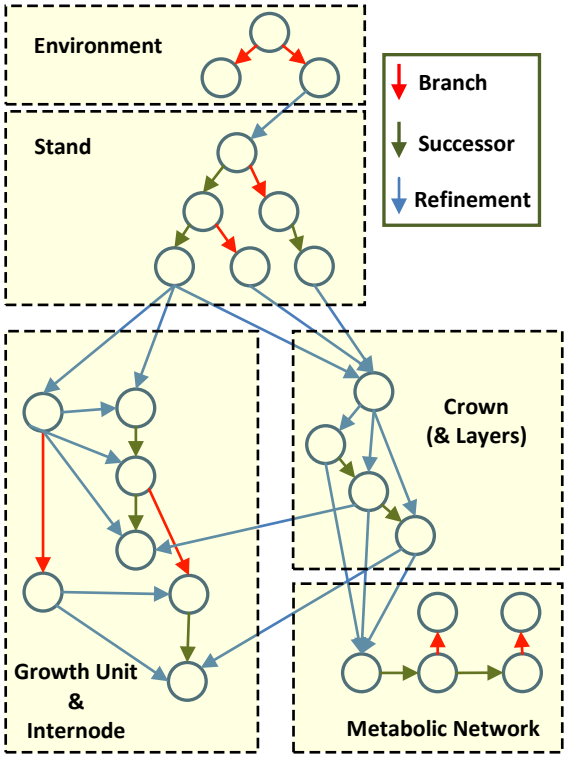

Fig. 2. Illustration of the dynamic graph model. Dotted boxes correspond to scales in the structure of scales. Individual circular nodes are instances of entities. Only important edge connections are shown.

RESULTS AND DISCUSSION

The multi-scale graph model and XL language extensions have enabled scale integration ranging from environmental and stand dynamics to beech functional-structural and metabolic processes. The basic data structure of our model is a directed graph, which is subject to restrictions given by a partially ordered set. This very general model backbone allows to represent scales in a coherent way which are incompatible in terms of refinement (e.g., topology: growth units versus geometry: crown layers). In its current version, our model serves as a proof-of-concept prototype and is not yet validated against field data.

The use of refinement edges between scales mandates customized graph traversal patterns in addition to classical turtle interpretation for graphical interpretation. Such traversal patterns are specified using rules in XL. The model size is computationally demanding and instantiation techniques (Smoleňová et al. 2012) to allow partially-unique trees are potentially useful in this aspect. Lastly, real-time level-of-detail visualization suitable for such increasingly large multi-scaled models is required for interactivity.

LITERATURE CITED

Abril N, Gion JM, Kerner R, et al. 2011. Proteomics research on forest trees, the most recalcitrant and orphan plant species. *Phytochemistry* **72(10)**:1219-1242.

Betz GA, Knappe C, Lapierre C, et al. 2009. Ozone affects Shikimate pathway transcripts and monomeric lignin composition in European beech (*Fagus sylvatica L.*). *European Journal of Forest Research* **128**:109-116.

Cieslak M, Seleznyova AN, Prusinkiewicz P, Hanan J. 2011. Towards aspect-oriented functional–structural plant modelling. *Annals of Botany* **108(6)**:1025-1041.

Cochard H, Coste S, Chanson B, Guehl JM, Nicolini E. 2005. Hydraulic architecture correlates with bud organogenesis and primary shoot growth in beech (*Fagus sylvatica*). *Tree Physiology* **25(12)**:1545-1552.

Denby B, Sundvor I, Cassiani M, de Smet P, de Leeuw F, Horálek J. 2010. Spatial Mapping of Ozone and SO_2 Trends in Europe. *Science of the Total Environment* **408**:4795-4806.

Godin C, Caraglio Y. 1998. A multiscale model of plant topological structures. *Journal of Theoretical Biology* **191**:1-46.

Hemmerling R, Kniemeyer O, Lanwert D, Kurth W, Buck-Sorlin G. 2008. The rule-based language XL and the modelling environment GroIMP illustrated with simulated tree competition. *Functional Plant Biology* **35**:739-750.

Kang MZ, de Reffye P. 2007. A mathematical approach estimating source and sink functioning of competing organs. *Function-Structural Plant Modelling in Crop Production* **22**:65-74.

Kerner R, Winkler JB, Dupuy JW, et al. 2011. Changes in the proteome of juvenile European beech following three years exposure to free-air elevated ozone. *iForest* **4**:69-76.

Kniemeyer O. 2008. *Design and implementation of a graph grammar based language for functional-structural plant modelling.* PhD Thesis, Brandenburg University of Technology, Germany.

Kurth W, Kniemeyer O, Sloboda B. 2012. Forest structure, competition and plant-herbivore interaction modelled with relational growth grammars. *Lesnícky casopis - Forestry Journal* **58(2)**:75-91.

Letort V, Cournède PH, Mathieu A, de Reffye P, Constant T. 2008. Parametric identification of a functional–structural tree growth model and application to beech trees (*Fagus sylvatica*). *Functional Plant Biology* **35**:951-963.

Maus C, Rybacki S, Uhrmacher AM. 2011. Rule-based multi-level modeling of cell biological systems. *BMC Systems Biology* **5**:166. doi:10.1186/1752-0509-5-166.

Olbrich M, Gerstner E, Bahnweg G, et al. 2010. Transcriptional signatures in leaves of adult European beech trees (*Fagus sylvatica L.*) in an experimentally enhanced free air ozone setting. *Environmental Pollution* **158**:977-982.

Ong Y. 2012. Multi-scale rule-based graph transformation using the programming language XL. In: Ehrig H, Engels G, Kreowski H-J, Rozenberg G, eds. *Graph Transformation.* Lecture Notes in Computer Science 7562, Springer, Berlin, 417-419.

Ong Y, Kurth W. 2012. A graph model and grammar for multi-scale modelling using XL. In: Gao J, Alhaij R, Dubitzky W, Ungar L, Wu C, Christianson A, Liebman M, Hu X, eds. *2012 IEEE International Conference on Bioinformatics and Biomedicine Workshops (BIBMW).* IEEE, 1-8. doi:10.1109/BIBMW.2012.6470293.

Scalfi M, Troggio M, Piovani P, et al. 2004. A RAPD, AFLP and SSR linkage map, and QTL analysis in European beech (*Fagus sylvatica* L.). *Theoretical and Applied Genetics* **108**:433-441.

Sinoquet H, Le Roux X. 2000. Short term interactions between tree foliage and the aerial environment: An overview of modelling approaches available for tree structure-function models. *Annals of Forest Science* **57**:477-496.

Smoleňová K, Kurth W, Cournède PH. 2012. Parallel graph grammars with instantiation rules allow efficient structural factorization of virtual vegetation. In: Echahed R, Habel A, Mosbah M, eds. *The Fourth International Workshop on Graph Computation Models (GCM 2012).* Bremen, 28.-29.9.2012, Proceedings, http://gcm2012.imag.fr/proceedingsGCM2012.pdf.

Strobel J. 2004. *Die Atmung der verholzten Organe von Altbuchen (Fagus sylvatica L.) in einem Kalk- und einem Sauerhumusbuchenwald.* PhD Thesis, University of Göttingen, Germany.

Proceedings of the 7th International Conference on Functional-Structural Plant Models, Saariselkä, Finland, 9 - 14 June 2013. Eds. Risto Sievänen, Eero Nikinmaa, Christophe Godin, Anna Lintunen & Pekka Nygren.
http://www.metla.fi/fspm2013/proceedings. ISBN 978-951-651-408-9.

Simulating the evolution of optimal rooting strategies in shallow soils and extreme climates

Michael Renton and **Pieter Poot**
School of Plant Biology and Centre for Climate Change Forest and Woodland Health, University of Western Australia, Crawley, WA 6009, Australia
**correspondence:* michael.renton@uwa.edu.au

Highlights: Functional-structural models of root development combined with evolutionary optimisation algorithms can provide insights into why plant species develop different strategies in different environments and conditions.

Keywords: evolutionary algorithm, ecological optimisation, resource acquisition, rooting strategies

INTRODUCTION

Through evolution, plants develop strategies to acquire the limited resources they need to survive, grow and reproduce, such as light, water and nutrients. These strategies would be expected to be adapted to the particular environment a plant experiences, with extreme conditions potentially leading to highly specific strategies. An example of such extreme conditions is that faced by perennial plants that grow in shallow soil in seasonally dry climates such as on rocky hills and ridges in the Mediterranean climate of southwest Australia; these plants usually germinate during the wet winter but then face a long summer drought in shallow soils that have very limited capacity to hold and provide water (e.g. Mishio 1992, Groom and Lamont et al. 1995).

There is evidence that water held within the underlying bedrock can be essential for meeting the transpiration demands of shrubs and trees during the dry season (e.g. Rose et al. 2003, Querejeta et al. 2007). Previous research has shown that species specialized for shallow soils in SW Australia have particular root morphologies that appear to be have evolved to improve their chance of finding fissures in the underlying rock that can provide access to such water; the shallow soil endemics tended to differ from related species from deeper soils by investing a larger portion of their biomass in roots, and distributing their roots faster and more evenly through the soil (Poot et al 2012, Poot and Lambers 2003a&b, Poot et al 2008, Poot and Lambers 2008). These results provide a possible explanation for the narrow endemism of many shallow-soil endemics because their root system traits seem to be adaptive in their own shallow-soil habitat in terms of obtaining access to fissures and water in the underlying rock, but are likely to be maladaptive in deeper soils. Indeed, it has been argued that the restricted range of shallow-soil endemics may be due to the high degree of root structure specialization required to survive in these extreme conditions, together with the fact that that these adaptations are relatively costly and are likely to provide relatively fewer benefits in deeper soil environments (Poot et al 2012).

Dynamic functional-structural models of plant growth (FSPMs) can potentially be used to predict the costs and benefits of different growth strategies in terms of resources gained and used, and how these costs and benefits vary according to differences in the temporal and spatial patterns in the availability of the resources. This can in turn provide insight into why different species develop and use different growth strategies in different environments and conditions. A computational model was developed to represent root development within a single growing season within a Mediterranean climate where rainfall is relatively plentiful for a period of the year and negligible for the remainder of the year (Renton et al 2012). The model is able to represent a wide range of relevant rooting strategies in a relatively simple and thus computationally efficient way. This allows computational evolutionary optimization algorithms (Fogel 1994) to be applied to the model, which in turn allows us to explore how ecological strategies evolve to best exploit available resources, and how this evolution of ecological strategies may vary with different patterns of resource availability.

TARSIERS

Our Tool for Analysis of Root Structures Incorporating Evolution of Rooting Strategies (TARSIERS) illustrates the potential of the approach of linking an FSPM with a computational evolutionary optimization algorithm. This tool is based on a computational FSPM that aims to capture the important processes involved

in root growth and development and water acquisition in a range of situations where water is the key limiting resource. The model was motivated by the southwest Australian shallow-soil case studies referred to above, but was constructed with the intention to be flexible enough to address questions about optimal rooting strategies in other conditions and species as well. The overall dynamics of the model are summarized and some different aspects of the model illustrated in Fig. 1, and details are available in Renton et al (2012). In brief, the model is based on a set of parameters that define various characteristics of the rainfall, soil, water uptake and biomass (known as Fixed Parameters, since they are assumed to be fixed for a particular environment), and another set of parameters that controls how the root structure develops over time (known as the Strategy Parameters, since they define the plant's growth strategy). The model employs a daily time step to simulate how the roots of a single plant grows through the soil after germinating at the start of the wet rainy season, and continues the simulation through this wet period until the start of a dry period. To keep the FSPM relatively computationally simple, we only represented the primary and secondary roots (we assume that these are the most important in defining the overall architecture of the root system and its access to water, both during the initial wet period and the subsequent drought period).

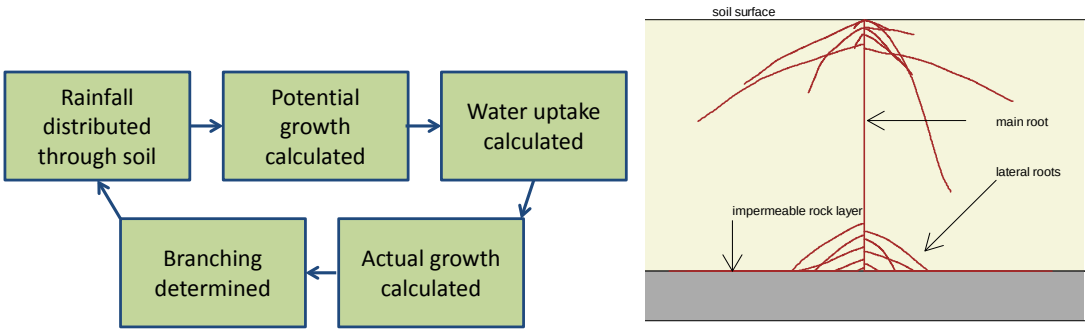

Fig. 1. Summary of dynamics of the FSPM at each time step (left) and illustration of FSPM components (right)

The full TARSIERS links the FSPM with an evolutionary optimisation algorithm that simulates the evolution of a plant population over time. An individual genotype is defined by a set of values for the Strategy Parameters, and a population is a number of such sets. The Fixed Parameters are defined to represent the conditions of interest (soil of a certain depth and water holding capacity, rainfall frequency and amount, frequency of fissures within the underlying rock etc) and a relative fitness is defined; for example, this could be zero if the plant has failed to access a wet fissure in the underlying rock to sustain it through the summer, and the biomass of the plant achieved by the start of the drought period if it has succeeded in finding a fissure. An initial population is then constructed and the evolution of that population is then simulated across a number of generations. For each generation, the FSPM is run separately for each individual in the current population and the resulting relative fitness of the individual is recorded. A new population is then constructed for the next generation. For each individual in the new population, a mother and father are randomly selected from the previous population based on a multinomial random distribution, where the weightings for each individual are its recorded relative fitness. The values for the Strategy Parameters defining the genotype of the new individual are the means of the corresponding values for the parents, plus a specified amount of random variation. When the new population has been defined, it is set to be the current population and the process continues until a fixed number of generations have been simulated.

RESULTS AND DISCUSSION

TARSIERS is able to successfully simulate the evolution of rooting strategies in particular conditions. The mean values of the Strategy Parameters change over the generations as more successful or 'fit' individuals in each generation have a higher probability of contributing to the next generation. The addition of random variation introduces novelty that allows new growth strategies to be explored (Fig 2). Moreover, different trajectories of evolution can be observed in different conditions, and the match between these trajectories and the conditions they are adapted for make ecological sense (Fig 2).

The FSPM in TARSIERS is relatively simple compared to more detailed existing root FSPMs (eg. Lynch et al 1997, Bidel et al 2000, Dunbabbin et al 2002), which makes it computationally feasible to link it with an evolutionary optimisation algorithm. Nonetheless, it includes enough detail and parameters to enable a wide range of developmental strategies to be explored. We plan to use TARSIERS to investigate how the rooting strategy evolves in different ways as a number of environmental assumptions are varied, including soil

depth, soil type, frequency of fissures in the underlying rock, wet season duration, frequency and amount of rainfall during the wet season, and spatial heterogeneity in soil characteristics. We also plan to extend the tool to account for competition between plants, soil nutrients, and phenotypic plasticity.

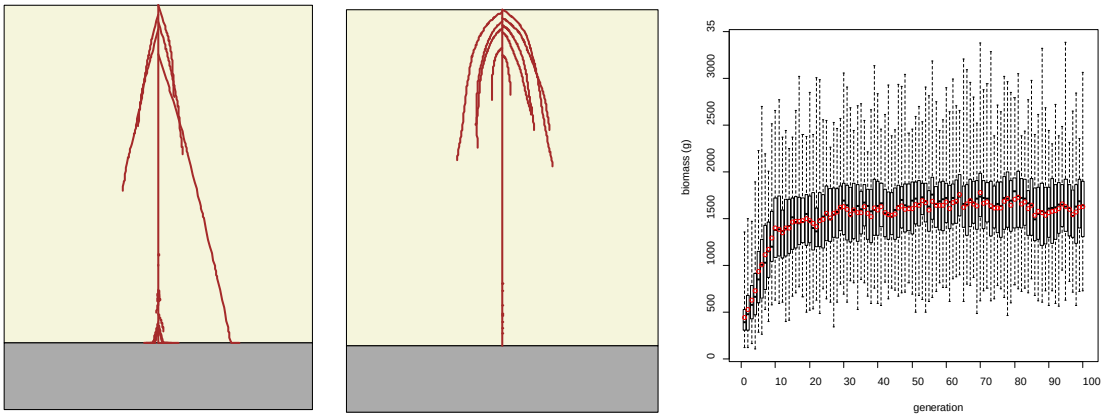

Fig. 2. Example outputs from using TARSIER to simulate the evolution of a plant species that initially has some adaptations to find fissures in underlying rock when 'fitness' is defined simply as biomass achieved at the start of the drought season (ie there is no advantage to finding fissures, only in making maximum use of water available over the wet period). Outputs include a typical example phenotype from an initial population (left), a typical example phenotype from the final population (centre) and boxplot showing values of the biomass achieved by individuals within the population changing over generations as evolution occurs (box: interquartile range, whiskers: range, red circle: mean). Note that the species has evolved to have a more superficial root system which leads to it achieving a higher biomass.

LITERATURE CITED

Bidel L, Pages L, Riviere L, Pelloux G, Lorendeau J. **2000**. MassFlowDyn I: a carbon transport and partitioning model for root system architecture. *Annals of Botany* **85**: 869.

Dunbabin VM, Diggle AJ, Rengel Z, Van Hugten R. **2002**. Modelling the interactions between water and nutrient uptake and root growth. *Plant and Soil* **239**: 19–38.

Fogel DB. **1994**. An introduction to simulated evolutionary optimization. *IEEE Transactions on Neural Networks* **5**: 3–14.

Groom PK, Lamont BB. **1995**. Leaf morphology and life form influence water relations of Hakea species on different soil substrates within south-western Australia. *Acta Oecologica* **16**: 609–620.

Lynch JP, Nielsen KL, Davis RD, Jablokow AG. **1997**. SimRoot: modelling and visualization of root systems. *Plant and Soil* **188**: 139–151.

Mishio M. **1992**. Adaptations to drought in five woody species co-occurring on shallow-soil ridges. *Functional Plant Biology* **19**: 539–553.

Poot P, Bakker R, Lambers H. 2008. Adaptations to winter-wet ironstone soils: a comparison between rare ironstone Hakea (Proteaceae) species and their common congeners. *Australian Journal of Botany* **56**: 574–582.

Poot P, Lambers H. 2003. Growth responses to waterlogging and drainage of woody Hakea (Proteaceae) seedlings, originating from contrasting habitats in south-western Australia. *Plant and soil* **253**: 57–70.

Poot P, Lambers H. 2008. Shallow-soil endemics: adaptive advantages and constraints of a specialized root-system morphology. *New Phytologist* **178**: 371–381.

Poot P, Hopper SD, Van Diggelen JMH. **2012**. Exploring rock fissures: does a specialized root morphology explain endemism on granite outcrops? *Annals of Botany*.

Poot P, Lambers H. **2003**. Are trade-offs in allocation pattern and root morphology related to species abundance? A congeneric comparison between rare and common species in the south-western Australian flora. *Journal of Ecology* **91**: 58–67.

Renton M, Poot P, Evers JB. 2012. Simulation of optimal rooting strategies: what's the best way to find a wet crack? *Proceedings of the Fourth International Symposium on Plant Growth Modeling and Applications (PMA12).* Shanghai: IEEE Computer Society.

Querejeta J, Egerton-Warburton L, Allen MF. **2007**. Hydraulic lift may buffer rhizosphere hyphae against the negative effects of severe soil drying in a California Oak savanna. *Soil Biology and Biochemistry* **39**: 409–417.

Rose K, Graham R., Parker D. **2003**. Water source utilization by Pinus jeffreyi and Arctostaphylos patula on thin soils over bedrock. *Oecologia* **134**: 46–54.

Proceedings of the 7th International Conference on Functional-Structural Plant Models, Saariselkä, Finland, 9 - 14 June 2013. Eds. Risto Sievänen, Eero Nikinmaa, Christophe Godin, Anna Lintunen & Pekka Nygren. http://www.metla.fi/fspm2013/proceedings. ISBN 978-951-651-408-9.

AMAPstudio: a 3D Interactive Software Suite for Plants Architecture Modelling

Sébastien Griffon[1] and **François de Coligny**[2]
[1]*Cirad, UMR AMAP, F-34000, Montpellier, France,* [2]*INRA, UMR AMAP, F-34000, Montpellier, France*
**correspondence:* sgriffon@cirad.fr

Highlights: Plants architecture modelling results in building complex models. Turning them into simulators requires strong interaction between scientists and software developers. The AMAPstudio project adapts a methodology that has been successfully conducted in the forestry modelling field for 12 years. It focuses on a long-term supported software environment and a strong customized technical backing to help modellers integrate their simulators in highly 3D interactive software.

Keywords: Plants architecture models, FSPM, AMAPstudio, modelling software

INTRODUCTION

Plants architecture (Barthélémy and Caraglio 2007) includes the plant's structure at a given time and its past development. Reading finely the current structure of a plant reveals what happened in its history and can lead to a highly detailed multi-level description. These botanical observations can be coded and handled by software in Multi-scale Tree Graphs (MTG) (Godin and Caraglio 1998) for further studies.

The AMAP laboratory has been building plants architecture modelling software since the 80's, both for structure and architecture analysis (Godin et al. 1999) and for simulation (Barczi et al. 2008). Several other contributions have been proposed since then, including the L-Studio/Vlab software (Prusinkiewicz and Lindenmayer 1990), GroIMP (Kniemeyer and Kurth 2008) and L-Py (Boudon et al. 2012) to simulate plants based on L-Systems with a set of rewriting rules, and OpenAlea (Pradal et al. 2008), a component based framework aiming at easing the integration and interoperability of models from different disciplines. The *VPlant* sub-package of the latter is dedicated to plant development and its control at the genetic and molecular level.

In parallel since 1999, the Capsis platform has been developed in AMAP to integrate forestry growth or dynamics models (Dufour-Kowalski et al. 2012). The Capsis methodology (de Coligny 2007) has been built in a collaborative way with the forestry modellers and the platform now contains more than 60 models of french or foreign partners.

The aim of this contribution is to propose an adaptation of the Capsis approach to the modelling of plants architecture.

SPECIFIC DESIGN OPTIONS

In order to share the effort, we decided to split the problem in two, this is why AMAPstudio (Griffon and Coligny 2012) contains two main software. *Xplo* is dedicated to the single plant level while *Simeo* works at the level of a scene made of several plants. The two software have the same structure, they are both based on a multi-operating systems, multi-projects Capsis kernel and they share some key components such as a common project manager and a central schematic 3D view. Both software rely on a common implementation of the MTG to handle a plant multi-scale description including topology and geometry with all elements having any attributes.

Xplo and Simeo bring *interactive editors* with classical import / export capabilities and some specific features. For instance, Xplo has an Excel like central table browser to edit all plant elements and their attributes, synchronized in real time with the 3D view, it proposes a configurable geometry reconstruction tool to add geometry to the plant, based on specific attributes or additional rules. It also comes with a set of flexible extraction features to quickly select some elements of the plants by creating new columns in an extraction table, filter the values on the fly and compute simple statistics. The resulting data can be plotted directly in Xplo or exported to other software for further analysis. Simeo proposes a set of plugins to layout plants according to several patterns. The terrain where the plants are added can either be flat, with a single slope or rely on any height map. It is possible to select the plants and move them with the mouse, set their coordinates very accurately through an editor or enter angles to rotate them. The customized scene can be exported to external biophysical simulators with plugins and the results added in new plant attributes. These

features were made interactive to be usable by any scientist or student needing to make simple actions quickly (Fig. 1). Most of them can be managed by AMAPstudio's undo / redo system.

Besides these editors for the daily routine work of importing, checking, editing and exporting data, AMAPstudio software can host *simulators for plant growth models*, at the individual level in Xplo or at the scene level in Simeo.

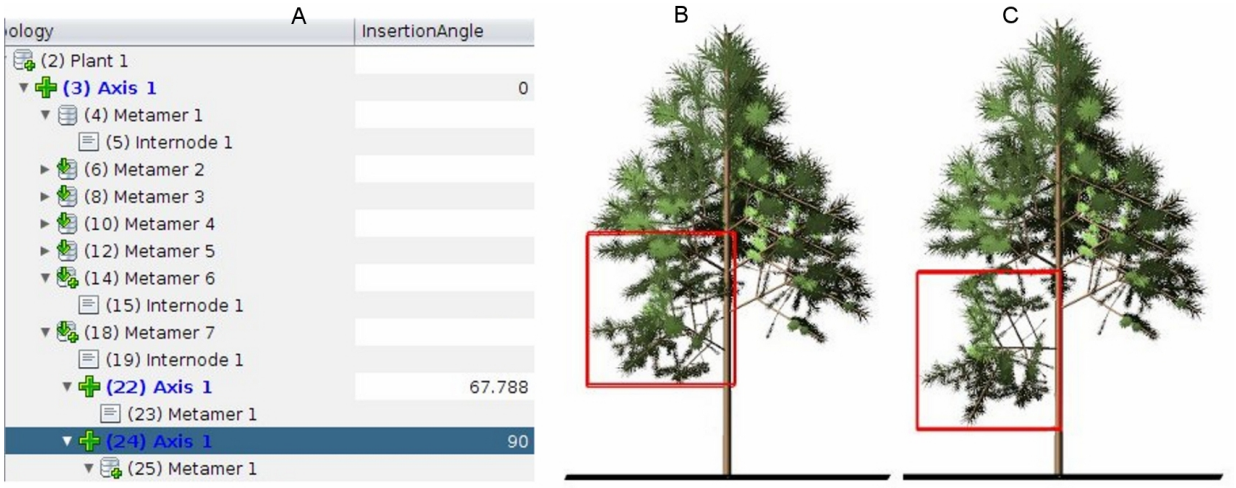

Fig. 1. Editing in the Xplo table view: (A) changing the insertion angle of the selected branch (B) of a juvenile Black pine tree is directly shown in the 3D view (C) when the on-the-fly geometric reconstruction is activated.

The modellers who decide to integrate their models in AMAPstudio have to read and accept the AMAPstudio charter describing the frame of the collaboration. Its main terms are the following: (i) the core software is distributed under the terms of a free license to make the partnerships easy, (ii) the modellers are in charge of the development of their models, (iii) they benefit from an initial training session, a customized starting stage and a permanent technical support, (iv) the ownership rules are clear: the models belong to their authors and they accept to share the source codes with all the other modellers adding their models into the project, (v) the charter also explicitly insists on the respect of each member's intellectual property.

Having a clear frame of rules facilitates the collaborations: each partner knows precisely from the beginning what investment he must make and what he can have in return. In particular, it is clear that the AMAPstudio developers - software engineers - will not help for the modelling work because they focus on the technical aspects for the modellers community: the scientists are the only authors of the models.

The project is based on the Java language which clearness and strictness help the scientists to develop with reasonable training and support.

Furthermore, its memory management makes it particularly convenient to build robust applications, its just-in-time native compilation features enable to get fast simulators.

The technical frame of the simulators comes from Capsis, there is no imposed modelling framework, the frame is about the minimal model usage: (i) initialisation of the departure situation and model configuration, (ii) parameters and stop criterion for the time loop. The model data structure is mainly a MTG in memory (or a MTG list) or any alternative plant description, the time step is free. The model evolution procedure calculates the successive states of the plant (or plant list) until the evolution limit is reached.

This loose framework can host very different models, including not exhaustively architectural models, functional-structural models, but also ecological models with environment interactions, including radiative balance or nutrients exchange with the soil.

All integrated models can be mixed with interventions or external events (e.g. pruning) to build scenarios and compare them. The simulations can be done with the interactive context or can be automated in specific scripts for long or repetitive tasks, concerning for instance heavy scenes with many highly detailed adult trees, running on dedicated calculation machines or clusters and writing their results in files for further analysis.

Because we know the importance of interoperability, AMAPstudio can import plant files through plugins, including MTG files, and all results can be exported the same way to MTG files or other standard formats to be reloaded in other applications.

CONCLUSION

AMAPstudio editors are used on a day to day basis by many students in the lab and by partners to load plant observations, check and edit them, reconstruct their geometry (Taugourdeau et al. 2010) and export extracted data to other software, e.g. Abaqus (Dassault Systèmes 2012).

Since late 2008, several plant level models have been integrated in AMAPstudio for various studies, including the aerial part of the plants: Greenlab (Feng et al. 2012), AMAPsim (Barczi et al. 2008), DRAFt (Taugourdeau et al. 2012), as well as the root part: DigR (Rey et al. 2011). Efforts are under progress to integrate libraries for radiative balance at the plant organ level (Dauzat et al. 2008) which can be used for ecological studies for a group of adult trees.

AMAPstudio is compatible with Windows, Linux and Mac OS, a web version can be downloaded on the project web site: http://amapstudio.cirad.fr.

LITERATURE CITED

Barczi JF, Rey H, Caraglio Y, de Reffye P, Barthélémy D, Dong Q, Fourcaud T. 2008. AMAPsim: an integrative whole-plant architecture simulator based on botanical knowledge, *Annals of Botany*, 101: 1125-1138.

Barthélémy D, Caraglio Y. 2007. Plant architecture: A dynamic, multilevel and comprehensive approach to plant form, structure and ontogeny, *Annals of Botany*, 99, 3: 375–407.

Boudon F, Pradal C, Cokelaer T, Prusinkiewicz P and Godin C. 2012. L-Py: an L-system simulation framework for modeling plant architecture development based on a dynamic language. *Front. Plant Sci.* 3:76.

Dassault Systèmes. 2012. The Abaqus product suite. http://www.3ds.com/fr/products/simulia/portfolio/abaqus/overview/ (17 Dec. 2012)

Dauzat J, Clouvel P, Luquet D, Martin P. 2008. Using virtual plants to analyse the light-foraging efficiency of a low-density cotton crop, *Annals of Botany*, 101: 1153-1166.

de Coligny F. 2007. Efficient Building of Forestry Modelling Software with the Capsis Methodology. In: Fourcaud T, Zhang XP, eds. *Plant Growth Modeling and Applications.* IEEE Computer Society, 216-222.

Dufour-Kowalski S, Courbaud B, Dreyfus P, Meredieu C, de Coligny F. 2012. Capsis: an open software framework and community for forest growth modelling. *Annals of Forest Science.* 69: 221–233.

Feng L, de Reffye P, Dreyfus P, Auclair D. 2012. Connecting an architectural plant model to a forest stand dynamics model—application to Austrian black pine stand visualization. *Ann For Sci.* 69: 245–255.

Godin C, Caraglio Y. 1998. A multiscale model of plant topological structures, *J. Theor. Biol.*, 191: 1–46.

Godin C, Guédon Y, Costes E. 1999. Exploration of a plant architecture databases with the AMAPmod software illustrated on an apple-tree hybrid family. *Agronomie*, 19 (3–4): 163–184.

Griffon S, de Coligny F. 2012. AMAPstudio: a Software Suite for Plants Architecture Modelling. In: Kang M, Dumont Y, Guo Y, eds. *Plant Growth Modeling, Simulation, Vizualization and Applications.* IEEE press, 141-147.

Kniemeyer O, Kurth W. 2008. The Modelling Platform GroIMP and the Programming Language XL. A. Schürr, M. Nagl, and A. Zündorf, Eds. *Lecture Notes In Computer Science, vol. 5088.* Springer-Verlag, 570-572.

Pradal C, Dufour-Kowalski S, Boudon F, Fournier C, Godin C. 2008. OpenAlea: a visual programming and component-based software platform for plant modelling, *Functional Plant Biology*, 35: 751-760.

Prusinkiewicz P, Lindenmayer A. 1990. *The algorithmic beauty of plants,* Springer-Verlag, New York, NY.

Rey H, Barczi JF, Jourdan C. 2011. DigR: how to model root system in its environment? 1 – the model. *XVIIIth International Botanical Congress*, Melbourne, Australia.

Taugourdeau O, Dauzat J, Griffon S, de Coligny F, Sabatier S, Caraglio Y, Barthélémy D. 2010. Retrospective analysis of fir sapling growth vs. light interception, In *Proceedings of 6th International Workshop on Functional-Structural Plant Models (FSPM),* 93-95.

Taugourdeau O, Barczi JF, Caraglio Y. 2012. Simulation of Morphogenetical Gradients Using a Minimal Functional-Structural Plant Model (FSPM). In: Kang M., Dumont Y., Guo Y., eds. *Plant Growth Modeling, Simulation, Vizualization and Applications*. IEEE press, 379-387.

Proceedings of the 7th International Conference on Functional-Structural Plant Models, Saariselkä, Finland, 9 - 14 June 2013. Eds. Risto Sievänen, Eero Nikinmaa, Christophe Godin, Anna Lintunen & Pekka Nygren. http://www.metla.fi/fspm2013/proceedings. ISBN 978-951-651-408-9.

Modelling Competition in Crop Populations via Reaction-Diffusion Foliage Dynamics. With an Outlook on Tree Modelling

Robert Beyer[1] and **Paul-Henry Cournède**[1]
[1]*Ecole Centrale Paris, Laboratory of Applied Mathematics, Ecole Centrale Paris, Laboratory of Applied Mathematics, Grande Voie des Vignes, 92295 Châtenay-Malabry, France*
**correspondence:* robert.beyer@ecp.fr

Highlights: Local leaf area index is considered as a spatially continuous variable, subject to dynamics of allocation, senescence and spatial propagation. This approach allows for inter-individual variability and competition while maintaining robustness – a key shortcoming of comparable models. Simulation results inspire a three-dimensional generalisation towards trees, alongside which an underlying dynamic branch system is devised, targeting finer morphological accuracy.

Keywords: leaf-area index, leaf area density, reaction-diffusion equations, optimisation

INTRODUCTION

Certain individual-based plant models applied in agronomy or forestry rely on a very precise geometric description of the plant, allowing for the radiative fluxes received by each plant organ to be computed by modelling the radiative exchanges in the whole canopy structure (Chelle et al. (2007) provide a review). Generally this geometry is difficult to obtain however and costly in terms of computation. Other approaches make use of competition indices, which are determined for each individual of a population according to the spatial configuration (Cournède et al., 2008; Pretzsch, 2002). Those in turn are usually restricted in terms of accuracy and extrapolation potential due to being based on empirical functions which are typically difficult to calibrate: They require heavy experimental data corresponding to detailed configurations and characteristics of all individual plants in various situations.

Aiming for a robust and adaptive technique to tackle scenarios of inter-individual competition for light, we explore a novel functional-structural approach leaving detailed geometry behind, while preserving macroscopic morphological properties. To this end, the spatiotemporal evolution of foliage is considered to be subject to certain partial differential equations, which stand out due to their inherent dynamic properties of self-organisation and spontaneous adaptation. First, this is done by considering the local leaf area index, LLAI, as the key variable. By contrast to the common LAI, it maps the non-constant course of the function that assigns to each position on the ground below a plant's foliage the number of layers of one-sided green leaf above this particular position. The thus derived model is afterwards tested on an experimental data set of sugar beet. The results motivate to consider in a similar way the LLAI's three-dimensional analogue, the local leaf area density, LLAD, which is embedded in a dynamical system modelling specifically tree growth.

MODEL FRAMEWORK

Let $L=L(x,y;t)$ denote a particular plant's LLAI at a ground position $(x,y)\in\square^2$ and time t. Following Beer-Lambert's law (Nilson 1971), its total biomass production at t reads

$$B(t)\propto PAR(t)\cdot\iint_{\square^2}1-e^{-\lambda\cdot L(x,y;t)}dxdy$$

with an extinction coefficient λ, and *PAR* denoting photosynthetically active radiation. This quantity is distributed among the plant organs. For the particular case of sugar beet, those are solely its root and its foliage. The respective time-dependent distribution ratios are readily determined empirically. The amount of produced biomass which is assigned to foliage, $B_{foliage}(t)$, is then spatially distributed: Here, this is done in the simple way that newly allocated leaf mass, $all=all(x,y;t)$, is proportional to the already existing amount of L in (x,y). Hence

$$all(t)\propto B_{foliage}(t)\cdot\frac{L(x,y;t)}{\iint_{\square^2}L(x,y;t)\,dxdy}$$

Leaf senescence, $sen=sen(x,y;t)$, is essentially chosen in a similar manner, deducting aged leaves from the set of photosynthetically active green leaves comprised in L.

Lastly and centrally, the spatial propagation of foliage, described by a dynamic flux term $\vec{\phi}$, is chosen according to a classical diffusion approach: It is said to follow foliage's negative gradient while being proportional to allocation. Hence

$$\vec{\phi}(x,y;t) \propto -\nabla L(x,y.t)\cdot all(t)$$

This reflects the morphogenetic idea that a plant tends to form new leaves in brighter rather than darker spots, i.e. those exhibiting lower rather than higher leaf-area surfacic density.

Combining allocation, senescence and this last spatial propagation term results in a two-dimensional partial differential equation, more precisely classifiable as reaction-diffusion equation. Minor adjustments suffice to take inter-individual competition for light, induced by overlapping foliage, into account. The generalisation for a population of plants can thus be derived, resulting in a coupled system of dynamic equations.

SIMULATION AND DATA COMPARISON

The complete model has been confronted to experimental data of three different spatial configurations of sugar beet populations, hence three distinct competition scenarios. Model parameters were partly chosen in accordance with Lemaire et al. (2009), additional ones were computationally estimated. The results are illustrated in Fig 1. The considerably different magnitudes of the production quantities, depending on field density are visibly well accounted for.

We emphasise that the set of model parameters is a single, global one – irrespective of field density. This is a desirable and not last a realistic feature, seeing that the simulated plant's response to a competitive situation is spontaneous, entirely handled by the adaptiveness of the dynamic model equations.

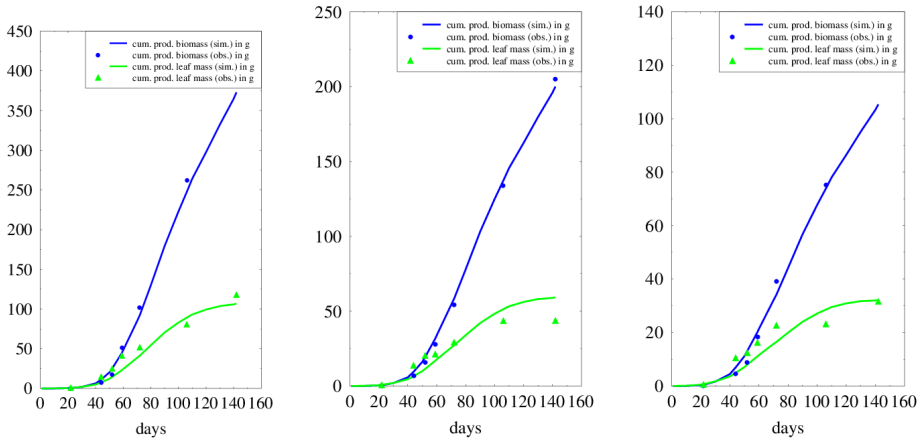

Fig. 1. Model simulation results for densities of arrangements of (from left to right) 5.4, 10.9, 16.4 plants per m^2 field. Shown quantities are per plant.

OUTLOOK: THREE-DIMENSIONAL EXTENSION

The purpose of tackling three-dimensional structure initiates the subsequent exploration of a model extension, developed specifically with a view to trees. The LLAI's three-dimensional counterpart is the local leaf area density LLAD, $L^*=L^*(x,y,z;t)$, defined as the total one-sided surface of green leaves in a ball centred in (x,y,z), at time t, divided by the ball's volume. (Formally, the ball's radius is infinitesimal; while in the context of numerical implementation as well as real data acquisition, cubes are used to prevent overlapping.) Hence $\int_0^\infty L^*(x,y,z;t)dz$ is nothing else but the LLAI in (x,y). Now, L^* can be assumed to be virtually continuous in x,y,z, making it possible to approach it with a similar reaction-diffusion technique as before.

The computation of biomass production is again carried out using Beer-Lambert's law. Yet, while the simplification of vertical light incidence was acceptable for sugar beet, it is not so for trees. Instead, for any given point $(x,y,0)$ on the ground and any time t we can now integrate L^* along the line connecting $(x,y,0)$ to

the sun's position, and thus compute the intercepted radiation. In this context, the effects of both self shading and of shading by a competitor, placed between the sun and the tree in question, come dynamically into play.

As for the spatial propagation, merely a straightforward transfer of the above diffusion flux is not productive. Instead, an additional element of structural heterogeneity is included to contribute to morphological realism: the tree's branch system. The basic principle, reflected in the respective differential equations, is to retain foliage's tendency to move from darker towards brighter regions – likewise in situations of inter-individual competition –, yet to impose a drift in order for it to remain close to the branch it corresponds to.

Having ticked off foliage dynamics, the dynamics of the branch system are addressed, namely in terms of the questions of the branches' own spatiotemporal propagation and growth, as well as ramification processes.

The former can be approached in terms of a mathematical optimisation problem: We assume that, at any point in time, the (infinitesimal) forward elongation of a branch is chosen to quantitatively optimise the tree's biomass production in the subsequent time step: Since LLAD dynamics are closely coupled to the growth of the branches, any change in the branch structure immediately affects foliage configuration, and thus biomass production. More specifically, the optimisation problem is formulated in the way that the *gain* of a potential elongation, in terms of an increment in future productivity, is weighted against its *cost.* This latter is chosen to be a function of the (infinitesimal) length and of the curvature of the elongation in question, notably taking into account hydraulic constraints.

As for the ramification processes we resort to a concept originally developed in botanical phyllotaxis, which is readily adapted in the present context and conceptually consistent with the further model framework. Brought forward by Snow & Snow (1952), it provides a principle to determine time and location of the formation of a bud at the apex, following the hypothesis that a new bud will only appear along the apical ring when and where there is enough space for it – the notion of 'enough' being related to a dynamic parameter. The principle is readily adapted to the ramification processes of a tree, for which the species-specific parameter evolution in the course of tree growth can be reconstructed by statistical means.

Once produced biomass is determined, as before, it needs to be distributed among foliage and wood. As for local foliage allocation, we assume that the increase of L^* in a position (x,y,z) is proportional to how much foliage at this position contributes to the overall biomass production. Meanwhile, biomass allocation to wood is provided by applying the (simplified) pipe model theory formulated by Shinozaki et al. (1964): For each additional unit of L allocated in (x,y,z), a "wooden" pipe is thought of to be installed, leading from (x,y,z) to the trunk base and below ground. Satisfying this principle determines the ratio of biomass partitioning among foliage and wood uniquely.

CONCLUSION

The two-dimensional LLAI model proved to be suitable for modelling production rates, handling arbitrary competition scenarios self-adaptively – a trait provided by the reaction-diffusion equations approach. The morphogenetic concept of spatial foliage formation, underlying the original model dynamics, has subsequently been utilized in a more complex model framework. This extension, tackling functional and structural properties at equal value for the case of a tree, was sketched and is subject to further exploration.

LITERATURE CITED

Cournède PH, Mathieu A, Houllier F, Barthelemy D, de Reffye P. 2008. Computing competition for light in the GreenLab model of plant growth: a contribution to the study of the effects of density on resource acquisition and architectural development. *Annals of Botany* **101(8)**:1207–1219.

Nilson, T. 1971. A theoretical analysis of the frequency of gaps in plant stands. *Agricultural and Forest Meteorology* **8**:25-38.

Chelle, M., & Andrieu, B. 2007. Modelling the light environment of virtual crop canopies. *Functional-Structural Plant Modelling in Crop Production* 22 :75–89.

Lemaire S, Maupas F, Cournède PH, de Reffye P. 2009. A Morphogenetic Crop Model for Sugar-Beet (Beta vulgaris L.). In: *Crop Modeling and Decision Support* (Cao W, White J, Wang E, eds.), Springer, 116–129.

Pretzsch H. 2002. The single tree-based stand simulator silva: construction, application and validation. *Forest Ecology and Management* **162**:3-21.

Shinozaki K, Yoda K, Hozumi K, Kira T. 1964. A quantitative analysis of plant form-the pipe model theory. I. Basic analyses. Jap. J. Ecol. **14**:97-105.

Snow M, Snow R. 1952. Minimum areas and leaf determination. *Proc. Roy. Soc.* **B139**: 545-566.

Proceedings of the 7th International Conference on Functional-Structural Plant Models, Saariselkä, Finland, 9 - 14 June 2013. Eds. Risto Sievänen, Eero Nikinmaa, Christophe Godin, Anna Lintunen & Pekka Nygren.
http://www.metla.fi/fspm2013/proceedings. ISBN 978-951-651-408-9.

Improving finite element models of roots-soil mechanical interactions

Ming Yang[1], **Pauline Défossez**[1] and **Thierry Fourcaud**[2]
[1]*INRA – UR1263 EPHYSE, 33883, Villenave d'Ornon, France,* [2]*CIRAD – UMR AMAP, Montpellier, France*
**correspondence:* thierry.fourcaud@cirad.fr

Highlights: Two finite element modelling approaches have been applied and compared to simulate direct shear tests of soils reinforced by roots. The "frictional behaviour" method used with solid elements predicted shear strength of the root-soil system 4.6-6.9% higher than that predicted with "embedded beam elements". This difference can be considered as negligible. Embedded beam elements were thus chosen to discretize digitized Maritime pine root systems in a tree anchorage model. Results exhibited contrasted mechanical responses when considering different root material properties.

Keywords: Tree anchorage, root architecture, simulation, biomechanics, overturning, failure, Abaqus

INTRODUCTION

The periodic wind storms recorded during the last decades in Europe have damaged several trees, sometimes killing people in urban areas. Moreover they were responsible of significant economic loss in the forest industry, also impacting the functioning of forest ecosystems. Tree overturning has been reported as a major mode of tree damage. Minimizing the risk of tree uprooting necessitates better understanding the mechanical interactions between roots and soil. Many studies were thus carried out on tree anchorage in the past, most of them using experimental approaches consisting in pulling trees to obtain force-displacement response curves (Cucchi et al. 2004; Abd Ghani et al. 2009; Mickovski and Ennos 2003). In addition, theoretical approaches based on numerical simulations were proposed in order to investigate in more detail the effect of root architecture on tree anchorage (Dupuy et al. 2005; Dupuy et al. 2007; Fourcaud et al. 2008), as well as the effect of individual roots on soil shear strength (Mickovski et al. 2011). However, the numerical models developed still need to be improved and validated with experimental data. In particular more attention must be paid to: 1- the modelling of root-soil interface; 2- the effect of successive root failures; 3- the realism of soil properties, e.g. considering soil heterogeneities and the effect of pore water pressure.

When complex root systems with several ramifications are considered, the first point above can result in extensive computation costs and give rise to convergence problems that constitute a severe limitation for the simulations. As an alternative to the use of solid elements to model the root phase, earlier simulations were performed with structural beam elements embedded in the soil matrix (Dupuy et al. 2005). The main weakness of such a simplification is that roots and soil are connected with rigid conditions, i.e. roots cannot slip within the soil. Another limitation of these previous models comes from the fact that successive root failures were not taken into consideration (as mentioned in point 2 above), thus neglecting an important component of root anchorage. The aim of this paper is: 1- to get an estimate of the discrepancy in the simulated mechanical response between models using embedded beams and solid elements with explicit surface-to-surface interaction respectively; 2- to incorporate a model of root failure in the simulations. The initial step 1 was carried out on a typical direct shear test of a soil reinforced with individual root elements, as experimental data were available. The second step was performed on a tree overturning model considering real digitized root systems of adult Maritime pine trees (*Pinus pinaster* Ait.) and varying root mechanical properties.

MODEL DESCRIPTION

First of all, a finite element model was constructed to simulate direct shear tests of reinforced soils previously carried out by Vanel (2011). The experimental system was composed of a block of soil of dimensions 50cmx50cmx32cm (Length x Width x Depth) containing 12 identical electric wires (mimicking roots) of length 24cm standing vertically in a plane perpendicular to the horizontal shear direction. The distance between two neighbouring wires was 4cm. A given pressure was applied at the top surface of the system prior to the shear test, putting bricks at the top surface of the soil. The soil was then sheared displacing the top half of the soil block with a constant (low) velocity. Resultant forces were measured during the displacement and the resulting force-displacement curves were analysed (Figure 1).

The above system was designed using the Abaqus Finite-Element package (http://www.3ds.com/products/simulia/portfolio/abaqus/overview/). The soil was modelled as an elasto-plastic material with the isotropic linear elastic part and the plastic part satisfying the Mohr-Coulomb criteria. Roots were considered to be isotropic linear elastic. The bottom part of the soil block was encastred, i.e. no displacement was allowed during the test. The top steel frame that constituted the shear box was modelled by a rigid plate. A reference point was associated to this frame, located at its centre, where the boundary conditions were imposed during the shear process. Two options were used to model the wires (roots). In the first option, roots were meshed with solid elements that were allowed slipping within the soil matrix. In the second option, structural beam elements embedded in the soil, i.e. with no possibility of slippage of roots within the soil matrix, were used.

Simulations were composed of two static calculation steps corresponding to the two stages mentioned above. In the first step, a given pressure force was applied at the top surface of the system, in addition to gravity, and the resulting soil pre-stress field was calculated. The second step corresponded to the shear test itself and was carried out displacing the reference point of the top frame up to 0.8-1.0cm. Corresponding resultant forces were computed during this last step. The resulting force-displacement curves were used to compare the two modelling options mentioned above.

In the first modelling option, root slippage was taken into consideration through a frictional law that consists in linking the transmitted shear force to the normal force across the surfaces in contact by using the Coulomb friction model. There was only one material (of soil or root) defined at each material point. Root parts were discretized with 8-node linear reduced-integration elements (C3D8R) and the soil part was discretized with 4-node linear tetrahedron elements (C3D4). The element names a referred from the Abaqus elements library. While in the second modelling option, the root parts (wires) were discretized with 2-node linear Timoshenko beam elements (B31) embedded in the soil.

For both methods, the plate was discretized with 4-node bilinear rigid quadrilateral elements.

The model of tree anchorage was composed of a digitized root system of a Maritime pine coming from measurements conducted by Danjon et al. (unpublished data) in the Nézer Forest, a soil block and a rigid stem where a horizontal displacement of 1.34 m is applied at the top. The discretization of roots and soil was the same as in the option “embedded element” mentioned above. The elastic-failure behaviour of roots was derived from the damage model of Fibre Metal Laminates developed by Linde et al. (2004). Two different datasets of root mechanical properties were considered for the simulations presented in this paper, one in the range of values found in the literature (Dupouy, 1992), and one corresponding to softer roots.

RESULTS AND DISCUSSION

Plastic strains at the end of shear test simulations are shown in Fig. 1 in the case of “embedded elements” and “frictional behaviour” respectively. In both cases, plastic strains began to accumulate in a narrow horizontal zone which appeared in the middle plane of the soil block, which is in accordance to the observation of real shear tests. However, the first case demonstrates an oblique shear region in the back of the displaced soil block.

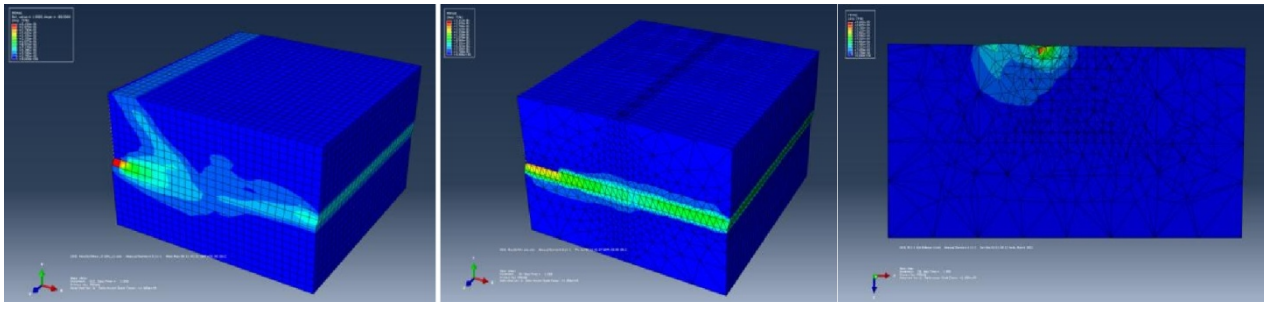

Fig 1. Distribution of equivalent plastic strain during a simulation of reinforced soil shear test using embedded beam elements (a), solid elements with frictional behaviour (b). Plastic strains during a tree overturning (c).

Results showed that both methods gave similar mechanical responses, with an increase in the reaction force in the elastic region, followed with a quick flattening of the curves that reach a maximum value which corresponded to the shear strength of the root-soil system. The recovery of the residual part after the decrease in shear stress can be explained by the reinforcing effect provided by roots. Shear strength increased with an increase in root-soil friction coefficient. Physically, this accounted for the fact that the rougher root-soil interface is, the more difficult it becomes to push the upper soil layer to move.

The model with embedded beam elements always underestimated shear strength compared with roots meshed with solid elements with frictional behaviour, but the difference does not exceed 4.6-6.9%. This result justifies using embedded beam elements in further studies of tree anchorage, as this method is much simpler to implement and the corresponding simulations are less time consuming. Simulations of tree overturning were thus performed using embedded beam elements.

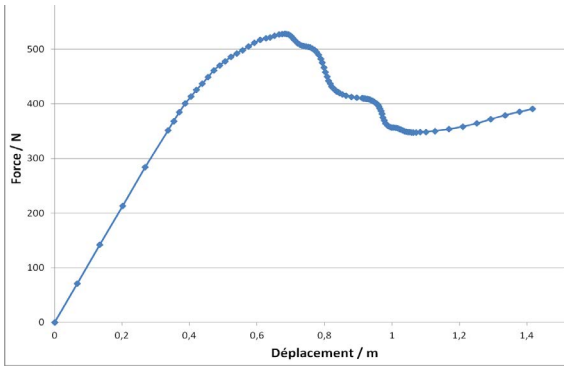

Fig. 2. Root anchorage response curve with the following root properties: Young's modulus: 20-40MPa; tensile strength: 1.35MPa; compressive strength: 0.9MPa

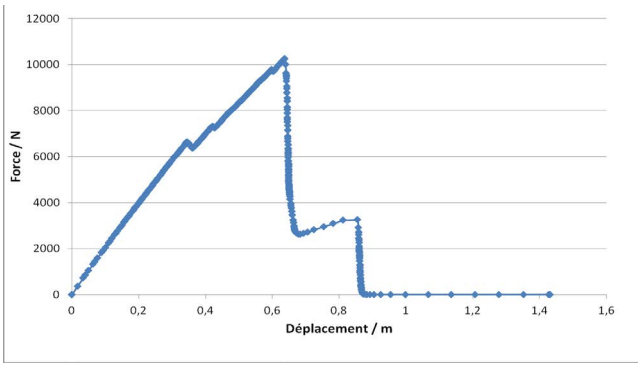

Fig. 3. Root anchorage response curve with *Pinus pinaster* root properties taken from Dupouy (1992): Young's modulus: 1-1.2GPa; tensile strength: 40MPa; compressive strength: 35MPa

The effect of successive root breakage can be observed on the response curves (Fig. 2&3). In Fig.2 the curve exhibit a peak value followed by a smooth decrease up to third of the critical force, followed by a new increase of the curve (hardening). In contrast, *Pinus pinaster* root properties (Fig. 3) induced an abrupt change of the reaction force that falls to zero at the end, which suggested a complete breakage of the system.

The present model based on previous studies (Dupuy et al., 2007) has incorporated the modelling of successive root breakage to give a more realistic modelling of tree anchorage. It could be applied to different tree species with different environmental conditions (soil conditions; roots damaged by parasites) by introducing appropriate values of the corresponding mechanical parameters. In our study this model aims to better understand the anchorage of *Pinus pinaster* and to extract key influential factors. Validation of the model will be carried out in a subsequent study, using experimental data.

LITERATURE CITED

Abd. Ghani M, Stokes A, Fourcaud T. 2009. The effect of root architecture and root loss through trenching on the anchorage of tropical urban trees (*Eugenia grandis* Wight). *Trees-Structure and Function* **23**:197-209.

Cucchi V, Meredieu, C, Stokes A, Berthier S, Bert D, Najar M, Denis A, Lastennet R. 2004. Root anchorage of inner and edge trees in stands of maritime pine (PinuspinasterAit.) growing in different podzolic soil conditions. *Trees: Structure and Function* **18**, 460-466.

Danjon F, Fourcaud T, Bert D. 2005. Root architecture and wind-firmness of mature Pinus pinaster. *New Phytologist* **168**: 387-400

Dupouy P. 1992. Condition d'encastrement d'un arbre dans le sol. Mémoire de DEA, Université de Bordeaux 1. 34p.

Dupuy L, Fourcaud T, Stokes A. 2005. A numerical investigation into the influence of soil type and root architecture on tree anchorage. *Plant and Soil* **278**: 119-134

Dupuy L, Fourcaud T, Lac P, Stokes A. 2007. A generic 3D finite element model of tree anchorage integrating soil mechanics and real root system architecture. *American Journal of Botany* **94**: 1506–1514.

Fourcaud T, Ji J-N, Zhang Z-Q, Stokes A. 2008. Understanding the impact of root morphology on overturning mechanisms: a modeling approach. *Annals of Botany* **101**: 1267-1280

Linde P, Pleitner J, de Boer H, Carmone C. 2004. Modelling and simulation of fibre metal laminates. 2004 Abaqu User's Conference

Mickovski SB, Ennos AR. 2003. Anchorage and asymmetry in the root system of Pinus peuce. *Silva Fennica* **37**: 161-173

Mickovski SB, Stokes A, van Beek R, Ghestem M, and Fourcaud T. 2011. Simulation of direct shear tests on rooted and non-rooted soil using finite element analysis. *Ecological Engineering* **37**:1523-1532.

Vanel Q. 2011. Étude de l'impact des différents traits architecturaux de systèmes racinaires sur la résistance au cisaillement du sol lors de glissements de terrain. Mémoire de Master, Ecole Pratique des Hautes Etudes. 28p.

Proceedings of the 7th International Conference on Functional-Structural Plant Models, Saariselkä, Finland, 9 - 14 June 2013. Eds. Risto Sievänen, Eero Nikinmaa, Christophe Godin, Anna Lintunen & Pekka Nygren. http://www.metla.fi/fspm2013/proceedings. ISBN 978-951-651-408-9.

Integrative models for analyzing jointly shoot growth and branching patterns

Jean Peyhardi[1,2], **Evelyne Costes**[3], **Yves Caraglio**[4], **Pierre-Éric Lauri**[3], **Catherine Trottier**[2] and **Yann Guédon**[1]

[1]*CIRAD, UMR AGAP and Inria, Virtual Plants, F-34095 Montpellier, France,* [2]*Université Montpellier 2, Institut de Mathématiques et de Modélisation de Montpellier, F-34095 Montpellier, France,* [3]*INRA, UMR AGAP, F-34398 Montpellier, France,* [4]*CIRAD, UMR AMAP, F-34398 Montpellier, France*

**correspondence:* guedon@cirad.fr

Highlights: The branching pattern of a shoot may be influenced by numerous factors varying along the shoot such as the internode length, the leaf surface or the local curvature. We introduce a generalization of hidden semi-Markov chains for categorical response variables that incorporates explanatory variables varying with the index parameter. Using this model, we demonstrate the influence of the growth pattern of a shoot on its immediate branching.

Keywords: branching pattern; generalized linear model; growth pattern; semi-Markov switching regression model.

INTRODUCTION

Branching patterns of a shoot often take the form of a succession of well-differentiated homogeneous branching zones where the composition properties, in terms of axillary productions, do not change substantially within each zone, but change markedly between zones. These branching patterns have been analysed using segmentation models and in particular hidden semi-Markov chains (Guédon et al. 2001). Branching patterns are modulated by both factors that have a global effect on the pattern and factors varying along the shoot that have differentiated effects on the successive axillary productions. We previously investigated the influence of the architectural position of a shoot, which can be viewed as a factor having a global effect, on apple tree branching patterns (Renton et al. 2006).

Here, we focus on factors varying along the shoot that modulate its branching pattern. For example, it has been shown that shoot growth modulates the branching pattern, in particular the immediate (or sylleptic) branching; see Lauri and Térouanne (1998) for an illustration in the apple tree case. Other potential factors include the local curvature of the shoot (Han et al. 2007). To this end, we introduce a new family of integrative models for analysing jointly the succession and length of branching zones and the modulation of the axillary productions within each zone by factors varying along the shoot. These models generalize hidden semi-Markov chains for categorical variables (Guédon et al. 2001) by incorporating explanatory variables and are called semi-Markov switching generalized linear models (SMS-GLMs). It should be noted that another family of semi-Markov switching regression models has been previously introduced for analysing forest tree growth components. More precisely, semi-Markov switching linear mixed models were used to identify and characterize the ontogenetic, environmental and individual growth components on the basis of tree main stems described by annual shoot and climatic data (Chaubert-Pereira et al. 2009).

RESULTS

The proposed approach is illustrated by the analysis of the immediate branching pattern of apple tree, cv. Fuji. The data set comprised 22 shoots of cumulative length 1494 (length between 63 and 73 nodes). For each tree, the first annual shoot of the trunk was described by node from the base to the top where, for each node, the type of axillary production chosen among latent bud, immediate short shoot and immediate long shoot, and the internode length (in cm) was recorded.

A semi-Markov switching generalized linear model, which is a two-scale segmentation model, was built on the basis of this data set. In this framework, the succession and length of branching zones (coarse scale) are represented by a non-observable semi-Markov chain while the axillary productions within a branching zone modulated by factors varying along the shoot (fine scale) are represented by generalized linear models attached to each state of the semi-Markov chain. A SMS-GLM combines three categories of variables: (i) “state” variable representing the non-directly observable branching zones, (ii) plant response categorical variable (types of axillary production), (iii) explanatory variables varying with the node rank (e.g., the internode length).

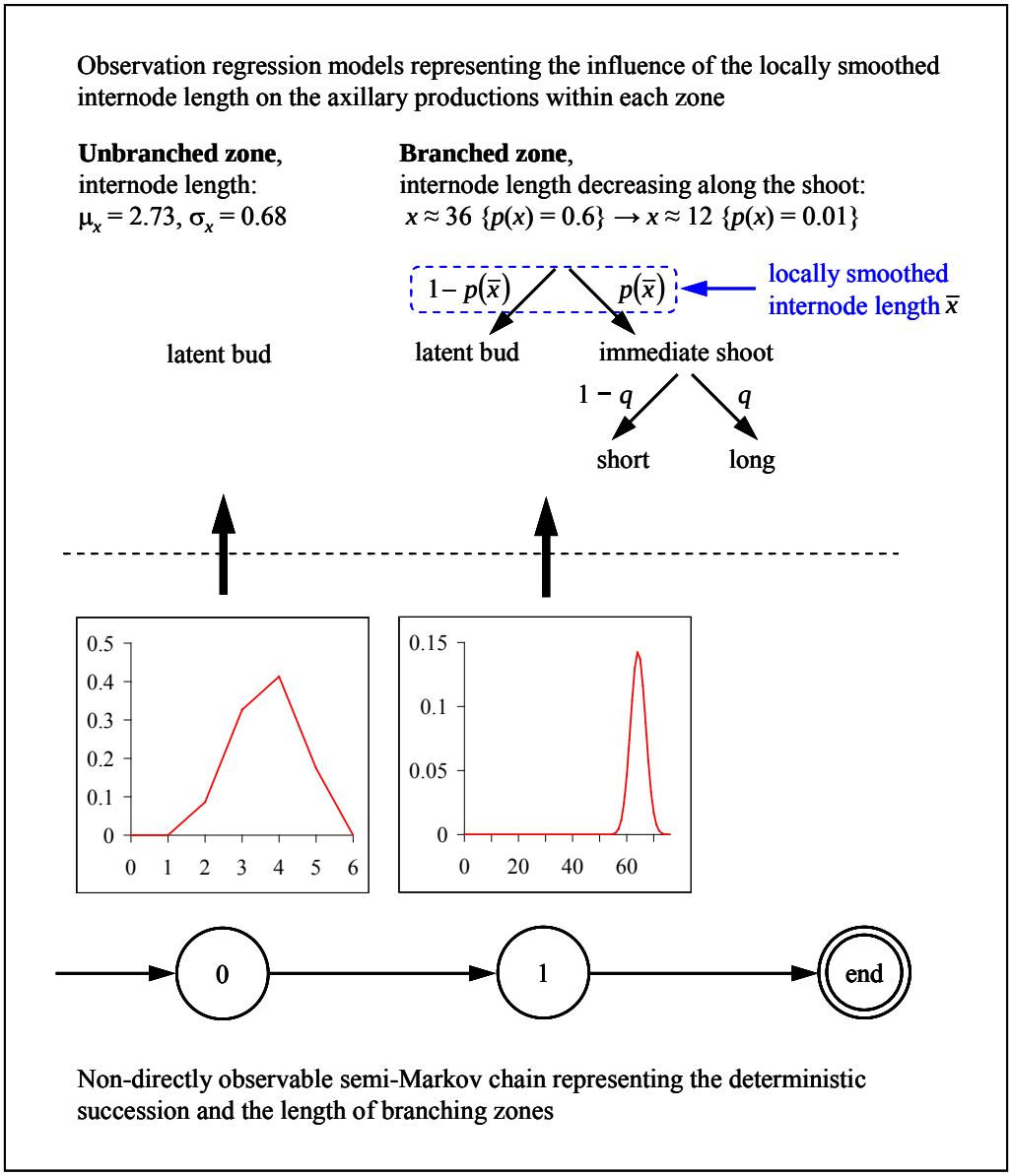

Figure 1. Semi-Markov switching generalized linear models. *Semi-Markov chain*: each state is represented by a vertex which is numbered. Vertices representing transient states are edged by a single line while the vertex representing the absorbing end state is edged by a double line. The possible transitions between states are represented by arcs (the attached probabilities are always 1). The arc entering in state 0 indicates that it is the only possible initial state. The occupancy distributions of the transient states are figured above the corresponding vertices. *Observation regression models*: for state 0 (unbranched zone), the observation model is degenerate since the only possible observation is latent bud. For state 1 (branched zone), the estimated branching probability p decreases with the internode length along the parent shoot. The locally smoothed internode length influences markedly the immediate shoot initiation but only slightly the subsequent growth of these immediate shoots (and the influence of the explanatory variable is only figured for the partition latent bud/immediate shoot).

The estimated SMS-GLM was composed of two transient states followed by a final absorbing end state modelling growth cessation (Renton et al. 2006); see Figure 1. The deterministic succession of states resulted from the iterative estimation procedure. We tested two types of transform of the measured internode length variable to build potential explanatory variables:

- shift of the variable, in particular backward shifts, since the internode elongation lasts about 12 days in apple tree and temporally overlaps the initiation of immediate shoots a few nodes below the apex.
- smoothing of the variable in order to remove the fluctuations and to extract the local internode length trend. This smoothing can be interpreted as an averaging over the internodes that elongate at a given time t.

The best model according to model selection criteria (Bayesian information criterion in this case) was obtained with no shift and a smoothing of the internode length obtained using a symmetric smoothing filter corresponding to the probability mass function of the binomial distribution of parameters 32 and 0.5 (95% of the mass concentrated on the 11 central values). This smoothing width appears to be consistent with the order of magnitude of the number of internodes that elongate at a given time *t*.

The unbranched zone of short internodes at the base of the shoot (state 0) corresponds to the preformed part of the shoot. The fact that the highest probability of branching and the longest internodes were found near the shoot base (around rank 10) likely resulted from the propagation mode of the observed young plants which issued from bud grafting on a one-year-old rootstock.

DISCUSSION

The example illustrates the fact that the definition of appropriate explanatory variables is a crucial step in the context of retrospective measurements. We are now investigating the extraction of explanatory variables on the basis of growth data follow up (e.g. leaf expansion). In this context, the extraction of explanatory variables requires two steps, (i) extraction of growth parameters using for instance nonlinear regression models (e.g. the maximum absolute growth rate deduced from the fit of a sigmoidal function), (ii) shifting and smoothing of growth parameters deduced from nonlinear regression models.

Concerning the observation regression models, a standard solution would have consisted of assuming that the categorical response variable was ordinal (with the following category order: latent bud, immediate short shoot and immediate long shoot) and to estimate an ordinal generalized linear model for the branched state. We chose to develop the more general framework of hierarchical models that enables to tackle not only the classical cases of nominal and ordinal categorical response variables but also the case of partially ordered categorical response variables. This framework relies on a recursive partitioning of categories into subsets. This hierarchical modelling is illustrated in the example where the categories are first partitioned into latent buds and immediate shoots, the immediate shoots being then partitioned into short and long shoots. Using this hierarchical modelling, it was possible to show applying model selection criteria that the locally smoothed internode length influences markedly the immediate shoot initiation but far less the subsequent growth of these immediate shoots which likely depended on environmental factors at this time.

Combining transform of explanatory variables and recursive partitioning of the axillary productions using hierarchical modelling, it was possible to test many assumptions concerning the influence of the growth pattern on the immediate branching pattern in our example.

This study together with the study of Chaubert-Pereira et al. (2009) illustrate the versatility of semi-Markov switching regression models where a semi-Markov chain can represent homogeneous branching zones at the node scale as well as growth phases at the annual shoot scale and where all the panoply of regression models can be incorporated depending on the type of the plant response variable (categorical variable for the type of axillary production and interval-scaled variable for the annual shoot length).

ACKNOWLEDGEMENTS

The authors thank Michael Renton for its participation to data collection.

LITERATURE CITED

Chaubert-Pereira F, Caraglio Y, Lavergne C, Guédon Y. 2009. Identifying ontogenetic, environmental and individual components of forest tree growth. *Annals of Botany* **104**(5): 883-896.

Guédon Y, Barthélémy D, Caraglio Y, Costes E. 2001. Pattern analysis in branching and axillary flowering sequences. *Journal of Theoretical Biology* **212**(4): 481-520.

Han HH, Coutand C, Cochard H, Trottier C, Lauri PÉ. 2007. Effects of shoot bending on lateral fate and hydraulics: invariant and changing traits across five apple genotypes. *Journal of Experimental Botany* **58**(13): 3537-3547.

Lauri PÉ, Térouanne É. 1998. The influence of shoot growth on the pattern of axillary development on the long shoots of young apple trees (*Malus domestica* Borkh). *International Journal of Plant Sciences* **159**: 283-296.

Renton M, Guédon Y, Godin, C, Costes E. 2006. Similarities and gradients in growth-unit branching patterns during ontogeny in 'Fuji' apple trees: A stochastic approach. *Journal of Experimental Botany* **57**(12): 3131-3143.

Proceedings of the 7th International Conference on Functional-Structural Plant Models, Saariselkä, Finland, 9 - 14 June 2013. Eds. Risto Sievänen, Eero Nikinmaa, Christophe Godin, Anna Lintunen & Pekka Nygren.
http://www.metla.fi/fspm2013/proceedings. ISBN 978-951-651-408-9.

Deciphering mango tree asynchronisms using Markov tree and probabilistic graphical models

Anaëlle Dambreville[1,3], Pierre Fernique[2], Christophe Pradal[2], Pierre-Eric Lauri[3], Frédéric Normand[1], Yann Guédon[2] and Jean-Baptiste Durand[4,2]*

[1]CIRAD, UPR HortSys, 97455 Saint-Pierre Cedex, Réunion Island, France, [2]CIRAD, UMR AGAP and INRIA, Virtual Plants, 34095 Montpellier, France, [3]INRA, UMR AGAP, 34098 Montpellier, France, [4]Grenoble University, Laboratoire Jean Kuntzmann, BP53, F-38041 Grenoble Cedex 9, France,
**correspondence:* jean-baptiste.durand@imag.fr

Highlights: Tree development is often characterised by complex dependencies between daughter growth units (GUs) deriving from a given mother GU, the so-called sister GUs. These dependencies directly affect the reproductive and vegetative phenological patterns that are at the origin of asynchronisms between adjacent GUs, eventually leading to within-canopy patchiness. These phenomena are rather common on tropical fruit-trees. We introduce new parsimonious statistical models to identify such dependencies. The proposed approach is illustrated on mango tree, a tropical species with a particularly complex timing of development. We focus especially on differences on fates and dates of burst between the daughter GUs issued from a same mother GU.

Keywords: growth asynchronism; growth unit; *Mangifera indica*; patchiness; spatio-temporal data analysis.

INTRODUCTION

As other tropical trees, mango tree is characterised by strong phenological asynchronisms between and within trees entailing patchiness (Chacko, 1986). Patchiness is characterized by clumps of either vegetative or reproductive development within the canopy: while some portions of the tree canopy develop vegetative GUs (i.e. portions of leafy axes developed during an uninterrupted period of growth), other portions may remain in rest or produce inflorescences at the same time. These asynchronisms often correspond to more or less large branching systems, e.g. scaffolds (Ramírez and Davenport, 2010). They entail various agronomical problems, such as the repeated use of pesticides to protect recurrent susceptible phenological stages from pests or a too extended period of fruit maturity, which may lead to difficulties to organize fruit harvesting.

If all terminal GUs produced both vegetative and reproductive daughter GUs in the same proportions and synchronously, i.e. at the same burst dates, all branching systems would grow synchronously and would have the same distribution of fates. Patchiness results from mutual exclusions, at the local scale of daughter GUs of a given mother GU, between some of their burst flushes (early, intermediate, or late) and / or some of their fates (vegetative or reproductive if it produces terminal or lateral inflorescences). These exclusions are observed, for example, when two kinds of daughter GUs cannot be produced by the same mother GU. Our final objective was to identify and characterise such exclusions and to open new perspectives to eventually connect them to patchiness at the canopy scale. Previous studies showed that the fate and burst date of a daughter GU are strongly affected by those of some ancestor GU (Dambreville *et al*., 2013). This approach, based on regression models, only made it possible to identify the effects of several factors (e.g. timing of development or fate of the mother GU, fruit load) on a single response variable, called GU feature (e.g. either the timing of development or the fate of a single daughter GU). This approach suffered from two main limitations: (i) multiple features of a GU cannot be predicted together in an obvious manner; (ii) a feature cannot be globally predicted for all daughter GUs if interactions exist between sister GUs, additionally to those with the mother GU.

The analysis of such interactions appears nevertheless essential to identify in which architectural and phenological contexts vegetative growth or flowering patches can occur. We present a new statistical methodology to reveal and describe these interactions using Markov tree and probabilistic graphical models (PGMs). Markov tree models allow the analysis of dependencies between a mother GU and its daughter GUs. They were introduced by Durand et al. (2005) to model plant architecture, assuming that sister GUs were independent given the mother GU. Here, the Markov tree model is generalised by introducing dependencies between sister GUs, in addition to their dependencies with their mother GU. The PMGs are used to unravel the dependencies between sister GUs, which express for example competition between these.

MATERIALS AND METHODS

The experimental orchard was located at the CIRAD (French Agricultural Research Centre for International Development) research station in Saint-Pierre, Réunion Island. Five trees of the Cogshall mango cultivar growing in the same plot were described at the GU scale (Dambreville *et al*., 2013). We defined the growing cycle as the period composed of the succession of a vegetative development period (appearance of new GUs) and a reproductive development period (flowering and possibly fruiting). Starting from the growing cycle of 2003, our experiment was carried out during the two following growing cycles in 2004 and 2005. We exhaustively described the development (fate, and in case of reproductive fate, number of terminal and lateral inflorescences, and burst date at the month scale) of all GUs appeared from sequential growth, i.e. located at the periphery of the canopy. Information on GUs burst in 2003 was limited to the fate, without distinction between terminal and lateral inflorescences for GUs that flowered. The 0.7% of GUs that burst after a two-year delay or more with respect to their mother GU were not considered in the study, and neither were their descendants.

The Markov tree models rely on three main assumptions: (i) the states of sister GUs (e.g. their fates) are independent from the states of their non-descendant GUs given the mother GU state (Markovian assumption); (ii) the joint distributions of the states of sister GUs are invariant under any permutation of the sisters (non-ordered sisters); (iii) these distributions do not depend on the position of the mother GU within the tree (homogeneity assumption). Let K denote the number of states and $\{0,\ldots,K-1\}$ the state space, let u be some non-terminal vertex and S_u its state variable. As a consequence of the three assumptions, the Markov tree model is entirely specified by the joint distributions of the numbers $(N_0,...,N_{K-1})$ of daughters with state 0,...,K-1 respectively, given the parent state $S_u=k$ (referred to as generation distributions).

Since the combinatorics induced by the variable number of sisters and the number of states is typically huge, the probability of occurrence cannot be reliably estimated by frequencies, and parsimonious parametric models must be used. In our approach, parsimony results from independence properties between the K count variables $N_0,...,N_{K-1}$, given $S_u=k$, summarised by a PGM; see Koller and Friedman (2009). The PGM vertices are the random variables $\{N_k\}$ and their connections correspond to conditional independence properties between the variables. Parametric models were obtained by combining discrete distributions and corresponding regression models (Fig. 1). Discrete distributions (chosen among Poisson, binomial, negative binomial and mixtures) were used to represent sources (vertices without parents) and the corresponding regression models were used to represent non-source vertices. To identify the PGM from data, an iterative algorithm was used to select edges, based on edit operations (deletion/insertion of edge, edge reversal). The PGM with maximum Bayesian information criterion (BIC) value was selected.

RESULTS AND DISCUSSION

To characterize dependencies (in particular, exclusions) between daughter GUs through their architectural and phenological context, it is necessary that the notion of GU state combines: (i) the period of growth of daughter GU, with respect to its mother GU burst date, i.e. immediate (I; i.e. during the same growing cycle) or one-year-delayed (D); (ii) the flush, i.e. early (E), Intermediate (I) or late (L); (iii) the fate, i.e. vegetative (V), reproductive with terminal flowering (T) or reproductive with lateral flowering (L). For GUs of 2003, the flush (U) and the position of flowering (F) were undefined. Thirteen states were defined for GUs as follows: U-V, IE-V, IL-V, DE-V, DI-V, DL-V, U-F, II-T, IL-T, DI-T, DL-T, II-L and DI-L.

Thus, 13 PGMs were identified, each one associated with one mother GU state. Since flushes were ordered (early, intermediate, late), and flowering mainly occurred for the last two flushes, states were partially ordered. As a consequence, the generation distributions simplified for states occurring late in the generation process, with respect to states occurring early.

We focus on the graph in Fig. 1 associated with the state II-L of the mother GU.

- No transition from the mother GU state II-L to the daughter GU states U-V, U-F, II-V, II-T, IL-V, IL-T, DE-V, nor II-L occurred. The states U-V and U-F (GUs produced in 2003) always preceded all the states. The other daughter GU states could theoretically follow II-L but this was not observed. This is translated in Fig.1 by isolated vertices with associated (quasi-) degenerate distributions for these eight states.
- The edges originating from source vertices DL-V and DL-T and pointing toward non-source vertex DI-V with associated negative regression parameters expressed mutual exclusion between DI-V on the one hand, and DL-V and DL-T on the other hand. The same mutual exclusion behaviour occurred between states DL-V and DI-L. This suggests that immediate intermediate GUs with lateral inflorescences (state II-L) could not have daughter GUs, the year after, successively at intermediate and then at late flushes.

Hence, mother GU in state II-L was a local context favourable to synchronism. This was consistent with the matrix of correlations between $\{N_k\}$ depicted in Fig. 2. However, despite a negative regression parameter associated with the edge pointing from vertex DI-T toward vertex DI-V, strict exclusion between both types of vertices did not strictly exist, since the correlation between the numbers of sister GUs in both states was non-negative (Fig. 2).

- The correlation matrix in Fig. 2 showed that the numbers of sister GUs in states DI-V and DI-L were quasi-uncorrelated, and that both are negatively correlated with the number of sister GUs in state DL-V. This was consistent with the selected PMG, which did not contain an edge between DI-V and DI-L.
- The numbers of sister GUs in states DL-T and DL-V were positively correlated, but it could be deduced from the PMG that this correlation was indirect, and was probably a consequence of their negative correlation with the number of sister GUs in state DI-V. This showed that daughter GUs with both vegetative (DL-V) and flowering (DL-T) fates may be produced synchronously, at flush L and with one-year delay, by mother GUs in the state II-L.

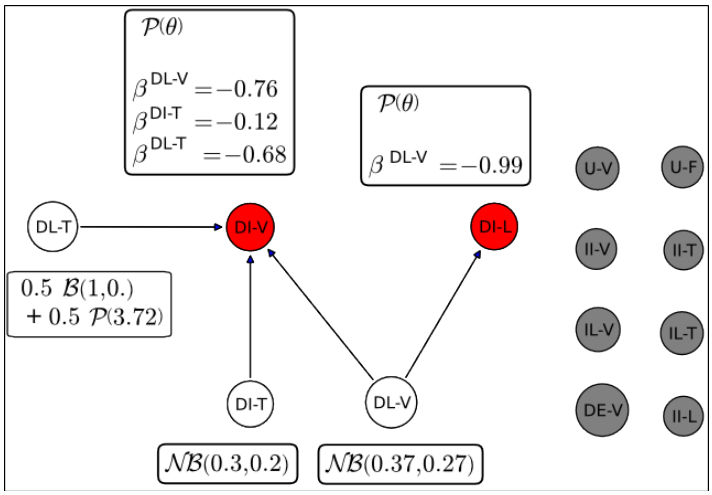

Fig. 1. PGM associated with the state II-L of the mother GU. Vertices of the PGM correspond to the random numbers of daughter GUs in each state. Grey vertices correspond to degenerate distributions. White vertices (source) and parameters correspond to univariate distributions ($\mathcal{P}$: Poisson, $\mathcal{B}$: binomial, $\mathcal{NB}$: negative binomial, and a mixture of $\mathcal{B}$ and $\mathcal{P}$ with weights 0.5 for vertex DL-T). Red vertices (non-source) correspond to univariate regressions. The parameter associated to the effect of variable i in the regression of the variable associated with a given vertex is denoted by β^i.

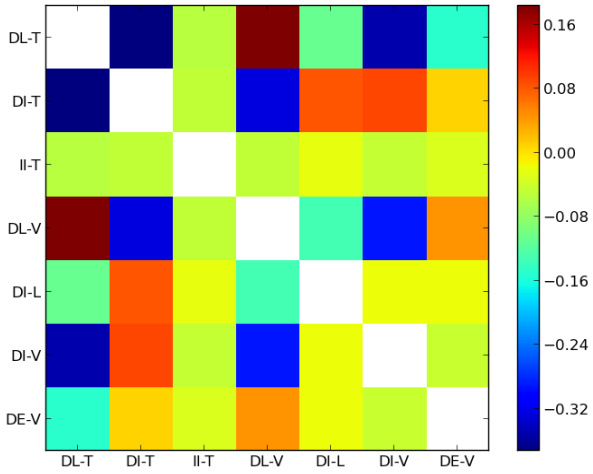

Fig. 2. Correlation matrix of the number N_k of daughter GUs in each state, given the mother GU state II-L (immediate intermediate flush with lateral flowering). Intensity of the correlation between N_j and N_k at location (j,k) is indicated using a colourmap. Blue tones correspond to negative correlations and red tones to positive ones. Some variables N_k with degenerate distributions are not represented.

These results show the ability of the Markov tree models to identify in which contexts a given mother GU can have or cannot have daughter GUs at different flushes or with different fates, which can be interpreted as the origin of asynchronism. This local point of view on asynchronism can be turned into a more integrated view by predicting, using our model, the total number of descendant GUs at each flush and each fate within a branching system, e.g. a scaffold, contributing to bring knowledge on the architectural determinants of patchiness. As a perspective, including explanatory variables into the generation distributions will allow to determine the effect of cultivar, growth conditions (climate) or horticultural practices (e.g. pruning or fruit thinning) on patchiness at different scales, and particularly at the whole-canopy level.

LITERATURE CITED

Chacko EK. 1986. Physiology of vegetative and reproductive growth in mango (*Mangifera indica* L.) trees. *Proceedings of the First Australian Mango Research Workshop*. CSIRO, Melbourne, 54–70.

Dambreville A, Lauri PÉ, Trottier C, Guédon Y, Normand F. 2013. Deciphering structural and temporal interplays during the architectural development of mango trees. *Journal of Experimental Botany doi 10.1093/jxb/ert105.*

Durand J-B, Guédon Y, Caraglio Y, Costes E. 2005. Analysis of the Plant Architecture via Tree-structured Statistical Models : the Hidden Markov Tree Models. *New Phytologist* **166**: 813-825.

Koller D, Friedman N. 2009. Probabilistic graphical models: principles and techniques. MIT press, 2009.

Ramírez F, Davenport TL. 2010. Mango (*Mangifera indica* L.) flowering physiology. *Scientia Horticulturae* **126**: 65-72.

Proceedings of the 7th International Conference on Functional-Structural Plant Models, Saariselkä, Finland, 9 - 14 June 2013. Eds. Risto Sievänen, Eero Nikinmaa, Christophe Godin, Anna Lintunen & Pekka Nygren. http://www.metla.fi/fspm2013/proceedings. ISBN 978-951-651-408-9.

OpenAlea 2.0: Architecture of an integrated modeling environment on the web

Christophe Pradal[1,2], Julien Coste[2], Frédéric Boudon[1,2], Christian Fournier[3] and **Christophe Godin[2]**
[1]CIRAD, UMR AGAP, F-34398 Montpellier, France, [2]INRIA, Virtual Plants, F-34398 Montpellier, France, [3]INRA, UMR 759 LEPSE, F-34060 Montpellier, France
**correspondence:* christophe.pradal@inria.fr

Highlights: Plant modeling is based on the use of a diverse set of design paradigms (L-systems, visual programming, imperative languages or sketch-based interfaces). In this poster, the architecture of a new multi-paradigm and integrated modeling environment is presented. This desktop application will become a distributed web application, allowing to run simulations on a cloud computing system and share virtual experiments on the web. The modeling environment will run on a web browser using HTML5 and WebGL technologies.

Keywords: Scientific workflow, Integrated modeling environment, Web 2.0, WebGL

The development of a model of plant or cellular tissue requires the use of a modeling paradigm: (i) imperative using a script or a compiled language, (ii) declarative to define a set of rewriting rules like in L-systems, (iii) interactive using a sketch-based interface for creating 3D models of plants, or (iv) visual programming to combine existing components. All these modeling paradigms have been developed in different software platforms in the plant modeling community, but, as of today, none of them provides all the modeling paradigms in an integrated software environment: vlab/LStudio (Prusinkiewicz et al. 2007), GroIMP (Hemmerling et al. 2008) and L-Py (Boudon et al. 2012) focus on L-systems; TreeSketch (Longay et al., 2012) focuses on sketch-based modeling of tree; and OpenAlea (Pradal et al., 2008) focuses on visual programming. However, the need to develop more complex and integrated models, often assembling many sub-models, leads us to consider a modeling environment capable of supporting multiple design paradigms and models, and make them interoperable.

In this poster, we will present the architecture of a new integrated modeling environment, based on OpenAlea, able to use different paradigms for plant modeling (e.g. L-systems and visual programming). The user will be able to construct virtual scenes and environmental models, and to simulate them using either of the preceding paradigms or a combination of them. It is possible to integrate different model applications in this environment and to share data between these applications via well-defined communication protocols. The first prototype takes the form of a desktop application, but will become a distributed web application, based on HTML5 and WebGL technologies.

LITERATURE CITED

Boudon F, Pradal C, Cokelaer T, Prusinkiewicz P. and Godin C. 2012 L-Py: an L-System simulation framework for modeling plant development based on a dynamic language. *Frontiers in technical advances in plant science*, vol. 3, Art. 76.

Hemmerling R, Kniemeyer O, Lanwert D, Kurth W, Buck-Sorlin G. 2008 The rule-based language XL and the modeling environment GroIMP illustrated with simulated tree competition. *Functional Plant Biology* **35**:739–750.

Longay S, Runions A, Boudon F, Prusinkiewicz P. 2012 Treesketch: interactive procedural modeling of trees on a tablet. In *Proceedings of the international symposium on sketch-based interfaces and modeling*. Eurographics Association 107-120

Pradal C, Dufour-Kowalski S, Boudon F, Fournier C and Godin C. 2008 OpenAlea: a visual programming and component-based software platform for plant modelling. *Functional Plant Biology* **35**:751-760.

Prusinkiewicz, P, Karwowski, R and Lane, B. 2007. The L+C plant modelling language. In Functional-Structural Plant Modelling in Crop Production, J. Vos et al. (eds.), Springer.

Proceedings of the 7th International Conference on Functional-Structural Plant Models, Saariselkä, Finland, 9 - 14 June 2013. Eds. Risto Sievänen, Eero Nikinmaa, Christophe Godin, Anna Lintunen & Pekka Nygren. http://www.metla.fi/fspm2013/proceedings. ISBN 978-951-651-408-9.

Rule-based integration of LIGNUM into GroIMP

Katarína Smoleňová*, **Michael Henke**, **Yongzhi Ong** and **Winfried Kurth**
Department Ecoinformatics, Biometrics and Forest Growth, Georg-August University of Göttingen, 37077 Göttingen, Germany
**correspondence:* ksmolen@gwdg.de

Highlights: LIGNUM is a functional-structural tree model combining the use of L-systems for structural development and the programming language C++ for modelling metabolic processes and radiation regimes. We show how both the structural and functional part of LIGNUM, used for a Scots pine model, can be translated into the rule-based language XL, thus offering new possibilities for model reuse and comparison.

Keywords: LIGNUM model, GroIMP, XL, FSPM integration

INTRODUCTION

LIGNUM is a generic functional-structural plant model (FSPM) designed and parameterized for modelling coniferous (e.g. Perttunen et al. 1998) as well as deciduous (e.g. Perttunen et al. 2001) tree species. These application areas justify the generic design of the LIGNUM model, which is implemented with the programming language C++. A tree is described in terms of four main structural units: tree segment, bud, branching point, and axis. While in conifers the foliage is modelled as a layer of a tree segment, in deciduous trees the leaves are modelled explicitly as ellipses or triangles (Perttunen 2008). Simplified modelling of root biomass is included. New structure is created at each time step (usually one year) by applying L-system rules, written in the language L (Perttunen and Sievänen 2005). The underlying data structure is a list. In LIGNUM, four generic algorithms for tree traversal have been identified: *ForEach*, *Accumulate*, *AccumulateDown*, and *PropagateUp* (Perttunen 2008). These are sufficient to cover the computation of all considered metabolic processes taking place throughout the tree, e.g., photosynthesis, respiration, senescence, or iterative allocation of new photosynthates into the organs. Light distribution is simulated by computing the mutual shading between all segments or by using a voxel space model. When modelling a concrete (new) species, new structural units, in the sense of C++ classes, need to be specified, e.g., *CfTreeSegment*, *PineSegment*, *ScotsPineSegment*, and also the rewriting rules for the architecture modelling, as well as species-specific metabolic processes. This design differs from another generic FSPM, GreenLab (Yan et al. 2004), where a fixed number of organ types is specified and architecture is modelled by a dual-scale automaton, corresponding to one generic rewriting rule (Smoleňová et al. 2012) – these are reparameterized for modelling different species, from simple plants to trees. Concerning metabolic processes, different implementations of submodels are available in GreenLab, too.

The question of reimplementation of the whole LIGNUM model using L-systems was raised in Perttunen and Sievänen (2005), but such a solution seemed not to be optimal because of the complexity of FSPMs. Note that the older version of LIGNUM applied to Scots pine (*Pinus sylvestris* L.) (Perttunen et al. 1996) was already translated into L-systems using the tool GROGRA (Kurth 1999). There, predefined sensitive functions were used inside the L-systems to simulate response to environment. The software platform GroIMP and its underlying language XL (eXtended L-system language) provide advanced features that allow to specify even complex relations addressed by FSPMs in terms of rule-based modelling. Here we show how to translate both, the structural and the functional part of LIGNUM (as described in Perttunen (2008)) into XL rules, with focus on the model parts necessary for the simulation of Scots pine.

IMPLEMENTATION DETAILS

The model presented here is implemented in the open-source platform GroIMP, version 1.4 (www.grogra.de), written in Java. The modelling language of GroIMP, the language XL, extends Java and allows combination of rule-based, object-oriented and imperative programming. The underlying data structure is a graph (see Kniemeyer (2008) for technical details).

The following structural components of LIGNUM were specified as XL modules (analogous to L-system symbols) with associated attributes and methods:

(1) modules for trees in general: *Tree*, *TreeSegment*, *Bud*, all extending *TreeCompartment*,

(2) modules specific for conifers, pine and Scots pine: *CfTreeSegment* (extends *TreeSegment*), *PineSegment* (extends *CfTreeSegment*), *PineBud* (extends *Bud*), *ScotsPineTree* (extends *Tree*), *ScotsPineSegment* (extends *PineSegment*), *ScotsPineBud* (extends *PineBud*).

Because of the general graph data structure, the main structural components *BranchingPoint* and *Axis* that were inevitable in LIGNUM were inherently expressed in XL.

The rules for architecture development were translated in a straightforward way. It was possible to write the XL rules in a more compact way, using *for*-loops for generation of new buds, which are not supported in the language L.

Generic algorithms of LIGNUM that are used to traverse the modelled tree and to perform functional computations were translated using selected features of the language XL (Kniemeyer 2008), e.g.:

(1) *Query expressions* are used to search for a specific pattern, enclosed in asterisked parentheses. The query

(sps:ScotsPineSegment, (sps.getLGAage() == 0) *)*

finds all newly created organs of type *ScotsPineSegment* with age 0, where age is accessed by the method *getLGAage()* and *sps* represents the current instance of *ScotsPineSegment*. Alternatively, age could be accessed using *sps[LGAage]*. Different edge patterns can be used inside of the queries to specify relations between searched organs, or to define transport in basipetal or acropetal direction.

(2) *Aggregate methods* collect multiple values and return one single value as result. Standard aggregate methods are for example *count*, *sum*, *first*, *last*. Aggregate methods can be combined with queries. The expression

sum((ScotsPineSegment *).getLGAP())*

searches for all organs of type *ScotsPineSegment*, obtains their photosynthate values (this is accessed by the method *getLGAP()*), and returns the sum of them.

(3) *Execution rules* are typically used to execute imperative statements for searched organs or update their attribute values, without changes in the topology. The following rule

sps:ScotsPineSegment ::> sps.photosynthesis();

computes photosynthesis for each *ScotsPineSegment*. In this case, the photosynthesis method was implemented inside the module *TreeSegment*.

A number of methods necessary for simulating the following metabolic processes have been translated into XL: photosynthesis, respiration, senescence, and allocation of photosynthates connected with tree segment elongation and diameter growth.

Two light models used in LIGNUM for computation of light distribution in single trees as well as the sky model (Perttunen 2008) were adapted into GroIMP. The first light model approach computes received radiation by tree segments influenced by shading caused by other segments. The second, voxel space model, reduces the radiation computation complexity by operating on voxels (regular boxes) into which the space where the tree grows is discretized. The light models were translated directly into GroIMP framework code (similarly as the light models already provided by GroIMP, i.e. the Monte-Carlo reversed path tracer, GPU-based raytracer supporting also spectral light simulation), but it would be possible to rewrite them in XL.

The following execution rule demonstrates how the light models can be called to compute radiation distribution in the tree:

sps:ScotsPineSegment ::> radiation.eval(sps);

where *radiation* is an instance of one of the light model classes. The amount of incoming and absorbed radiation by a tree segment can then be obtained by calling *sps.getLGAQin()* and *sps.getLGAQabs()* respectively.

DISCUSSION AND OUTLOOK

The advanced features of the modelling language XL allow to translate even complex models like LIGNUM into rule-based models. While structural development was translated using rules similar to classical L-systems, further features (e.g., graph traversal, query and aggregate expressions, execution rules) were necessary for simulation of metabolic processes. The two radiation models and the sky model were added to GroIMP, and therefore their code is hidden from the user, although an implementation in XL would also be possible. Furthermore, besides the fact that rule-based description of plant growth and development is more intuitive, the rule-based integration of LIGNUM into GroIMP supports model reuse and opens new possibilities for testing and comparison of different submodels. On one hand, the submodels already existing in XL could be integrated into the translated LIGNUM along with potential extensions. This will make a

direct comparison, for instance of different hypotheses and approaches of light simulation or biomass partitioning, possible. On the other hand, LIGNUM submodels could be integrated into other XL models. However, both possibilities would require some model adaptations, either in LIGNUM or in (existing) XL models. Another interesting issue concerns model comparison for one selected species, simulated using different models, in terms of generated output values, based on the same input data set (cf. Baey et al. 2012). This way, one could compare outputs (e.g. biomass) generated by GreenLab and LIGNUM simulations of the same species, e.g. Scots pine.

ACKNOWLEDGEMENTS

This research was funded by the German Research Foundation (DFG) under project identifier KU 847/8-1. We thank A. Brinkmann for his work on translating LIGNUM's light models into GroIMP. We also thank J. Perttunen and R. Sievänen for explanation of the LIGNUM model and for hosting the first author at Finnish Forest Research Institute Metla, Vantaa.

LITERATURE CITED

Baey C, Song L, Cournède PH, Lemaire S, Maupas F. 2012. Evaluation of the predictive capacity of five plant growth models for sugar beet. In: Kang MZ, Dumont Y, Guo Y, eds. *Proc. IEEE 4th International Symposium on Plant Growth Modeling, Simulation, Visualization and Applications*. IEEE, Beijing, 30–37.

Hemmerling R, Kniemeyer O, Lanwert D, Kurth W, Buck-Sorlin G. 2008. The rule-based language XL and the modelling environment GroIMP illustrated with simulated tree competition. *Functional Plant Biology* **35**: 739-750.

Karwowski R, Prusinkiewicz P. 2003. Design and implementation of the L+C modeling language. *Electronic Notes in Theoretical Computer Science* **86**: 134–152.

Kniemeyer O. 2008. Design and implementation of a graph grammar based language for functional-structural plant modelling. PhD Thesis, BTU Cottbus, Germany.

Kurth W. 1999. *Die Simulation der Baumarchitektur mit Wachstumsgrammatiken*. Berlin: Wissenschaftlicher Verlag.

Perttunen J. 2008. The LIGNUM functional-structural tree model. PhD Thesis, Helsinki University of Technology, Finland.

Perttunen J, Sievänen R. 2005. Incorporating Lindenmayer systems for architectural development in a functional-structural tree model. *Ecological Modelling* **181**: 479–491.

Perttunen J, Nikinmaa E, Lechowicz MJ, Sievänen R, Messier C. 2001. Application of the functional-structural tree model LIGNUM to sugar maple saplings (*Acer saccharum* Marsh) growing in forest gaps. *Annals of Botany* **88**: 471–481.

Perttunen J, Sievänen R, Nikinmaa E, Salminen H, Saarenmaa H, Väkevä J. 1996. LIGNUM: a tree model based on simple structural units. *Annals of Botany* **77**: 87–98.

Perttunen J, Sievänen R, Nikinmaa E. 1998. LIGNUM: a model combining the structure and the functioning of trees. *Ecological Modelling* **108**: 189–198.

Smoleňová K, Henke M, Kurth W. 2012. Rule-based integration of GreenLab into GroIMP with GUI aided parameter input. In: Kang MZ, Dumont Y, Guo Y, eds. *Proc. IEEE 4th International Symposium on Plant Growth Modeling, Simulation, Visualization and Applications*. IEEE, Beijing, 347–354.

Yan HP, Kang MZ, de Reffye P, Dingkuhn M. 2004. A dynamic, architectural plant model simulating resource-dependent growth. *Annals of Botany* **93**: 591–602.

Proceedings of the 7th International Conference on Functional-Structural Plant Models, Saariselkä, Finland, 9 - 14 June 2013. Eds. Risto Sievänen, Eero Nikinmaa, Christophe Godin, Anna Lintunen & Pekka Nygren.
http://www.metla.fi/fspm2013/proceedings. ISBN 978-951-651-408-9.

An extension of the graph-grammar based simulator GroIMP for visual specification of plant models using components

Michael Henke,[1]* **Katarína Smoleňová,**[1] **Yongzhi Ong**[1] and **Winfried Kurth**[1]
[1]*Department Ecoinformatics, Biometrics and Forest Growth, Georg-August University of Göttingen, Büsgenweg 4, 37077 Göttingen, Germany*
**correspondence:* mhenke@uni-goettingen.de

Highlights: The FSPM platform GroIMP was extended by a graphical editor for components of rule-based models, enabling a better re-use and comparison of submodels. Components can be arbitrarily nested and can have several types of connectors with different semantics. The new tool provides a parallel maintenance of model code and of the graphical view showing the component structure.

Keywords: components, visual programming, software for modelling, GroIMP platform, XL language

INTRODUCTION

The most frequently used formalism to specify functional-structural plant models (FSPMs) are L-systems. A powerful generalization are parallel graph grammars. The programming language XL combines these with the power of the general-purpose, object-oriented language Java and gives thus support to the combination of process-based and rule-based submodels (Kniemeyer 2008). However, when applied to complex tasks, models specified in XL like those in other languages still tend to grow in an intransparent manner. Methods which are commonly used in software engineering are not yet supported (this being a general problem for scientific software, see Wilson 2006). As a further step towards a more transparent and flexible modelling process, we have enhanced the language XL and the open-source development platform GroIMP by tools supporting the creation of independent components, fostering also the interchangeability and comparison of submodels (e.g., for photosynthesis, structure formation, etc.). Interactive graphical visualization tools will make this approach also accessible to scientists with low experience in classical programming.

The issue of component-based development of FSPMs was already addressed by the open-source platform OpenAlea (Pradal et al. 2008), a framework which provides the possibility to create plant models by connecting components and to extend the available set of components by user-defined ones. However, OpenAlea has been designed for model integration and connection rather than for modelling feedback and retroaction between submodels. Furthermore, graph-transformation based models are not yet supported by it.

In the field of software engineering, the component-based approach has been successfully established and has led to divese tools and models, like CORBA (Mowbray & Ruh 1997), .NET (Box & Sells 2002) and JavaBeans (Sun Microsystems 2009). According to Szyperski (2002), components are "executable units of independent production, acquisition, and development that can be composed into a functioning system". Typical features are a useful functionality, encapsulation, re-usability, configurability, independent deployment and GUI-aided design. Usually, each component has its specific interfaces or *slots* which can either send or receive information to / from other components.

THE GRAPH MODEL

The composition of a model in terms of nested and interconnected components is represented by a directed graph $(C \cup S, E)$. Its nodes stand for the components C and their slots S; its edges belong to one of the three disjoint subsets E_C (refinement or "contains" edges between components), E_{SC} (slot-component incidence edges which indicate that a slot is an entrance or exit point of a component) and E_S (connectors between slots of different components). The connectors carry the information flow within the model. The edges between the different sorts of nodes of the graph have to conform to certain restrictions which we cannot list here exhaustively; we mention only the most important ones:

(1) The restriction of the graph to node subset C is acyclic. It reflects the "containment" relationship between components, or, in the hierarchical view, their nestedness.

(2) For each slot $s \in S$ there is exactly one adjacent component $c \in C$, i.e., there is exactly one edge (s, c) or (c, s) in E_{SC}. c is the component to which s "belongs". In our current implementation, the components

carry all functionality (similar to classes in the sense of object-oriented programming), but principally, slots could also be equipped with some functional abilities, e.g., for checking correctness of input data.

(3) Edges from E_S can only connect components which are at most one refinement level apart. If same-level components are connected, they must belong to the same supercomponent at the next-coarser level.

In the literature, different types of connectors and their characterization by algebraic properties are discussed (Bruni et al. 2011). Our graph model is designed for two types, "signal" and "call/receive" connectors, but could easily be extended to include more than two types. A "signal" connector mediates an unidirectional signal which can trigger an event in the receiving component. "Signal" connectors have thus a "push" semantics. A variant of "signal" connectors are "send" connectors which can transport a data stream. A "call/receive" connector mediates a function or method call or a request for a service. It carries information in both directions (the request in one direction, and the delivered result from the addressed component in the opposite direction). It has thus a "pull" semantics. In our current implementation, only "call/receive" and "send" connectors are realized.

Fig. 1 shows a simple example of a component structure. On the left-hand side, we see the classical graph view with the components as labelled circles, the slots as triangles and all edges as arrows. Edges marked with "/" are from E_C , they stand for the "containment" relationship. The dotted edge sends the output of the model (the result of some calculation in "structure") to the exterior output slot at the coarsest level, it is thus a "send" connector. The right-hand side shows the same component structure in a hierachical, nested view. The "plant" component (at the coarsest level) contains (visually) the three other components. Only edges from E_S are shown as arrows here.

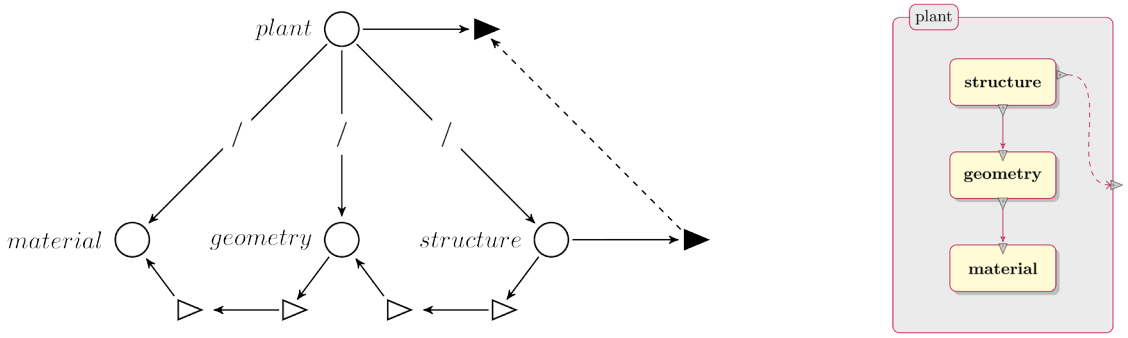

Fig. 1. A graph representing a component structure of a plant model, shown in two alternative views. Left: classical graph view. Right: hierarchical view, "containment" relationships are visualized by geometric inclusion of rectangles.

RESULTS

The here-discussed framework is written as an extension of the software GroIMP (Growth-grammar related Interactive Modelling Platform, Kniemeyer et al. 2007; http://sourceforge.net/projects/groimp/), a 3-d modelling platform based on graph transformations and employed for model implementation and visualization of results. GroIMP is designed as an integrated platform which incorporates modelling, simulation, visualization and user interaction, and provides a compiler and development tools for the rule-oriented language XL with specialized facilities for plant modelling. GroIMP's basic data structure is an attributed graph, with the nodes generally standing for objects (e.g., plant organs) and the edges for relationships. This graph can undergo transformations, specified in XL. The GroIMP graph offers itself in a natural way to represent the component structure of a model, expressed by the above-described graph, as well. Each node from C is then associated with a piece of code which represents the functionality of the corresponding component. Currently, all components have to be encoded in XL or Java and have to be accessible for the integrated XL compiler of GroIMP. Frequently used components can be kept permanently in an inherent library of GroIMP and are then accessible by a browser. With drag-and-drop, the user can take them from the browser window and link them graphically to other components in the component editor window.

The component editor offers two alternative views, corresponding to the two graph representations in Fig. 1. Furthermore, the XL code of each component can be directly accessed in a code window. With this, we deliberately violate the "black-box principle" of strict component-oriented development, thus answering to the demands of modellers from the FSPM community who have expressed their wish to have full insight and control of the software components they are expected to use. An additional developer environment with a

template component as a base allows such users to implement their own components quickly.
As example we use the simple tree with dichotomous branching and with coloured, spherical buds which comes along as a basic L-system template code within the GroIMP software (activate "open File" / "New" / "RGG project"). A separation of the XL code into the three components "structure", "geometry" and "material" is possible and leads to the structure shown in Fig. 1 (without the output slots pointing to the right; code not shown). In the "structure" component the morphological plant structure is defined, while the "geometry" component associates geometrical objects to the L-system labels used in "structure". The "material" component finally encapsulates the visual representation of the geometrical objects (plant organs) for the 3-d view. This example demonstrates that components can be used in XL to realize *aspect-oriented programming* in the sense of Cieslak et al. (2011). Aspects are the result of decomposing an organism into sub-entities which represent functionalities rather than spatial units. In this simple example, topological functions or rules reside in "structure", geometrical ones in "geometry", and optical properties are confined to "material".

A considerable amount of information is exchanged along the "call/receive" edges in this example, namely, the complete graph which represents the plant. E.g., the "geometry" component makes use of interpretive rules to insert some rotation nodes into the graph provided by "structure". Thus, the complete graph must be accessed by the components. This is somewhat contradictory to the parsimony principle of component-based development, which demands that inter-component information flow is small and strictly gate-kept by the slot specifications. Again, practical demands justify our wide interpretation of the component-based paradigm.

DISCUSSION AND OUTLOOK

It is our expectation that our component framework for XL will considerably improve the reusability of graph-transformation based submodels of FSPMs and will thus reduce the development time for plant models and enable a better maintenance and exchange between different teams. Although the development of the framework itself is not yet finished, we have started to create a library of ready-to-use components. Particularly, a set of photosynthetic rate models was implemented in XL, differing in their complexity from simple light-response curves to biochemical Farquhar-type models. In the future, we want to enable the usage of components written in other languages by utilizing wrapper components with Babel as glue (cf. Dahlgren et al. 2009).

ACKNOWLEGEMENTS

This research was funded by DFG under project identifier Ku 847/8-1.

LITERATURE CITED

Box D, Sells C. 2002. *Essential .NET. Vol. I: The Common Language Runtime.* Addison Wesley Professional.

Bruni R, Melgratti H, Montanari U. 2011. A connector algebra for P/T nets interactions. In: Katoen JP, König B (eds.): *CONCUR 2011*, *LNCS* **6901**, Springer, Berlin, 312-326.

Cieslak M, Seleznyova AN, Prusinkiewicz P, Hanan J. 2011. Towards aspect-oriented functional-structural plant modelling. *Annals of Botany* **108**(6):1025-1041.

Dahlgren T, Kumfert G, Epperly T, Leek K. 2009. Babel user's guide. Technical Report UCRL-SM-230026, Center for Applied Scientific Computing, Lawrence Livermore Nat. Lab., PO Box 808, Livermore, Cal.

Kniemeyer O. 2008. Design and Implementation of a Graph Grammar Based Language for Functional-Structural Plant Modelling. PhD thesis, University of Cottbus, http://nbn-resolving.de/urn/resolver.pl?urn=urn:nbn:de:kobv:co1-opus-5937

Kniemeyer O, Buck-Sorlin G, Kurth W. 2007. GroIMP as a platform for functional-structural modelling of plants. In: Vos J, Marcelis LFM, deVisser PHB, Struik PC, Evers JB (eds.), *Functional-Structural Plant Modelling in Crop Production*. Springer, Dordrecht, 43-52.

Mowbray TJ, Ruh WA. 1997. *Inside CORBA. Distributed Object Standards and Applications.* Pearson.

Pradal C, Dufour-Kowalski S, Boudon F, Fournier C, Godin C. 2008. OpenAlea: A visual programming and component-based software platform for plant modeling. *Functional Plant Biology* **35**:751-760.

Sun Microsystems. 2009. *JavaBeans specification.*

Szyperski C. 2002. *Component Software. Beyond Object-Oriented Programming.* Addison-Wesley, London.

Wilson G. 2006. Where's the real bottleneck in scientific computing? *American Scientist* **94**(1):5.

Proceedings of the 7th International Conference on Functional-Structural Plant Models, Saariselkä, Finland, 9 - 14 June 2013. Eds. Risto Sievänen, Eero Nikinmaa, Christophe Godin, Anna Lintunen & Pekka Nygren. http://www.metla.fi/fspm2013/proceedings. ISBN 978-951-651-408-9.

Global sensitivity analysis of the NEMA model for its parameterization and biological diagnosis

Qiongli Wu [1], **Jessica Bertheloot**[2] and **Paul-Henry Cournède** [1]
[1]*Lab MAS, Ecole Centrale Paris, 92295, Châtenay-Mâlabry Cedex, France*
[2]*INRA,UMR 0462 SAGAH, Beaucouzé Cedex, France*
**correspondence: qiongli.wu@gmail.com*

Highlights: A new comprehensive methodology of global sensitivity analysis is applied to the NEMA model. Besides the common objective of global sensitivity analysis for ranking the importance of individul input factors, we also analyze specifically the functional modules corresponding to the different processes involved in the model, in order to get useful information about the importance and interactions of these physical processes. The results are helpful in the parameterization process and provide new biological insights and diagnosis for NEMA.

Keywords: NEMA, nitrogen, wheat, global sensitivity analysis, SRC, Sobol's method

INTRODUCTION

Functional-structural models of plant growth (FSPM) aim at describing the structural development of individual plants combined with their eco-physiological functioning (photosynthesis, biomass allocation, in interaction with the environment) [Godin and Sinoquet, 2005]. The multi-biophysical processes described in FSPMs and their complex interactions make it difficult to identify the key processes, control variables and parameters driving plant growth. Sensitivity analysis (SA) can help to provide useful insights about the model. First, it helps to simplify parameter estimation by screening the non-influential parameters. Moreover, SA can also provide new biological diagnosis and understanding by the quantitative analysis of interactions between the sub-models corresponding to different processes involved in plant growth.

NEMA (Nitrogen Economy Model within plant Architecture) [Bertheloot et al.,2011] is typically an FSPM with many parameters and many sub-models (modules) describing multi-physical processes in interaction. The main objective of this paper is to perform SA for NEMA to identify the most influential model parameters, processes, and the interactions between them, by taking advantage of several complementary global SA methods.

MATERIALS AND METHODS

From a methodology point of view, there exist different sensitivity analysis methods with different objectives and adapted to different types of models. First of all, the aims of sensitivity analysis need to be considered: Factor prioritization, factor fixing, variance cutting or factor mapping [Saltelli et al.,2008]. Each aim involves different methods. Moreover, the computing cost issue related to the complexity of the models also needs to be considered. For instance, the Standard Regression Coefficients (SRCs) [Cariboni et al., 2007] can be viewed as an interesting trade-off between the accuracy of the analysis and the computing cost, but it is only valid when model's linearity is high. Sobol's method can help us get the interaction information for parameters and functional modules, but the sampling-based Monte-Carlo simulation makes Sobol's method sometimes prohibitive from a computation point of view [Wu et al., 2011]. Especially when we make the module analysis, the interactions between modules are the diverse combinations of interactions between factors within the modules with a lot of higher order Sobol's indices. To circumvent this problem, we propose an adaptation of Sobol's method to group of factors which allows an efficient computation of intra-module and inter-module interactions using the decomposition of total-order indices for group factors associated with sub-modules of the model.

The methodology can be summarized into 5 steps:

1) Non-linearity analysis using SRCs: it gives out the evolution of model non-linearity and a general view of the model dynamic property. This preliminary information is also useful to adapt the following stategy accordingly.

2) Group analysis: it provides the evolution of module importance by computing the evolution of the sensitivity indices of the total set of parameters corresponding to each module of the model. We define the set of factors Ω_m gathering the inputs of one module. Group indices are computed: first order group index

$S^g_{\Omega_m}$ (The main effect of Ω_m) and total order group index $ST^g_{\Omega_m}$ (The total effect of Ω_m). The inter-module interaction is given by $ST^g_{\Omega_m} - S^g_{\Omega_m}$ (it is the sum of interactions of all orders between factor set Ω_m and the other sets).

3) Module by module parameter screening: we compute Sobol's first order index S_i (the main effect of factor X_i, mainly used for 'factor prioritization'), Sobol's total order index ST_i (The total effect of factor X_i, mainly used for 'factor fixing' or screening), $ST_i - S_i$ (The sum of interactions of all orders between factor X_i and the other factors) and Sobol's second order index S_{ij} (The interaction between factors X_i and X_j). We run the SA module by module based on the same sampling points, so that to provide index ST_i of each parameter for screening. For this purpose, we use a time averaging index called TGI [Wu, 2012] to reduce the time dimension of the sensitivity indices.

4) Quantitative intra-module and inter-module interaction analysis: we consider the results from step 2 and step 3 and write the following decomposition $ST^g_{\Omega_m} = \sum_{i\in m} S_i + (S^g_{\Omega_m} - \sum_{i\in m} S_i) + (ST^g_{\Omega_m} - S^g_{\Omega_m})$. $\sum_{i\in m} S_i$ is the main effect brought by all the factors with module *m*, while $S^g_{\Omega_m} - \sum_{i\in m} S_i$ stands for the intra-module interactions and $ST^g_{\Omega_m} - S^g_{\Omega_m}$ is the inter-module interactions as indicated in step 2.

5) Complete analysis for model with the selected parameters.

NEMA [Bertheloot et al.,2009] is a complex functional-structural model describing carbon (C) and nitrogen (N) acquisition by a wheat plant as well as C and N distributions between plant organs after flowering. Nitrogen content of each photosynthetic organ and its remobilization following RubisCO turnover are simulated. The turnover depends on light intercepted and a mobile nitrogen pool, which is enriched by root uptake and nitrogen release from vegetative organs, which is depleted by grain uptake and protein synthesis in vegetative organs. It also accounts for the negative feedback of circulating nitrogen on root uptake, which is formalized following high affinity transport system (HATS) and low affinity transport system (LATS) activities. Organ nitrogen content and light intercepted determine dry matter production by photosynthesis, which is distributed between organs according to their respective demand [Bertheloot et al.,2011]. C assimilation is predicted from the N content of each photosynthetic organ. Inputs of Nitrogen fertilizers are fundamental to get high-yielding crops and a production of high quality with the required protein content. This required a proper understanding of root N uptake regulation and of N determinism on yield and production. Complex interactions exist between root N uptake, N remobilization to grains, and photosynthesis, whose regulatory mechanisms remain far from clear. All the parameters involved for the analysis are given in [Bertheloot et al.,2011].

Basic biological modules are identified for NEMA: Carbon distribution (DMflux), Nitrogen distribution (Nflux), Carbon acquisition via photosynthesis (Photosynthesis), Nitrogen acquisition by roots (RootNuptake), Senescence (TissueDeath). We use subscrips to identify the factors for different plant organs as follows: g for grain, r for root, La for Lamina, Sh for Sheath, In for internode, Pe for Peduncle, Ch for Chaff. Several outputs of interest are considered for both intra-module and inter-module interaction analysis: a) total green area of the plant (AreaGreenTotal), b) total dry mass production of the plant (Production), c) dry mass of the grains (DMgrains), d) Nitrogen mass of the grains (Ngrains) and e) root Nitrogen uptake (RootNuptake). For each output of interest, we did all the 5 steps in the methodology. The evolution of the sensitivity indices are computed for a better investigation of the dynamics of plant growth, but when we aim at screening parameters, we consider the TGI index. The full model involves 83 parameters. We used the parameterization in [Bertheloot et al., 2011].

RESULTS AND DISCUSSION

We select output AreaGreenTotal as a demonstration of how our analysis can provide useful biological insights. The 'non-linearity analysis' and 'group analysis' are shown in Fig.1. Quantitative results for module by module analysis are given directly. A summary of selected parameters for different outputs of interest is also given in Fig.2 to show how 'parameter screening' works for model parameterization.

In Fig.1., with AreaGreenTotal as the output of interest, between 374 ^{o}Cd and 531^{o}Cd, there is one valley for the linearity, during which the lowest linearity appears at 417^{o}Cd to the linearity of 0.48. Such a period in which a strong non-linearity occurs may be characteristic of very specific biological phenomena during plant growth and of high level of interactions between parameters, either known by the modeler or unknown, in which case they should probably be investigated more. The first order sensitivity mainly goes to module DMflux and Nflux, and for a short period to the module Tissuedeath. The interactions between modules

mainly exist for DMflux and Nflux. We also noticed that the module Photosynthesis and RootNuptake contribute little to the variance of the output from the beginning to the end. Moreover, the inter-module interactions for the two modules are also very low at all stages. In module by module analysis, we managed to see these interactions more quantitatively. With TGI in step 4, most intra-module interactions exist in module DMflux, which is as high as 8.75% while the total intra-module interactions for all the five modules is 8.79%. The inter-module interactions between DMflux and Nflux reaches 4.9%.

In Fig.2, 17 factors are selected out of 83 and explain most of the variance of the system. This result has already been used in the parameterization process. The most important factors for module Nfluxe are pretty steady for all the outputs: 1) γ standing for the relative rate of potential grain N filling during cell division, 2) $\sigma_{La}^{N_{ph}}$ standing for relative rate of photosynthetic N synthesis associated to xylem flux for entity Lamina, 3) δ_{La}^{N} standing for relative degradation rates of remobilizable N for entity Lamina. γ rules all the outputs and most of the time has the highest ranking. If we categorize the factors selected in Fig.2 by organs, we can see that in the 4 types of parameters for module DMflux, the ones for organ grain and root tend to have significant effect for all outputs. The parameter of lamina tend to control Nflux, Tissuedeath and Photosynthesis.

The consequences of this study are crucial in several aspects: for parameterization, stressing on which module and on which parameter within each module more care should be taken, but also on whether each module can be parameterized independently (from different experiments for example). Moreover, studying dynamically the interactions between parameters and modules may reveal some biological phenomena of interests, non-visible through simple simulations. In this regards, SA offers new tools in integrative biology.

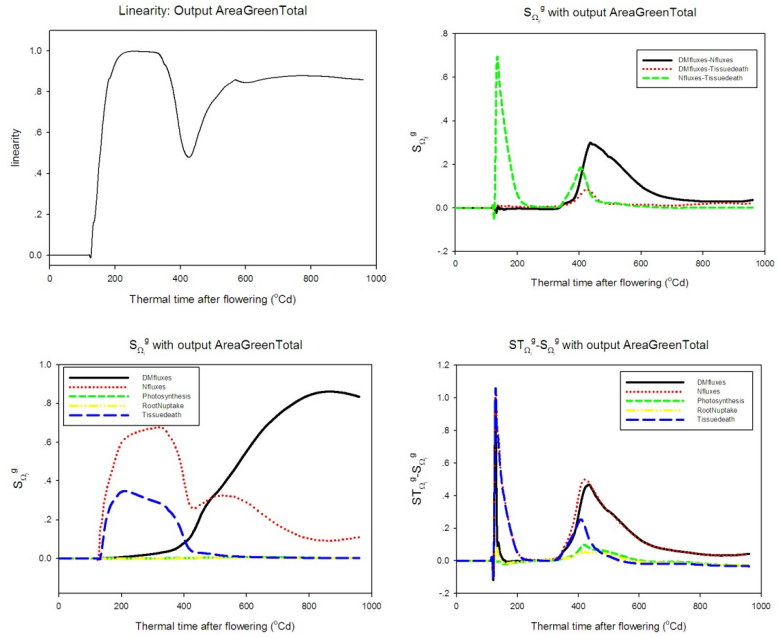

Fig.1. 'non-linearity analysis' and 'group analysis' for output AreaGreenTotal.

S_i ranking	a	b	c	d	e
Module:DMfluxes					
σ_g^M	6	8	4	-	5
α_g	-	12	2	-	8
β_g	21	13	5	-	9
tt_g^{Macc}	9	7	1	7	3
σ_r^M	5	5	-	4	4
α_r	7	6	-	5	6
β_r	3	3	-	3	2
tt_r^{Macc}	1	1	13	2	1
tt_{La}^{Macc}	-	-	8	-	16
tt_{Sh}^{Macc}	-	-	9	-	32
tt_{Ip}^{Macc}	-	-	10	-	17
tt_{Ch}^{Macc}	17	-	-	-	15
Module:Nfluxes					
γ	2	2	11	1	7
$\sigma_{La}^{N_{ph}}$	8	10	7	-	14
δ_{La}^{N}	4	4	6	-	10
Module:Tissuedeath					
d_{La}	11	-	-	-	-
Module:Photosynthesis					
$\omega_{La,2}$	-	9	3	-	11

Fig.2. Selected factor's Si ranking for the complete model for the different outputs

LITERATURE CITED

Godin C, Sinoquet H. 2005. Functional-structural plant modeling. *New Phytologist* **166**:705–708.

Bertheloot J, Cournède P-H, and Andrieu B. 2011. NEMA, a functional–structural model of nitrogen economy within wheat culms after flowering. I. Model description. *Annals of Botany*, **108 (6):** 1085-1096.

Saltelli A, Ratto M, Andres T, Campolongo F, Cariboni J, Gatelli D, Saisana M, Tarantola S. 2008. *Global Sensitivity Analysis*. John Wiley&Sons, the primer edition, **24-33**.

Cariboni J, Gatelli D, Liska R, and Saltelli A. 2007. The role of sensitivity analysis in ecological modelling, *Ecological modelling* **203**: 167-182.

Wu Q, Cournède P-H, and Mathieu A. 2012. An efficient computational method for global sensitivity analysis and its application to tree growth modelling. *Reliability Engineering & System Safety* **107**:35-43.

Wu Q. 2012. Sensitivity analysis for functional structural plant modeling, *PhD thesis, Ecole Centrale Des Arts et Manufactures (Ecole Centrale Paris)*, 91-93.

Proceedings of the 7th International Conference on Functional-Structural Plant Models, Saariselkä, Finland, 9 - 14 June 2013. Eds. Risto Sievänen, Eero Nikinmaa, Christophe Godin, Anna Lintunen & Pekka Nygren.
http://www.metla.fi/fspm2013/proceedings. ISBN 978-951-651-408-9.

Reconstruction of leaf area time series using data assimilation on the GreenLab plant growth model and remote sensing

Xing Gong[1,2] , **Thomas Corpetti**[1], **Mengzhen Kang**[2] , **Baogang Hu**[2] , **Laurence Hubert-Moy**[1]
[1]*Costel, Univ Rennes 2, UMR CNRS 6554 LETG, Rennes, France.* [2]*LIAMA, Institute of Automation, Chinese Academy of Sciences, 100080, Beijing, China*
**correspondence:* xgong.nlpr@gmail.com

Highlights: The GreenLab plant growth model is a powerful and complex tool able to simulate plant growth evolution. The calibration of GreenLab model for a specific plant usually requires field experiments with destructive sampling periodically done on individual plants in order to characterize growth and organogenesis. However when one is merely interested on particular aspects of plant growth, such as leaf area evolution or fruit harvest, we demonstrate in our work that a substantially simplified GreenLab model, associated with data assimilation methods, is able to provide satisfactory performances. Based on these techniques, we have successfully applied GreenLab to remote-sensing area where the observation data is highly limited. Experimental results show that qualitative and quantitative criteria on leaf area reconstructed time series are of good quality.

Keywords: GreenLab model, data assimilation, remote-sensing

INTRODUCTION

GreenLab Plant Growth model

The Greenlab plant growth model is an iterative technique that produces complex and variable plant architectures using some model parameters that depend on the kind of plant (Yan et al. 2004). These parameters are generally classified into two categories: those which can be estimated from direct, likely destructive, plant measurements and the hidden parameters deeply implied in the simulation process. The parameters of the first category are connected to the internal structure of the plant and comprise for example its geometry, weight and number of fruits, internodes, leaves, petals, etc. The parameters of the second category include external effects as the photosynthesis efficiency or the biomass demand of various organs.

Practical problems

Obviously, a manual collection of adequate observations and measurements required by Greenlab would be time-consuming and work-intensive. This indeed requires cultivating a plantation of given plant species, to dig out a small amount of individual plant units at a regular time interval and to perform extensive and destructive measurements (Guo Y et al., 2006; Zhan et al., 2003). In a large number of applications, this requirement for observation and measurement is too strong and unlikely to be satisfied.

Core idea: simplify GreenLab, compensating for these simplifications with remote sensing and data assimilation

Fortunately, as is shown in our work, when we are merely interested in certain aspects of plant growth, a simplified Greenlab model with significantly reduced number of parameters can be adequate. With the help of data assimilation methods (Evensen 1994), we are entitled to combine the information provided both by the plant growth model and up-to-date observations.

SHORT PRESENTATION OF GREENLAB

As other plant growth models, the goal of GreenLab is to simulate the growing process by dividing it into a number of consecutive growth cycles (Evers et al. 2007; Yan et al. 2004). In each cycle, depending on influential factors of plant and environmental context, biomass is produced by plant's photosynthesis. After its production, biomass is redistributed among all organs of the plant. The biomass generation formula reads:

$$\mathrm{Q(i)} = \mathrm{E(i)} \cdot S_p \cdot \frac{1}{r}\left(1 - \exp\left(-k \cdot \frac{S(i)}{S_p}\right)\right) \quad (1)$$

In the above equation, Q(i) stands for biomass generated at i_{th} growth cycle, E(i) is the environmental factor, S_p is the land area occupation, k is related to plant photosynthesis efficiency, r is a scale parameter, $S(i)$ represents the total leaf area at i_{th} growth cycle. Among above parameters, r, k are species-dependent

and have to be determined with learning techniques; $S(i)$ is both an intermediate and final biological index and plays a key role in our application.

Once the biomass is produced, it has to be redistributed among different organs of the plant, when simplifying the model, we adhere to GreenLab's *sink-demand* strategy for biomass partition: all organs of a plant share a common biomass pool generated by photosynthesis (Eq.1). Organs have to compete with each other for available biomass, and their partition lies upon their *demand* ratio of the whole plant. The organ's biomass accumulation $\Delta_{q_0(i)}$ is regarded as its growth.

In our application we are particularly interested in the leaf area evolution of agricultural plants that can be measured from remote sensing images. The iterative transition of leaf area $S(i)$ at i_{th} growth cycle is modeled as:

$$S(i) = \alpha \cdot (S(i-1) - \beta_i) + \Delta_{q_l(i)} \quad (2)$$

In the above equation, the withering of leaves at i_{th} growth cycle is denoted as β_i. It depends on leaf biological age and life span, and can be easily computed based on GreenLab structural sub-model. $\Delta_{q_l(i)}$ represents leaf's biomass partition at i_{th} growth cycle. The parameter α is in [0,1] and stands for the spoilage in natural growths. It is in practice estimated with learning techniques.

DATA ASSIMILATION

Data assimilation consists in estimating the state of a system by combining different sources of information, namely observation and prior knowledge represented as mathematical dynamical models and statistics. It is a widespread mathematical tool in various research areas such as fluid mechanics, atmosphere physics, oceanology and even pattern recognition (Evensen. 1994).

Among possible solutions to perform data assimilation, we rely in this study on stochastic techniques (Nummiaro et al. 2003, Bonet et al, 1999), mainly because of the non-linearity of the GreenLab model. The overall strategy consists in using two sub-models: i) state transition. ii) correction with observation. On the one hand, many external factors are likely to disturb a theoretical evolution of the plant, and therefore the GreenLab outputs are not guaranteed to fit with observations. On the other hand, using remote sensing, several observations per year can be obtained. This kind of observation is however noisy and even corrupted due to atmosphere disturbance and cloud occultation. In our work, we intend to combine model outputs and observations to reconstruct the mean leaf area evolution over agricultural crops observed from remote sensing.

Because of the complexity of the GreenLab model and the impossibility to assess all the parameters, we decided to simplify the model and to compensate these simplifications with data assimilation strategies. We in addition reformulated the deterministic GreenLab model into a probabilistic one by adding gaussian white noise to biomass production in Eq.1. This probabilistic GreenLab could be regarded as state transition model. The observation model is the satellite imaging process. The combined PROSPECT leaf optical properties model and SAIL canopy bidirectional reflectance model, also referred to as PROSAIL, has been used to estimate the Leaf Area Index from remote sensing images (Jacquemoud et al. 2009). In our application, we also mix the PROSAIL with gaussian additive white noise to make it probabilistic and deal with as the observation model.

RESULTS AND DISCUSSION

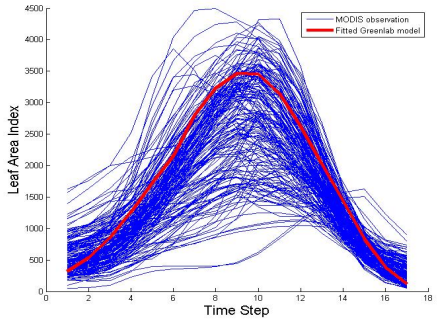

Fig. 1. Leaf area observation sequences of cereal and fitted GreenLab model output. Blue lines are noisy sample sequences calculated with PROSPECT from MODIS data, red line is the output of GreenLab which is fitted with non-linear least square method

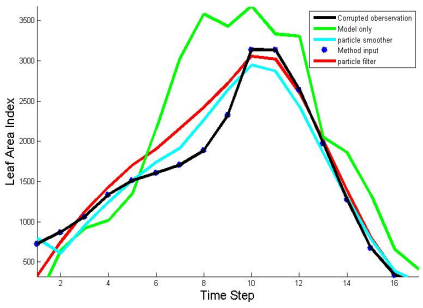

Fig. 2. Result of GreenLab with data assimilation applied to corrupted observation sequence. Dark line are corrupted MODIS observation, red line is the result of GreenLab with particle filter, cyan line from particle smoother, and green line from model only.

The goal of our application is to reconstruct leaf area sequence using GreenLab model with data assimilation methods from medium remote sensing observations, namely temporal series of MODIS images. The area of interested is in Brittany, France. MODIS took a multi-spectral snapshot at a time interval of 10 days, yielding a sequence of 36 observations at each location for a single year. Yet we are only interested on the growth process, which is centered on peak time in summer and extends about 170 days. For this period, leaf area index (LAI) sequences of cereal at various agricultural fields are computed with PROSAIL model and shown with the blue lines in Fig. 1. Because of the atmosphere disturbance and cloud occultation, MODIS data are quite noisy and sometimes even corrupted.

Even though we have significantly reduced the complexity of GreenLab model in our implementation, we still need to estimate three parameters that are r and k from Eq. 1 and α from Eq. 2. We have in practice estimated them automatically using non-linear least square method (Guo et al. 2006, Zhan et al. 2003) on input data. Examples of results are shown in Fig. 1 (a) where the red line is the result of GreenLab with fitted parameters from a set of series.

Tab. 1. Sum of square error (SSE) from different methods at various situation for synthetic data

	Model	**Observe**	**Filter**	**Smoother**	**Sparse**	**Missing**
SSE	346.1	288.6	80.75	70.40.	113.7	293.2

However in practice, because of some problems in the acquisition (aerosols, clouds, etc.), remote sensing data are often noisy and sometimes corrupted. From this noisy & corrupt data, the reconstruction of the LAI is performed using data assimilation. We have tested two variations of stochastic methods: particle filter and particle smoother. Results are shown in Fig. 2 (b). The dark line is a sample of MODIS input data. If we only had the probabilistic GreenLab model (prior knowledge), the green line would be the result we could obtain. After a data assimilation process that combines model (green line) and observations (dark line), the red and cyan lines can be extracted and respectively correspond to the results of particle filter and smoother. From a visual inspection, the data assimilation methods have extracted interesting results. From a quantitative point of view, we have applied our algorithms on synthetic data. The synthetic noisy observation data are generated by adding gaussian noise to a real and uncorrupted observation and by randomly removing 10 points, yielding a time series of 7 points instead of 17. Quantitative results are shown in Tab. 1. As one can observe, the sum of square error (SSE) of corrupted observation is large and this error reduces with assimilation techniques, yielding the particle smoother very efficient.

REFERENCES

Bonet J, Lok T.S. 1999. Variational and momentum preservation aspects of smooth particle hydrodynamic formulations. *Computer Methods in applied mechanics and engineering*. **180(1)**:97-115.

Evensen G. 1994. Sequential data assimilation with a nonlinear quasi-geostrophic model using Monte Carlo methods to forecast error statistics. *Journal of Geophysical Research-All Series*, **99**:10-10.

Evers JB, Vos J, Fournier C, Andrieu B, Chelle M, Struik PC. 2007. An architectural model of spring wheat: evaluation of the effects of population density and shading on model parameterization and performance.. *Ecological Modelling*, **200**:308-320.

Guo Y, Ma YT, Zhan ZG, Li BG, Dingkuhn M, Luquet D, de Reffye P. 2006. Parameter optimization and field validation of the functional-structural model GreenLab for maize. *Annals of Botany* **97**:217-230.

Jacquemoud S, Verhoef W, Baret F, Bacour C, Zarco-Tejada P.J, Asner G.P, François C, Ustin S.L. 2009, PROSPECT + SAIL models: a review of use for vegetation characterization. *Remote Sensing of Environment*, **113**:S56-S66.

Nummiaro K, Koller-Meier E, Van Gool L. 2003. An adaptive color-based particle filter. *Image and Vision Computing*, **91(1)**:99-110.

Yan HP, Kang MZ, de Reffye P, Dingkuhn M. 2004. A dynamic, architectural plant model simulating resource dependent growth. *Annals of Botany* **93**:591-60.

Zhan ZG, Wang YM, de Reffye P, Wang BB, Xiong FL. 2003. Fitting a functional-structural growth model with plant architectural data. In: Hu BG, Jaeger M, eds. *Plant growth modeling and application*, Beijing: Tsing Hua University Press/Springer-Verlag, 108-117.

GROWTH AND DEVELOPMENT OF PLANT COMMUNITIES

Proceedings of the 7th International Conference on Functional-Structural Plant Models, Saariselkä, Finland, 9 - 14 June 2013. Eds. Risto Sievänen, Eero Nikinmaa, Christophe Godin, Anna Lintunen & Pekka Nygren. http://www.metla.fi/fspm2013/proceedings. ISBN 978-951-651-408-9.

Plant structure in crop production: considerations on application of FSPM

Jan Vos and **Jochem B. Evers**
Centre of Crop Systems Analysis, Wageningen University, PO Box 430, 6700 AK Wageningen, the Netherlands
**correspondence:* jan.vos@wur.nl

Highlights: Cereals, potato and glasshouse cut rose, representing monocot annuals, vegetative propagated dicot annual and woody perennials, have different structural development. 'Bud break', initiating tillering (monocots) and branching (dicots) is a key process determining plant structure. Plant population density is affecting bud break in each of these three species. The mechanisms explaining these observations and the application in models will be discussed, primarily carbon source : sink ratio and light quality (i.e. red : far red ratio.

Keywords: barley, maize, wheat, potato, cut rose, carbon source sink, red : far red ratio

INTRODUCTION

Growers apply crop management measures that modulate crop structure in order to influence the yield and properties of the produce, e.g. the size distribution. Examples of the latter are grain size distribution of malting barley, tuber size distribution in potato and length and diameter of flower shoots in glasshouse cut roses. Management starts already with decisions on planting density and plant configuration. In cereals, the desired degree of tillering has always been a subject of discussions on the preferred ideotype. Understanding plant structure, how it comes about, how it can be manipulated are therefore key questions in production-oriented plant sciences. Plants can modulate their structure by adaptation of sizes of individual organs, but more importantly by a variable degree of tillering (cereals, grasses) or branching (dicots). Insight in the mechanisms determining the degree of branching and tillering is a central issue for modelling plant structure. A special, but so far virtually neglected issue is the variation among individuals and if this degree of variation can be explained and perhaps managed.

The objectives of this paper include (i) to highlight the essential features of structural development of some different crop species, (ii) summarize the main factors determining the degree of tillering and branching, (iii) address the concepts used to model tillering and branching, using functional-structural plant models (FSPM). Endeavours to construct FSPMs reveal knowledge gaps on the one hand, and if solved or circumvented, provide the opportunity to analyze how organ properties evolve from ontogeny and plant plasticity and how management could make a difference in properties of organs, e.g. size distributions. FSPM can improve our understanding of the efficacy of management options.

This paper is limited to cereals, i.e. maize (*Zea mays*) and the small grain species barley (*Hordeum vulgare*), wheat (*Triticum aestivum*) and rice (*Oryza* spp.), as opposed to potato (*Solanum tuberosum*) and glasshouse cut rose (*Rosa hybrida*); cereals being representatives of monocotyledonous annual species, potato representing vegetatively propagated dicot annual species and cut rose representing dicot perennial species.

STRUCTURAL DEVELOPMENT OF CEREALS, POTATO AND CUT ROSE

Early work on the development of FSPM to field crops dealt with describing the structural development of maize in a model called ADELmaize (Fournier and Andrieu, 1999). Maize does not produce tillers under practical conditions, simplifying modelling of the structural development. The main issues were (i) quantifying the plastochron, the phyllochron, and the size distributions of the leaf blades, leaf sheaths and internodes (if extended).

Though temperature is the dominant driver of rate of development, it appeared that plant population density (Andrieu et al., 2006) and level of irradiance (Bos et al., 2000) affected the rate of development in maize. Andrieu and Fournier postulated that initiation, extension, and appearance of successive organs are highly coordinated processes, where environmental effects on rate and/or duration of one component process has consequences for the timing of all succeeding developmental events.

The structural analysis applied to maize was also applied to wheat (Fournier et al., 2003, Evers et al.,

2005), barley (Buck-Sorlin et al., 2007) and rice (Xu et al., 2011). In these small grain cereals the degree of tillering is a prime mechanism to adapt plant structure to available resources. Fundamental insight in the regulation of tillering is key to adequate modelling of canopy structure and the consequences for issues such as grain size distribution.

The potato tuber can be regarded a stack of swollen phytomers, with axillary buds, called 'eyes', in phyllotactic arrangement on the tuber's surface. Stems arising from a bud are called main stems. The structure of a potato plant is primarily determined by the number of main stems per plant. That number depends on many factors including number of eyes per planted tuber and fraction bud break. The second main determinant of the structure of the crop is branching. Buds in leaf axils just below and above the soil surface can break to produce basal lateral branches (Vos, 1995). The main stem apex produces a terminal inflorescence. Apical branching is of sympodial nature with apical branches commonly occurring from the axils of the second and third leaf below the flowers. Two primary apical branches can produce four secondary branches, which could produce eight tertiary branches, etc. The basal laterals can also produce inflorescences and apical laterals, adding to the complexity of the structure.

Rose crops commonly start from nodal cuttings. The primary shoot is commonly bent down near the time it would flower. It will branch in horizontal direction; any upright growth being re-bent or removed. The 'bent canopy' that develops in this way serves as a source of assimilates for vertically growing shoots which are harvested and sold. Axillary shoots emerging from the base of the primary shoot, called bottom breaks, form the basis of the woody structure from which vertically growing harvestable flower canes emerge continuously over 4-7 years. When a flower cane is harvested, commonly a shoot remainder is left with some nodes and axillary buds. Variable fractions of buds below the cut end may break and produce new shoots. When new shoots grow from shoot remainders of the preceding harvested shoot, each new generation of harvested flowers originates from a next higher level of branching. This is associated with intrinsically thinner shoots than the previous harvest. At 'some stage' the grower will decide to cut back the structure to stimulate branching from buds on lower orders of branching. Managing the crop so as to achieve continuous production of shoots of the desired dimensions is a complicated game involving management of woody structure, the number of shoots allowed to grow and glasshouse climate. There are practical experiences how to do this, but there is no solid theory explaining how a grower can achieve his/her objectives at minimum interference, i.e. at minimum cost.

MODELLING CROP STRUCTURE

The plant species considered, cereals, potato and cut rose, differ in many morphological and physiological respects. For cereals, concepts for modelling structural development are most advanced, allowing quite accurate prediction of the time when a next leaf or a next tiller will appear, *if* it is going to appear. For rose there is a prototype structural model (Buck-Sorlin et al., 2011) and for potato there is interest to develop it. Apart from simulating adaptation in organ sizes, the common challenge is to design concepts when buds will grow out to become a tiller or branch. In general, the number of tillers or branches declines with increase in plant population density. This is true in cereals (Darwinkel, 1978, Evers et al., 2006) and potato (Vos, 1995) and likely in rose (Wubs et al., in preparation). Ample availability of nitrogen (N) stimulates tillering (Longnecker et al., 1993) and branching (Vos, 1995). Soil N and P (phosphorus) as well as red : far red ratio of light in the canopy affect the plant's hormonal signalling system controlling bud break (Domagalska and Leyser, 2011). Experimental evidence shows that the degree of tillering responds to the imposed red : far red ratio of the light regime (Casal et al., 1987, Skinner and Simmons, 1993). Literature search did not yield information on effects of red : far red ratio on (basal) branching of potato. In rose explants far-red illumination inhibited bud break, whereas red, blue and white light promoted bud break (Girault et al., 2008). When whole rose plants were illuminated with higher red:far-red ratios, more buds sprouted (Mor and Halevy, 1984). However, Wubs et al. (in preparation) did not find such effects of red and far-red on bud break in rose; higher irradiance on buds was associated with more bud break rather than spectral composition of light absorbed by the bud.

Information from 'dose – response experiments' on factors affecting bud break can generally not be used directly in mechanistic modelling. A mechanism explaining the observations has to be deduced using insights from physiology. Effects of plant population density fuelled the idea that trophic relations determine branching and tillering: with more plants growing per unit area, less light can be absorbed and fewer assimilates produced per plant. Too many sinks (growing organs) and associated low levels of available carbohydrate per sink would act as, or be translated into, signals precluding further bud break. The effect of

nitrogen could fit in this picture, because N limitation feeds back on assimilate production per plant, i.e. source capacity. Many models use, with variable degree of conviction, carbon source-sink ratios as a regulator to simulate aspects of growth and development, e.g. the Greenlab series (Ma et al., 2008). Evers et al. (2007) used a reaction norm of bud growth to red : far red ratio to simulate cessation of tillering, but this descriptive approach needs mechanistic substantiation. Detailed models simulating bud break as emergent from internal hormonal interactions and external environmental cues may yield rules that can be implemented in plant and crop models (Evers et al., 2011). In rose, in spite of much effort (Girault et al., 2008), no consistent concept was found to model bud break in crop situations (Buck-Sorlin et al., 2011; Wubs et al., in preparation). Do we need paradigm shifts to make progress?

LITERATURE CITED

Andrieu B, Hillier J, Birch C. 2006. Onset of sheath extension and duration of lamina extension are major determinants of the response of maize lamina length to plant density. *Annals of Botany,* **98**: 1005-1016.

Bos HJ, Tijani-Eniola H, Struik PC. 2000. Morphological analysis of leaf growth of maize: responses to temperature and light intensity. *NJAS - Wageningen Journal of Life Sciences*, **48**: 181-198.

Buck-Sorlin G, de Visser PHB, Henke M, Sarlikioti V, van der Heijden GWAM, Marcelis LFM, Vos J. 2011. Towards a functional–structural plant model of cut-rose: simulation of light environment, light absorption, photosynthesis and interference with the plant structure. *Annals of Botany,* **108**: 1121-1134.

Buck-Sorlin G, Kniemeyer O, Kurth W. 2007. A grammar-based model of barley including virtual breeding, genetic control and a hormonal metabolic network. In: Vos J, L.F.M. Marcelis, P.H.B. de Visser, P.C. Struik, J.B. Evers ed. *Functional-structural plant modelling in crop production.* Dordrecht, Springer.

Casal JJ, Sáchez RA, Deregibus VA. 1987. Tillering Responses of Lolium multiflorum plants to changes of red/far-red ratio typical of sparse canopies. *Journal of Experimental Botany,* **38**: 1432-1439.

Darwinkel A. 1978. Patterns of tillering and grain production of winter wheat at a wide range of plant densities. *Netherlands Journal of Agricultural Science,* **26**: 383-398.

Domagalska MA, Leyser O. 2011. Signal integration in the control of shoot branching. **12**: 211-221.

Evers JB, van der Krol AR, Vos J, Struik PC. 2011. Understanding shoot branching by modelling form and function. *Trends in Plant Science,* **16**: 464-467.

Evers JB, Vos J, Andrieu B, Struik PC. 2006. Cessation of tillering in spring wheat in relation to light interception and red : far-red ratio. *Annals of Botany*, **97**: 649-658.

Evers JB, Vos J, Chelle M, Andrieu B, Fournier C, Struik PC. 2007. Simulating the effects of localized red:far-red ratio on tillering in spring wheat (*Triticum aestivum)* using a three-dimensional virtual plant model. *New Phytologist,* **176**: 325-336.

Evers JB, Vos J, Fournier C, Andrieu B, Chelle M, Struik PC. 2005. Towards a generic architectural model of tillering in Gramineae, as exemplified by spring wheat (*Triticum aestivum*). *New Phytologist,* **166**: 801-812.

Fournier C, Andrieu B. 1999. ADEL-maize: an L-system based model for the integration of growth processes from the organ to the canopy. Application to regulation of morphogenesis by light availability. *Agronomie,* **19**: 313-327.

Fournier C, Andrieu B, Ljutovac S, Saint-Jean S. 2003. ADEL-wheat: a 3D architectural model of wheat development. In: Hu BG, Jaeger M eds. *International Symposium on Plant Growth Modeling, Simulation, Visualization, and their Applications.* Beijing, China PR, Tsinghua University Press / Springer.

Girault T, Bergougnoux V, Combes D, Viemont J-D, Leduc N. 2008. Light controls shoot meristem organogenic activity and leaf primordia growth during bud burst in *Rosa* sp. *Plant, Cell & Environment,* **31**: 1534-1544.

Longnecker N, Kirby EJM, Robson A. 1993. Leaf emergence, tiller growth, and apical development of nitrogen-deficient spring wheat. *Crop Science,* **33**: 154-160.

Ma Y, Wen M, Guo Y, Li B, Cournede P-H, de Reffye P. 2008. Parameter optimization and field validation of the functional-structural model GREENLAB for maize at different population densities. *Annals of Botany,* **101**: 1185-1194.

Mor Y, Halevy AH. 1984. Dual effect of light on flowering and sprouting of rose shoots. *Physiologia Plantarum,* **61**: 119-124.

Skinner RH, Simmons SR. 1993. Modulation of leaf elongation, tiller appearance and tiller senescence in spring barley by far-red light. *Plant, Cell & Environment,* **16**: 555-562.

Vos J. 1995. The effects of nitrogen supply and stem density on leaf attributes and stem branching in potato (*Solanum tuberosum* L.). *Potato Research*, **38**: 271-279.

Xu L, Henke M, Zhu J, Kurth W, Buck-Sorlin G. 2011. A functional–structural model of rice linking quantitative genetic information with morphological development and physiological processes. *Annals of Botany,* **107**: 817-828.

Proceedings of the 7th International Conference on Functional-Structural Plant Models, Saariselkä, Finland, 9 - 14 June 2013. Eds. Risto Sievänen, Eero Nikinmaa, Christophe Godin, Anna Lintunen & Pekka Nygren. http://www.metla.fi/fspm2013/proceedings. ISBN 978-951-651-408-9.

Re-parametrisation of Adel-wheat allows reducing the experimental effort to simulate the 3D development of winter wheat

Mariem Abichou[1], Christian Fournier[2], Tino Dornbusch[1], Camille Chambon[1], Rim Baccar[1], Jessica Bertheloot[3], Tiphaine Vidal[1], Corinne Robert[1], David Gouache [4], Bruno Andrieu[1,*]

[1] INRA, AgroParisTech, UMR1091 EGC, F-78850 Thiverval-Grignon, France, [2] INRA, SupAgro, UMR759 LEPSE, F-34090 Montpellier, France, [3]INRA, AgroCampus Ouest, UMR1345 IRHS, F-49071 Beaucouzé Cedex, [4]ARVALIS-Institut du végétal, Service GPP, F-91405 ORSAY CEDEX, France

[*] Correspondence: andrieu@bcgn.grignon.inra.fr

Highlights: A parameterisation of wheat architecture was developed, having high flexibility to simulate contrasted genotypes and growth conditions with a reasonably low number of parameters. Field measurements at 4-5 dates allowed to simulate crops from emergence to maturity with a good agreement between simulated and measured ground cover and GAI. Dynamics of leaf angles were shown to impact strongly ground cover.

Keywords: 3D modelling, parameterisation, tillering, architecture, phyllochron, geometry

INTRODUCTION

Functional-structural plant models (FSPM) simulate plant development and growth, by combining models of physiological and developmental processes within a representation of the three-dimensional (3D) structure of plants. Structural 3D plant models rather aim at mimicking the dynamics of plant and crop structure based on experimental data. Structural 3D plant models, interfaced with physical models, can be used as tool to investigate how plant structure modulates various processes such as emission, deposition and transfer of biotic (e.g. fungal spores) and abiotic entities (e.g. water, light, pesticides) in the canopy. In this paper, we focus on improvement and validation of Adel-wheat (Fournier *et al*., 2003), which is a structural model of winter wheat. Adel-wheat is based on a small set of coordination rules relating organ extension patterns with leaf emergence patterns, and a rather detailed and extensive set of parameters describing plant architecture at the individual organ level. It allows simulating the dynamics of wheat architecture over time, with flexibility allowing to represent morphological differences between genotypes and plasticity in response to growth conditions. Still the model requires intensive field data acquisition and had not been carefully assessed for the properties of the simulated canopies. In this work we: (i) set up a new parameterisation to improve the compromise between flexibility and complexity, (ii) assessed the quality of the model (iii) defined a protocol for acquisition of experimental data and (iv) implemented a routine to estimate model parameters and input variables from experimental data.

METHODOLOGY

Developing and improving Adel-wheat parameterisation

Adel-wheat uses a coordination scheme of organ extension, senescence and disappearance in which the beginning and the end of events for each botanical module (lamina, sheath, and internode) are determined by the Haun Stage dynamic (HS) and the shoot senescence index (SSI). The dynamics for HS and SSI for each axis need to be provided as input in the model; just like functions representing dimensions of the fully developed organs depending on their position on the axis. Based on a set of experiments representing various cultivars, cultural practices (sowing date, planting density, and fertilization) and climatic conditions, we defined more synthetic parameterisations of the HS, the SSI, the dynamic of tiller population, the axis final leaf number and the final organ dimensions. For tillers, the dynamics of organ extension and senescence and dimensions of mature organs are derived from those simulated on the main stem. All dynamics are expressed in thermal time, which can be calculated taking into account either a linear or a non-linear temperature response. The objective of the new parameterisation was to keep sufficient flexibility to be fitted in a large range of plasticity whilst keeping the number of parameters reasonably low (3-6 for each aspect). We also seek at proposing parameters that have simple interpretation and are easy to derive from field measurements.

The Haun Stage dynamic HS(τ) over the growth cycle was either linear with a constant phyllochron or bilinear with a break-point. The HS sub-model allows for these two possible behaviours (Fig.1). Depending on HS behaviour, either four or five parameters are required to calibrate the model, taking into account both main stem and tillers.

The Shoot Senescence Index (SSI) describes the number of senescent leaves on an axis. We defined a simple empirical description of leaf senescence in which the SSI dynamic is derived from the number of green leaves GL(τ) and the Haun Stage: SSI(τ)= HS(τ) - GL(τ). As a prerequisite, we need to know HS(τ) and 6 parameters have to be measured to calibrate GL(τ). Fig.1 illustrates this parameterisation.

Tillers are divided into cohorts according to their date of emergence, which is synchronized with MS leaf emergence. When a primary tiller exists, the conditional probability of emergence of a secondary tiller is taken equal to those of a primary tiller of the same cohort. The number of active tillers decreases linearly during the phase of fast internode elongation: the youngest tillers stop first. Consequently, the number of active axes follows a curve with 4 phases. The parameters to calibrate this sub-model are: the emergence probabilities of primary tillers, the number of elongated internodes and the number of ear-bearing tillers.

Dimensions of mature organs on tillers are derived from those on the main stem. For this, we defined correspondence functions based on to the date of phytomer emergence and/or the position of the phytomer along the axis (Fig.2). The variables required as input are the dimension of main stem organs (laminas, sheath, internode, peduncle, and ear).

Leaf curvature is not parameterised with a mathematical function: the model select leaf curvatures in a database of measured ones. The function used for this could however be re-parameterised. In the previous version, selection within the leaf curvature database, depended only of the phytomer position along the axis. In this work, we showed that leaf curvature varies significantly not only with leaf position but also with phytomer age. In the new version, both leaf position and leaf age are considered in the selection function (Fig.3).

A reference experiment for model evaluation

The winter wheat cultivar *T. aestivum* 'Maxwell' was sown with typical agronomic conditions (220 plants/m², sowing on October, 26th of 2010). Plants were grown under non limiting conditions of water and nutrients and kept free of disease and weeds. The layout includes four blocs treated as repetitions. Two types of data were collected: data at plant scale that were used as input in the model, and data at crop scale used to evaluate the model by comparing them with simulations. Data collection included 3 parts: First, sixty tagged plants were followed weekly to estimate: (i) kinetics of laminas leaf extension and senescence, (ii) organ final size (laminas, sheath, internode, peduncle and ear) (iii) evolution of active axes number. Second, destructive samplings were carried out at 6 dates in order to complement the dataset of dimension and to calculate variables at crop level (leaf and global area index: GAI and LAI). Geometric data (leaf shape and curvature) are also collected for each date. Third ground cover (GC) photographs were taken weekly with two angle of view: vertical (0°) and oblique (57.5°).

The simplified experimental protocol

We (i) defined an experimental protocol that minimizes the measurement effort and allow estimating the required parameters and (ii) developed an application that generates Adel-wheat detailed input based on the parameters values. Finally the procedure allows for simulating the 3D crop dynamics from emergence to grain maturity by only performing detailed measurements at four dates: HS=4~5, 1 node, 2 nodes and flowering, plus simple measurements of green leaf number at one or two dates during grain filling. Measured data consist in: HS, SSI and organ dimension of MS, probability of primary tiller appearance, final axis number and the moment of start elongation and flowering. Detailed evaluation of this application will be presented in the oral communication.

RESULTS

The parameterisations that had been defined with the large set of experimental conditions could be fitted to represent with a high degree of accuracy the plant behaviour observed in the reference experiment. The figures below illustrate results relative to parameterisation of: the dynamic of Shoot Senescence Index (Fig.1) and the length of laminas (Fig.2).

When comparing simulated GAI and gap fraction dynamics with field measurements, differences were within the range of experimental errors. Figure 3 illustrates the importance of leaf curvature dynamic. Pooling leaf curvature data independently of leaf age resulted in significant deviations between model and simulations that vanished when data of leaf curvature were separated according to leaf age.

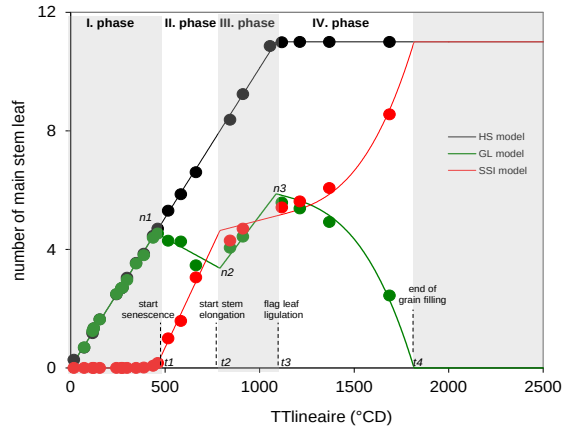

Fig.1. Dynamic of leaf number vs. thermal time for a main stem. Lines represent the parameterisation: total (HS, black), green (GL; green), senescent (SSI; red). Background (white/grey) shows the phases of senescence. I: No senescence. II: linear decrease of GL until stem elongation. III: linear increase in GL until flag leaf ligulation. IV: polynomial function for kinetics of GL after flowering. Dots show measurements in the reference experiment; each dot is a median calculated over 60 plants.

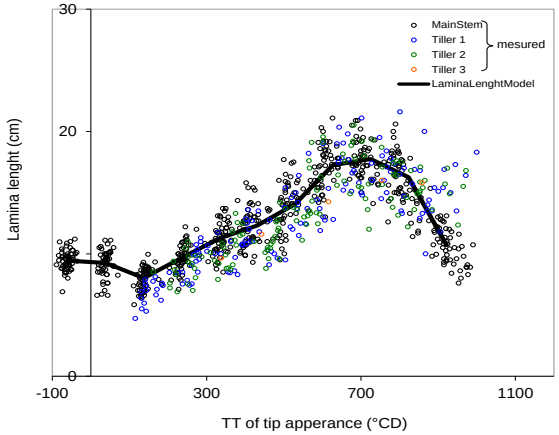

Fig.2. Length of fully developed laminas vs. thermal time of tip appearance; black line represents the function fitted to main stem data and symbols represent length of individual laminas of main stem (black), tiller 1 (blue) and tiller 2 (red) measured during the reference experiment. A same curve could be used for the main stem and tillers.

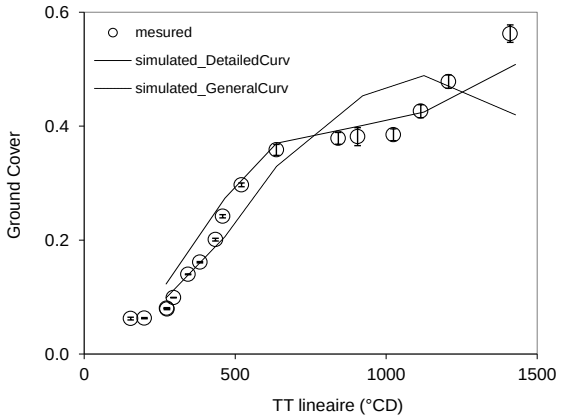

Fig.3. Ground cover vs. thermal time in the reference experiment; symbols represent measurements. Lines represent model simulation using (i) collections for leaf curvature depending on position and age of the leaf (solid line) or (ii) collections of leaf curvature depending on leaf position but pooled independently of time after ligulation (dashed line).

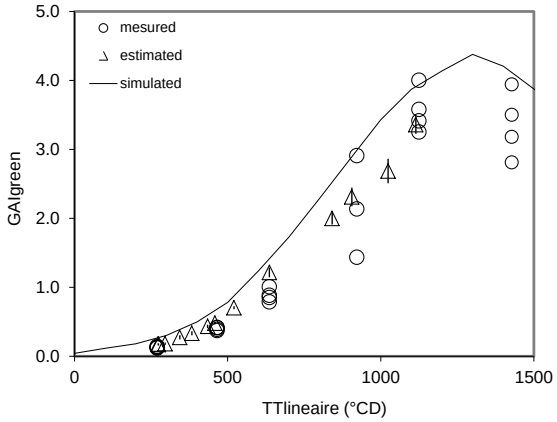

Fig.4. Global green area index vs. thermal time in the reference experiment; "o" represent direct measurements and "Δ"represent estimates from photographs at 57°. The line shows simulation with Adel-wheat virtual cover.

CONCLUSION

The major outcomes of this work are: (i) 3D reconstruction is now possible for the full cycle, from sowing to maturity; (ii) the protocol for data acquisition has been simplified and a routine was developed so that 3D simulations can be done in applied projects (Fournier et al 2013); (iii) the parameterization, while having the flexibility to be fitted to a wide range of conditions, was shown to be able to adjust a specific condition with a high accuracy; (iv) the leaf curvature dynamics after ligulation was shown to be an important variable that deserves further attention.

LITERATURE CITED

Fournier C, Andrieu B, Ljutovac S., Saint-Jean S, 2003. ADEL-wheat: A 3D architectural model of wheat development. In: Hu, B.-G., Jaeger, M. (Eds.), *Plant Growth Modelling and Applications, Proceedings of 2003 International Symposium.* Tsinghua University Press - Springer Verlag, Beijing, CHN pp. 54-63.

Fournier C, Pradal C, Abichou M et al., 2013. An integrated and modular model for simulating and evaluating how canopy architecture can help reducing fungicide applications. In these proceedings.

Proceedings of the 7th International Conference on Functional-Structural Plant Models, Saariselkä, Finland, 9 - 14 June 2013. Eds. Risto Sievänen, Eero Nikinmaa, Christophe Godin, Anna Lintunen & Pekka Nygren. http://www.metla.fi/fspm2013/proceedings. ISBN 978-951-651-408-9.

Perspectives for improving carbon and nitrogen allocation in forest models from stand to global scale

Oskar Franklin[1] & Peter M. van Bodegom[2]

[1]IIASA, International Institute for Applied Systems Analysis, Laxenburg, Austria, [2]VU University Amsterdam, department of Ecological Science, subdepartment of Systems Ecology, de Boelelaan 1085, 1081 HV Amsterdam, the Netherlands

Email for correspondence: franklin@iiasa.ac.at

Highlights: We show that using a fixed foliage: fine-root ratio leads to unrealistic modeled responses of forest growth to environmental variability (in particular to soil nitrogen availability). Not only the relative growth of organs (carbon allocation) will be off but also gross primary productivity predictions indirectly suffer from a lack of allocation flexibility. We suggest that applying evolution-based optimization principles to account for allocation plasticity is a key measure to improving future forest models and dynamic global vegetation models (DGVMs).

Keywords: Productivity, tree, uptake, N:C ratio, nitrogen concentration

INTRODUCTION

In times of rising atmospheric carbon dioxide, forest carbon (C) allocation has drawn interest due to its responsiveness and potential effect on the global carbon balance. The differences in lifespan and decomposition rates among tree organs, such as stems and leaves, imply that C allocation in trees strongly influences forest carbon cycling rates. Both productivity and allocation is often controlled by nutrient availability, in particular nitrogen (N) availability, pointing to the fundamental importance of C-N interactions. Whereas the importance of C allocation and its link to N availability is undisputed, there is little consensus on how it should be modeled. Consequently, allocation is the Achilles' heel of most forest models (Landsberg 2003; Le Roux et al. 2001). Although many promising approaches have been developed for the purpose of scientific insight, it is remarkable how rudimentary the representation of C allocation is in comparison to C assimilation (photosynthesis) in most applied forest models. For example, most dynamic global vegetation models (DGVMs) have fixed or only water-dependent C allocation (Ostle et al. 2009). While N limitation has now been included in a number of DGVMs, the underlying assumptions vary and are not always supported by proven mechanisms. For example, some models impose a sudden switch from C to N limitation if N supply does not meet demand set by C productivity. Others models let N limitation control photosynthesis via leaf N:C ratio, while linking N:C of all tissues through proportionality constants. While these assumptions serve to impose N limitation on growth they do not link N limitation to C allocation, although changes in C allocation is an important means for plants to equalize limiting effects of C and N. Another factor that influences allocation is the degree of competition (e.g. for soil N), which has never been considered in large scale models. However, it is not well known how all these potential shortcomings affect DGVM predictions and which aspects should be most urgently addressed.

In contrast to bottom-up and ad-hoc methods of adding N limitation and allocation to existing models, we suggest that plasticity (variability) in growth and allocation can only be properly understood -and therefore efficiently modeled- on the basis of the underlying principles that ultimately control plant behavior as a whole. These evolution-based principles can often be approximated by optimization assumptions (Franklin et al. 2012). Here we present a forest stand model based on well established structural and physiological assumptions assuming that the trees optimize N and C allocation to maximize fitness in response to environmental variables. We evaluated the importance of plasticity in C allocation and N:C ratio as well as the effect of competition for predictions of forest productivity at the stand level and globally.

MODEL

The model is based on a previous model (Franklin et al. 2009) used to explain the forest responses to elevated CO2 and N availability in free air carbon dioxide experiments (FACE). In this model trees respond to CO_2 and N availability by adjusting C allocation, canopy N content, and leaf area index (LAI).

Photosynthesis is modeled based on leaf N per area and photosynthetically active radiation (PAR). N uptake is a function of fine-root biomass and soil N availability. This model was extended to account for competition among trees for soil N (as done in Franklin et al. 2012), and plasticity in leaf- and wood N:C ratio, which influences N and C demands as well as the relationship between LAI and photosynthetic capacity. Wood N:C ratio was assumed to change in proportion to leaf N:C ratio.

To evaluate the importance of the three factors (i) leaf: root allocation plasticity, (ii) leaf N:C ratio responses, and (iii) root competition, we ran the model with and without each of these effects. The evaluation was done first for the Oak Ridge National Laboratory (ORNL) FACE forest based on data from Franklin et al. (2009) and, second, for potential GPP of a temperate forest stand (parameterized for ORNL FACE site) simulated globally based on gridded data (restricted to non water-limited forest covered grid cells) on PAR, day length, length of growing season, and soil N mineralization.

RESULTS AND DISCUSSION

Previous work has proven the valididty of the allocation optimization approach by predicting the observed C allocation shift from wood to fine-roots in response to elevated CO_2, and its reversal after N addition, in FACE experiments (Franklin et al. 2009). It was therefore not surprising that replacing allocation optimization with N:C ratio optimization made the model unable to capture the allocation patterns typically observed in response to changes in soil N availability (Fig. 1). More surprising is that this assumption also led to a much steeper response of GPP to soil N availability than if the trees are allowed to adjust allocation (Fig. 1a). Allowing optimization of leaf N:C ratio in addition to allocation optimization did not change GPP significantly, but it enhanced leaf growth response at low soil N availability (Fig. 1).

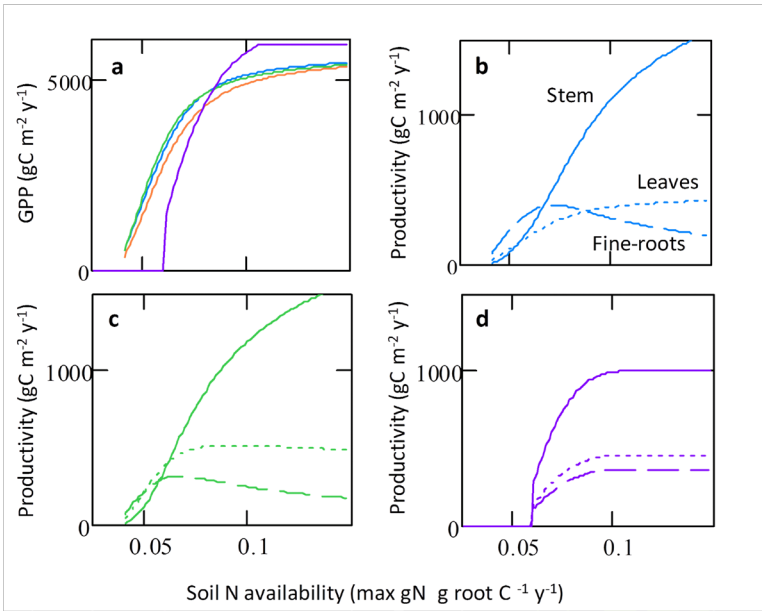

Figure 1. Modeled productivity as a function of soil N availability in the Oak Ridge National Laboratory Free Air Carbon dioxide Experiment (ORNL FACE) site, showing GPP (**a**) and growth of leaves, stem and fine-roots (**b-d**). Trees maximize net growth under alternative optimization variables: stem:leaves:root ratio (**b**-blue lines), stem:leaves:root ratio and leaf N:C ratio with and without root competition, respecetively (**c**-green lines, orange line), and leaf N:C ratio assuming fixed fine-root: foliage ratio (**d**-purple lines). Observed responses largely agree with model **b** and **c** (Franklin et al. 2009).

The global latitudinal analysis showed that assuming that trees acclimate to their environment only via their N:C ratio in foliage (and stem) leads to much stronger, and partly unrealistic, latitudinal variability in gross primary productivity (GPP) than if they are assumed to acclimate C allocation (Fig. 2). Furthermore, in this scenario the model was sometimes not able to find an optimal leaf N:C ratio within the range of realistic values (gaps in the purple line in Fig. 2). If allocation optimization was enabled, simultaneous optimization of leaf N:C had a relatively small additional impact, slightly moderating the latitudinal response. These results suggest that adjustment of C allocation is a much more important response to environmental conditions across a globally latitudinal range than adjustment of leaf (and wood) N:C ratios.

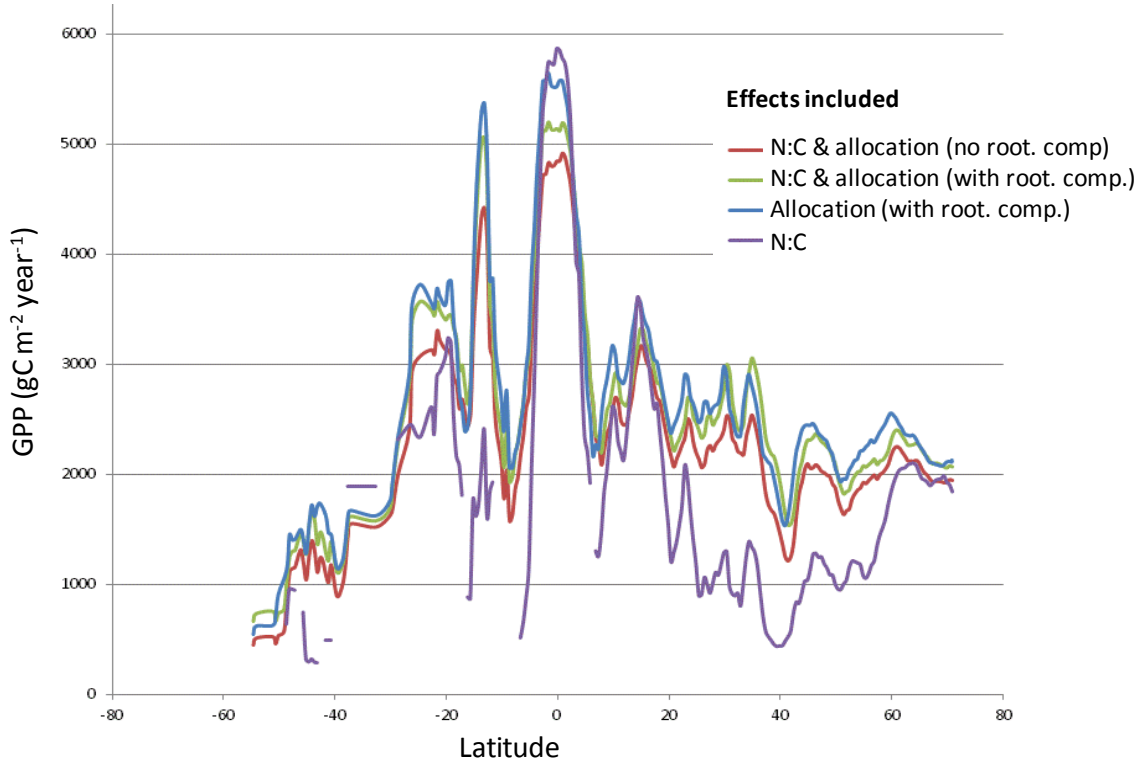

Figure 2. Potential gross primary productivity (GPP) of temperate broadleaf forest (parameterized for the Oak Ridge National Laboratory Free Air Carbon dioxide Experiment- ORNL FACE site) modeled for all grid cells (0.5 x 0.5 degrees) dominated by forest that are not significantly water-limited. The trees adjust to the environment (PAR, length of growing season, day-length, and soil N mineralization) by maximizing net growth (wood growth + reproductive production) by optimizing: leaf N:C ratio (purple line), C allocation (blue line), or leaf N:C and allocation including the effect of root competition (green line) or not (red line).

The inability of the model with fixed root:foliage ratio to match observed allocation patterns at the stand level point to the importance of flexible allocation in forest modeling, not only for growth of different organs but also for GPP (Fig. 1). The global level analysis suggest that this conclusion is relevant also for global modeling of GPP by showing a large effect of allocation optimization on the GPP response to a global latitudinal environmental gradient (Fig. 2). We suggest that applying evolution-based optimization principles to account for allocation plasticity should be a priority measure to improve future forest models and DGVMs, whereas plasticity in N:C ratios and root competition are of secondary importance.

REFERENCES

Franklin O, Johansson J, Dewar RC, Dieckmann U, McMurtrie RE, Brännström Å, Dybzinski R. 2012. Modeling carbon allocation in trees: a search for principles. Tree Physiology. **32**, 648-666.

Franklin O, McMurtrie RE, Iversen CM, Crous KY, Finzi AC, Tissue DT, Ellsworth DS, Oren R, Norby RJ. 2009. Forest fine-root production and nitrogen use under elevated CO2: Contrasting responses in evergreen and deciduous trees explained by a common principle. Global Change Biology. **15**, 132–144.

Landsberg J. 2003. Modelling forest ecosystems: State of the art, challenges, and future directions. Canadian Journal of Forest Research. **33**, 385-397.

Le Roux X, Lacointe A, Escobar-Gutiérrez A, Le Dizès S. 2001. Carbon-based models of individual tree growth: A critical appraisal. Annals of Forest Science. **58**, 469-506.

Ostle NJ, Smith P, Fisher R., Woodward F Ian, Fisher JB, Smith JU, Galbraith D, Levy P, Meir P, McNamara NP, Bardgett RD. 2009. Integrating plant-soil interactions into global carbon cycle models. Journal of Ecology. **97**, 851-863.

Proceedings of the 7th International Conference on Functional-Structural Plant Models, Saariselkä, Finland, 9 - 14 June 2013. Eds. Risto Sievänen, Eero Nikinmaa, Christophe Godin, Anna Lintunen & Pekka Nygren. http://www.metla.fi/fspm2013/proceedings. ISBN 978-951-651-408-9.

Photosynthesis, Transpiration and LAI: scale effects of spatial patterns

Moritz Kupisch[1], **Anja Stadler**[1], **Matthias Langensiepen**[1] and **Frank Ewert**[1]
[1]*Institute of Crop Science and Resource Conservation, Katzenburgweg 5, D-53315 University of Bonn, Germany*
**correspondence:* mkupisch@uni-bonn.de

Highlights: Field level fluxes of CO_2 and H_2O as well as LAI are highly dependent on the underlying spatio-temporal patterns of environmental factors. Process models at the field scale have to consider the interaction with distribution and spatial patterns of input parameters applied on different plant response processes at the underlying leaf- and canopy-level.

Keywords: Photosynthesis, transpiration, spatial heterogeneity, GECROS model, upscaling

INTRODUCTION

Exchange of CO_2 and water vapor between plant surfaces and the atmosphere are important processes that determine plant growth and yield. They are affected by changes in physical boundary conditions and their magnitudes differ greatly between plant species (Arora *et al*., 2001; Monti *et al*., 2006). The temporal variability of gas exchange in crops has been extensively studied (Reicosky *et al*., 1994; Mo and Liu, 2001; Wang *et al*., 2006), but less is known about its spatial variability in fields. Understanding the spatio-temporal variability of gas exchange is necessary for modeling and estimating the dynamics of soil-vegetation-atmosphere processes at field and larger scales. Most crop modeling efforts ignore the spatial variability of gas exchange and plant structural development processes within fields which are influenced by heterogeneous soil conditions. Detailed representations of plant physiological processes at a single point within a field are typically assumed to represent the entire field. Little work has been done on scaling up from the single point to the entire field, not least due to the limited availability of experimental data.

Observations in wheat and sugar beet field experiments carried out in Western Germany at Selhausen (50° 52′ N, 6° 26′ E) during the 2010 and 2011 vegetation seasons revealed strong spatial heterogeneities in CO_2 and H_2O canopy fluxes across the fields. While canopy measurements showed temporal variability with distinct diurnal and seasonal patterns, the temporal and spatial variability of leaf level photosynthesis and transpiration rates were comparably small. Further analyses suggested that the observed spatial and seasonal variability of canopy measurements were mainly caused by field heterogeneities in LAI and less by gas exchange rates per unit leaf area. However, both crops differed in their responses to drought stress. While wheat responded mainly through irreversible reduction in green leaf area, the canopy assimilation rate of sugar beets decreases only temporarily with no observed effects in LAI.

The obtained datasets from both years are the basis for parameterizing different plant and crop growth models with varying complexities at the point level. The study below focuses on simulation experiments which characterize the effects of up-scaling methods on field level fluxes and their interaction with distribution and aggregation of spatial patterns of input parameters applied to different plant response processes at the underlying leaf- and canopy-levels.

SIMULATIONS

The simulations comprise calculations of instantaneous photosynthesis (Farquhar model, Farquhar *et al*. 1980) and transpiration (Penman-Monteith equation, Monteith 1973) rates at leaf and cannopy scales as well as an application of the crop growth model GECROS (Yin and van Laar, 2005) over the whole season in dependance on spatially varying inputs. Each simulation was executed for six different spatial patterns (Fig. 1) with different edge lengths resolutions, ranging from a minimum value of 1 m to 280 m, which is the mean of the whole field. The patterns differ only in their spatial arrangement but not with respect to their underlying frequency distributions. The distribution of the general patterns range from 0 to 1 and are subsequently applied to specific ranges of temperature, PAR, leaf nitrogen content and VPD. During each simulation run, all other parameters were kept constant, i. e. no co-variation was analysed. For the simulations with the crop model, only the amount of daily water supply was used as a spatial input parameter. For each simulation scenario, the corresponding models were run for every square meter, i. e. at the lowest resolution size, whereas the output was calculated as a mean value of the total field per m^2.

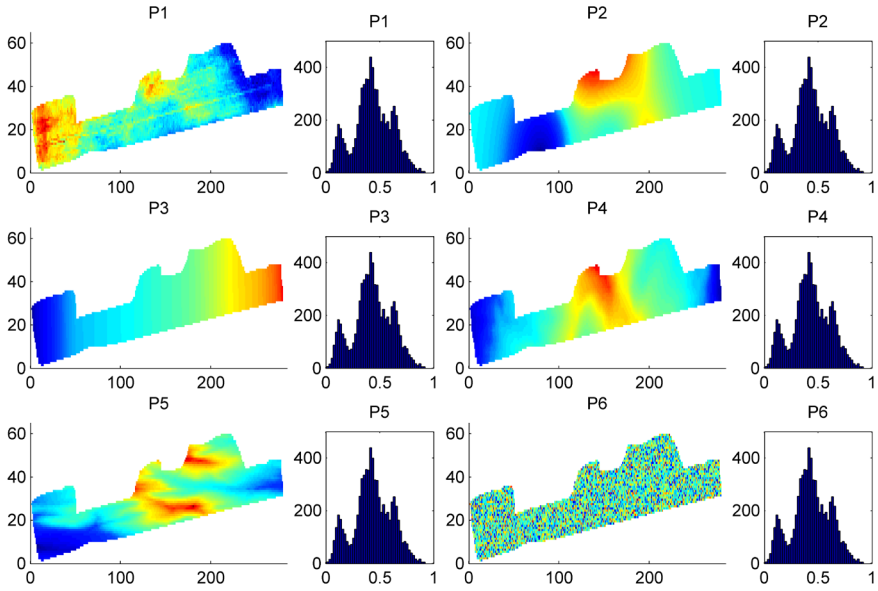

Fig. 1. Spatial patterns P1 – P6 with the same underlying frequency distribution applied to different parameters (temperature, VPD, daily water supply) used as inputs for models at the leaf-, canopy- and seasonal crop scale.

RESULTS AND DISCUSSION

Simulations resulted in highly fluctuating responses of photosynthesis, transpiration and LAI, depending on the aggregation of input parameter step-sizes (Fig. 2 and 3). The first and the last value of all scenarios were the same for all input patterns as they represented either the response to the original frequency distribution (cf. Fig. 1) or the mean of the total field. The values in between represented the response to the changed distribution due to the effect of aggregating different spatial patterns. Regarding fluxes of CO_2 and H_2O one could observe significant similarities in the courses relating to one input pattern, although applied to different parameters (temperature, VPD and water supply) and functional scale (leaf, canopy and crop growth). At the level of seasonal crop growth, the output patterns of maximum LAI were decoupled from the patterns of photosynthesis and transpiration. Model responses to other distributions showed also effects of spatial patterns, but with a different extent (not shown here). No effects of input aggregation has been observed if the response variable was linearily dependent on the input, e. g. leaf nitrogen content (not shown here).

Results indicated that it is important to consider field heterogeneity for parameterizing plant, crop and large-scale soil-vegetation-atmosphere-transport models. Moreover, the spatial pattern of a given distribution has a significant effect on overall field level fluxes. Ongoing work will focus on the interaction of spatial patterns and multiple input parameters with models of varying complexity.

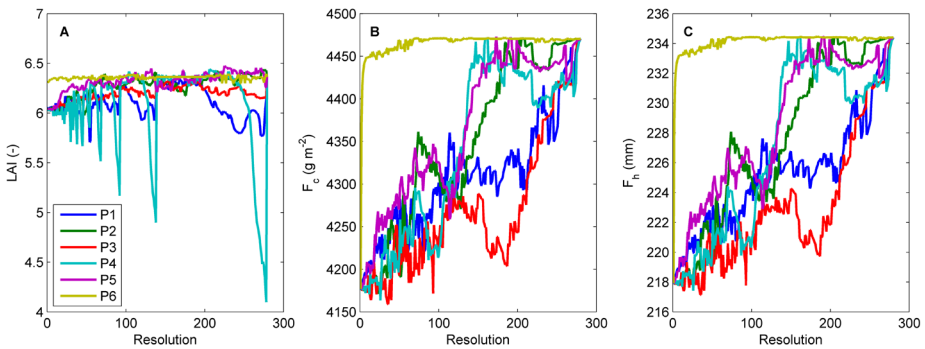

Fig. 2. Mean maximum LAI (A), mean cumulative gross canopy photosynthesis (B) and transpiration (C) as calculated by GECROS model in dependance on the resolution of the underlying input patterns applied to daily water supply.

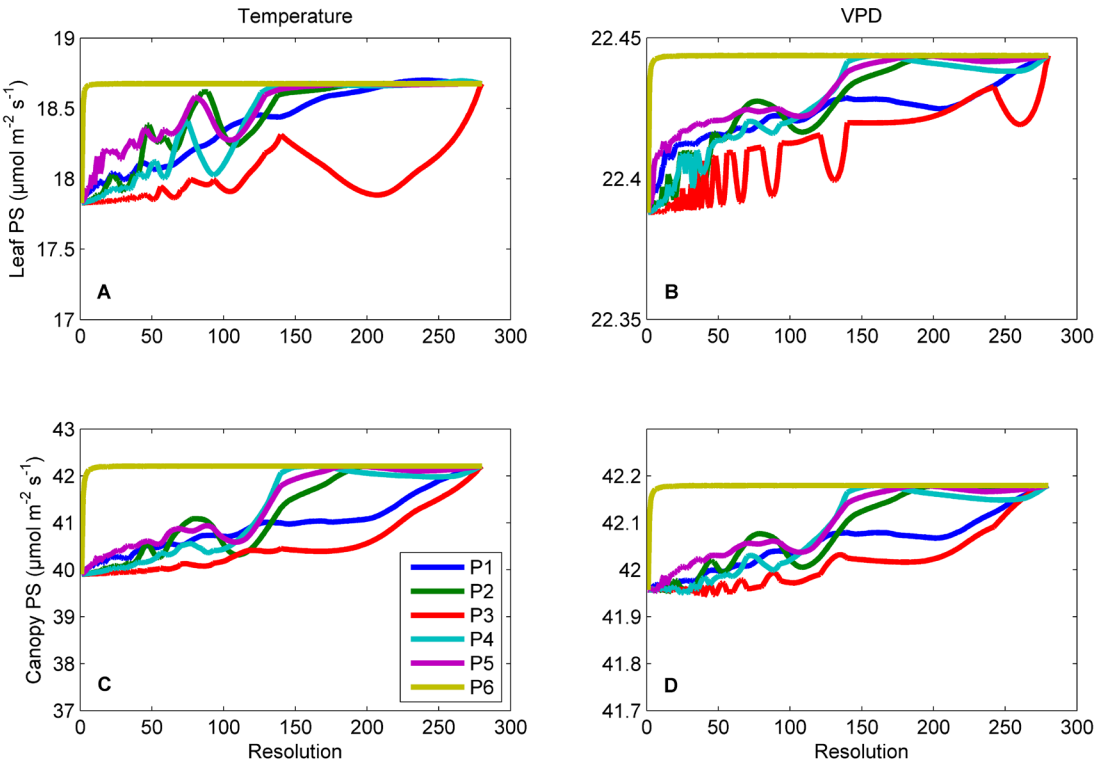

Fig. 3. Mean instanteneous leaf (A, B) and canopy photosynthesis (C, D) in dependance on the resolution of the underlying input patterns applied to temperature (A, C) and VPD (B, D).

LITERATURE CITED

Arora A, Singh VP, Mohan J. 2001. Effect of nitrogen and water stress on photosynthesis and nitrogen content in wheat. *Biologia Plantarum* **44**, 153–155.

Farquhar GD, von Caemmerer S, Berry JA. 1980. A biochemical model of photosynthetic CO_2 assimilation in leaves of C_3 species. *Planta* **149**, 78–90.

Mo X, Liu S. 2001. Simulating evapotranspiration and photosynthesis of winter wheat over the growing season. *Agricultural and Forest Meteorology* **109**, 203–222.

Monteith JL. 1973. Principles of environmental physics. *Edward Arnold, London*, 241 pp.

Monti A, Brugnoli E, Scartazza A, Amaducci MT. 2006. The effect of transient and continuous drought on yield, photosynthesis and carbon isotope discrimination in sugar beet (Beta vulgaris L.). *Journal of Experimental Botany* **57**, 1253–1262.

Reicosky DC, Brown PW, Moran MS. 1994. Diurnal trends in wheat canopy temperature, photosynthesis, and evapotranspiration. *Remote Sensing of Environment* **49**, 235–245.

Wang J, Yu Q, Li J, Li LH, Li XG, Yu GR, Sun XM. 2006. Simulation of diurnal variations of CO2, water and heat fluxes over winter wheat with a model coupled photosynthesis and transpiration. *Agricultural and Forest Meteorology* **137**, 194–219.

Yin X, van Laar HH. 2005. Crop systems dynamics. An ecophysiological simulation model for genotype-by-environment interactions. *Wageningen Academic Pub*.

Proceedings of the 7th International Conference on Functional-Structural Plant Models, Saariselkä, Finland, 9 - 14 June 2013. Eds. Risto Sievänen, Eero Nikinmaa, Christophe Godin, Anna Lintunen & Pekka Nygren.
http://www.metla.fi/fspm2013/proceedings. ISBN 978-951-651-408-9.

Plant diversity and drought

Magnus Lindh[1], **Lai Zhang**[1], **Daniel Falster**[3], **Mark Westoby**[3], **Oskar Franklin**[2] and **Åke Brännström**[1]
[1]*Department of Mathematics and Mathematical Statistics, 901 87 Umeå University, Sweden*
[2]*International Institute for Applied Systems Analysis, Schloßplatz 1, 2361 Laxenburg, Austria*
[3]*Department of Biological Sciences, Macquarie University, Sydney, NSW 2109, Australia*
**correspondence:* magnus.lindh@math.umu.se

Highlights: We find a phase transition from no species to a highly diverse community, as the drought mortality and water table sharpness increases, but this is not true for water table depth. The species richness is decreasing with drought mortality and water table depth, but not with water table sharpness. Thin crown and intermediate values of photosyntetic efficiency (i. e. productivity) has the highest diversity.

Keywords: root, shoot, evolution, adaptive dynamics, drought

INTRODUCTION

Extreme temperatures and droughts will cause a loss of plant species according to recent studies (Thuiller et al. 2005). Water limitation is a severe obstacle for plant growth and survival. Droughts can cause irreparable damages as air enters the water transportation system, in a process known as cavitation. One way to avoid such damages is that the plant invests in a deep root, a so called taproot.

The conditions for coexistence for plants in a dry environment has not received much attention. Here we extend a static shoot model by Iwasa et al. (1984) with a taproot, able to reach for deep water, and we investigate the model with the techniques of adaptive dynamics. The deep soil water abundance, or potential, is increasing with depth corresponding to a situation often encountered in regions with drought. A taproot reduces mortality, but it is also costly, so investing in a taproot is a strategy with a trade-off.

We find that the shoot and root can coevolve to a common evolutionarily stable strategy (ESS). For the shoot, evolutionary divergence is possible only for large mutational steps. For the root we find one stable strategy, one unstable strategy, and one stable strategy with no root. Surprisingly the stable strategy with a root can result in a larger shoot than the strategy without a root. Deeper soil water levels tend to decrease diversity but more unexpectedly we find a phase transition from zero diversity to high diversity as the drought mortality increases.

SIMULATIONS

We extend the Iwasa el al. (1985) model with a root, which has a quadratic cost like in the original model. There is no competition (or in other words density dependence) for the root. The depth of the root is reducing the non-density dependent mortality from droughts. The reduction is modelled with a logistic function, with initially very low reduction in mortality, an intermediate reduction in mortality when the roots reach the ground water table, and a high reduction at greater depths. Our model has two traits: height of the shoot and depth of the roots. We are interested in the conditions for coexistence and evolutionary divergence.

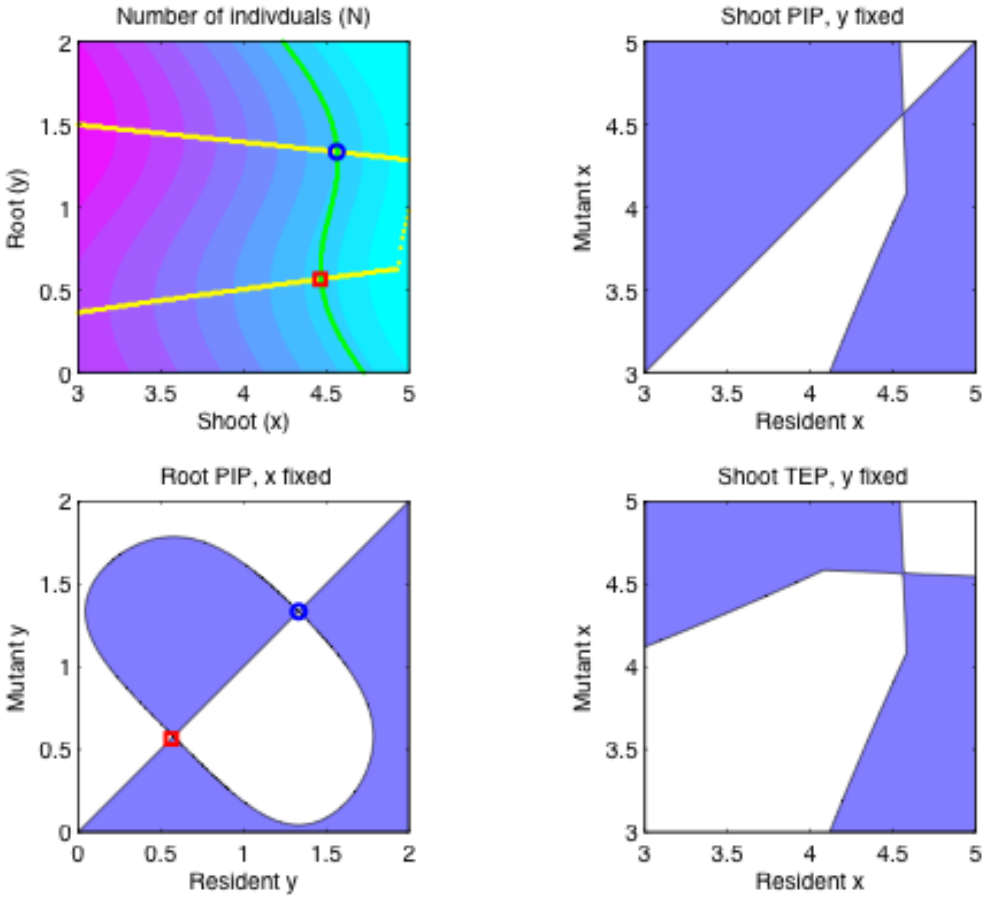

Fig. 1. Isoclines of shoot (green) and root (yellow) plotted on top of the number of individuals (top left). The stable (blue circle) and unstable (red square) intersection of the isoclines is marked in the root PIP (bottom left). The shoot PIP (top right) is always convergence stable, but not evolutionarily stable for large steps. The coexistence area is marked blue in the shoot TEP (bottom right).

We use graphical methods to investigate the evolutionary dynamics of our model. A standard tool used in adaptive dynamics is the pairwise invisibility plot (PIP). In this plot the invasion fitness F of a mutant strategy in the presence of a resident strategy is marked either as positive or negative. In the PIP's in Fig. 1 we have marked the positive invasion fitness as blue, and the negative invasion fitness as white. Along the diagonal, when the resident strategy is equal to the mutant strategy we have a zero invasion fitness. A singular evolutionary strategy is easily found in the PIP (Geritz 1998). The singular strategy could be either convergence stable or unstable. If we have a convergence stable strategy (CSS), evolution will move towards this strategy, and if it is convergence unstable evolution will be repelled by this strategy. Once evolution reaches the CSS it can stop there, in this case we have an evolutionarily stable strategy (ESS), or diverge into two new stable strategies. In the root PIP in Fig. 1 the stable point (ESS+CSS) is marked with a green circle and the unstable point with a red square. There is also a stable strategy with no root but this is not marked in the figure, since it is just the point at origo. For the shoot we only find one convergence stable strategy (CSS). This strategy is an ESS for small mutational steps but not for large mutational steps, as can be seen in the blue coexistence area in the shoot trait evolutionary plot (TEP) in Fig. 1 (bottom right). In the TEP the PIP is flipped along the main diagonal and superimposed on the original PIP and the points where both the original and the flipped PIP's are positive are marked as positive (blue) or negative (white). By tracing the singular strategies of one trait as the other trait is varied we can draw isoclines for the traits. When the isoclines cross we have a common singular point for both traits that can be stable or unstable. In Fig. 1 there are two common singular points at the crossing of the shoot isocline (green) and the root isocline (yellow).

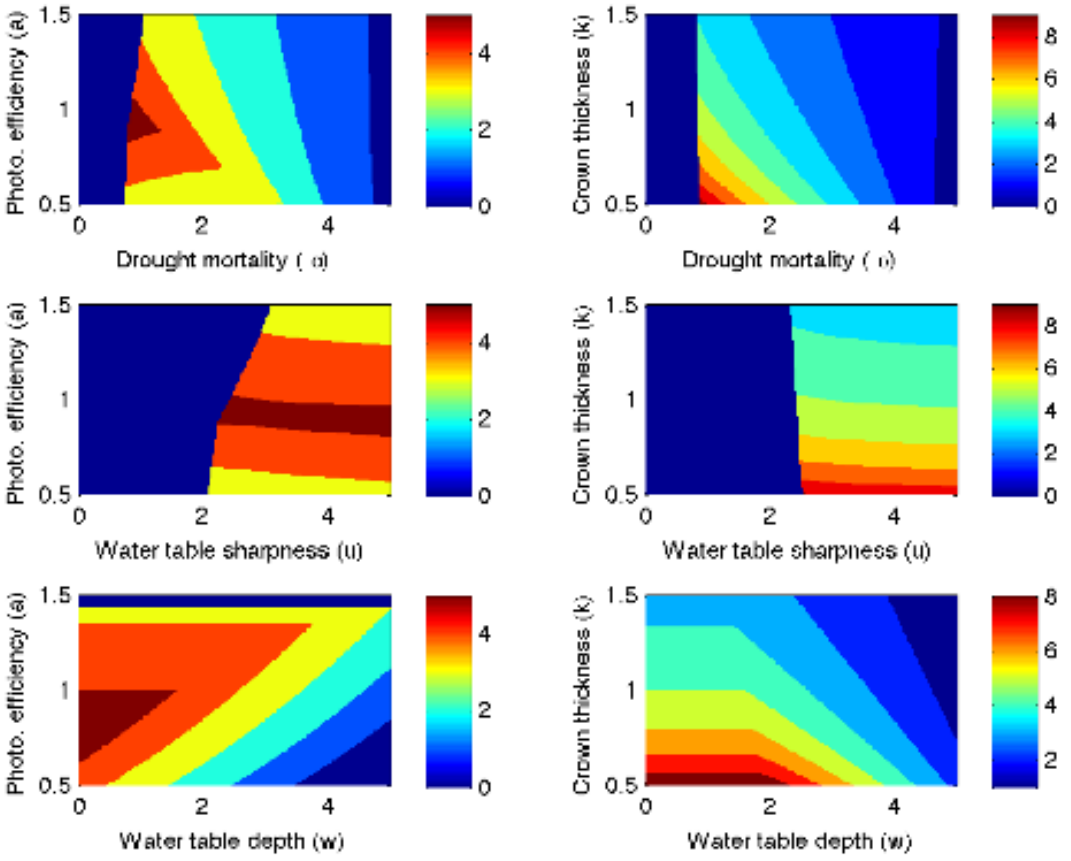

Fig. 2. Number of coexisting species with a taproot, depending on root and shoot parameters.

We investigate the number of coexisting plants dependence on the shoot and root parameters. We find the highest diversity for intermediate levels of photosynthetic efficiency, and low thin crowns (Fig. 2). The diversity is zero for low values of the drought mortality. In this case there is no point in investing in a root, the root and shoot isoclines never cross (Fig. 1), so there is no common singular point. For increasing drought mortality the there is a fast transition to high diversity, and then it decreases slowly. The ground water sharpness has a similar behaviour as the drought mortality but here the high diversity for intermediate values is not disappearing at higher values, and diversity is only affected slightly as drought mortality is increasing. The ground water table depth is lowering the diversity linearly with increasing depth. There is no phase transition as in the case for drought mortality and water table sharpness. For the shoot traits we find the highest diversity for intermediate photosynthetic efficiency, and thin crowns. This pattern disappears for large drought mortality, but not for large water table sharpness.

LITERATURE CITED

Geritz SAH, Kisdi É, Meszéna G & Metz JAJ. 1998. Evolutionarily singular strategies and the adaptive growth and branching of the evolutionary tree. *Evolutionary Ecology* **12**: 35-57

Iwasa Y, Cohen D, Leon JA. 1984. Tree Height and Crown Shape, as Results of Competitive Games. *J. theor biol* **112**, 279-297.

Thuiller W, Lavorel S, Araújo MB, Sykes MT, Prentice IC. 2005. Climate change threats to plant diversity in Europe. *PNAS* vol. 102.

Proceedings of the 7th International Conference on Functional-Structural Plant Models, Saariselkä, Finland, 9 - 14 June 2013. Eds. Risto Sievänen, Eero Nikinmaa, Christophe Godin, Anna Lintunen & Pekka Nygren. http://www.metla.fi/fspm2013/proceedings. ISBN 978-951-651-408-9.

Quantifying the potential yield benefit of root traits in a target population of environments

Mathieu Veyradier[1], John (Jack) T Christopher[1,2], Karine Chenu[1,2]
[1] *Agri-Science Queensland, DAFF, QPI&F, APSRU, 203 Tor Street, Toowoomba, 4350 Qld, Australia.*
[2] *The University of Queensland, QAAFI, 203 Tor Street, Toowoomba, 4350 Qld, Australia*
**correspondence:* karine.chenu@uq.edu.au

Highlights: Despite their importance, roots characteristics and their influence on crop growth remain poorly understood. A modelling approach was used to evaluate the potential impact of different root traits in targeted environments. Increased root extractable water at depth gave some substantial advantage to crops in all regions of the Australian wheatbelt, while increased root growth rate was only advantageous in the West of the belt.

Keywords: root, drought, water deficit, wheat, APSIM model, genotype-environment interaction.

INTRODUCTION

In rain-fed agriculture, crop yield greatly varies depending on the timing and intensity of water-deficit. While shoot traits have been extensively studied in such environments, root traits remain poorly understood, mainly due to technical difficulty associated with their assessment. Historical yield improvement is nevertheless thought to be substantially related to improvement of the root system architecture and water capture in crops like maize (Hammer et al., 2009). Understanding genotype-environment interactions of root characteristics and their impact on yield is thus an active area of research (e.g. Richards et al., 2010). Root traits with potential yield benefit in water-limited environments include increased root depth and root elongation rate (Hurd, 1974; Lopes and Reynolds, 2010), higher root distribution at depth (Hurd, 1974; Manschadi et al., 2006; Fig. 1), narrow seminal-root angle (Nakamoto and Oyanagi, 1994; Manschadi et al., 2008), decreased root:shoot biomass ratio (Siddique et al., 1990) and decreased xylem vessel diameter to increase hydraulic resistance, thus allowing some water saving for later more crucial stages (Richard and Passioura, 1989). The value of these traits, however, depends on the environment.

A modelling approach was used to quantify the impact of root-related traits in a broad range of environments that reflects the variability of soil and climates of the Australian wheatbelt ('target population of environments'; Chenu et al., 2011 and 2013). The considered traits included (1) root-front growth rate, water extraction rate in (2) shallow and (3) deep soil layers, as well as (4) water extractability at depth.

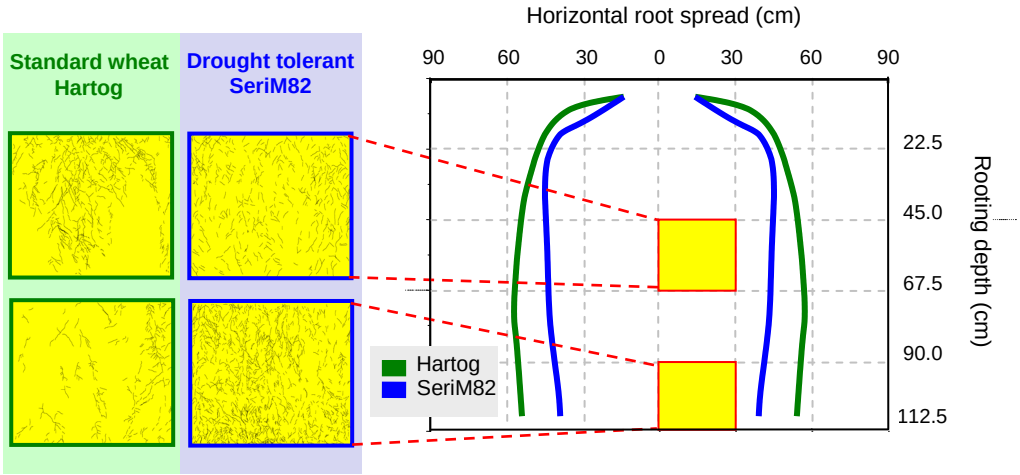

Fig. 1. Spatial root occupancy of the drought-tolerant cultivar SeriM82, and the check cultivar Hartog in a root chamber experiment at crop maturity. On the right, zone occupied by the roots of the two cultivars (green, Hartog; blue, SeriM82) within the root chamber. On the left, distribution of roots in the some sections of the root chamber. Figure adapted from Manschadi et al. (2006).

SIMULATIONS

The impact of root traits was simulated across the Australian wheatbelt over 123 years, using the APSIM-wheat crop model (e.g. Wang et al., 2002). The complete APSIM cropping system simulation platform is documented at www.apsim.info, and a detailed description of the wheat crop model and the soil modules is given at http://www.apsim.info/Wiki/APSIM-Documentation.ashx.

To represent the Australian wheat cropping system, simulations were performed in 60 locations, each representing between ~130,000 and 230,000 hectares of planted wheat (averaged data from 1975-2000, 2005 and 2006; source: Australian Bureau of Statistics). The simulations used a standard management system representing current grower practice from the region, and weather records for 1889-2011 (SILO Patched Point Dataset; http://www.longpaddock.qld.gov.au/silo/).

The simulations were conducted for the check wheat cultivar 'Hartog' with the following traits modified singly or in combination to produce 'virtual genotypes':

- Rate of downward root growth ('root-front growth rate') that ranged from 22.5 to 45 mm day^{-1} (Hartog: 30 mm day^{-1}) to capture the genetic variability reported in wheat root growth rate (from 0.84 to 1.8 mm ºCd^{-1}; Kirkegaard and Lilley, 2007),
- Water extraction rate ('*kl*' parameter in APSIM) in the top 50-cm soil layers, ranging from -20% to +20% compared to the reference cultivar (*kl* values typically decrease with depth, and vary among soil types),
- Water extraction rate (*kl*) in soil layers below 50-cm deep, ranging from -20% to +20% compared to the reference cultivar,
- Water extractability below 50 cm of depth (defined as the lowest soil water content to which the crop can extract water; '*lower limit*'), which varied from -20% to +20% from the value of reference cultivar.

All possible combinations of these root-related traits were considered, and their simulated yield and water extraction were compared to the reference genotype. Overall, 500 virtual genotypes (4 root-front growth rates x 5 shallow water extraction rate x 5 deep water extraction rate x 5 deep water extractability) were generated and these crops were simulated in 7380 environments (60 locations x 123 years), which resulted in a total of over 3.5 million simulations.

In each location, the yield advantage resulting from extra water uptake after flowering was calculated as the slope between (1) the extra grain yield produced by the virtual genotype compared to the reference genotype, and (2) the extra water uptake of the virtual genotype between flowering and maturity. Unstressed crops (<5% of the simulations) were removed from the analysis, as in these conditions, any extra water uptake had little impact on yield.

Results are presented as the average per region for yield advantage compared to the reference genotype, and for yield advantage per extra water uptake (Fig. 2).

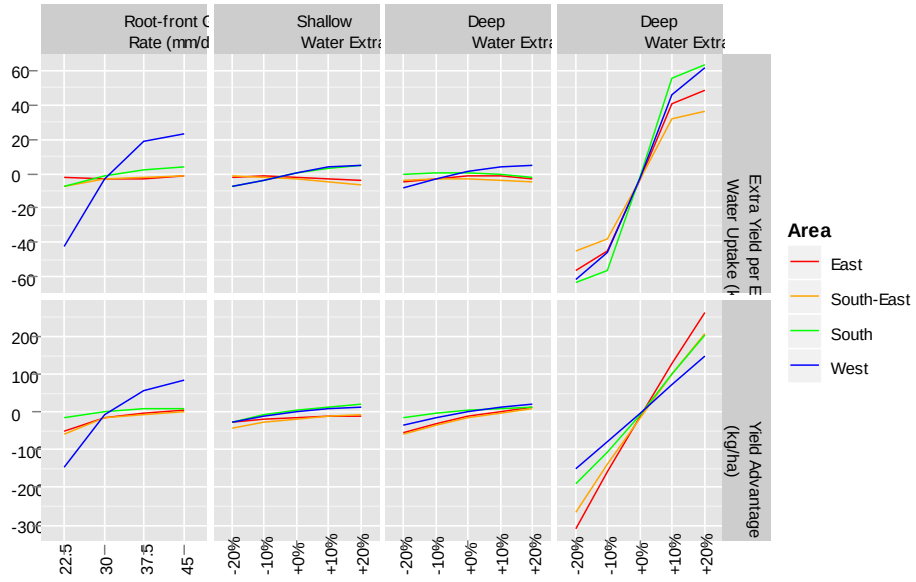

Fig. 2. Average impact of four root-related traits across the main areas of the Australian wheatbelt. The impact is presented in terms of (1) yield advantage per extra mm of post-flowering water uptake; (2) yield advantage compared to the reference genotype (Hartog).

RESULTS AND DISCUSSION

Out of the four integrated root-related traits studied, only increased water extractability below 50 cm conferred a substantial yield advantage in all regions (Fig. 2). Increasing the water extraction rate by up to 20% in either shallow or deeper soil layers (or both) did not change yield average greatly, irrespectively of whether crops were subjected to high or low in-season rainfall patterns, or whether they were grown in light or heavy soils. The rate of penetration of the deepest roots ('root-front growth rate') only substantially impacted yield in the West where wheat crops are produced on sandy-loamy soils with a relatively low water holding capacity, so that crops rely on the in-season rainfall. Thus, greater root penetration rate may increase the plant ability to chase water as it drains rapidly down the soil profile.

Importantly, the yield advantage conferred by all 'beneficial' traits was related to an increase in water uptake after flowering (Fig. 2), when water is required to maintain a green canopy (stay-green phenotype) and sustain carbon assimilation to fill the grains. Some research in this area has revealed that the stay-green drought-tolerant genotype 'SeriM82' has an adaptive root architecture (Manschadi et al., 2006; Christopher et al., 2008). The SeriM82 root system is more compact, and more uniformly distributed than the reference genotype Hartog, with greater root length at depth (Fig. 1; Manschadi et al., 2006). The greater root-length density at depth allows SeriM82 to have a greater water-extraction rate, while the better root 'occupancy' (more even root-branching) gives the crop a ~10% increase in water extractability below 50 cm (Manschadi et al., 2006). In accordance with experimental observations, simulations for this 'adapted' genotype showed a net yield advantage in the East area. When extended to a wider range of traits and to the entire wheatbelt, this modelling approach revealed that water extractability below 50 cm was beneficial in all areas, and that this trait had a greater impact than the rate of water extraction (at least for increase up to a 20%). Such results can help focus research on root traits with greatest potential to improve adaptation in the target population of environments. This study indicates that increased root occupancy at depth is one such trait.

LITERATURE CITED

Chenu K, Cooper M, Hammer GL, Mathews KL, Dreccer MF, Chapman SC. 2011. Environment characterization as an aid to wheat improvement: Interpreting genotype-environment interactions by modelling water-deficit patterns in north-eastern Australia. *Journal of Experimental Botany* **62**: 1743-1755.

Chenu K, Deihimfard R, Chapman SC. 2013. Large-scale characterization of drought pattern: A continent-wide modelling approach applied to the Australian wheatbelt - Spatial and temporal trends. *New Phytologist,* doi: 10.1111/nph.12192.

Christopher JT, Manschadi AM, Hammer GL, Borrell AK. 2008. Developmental and physiological traits associated with high yield and stay-green phenotype in wheat. *Australian Journal of Agricultural Research* **59**: 354-364.

Hammer GL, Dong ZS, McLean G, Doherty A, Messina C, Schusler J et al. 2009. Can changes in canopy and/or root system architecture explain historical maize yield trends in the US Corn Belt? *Crop Science* **49**: 299-312.

Kirkegaard JA, Lilley JM. 2007. Root penetration rate - a benchmark to identify soil and plant limitations to rooting depth in wheat. *Australian Journal of Experimental Agriculture* **47**: 590-602.

Lilley JM, Kirkegaard JA. 2011. Benefits of increased soil exploration by wheat roots. *Field Crops Research* **122**: 118-130.

Lopes MS, Reynolds MP. 2010. Partitioning of assimilates to deeper roots is associated with cooler canopies and increased yield under drought in wheat. *Functional Plant Biology* **37**: 147-156.

Manschadi AM, Christopher J, Devoil P, Hammer GL. 2006. The role of root architectural traits in adaptation of wheat to water-limited environments. *Functional Plant Biology* **33**: 823-837.

Manschadi AM, Hammer GL, Christopher JT, deVoil P. 2008. Genotypic variation in seedling root architectural traits and implications for drought adaptation in wheat (Triticum aestivum L.). *Plant and Soil* **303**: 115-129.

Nakamoto T, Oyanagi A. 1994. The direction of growth of seminal roots of *Triticum aestivum* L. and experimental modification thereof. *Annals of Botany* **73**: 363-367.

Richards RA, Passioura JB. 1989. A breeding program to reduce the diameter of the major xylem vessel in the seminal roots of wheat and its effect on grain yield in rain-fed environments. *Australian Journal of Agricultural Research* **40**: 943-950.

Richards RA, Rebetzke GJ, Watt M, Condon AG, Spielmeyer W, Dolferus R. 2010. Breeding for improved water productivity in temperate cereals: phenotyping, quantitative trait loci, markers and the selection environment. *Functional Plant Biology* **37**: 85-97.

Siddique KHM, Belford RK, Tennant D. 1990. Root:shoot ratios of old and modern, tall and semi-dwarf wheats in a Mediterranean environment. *Plant and Soil* **121**: 89-98.

Wang E, Robertson MJ, Hammer GL, Carberry PS, Holzworth D, Meinke H et al. 2002. Development of a generic crop model template in the cropping system model APSIM. *European Journal of Agronomy* **18**: 121-140.

Proceedings of the 7th International Conference on Functional-Structural Plant Models, Saariselkä, Finland, 9 - 14 June 2013. Eds. Risto Sievänen, Eero Nikinmaa, Christophe Godin, Anna Lintunen & Pekka Nygren. http://www.metla.fi/fspm2013/proceedings. ISBN 978-951-651-408-9.

X-Palm, a functional structural plant model for analysing temporal, genotypic and inter-tree variability of oil palm growth and yield

Benoît Pallas*, **Jean-Christophe Soulié, Grégory Aguilar, Lauriane Rouan** and **Delphine Luquet**
CIRAD, UMR AGAP, Avenue d'Agropolis, F-34398 Montpellier cedex 5
**correspondence:* pallas@supagro.inra.fr

Highlights: Oil palm yield depends on many component traits that are determined during about 4 years between inflorescence meristem initiation and harvest. Yield also presents large inter-month variability as well as variability among trees in the field. To simulate this complex system we developed a plant growth model using i) plant source-sink relationships as drivers of plant phenotypic plasticity and ii) stochastic rules relating inflorescence characteristics to plant nutritional status.

Keywords: Carbon balance, yield components, *Elaeis guinensis*, stochastic model, organogenesis

INTRODUCTION

Oil palm is the most important oil crop in the world but no relevant model was built to simulate and predict oil palm growth and yield variability. This can be explained by the complexity of yield elaboration for oil palm. Throughout its productive period, each phytomer can bear a female or male inflorescence or none at all if abortion occurs. Yield also depends on other components such as the number of fruits per inflorescence, individual fruit weight or oil content in fruits. Previous studies (Combres et al., 2013) showed that each of these yield components is determined during specific phases of the whole inflorescence development (4 years). Several factors can indeed differently affect each yield component. Plant source-sink balance for carbohydrates was observed to be one of the main factors affecting yield (Pallas et al., 2013). Each tree in a plantation can also present its own production rhythm resulting in trees that are out of phase. Accordingly, depending on the genotype propensity to have desynchronized trees and on environmental conditions, production at the plantation level will be either rhythmic or continuously distributed along years (Corley and Tinker, 2003). To simulate this pattern deterministic models based on response curves at the plantation level are not fully adequate. Different modelling approaches were performed, in particular stochastic models, to predict growth variability in the field (e.g. Kang et al., 2009) but these approaches showed limits in modelling such complex system of dynamic source-sink relationships and their genotypic and environmental determinisms. The study presents an original (X-Palm) model dedicated to analyze the dynamic source/sink relationships underlying yield elaboration and predict the periodicity of oil palm plantation production.

MODEL STRUCTURE

Using object-oriented modelling, X-Palm is based on an explicit topological representation of all the growing units. The plantation is represented as a sum of individual trees, each of them are composed of a cohort of phytomers bearing organs (internode, leaf and bunch). Each organ is decomposed into 'sub-organs' (e.g. peduncle, rachilla, fruit for bunches). Each organ is characterized by both quantitative (weight, thermal time since appearance...) or qualitative (inflorescence state...) variables. X-Palm is based on the concept of competition among sinks driving biomass partitioning and on retroaction loops between source/sink ratio and morphogenesis (Luquet et al., 2006). At each time step a plant carbon balance is computed. This carbon balance takes into account assimilate demand for organ growth and maintenance respiration and assimilate supply from photosynthesis and reserve mobilization. Estimation of organ assimilate demand is based on its potential organ growth according to its physiological age and on its biomass composition. Assimilate supply is estimated using the Monteith formalism and the Beer-Lambert law. A competition index (ratio between C supply and demand, *Ic*) is then computed at the plant level. Water deficit, as previously suggested (Combres et al., 2013), directly acts on the assimilation rate on thus leads to decrease *Ic*. The main originality of this model is to formalize the sequence and interdependency of yield elaboration processes each having its own sensitivity to plant nutritional status represented by *Ic* (Fig. 1A,B; Pallas et al., 2013). During these specific stages of sensitivity, probability laws are used to determine inflorescence status (aborted, female, male) according to *Ic*. Similarly, quantitative relationships are used to regulate other yield components depending on *Ic* (number of flowers per inflorescence, fruit-set). The probabilities linking the different inflorescence states and *Ic* are computed according to two parameters, *Ic_slope* : the regression slope between *Ic* during specific phases and the probability for producing female inflorescence (becoming productive) and *Ic_int* : the

intercept of the linear relationship between *Ic* and the probability for producing female inflorescence (Fig. 1B). These formalisms enable the model to simulate trade-offs between yield components at plant scale (competition among bunches) and at bunch scale (competition between fruit size and number). The model also simulates a reserve pool of carbon assimilate resulting from above mentioned source/sink balance.

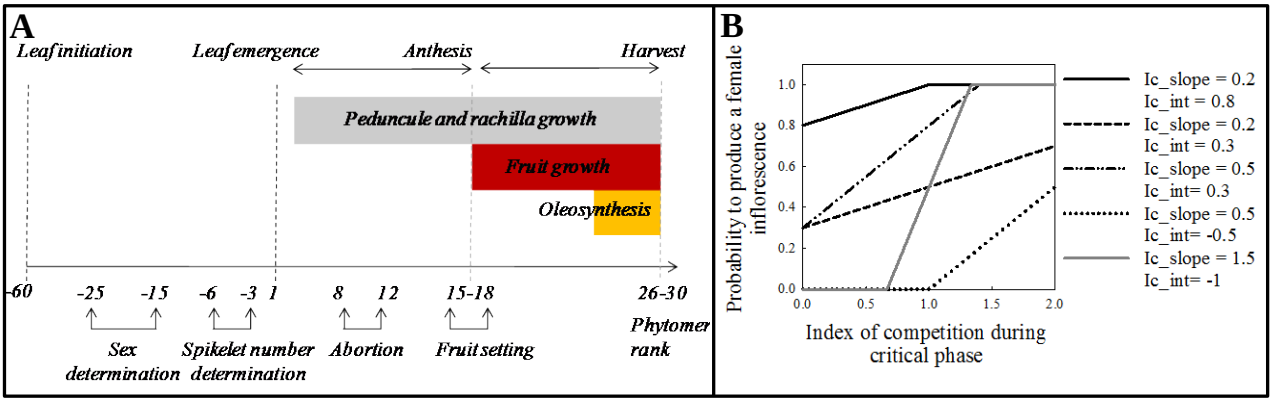

Fig. 1. Sub-model for (A) yield component elaboration and (B) the probability to produce a female inflorescence.

MODEL VALIDATION

The model was calibrated on a long-term experiment (10 years) performed in Indonesia on a commercial hybrid (Pallas et al., 2013). This experiment enabled to calibrate the relationships between *Ic* and yield components as well as model parameters dealing with organ potential growth or phytomer production rate. The model was then validated on trees of the same genotype grown in the same environmental conditions but subjected to two pruning practices to artificially modify source/sink relations at tree level. For the trees under leaf pruning treatment (LPT) more than 50% of the leaves were pruned to decrease the source/sink ratio and for the trees under fruit pruning treatment (FPT) all bunches were removed to increase the source/sink ratio. Since the model is not deterministic, simulations were performed with the same number of trees than observed on the experimental plot (6 trees per treatment). As observed experimentally LPT decreased bunch production (simulated: -26%, observed: -21%) whereas bunch production was strongly increased for trees under FPT after the end of bunch ablation practices (simulated: +102%, observed: +189%) (Fig. 1A). No clear seasonal periodicity in bunch production was observed and simulated in this environment. This roughly continuous production mainly results from the absence of dry season in Indonesia that leads to reasonably constant seasonal carbon balance (*Ic*).

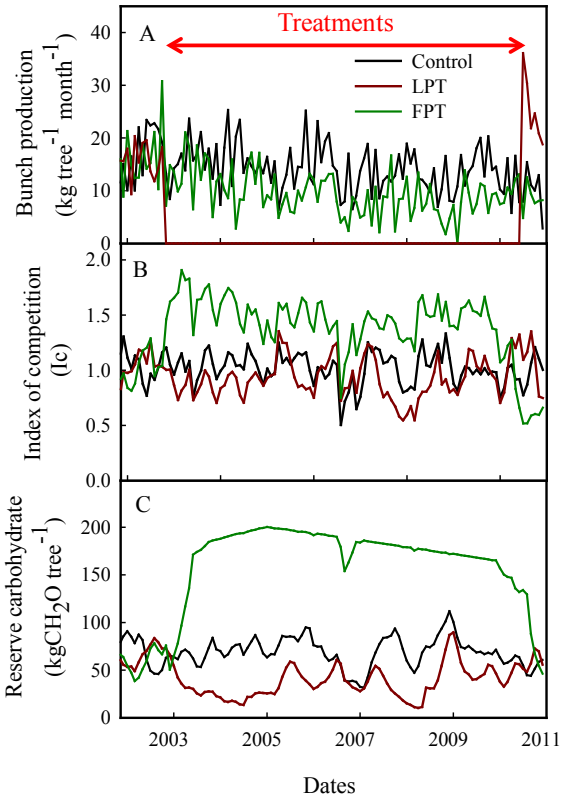

Fig. 2. Simulation of (A) bunch production per tree, (B) monthly index of competition and (C) whole reserve carbohydrate biomass per tree for the three treatments. LPT: leaf pruning treatment, FPT: fruit pruning treatment. Results are the average values of 6 simulated trees.

Simulation results showed strong impact of treatments on *Ic* (mean values = 1.03, 0.96 and 1.45 for Control, LPT and FPT) (Fig. 2B) and on the amount of carbohydrates in the reserve pool (Fig. 2C), the former showing strong temporal fluctuations. The average values of *Ic* as well as the relative differences in carbon reserve are close to that calculated on experimental data (Pallas et al., 2013). Both *Ic* and reserve pool simulations provide a conceptual validation of the model. Due to observed and simulated inter-tree variability of the variables related to carbohydrate balance a dynamic validation of the model is difficult at

this stage. As a consequence model validation was also performed using final yield component variables. The model represents the impact of each treatment on the different yield components during the leaf pruning treatment period for trees under LPT or after the cessation of treatments for trees under FPT (Table 1). The variability of each yield component among trees and months is also represented (Fig. 3). The model was also able to simulate the evolution of fruit and leaf growth according to their age and the trade-offs between yield components especially between individual fruit weight and fruit number per bunch (not shown).

Table 1. Simulated and observed yield components for Control, LPT (leaf pruning treatment) and FPT (fruit pruning treatment). Results are the average values of 6 simulated trees.

	Control (observed)	Control (simulated)	LPT (observed)	LPT (simulated)	FPT (observed)	FPT (simulated)
Number of harvested inflorescences (tree^{-1} month^{-1})	1.28	1.21	0.91	0.93	1.73	1.66
Number of fruits per inflorescence	1627	1678	1209	1395	2910	2770
Individual fruit dry weight (g)	6.6	6.2	6.5	5.9	5.9	5.9
Oil content (g g^{-1})	0.79	0.75	0.79	0.76	0.76	0.74

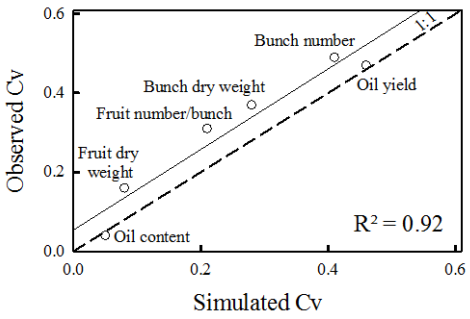

Fig. 3. Simulated and observed coefficients of variation (Cv) for the 6 control trees during the experiments.

SENSITIVITY ANALYSIS AND GENETIC VARIABILITY

A set of model sensitivity analyses were performed to quantify yield sensitivity to each of its component. In particular, the impact of parameters *Ic_slope* and *Ic_int* controlling the probability to produce bunches according to *Ic* was tested to further analyse and explain existing genotypic differences in term of bunch production periodicity and intensity (Corley and Tinker, 2003). Meteorological data originated from Ivory Coast were used. In this zone, seasonal water deficit resulting in periodic low *Ic* values are observed (Fig. 4B). Both parameters (*Ic_slope* and *Ic_int*) displayed strong impact on inter-tree variability and thus plantation production periodicity (Fig. 4A). The model needs to be further validated on contrasted genotypes and environments to further explore traits of interest for oil-palm breeding in non-optimal cultivation zones.

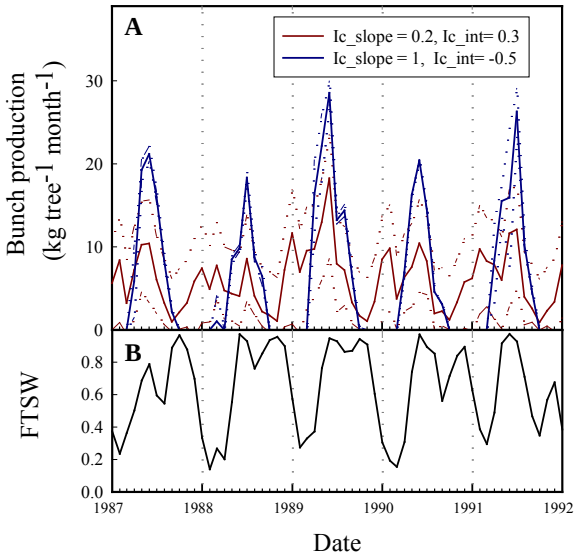

Fig. 4 (A) Simulation of bunch production in Ivory Coast for two "virtual" genotypes with different sensitivity to *Ic*. Simulations were performed with 70 trees. Solid line is the mean value and dashed line is the standard deviation. (B) Evolution of the fraction of transpirable soil water.

LITERATURE CITED

Combres JC, Pallas B, Rouan L, Bonnal V, Mialet-Serra I, Caliman JP, Braconnier S, Soulié JC, Dingkuhn M. 2013. Simulation of inflorescence dynamics in oil palm and estimation of environment sensitive phenological phases. A model based analysis. *Functional Plant Biology* **40:** 263-279.

Corley RHV, Tinker PB. 2003. *The oil palm*, 4th edn. Oxford : Blackwell Science.

Kang M, Cournède PH, (de) Reffye P, Auclair D, Hu G. 2008. Analytical study of a stochastic plant growth model : application of the GreenLab model. *Mathematics and Computers in Simulation* **78:** 57-75.

Luquet D, Dingkuhn M, Kim H, Tambour L, Clement-Vidal A. 2006. *EcoMeristem*, a model of morphogenesis and competition among sinks in rice. 1. Concept, validation and sensitivity analysis. *Functional Plant Biology* **33**: 309-323.

Pallas B, Mialet-Serra I, Rouan L, Clément-Vidal A, Caliman JP, Dingkuhn M. 2013. Effect of trophic competition on yield components, growth dynamics and structure of bunches in oil-palm (*Elaeis guineensis*). *Tree Physiology* in press.

Proceedings of the 7th International Conference on Functional-Structural Plant Models, Saariselkä, Finland, 9 - 14 June 2013. Eds. Risto Sievänen, Eero Nikinmaa, Christophe Godin, Anna Lintunen & Pekka Nygren.
http://www.metla.fi/fspm2013/proceedings. ISBN 978-951-651-408-9.

Modeling forest stand structure within a process-based model

Joannès Guillemot[1*], **Nicolas Delpierre[1]**, **Patrick Vallet[2]**, **Christophe François[1]**, **Kamel Soudani[1]**, **Manuel Nicolas[3]**, and **Eric Dufrêne[1]**
[1]ESE Lab (UMR 8079), Paris Sud University, CNRS, AgroParisTech, F-91405 Orsay, France; [2]Irstea, Research Unit 'Forest Ecosystems', F-45290 Nogent-sur-Vernisson, France ; [3]National forest office, F-77300 Fontainebleau, France
**correspondence:* joannes.guillemot@u-psud.fr

Highlights: A new empirical between-tree interaction module was implemented in the CASTANEA process-based forest stand model. The resulting functional-structural plant model demonstrates its ability to predict the morphological trajectories of individual trees grown in contrasted site condition. The presented stand structure modeling can be profitably used to investigate forest responses to global changes and to design new silvicultural guidelines.

Keywords: process-based model, CASTANEA, stand structure, forest management, tree competition

INTRODUCTION

In the context of global changes, process-based (PB) models validated at the stand rotation time scale (i.e. 100-150 years) have become important tools in forest sciences. Most of them simulate the functioning of an "average tree" to predict growth, or carbon (C) and water fluxes at the stand scale, where they obtain more robust results than aggregated predictions from tree-centered models (Cao, 2006). By definition, these models are not able to simulate the realistic evolution of the stand structure, i.e. the morphological changes of the individual trees. In particular, they fail to predict the circumference and volume increments of the individual trees, as well as the evolution of the tree density along the forest rotation.

This shortcoming strongly limits their explorative capacity and their potential applications. First, they cannot accurately simulate forest management, precluding i) the design of adaptive silvicultural guidelines taking into account current and future impacts of climate changes ii) the accurate assessment of biomass stocks and sink capacities of the increasingly managed part of the world's forests (Bellassen *et al.*, 2010). Secondly, "average tree" models cannot be directly validated with the most abundant available data: dendrometric measurements from forest inventories (tree density or basal area) and dendrochronological series, both being obtained from the aggregation of individual measurements. The simulation of the stand structure at individual tree scale would therefore allow modelers to formalize and to test functional hypothesis at larger time and spatial scales, e.g. along contrasted conditions of regional or continental gradients. Finally, the explicit representation of within-stand heterogeneity in multi-decade simulations would allow for investigation of long-term processes potentially involved in drought-induced forest diebacks, such as competition or individual C balances.

By contrast to the PB approach, empirical tree - centered growth models proved their ability to predict the retrospective evolution of forest structure on a purely statistical basis. The way resources, and therefore growth increment, are distributed within the individual trees is the focal point of these morphological models. Resources distribution partly depends on the mode of tree competition, which can be size-symmetric (i.e. the growth is proportional to the size) in the case of below-ground resources limitation or size-asymmetric when growth is limited by light. Recent papers have shown that the mode of competition strongly varies spatially, along fertility gradients, but also temporally (Metsaranta and Lieffers, 2010), making it an important stand structure driver which is poorly considered in tree - centered growth models. In any case, these empirical models cannot be used to predict future impacts of climate changes on forest functioning as they do not rely on explicit biological mechanisms.

In this study, our aim was to couple the CASTANEA forest PB model to a new empirical stand structure module (SSM) which we used to study the spatial and temporal variability of the tree competition mode. An attempt to couple forest management module to global vegetation model has recently been made (Bellassen *et al.*, 2010), but an approach allowing new insights in species-specific functioning and management is still lacking. The resulting functional-structural plant model (FSPM) has been validated on forest inventories data from 11 beech (*Fagus sylvatica*) permanent plots distributed on the French territory.

DATA AND MODELING METHODOLOGY

Growth data were obtained from the French permanent plot network RENECOFOR. Dendrochronological series were extracted on all plots in 1994. Additionally, circumference inventories were conducted regularly from 1991 to 2009, time intervals between 2 measurements ranging from 1 to 5 years.

We first studied the spatial and temporal variability of the competition mode in *F. sylvatica* by relating the stand productivity to an index of competition asymmetry. The stand productivity (obtained from site index for the study of spatial variability and annual circumference increments for the study of time variability) has been used as a proxy to characterize the stand growing conditions (Metsaranta and Lieffers, 2010). The competition index (γ_{data}) is the slope of the linear regression between tree circumferences in year (n) and their respective basal area increments. Statistical analyses were conducted within the linear framework and results, after check of the underlying test hypotheses, were used to calibrate the SSM.

The CASTANEA model (Dufrêne *et al*., 2005) has been thoroughly used and validated in long term growth and flux simulation (Delpierre *et al*., 2009). A new allocation scheme for *F. sylvatica* has recently been validated on stand growth across France (C. François, *unpubl. res.).* The SSM structure is inspired from the growth and yield model FAGACÉES, successfully used for 2 decades on beech even-aged forests in France (Le Moguedec and Dhôte, 2011). SSM allocates annually the biomass increment calculated by CASTANEA to a distribution of individual trees, through a non-linear relationship with 2 parameters: σ and $\gamma_{castanea}$, which are respectively the slope and threshold of the relationship between tree circumferences in year (n) and their respective basal area increments (Fig. 1). SSM is also able to simulate silvicultural thinning or competition-induced mortality (i.e. self-thinning). It includes a forest management module, which allows for the setting of multiple silviculture guidelines and different biomass export scenarios. SSM finally returns back to CASTANEA the changes in LAI and in biomass stocks resulting from the mortality simulation.

We initialized simulations with field measurement (e.g. LAI, leaf nitrogen, soil water capacity, biomass), completed with species-specific parameters from the bibliography. The SAFRAN database was used for half-hourly climatic forcing. On each year of inventory, the tree distribution simulated by the FSPM was compared with measurements, through usual dendrometric variables (stand basal area and mean circumference, see Fig. 1). The distribution was then re-initialized with the corresponding data.

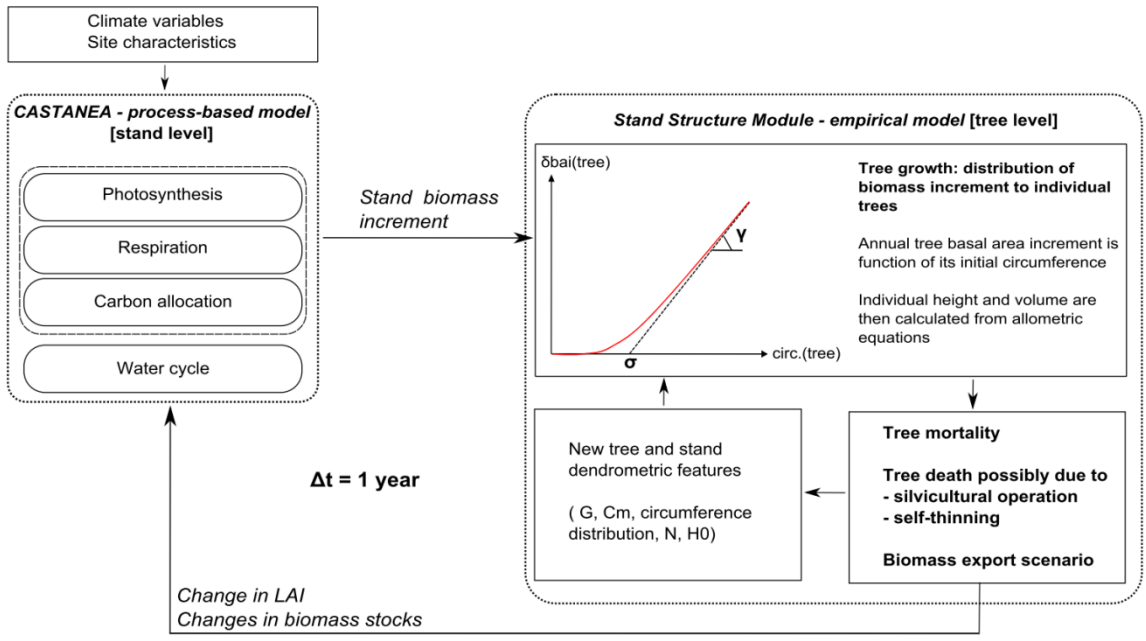

Fig. 1. Conceptual diagram of the coupled CASTANEA – SSM model. Abbreviations*: G (Stand Basal Area), Cm (mean circumference), N (stem density), H0 (dominant height), circ. (circumference), δbai (basal area increment.)*

RESULTS AND DISCUSSION

As expected, the index of competition asymmetry γ_{data} was positively correlated to stand productivity. The correlation was high along the spatial gradient (*p-value* < 0.001, $R^2 = 0.53$). Similarly, the

within-site index variability was well explained by the annual productivity (*p-value* < 0.001, $R^2 = 0.71$). The annual calibration of SSM was then designed as follows: 1) σ, which corresponds to the minimum circumference of trees with access to direct sunlight, was estimated from an empirical model fitted on the inventory data (σ = 0.43 * Cm + 0.04 * V – where Cm and V represent mean circumference and stand volume, respectively – , *p-value* < 0.001, $R^2 = 0.87$). 2) $\gamma_{castanea}$ is then adjusted so that the resulting individual circumferences increments was consistent with CASTANEA stand growth simulations. SSM simulates explicitly the observed temporal and spatial variability of the mode of tree competition, through the $\gamma_{castanea}$ positive dependence on CASTANEA stand growth predictions. The resulting FSPM predicted efficiently both stand volume (Fig. 2A) and stand structure evolutions (Fig. 2B & C) of the 11 beech plots over the 1991-2009 period, without systematic bias. The empirical modeling of the between-tree interaction allowed the CASTANEA physiologically-based stand model to reproduce morphological trajectories of individual trees, grown in contrasted site conditions. There is a strong need of the forest science community to upscale knowledge obtained from tree-centered FSPM to stand level for decision support, and some attempts have been made in this way (e.g. Sievänen *et al*., 2008). However they did not so far obtain the required predictive capacity to be profitably used in forest applications (Cournède *et al*., 2010). The presented new FSPM, which considers structure at the stand scale in a "top-down" approach, can alternatively be useful to investigate forest responses to global changes and to design new adaptive silvicultural guidelines.

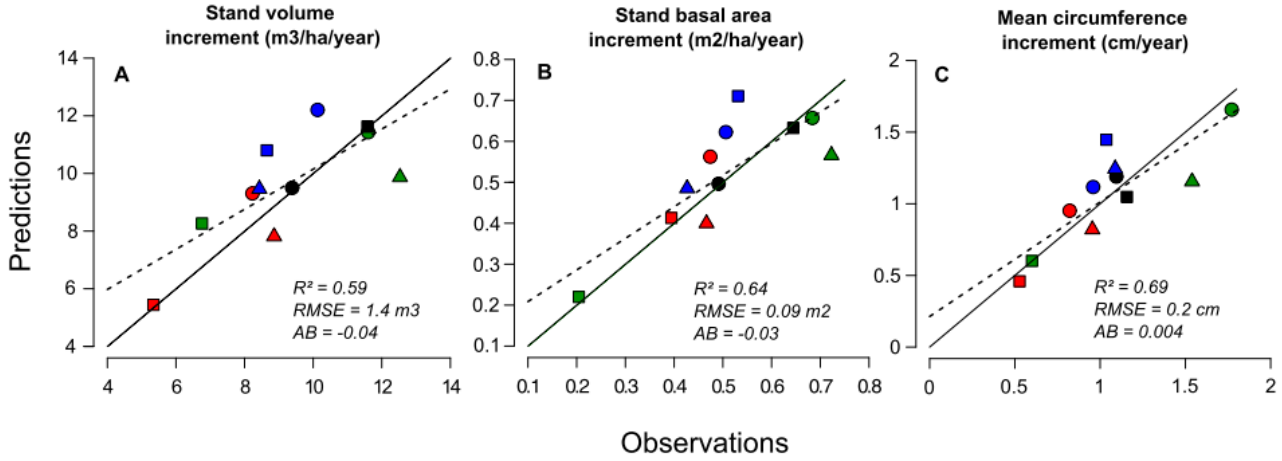

Fig. 2. Spatial validation of the FSPM. Each symbol is the averaged increment (over the 1991-2009 period) of the corresponding variable on one of the 11 plots. Solid and dashed lines are first bisector and regression line. AB and RMSE are average bias and root mean square error.

LITERATURE CITED

Bellassen V, Le maire G, Dhôte JF, Ciais P, Viovy N. 2010. Modelling forest management within a global vegetation model – Part1: Model structure and general behaviour. *Ecological Modelling* **221**:2458-2474.

Cao QV. 2006. Predictions of individual-tree and whole-stand attributes for loblolly pine plantations. *Forest Ecology and Management* **236**:342-347.

Cournède PH, Guyard T, Bayol B, *et al.* 2010. A forest growth simulator based on functional-structural modeling of individual trees. In: *PMA09, 3rd international symposium on plant growth modeling, simulation, visualization and applications*. Beijing (China), 09-13/11/2009.

Delpierre N, Soudani K, François C, Köstners *et al.* 2009. Exceptional carbon uptake in European forests during the warm spring of 2007: a data-model analysis. *Global Change Biology* **15***:*1455–1474.

Dufrêne E, Davi H, François C, Le Maire G, Le Dantec V, Granier A. 2005. Modelling carbon and water cycles in beech forest Part I: Model description and uncertainty analysis on modeled NEE**.** *Ecological Modelling* **185**:407-436.

Le Moguedec G, Dhôte JF. 2011. Fagacées: a tree-centered growth and yield model for sessile oak (*Quercus petraea* L.) and common beech (*Fagus sylvatica* L.). *Annals of Forest Science* **69**:257-269.

Metsaranta JM, Lieffers VJ. 2010. Patterns of inter-annual variation in the size asymmetry of growth in Pinus banksiana. *Oecologia* **163**:737-745.

Sievänen R, Perttunen J, Nikinmaa E, Kaitaniemi P. 2008. Toward extension of a single tree functional-structural model of Scot pine to stand level: effect of the canopy of randomly distributed, identical trees on development of tree structure. *Functional Plant Biology* **35**:964-975.

Proceedings of the 7th International Conference on Functional-Structural Plant Models, Saariselkä, Finland, 9 - 14 June 2013. Eds. Risto Sievänen, Eero Nikinmaa, Christophe Godin, Anna Lintunen & Pekka Nygren. http://www.metla.fi/fspm2013/proceedings. ISBN 978-951-651-408-9.

Effects of defoliation intensity on the genetic and phenotypic composition of virtual ray-grass populations

D. Combes, I. Litrico, S. Grenier, Ph. Barre, A.J. Escobar-Gutiérrez, G. Louarn
INRA, UR4 P3F, Equipe Ecophysiol Plantes Fourrageres, Le Chêne - RD 150, BP 6, 86600 Lusignan, France
**correspondence:* didier.combes@lusignan.inra.fr

Highlights: A modeling approach to simulate a successive generation of plants submitted to defoliation cylcles was built upt using the L-Grass FSPM model coupled with a simple genetic model. The model allows analyzing the phenotype of simulated successive plant generation resulting from genetics and light competition processes.This study showed the use of the FSPM approach for analyzing evolution of plant population in grassland system

Keywords: L-GRASS model, selective pressure, phenotypic plasticity, genetic selection, *Lolium perenne* L.

Grasslands Biomass production and quality respond to multi-factor dynamics including management such as frequency of defoliation, climatic conditions, soil properties or the floristic composition of the grassland. One of the challenges is to understand the determinants implied in the perinnity of grassland productivity. These determinants are related to the fitness of plants that constitute the grassland and the fitness of plant depends on environmental conditions. Canopy structure, that is to say the pattern of the spatial distribution of the plant items, is equally a factor that shall be considered especially in interactions among individual plants such as light competition which are involved in the dynamics of plant population.

The aim of the present work was there to build up a modeling approach to simulate a successive generation of plants submitted to defoliation cylcles. This approach is based on the coupling of an existing FSPM L-Grass (Verdenal *et al.*, 2008) with a module dealing with genetic properties and reproduction.

The plant model L-Grass (Verdenal et al., 2008) consists in the realistic simulation of the 3D development of the aerial parts of plants in the vegetative phase. Grasses have the particularity, in the vegetative phase, of not elongating their internodes so that the plant is mainly constituted of tillers, which are themselves made of leaves emitted at the basis of the plant, by the apical meristems. Consequently, a realistic representation of the architecture can be obtained by a faithful description of the topology of the plant and of the leaf dynamics (e.g. growth kinetic, lifespan, geometry) at different levels of organization.

The estimation of the biomass production was based on the linear relationship between dry weight accumulation (DW) and intercepted PAR radiation cumulated over time (PARc), which is consistently observed for crop canopies in conditions where neither water nor mineral nutrients are limiting.

A generation G1 of plants originating from the G0 population was obtained using the harvest index principle which determine the number of seed per individual as a function of its total biomass through an empirical relationship parametrized from observed data. Genetic information for each seed was simulated with a bottom-up approach from genes to individual using a L-Grass parameter representing the phenotype of each individual. The simple genetic model is based on the additive hypothesis of quantitative effect of each gene contributing to the expression of the phenotype.

This modeling approach shows the capacity of the L-Grass model to simulate the virtual plant population submitted to cylcles of defoliations. The model allows analyzing the phenotype of simulated successive plant generation resulting from genetics and light competition processes. This study showed the use of the FSPM approach for analyzing evolution of plant population in grassland system.

LITERATURE CITED

Verdenal A, Combes D, Escobar-Gutiérrez AJ. 2008. A study of ryegrass architecture as a self-regulated system, using functional-structural plant modelling. *Functional Plant Biology,* **35**: 911-924.

Proceedings of the 7th International Conference on Functional-Structural Plant Models, Saariselkä, Finland, 9 - 14 June 2013. Eds. Risto Sievänen, Eero Nikinmaa, Christophe Godin, Anna Lintunen & Pekka Nygren.
http://www.metla.fi/fspm2013/proceedings. ISBN 978-951-651-408-9.

Formation of crown structure in Scots pine trees

Kourosh Kabiri Koupaei*, **Eero Nikinmaa** and **Pertti Hari**
Department of Forest Sciences, PO Box 27, 00014 University of Helsinki, Finland
**corresponding author:* kourosh.kabiri@helsinki.fi

Highlights: The ecosystem model MicroForest describes the development of trees, ground vegetation and forest soil in a Scots pine stand based on coupling carbon and nitrogen fluxes in the system. Here, we simulated the crown development in a mature Scots pine stand assuming the semi-autonomous behaviour of the branches with optimizing C and N allocation simultaneously.

Keywords: Carbon balance, nitrogen allocation, SMEAR II, MicroForest, structural regularities

INTRODUCTION

Scots pine forms a whorl of branches each year at the top of the tree. Thereafter the branches grow annually, new needles are formed and the length and diameter of the branches increase. The growth is strong in a young branch, it slows down and finally the branch dies. The needles in the branch are, however, unable to photosynthesize without water that is taken up by roots and transported in the woody structures from roots to needles. At the same time proteins are needed for photosynthesis since pigment complexes, enzymes and membrane pumps carry out the synthesis of sugar. The high nitrogen concentration of proteins (15 – 17 %) explains the crucial role of nitrogen in the metabolism of trees where carbon and nitrogen uptake are connected with each other

We consider that whorls are the functional units of Scots pine trees; the needles, water transport system and fine roots for water and nitrogen uptake form the whorl. The sugars synthesized in the needles and the nitrogen taken up from the soil and obtained from the senescent needles are used for the growth and maintenance of the whorl and for the growth of the treetop. The sugars are used mainly for the synthesis of cellulose, lignin, lipids and starch while the nitrogen is crucial for the synthesis of proteins.

The allocation of sugars and nitrogen for needles, water pipes and fine roots is a very demanding task for the biochemical regulation system of the tree. We assume that the regulation system is powerful and it is able to utilize the resources in an efficient way. There must exist a balance between the transpiration from needles and the water transport capacity in the branches, stem and in transport roots. The commonly observed linear relationship between needle mass and sap wood area (Hari *et al*., 1986, Nikinmaa, 1992 and Perttunen *et al.*, 1996) is a result of the action of the biochemical regulation system and it makes the balance between the transpiration from needles and water transport in the stem.

The relationship between the sapwood area and needle mass determines the amount of new water pipes needed for a gram of needle growth in a whorl. Thus we can obtain the amount of sugars used for water pipes from the needle growth in the whorl. The tissues have characteristic nitrogen concentrations, high in needles and fine roots and low in woody structures. The amount of fine roots must be such that the fine roots can provide the nitrogen needed for the synthesis of proteins in the needles, fine roots and water pipes. We formulate the above ideas as carbon and nitrogen balance equations. We assume that the action of the biochemical regulation system produces such structures that they fulfil the carbon and nitrogen balance equations.

The carbon and nitrogen balance equations include two unknowns; needle and fine root growth. We solve these unknowns and thereafter we determine the growth of the woody structures. We obtain branch elongation from the requirement that needle density is constant. The whorls form the crown of a pine tree and we obtain the crown development from the growth of the whorls in the tree.

The ecosystem model MicroForest (Hari *et al.*, 2008; Hari *et al.*, 2013) describes the development of trees, ground vegetation and forest soil in a Scots pine stand. Here, we introduce MicroForest as an ecosystem model which can predict the development of stand from an early initial state of stand establishment. Our aim is to present a theoretical framework for structural regularities in crown development in Scots pine and test it. The crown development is based on carbon and nitrogen balance both as a function of needle mass. Thus we can simulate the crown development with MicroForest from an initial state. Then

the reduction of photosynthesis per needle mass caused by shading is introduced into the simulations through stand development.

SIMULATIONS

We selected the stand around SMEAR II (Hari and Kulmala, 2005) measuring station for demonstration of the behaviour of our crown model. The needle growth in a branch have a clear pattern, first rapid growth following a stabilization phase and finally a slow decline (Fig.1). The pattern of branch elongation is also clear as a saturating function where a slow declining trend is dominating (Fig.2). The crowns in dominating and suppressed trees are rather different (Fig.3). Based on the simulated needle mass profile and branch elongation model we are able to predict crown size development for Scots pine trees. We will test the simulations with measurements done in the spring 2013.

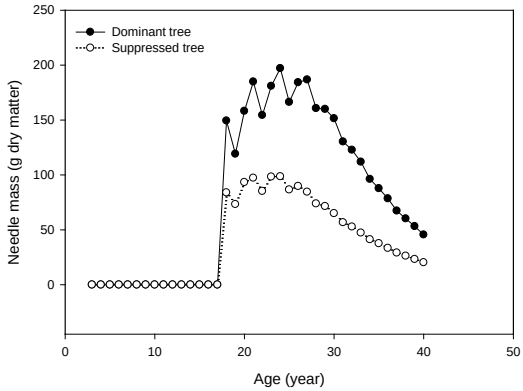

Fig.1. Needle mass growth in a whorl formed at age 18 in a dominant and suppressed tree.

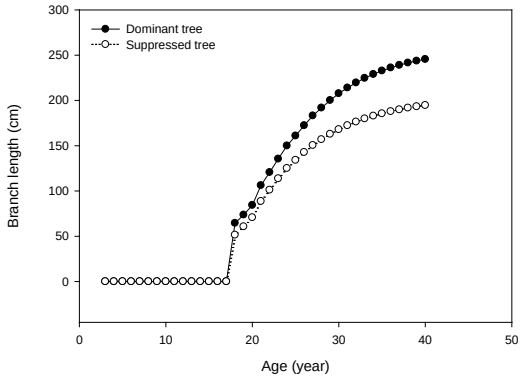

Fig.2. Branch elongation onset at age 18 years in a dominant and suppressed tree.

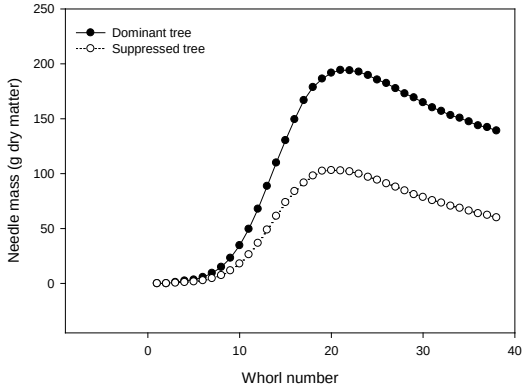

Fig.3. Needle mass distribution in a crown profile at age 40 in a dominant and suppressed tree.

LITERATURE CITED

Hari, P., Heikinheimo, P., Mäkelä, A., Kaipiainen, L., Korpilahti, E. and Salmela, J. 1986. Trees as water transport system. *Silva Fennica.* 20: 205-210.

Hari, P., Kulmala, M., 2005. Station for measuring ecosystem–atmosphere relations (SMEAR II). *Boreal Environment Research.* 10: 315–322.

Hari, P., Salkinoja-Salonen, M. S., Liski, J., Simojoki, A., Kolari, P., Pumpanen, J., Kähkönen, M., Aakala, T., Havimo, M., Kivekäs, R. and Nikinmaa, E. 2008. Growth and development of forest Ecosystems: the MicroForest model. In: *Boreal forest and climate change*. Hari, P. & Kulmala, L. (editors.) Springer s. 433-461. 29 (Advances in global change research; 34).

Hari, P., Havimo, M., Kabiri Koupei, K., Jögiste, K., Kangur, A., Salkinoja-Salonen, M., Aakala, T., Aalto, J., Schiesl-Aalto, P., Liski, J. and Nikinmaa, E. 2013. Dynamics of carbon and nitrogen fluxes and pools in forest ecosystem. In: *Physical and physiological forest ecology*. Hari, P., Heliövaara, K. & Kulmala, L. (editors.) Springer s. 346-396.

Nikinmaa, E. 1992. Analyses of the growth of Scots Pine: matching structure with function. *Acta Forestalia Fennica.* 235.

Perttunen, J., Sievänen, R., Nikinmaa, E., Salminen, H., Saarenmaa, H. and Väkevä, J. 1996. LIGNUM: a tree model based on simple structural units. *Annals of Botany* 77: 87-98.

Proceedings of the 7th International Conference on Functional-Structural Plant Models, Saariselkä, Finland, 9 - 14 June 2013. Eds. Risto Sievänen, Eero Nikinmaa, Christophe Godin, Anna Lintunen & Pekka Nygren. http://www.metla.fi/fspm2013/proceedings. ISBN 978-951-651-408-9.

FSM-Rice: a simulation study on rice morphology using functional–structural plant modeling

Liang Tang, LeiLei Liu, Yonghui Zhang, Dongxiang Gu, Weixing Cao and **Yan Zhu**
National Engineering and Technology Center for Information Agriculture, Ministry of Industry and Information Technology/Key Laboratory for Information Agriculture, Science and Technology Department of Jiangsu Province/College of Agriculture, Nanjing Agricultural University, Nanjing 210095, P.R.China
**correspondence: yanzhu@njau.edu.cn*

Highlights: A functional-structural plant model for rice (FSM-Rice) was developed by linking an existing rice growth model (RiceGrow) with a detailed morphological model (RiceMoph) to realize dynamic visualization of 3D rice plant at organ, individual and population scales under different growth conditions and cultivars.

Keywords: Rice, OpenGL, visualization, morphological model, RiceGrow, functional–structural plant model (FSPM)

INTRODUCTION

Rice (*Oryza sativa* L.) is one of the most important grain crops in China, its planting area accounting for 30% of all grain crops, and its yield for 40% of the grain yields. Rice plant architecture is one of the key factors related to its yield, which affects light distribution and photosynthesis in canopy. The modeling approach functional-structural plant model concerned with integration of architecture and resource allocation as aspects of plant function was developed in the mid-1990s. However, rice modeling using FSPM should be improved and developed in physiology and organ architecture descriptions. This study aimed at plant architecture modeling and visualization in rice, was to develop a functional-structural plant model in rice (FSM-Rice) by linking an existing physiological model in rice, RiceGrow (Tang et al. 2009), with a detailed morphological model (RiceMoph) which developed under different environmental conditions and cultivar types.

RESULTS

Based on time-course observations on morphological characteristics of organs (leaf, stem (tiller), panicle, and root) in rice under different environmental conditions and cultivar types, a morphological model (RiceMoph) was developed with growing degree days (GDD). The RiceMoph model allowed dynamic construction of geometric structure of rice plant, including morphological characteristics of leaf (length, width, angle and curvature), sheath and internode (width, length), panicle (length, width, curvature, branch, grain), root (length, number, diameter), and organ color sub-models. RiceGrow is a field scale, weather-driven, process-based dynamic simulation model, including 6 submodels for simulating phasic and phenological development, morphological and organ formation, photosynthesis and dry matter accumulation, yield and quality formation, soil water relations and dynamic nitrogen balance. FSM-Rice was developed by integration of RiceGrow model and RiceMoph model. The RiceGrow ran continuously and independently, was driven by data of weather, variety, soil and management, simulated the functional processes of rice growth and development and provided basic inputs for RiceMoph model, including development rate, population architecture, assimilate accumulation and partitioning, water and nitrogen factors. Visualization model was also developed to make the virtual rice more realistic by using OpenGL technology, including geometry, realistic rendering, organ deformation, texture, and illumination submodels. Dynamic visualization of 3D rice plant at organs, plant individuals and population scales under different cultivars and growth conditions were realized by using C# on the platform of .Net. Comparisons between virtual rice and real rice showed that visualization of 3D rice plant had a good prediction for dynamic changes of spatial morphology and color in rice plant. The results would support for rice production, breeding, research, and teaching.

LITERATURE CITED

Tang L, Zhu Y, Hannaway D, Liu LL, Chen L, Zhu Y, Cao WX. 2009. RiceGrow: A rice growth and productivity model. *NJAS -Wageningen Journal of Life Sciences* **57**: 83–92.

Proceedings of the 7th International Conference on Functional-Structural Plant Models, Saariselkä, Finland, 9 - 14 June 2013. Eds. Risto Sievänen, Eero Nikinmaa, Christophe Godin, Anna Lintunen & Pekka Nygren. http://www.metla.fi/fspm2013/proceedings. ISBN 978-951-651-408-9.

Parameterisation and evaluation of stand level process-based PipeQual-model for Norway spruce

Tuomo Kalliokoski[1,2], Harri Mäkinen[2] and **Annikki Mäkelä[1]**
[1]*Department of Forest Sciences, P.O. Box 27, 00014 University of Helsinki, Finland*
[2]*Finnish Forest Research Institute, Vantaa Research Unit, P.O. Box 18, 01301 Vantaa, Finland*
**correspondence:* tuomo.kalliokoski@metla.fi

Highlights: We evaluated the process-based stand growth mode, PipeQual, with the data from the long-term experiments. Slope values between observations and simulations ranged from 0.96 to 1.05 depending on the variable illustrating the applicability of PipeQual for predicting forest stand growth in the future climate.

Keywords: *Picea abies*, growth simulation model, validation

Process-based simulation models provide means for depicting the growth and development of the forest stands in the future climate. The premise of predicting forest growth in future climate is that the model produces consistent results with the observed forests growth in past and current climate. In this study, we parameterisized and evaluated the PipeQual model using dataset collected from 19 long-term thinning experiments in even-aged Norway spruce (*Picea abies* L. Karst) stands in southern and central Finland. PipeQual model is a process-based carbon balance model, in which stand is divided to size classes. Within each class mean tree acquires carbon and allocates it to foliage, branches, stem and roots based on structural regulations. The growth of each size class is described by this mean tree and the number of trees in the class. To ensure observed flexibility of Norway spruce crown structure, the built-in empirical relationships between needle mass and crown length, and between branch and crown length were made dependent of light environment. Due to these modifications, tree crowns grow denser in more intense light and wider with lower crown coverage. After these modifications, the model accuracy at the whole dataset level was high, slope values between observations and simulations ranging from 0.96 to 1.05 depending on the variable. The predicted mortality of trees was slightly higher than observed in a few cases. The average bias in stand dominant height was 0.44 m, 0.77 cm in stand mean diameter, 3.1 m^2 in stand basal area and 22 m^3 in stand total stem volume. Stand dynamics over time also followed generally quite closely the observed patterns (Fig. 1). Reasonable accurate predictions illustrate the applicability of PipeQual model for predicting forest stand growth in the future climate.

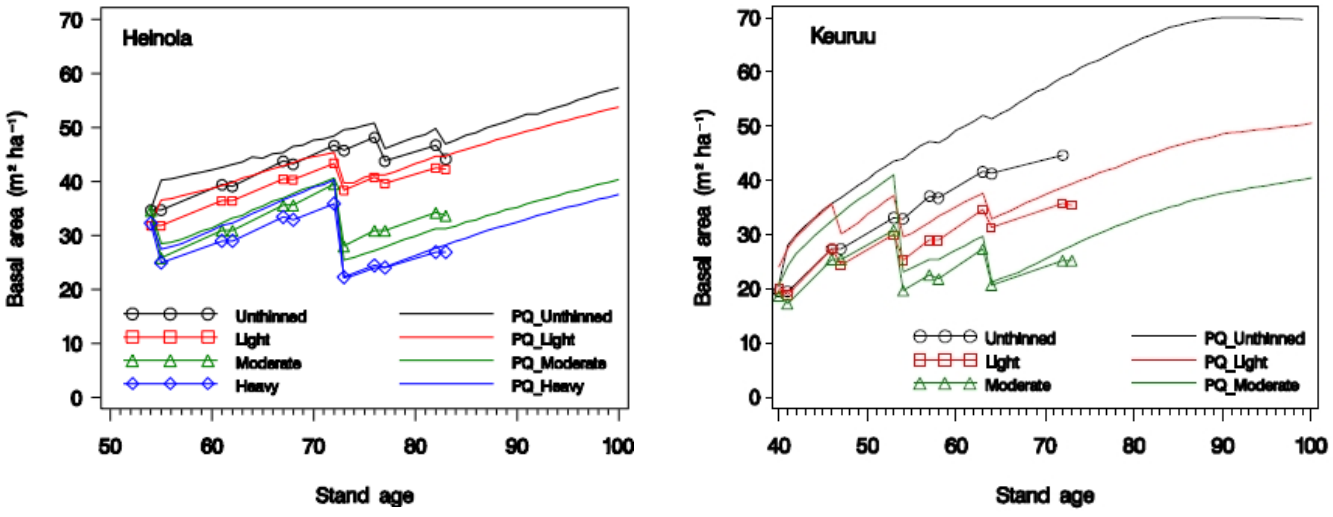

Fig. 1. Stand basal area plotted against stand age in two different experiments with plots of varying thinning intensity. Lines with the markers are the observations, lines without markers are the predictions of PipeQual model.

Proceedings of the 7th International Conference on Functional-Structural Plant Models, Saariselkä, Finland, 9 - 14 June 2013. Eds. Risto Sievänen, Eero Nikinmaa, Christophe Godin, Anna Lintunen & Pekka Nygren. http://www.metla.fi/fspm2013/proceedings. ISBN 978-951-651-408-9.

The model of root spreading and belowground competition in boreal mixed forests

Vladimir Shanin[1], **Maxim Shashkov**[1], **Natalia Ivanova**[2,3], **Svetlana Moskalenko**[1], **Maria Bezrukova**[1], **Raisa Mäkipää**[4], **Kapitolina Bobkova**[5], **Alexey Manov**[5], and **Alexander Komarov**[1]

[1]Institute of Physicochemical and Biological Problems in Soil Science, Russian Academy of Sciences, Russian Federation; [2]Institute of Mathematical Problems of Biology, Russian Academy of Sciences, Russian Federation ;[3]Pushchino State Institute of Natural Sciences, Russian Federation; [4]Finnish Forest Research Institute, Finland; [5]Institute of Biology, Komi Scientific Centre, Ural Branch, Russian Academy of Sciences, Russian Federation

**correspondence:* shaninvn@gmail.com

Highlights: New model of belowground competition is proposed. The model is operating on simulation grid and can simulate growth of root systems in mixed stands taking into account the irregularity in horizontal and vertical distribution of roots' biomass. The main outputs are the density of roots in each cell and amount of nutrients captured by each tree.

Keywords: belowground competition, root systems, mixed forests

The model is spatially-explicit. It allows describing the competition between trees for soil nutrients. The area of simulation is represented as two-dimensional grid consisting of cells of equal size. Each tree has exact spatial location, and its zone of nutrition is represented as array of cells. The tree-specific area of nutrition is calculated on the basis of average (*l_avg*) and maximal (*l_max*) root spreading distance. These two parameters, in turn, are calculated on the basis of stem diameter at breast height using logistic equation $l=a/(1+b*e^{-c*DBH})$. The coefficients *a*, *b*, *c* of equation were calculated from the experimental data using regression analysis. Since maximal and average root spreading distances decrease with increasing soil fertility and moisture, these parameters have site-specific modifiers: $l=l*m_{moist}*m_{fert}$. In the first stage of simulation, potential area occupied by rooting system is calculated based on average root spreading distance as square of circle with radius equal to *l_avg*: $S_{n\_zone}=Pi*l\_avg^2$. The next stage is the determination which cells are occupied by rooting system of the tree. To calculate the preferability of including of each cell into the area of nutrition the parameter *p* is used. It is calculated as $p=d^{-1}*m^{-1}*n$, where *d* is the distance between current cell and the rooting cell of focal tree, *m* is the mass of roots of other species, and *n* is the amount of available nutrients (nitrogen etc.) in the current cell. Parameter *p* is calculated for all cells inside the potential zone of nutrition (circle with *R=l_max*) but not included into the actual zone of nutrition yet. Therefore, the cells with the highest values of *p* will be included first. There are two restrictions which should be taken into account: (1) the distance from each cell included into the nutrition area to the rooting cell cannot be more than maximal root spreading distance for the given tree and (2) all cells, forming the area of nutrition of the given tree, must be arranged in continuous connected contour. Nutrition zones of different trees can overlap. The horizontal distribution of biomass of roots is depended on the distance from the stem. Vertical distribution (implemented as independent calculation of root portion for forest floor and mineral soil) depends on species-specific features, soil characteristic and strength of belowground competition (amount of roots of other plants). Model independently calculates distribution for coarse and fine roots. The nutrients from each cell are distributed between competing trees proportionally to the biomass of their fine roots in given cell with species-specific modifiers. The main outputs from the model are the spatial distribution of biomass of roots and the amount of nutrients captured by each tree. This will allow simulating asymmetric competition between different species, which gives comprehensive facilities for realistic modelling of mixed forests. The value of uptake of nutrients can be used as driving variable for calculation of annual increment of biomass of tree. The model also can be used for simulation of vegetative propagation of trees. This work was supported by the Russian Foundation for Basic Research, grant number 12-04-31635 and the Academy of Finland, project numbers 140766 and 257845.

Proceedings of the 7th International Conference on Functional-Structural Plant Models, Saariselkä, Finland, 9 - 14 June 2013. Eds. Risto Sievänen, Eero Nikinmaa, Christophe Godin, Anna Lintunen & Pekka Nygren.
http://www.metla.fi/fspm2013/proceedings. ISBN 978-951-651-408-9.

Analysis of hybrid vigor for cucumber with Functional-Structural plant model Greenlab

Xiujuan Wang[1], **Mengzhen Kang**[1,*], **Lili Yang**[2], **Baogui Zhang**[2], and **Philippe de Reffye**[3]
[1]*State Key Laboratory of Management and Control for Complex Systems, Institute of Automation, Chinese Academy of Sciences, 100190 Beijing, China,* [2]*China Agricultural University, 100193 Beijing, China,*
[3]*CIRAD, UMR 51 AMAP 34398 Montpellier cedex 5, France*
**correspondence:* mengzhen.kang@ia.ac.cn

Highlights: To analyze the hybrid vigor between parent and hybrid plants, three cucumber cultivars were used (Parents: A, B; F1 hybrid: C). Continuous observations and destructive samplings were made throughout the growth of plants. Experimental results indicate that cyclic changes occur in the dry weights of organs (internode, leaf and petiole) of different positions along the stem. The yield, organ sizes and fruit numbers of the three cultivars were different. To analyze these differences, a Functional-structural model 'Greenlab' was applied to compute the parameters of source sink for organs. The results demonstrate that plant architecture plays an important role in heterosis breeding. This study is a first step to build a tool to provide the guidance of heterosis breeding for breeders on cucumber.

Keywords: Hybrid vigor, Cyclic variation, Greenlab model, Cucumber, Sink-source ratio, Fruit set

INTRODUCTION

Hybrid vegetable technology is one of the better options to improve cucumber yield, particularly because the full potential of hybrids has not been completely exploited in vegetable crops, as compared to several cereals. Hybrid vigour can be expressed by total yield and the increased yield due to larger number of fruits/plant. Yield and fruit quality are some of the most frequent traits influenced by heterosis. In cucumber, Hayes & Jones (1916) first observed heterosis for fruit size and fruit number per plant. The highest yielding hybrids gave higher yield and showed an increase in fruit size compared with corresponding parents.

In recent years with the rapid development of molecular biology and genomics progress has been made in the study of characters of high yield and the mechanisms for high yielding and their related genes. Plant type is one of the important factors to determine the yield (Du et al., 2007). The length of internode, the size and angle of leaves are three most characters of agronomic importance in cucumber. Ghaderi & Lower (1978) suggested that heterosis in yield components such as number or weight of leaves, branches, and roots should have a direct effect on fruit yield. F1 hybrids may have greater photosynthetic activity than their parents leading to higher yield. It is well known that the yield depends on the production and allocation of assimilates of plants, which is linked to source-sink ratio (Marcelis, 1994). The aim of the current study was to quantify the link between source-sink ratio and fruit-set for cucumber plants with different cultivars, compare the difference of organ growth, photosynthesis and biomass production between the F1 hybrid and parent plants using the Functional-Structural model 'Greenlab' to compute the source sink parameters of organs for cucumber plant. Thus, the model can analyse the heterosis and provide a virtual experimental tool for breeding.

MATERIALS AND METHODS

1. Experiment setup and measurements

The experiment was carried out in the greenhouse of China Agricultural University from April to July 2010. Plant material was cucumber (three cultivars: A, B and C). The cultivar C is F1 hybrid of A and B. Seeds of the three cultivars were sowed on March 9 2010. Cucumber seedlings with four leaves were implanted into 25-cm pots at April 10. The pots were filled with 70% peat, 20% vermiculite and 10% pearlite. 20, 20 and 10 pots of plants were planted for A, B and C, respectively. There were no water and fertilization stresses. Destructive measurements and continuous observations were made. In destructive measurements, 2 plants were selected to measure the dry weight of organs (internode, blade, petiole and root) and blade surface for three cultivars, at six stages along the growing period (10 April, 26 April, 17 May, 31 May, 16 June and 3 July. The measured data of the last four stages were used to estimate the source sink parameters of model for each cultivar. Continuous observations were made on 6 plants for each cultivar, twice per week. Detailed topological observations included the number of metamers (internodes, leaves and flowers and fruits), and the stage of development (flower bud, flower and fruit or abortion) for each position for the three cultivars.

2. Greenlab model

GreenLab (Yan et al, 2004) is a generic plant model simulating two basic processes of plant: development (organogenesis) and growth (organ expansion). The organogenesis is simulated with a dual-scale automaton, which gives the number of organs that participate in biomass production and allocation. At each time interval, called Growth Cycle (GC), plant structure is updated according to the organogenesis model. Biomass production *Q(i)* is calculated according to the initial biomass from the seed, total leaf area and ground projection area of plant at each GC. Biomass is distributed into growing organs according to their sink strengths. The ratio *Q(i)* and the total demand of plant *D(i)* represents the biomass availability for each organ, called source-sink ratio. The total biomass of organs can be computed by summing up the biomass of all individual organs of the same property, which can be measured in reality.

RESULTS

1. Experiment results

The phyllochron has no significant difference for the three cultivars. Thus, we can use the same time step in the model to compute the source sink parameters. The biomass and sizes of organs, biomass allocation at the plant level, total plant biomass, organ number and position changed for the three cultivars. Plants of cultivar A had larger biomass and organ sizes for internode, blade and petiole. By contrast, the cultivar B had less biomass and smaller organ sizes than A, while the cultivar C showed intermediate values (Data not shown). To take an example for fruits, total mean fruit dry weight per plant was C>B>A, while the maximum individual fruit dry weight was A>C>B at final harvest (Table 1).

Table 1 Comparison of fruit number and average weight per plant and standard error between the three cultivars.

	Mean No. Fruits	Mean total fruit dry weight (g)	Maximum individual fruit dry weight (g)
A	1.0±0.0	12.1±3.5	14.6
B	6.0±0.8	22.8±9.0	7.64
C	3.5±0.6	31.5±0.9	12.9

2. Estimation results

Target data for one plant from different sampling dates were fitted simultaneously, including the dry weights of individual internode, blade, petiole, fruit, and the total dry weight of each component. Following our observations, the maximum duration of expansion was set to 30 growth cycles for leaves and internodes, and 35 cycles for fruits. The duration of function was set to 40 growth cycles for each organ. An example for Cultivar A of fitting results on organ-level data is shown in Fig. 1.

A set of source sink parameters was identified for each cultivar, as shown in Table 2. Petiole and internode sink strength (P_i, P_p and P_b) was similar for cultivars A and C. The same trend appeared for the sink variation parameters of blade, petiole, internode and fruit (B_b, B_p, B_f and B_i). Only fruit sink strength (P_f) differed. These parameters for cultivar B were smaller than the cultivar A and C. The estimation results are consistent with that of experiments (Table 1). A had larger individual fruit and B had smaller one. Regarding source parameters, the projection area (S_p) were stable for the three cultivars. The light use efficiency (r_P) was larger for the cultivar B.

Table 2 Estimated parameter values for three cultivars

	A	B	C
P_i	0.37	0.25	0.33
P_p	0.19	0.18	0.18
P_f	22.1	8.69	11.9
B_i	4.78	3.00	5.47
B_b	3.52	3.47	3.84
B_p	3.01	2.93	2.87
B_f	3.08	0.93	2.85
S_p	139.0	142.8	154.5
r_p	125.7	226.4	154.0
R^2	0.984	0.942	0.932

P_o is the coefficient of sink strength, B_o is the parameter of the beta function for organ expansion, S_p is the projected surface area of the plant, o=i(internode), b(blade), p(petiole), f(fruit).

Using these parameter values, the ratio between biomass supply and demand (Q/D) was computed, as shown in Fig. 2. The Q/D ratio of A and C was larger than that of B, and all three values decreased after their peak values when the fruit appears. This indicates that the growth of organs is influenced by the source sink ratio.

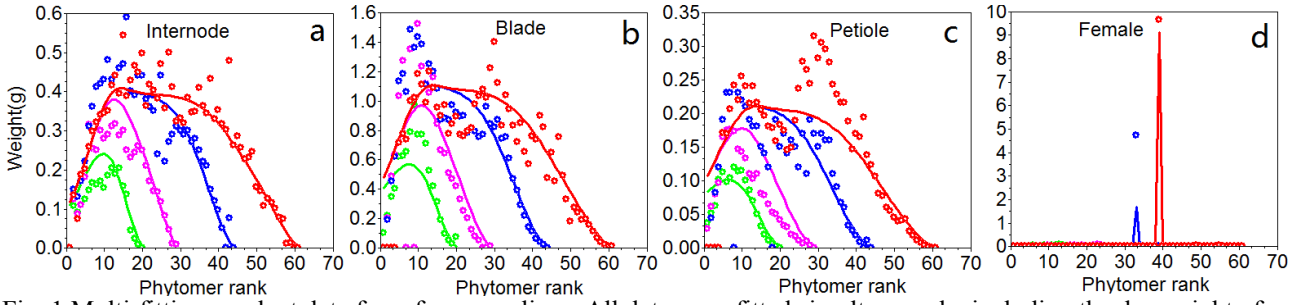

Fig. 1 Multi-fitting on plant data from four samplings. All data were fitted simultaneously, including the dry weight of individual internodes (a), blades (b), petioles (c), and fruits (d), shown with cultivar A. Dots represent the measured data, lines represent the computed data, respectively.

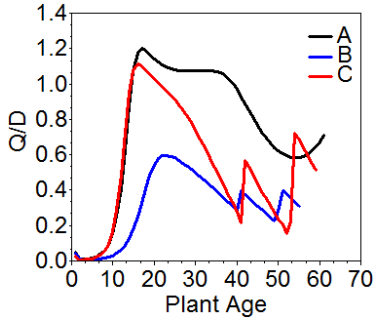

Fig. 2 Computed evolution of plant demand per cycle for the three cultivars.

DISCUSSION

The aim of the current study is to quantify the link between source–sink ratio and fruit-set for cucumber plants for different cultivars. Our model can compute the source sink parameters of organs per plant. The model results are consistent with the experiments. Cultivar A has larger leaves and individual fruit, but fewer fruits, in contrasts, cultivar B had smaller leaves and individual fruits, but more fruits; the F1 hybrid C had large leaves and fruits, also more fruits. The total yield of cultivar C is larger than A and B (Table 1). As shown in Fig.2, the fruit sink strength of F1 hybrid (cultivar C) may depend on the parent A, while the fruit sets depend on the parent B. Although source–sink ratio has been regarded as the principal factor determining fruit-set and organ growth, the cyclic pattern cannot be fitted very well using our model, as shown in the Fig. 1. Moreover, the cyclic pattern still exists even if fruits aborted there. This could result from flower bud differentiation, which may influence the cell number of organs, and in turn, its size (Ramirez-Parra et al, 2005) at the flowering stage for cucumber. The development of fruit relates to cell division and cell expansion. Factors affecting cell division before and after anthesis can bring about a failure of fruit-set. For modelling it is necessary to distinguish the time period which factors influence the size of organs during the growth.

The model can simulate the difference of organs and yields between cultivars by computing the source sink parameters of plant organs. The F1 hybrid can obtain the heterosis by combining the advantages of the parents. The model is helpful for breeders to understand the mechanism of hybrid vigor.

LITERATURE CITED

Du Y, Wang Y, Wang XH, Sun LL, Yang JC. 2007. Comparisons of plant type, grain yield, and quality of different japonica Rice cultivars in Huanghe-Huaihe River Area[J]. Acta Agronomica Sinica **33(07)**: 1079-1085.

Ghaderi A, Lower RL. 1978. Heterosis and phenotypic stablility of F1 hybrids in cucumber under controlled environment. Journal of the American Society for Horticultural Science 103: 275-278.

Guo M, Rupe MA, Dieter JA, Jijun Z, Spielbauer D, Duncan KE, Howard RJ, Hou Z, Simmons CR. 2010. Cell Number Regulator1 Affects Plant and Organ Size in Maize: Implications for Crop Yield Enhancement and Heterosis. The Plant Cell, 22: 1057-1073.

Hayes HK, Jones DF. 1916. First generation crosses in cucumbers. Connecticut Agricultural Experiment Station Annual Report: 319-322.

Marcelis L. 1994. A simulation model for dry matter partitioning in cucumber. Annals of Botany, 74: 43-52.

Ramirez-Parra E, Desvoyes B, Gutierrez C. 2005. Balance between cell division and differentiation during plant development. Int Journal of Developmental Biology. 49: 467-477.

Yan H, Kang M, de Reffye P, Dingkuhn M. 2004. A dynamic, architectural plant model simulating resource-dependent growth. Annals of Botany **93**: 591–602.

Proceedings of the 7th International Conference on Functional-Structural Plant Models, Saariselkä, Finland, 9 - 14 June 2013. Eds. Risto Sievänen, Eero Nikinmaa, Christophe Godin, Anna Lintunen & Pekka Nygren.
http://www.metla.fi/fspm2013/proceedings. ISBN 978-951-651-408-9.

"Virtual grassland": an OpenAlea package to deal with herbaceous plant architecture and grassland community dynamics

Gaëtan Louarn*, Abraham Escobar-Guttierrez, Didier Combes
INRA, UR4 P3F, BP6, F-86600 Lusignan, France
* gaetan.louarn@lusignan.inra.fr

Highlights: The "Virtual grassland" OpenAlea package was developed to provide herbaceous plant models and coupling methods with soil and light transfer modules. It aims at simulating the effects of competition and facilitation interactions at the population and community levels in grasslands.

Keywords: Architecture, grass, legume, community, dynamics

Grasslands are the major source of forages worldwide. They are exploited via grazing and mowing and can be natural or cultivated. Their agricultural use-value depends on the structure of their canopy and on their botanic composition (most are indeed multi-specific). Both determine the quantity and the quality of the biomass harvested by grazing or mowing. In temperate grasslands, perennial grasses and forage legumes dominate the floristic composition of grasslands and are generally intended to be grown in mixtures because of their agronomic (feeding value) and ecological (resource capture and use) complementarities. An appropriate species balance is however difficult to maintain in such non-equilibrium communities. The proportion of forage legumes fluctuates both from year-to-year and within a single growth period as a result of species interactions and management. In spite of its agronomic significance, most grassland models developed so far ignore plant-plant interactions and the community dynamics of grasslands. Efforts have been done mainly on white clover based mixtures for which a gain of understanding of coexistence conditions was achieved thanks to individual-based models. White clover has however rather atypical colonisation strategy and persistence habit among forage legumes and these predictions may present a limited interest for other grass-legume combinations. To deal with this question, the "Virtual grassland" package was developed under the OpenAlea platform (Pradal et al. 2008) to simulate the architecture of various grass and legume species and predict the effects of competition / facilitation interactions at the population and community levels.

The "Virtual grassland" package provides i) two generic plant models accounting respectively for grass (L-grass) and legume (L-egume) morphogenesis above- and below-ground, and considering responses to defoliation (Verdenal et al. 2008), ii) coupling methods (in the form of OpenAlea nodes) between the MTG central data structure for plant architecture and environmental models above- (light) and belowground (water and soil N) available through the platform and finally iii) dataflows enabling to scale up from plant to community and ecosystem (soil-plants-atmosphere) levels by combining the different plant and environmental models together, and providing a graphical interface to manage model input parameters and visualise simulation results. The two plant models are based on the l-system formalism (L-py software) and aim at accounting for intra- and inter- specific variations in morphogenesis, dry matter production and C/N composition. In the legume functional group, different growth habit in terms of shoot growth (erect/prostrate), branching, coordination of organ growth and ability to develop adventitious roots/shoots enable to distinguish between colonisation strategies ranging from herbs perennating by formation of a single taproot (such as alfalfa or red clover) to clonal patches resulting from rhizome spreading (creeping lucerne) or rooted shoots at the soil surface (white clover). Similarly, in grasses, differences in the self-regulation of leaf growth and tiller development enable to account for growth habit ranging from long-leaf forage species/cultivars to short-leaf turfs. Leaf gas-exchange is simulated using the Farqhar model. A simple soil model adapted from the STICS soil module is currently tested for water and nitrogen acquisition. The coupled soil-plant-atmosphere model is currently being assessed both for the behaviour of isolated plants, and the dynamic of plant populations into binary species mixtures.

LITERATURE CITED

Pradal C, Dufour-Kowalski S, Boudon F, Fournier C, Godin C. 2008. OpenAlea: a visual programming and component-based software platform for plant modelling. *Functional Plant Biology* **35**(10): 751-760.

Verdenal A, Combes D, Escobar-Gutiérrez AJ. 2008. A study of ryegrass architecture as a self-regulated system, using functional–structural plant modelling. *Functional Plant Biology* **35**: 911–924.

STRUCTURAL DEVELOPMENT OF PLANTS AND LIGHT ENVIRONMENT

Proceedings of the 7th International Conference on Functional-Structural Plant Models, Saariselkä, Finland, 9 - 14 June 2013. Eds. Risto Sievänen, Eero Nikinmaa, Christophe Godin, Anna Lintunen & Pekka Nygren. http://www.metla.fi/fspm2013/proceedings. ISBN 978-951-651-408-9.

KEYNOTE: A critical role for root models in feeding 10^{10} people

Jonathan P. Lynch
Dept. Plant Science, The Pennsylvania State University, University Park, PA, 16802, USA
correspondence: JPL4@psu.edu

Highlights: There is an urgent need to develop crops with reduced nutrient and water requirements. The complexity of relevant processes overwhelms conventional empirical approaches. Structural-functional modeling of root systems has a unique role in providing important insights into the root phenome, which will focus empirical research on the most productive avenues, and inform crop ideotype development.

Keywords: root traits, modeling, food security

We confront a global crisis. Approximately 1B people are chronically hungry, soil and water resources are degrading, climate is changing, and the human population is expected to reach 10B in a few decades. The greatest challenge facing humanity today is the need to develop systems to sustainably support our species.

Food production requires water and nutrients. In rich nations the intensive use of fertilizers and irrigation are causing significant environmental degradation, while in poor nations drought and low soil fertility are primary limitations to crop yields, food security, and economic development. It is unrealistic to expect poor nations to adopt the input-intensive agriculture of rich nations for both economic and environmental reasons, as well as inherent limits to the supply of resources including fresh water and high grade phosphorus ore deposits. In both rich and poor nations, new crops and crop varieties with reduced water and nutrient requirements would have great value.

Fortunately, substantial genetic variation exists within crops for growth and yield in stressful soil environments. Much of this variation is related to root traits. However, we do not understand root/soil interactions very well, in large part because of the complexity of the problem. Root systems are highly dynamic, complex structures, interacting with the soil, which is a highly complex, dynamic, diverse, and opaque environment. It is very difficult to conceptualize how a root trait might affect crop growth in the context of this complexity. Structural-functional plant models therefore have unique value in helping us understand the acquisition of soil resources by plant roots. Such models have heuristic value in identifying knowledge gaps, key processes, and potential outcomes and interactions, that are useful for guiding empirical research. Empirical research is in turn useful in parameterizing and guiding model development.

An example of the application of root modeling for the improvement of crop stress tolerance is the search for root traits to improve water and N acquisition by maize.

An ideotype to optimize water and N acquisition by maize root systems is called “steep, cheap, and deep”; ‘steep’ representing architectural traits, ‘cheap’ representing anatomical traits that reduce the metabolic cost of soil exploration, and ‘deep’ representing the goal of placing roots deeper in the soil profile, where water and nitrate resources are often found under stressful conditions (Lynch, 2013). The ideotype includes 1) a large diameter primary root with few but long laterals and tolerance of cold soil temperatures, 2) many seminal roots with shallow growth angles, small diameter, many laterals, and long root hairs, or as an alternative, an intermediate number of seminal roots with steep growth angles, large diameter, and few laterals coupled with abundant lateral branching of the initial crown roots, 3) an intermediate number of crown roots with steep growth angles, and few but long laterals, 4) one whorl of brace roots of high occupancy, having a growth angle that is slightly shallower than the growth angle for crown roots, with few but long laterals, 5) low cortical respiratory burden created by abundant cortical aerenchyma, large cortical cell size, an optimal number of cells per cortical file, and accelerated cortical senescence, 6) unresponsiveness of lateral branching to localized resource availability, and 7) low Km and high Vmax for nitrate uptake. Some elements of this ideotype have experimental support, but most are hypothetical.

The structural-functional root model *SimRoot* has been very useful in assessing various aspects of this ideotype. *SimRoot* is a dynamic model that simulates the growth and development of root systems and nutrient acquisition from the soil (Lynch *et al.*, 1997; Postma and Lynch, 2011).

One application of *SimRoot* was to quantitatively evaluate the hypothesis that the formation of root cortical aerenchyma (RCA) is a useful adaptation to suboptimal availability of phosphorus, nitrogen, and potassium by reducing the metabolic costs of soil exploration. Empirical data shows that RCA formation reduces the respiration and nutrient content of root segments, but it was not known if these effects could

significantly benefit plant growth, considering the spatiotemporal complexity of RCA expression, and the autocatalytic effects of reduced root metabolic costs on soil resource acquisition. *SimRoot* showed that RCA could increased the growth of simulated 40-d-old maize plants substantially under conditions of suboptimal nitrogen, phosphorus, or potassium, and that RCA could also reduce critical fertility levels in high-input systems (Postma and Lynch, 2011). The utility of RCA depended on other root phenes and environmental factors. In low-phosphorus soils, the utility of RCA was greater in plants with increased lateral branching density. In low-nitrate soils, the utility of RCA formation was greater in coarser soils with high nitrate leaching. These results were supported by field results showing that high RCA maize lines have greater rooting depth, better drought tolerance, and better growth under limited N.

SimRoot was also used to assess the potential value of several architectural phenes, including nodal root growth angle and branching. These results indicate that moderately steep nodal root growth angles are best for N acquisition, but that the magnitude of the benefit depends on the rate of nitrate leaching, which in turn depends on the soil texture, precipitation, and N fertility regime. Planting density also effects the optimal root branching angle by affecting interplant competition. Variation in lateral branching was also related to nitrate capture. Root phenotypes with few, long lateral branches had the best nitrate capture. However, for phosphorus capture, the best root phenotype had many, short lateral roots. This functional tradeoff is an example of the complexity that modeling can elucidate.

The 'steep, cheap, and deep' ideotype is composed of multiple architectural, anatomical, and physiological traits. Some of these traits have interactions with each other, including synergism (positive interaction) and antagonism (negative interaction). The possible combinations of these traits generates millions of potential root phenotypes, the utility of which will be affected by several environmental variables including precipitation, soil type, nutrient availability, soil temperature regime, etc. Simulation modeling is the only feasible way to explore this 'fitness landscape' and guide empirical research to the most promising avenues.

Root modeling has great value in helping us understand the complexity of the interactions between plant root systems and soil. Linking root modeling efforts with empirical research and crop breeding is more powerful than modeling in isolation. Currently the field is limited by inadequate research and training investment outside of the EU. This must change if we are to realize the benefit of this tool for improving global food security.

LITERATURE CITED

Lynch JP. 2013. 2013. Steep, cheap, and deep: an ideotype to optimize water and N acquisition by maize root systems. *Annals of Botany* doi:10.1093/aob/mcs293.

Lynch JP, Nielsen KL, Davis RD, Jablokow AG. 1997. *SimRoot*: Modelling and visualization of root systems. *Plant and Soil* **188**: 139-151.

Postma JA, Lynch JP. 2011. Root cortical aerenchyma enhances the growth of maize on soils with suboptimal availability of nitrogen, phosphorus, and potassium. *Plant Physiology* **156**: 1190-1201.

Postma JA, Lynch JP. 2011. Theoretical evidence for the functional benefit of root cortical aerenchyma in soils with low phosphorus availability. *Annals of Botany* **107**: 829-841.

Proceedings of the 7th International Conference on Functional-Structural Plant Models, Saariselkä, Finland, 9 - 14 June 2013. Eds. Risto Sievänen, Eero Nikinmaa, Christophe Godin, Anna Lintunen & Pekka Nygren. http://www.metla.fi/fspm2013/proceedings. ISBN 978-951-651-408-9.

Integration of root system in a ryegrass perennial model based on self-regulation

Vincent Migault[1], **Didier Combes**[1], **Gaëtan Louarn**[1], **Loïc Pagès**[2] and **Abraham Escobar-Gutiérrez**[1*]
[1]*INRA, UR4 URP3F, BP 6, F-86600 Lusignan, France*, [2]*INRA centre d'Avignon, UP 115 PSH Site Agroparc, 84914 Avignon Cedex 9, France*
**correspondence:* abraham.escobar@lusignan.inra.fr

Highlights: An individual-based functional-structural model of heterogeneous mini populations of ryegrass plants can be a useful tool to improve our understanding of the grassland use-value creation. Here we present the L-grass model that allows simulating the shoot and root development of plants with different morphologies using self-regulation rules in an auto-organized architectural system.

Keywords: L-system, perennial ryegrass

INTRODUCTION

Grasslands are one of the major sources of forage in Europe. They are exploited via foraging and mowing. In the European changing political context regarding environmental questions, social perception of grasslands has shifted. Grasslands are now seen as important due to two main functions: forage production and environmental roles (biodiversity preservation, carbon sequestration, soil conservation). They are well inserted in the multifunctional paradigm. In addition, compared with other land uses, grasslands present some particularities that justify their specific study. For example, they are perennials populations repeatedly exploited via defoliation-regrowth cycles while growing under changing conditions. Grasslands also show high intra and inter specific variability.

Both the canopy structure and the genotypic composition of the population are determinants of the grassland use-value (quantity and quality of the harvested biomass) as well as of its environmental roles. Canopy structure and the genotypic composition of the population are emergent properties resulting from the behaviour of individual plants and their interactions during the grassland lifespan. Thus, the study of the morphogenesis of the individual is a relevant element to better understand the dynamic of the canopy structure and the population composition.

Several major environmental factors affect plant morphogenesis such as: light resource (trophic and photomorphogenetic signals), intensity and frequency of defoliation, nutrient supply, water availability, and temperature dynamics. However, it is difficult to quantify the contribution of each of these factors to the phenotypic plasticity because of their multiple interactions.

OBJECTIVES

Our aim is to build up an individual-based functional-structural model of heterogeneous mini populations of perennial ryegrass plants. A functional-structural model of shoot morphogenesis exists (Verdenal *et al.*, 2008). It dynamically simulates the shoot structure of the plant by using auto-regulation rules in an auto-organized system (Verdenal *et al.*, 2012). In its current version, the model is based on the assumption that resources from the soil are not limiting plant growth. Nevertheless, in order to better understand the impact of soil resources on the shoot architecture and therefore on the biomass harvested, our objective is to endow the model with a module of root morphogenesis.

THE MODEL

Our L-grass model is based on the L-system formalism (Lindenmayer, 1968; Prusinkiewicz, 1999) using the L-Py simulation framework (Boudon *et al.*, 2012) from OpenAlea platform. The topology of the whole plant is modelled using the MTG package (Godin *et al.*, 1999).

The plant model simulates the 3D development of the shoot and root parts of plants in the vegetative phase. It is largely inspired from a shoot morphogenesis model (Verdenal *et al.*, 2008) and the root system model ArchiSimple (Pagès *et al.*, 2012). The model ArchiSimple allows the root system to be simulated with a low number of parameter. Moreover, carbon resources provided by shoot are considered in this model.

Establishment of plant topology

The plant is represented by a set of phytomers organized as a tree. Each branch of the tree represents a tiller. Phytomers are composed of internode, leaf, root bud, and axillary buds. This composition of phytomers is inspired from a representation of another poaceae, the rice plant (Nemoto *et al.*, 1995). The rate of phytomer production is a function of leaf emergence from sheaths. Emission of new primary root, from a root bud, depends on the tiller rank (primary tiller, secondary tiller,…) and on the number of phytomers in the tiller.

Elongation of organs

Elongation of a leaf starts when its phytomer is created. Leaf parameters such as final length, elongation duration, and proportion of sheaths and blades, are determined as functions of the time that the leaf spends growing within the whorl. Thus, they are partially determined by the sheath length of the previous leaf.

Root development is inspired from the model ArchiSimple (Pagès *et al.*, 2012). It allows to represent the 3D architecture of roots using nine parameters (such as inter-branching distance, tip diameter of emitted roots) estimated from rhizotron and pot experiments. Elongation of the root is regulated by the behaviour of the shoot by an allometric relationship. Indeed, root tips have a growth potential (defined as function of root tip diameter), which is achieved only if the shoot part of the plant provides enough carbon resources for growth and associated respiration.

RESULTS AND DISCUSSION

The model allows simulating the development of ryegrass plants with different morphologies. For example, two contrasting genotypes (Hazard *et al.*, 1996) developing short or long leaves were simulated (Fig. 1).

Fig. 1. Results of simulations of two ryegrass plants with different morphologies, at the same age of development, (Short Leaves (left); Long Leaves (right))

The model allows simulating different root system morphologies without changing root parameters. Indeed, the plasticity of the root system architecture is related to the plasticity of the aerial part transmitted via a self-regulation rule that triggers the emission of new primary roots and the tip growth potential that depends on leaf area. In addition, simulations of different cutting management regimes are also possible (Fig. 2). Indeed, a cut reduces significantly the leaf area thus the effective growth of roots becomes quasi null. The development of the root system, at this time, is thus very slow. Simulation results are in good agreement with observations.

Fig. 2. Sequence illustrating the simulation of the development of a plant undergoing defoliation at 300 °C.d (A1 to A4) and without cutting (B). A1 and A2 represent the plant just before and after the cut. A3 and A4 represent the plant regrowth at time 350 °C.d and 400 °C.d.

The root system representation using all the architecture details is CPU-consuming. Therefore, simulations of canopy undergoing different management could result long and unpractical.

PERSPECTIVES

Time-consuming. In order to overcome the time-consuming calculation due to an explicit architecture of the root system, the use of the root density approach (Dupuy *et al.*, 2010) could be explored.

Environmental condition. Inclusion of a virtual soil (water and nitrogen availabilities) in the model is possible. Estimation of the quantity of resources uptake from soil could modify leaf growth potential, and thus the architecture of the shoot. Thus aerial architecture will be modified and therefore the root system architecture too. These kinds of simulation will help to understand the aerial architectural (so the grassland use-value) response to modification of water and nutrient supply.

KNOWLEDGEMENTS

This research is partially funded by “La Région Poitou-Charentes”, France.

LITERATURE CITED

Boudon F, Pradal C, Cokelaer T, Prusinkiewicz P and Godin C. 2012. L-Py: an L-System simulation framework for modeling plant development based on a dynamic language.

Dupuy L, Gregory PJ and Bengough AG. 2010. Root growth models: towards a new generation of continuous approaches. *Journal of Experimental Botany*, **61**:2131-2143.

Godin C, Costes E and Sinoquet H. 1999. A method for describing plant architecture which integrates topology and geometry. *Annals of Botany*, **84**:343-357.

Hazard L, Ghesquiere M and Barraux C. 1996. Genetic variability for leaf development in perennial ryegrass populations. *Canadian Journal of Plant Science*, **76**:113-118.

Lindenmayer A. 1968. Mathematical models for cellular interaction in development, Parts I and II. *Journal of Theoretical Biology*, **18**:280–315.

Nemoto K, Morita S and Baba T. 1995. Shoot and root development in rice related to the phyllochron. *Crop Science*, **35**:24-29.

Pagès L, Moreau D, Sarlikioti V, Boukcim H and Nguyen C. 2012. ArchiSimple: a Parsimonious Model of the Root System Architecture. *IEEE 4th International Symposium on Plant Growth Modeling, Simulation, Visualization and Applications*.

Prusinkiewicz P. 1999. A look at the visual modeling of plants using L-systems. pp. 211-224.

Verdenal A, Combes D and Escobar-Gutierrez A. 2012. Programmable and Self-Organised Processes in Plant Morphogenesis: The Architectural Development of Ryegrass. In *Morphogenetic Engineering*: Springer Berlin Heidelberg, pp. 501-517.

Verdenal A, Combes D and Escobar-Gutierrez AJ. 2008. A study of ryegrass architecture as a self-regulated system, using functional-structural plant modelling. *Functional Plant Biology*, **35**:911-924.

Proceedings of the 7th International Conference on Functional-Structural Plant Models, Saariselkä, Finland, 9 - 14 June 2013.
Eds. Risto Sievänen, Eero Nikinmaa, Christophe Godin, Anna Lintunen & Pekka Nygren.
http://www.metla.fi/fspm2013/proceedings. ISBN 978-951-651-408-9.

Modelling Sugar maple development along its whole ontogeny: modelling hypotheses and calibration methodology

Taugourdeau O[1], Delagrange S[2], de Reffye P[3] and Messier C[1-2]
[1]*: Chaire CNRSG/Hydro-Québec, Dép. Sc. Biol. – UQAM, Montréal, Québec, Canada;* [2]*: ISFORT-UQO, Ripon, Québec, Canada;* [3]*: CIRAD-UMR AMAP, Montpellier, France.*
Correspondence: o.taugourdeau@gmail.com

Highlights: Relevant GreenLab model hypotheses can be used to model sugar maple development along its whole ontogeny. A dedicated methodology is presented for model calibration (from measurement to parameter calibration). It allows the modelling of long lived trees with highly complex structures.

Keywords: GreenLab model, Sink-source, Biomass partitioning, Factorization, Simulation, virtual plant, *Acer saccharrum* Marsh.

INTRODUCTION

Modelling tree development is a difficult task due to their long lifespan and complex crown structure. Traditionally in forestry, vertical complexity is represented by simple measures (e.g. Diameter at Breast Height (DBH), tree height) and the temporal scale is assessed by survey or ring and stem analysis. When more precise modelling is required (e.g. crown shape and branches sizes), plant architectural analysis provides a relevant framework to analyse and simulate tree structure development over time (Barthélémy & Caraglio 2007).

Dealing with long lifespan and spatial complexity is also an issue for computer simulations, mainly because as plants age, there is an exponential increase in the number of organs. For example, light interception simulation at the leaf level is often possible only on saplings (Perttunen *et al.* 2001).

The aim of this study is to provide a simple and accurate modelling approach for tree growth, architecture and biomass partitioning -across all ontogenetic stages- based on the GreenLab model (de Reffye & Hu 2003) and driven by tree scale constraints. GreenLab model presents desirable properties for tree modelling and simulation: (i) structure factorization based on botanical knowledge, (ii) possibility of doing simulation with or without tree geometrical reconstruction and (iii) data driven approach (hidden parameters estimation). We use Sugar maple (*Acer saccharrum* Marsh.) as a model species due to its ecological and economic importance in Eastern North-America temperate forests and the abundant existing ecophysiological knowledge of the species.

MODELLING HYPOTHESIS

Modelling scale

GreenLab is based on discrete time step modelling. In this study, each time step corresponds to a year and the structural unit is the annual shoot (i.e all organs produced by a single shoot apical meristem during a single year). Each time step is divided into two successive substeps: structure development (i.e. organogenesis), and organ functioning (i.e. assimilation and growth).

Structure development

Structure development is based on physiological age modelling assumptions (Barthélémy & Caraglio 2007): (i) each annual shoot produced by the tree can be labelled with a given Physiological Age (PA) and (ii) all annual shoots produced the same year and with the same PA behave the same way. This last property allows structure factorization that largely reduces computing limitations related to time and memory use. Structure development is modelled by a set of determinist (axes drift and base effect) and stochastic (branching and mortality) processes.

Branching and mortality rules were defined at PA scale. Branching corresponded to a square matrix with $n_{i,j}$ the average number of annual shoots of each PA j hold by an annual shoot of PA i. Mortality is modelled as a sigmoid function of axes age (i.e. age of the first annual shoot)

Axes drift (Barthélémy & Caraglio 2007) is modelled as a transition from a PA to another one along successive annual shoots of an axis.

Base effect (Barthélémy & Caraglio 2007) is modelled by constraining the number of internodes –and ultimately the number of lateral axis- produced by each PA with empirical ontogenetic rules.

Organ functioning

Biomass partitioning at each time step is based on sink-source equations:

$$q_i(t)=d_i(t)*Q(t-1)/(\sum_i (d_i(t))+ Dwood(t)) \quad (1)$$

with $q_i(t)$ increment of organ biomass at time t, $di(t)$ organ demand at time t, $Q(t-1)$ biomass assimilated by the tree at time t-1, $\sum_i (d_i(t))+Dwood(t)$ the total plant demand at time t that include plant demand for wood production ($Dwood(t)$). $Q(t=0)$ correspond to seed mass. Three different types of demands and allocations are considered: leaf demand, internode demand for primary growth and plant demand for secondary growth. The first two types only occur during the year of organ development and depend of annual shoots PA (i.e. one demand parameter per organ type and PA). Plant demand for secondary growth is proportional, with a parameter Pc, to the total leaf number. Internodes allocations to secondary growth are based on pipe model assumptions (surface section conservation).

Biomass assimilation is modelled as asymptotic function of leaf area:

$$Q(t)= 1/R * Sp (1-exp(-k.Sf(t)/Sp)) \quad (2)$$

with $Sf(t)$ the tree total leaf area at time t which is related to tree leaf biomass and Leaf Mass per Area ratio empirically calibrated (range from 40g.m-2 to 180g.m-2 along tree ontogeny), R a scaling factor, Sp the available surface for the tree (i.e. Sp/R correspond the maximal quantity of biomass the plant can assimilated per year given the environment and $Sf(t)/Sp$ to the LAI), k correspond to a calibration coefficient related to the efficiency of leaf displacement (i.e. self-shading).

CALIBRATION

Biological dataset (on AmapStudio)

To minimize phenotypic variation driven by environmental factors, dominant or co-dominant trees of various sizes (from seedlings to 74cm of DBH) were identified in summer 2012. To do this, maple forest stands originating from clear cuts of contrasting ages (from 5 years to 34 years) were visited to obtain individuals ranging in size from seedling to 20 cm DBH. Larger individuals (up to 74 cm DBH) were sampled from uneven aged forest stands. Total sample consisted of 48 individuals.

In September after cessation of growth, the last 3-years of growth were sampled for the main stem, or for one of the main stems for reiterated trees. All the annuals shoots of these branching systems were labelled and the following traits were measured: topological location (following MTG formalism), annual shoot dry biomass, internodes lengths, leaf number, fresh leaf surface and leaf dry biomass.

Physiological age identification (on R)

A semi-automated algorithm was developed to perform PA labelling on measured annual shoots. The goal was to characterize a PA based on annual shoots morphological measurements (annual shoot length, number of leaves, average internodes length) and the estimated PA of its lateral axes. The initialization is made on the ultimate PA that can be recognized by the lack of any lateral axes development.

- Step 0: main stem annual shoots are associated with the first PA and were removed from following steps:
- Step 1: estimating a linear discriminant model on the occurrence of lateral axes on 2011 annuals shoots (unbranched vs. branched) based on morphological measurements.
- Step 2: predicting the PA of 2012 annual shoots: due to one-year delayed branching none of them already express branching.
- Redo step 1-2 with a supplementary group: unbranched 2011 annual shoots, branched 2011 annual shoots that hold ultimate PA axes (according to step 2 predictions) and other 2011 annual shoots.
- Redo step 1-2 with a supplementary group …

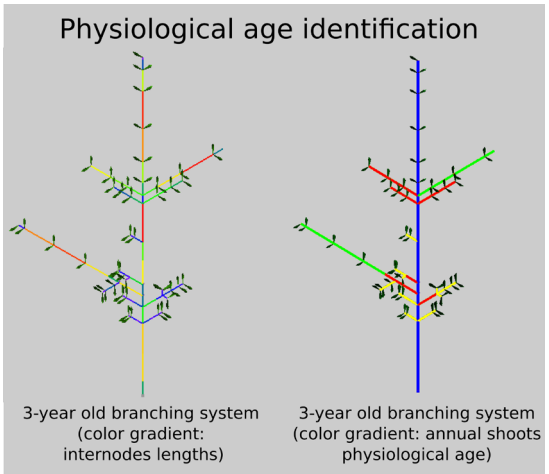

Fig. 1: Physiological age identification based on morphological measurements. Left: Internodes colours correspond to their respective lengths (long internodes in red and short internodes in blue). **Right:** Annual shoots colours correspond to their physiological age (GreenLab color code convention).

The recursive algorithm is stopped when the "other 2011 annual shoots" contains too few annual shoots that can be recognized as main stem reiterations.

The R implementation of the algorithm takes as input a matrix of data at annual shoot scale that includes branching relationships between annual shoots. Data extraction was made with AmapStudio.

In our case, four PA were characterized (**Fig. 1**).

Branching, Mortality and ontogeny rules calibration (on R)

Based on PA identifications, branching rules were calibrated by the mean number of lateral axes of PA*j* hold by PA*i* 2011 annual shoots (i.e. a given annual shoot can hold different type of lateral axes simultaneously).

Mortality rules were estimated by making complement measurements on labelled trees. The proportion of dead lateral axes per PA was recorded, along 65 axes of various sizes. A two-parameter logistic curve was estimated per PA of lateral axes.

The ontogenetic changes of the number of internodes per annual shoots (i.e. ontogenetic rules) were described empirically with five control points with linear interpolation between each of them. As the real age of each tree remains unknown, the empirical functions were calibrated with tree DBH (or tree base diameter for smallest trees). Tree diameter was later converted to tree age based on ring width measurements.

Sink-source parameters calibration (on Matlab)

All parameters related to supply (*R*, *Sp* and *k*) and demand (*Q(t=0)*, *Pc* and leaves and stem demand per PA) computations were calibrated together. Data used correspond to the leaves and stem dry biomass per PA and per year (only the last for leaves) measured on the 48. Structure development rules were used to provide, for each time step, the number of annual shoots of each PA and each age. Gauss-Newton gradients were used for parameter estimations. Results of this analysis will be provided at the conference.

DISCUSSION AND PERSPECTIVES

In previous applications of GreenLab on trees, the development sub-model was by-passed thanks to an exhaustive topology description based on expert physiological age identification (e.g. Guo *et al.* 2012). To our knowledge, the current methodology is the first GreenLab application that allowed the stochastic development sub-model calibration (e.g. branching probabilities and branch mortality) for long-lived trees, which prevent any exhaustive measurements.

The physiological age identification algorithm appeared as an efficient way toward automation of the stochastic development sub-model calibration. An open question is to quantify the consistence of this algorithm with: botanical expertise, hidden Markov tree modelling (Durand *et al.* 2005) and other clustering methods (e.g. kmeans).

Based on accurate structure development and organ functioning calibration, several opportunities are possible: (i) tree growth simulation along 150 years; (ii) replacing ontogenetic rules by functional ones to get a feedback between structure complexity and environmental constraints and (iii) testing some pruning scenarios during simulations.

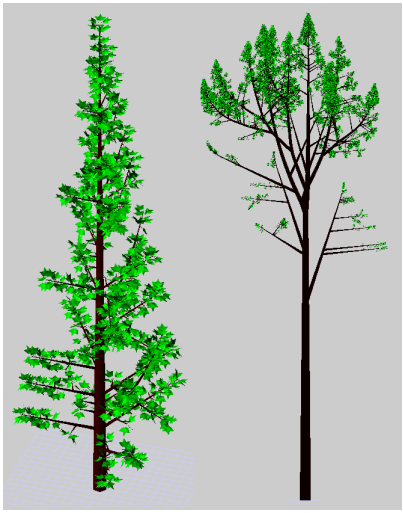

Fig. 2: The same virtual tree at two different time step. left: 15 years old; **right:** 90 years old (scales are not respected). Calibrated developmental parameters were used to calibrate AmapSim, thanks to AmapSim compatibility with developmental part of GreenLab. Visualisation was made in AmapStudio.

ACKNOWLEDGEMENTS

OT postdoctoral fellowship was funded by the Chaire de recherche CNRSG/Hydro-Quebec. The venue of PdR in Québec was funded by the CEF-CFR. B. Lecigne, J. Poirier, M.-E. Roy, R. Pouliot and S. Raposo provided useful help during measurements. J.-F. Barczi provided useful help for AmapSim parameterization (**Fig 2.**). C. Nock provided relevant comments on the manuscript.

LITERATURE CITED

Barthélémy D, Caraglio Y. 2007. Plant architecture: A dynamic, multilevel and comprehensive approach to plant form, structure and ontogeny. *Annals of Botany* **99** (3): 375-407.

Durand J-B, Guédon Y, Caraglio Y, Costes E. 2005. Analysis of the plant architecture via tree-structured statistical models: the hidden Markov tree models. *New Phytologist* **166**: 813–825.

Guo H, Lei X, Cournede P-H, Letort V. 2012. Characterization of the effects of inter-tree competition on source–sink balance in Chinese pine trees with the GreenLab model. *Trees* **26**: 1057–1067.

de Reffye P, Hu BG. 2003. Invited talk. Relevant qualitative and quantitative choices for building an efficient dynamic plant growth model: GreenLab case. *Plant Growth Modeling and Applications, Proceedings*: 87-107.

Perttunen J, Nikinmaa E, Lechowicz MJ, Sievänen R, Messier C. 2001. Application of the functional-structural tree model LIGNUM to sugar maple saplings (*Acer saccharum* Marsh) growing in forest gaps. *Annals of Botany* **88** (3): 471–481.

Proceedings of the 7th International Conference on Functional-Structural Plant Models, Saariselkä, Finland, 9 - 14 June 2013. Eds. Risto Sievänen, Eero Nikinmaa, Christophe Godin, Anna Lintunen & Pekka Nygren. http://www.metla.fi/fspm2013/proceedings. ISBN 978-951-651-408-9.

Characterizing the balance between ontogeny and environmental constraints in forest tree development using growth phase duration distributions

Yann Guédon[1], **Olivier Taugourdeau**[2], **Yves Caraglio**[3] and **Sylvie Sabatier**[3]
[1]*CIRAD, UMR AGAP and Inria, Virtual Plants, F-34095 Montpellier, France,* [2]*Université Montpellier 2, UMR AMAP, F-34398 Montpellier, France,* [3]*CIRAD, UMR AMAP, F-34398 Montpellier, France*
**correspondence:* guedon@cirad.fr

Highlights: We built segmentation models to identify tree growth phases on the basis of retrospective measurement of annual shoot characteristics along the main stem. Growth phase duration distributions estimated within these models characterize the balance between ontogeny and environmental constraints in tree development at the population scale. These distributions have very contrasted characteristics in terms of shape and relative dispersion between ontogeny-driven and environment-driven tree development.

Keywords: developmental plasticity; growth trajectory; hidden semi-Markov chain; segmentation model.

INTRODUCTION

Tree developmental plasticity is a key determinant of forest dynamics and composition. This study aimed to identify robust indicators that summarize the balance between ontogeny and environmental constraints in tree development using different species growing in contrasted conditions.

Observed apical growth, as given for instance by the length of successive annual shoots along a tree main stem, results mainly from an ontogenetic component and an environmental component. In this study, the ontogeny was viewed as a developmentally programmed growth trajectory preadjusted to the most likely environments (Yagi 2009). The ontogenetic component is assumed to be structured as a succession of roughly stationary growth phases that are asynchronous between individuals (Guédon et al. 2007). We applied segmentation models to identify growth phases on the basis of characteristics measured retrospectively on successive annual shoots along a tree main stem. When building segmentation models for different tree species growing in contrasted conditions (Guédon et al. 2007; Chaubert-Pereira et al. 2009; Taugourdeau et al. 2011), growth phase duration distribution emerged as a potential indicator that could summarize the balance between ontogeny and environmental constraints in tree development at the population scale. Growth phase duration distributions ranged from bell-shaped distributions with small relative dispersions for trees growing in open field conditions to right-skewed distributions with larger relative dispersions for trees growing in understorey. The objective here is thus to investigate systematically this indicator.

RESULTS

The analysis of the duration of growth phases is illustrated by both evergreen (Corsican pine and silver fir) and deciduous (sessile oak and Persian walnut) tree species growing in contrasted conditions ranging from managed forest stands (Corsican pine and sessile oak) to unmanaged understoreys (silver fir and Persian walnut). All these data sets include a large number of individuals (between 65 and 208) and correspond mostly to young trees before their maximum growth. For each data set, a hidden semi-Markov chain (HSMC), which is a two-scale segmentation model (Guédon et al. 2007), was built. In this framework, the succession and duration of growth phases (coarse scale) are represented by a non-observable semi-Markov chain while annual shoot characteristics (e.g. length, number of growth units) within a growth phase (fine scale) are represented by observation distributions attached to each state of the semi-Markov chain. Hidden semi-Markov chains were compared with simple hidden Markov chains (HMCs) which corresponds to the purely opportunistic development assumption driven by changing environmental constraints (Taugourdeau et al. 2011). In a HSMC, the duration of each growth phase is explicitly modelled by a dedicated parametric discrete distribution, while in a HMC, the duration of each growth phase is implicitly modelled by a geometric distribution, which is the unique “memoryless” discrete distribution. The assumption of geometric state occupancy distributions (the shorter the growth phase duration, the more probable it is) should here be viewed as a limiting case and a minimal duration > one year in a given growth

phase is a more realistic assumption. HSMCs and HMCs were estimated on the basis of bivariate sequences along the main stems with the annual shoot length as first variable (the index parameter of the sequence was thus the year) and as second variable:

- the number of branches per tier for Corsican pine and silver fir,
- the number of growth units for sessile oak,
- the absence/presence of branches for Persian walnut.

There were three states (i.e. two successive transient states followed by a final absorbing state) for Corsican pine, silver fir and Persian walnut and two for sessile oak. As the last year of measurement was arbitrary with regard to tree development, the duration of the last growth phase was assumed to be systematically truncated and could not be modelled.

As a result of the estimation procedure, the succession of states was deterministic for each estimated model. This deterministic succession of states supports the assumption of a succession of growth phases. The integrated completed likelihood criterion (a model selection criterion which takes account of the segmentation objective) clearly favoured the estimated HSMC in the Corsican pine and sessile oak cases while the estimated HSMC and HMC were quite close according to this criterion in the silver fir and Persian walnut cases. While the Corsican pine and sessile oak developments were far from an opportunistic development driven by changing environmental constraints, the silver fir and Persian walnut developments were close to an opportunistic development. Using different methods (Guédon et al. 2007), we checked that the estimated state occupancy distributions representing growth phase durations reflected mainly between-individual differences rather than within-individual differences (i.e. different possible segmentations of a given individual) and were readily interpretable as population parameters.

Table 1. State occupancy distributions estimated for each HSMC: parametric definition, mode and coefficient of skewness.

	State 0			State 1		
	Distribution	Mode	Skewness	Distribution	Mode	Skewness
Corsican pine	B(1, 6, 0.36)	3	0.26	NB(1, 3.26, 0.44)	3	1.15
Sessile oak	B(1, 9, 0.42)	4	0.11			
Silver fir	NB(1, 1.95, 0.092)	10	1.43	NB(1, 2.89, 0.17)	10	1.18
Persian walnut	NB(1, 1.83, 0.12)	6	1.48	NB(1, 1.74, 0.15)	5	1.52

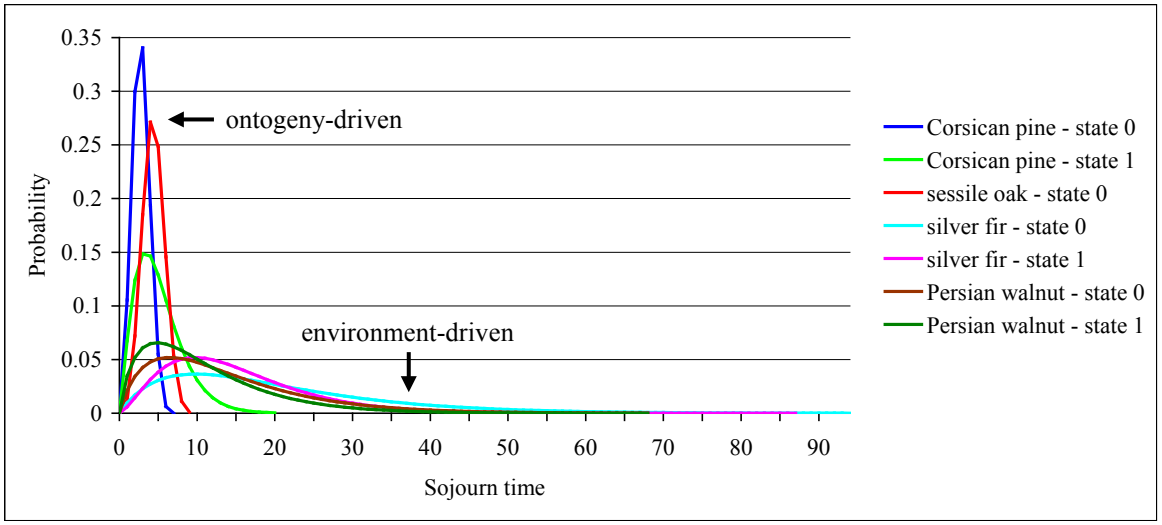

Figure 1: Estimated state occupancy distributions.

All the estimated state occupancy distributions were 1-shifted binomial distributions B(1, n, p) or negative binomial distributions NB(1, r, p); see Table 1. The estimated state occupancy distributions were very different in terms of shape, ranging from bell-shaped distributions (state 0 for Corsican pine and sessile oak) to distributions tending toward reverse-J-shaped distributions (states 0 and 1 for Persian walnut, state 0 for silver fir); see Figure 1. The estimated state occupancy distributions can be compared on the basis of their coefficient of skewness and their shape parameter r for negative binomial distributions; see Table 1. The

coefficient of skewness is a dimensionless measure of the asymmetry of a distribution. In our case of positive skewness, the magnitude of this coefficient quantifies how the bulk of the values lies to the left of the mean. The proximity of the coefficient of skewness to 2 (approximate coefficient of skewness of the implicit geometric state occupancy distributions of the estimated HMCs in our case) can be interpreted in terms of proximity to the geometric distribution. In the case of a negative binomial distribution, the proximity of the shape parameter *r* to 1 (the shape parameter of the geometric distribution) can be also interpreted in terms of proximity to the geometric distribution. The estimated state occupancy distributions can be ranked from the closest to the farthest from geometric distributions:

1. states 0 and 1 for Persian walnut, state 0 for silver fir,
2. state 1 for silver fir and state 1 for Corsican pine,
3. state 0 for Corsican pine and sessile oak.

For 1-shifted binomial distributions (state 0 for Corsican pine and sessile oak), we have $\mu - 1 > \sigma^2$ while for 1-shifted negative binomial distributions (all the other states), we have $\mu - 1 < \sigma^2$. Hence, the three groups of state occupancy distributions defined above also correspond to different variance to mean ratios.

DISCUSSION

If it is assumed that forest gaps occur with a constant probability at a given location in unmanaged forest understorey (Spies et al. 1990), trees within the population will be randomly affected by a marked change in the light environment that suddenly will become favourable and likely induce a growth phase transition. In this case, we expect growth phase duration distributions to be close to geometric distributions, the unique discrete memoryless distribution, reflecting opportunistic development at the population scale. When tree development is mainly driven by changes in the local environment (mainly light environment), we will speak of environment-driven development. When the changes in the local environment are gradual, small in magnitude, and only slightly modulate tree ontogeny, we will speak of ontogeny-driven development. At first sight, the Corsican pine and sessile oak examples illustrate ontogeny-driven development while the Persian walnut and silver fir examples illustrate environment-driven development.

The modes of the two estimated growth phase duration distributions were similar in the different three-state models (Corsican pine, silver fir and Persian walnut); see Table 1. The four examples may be ranked in order of increasing mode of growth phase duration distributions:

- Corsican pine and sessile oak: trees growing in managed stands with a rather low level of competition;
- Persian walnut: trees growing in the understorey of a riparian forest;
- Silver fir: trees growing in the understorey of a mountain forest.

We therefore assume that the mode of growth phase duration distributions is an indicator of the growing potential of a species in a specific location (independently of competition level). In the case of a highly heterogeneous light environment, the growth phases lengthen for a certain proportion of the population and the growth phase duration distributions become highly right-skewed.

Since each example corresponded to a specific species growing in a specific environment, we focused on dimensionless characteristics of growth phase duration distributions such as the coefficient of skewness. An avenue for future work would be to study species with different adaptative strategies (e.g. shade avoidance and shade-tolerant species) in a given location or to compare the development of a given species in different environments in order to study the phenotypic plasticity of this species.

LITERATURE CITED

Chaubert-Pereira F, Caraglio Y, Lavergne C, Guédon Y. 2009. Identifying ontogenetic, environmental and individual components of forest tree growth. *Annals of Botany* 104(5): 883-896.

Guédon Y, Caraglio Y, Heuret P, Lebarbier E, Meredieu C. 2007. Analyzing growth components in trees. *Journal of Theoretical Biology* **248(3)**: 418-447.

Spies TA, Franklin JF, Klopsch M. 1990. Canopy gaps in Douglas-fir forests of the Cascade Mountains. *Canadian Journal of Forest Research* **20(5)**: 649-658.

Taugourdeau O, Chaubert-Pereira F, Sabatier S, Guédon Y. 2011. Deciphering the developmental plasticity of walnut saplings in relation to climatic factors and light environment. *Journal of Experimental Botany* **62(15)**: 5283-5296.

Yagi T. 2009. Ontogenetic strategy shift in sapling architecture of *Fagus crenata* in the dense understorey vegetation of canopy gaps created by selective cutting. *Canadian Journal of Forest Research* **39**(6): 1186-1196.

Proceedings of the 7th International Conference on Functional-Structural Plant Models, Saariselkä, Finland, 9 - 14 June 2013. Eds. Risto Sievänen, Eero Nikinmaa, Christophe Godin, Anna Lintunen & Pekka Nygren.
http://www.metla.fi/fspm2013/proceedings. ISBN 978-951-651-408-9.

Influence of canopy architecture and parameters of leaf level photosynthesis on dry matter production in greenhouse cucumber

Dirk Wiechers[1], Katrin Kahlen[2], Hartmut Stützel[1]
[1] Leibniz Universität Hannover, Herrenhäuserstr. 2, 30419 Hannover, Germany
[2]University Geisenheim, von-Lade-Str. 1, 65366 Geisenheim, Germany
correspondence: wiechers@gem.uni-hannover.de

Highlights: Productivity of crops highly depends on structural and physiological parameters. Using a FSPM we analyzed the sensitivity of key parameters revealing the strong influence of structural differences as well as the dominant role of light and stomatal control on the physiological parameters.

Keywords: L-System, photosynthesis, canopy structure, modeling

INTRODUCTION

Indeterminately growing plants like cucumbers (*Cucumis sativus* L.) are continuously producing new fruits. In these crops, variations in yield and individual fruit growth depend on the plant arrangement and plant density (Kahlen, 2007; Wiechers et al., 2011a). The photosynthetic activity of the leaves is one of the key physiological processes in plants determining dry matter production, driven by the available quantity of light as one of the major environmental factors (Chenu et *al.*, 2005). The model of leaf photosynthesis developed by Farquhar and coworkers (Farquhar et al., 1980) is capable of predicting the rate of photosynthesis for a variety of environmental factors like: CO_2 concentration, light, temperature and relative humidity (von Caemmerer, 2000). In the Farquhar model, the stomatal conductance (g_s) and the internal conductance (g_i) are major influences on the apparent rate of photosynthesis. The model contains multiple input variables, parameters, constants and equations for which different methods of parameterization are proposed (e.g. Sharkey et al., 2007; Dubois et al., 2007). A combination of the Farquhar model and a model of stomatal conductance (g_s) (Ball et al., 1987) was developed to simulate the photosynthesis of single leaves (Kim and Lieth, 2003). To be able account for the strong variability of leaf photosynthesis over the plant, a leaf level model needs information about the plant and canopy structure. A precise description of the plant structure is of special importance in vertically trained row canopies like greenhouse cucumber with their discontinuous canopy structures, which causes the spatial distribution of light to be highly uneven and variable with time (Wiechers et al., 2011b). Besides the rate of photosynthesis the rate of respiration also plays a major role for the determination of plant productivity. Commonly the concept of growth and maintenance respiration has been used to account for respiration in plant models (Amthor, 2000). Thus, to simulate the environmental influences on the yield formation and the development of individual organs, models which are capable of accounting for interactions between organ based physiological processes and plant morphology influenced by the canopy structure are essential (Fourcaud et al., 2008).

The objective of this study is to gain a better understanding of the importance of the key structural and physiological based factors of plant productivity. Therefore, we extended the established L-Cucumber (Kahlen et al., 2008) model to analyze the influence of structural and physiological factors on dry matter production.

SIMULATIONS

The capability to track structural changes is analyzed by simulating four canopies with different plant spacing's, a dense and a wide variant of both, a row canopy and an isometric canopy (Table 1).

Table 1. Plant spacing of the four measured and simulated canopy architectures

Distance (m)	Sparse Isometric (I1)	Dense Isometric (I2)	Sparse Row (R1)	Dense row (R2)
In row	1.08	0.54	0.54	0.27
Between row	0.93	0.93	1.86	1.86

Into the existing dynamical FSPM L-Cucumber (Kahlen et al., 2008) the model of leaf photosynthesis (Kim and Lieth, 2003) based on own measurement for cucumber was implemented. The model parameterization was not changed for the simulations of the four canopy structures. Main functional traits considered in this study are parameters of the photosynthesis like the maximum rate of electron transport (J_{max}), the maximum rate of carboxylation (V_{cmax}), g_s and g_i. Hourly leaf level light intensities were calculated with the radiosity based Caribu light model (Chelle et al., 1998). To avoid artifacts due to overestimations of the vegetative plant part the maximum leaf size and the specific leaf area (SLA) of the four canopy structures were taken as input in to the model. Plant morphology only differed due to the shade avoidance adaption of the leaves. Simulations were run until day 47 after transplanting with daily measured light and temperature values of the actual experiments as input. Detailed information about assimilate partitioning of the model can be found elsewhere (Wiechers et al., 2011a). Simulation results were compared to data of non-destructive measurements of the vegetative and fruits plant parts as well as final harvest data of four different canopy architectures.

RESULTS AND DISCUSSION

Differences in canopy architecture nearly doubled the final fruit dry mass in the experiment (Fig. 1). We implemented individual coefficients for growth respiration of fruits (30 %) and vegetative parts (10 %), related to the newly produced dry matter, as well as a maintenance respiration coefficient for the fruit part (2 %), related to the standing dry mass. Figure 1 shows exemplarily the close simulation of the measured dry matter production per plant in the different plant architectures for the row canopies. Maintenance respiration of the leaves was assumed to be covered by the respiration term of the Farquhar model. The low respiration coefficients of the fruits can be explained by the relatively low physiological activity of the fruit tissue and the excluding of photosynthetic activity of fruits by the model (Schapendonk & Challa, 1981; Marcelis & Baan Hofman-Eijer, 1995a, b). The maximum deviation of the simulations ranged between 15 % overestimation and 11 % underestimation for the final fruit dry mass. The bigger deviations at the end of the simulation can be related to change in fruit growth due to a topping of the plants (downwards arrows in Fig. 1).

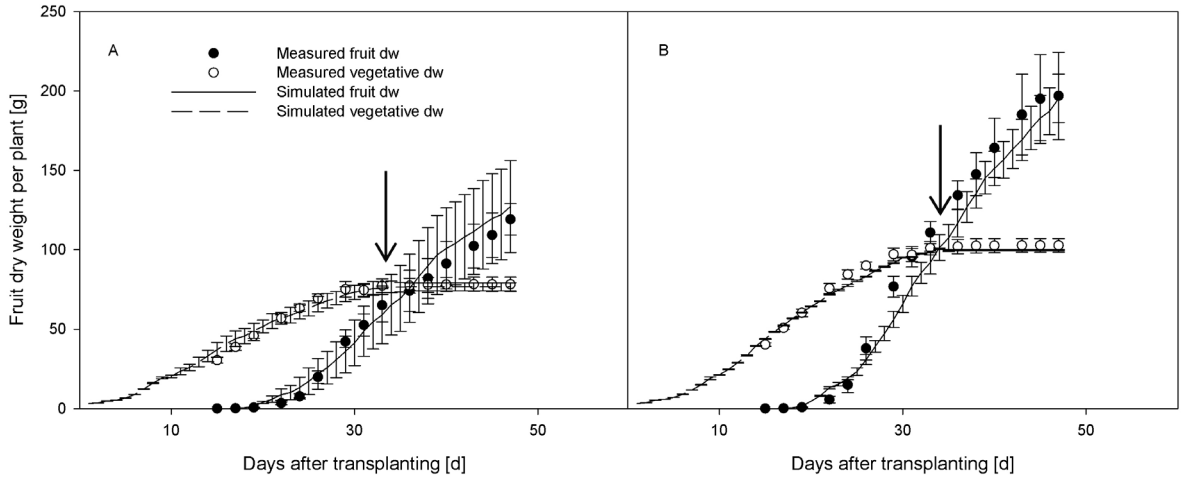

Figure 1. Measured and simulated fruit and vegetative dry weight (dw) per plant in a row canopy with 2 plants per m² (A) and 1 plant per m² (B). Downward arrows indicate topping. Error bars represent standard deviations.

Analyzing the impact of key parameters of leaf level photosynthesis shows clear differences in the sensitivity of a change of individual parameters (Table 2). Starting from the parameterization for cucumber four scenarios for each parameter were simulated with -20 %, -10 %, +10 %, +20 % change of the parameter. Internal conductance and maximum rate of carboxylation were less sensitive to a change of the parameter value compared to changes in the stomatal conductance and the maximum rate of electron transport. The results are in line with the common knowledge that the canopy productivity is mainly influenced by the availability of light and the regulation by the stomata (Trouwborst et al., 2010).

Table 2. Average change (%) over four canopy architectures of internal conductance (g_i), stomatal conductance (g_s), maximum rate of electron transport (J_{max}) and maximum rate of carboxylation (V_{cmax}) per 10 % change of parameter on the final fruit dry weight (FFDW) .

	Change in FFDW (%) per 10% change of parameter			
Parameter	g_i	g_s	J_{max}	V_{cmax}
Mean	0.65	2.83	4.17	0.70
SD	0.60	0.25	0.99	0.91

Extending the existing L-Cucumber model with an implementation of a leaf level model of photosynthesis shows that the presented FSPM provides the possibility to account for physiological factors and factors induced by the spatial structure of the plant and the canopy, which are necessary for an accurate estimation of plant productivity. Relating the physiological changes to the structural differences clearly emphases the importance of a precise description of the plant structure.

Further simulations extending the set of parameters and their interaction should strengthen the usability of the model for analysis of the impact of the different plant parameters on dry matter production. Thus, the FSPM could serve as a tool to analyze the impact of environmental control strategies on productivity for greenhouse production.

REFERENCES

Amthor JS. 2000. The McCree-de Wit-Penning de Vries-Thornley Respiration Paradigms: 30 Years Later. *Annals of Botany* 86: 1-20.

Ball JT, Woodrow IE, Berry JA. 1987. A model predicting stomatal conductance and its contribution to the control of photosynthesis under different environmental conditions. *Progress in Photosynthesis Research* 4: 221-224.

Chelle M, Andrieu B, Bouatouch K. 1998. Nested radiosity for plant canopies. *The Visual Computer*,14: 109-125.

Chenu K, Franck N, Dauzat J, Barczi JF, Rey H, Lecoeur J. 2005. Integrated responses of rosette organogenesis, morphogenesis and architecture to reduced incident light in Arabidopsis thaliana results in higher efficiency of light interception. *Functional Plant Biology* 32: 1123-1134.

Dubois JJB, Fiscus EL, Booker FL, Flowers MD, Reid CD. 2007. Optimizing the statistical estimation of the parameters of the Farquhar-von Caemmerer-Berry model of photosynthesis. *New Phytologist* 176: 402-414.

Farquhar GD, von Caemmerer S, Berry JA. 1980. A biochemical model of photosynthetic CO_2 assimilation in leaves of C_3 species. *Planta* 149: 78-90.

Fourcaud T, Zhang X, Stokes A, Lambers H, Körner C. 2008. Plant Growth Modelling and Applications: The Increasing Importance of Plant Architecture in Growth Models. *Annals of Botany* 101: 1053-1063.

Kahlen K. 2007. Towards functional-structural modelling of greenhouse cucumber In: Vos J, Marcelis LFM, de Visser PHB, Struik PC, Evers JB eds. Functional-Structural Plant Modelling in Crop Production. Dordrecht: Springer.

Kahlen K, Wiechers D, Stützel H. 2008. Modelling leaf phototropism in a cucumber canopy. *Functional Plant Biology* 35: 876-884.

Kim SH, Lieth JH. 2003. A coupled model of photosynthesis, stomatal conductance and transpiration for a rose leaf (Rosa hybrida L.). *Annals of Botany* 91: 771-781.

Marcelis LFM, Baan Hofman-Eijer LR. 1995a. The contribution of fruit photosynthesis of cucumber fruits as affected by irradiance, temperature and ontogenity. *Physiologia Plantarum* 93: 476-483.

Marcelis LFM, Baan Hofman-Eijer LR. 1995b. Growth and maintenance respiration costs of cucumber fruits as affected by temperature and ontogenity and size of the fruits. *Physiologia Plantarum* 93: 484-492.

Schapendonk AHC, Challa H. 1981. Assimilate requirements for growth and maintenance of the cucumber fruit. *Acta Horticulturae* 118: 73-82.

Sharkey TD, Bernacchi CJ, Farquhar GD, Singsaas EL. 2007. Fitting photosynthetic carbon dioxide response curves for C3 leaves. *Plant, Cell & Environment* 30: 1035-1040.

Trouwborst G, Oosterkamp J, Hogewoning SW, Harbinson J, Van Ieperen W. 2010. The responses of light interception, photosynthesis and fruit yield of cucumber to LED-lighting within the canopy. *Physiologia Plantarum* 138: 289-300.

von Caemmerer S. 2000. Biochemical models of leaf photosynthesis Collingwood, CSIRO Publishing.

Wiechers D, Kahlen K, Stützel H. 2011a. Dry matter partitioning models for the simulation of individual fruit growth in greenhouse cucumber canopies. *Annals of Botany* 108: 1075-1084.

Wiechers D, Kahlen K, Stützel H. 2011b. Evaluation of a radiosity based light model for greenhouse cucumber canopies. *Agricultural and Forest Meteorology* 151: 906-915.

Proceedings of the 7th International Conference on Functional-Structural Plant Models, Saariselkä, Finland, 9 - 14 June 2013. Eds. Risto Sievänen, Eero Nikinmaa, Christophe Godin, Anna Lintunen & Pekka Nygren. http://www.metla.fi/fspm2013/proceedings. ISBN 978-951-651-408-9.

Light signal perception in Arabidopsis rosettes

Jochem B. Evers[1*], **Ronald Pierik**[2], and **Alexander R. van der Krol**[3]
[1]*Crop Systems Analysis, Wageningen University, PO Box 430, 6700 AK, Wageningen, the Netherlands*
[2]*Plant Ecophysiology, Utrecht University, PO Box 800.84, 3508 TB, Utrecht, the Netherlands*
[3]*Plant Physiology, Wageningen University, PO Box 430, 6700 AK, Wageningen, the Netherlands*
**correspondence:* jochem.evers@wur.nl

Highlights: Light signals are important signals for future and present competition. We used an architectural model of Arabidopsis development to show that vertical growth of neighboring vegetation is more important than proximity for early detection of competition. Self-signaling is greatly enhanced when own organs grow more vertically, and signal strength differs between signal perception at the apex compared to the leaves.

Keywords: Arabidopsis, light signaling, shade avoidance, competition

INTRODUCTION

Plants are able to adapt their development to the level of competition for light with neighboring plants, by increased height growth (Franklin and Whitelam, 2005), increased hyponasty (leaf angle) (De Wit et al., 2012, Vandenbussche et al., 2005) and reduced branching (Finlayson et al., 2010, Casal et al., 1987) among others. These responses are termed the shade avoidance syndrome (SAS), and together they result in allocation of biomass in regions of the canopy where competition for light is minimal. In order to accurately judge the intensity and timing of future and present competition for light, plants are equipped with an array of neighbor-sensing mechanisms. Next to mechanisms based on gaseous ethylene perception (Pierik et al., 2003) and physical touching (De Wit et al., 2012), plants use light signals such as the red/far-red ratio (R:FR) (Ballaré et al., 1990) and blue light intensity (Pierik et al., 2004). Light reflected or transmitted by plant organs have a low R:FR and blue intensity (red and blue light are mostly absorbed by green tissues whereas far-red light is mostly scattered) which makes them suitable to be interpreted as signals for competition. To do so plants are equipped with photoreceptors such as phytochromes and cryptochromes (Franklin, 2008) that translate the strength of the light signal into a physiological state, enabling the plant to respond accordingly.

Photoreceptors are generally found throughout the plant body, but there are still many questions regarding the location of signal perception in relation to their orientation in the canopy. In gramineous species, vertically oriented organs such as the stem base and young elongating leaf blades are sensitive to low R:FR (Skinner and Simmons, 1993) as light travelling more or less parallel to the soil surface is most likely to have been scattered by surrounding vegetation. Indeed, in Arabidopsis (*Arabidopsis thaliana*) the vertical orientation of leaves heavily determines R:FR signal strength (De Wit et al., 2012). In other dicots, both internodes, leaves and axillary buds have been reported to be sites of R:FR perception (Girault et al., 2008, Casal and Smith, 1988, Morgan et al., 1980). In both dicots and monocots the phytochrome and cryptochrome receptor genes show expression in all organs, but the link between the individual photoreceptor signaling pathways and other processes like hormone synthesis may differ between organs (Evers et al., Submitted). No information is available to date about what are the sites of perception for low blue light-induced shade avoidance.

Also, the extent to which a plant is exposed and reacts to light signals created by its own leaves and stems is unclear. The light that influences plant development is a combination of sky light, light reflected from neighboring structures and from the plant's own organs, but the proportion self-signaling to total signaling in relation to the vegetation density is unknown. Plant simulation models are suitable to address such questions

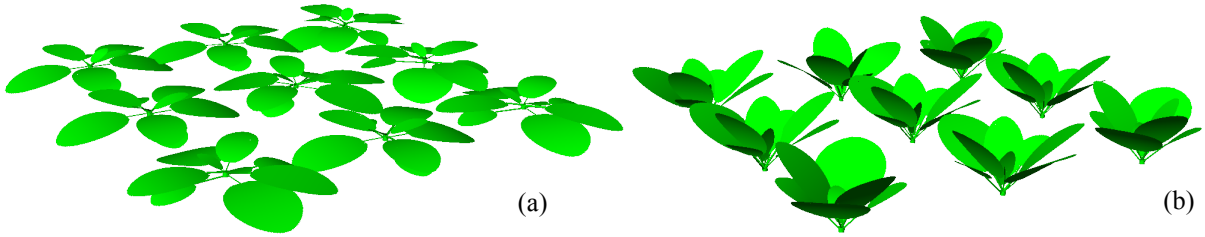

Fig. 1. Example of the visual output of the Arabidopsis rosette model showing virtual canopies after 225 hours at a plant distance of 2 cm; (a) normal leaf inclination, (b) 50% increased leaf inclination.

Table 1: Canopy composition and leaf angle in the simulated treatments

Treatment		Leaf angle increase focal plant	Leaf angle increase border plant
1	Single plant	0 %	-
2	Plot	0 %	0 %
3	Plot	0 %	50 %
4	Single	50 %	-
5	Plot	50 %	50 %

related to signal perception. The purpose of this simulation study was to assess to what extent different plant components of Arabidopsis rosettes receive R:FR and blue light signals in relation to the density and structure of neighboring vegetation and to their own plant structure.

SIMULATIONS

We used a descriptive simulation model of Arabidopsis rosette development (Evers et al., Submitted, De Wit et al., 2012), which was constructed using the simulation platform GroIMP v1.4.1 (Hemmerling et al., 2008). Simulation of the light environment was done using the GroIMP radiation model. All rosette organs were provided with values for reflectance, transmittance and absorbance of red, far-red and blue light based on measured data from greenhouse-grown Arabidopsis plants using a Perkin Elmer Lambda 9 Spectrometer (Perkin Elmer, Waltham, USA). Light signal perception was defined for leaf blades as well as for the shoot apex (represented by an invisible spherical sensor in the center of the rosette).

Arabidopsis plants were simulated individually as well as in stands of nine plants in a 3×3 square grid at 2, 4 and 6 cm plant distance (Fig. 1), of which the middle plant (the focal plant) was used for analysis. Due to model stochasticity, simulations were done five times. Orientation in the x-y plane of simulated plants was chosen at random for each plant. To assess the effect of hyponasty on light signaling, in a second set of simulations the inclination of all leaves was increased by 50% (Fig. 1b). Finally, a third set of simulations of nine plants was done in which the focal plant were non-hyponastic and the border plants had 50% increased leaf inclination (table 1). R:FR of the incoming light was 1.2. For the range 150 to 250 hours, R:FR and blue light levels at the apex and on all leaf blades were recorded and averaged.

RESULTS AND DISCUSSION

The apex perceived lower R:FR values than the leaves across treatments (Fig. 2a) due to the shielded location of the apex in the rosette, receiving mostly light scattered from its own leaves. R:FR perceived at the apex and on the leaves decreased with the addition of non-hyponastic neighbors, and decreased further in case neighbors were hyponastic (i.e. had more vertically oriented leaves). A more pronounced drop occurred

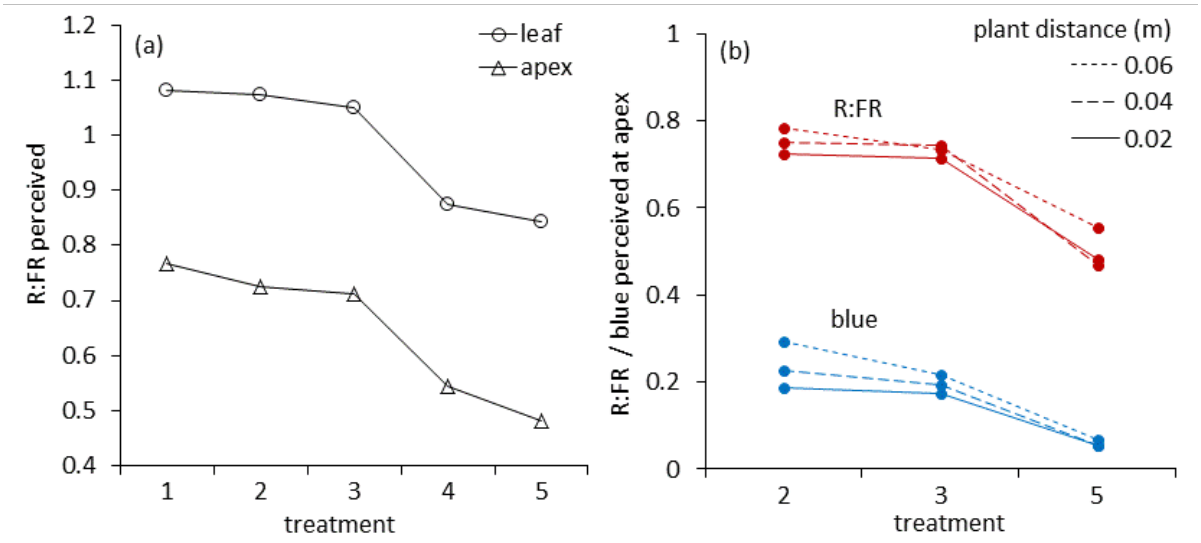

Fig. 2. (a) R:FR perceived by the leaves (circles) and the apex (triangles) in treatments 1 to 5. Treatments sorted with decreasing value of R:FR perceived. (b) R:FR and blue light (expressed as a fraction of incoming blue light intensity) perceived by the apex in treatments 2, 3 and 5 at three plant distances.

when the focal plant itself was hyponastic and largest decrease in R:FR occurred at the combination of both hyponastic focal and border plants. Hyponasty in the focal plant clearly had a much larger effect on R:FR perceived by both apex (34.1%) and leaves (64.1%) than adding neighbors. Adding neighbors never contributed more than 9.1% in case neighbor and focal plant leaf angle were identical. Adding hyponastic neighbors to a non-hyponastic focal plant provided an additional R:FR drop up to 22.1%, showing the relevance of vertical growth for R:FR signaling. This trend was observed for all plant distances (Fig. 2b). Plant distance hardly affected R:FR perceived by the apex. Blue light signaling was only affected in non-hyponastic situations: blue light fractions ranged from 0.19 to 0.29 when increasing plant distance from 0.02 to 0.06 m). In a fully hyponastic canopy, blue light signaling at the apex was not affected by plant distance.

This exercise highlights the relative importance of vertical neighbor growth in plant competition. Even if competitors are relatively close, they will not be noticed through light signaling if they do not show significant vertical growth. This strengthens the conclusions of De Wit *et al.*. (2012) that touch rather than light signals provide the strongest early signals for competition in 'flat' canopies such as those composed by Arabidopsis rosettes. Furthermore, the observed differences in light signal perception between apex and leaves gives interesting questions regarding signal integration and site of perception. For example, increased petiole extension leading to local exploration of space is a local response to R:FR perception by the attached blade (Kozuka et al., 2010), for which relatively mild drops in R:FR may be sufficient (Fig. 2a). However shoot branching regulation by auxin (Domagalska and Leyser, 2011) may be modulated at least partly by R:FR at the apex, since leaf blades do not respond to low R:FR in terms of auxin activity (Evers et al., Submitted), in which case our model predicts more severe drops in R:FR are required. Further experimental and simulation studies will be conducted to assess how the different signals act in concert to give rise to the various responses in the shade avoidance syndrome.

LITERATURE CITED

Ballaré CL, Scopel AL, Sánchez RA. 1990. Far-red radiation reflected from adjacent leaves: an early signal of competition in plant canopies. *Science,* **247**: 329-332.

Casal JJ, Sánchez RA, Deregibus VA. 1987. Tillering responses of *Lolium multiflorum* plants to changes of red/far-red ratio typical of sparse canopies. *Journal of Experimental Botany,* **38**: 1432-1439.

Casal JJ, Smith H. 1988. Persistent effects of changes in phytochrome status on internode growth in light-grown mustard: occurence, kinetics and locus of perception. *Planta,* **175**: 214-220.

De Wit M, Kegge W, Evers JB, Vergeer-van Eijk MH, Gankema P, Voesenek LACJ, Pierik R. 2012. Plant neighbor detection through touching leaf tips precedes phytochrome signals. *Proceedings of the National Academy of Sciences,* **109**: 14705-14710.

Domagalska MA, Leyser O. 2011. Signal integration in the control of shoot branching. *Nature Reviews Molecular Cell Biology,* **12**: 211-221.

Evers JB, Vos J, Bouwmeester H, Van der Krol AR. Submitted. Light signalling in hormone-regulated shoot branching.

Finlayson SA, Krishnareddy SR, Kebrom TH, Casal JJ. 2010. Phytochrome regulation of branching in arabidopsis. *Plant Physiology,* **152**: 1914-1927.

Franklin KA. 2008. Shade avoidance. *New Phytologist,* **179**: 930-944.

Franklin KA, Whitelam GC. 2005. Phytochromes and shade-avoidance responses in plants. *Annals of Botany,* **96**: 169-175.

Girault T, Bergougnoux V, Combes D, Viemont JD, Leduc N. 2008. Light controls shoot meristem organogenic activity and leaf primordia growth during bud burst in Rosa sp. *Plant, Cell and Environment,* **31**: 1534-1544.

Hemmerling R, Kniemeyer O, Lanwert D, Kurth W, Buck-Sorlin GH. 2008. The rule-based language XL and the modelling environment GroIMP illustrated with simulated tree competition. *Functional Plant Biology,* **35**: 739-750.

Kozuka T, Kobayashi J, Horiguchi G, Demura T, Sakakibara H, Tsukaya H, Nagatani A. 2010. Involvement of auxin and brassinosteroid in the regulation of petiole elongation under the shade. *Plant Physiology,* **153**: 1608-1618.

Morgan DC, O'Brien T, Smith H. 1980. Rapid photomodulation of stem extension in light-grown *Sinapis alba* L. *Planta,* **150**: 95-101.

Pierik R, Visser EJW, de Kroon H, Voesenek LACJ. 2003. Ethylene is required in tobacco to succesfully compete with proximate neighbours. *Plant, Cell & Environment,* **26**: 1229-1234.

Pierik R, Whitelam GC, Voesenek LACJ, De Kroon H, Visser EJW. 2004. Canopy studies on ethylene-insensitive tobacco identify ethylene as a novel element in blue light and plant-plant signalling. *Plant Journal,* **38**: 310-319.

Skinner RH, Simmons SR. 1993. Modulation of leaf elongation, tiller appearance and tiller senescence in spring barley by far-red light. *Plant, Cell & Environment,* **16**: 555-562.

Vandenbussche F, Pierik R, Millenaar FF, Voesenek LACJ, Van der Straeten D. 2005. Reaching out of the shade. *Current Opinion in Plant Biology,* **8**: 462-468.

Proceedings of the 7th International Conference on Functional-Structural Plant Models, Saariselkä, Finland, 9 - 14 June 2013. Eds. Risto Sievänen, Eero Nikinmaa, Christophe Godin, Anna Lintunen & Pekka Nygren.
http://www.metla.fi/fspm2013/proceedings. ISBN 978-951-651-408-9.

How do variations of architectural parameters affect light partitioning within wheat - pea mixtures? A simulation study based on a virtual plant approach.

Romain Barillot[1], **Christian Fournier**[2,3], **Pierre Huynh**[1], **Abraham J Escobar-Gutiérrez**[4] and **Didier Combes**[4*]

[1]*LUNAM Université, Groupe Ecole Supérieure d'Agriculture, UPSP Laboratoire d'Ecophysiologie Végétale & Agroécologie, 55 rue Rabelais, BP 30748, F-49007 Angers cedex 01, France.*

[2]*INRA, UMR 759 LEPSE, F-34060 Montpellier, France*

[3]*SupAgro, UMR 759 LEPSE, F-34060 Montpellier, France*

[4]*INRA, UR4 P3F, Equipe Ecophysiologie des plantes fourragères, Le Chêne - RD 150, BP 6, F-86600 Lusignan, France.*

**correspondence:* didier.combes@lusignan.inra.fr

Highlights: 3D and dynamic models of wheat and pea were used to study light partitioning in virtual wheat-pea mixtures. Our results showed that architectural parameters defined at plant scale (*e.g.* branches, internode length) significantly affect the interception of light by each component species. The modifications performed on the architectural parameters of both models led to asymmetric variations of light partitioning.

Keywords: *Pisum sativum*, plant architecture, *Triticum aestivum*, virtual plant model, wheat-pea mixture

INTRODUCTION

Light partitioning among intercropped species is highly related to the physical structure of the canopy (Barillot *et al.*, 2011) emerging from the architecture of the individuals growing within the stand (Barillot *et al.*, 2012). Plant architecture is defined as the resultant of i) the inventory of the plant components, ii) the topological relations between these components, and iii) their geometry (Godin, 2000). The multiscale description of the canopy structure reveals the importance of the architectural parameters as underpinning factors that determine light partitioning within mixed cropped systems.

Modelling approaches such as Functional – Structural Plant Models (FSPMs, DeJong *et al.*, 2011) have been proved to be well suited for studying light partitioning within contrasting canopies (Barillot *et al.*, 2011). As a consequence, these models can be considered as pertinent frameworks for assessing the relations between architectural parameters and light partitioning among the component species of intercropping systems.

The aim of the present study was therefore to assess the effect of architectural variations on light partitioning within wheat – pea mixtures. To this end, virtual mixtures were built up from architectural models of both species for which a strong variability of the architecture has been showed among genotypes and environmental conditions (Baccar *et al.*, 2011, Dornbusch *et al.*, 2011, Barillot *et al.*, 2012).

SIMULATIONS

Virtual wheat – pea mixtures were generated from architectural models of wheat and pea. First, we used a dynamic model of wheat development (Adel-Wheat, Fournier *et al.*, 2003). Then an architectural model of pea, hereafter called L-Pea, was built up using the L-Py platform (Boudon *et al.*, 2012). A detailed description of the model will be given in a companion poster (Barillot *et al.*, 2013). Briefly, the development of pea architecture is modelled as a function of the growing degree day. Kinetics of phytomer and branch production are described in a *vegetative module*, based on an experiment conducted in

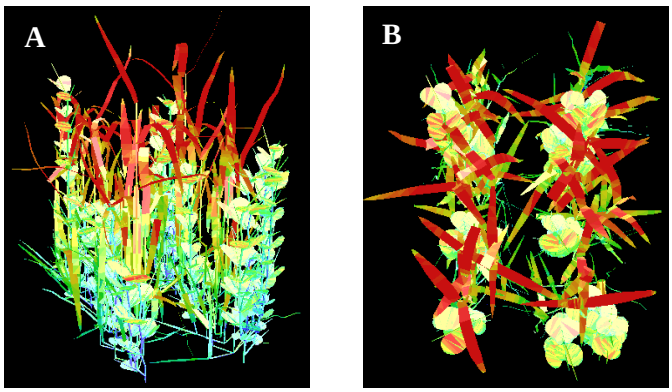

Fig. 1. Illustrations of a virtual wheat – pea mixture. The gradient of colour is a function of the light intercepted by organs (from blue to red).

field on cultivar Lucy grown in mixture with wheat. The elongation and coordination of the organs generated by the *vegetative module* are handled by a *growth module*. L-pea model was then implemented into the OpenAlea platform (Pradal *et al.*, 2008) in order to generate virtual wheat – pea mixtures (Fig. 1). Sowing densities were set to 125 and 45 plant m^{-2} for wheat and pea respectively. Finally, virtual wheat – pea mixtures were interfaced with the radiative transfer model Caribu (Chelle and Andrieu, 1998) that allows to estimate the dynamic of light partitioning at each step of the growing cycle. Simulations were processed from 0 to 2000 GDD with a time step of 50 GDD.

Architectural parameters were selected as a function of their contribution to the Leaf Area Index (LAI) and plant height (Table 1) that are known to affect light interception.

Table 1: Architectural parameters selected for modifying the species LAI and height.

Species	Variable	
	LAI	Height
Wheat	Number of tillers (± 25 and 50%)	Internode length (± 25 and 50%)
Pea	Number of branches (± 25 and 50%)	Internode length (± 25 and 50%)

A first simulation with unmodified architectural parameters for both wheat and pea models was run and called *reference simulation*. Based on this simulation, the architectural parameters of wheat and pea were then modified by ± 25 and ± 50%.

RESULTS AND DISCUSSION

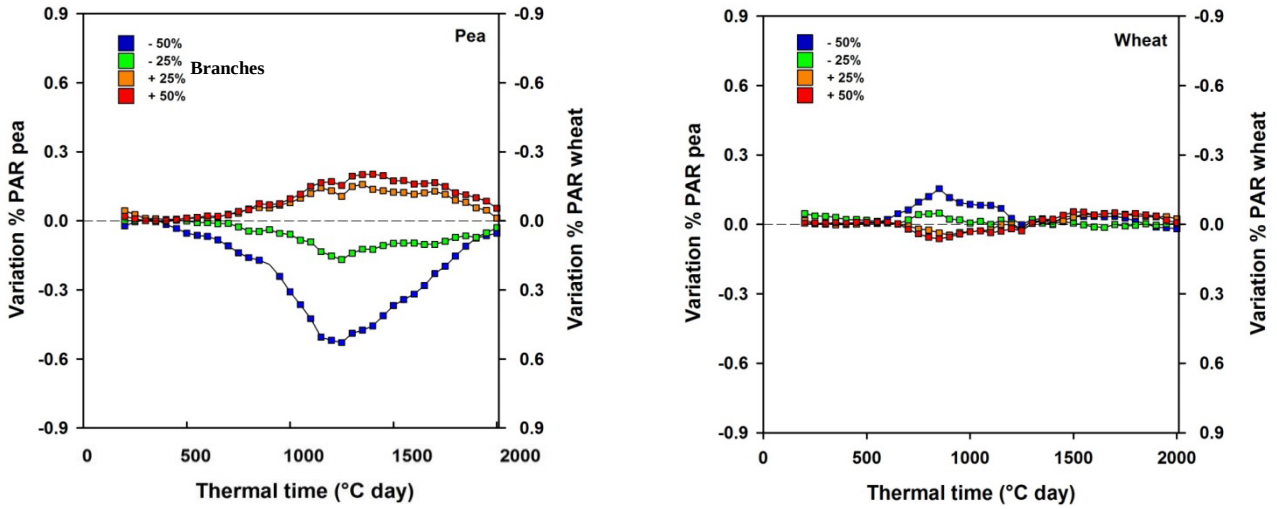

Fig. 2. Relative variations of light interception (%PAR, estimated from the reference simulation) by pea and by wheat (secondary axis in reverse order). Light interception was computed consecutively to a modification in the number of i) branches of pea (left) and ii) tillers of wheat following the gradient of colours.

The modifications performed on the final number of branches and tillers led to variations of light partitioning compared to the *reference* simulation (Fig. 2). The highest variation of light partitioning resulted from a reduction by 50 % in the number of branches of pea (Fig. 2, left). Lower absolute variations of light partitioning were observed consecutively to an increase of the number of pea branches, thus defining *asymmetric* variations. Compared to pea, alterations of the number of tillers produced by wheat (Fig. 2, right) led to slighter relative variations of light partitioning (at most 15 %).

Modifications of internode length appeared to have the most dramatic effects on light partitioning compared to branching (Fig. 3). These effects were observed earlier in pea, since the internode elongation of wheat began around 1000 GDD. A strong asymmetry was found in the variations of light partitioning between plants subjected to an increase of their internode length and those whose internodes were reduced. Similar variations of light partitioning were observed after an increase of the internode length of pea or an

equivalent reduction of wheat internodes. In contrast, increasing the internode length of wheat did not bring a similar gain of light interception as an equivalent reduction of pea internodes.

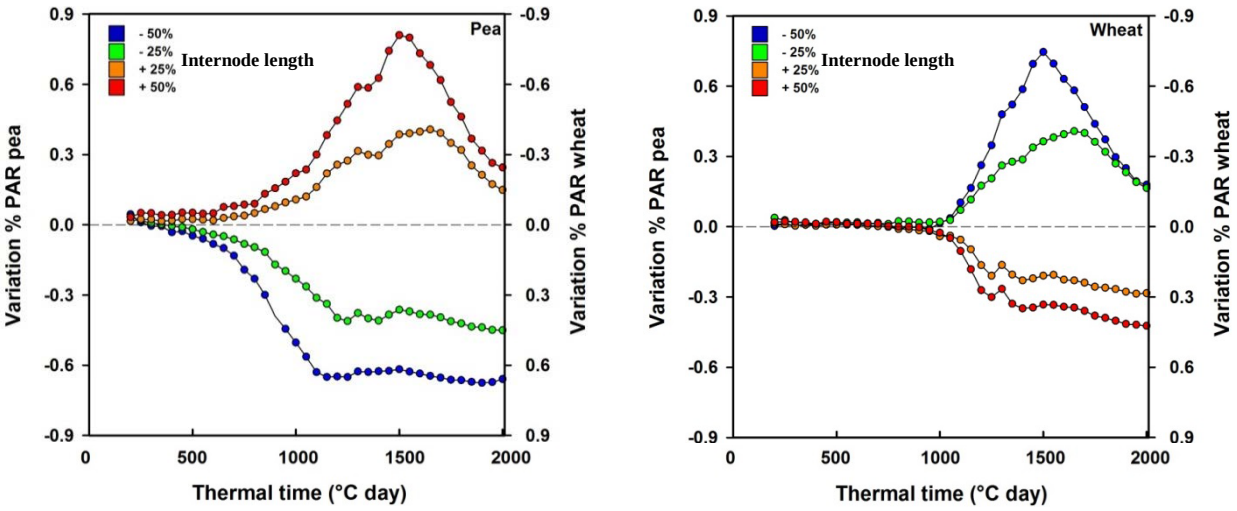

Fig. 3. Relative variations of light interception (%PAR, estimated from the reference simulation) by pea and by wheat (secondary axis in reverse order). Light interception was computed consecutively to a modification of internode length for pea (left) and wheat (right) following the gradient of colours.

The preliminary results presented here stemmed from a simulation study where the plasticity of plants in response to environmental variations was not included in the model. Therefore, further works have to be conducted in order to study how morphological variations can affect the interactions between the component species and their development. However, we used the FSPM approach to assess the *theoretical* sensitivity of light partitioning to the architecture of wheat and pea plants. These results therefore provide information that enables to identify / design suitable cultivars / ideotypes for intercropping systems towards light partitioning.

LITERATURE CITED

Baccar R, Fournier C, Dornbusch T, Andrieu B, Gouache D, Robert C. 2011. Modelling the effect of wheat canopy architecture as affected by sowing density on *Septoria tritici* epidemics using a coupled epidemic-virtual plant model. *Annals of Botany*, **108**: 1179-1194.

Barillot R, Combes D, Chevalier V, Fournier C, Escobar-Gutiérrez AJ. 2012. How does pea architecture influence light sharing in virtual wheat-pea mixtures? A simulation study based on pea genotypes with contrasting architectures. *AoB Plants*, **pls038**.

Barillot R, Huynh P, Escobar-Gutiérrez AJ, Combes D. 2013. L-Pea: an architectural model of pea (Pisum sativum) development. *7th International Workshop on Functional-Structural Plant Models.* Saariselkä, Finland.

Barillot R, Louarn G, Escobar-Gutiérrez AJ, Huynh P, Combes D. 2011. How good is the turbid medium-based approach for accounting for light partitioning in contrasted grass-legume intercropping systems? *Annals of Botany*, **108**: 1013-1024.

Boudon F, Pradal C, Cokelaer T, Prusinkiewicz P, Godin C. 2012. L-Py: an L-System simulation framework for modeling plant development based on a dynamic language. *Frontiers in Plant Science*, **3**.

Chelle M, Andrieu B. 1998. The nested radiosity model for the distribution of light within plant canopies. *Ecological Modelling*, **111**: 75-91.

DeJong TM, Da Silva D, Vos J, Escobar-Gutiérrez AJ. 2011. Using functional–structural plant models to study, understand and integrate plant development and ecophysiology. *Annals Of Botany*, **108**: 987-989.

Dornbusch T, Baccar R, Watt J, Hillier J, Bertheloot J, Fournier C, Andrieu B. 2011. Plasticity of winter wheat modulated by sowing date, plant population density and nitrogen fertilisation: Dimensions and size of leaf blades, sheaths and internodes in relation to their position on a stem. *Field Crops Research*, **121**: 116-124.

Fournier C, Andrieu B, Ljutovac S, Saint-Jean S. 2003. ADEL-wheat: A 3D architectural model of wheat development. *Proceedings of the 2003 Plant Growth Modeling, Simulation, Visualization, and Applications.* Beijing, China, IEEE Computer Society.

Godin C. 2000. Representing and encoding plant architecture: A review. *Annals of Forest Science*, **57**: 413-438.

Pradal C, Dufour-Kowalski S, Boudon F, Fournier C, Godin C. 2008. OpenAlea: a visual programming and component-based software platform for plant modelling. *Functional Plant Biology*, **35**: 751-760.

Proceedings of the 7th International Conference on Functional-Structural Plant Models, Saariselkä, Finland, 9 - 14 June 2013. Eds. Risto Sievänen, Eero Nikinmaa, Christophe Godin, Anna Lintunen & Pekka Nygren. http://www.metla.fi/fspm2013/proceedings. ISBN 978-951-651-408-9.

Influence of the genetic variation of branching during early growth on light interception efficiency of apple trees: a modelling study with MAppleT

David Da Silva[1], Liqi Han[2], Robert Faivre[3] and Evelyne Costes[1*]

[1]*INRA, UMR 1334 Plant Genetic Improvement and Adaption (AGAP), Montpellier, France*
[2]*School of Computer Engineering, Weifang University, Weifang, China*
[3]*INRA, UR 875 Biometry and Artificial Intelligence (BIA), Castanet-Tolosan, France*
[*]*correspondence:* costes@supagro.inra.fr

Highlights: Light interception is a key parameter to optimise fruit tree production. Assuming that genetic variability of branching along trunks impacts tree development, total leaf area and light interception in the consecutive years, we estimated STAR values on 1 to 5 years old simulated apple trees. We analyse the relative impact of proleptic and sylleptic shoots, and depending on their length category on STAR variance.

Keywords: STAR, Modeling, Leaf Area, Branching, Sensitivity analysis, *Malus x domestica*

INTRODUCTION

The architecture of a tree has an impact on light interception, water transport and transpiration as well as carbon acquisition and allocation. Therefore, the optimisation of tree architectures is desirable in fruit tree culture to improve fruit production in quantity, regularity and quality. For apple tree, most architectural traits vary genetically, particularly during the first years of tree life (Segura *et al.*, 2008). However, it remains difficult to integrate these traits in breeding programs, because their values change during tree development (Laurens *et al*., 2000). Considering the complexity of apple tree architecture over years of growth and the large number of trees required for quantitative genetics studies, it is not convenient to grow and measure phenotypes in the field especially at fine scales. For that reason, we rely on modelling strategies (DeJong *et al*., 2011) as well as environmental simulation tools to perform computer-based virtual experiments.

Our strategy makes use of MAppleT, i.e. Markov Apple Tree, a FSPM which simulate apple tree topology and geometry for Fuji cultivar (Costes *et al*., 2008). The light interception of the simulated trees was estimated using MµSLIM, namely Multi-Scale Light Interception Model, included in OpenAlea (Da Silva *et al*., 2008). This research aims at demonstrating that a sensitivity analysis could be used to investigate the impact of the known genetically variable architectural traits on light interception efficiency. In a previous study, we analysed the impact and interactions of a limited number of geometrical traits on the whole tree light interception (Han *et al*., 2012). The contribution of the stochastic part of Markov models to the total variance of the output was also examined and was particularly low. Here, we complemented our approach by considering the variation in the trunk first annual shoot branching of the same apple hybrids, and examining the variability induced on light interception, when 5 years old (yo).

MATERIALS AND METHODS

The tree simulations were initiated with trunks sequences previously observed within a segregating population of apple hybrids (Segura *et al.*, 2008). Different axillary shoots types were considered: in the first year of growth, each axillary bud could develop immediately into a sylleptic shoot or remain latent until next budbreak when they could develop into proleptic shoots, or still remain latent. Both sylleptic and proleptic shoots could be short, medium or long. A sample of initial (1yo) and resulting final (5yo) simulated tree architectures are shown in Fig.1. The number of sylleptic and proleptic shoots in each category along the 1yo trunks was considered and divided by the corresponding annual trunk length, in order to express a branching density. All the other parameters of the model were kept with default values (Costes *et al*., 2008). In particular, the Markov models estimated for Fuji cultivar were used to simulate the type of growth unit and axillary shoots developed from each bud, either terminal or axillary, in the consecutive years. The simulated trees thus differed only because of the different initial branching sequences.

For light interception efficiency evaluation, the Silhouette to Total Area Ratio (STAR) (Oker-Blom and Smolander, 1988), was used. The STAR of a whole tree, for one direction, is the ratio of its Projected Leaf Area (PLA) to its Total Leaf Area (TLA) . For the light environment simulation, the diffuse mode available in MµSLIM was used to simulate the radiance of an overcast sky. The integrated STAR value was obtained by averaging the STAR from 46 directions with weighting coefficients derived from the standard overcast sky radiance (Moon and Spencer, 1942). The virtual experiments covered five years growth of a set of 111 trees and the whole tree STAR was calculated on June 30 of each year.

For investigation of our model response, we preferred a metamodelling approach (or response surface modelling) rather than sensitivity analysis methods based on eFAST or Sobol (Slatelli *et al*., 2000), because

$$STAR_i = \sum_k f_k(X_{k,i}) + \varepsilon_i$$

the latter options require much higher number of simulations. Among metamodelling approaches, a Generalized Additive Model (GAM) (Wood, 2006) was used, by which STAR was viewed as an additive sum of nonparametric functions of each input parameter:
where k is the number of parameters X for tree i and ε is its residual error term.

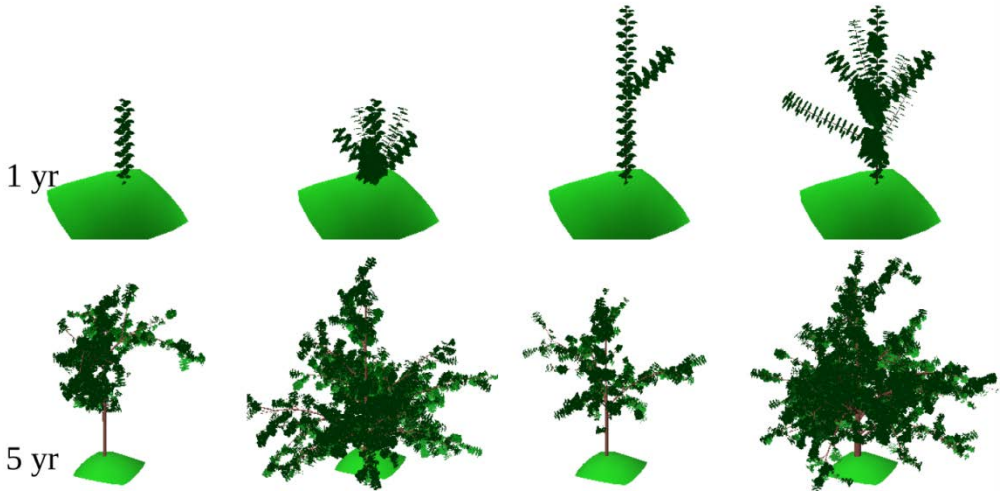

Fig. 1. Visualization of simulated apple tree architectures. These sample architectures were produced by MAppleT with different branching sequences for the trunk first annual shoots.

Results and Discussion

The TLA of the simulated trees increased rapidly in both mean and variance, from the first to the fifth year of growth (Fig. 2.), with a stabilization of variance in the fifth year. By contrast, the STAR values decreased, and then stabilized in both mean value and variance in the fourth and fifth years, with a variance notably smaller than that observed in TLA.

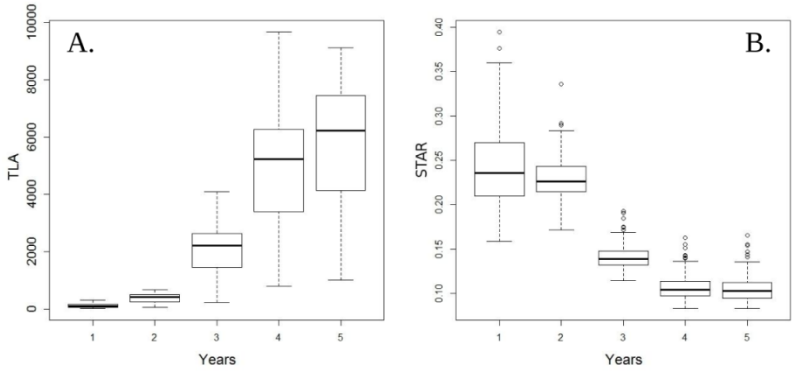

Fig. 2. Mean values and variation of simulated TLA and STAR values for 111 apple trees from 1 year to 5 years.

The prediction of STAR values with GAM model was performed for two specific combinations of input parameter values. First, the number of proleptic and sylleptic laterals per unit length was considered. The approximate effects on STAR revealed significant influences of proleptic shoots in the second year of growth, whereas the effect of sylleptic shoots was the highest in the first year of growth and remained significant until the fifth year (Table 2. left). The estimated GAM explained 76.14% to 22% (adjusted R^2) of the total variation of STAR values. Fluctuations in shape of the output variable responses are revealed by the value of estimated degree of freedom (edf). Second, the number of each type of sylleptic (long, medium and short) per unit length was considered. All showed significant effects in the first year, long and medium sylleptics continued their significance in the second year, and only long sylleptics remained significant in the consecutive years (Table 2. Right). The estimated GAM explained 78.2% of the total variation of STAR values in the first year of growth and then decreased to approximately 30%. The function of STAR responses to long sylleptic shoots had the highest edf value, indicating a higher number of fluctuations.

Thus, branching along the first annual shoot of the trunks enhances the variability in tree architecture and

TLA. However, when reaching year 4 or 5, the STAR values show small variance despite of the high variance of TLA which is the STAR normalizing term. This suggests a light interception optimization within trees showing lower TLA and a threshold of efficiency that is not overcome by the sole increase of leaf area. In terms of carbon capture efficiency, even though the gross photosynthesis increases with TLA, it is actually more related to PLA and therefore the photosynthesis per unit leaf area is more likely to follow STAR pattern.

Table 2. Approximate effects of the input parameters on STAR values with a GAM. Input variables were the number of sylleptic (s) and proleptic (p) shoots per unit length ($.l^{-1}$), for the left table and the three types of sylleptic shoots, long (sl), medium (sm) and short (ss) per unit length ($.l^{-1}$), for the right table.

Years		edf	F	p-value		R^2
1	$s.l^{-1}$	4.41	59.36	<2e-16	***	76.1
	$p.l^{-1}$	2.70	1.61	0.18		
2	$s.l^{-1}$	1.52	23.26	7.77e-09	***	32.3
	$p.l^{-1}$	1.00	6.90	0.009	**	
3	$s.l^{-1}$	1.12	17.90	1.19e-05	***	17.1
	$p.l^{-1}$	1.00	0.47	0.49		
4	$s.l^{-1}$	1.88	12.28	4.25e-06	***	22.6
	$p.l^{-1}$	1.00	0.09	0.76		
5	$s.l^{-1}$	1.89	12.33	3.84e-06	***	22.6
	$p.l^{-1}$	1.00	0.05	0.82		

Years		edf	F	p-value		R^2
1	$sl.l^{-1}$	5.52	22.38	<2e-16	***	78.2
	$sm.l^{-1}$	1.00	18.52	3.89e-05	***	
	$ss.l^{-1}$	2.54	3.67	0.0129	*	
2	$sl.l^{-1}$	2.01	5.97	0.00167	**	33.0
	$sm.l^{-1}$	1.00	10.12	0.00192	**	
	$ss.l^{-1}$	1.00	0.34	0.55609		
3	$sl.l^{-1}$	2.12	6.83	0.000529	***	24.5
	$sm.l^{-1}$	1.00	0.80	0.370685		
	$ss.l^{-1}$	1.00	1.01	0.315264		
4	$sl.l^{-1}$	2.37	10.04	7.89e-06	***	32.6
	$sm.l^{-1}$	1.00	0.51	0.475		
	$ss.l^{-1}$	1.00	1.55	0.216		
5	$sl.l^{-1}$	2.49	10.72	2.42e-06	***	34.3
	$sm.l^{-1}$	1.00	0.43	0.510		

Here, the GAM approach was selected because of its robustness with correlated variables, like the different types of sylleptic shoots. However it does not take into account the interactions between variables, and further study using variable selection (Wood, 2006) would certainly allow a more refined analysis. Comparing the present results with those obtained in Han *et al*. (2012) highlights a higher impact on STAR when varying organ geometry than early branching. This may be due to the repeated occurrence of individual organs over the years whereas the topology has a declining effect linked to tree ontogeny. Even though the improvement of light penetration within tree canopies has been a constant objective of fruit tree architecture manipulation through the setting up of training systems (Willaume *et al.*, 2004), breeding and genetic selection could open new avenue for light interception optimization, and could be more efficient for saving time, labour and resources than yearly topology manipulation through pruning.

LITERATURE CITED

Costes, E., Smith, C., Renton, M., Guédon, Y., Prusinkiewicz, P., and Godin, C., 2008. MAppleT: simulation of apple tree development using mixed stochastic and biomechanical models. *Functional Plant Biology* **35**: 936-950.

Da Silva, D., Boudon, F., Godin, C., and Sinoquet, H., 2008. Multiscale framework for modeling and analyzing light interception by trees. *Multiscale Modeling and Simulation* **7**: 910-933.

DeJong, T. M., Da Silva, D., Vos, J., and Escobar-Gutiérrez, 2011. Using functional-structural plant models to study, understand and integrate plant development and ecophysiology. *Annals of Botany* **108**: 987-989.

Han, L., Da Silva, D., Boudon, F., Cokelaer, T., Pradal, C., Faivre, R., and Costes, E., 2012. Investigating influence of geometrical traits on light interception efficiency of apple trees: a modelling study with MAppleT. in *IEEE Computer Society; Proceedings of PMA12.* M. Kang and Y. Dumont, Eds.152-159.

Laurens, F., Audergon, J. M., Claverie, J., Duval, H., Germain, E., Kervella, J., Lezec, M., Lauri, Lespinasse, J. M., and Others, 2000. Integration of architectural types in French programmes of ligneous fruit species genetic improvement. *Fruits* **55**: 141-152.

Moon, P., and Spencer, D. E., 1942. Illumination from a non-uniform sky. *Transactions of the Illumination Engineering Society* **37**.

Oker-Blom, P., and Smolander, H., 1988. The ratio of shoot silhouette area to total needle area in scots pine. *Forest Science* **34**: 894-906.

Saltelli, A., Chan, K., and Scott, E. M., 2000. *Sensitivity Analysis: Gauging the Worth of Scientific Models*. Wiley Eds.

Segura, V., Cilas, C., and Costes, E., 2008. Dissecting apple tree architecture into genetic, ontogenetic and environmental effects. *New Phytologist* **178**: 302–314.

Wood, S.N., 2006. *Generalized additive models: an introduction with R*. Chapman & Hall/CRC.

Willaume, M., Lauri, P. E., and Sinoquet, H., *et al.*, 2004. Light interception in apple trees influenced by canopy architecture manipulation. *Trees* **18**: 705-713.

Proceedings of the 7th International Conference on Functional-Structural Plant Models, Saariselkä, Finland, 9 - 14 June 2013. Eds. Risto Sievänen, Eero Nikinmaa, Christophe Godin, Anna Lintunen & Pekka Nygren. http://www.metla.fi/fspm2013/proceedings. ISBN 978-951-651-408-9.

Quantitative characterization of clumping in Scots pine crowns

Pauline Stenberg[1], **Matti Mõttus**[2], **Miina Rautiainen**[1] and **Risto Sievänen**[3]
[1]*Department of Forest Sciences, PO BOX 27, FI-00014 University of Helsinki, Finland*
[2]*Department of Geosciences and Geography, PO BOX 64, FI-00014 University of Helsinki, Finland*
[3]*Finnish Forest Research Institute, PO BOX 18, FI-01301 Vantaa, Finland*
**correspondence:* pauline.stenberg@helsinki.fi

Highlights: The stochastic approach of modeling tree crowns as geometric shapes filled with a random medium was tested on twelve Scots pine trees generated with the LIGNUM model. Results supported the capability of the stochastic approach in characterizing clumping in crowns given that the outer shell of the tree crown is well represented.

Keywords: photon recollision probability, LIGNUM, STAR, crown shape, canopy structure

INTRODUCTION

The spatial aggregation of plant elements in a canopy, also referred to as 'clumping', is an adaptive strategy of individual plants and plant communities. The spatial distribution of foliage controls the interaction of radiation with vegetation, and thus indirectly also plant growth and reproduction. Clumping can occur at various hierarchical scales from microscale (shoots in coniferous canopies) to macroscale (spatial tree patterns in forest stands). Clumping causes a decrease in the fraction of sunlit leaf area and a downward shift in the vertical distribution of the sunlit leaf area. From the production ecological point-of-view, these effects may be translated into a decrease in the fraction of absorbed photosynthetically active radiation (FAPAR) but a more even distribution of irradiance on the canopy leaf area and, thus, higher light use efficiency. Especially for canopies carrying a high leaf area index (LAI) the combined effect may be beneficial for the photosynthetic production (Stenberg 1998).

Proper characterization of the clumped structure of forests allowing, e.g., calculation of scattered and absorbed radiation regimes and photosynthetic production in different parts of the canopy, has proved to be a challenging task. This concerns in particular statistical canopy radiation models, where probability density functions are used to describe the spatial distribution and orientation of foliage, and the transfer of radiation is described using a stochastic variable – the gap probability. Another option is to use deterministic three dimensional (3D) structural models, where the plant elements have exact locations and the radiation reaching any specific point in the canopy can be determined by ray tracing. Limitations of such models, however, are their reliance on detailed descriptions of canopy architecture and lack of generality. Statistical models would be preferred for many larger scale applications, given that the models are realistic enough to produce reasonable results. Uncertainties in statistical models depend on how well the within-crown structure is characterized by the models which typically are based on oversimplifications.

In this paper, the focus of our interest is on the degree and quantitative characterization of within-crown clumping in Scots pine (*Pinus sylvestris* L.). Using a statistical (nested Poisson) model, we first present a theoretical analysis of the clumping of the canopy and how it is related to the spherically averaged silhouette to total area ratio (STAR) of shoots and crown. The latter is directly related to a novel and powerful concept in quantifying canopy structure, the photon recollision probability (p). A series of differently-sized pine trees is constructed using the LIGNUM model (Perttunen et al. 1996), by which the crown silhouette area and amount of self-shading can be exactly calculated. These exact values are compared to results produced by the statistical model to examine how well the statistical models are able to characterize the within-crown clumping.

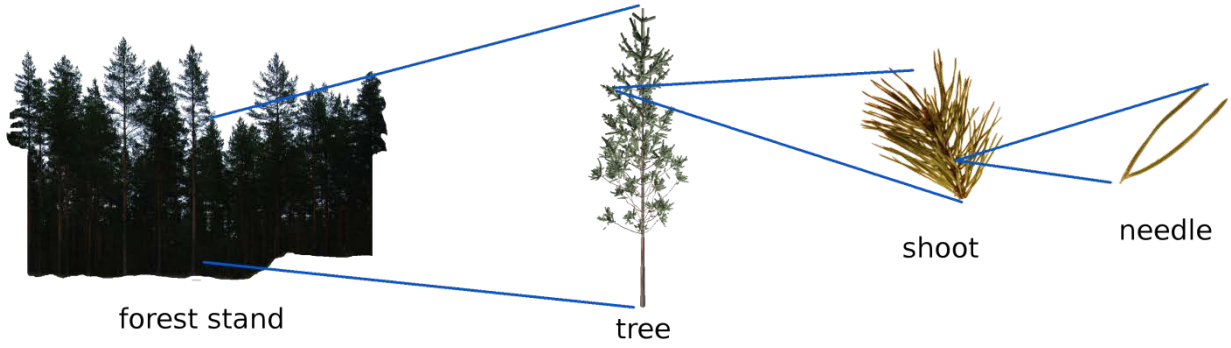

Fig. 1. The different structural levels used in describing the structure of a coniferous stand.

PHOTON RECOLLISION PROBABILITY

The spectrally invariant parameter *p* is defined as the probability by which a photon scattered from a leaf or needle in the canopy will interact within the canopy again (Smolander and Stenberg 2003). It provides a link between the absorption and scattering properties at different canopy structural levels, e.g., between the levels of the whole canopy and the shoot, or the levels of the shoot and the needle. The different structural levels commonly used in modeling a forest canopy are shown in Fig. 1. However, additional intermediate levels can be introduced if necessary and when data are available, e.g., those of a branch or a whorl.

If canopy structure is described as a nested Poisson process, where the hierarchical levels ("clumps") at which clumping of foliage occur are Poisson distributed, the canopy p value can be decomposed as:

$$p(\text{canopy}) = p_1 + (1-p_1)p_2 + \cdots + (1-p_1)..(1-p_{n-1})p_n\ , \qquad (1)$$

where *n* is the number of levels and p_i is the probability that a photon leaving a "clump" at the hierarchical level *i*-1 will collide with a clump at level *i*. In the case with Poisson distributed trees and shoots within the tree crowns (n=3), p_1 in Eq. 1 would represent the recollision probability within a shoot, p_2 the recollision probability of a shoot leaving photon within the crown, and p_3 the recollision probability of a crown leaving photon with another crown. Smolander and Stenberg (2003) showed that a close to perfect linear relationship exists between the *p* value of an individual coniferous shoot (p_{shoot}) and its spherically averaged silhouette to total area ratio ($STAR_{shoot}$). Mathematically, the observed linear relationship:

$$p_i = 1 - \ \mathrm{STAR}_i/STAR_{i-1}, \qquad (2)$$

where $STAR_0$=1/4 is the spherically averaged silhouette to total area ratio of an individual needle, applies to all structural levels *i*. Thus, the knowledge of tree-level STAR would enable to quantify the relationship between the optical properties of a forest stand and those of a single needle.

TREE CROWN MODELS

We used LIGNUM to generate 12 realistic pine trees with heights of 3, 6, 9, 12, 15 and 18 m. Two needle area configurations were used when generating the trees: "dense" and "sparse". The two configurations were chosen to simulate varying growth conditions and between-tree competition scenarios. Total (all-sided) needle areas for the generated trees varied between 15 and 200 m^2 (Table 1). The projection areas for the computer-generated trees were calculated at 15-degree steps from the horizontal direction to vertical. Using appropriate weights for the directions, we calculated the hemispherically averaged $STAR_{crown}$ (Table 1).

Next, we tested the suitability of different simple geometric crown shape models for scaling between the canopy structural levels. We divided the realistic pine tree crown (Fig. 2 left) into segments with a thickness of 30 cm, calculated the maximum extent of the crown in each segment, and represented the tree crown as a stack of cylindrical segments (Fig. 2 middle). To test the suitability of an even simpler crown shape model, we determined the maximum horizontal and vertical extents of a tree crown and modeled the crown as an ellipsoid of rotation (Fig. 2 right). We assumed a uniform distribution of shoots (exponential attenuation) within the geometric volumes to calculate the silhouette areas of the crowns.

Table 1. Basic characteristics of LIGNUM-generated trees.

Tree height (m)	3.0	6.0	9.0	12.0	15.0	18.0
Needle area (sparse) (m^2)	15.9	35.5	69.4	101.6	117.2	164.6
Needle area (dense) (m^2)	23.8	42.5	96.5	110.3	144.2	188.1
Crown STAR (sparse)	0.067	0.060	0.061	0.058	0.062	0.059
Crown STAR (dense)	0.059	0.059	0.057	0.061	0.055	0.056

Fig. 2. A sample computer-generated tree (height 9 m, sparse) and the corresponding geometric crown shapes.

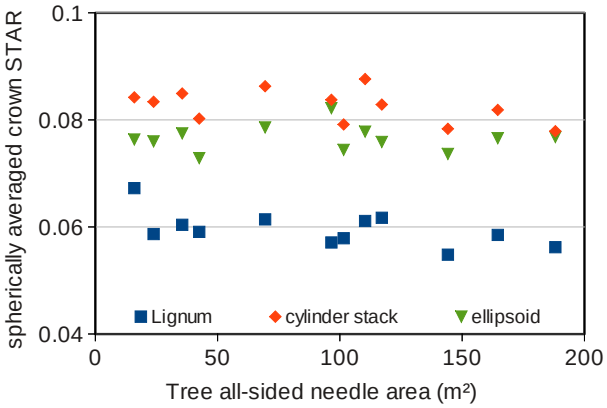

Fig. 3. $STAR_{crown}$ values calculated using the three crown models presented in Fig. 2 plotted against crown all-sided needle area.

RESULTS AND DISCUSSION

The crown STAR (and thus *p*) was rather independent of tree height, needle area or growth conditions (Fig. 3). Although a slightly decreasing trend with needle area may be noted, LIGNUM predicts a species-specific value of $STAR_{crown}$=0.06. The two other approaches used in the study considerably overestimated $STAR_{crown}$. However, this does not invalidate the stochastic approach (modeling tree crowns as geometric shapes filled with a random medium). Indeed, the crown shape determination method presented here was chosen to simulate a visual measurement in a forest where a person performing the measurements would determine the maximum extent of the crown at different heights. By doing so, we (and the measurer) have included a considerable amount of empty space into the crown. As actual tree crowns are not rotationally symmetric and their projected width depends on direction, using the maximum extent overestimates average crown width. Thus, we have decreased the needle area density within the crowns, increased average crown transmittance and its projected area.

The near-constant difference between the $STAR_{crown}$ values produced by the two geometric models and and LIGNUM (Fig. 3) gives evidence of the applicability of the stochastic approach (and thus also p-theory) inside individual tree crowns. However, for quantitatively accurate results, a more physical method for determining the outer shell of a tree crown has to be developed.

Interestingly, modeling the crown as an ellipsoid yields better results than the more detailed stack model. This indicates that the scaling approach based on photon recollision probability can be applied robustly with a small number of input parameters. This finding, together with the small variation in the value of $STAR_{crown}$, supports further development of the *p*-theory as a reliable method to connect the smallest and the largest scales in a forest canopy.

LITERATURE CITED

Perttunen J, Sievänen R, Nikinmaa E, Salminen H, Saarenmaa H, Väkevä J 1996. LIGNUM: A tree model based on simple structural units. *Annals of Botany* **77**: 87-98.

Smolander S, Stenberg P 2003. A method to account for shoot scale clumping in coniferous canopy reflectance models. *Remote Sensing of Environment* **88:** 363-373.

Stenberg P 1998. Implications of shoot structure on the rate of photosynthesis at different levels in a coniferous canopy using a model incorporating grouping and penumbra. *Functional Ecology* **12**: 82-91.

Proceedings of the 7th International Conference on Functional-Structural Plant Models, Saariselkä, Finland, 9 - 14 June 2013. Eds. Risto Sievänen, Eero Nikinmaa, Christophe Godin, Anna Lintunen & Pekka Nygren. http://www.metla.fi/fspm2013/proceedings. ISBN 978-951-651-408-9.

Towards three-dimensional modeling light capture of crop canopy considering regional variation of incident radiation

Tongyu Hou[1], Tao Duan[1], Zhaoli Xu[2], Yuntao Ma[1], Bangyou Zheng[3], Yuhong Yang[2] and **Yan Guo[1,*]**
[1]*College of Resources and Environment, China Agricultural University, Beijing 100193, China ,*[2]*Yunnan Academy of Tobacco Agricultural Sciences, Kunming 650021, China,* [3]*CSIRO Plant Industry, Queensland Bioscience Precinct, 306 Carmody Road, St. Lucia, 4067, Brisbane, Australia*
**correspondence:* yan.guo@cau.edu.cn

Highlights: A GIS-based model was adopted to simulate the regional variation of incident photosynthetically active radiation (PAR) in mountainous area. The PAR capture of rice and tobacco canopies at four special eco-sites was calculated utilizing three-dimensional modeling. This provides the basis for using functional-structural models to simulate crop growth and assess plant types at different regions accurately.

Keywords: crop growth simulation, functional-structural plant modeling, GIS, PAR, regional variation

INTRODUCTION

Crop growth and yield is greatly affected by environmental conditions. For instance, mean radiation of 20-21 MJ m^{-2} d^{-1} is needed for potential growth of rice (Peng et al. 2004). Reduction of incident radiation in rainy season in tropical and subtropical regions can limit rice growth significantly, and rice yield may decrease 30% if the incident radiation drop 50% during reproductive period (Singh 2005). Rice yield in mountainous area of Yunnan, China, could be 90% higher comparing to the major rice producing areas in the middle and lower reaches of Yangtze River Plain, although they all belong to subtropical region (Li et al. 2009). Studies showed that mild air temperature is one of the main environmental factors for high yielding in Yunnan (Ying et al. 1998; Katsura et al. 2008), and high incident radiation also plays an important role for high yielding in this region. Despite of mountain shading, incident radiation in Yunnan is significantly higher than that in Yangtze River Plain because of its lower latitude and high altitude (Li et al. 2009). Incoming radiation and other environment factors can be modified substantially by terrain. In order to accurately simulate crop growth at different regions, accurate simulation of the environmental conditions by considering regional variations is required. Rice and tobacco crop rotation is commonly used in Yunnan. The objectives of this paper are: using a GIS-based model to quantify diurnal incident radiation in different regions of Yunnan; simulating light interception of rice and tobacco based on three-dimensional canopy architectural models. This study can provide a preliminary exploration for crop growth simulation and quantitative assessment of plant types under different environmental conditions.

SIMULATIONS

The digital elevation model (DEM) of Yunnan province (Fig. 1a) was divided into 90 square units with the span of 1° × 1° latitude and longitude in ArcGIS (Esri, USA). Solar elevation angle, azimuth and extraterrestrial radiation for each given moment in a day were calculated for each square unit according to its center position. The solar radiation for each raster grid (1 km × 1km) was calculated using Hybrid model (Yang and Koike 2005; Gueymard 2012). The input parameters include: the altitude, air temperature and relative humidity. Direct and diffuse radiative transmittances were calculated separately by considering the extinction of ozone thickness, precipitable water and aerosols to radiation. The surface pressure, ozone thickness, precipitable water, turbidity coefficient were all calculated by empirical functions with input parameters. Then the radiation on the earth surface was calculated via extraterrestrial radiation and direct or diffuse radiative transmittance. Conversion parameter of 1.9 was used to transfer broadband radiation (W m^{-2}) output by Hybrid model to photosynthetically active radiation (PAR, μmol m^{-2} s^{-1}, Wang et al. 2007).

The shading to each raster grid in each square unit was determined via ArcGIS Spatial Analyst tool Hillshade. The temperature lapse rate, i.e. the rate of decrease of atmosphere temperature with the increase of altitude, was calculated by linear regression of daily mean air temperature and altitude of each meteorological station in Yunnan (Fig. 1b). Daily mean air temperature error was calculated by subtracting measured values at meteorological stations from the values computed with temperature lapse rate. Inverse Distance Weighted (IDW) method in ArcGIS Spatial Analyst was used to interpolate daily mean air temperature error. The daily mean air temperature of each raster grid was calculated by temperature lapse

rate and compensated with temperature error. The relative humidity of each meteorological station was directly interpolated for each raster grid with IDW method in ArcGIS. Meteorological data was downloaded from China Meteorological Data Sharing Service System (http://www.cma.gov.cn/2011qxfw/2011qsjgx/).

The architecture data of rice cultivar Y58S/9311 was adopted from Zheng et al. (2008). The architecture data of tobacco cultivar K326 was collected using FastSCAN^{TM} (Polhemus, USA) at the Zhaowei experimental site (24.35N, 102.52E, 1642 m) in 2012. Scenario analyses of diurnal PAR distributions were conducted for Lijiang (27.13N, 101.03E, 1170 m), Xundian (25.56N, 103.25E, 1883 m), Yuxi (24.35N, 102.52E, 1642 m) and Puer (23.02N, 101.28E, 1360 m). The PAR interception of crop canopy was simulated using DSHP model (Wang et al. 2006).

RESULTS AND DISCUSSION

The simulated results at 12:00 on July 6, 2011 showed that there was more direct PAR but less diffuse PAR in higher altitude regions of Yunnan province under clear sky (Fig. 1c, 1d), due to the decrease of substance contents in the atmosphere which can absorb and scatter radiation with the increase of altitude.

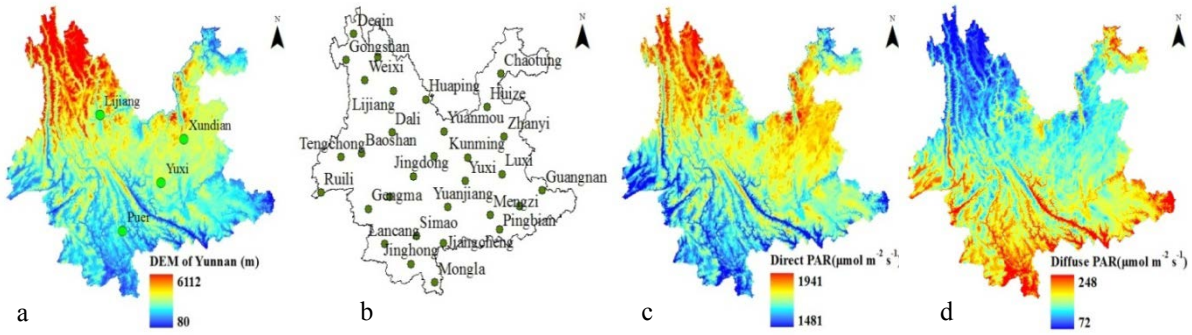

Fig. 1. The digital elevation model of Yunnan province and positions of the four specific eco-sites (a), the distribution of meteorological stations in Yunnan (b), the direct (c) and diffuse (d) PAR distribution in Yunnan at 12:00 on July 6, 2011

Diurnal courses of incident PAR were similar for the four eco-sites under clear sky. The differences of incident PAR can be identified among the four eco-sites although they were mild (Fig. 2a, 2b). The simulated diurnal courses of PAR interception of rice and tobacco canopies at the four eco-sites are showed in Fig. 2c, d. No significant differences were observed at early morning (7:00-9:00) or late afternoon (17:00-18:00) between the PAR interception of rice (Fig. 2c) and tobacco (Fig. 2d) canopy. In contrast, rice canopy intercepted more PAR than tobacco at higher solar elevation angles (10:00-16:00), as rice leaf area index (8.1) was substantially higher than that of tobacco (2.8). The decrease of PAR interception of rice canopy occurred at 13:00 (Fig. 2c) because of its steep leaf angle coincide with high solar elevation angle (ca. 85°). It was not the case for tobacco canopy because of its rather flat leaves (Fig. 2d).

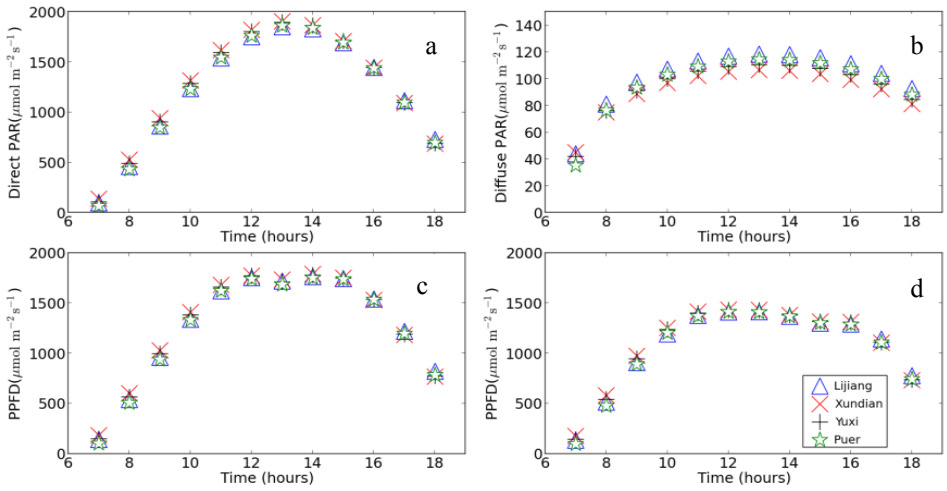

Fig. 2. The simulated diurnal courses of incident direct (a) and diffuse (b) PAR, the PAR interception of rice (c) and tobacco (d) canopies at the four specific eco-sites in Yunnan under clear sky on July 6, 2011

The visualizations of PAR distribution within rice and tobacco canopies in Yuxi at 12:00 were shown in

Fig. 3. In current study, the model test was not implemented yet because of the lack of measured data, and only scenario in clear sky condition was analyzed. As accurate simulation of incoming radiation is substantially affected by sky cloud cover in mountainous area, this will be incorporated in the future work. Currently our simulation was conducted based on the static canopy model. Dynamic model can be adopted in future to assess the effects of regional variation of incident radiation on crop growth.

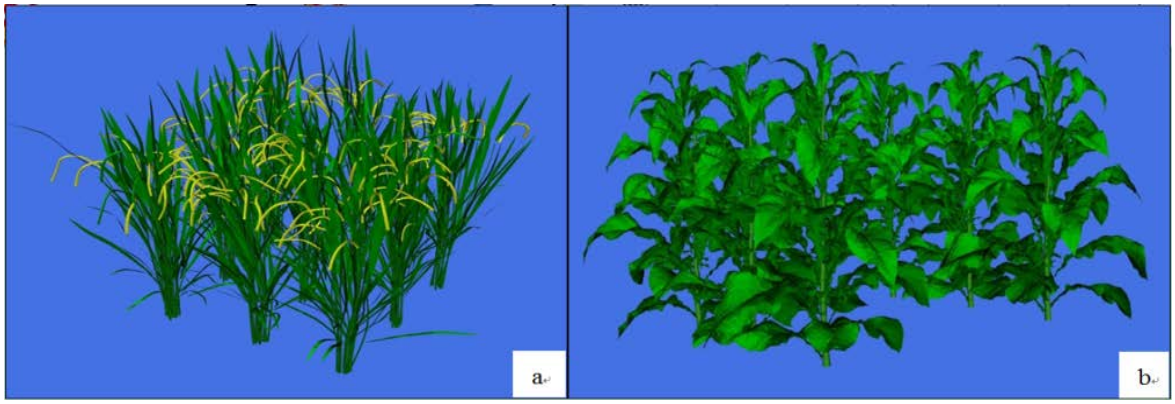

Fig. 3. Visualization of PAR distribution in rice (a) and tobacco (b) canopies in Yuxi at 12:00 on July 6, 2011

ACKNOWLEDGMENT

This research was sponsored by China National Tobacco Corporation Yunnan Province Company (2011YN08) and National Scientific and Technological Support Plan (2012BAD35B02).

LITERATURE CITED

Gueymard CA. **2012**. Clear-sky irradiance predictions for solar resource mapping and large-scale applications: Improved validation methodology and detailed performance analysis of 18 broadband radiative models. *Solar Energy* **86**: 2145–2169.

Katsura K, Maeda S, Lubis I, Horie T, Cao W, Shiraiwa T. **2008**. The high yield of irrigated rice in Yunnan, China:"A cross-location analysis". *Field crops research* **107**: 1–11.

Li GH, Xue LH, Gu W, Yang CD, Wang SH, Ling QH, Qin X, Ding YF. **2009**. Comparison of yield components and plant type characteristics of high-yield rice between Taoyuan, a "special eco-site" and Nanjing, China. *Field Crops Research* **112**: 214–221.

Peng SB, Huang JL, Sheehy JE, Laza RC, Visperas Romeo M., Zhong XH, Centeno GS, Khush GS, Cassman Kenneth G. 2004. Rice yields decline with higher night temperature from global warming. *Proceedings of the National Academy of Sciences of the United States of America* **101**: 9971–9975.

Singh S. **2005**. Effect of low-light stress at various growth phases on yield and yield components of two rice cultivars. *International Rice Research Notes* **vol 30 (2) :**36-37.

Wang Q, Kakubari Y, Kubota M, Tenhunen J. **2007**. Variation on PAR to global solar radiation ratio along altitude gradient in Naeba Mountain. *Theoretical and Applied Climatology* **87**: 239–253.

Wang XP, Guo Y, Li BG, Wang XY, Ma YT. **2006**. Evaluating a three dimensional model of diffuse photosynthetically active radiation in maize canopies. *International journal of biometeorology* **50**: 349–357.

Yang K, Koike T. **2005**. A general model to estimate hourly and daily solar radiation for hydrological studies. *Water Resources Research* **41**: W10403.

Ying JF, Peng SB., He QR, Yang H, Yang CD., Visperas R. M., Cassman K. G. 1998. Comparison of high-yield rice in tropical and subtropical environments: I. Determinants of grain and dry matter yields. *Field Crops Research* **57**: 71–84.

Zheng BY, Shi LJ, Ma YT, Deng QY, Li BG, Guo Y. **2008**. Comparison of architecture among different cultivars of hybrid rice using a spatial light model based on 3-D digitising. *Functional Plant Biology* **35**: 900–910.

Proceedings of the 7th International Conference on Functional-Structural Plant Models, Saariselkä, Finland, 9 - 14 June 2013. Eds. Risto Sievänen, Eero Nikinmaa, Christophe Godin, Anna Lintunen & Pekka Nygren.
http://www.metal.fi/fspm2013/proceedings. ISBN 978-951-651-408-9.

Modeling Seasonal Patterns of Carbohydrate Storage and Mobilization in Peach Trees

David Da Silva*, Liangchun Qin, Carolyn Debuse and Theodore M. DeJong
Department of Plant Sciences, University of California Davis, Davis CA 95616, USA
**correspondence:* dodasilva@ucdavis.edu

Highlights: Storage of carbohydrate is essential for perennial plants survival, but its modeling is often unsatisfactory. We studied the dynamics of reserve storage and mobilization in Peach trees and introduced a modeling approach that consider storage as an active sink rather than a passive buffer as frequently done in carbon-based models of tree growth.

Keywords: carbon budgets, carbon reserves, stored carbohydrates, perennial plants, tree carbon budget modeling, xylem storage

INTRODUCTION

Carbohydrate reserves, defined as carbohydrate resources accumulated in plant tissues that can mobilized at a later date, are recognized to play an essential role in the survival and productivity of temperate deciduous fruit trees. They provide a source of carbohydrate for growth and metabolism during periods when current photosynthetic supply of carbohydrates is not adequate to meet demands required to sustain normal organ growth and functioning. Carbohydrate reserves have been studied in many types of forest and fruit trees (Priestley 1970, Oliviera and Priestley 1988, Kozlowski 1992). There is not a clear understanding about how allocation of carbohydrates to storage reserves occurs in trees. The prevailing view has been that trees store carbohydrate reserves during times of "excess" photosynthate production and deplete reserves when the potential rate of carbohydrate utilization exceeds the rate of current photosynthate production (Oliviera and Priestley 1988, Kozslowski *et al.* 1991, Millard and Grelet 2010). In 1994, Cannell and Dewar challenged this concept and argued that because storage reserves are so important for the survival of perennial plants at times when current photosynthates are inadequate to meet growth demands, it may not be correct to treat storage sinks as passive reservoirs.

The lack of understanding and clear concepts regarding the dynamics of reserve storage and mobilization in perennial plants has been a major limitation in carbon-based models of tree growth (Lacointe 2000, Le Roux *et. al.* 2001), and was often ignored (Génard *et al*. 2008). Viewing reserve storage as a passive buffer means that carbohydrate partitioning into storage is modeled passively when all other sinks are satisfied. However, seasonal patterns of reserve storage and mobilization indicates that some storage often occurs when there are many other active carbohydrate sinks. Thus the concept of active carbohydrate reserve sinks and sources proposed by Cannell and Dewar (1994) seems more appropriate.

The first objective of this research was to experimentally determine the concentration of non-structural carbohydrates present in the bark and wood of mature peach trees under conditions when it was likely that those concentrations would represent the maximum and minimum concentrations during a growing season. The second objective was to use the data from the field experiment to fully implement the long term carbohydrate storage sub-model in the functional-structural L-PEACH model.

MATERIALS AND METHODS

To achieve the first objective and insure that the results of the field study would reflect the "capacity" of peach trees to mobilize and replenish carbohydrate reserves in their trunks we used an experimental treatment that was designed to "maximize" utilization of reserves. On March 1, prior to bud-break, 24 16-year-old peach trees ('O'Henry' scion grafted on 'Lovell' rootstock) growing in a semi-commercial orchard at the University of California Wolfskill Experimental Orchard, were selected for uniformity. At that time six trees were cut down and the stumps and major roots were removed from the soil. Two radial slices (~1cm thick) of the trunk (~20 cm above the graft union) and root crown (~10 cm below the graft union) were sampled for carbohydrate analyses. The top of the two main scaffolds of 18 remaining trees were removed to a height of about 1 m above the ground. This treatment was designed to eliminate reproductive sinks and stimulate strong vegetative regrowth in the form of epicormic shoots (Pernice *et al.* 2006) and therefore, mobilize all available carbohydrate reserves. On June 6, August 5 and November 5, six additional trees were cut down, removed

from the soil and sample slices of the trunk and root crown were obtained as described above for the initial six trees. The tissue samples were subsequently dried to a constant mass at 60 °C, weighed, ground to pass a 40-mesh (0.60 mm) screen, and analyzed for starch and soluble nonstructural carbohydrates by standard methods (Smith 1968). Starch was hydrolyzed with amyloglucosidase, and glucose, sucrose, fructose and sorbitol were analyzed by HPLC (Johansen *et al.* 1996) with a fast carbohydrate column. Concentrations of total glucose after starch hydrolysis, sucrose, fructose and sorbitol were summed to give an estimate of total nonstructural carbohydrates (TNC).

MODELING

The L-PEACH functional-structural plant model (Allen *et al*., 2005, Lopez *et al.* 2008) simulates the development and growth of a plant's architecture based on carbon and water exchanges (Da Silva *et al.* 2011). This model has no set carbohydrate allocation patterns; instead carbohydrate distribution is driven by competition among individual plant organs acting as semi-autonomous components sensitive to local availability of carbon and water as well as environmental factors. In this model the underlying mechanism for carbon transport treats the plant as a network of components and uses an analogy with an electrical circuit to compute the flow of carbohydrate between every component. The stored carbohydrate that can be mobilized was modeled as a capacitor within the electrical sub-circuit representing the organ storage. This capacitor discharged when carbohydrate storage was mobilized, thus acting as an active source, and charged when storage was a sink. However, the switch between source and sink, i.e. the remobilization period, was user-defined. Moreover, the carbohydrate demand of the storage sink and the maximum carbohydrate available for mobilization needed to be defined and quantified. Since storage in woody tissue represents the majority of carbohydrates stored in perennial tissues of deciduous trees, the concentration of stored carbohydrates in the active sapwood of a tree under conditions in which the storage sinks would be expected to be saturated, was used as the potential sink storage. By the same reasoning the maximum carbohydrates available for mobilization was assumed to be represented by the difference between the maximum concentration of carbohydrates in the sapwood and the minimum concentration under conditions when it would be expected that all available reserves have been mobilized, the severe pruning treatment in our study. The corresponding experimental values that were used for parametrization are shown in Table 1.

Table 1: Mean (± SE) non-structural carbohydrate concentrations (% dry wt.) for root crown and trunk tissues of peach trees at their potential, (March) and at the sampling date when the minimum was measured (June), and the percent decline in the concentration between the two sampling dates.

	Potential	Min	% Decline
Root	12.89 ± 0.48	7.08 ± 0.16	45.05 ± 3.91
Trunk	8.48 ± 0.34	4.86 ± 0.35	42.71 ± 5.55

In the electrical analogy, sources and sinks are defined by their electromotive force (*ef*) that can be viewed as their "strength". The electromotive forces of the whole system are subsequently used to determine the voltage (or carbohydrate concentration) at each attachment point of sources and sinks. Simply put, for a pure sink *ef* = 0 while for a pure source *ef* = 1. In the case of a process that can act as both, source and sink, a shift between these values is necessary to simulate the passage from sink to source and vice-versa. However, such a drastic change is unlikely to be a natural process and moreover, it requires additional information about when and why this switch occurs. To tackle this, we defined the storage *ef* as a function of the capacitor charge, it is 0 as long as the TNC is below the minimum value (Table 1. Min) and increases along a simple logistic curve to reach the value of 1 when TNC reaches its potential value (Table 1. Potential). In that way, source or sink activity depends on the local conditions of carbohydrate allocation and, as the pattern of TNC along the season, is an emergent property of the model.

RESULTS AND DISCUSSION

The simulated results were obtained on the 6th year run of a tree that was severely pruned to reproduce the field experiment. During the first 5 years, the tree was grown and pruned to simulate the commercial practices of the orchard. As shown in Fig.1, the TNCs at the beginning of the season were the potential ones as defined in Table 1. The TNCs then decrease, as storage mobilization takes place, and reach a minimum value slightly

above the one indicated in Table 1. The mobilization period is followed by a period when carbohydrates are accumulated again toward their initial ratio. The overall behavior of mobilization and refill of storage carbohydrate matches the experimental pattern (whisker dots in Fig1). However its slight offset suggests that mobilization occurs sooner than only as a function of demand. It is likely that spring carbohydrate mobilization starts as a signal activated process with stored starch being hydrolyzed and sugars being unloaded into xylem vessels (Sauter *et al.* 1973). Additionally, replenishing storage sinks appears to be a slower process than mobilization and what occurred in the simulations. The slower rate of storage refill might be due to the differences between the biochemical processes necessary to transform starch into sugar and those to hydrolyze starch in the spring. Further research is needed before this can be explicitly modeled within the framework of L-PEACH since, at present, all carbohydrate allocation in the model is sink driven.

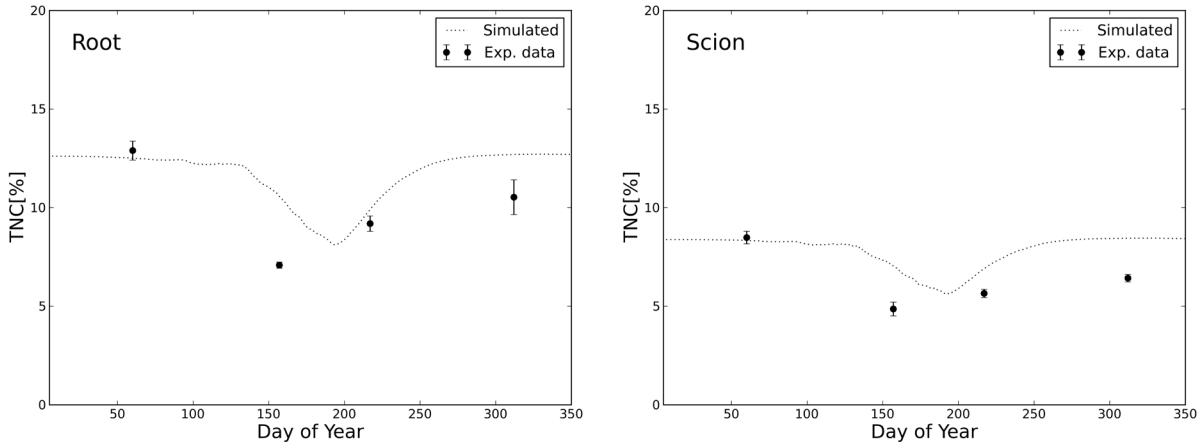

Figure 1: Seasonal patterns of TNC for root (left) and scion (right). Experimental data are displayed as points representing the mean (± SE) TNC measured at the different sampling dates. The dashed lines are the simulated patterns.

These improvements allowed the model to reproduce the general pattern of TNC using a simple approach and without a user-defined period of mobilization. However, the discrepancies in behavior suggest that additional mechanisms are involved and detailed modeling of these processes may require specific parameterization for a given species. Indeed, the more detail we incorporate into modeling specific processes, the closer we get to a connection with genetic specificity. Being able to determine what parameters/processes are genetically altered among genotypes and incorporating them into functional-structural models is a major challenge for the future.

LITERATURE CITED

Allen, M.T., P. Prusinkiewicz and T.M. DeJong. 2005. Using L-systems for modeling source-sink interactions, architecture and physiology of growing trees: the L-PEACH model. *New Phytologist* **166**:869-888.

Cannell, M.G.R. and R.C. Dewar. 1994. Carbon allocation in trees: A review of concepts for modeling. In *Advances in Ecological Research*, Academic Press, London, **25**:59-104.

Da Silva, D., R. Favreau,I. Auzmendi, and T. M. DeJong, 2011. Linking water stress effects on carbon partitioning by introducing a xylem circuit into L-PEACH. *Annals of Botany* **108** (6): 1135-1145.

Génard, M., J. Dauzat, N. Franck, F. Lescourret, N. Moitrier, P. Vaast, and G. Vercambre, 2008. Carbon allocation in fruit trees: from theory to modelling. *Trees - Structure and Function* **22**:269-282.

Johansen, H.N., V. Glitso and K.E.B. Knudsen. 1996. Influence of extraction solvent and temperature on the quantitative determination of oligosaccharides from plant materials by high-performance liquid chromatography. *J. Agric. Food Chem.* **44**:1470-1474.

Kozlowski, T.T. 1992. Carbohydrate sources and sinks in woody plants. *Botanical Review* **58**: 107-222.

Lacointe, A. 2000. Carbon allocation among tree organs: A review of basic processes and representation in functional-structural plant models. *Annals of Forest Sciences* **57**: 521-533.

Le Roux, X., A. Lacointe, A. Escobar-Gutierrez and S. Le Dizes. 2001. Carbon-based models of individual tree growth : A critical appraisal. *Annals of Forest Sciences* **58**:469-506.

Lopez, G., R. Favreau, C. Smith, E. Costes, P. Prusinkiewicz and T. DeJong, 2008. Integrating simulation of architectural development and source–sink behaviour of peach trees by incorporating markov chains and physiological organ function submodels into L-PEACH. *Functional Plant Biology* **35** (10): 761-771.

Millard, P. and G.A. Grelet, 2010. Nitrogen storage and remobilization by trees: ecophysiological relevance in a changing world. *Tree Physiology* **30**:1083-1095.

Oliviera, C.M. and C.A. Priestley. 1988. Carbohydrate reserves in deciduous fruit trees. *Horticultural Reviews* **10**:403-430.

Pernice, F., L. Solari and T.M. DeJong. 2006. Comparison of growth potentials of epicormic shoots of nectarine trees grown on size-controlling and vigorous rootstocks. *J. Hort. Sci. and Biotechnology* **81**:211-218.

Priestley, C.A. 1970. Carbohydrate storage and utilization. In *Physiology of Tree Crops*. Academic Press, London, 113-127.

Sauter, J., W. Iten and M.H. Zimmermann, 1973. Studies on the release of sugar into the vessels of sugar maple (*Acer saccharum*). Canadian Journal of Botany **51**:1-8.

Smith, D. 1968. Removing and analyzing total nonstructural carbohydrates from plant tissue. *Wisconsin Agric. Exp. Sta. Res.* Report 41, Madison, WI.

Proceedings of the 7th International Conference on Functional-Structural Plant Models, Saariselkä, Finland, 9 - 14 June 2013. Eds. Risto Sievänen, Eero Nikinmaa, Christophe Godin, Anna Lintunen & Pekka Nygren.
http://www.metla.fi/fspm2013/proceedings. ISBN 978-951-651-408-9.

Simulation of small footprint full waveform LiDAR signals from seedling stand vegetation using Monte Carlo ray tracing and statistical models of 3D vegetation structure

Aarne Hovi[1] and **Ilkka Korpela**[1]
[1]*Department of Forest Sciences, PO Box 27, 00014 University of Helsinki, Finland*
aarne.hovi@helsinki.fi

Keywords: Radiative transfer modeling, LiDAR, ray tracing, statistical model, leaf angle distribution

Accuracy of small footprint airborne light detection and ranging (LiDAR) in predicting stand mean characteristics such as stem volume was first demonstrated 10–15 years ago, and LiDAR is currently being applied in practical scale forest inventory in many countries. Despite the accuracy, method development is still needed for solving certain problems, e.g. tree species recognition and detecting the need for stand treatments. Simulation tools can be useful in studying effects of different sensor and target properties on the obtained signal. Monte Carlo ray tracing (MCRT) is computationally intensive, but generally considered as one of the most accurate methods for radiative transfer modeling in vegetation canopies as it aims at modeling the real photon paths (Widlowski et al. 2008). For input, a representation of geometric-optical properties of the scene is needed. Recent studies demonstrate use of MCRT with explicit, leaf/needle level 3D models in remote sensing studies, including LiDAR (Hancock et al. 2012; North et al. 2010).

The overall aim of this study was to develop a LiDAR simulator based on MCRT. More detailed aims were 1) to evaluate the simulator performance by comparing simulated signals against real data, and 2) to use the simulator for finding best suitable sensor characteristics for classification of common species in Finnish seedling stands. Statistical models of the 3D structure of three common species, silver birch (*Betula pendula*), raspberry (*Rubus idaeus*) and fireweed (*Epilobium angustifolium*), were used. The model of silver birch was obtained from Lintunen et al. 2011. For the other species, measurements on the shoot structure were made in the field, and the amount of shoots per square meter was linked to leaf area index (LAI). The validation dataset consists of field samples in Hyytiälä, Southern Finland (61°50′N, 24°20′E), and two separate LiDAR acquisitions.

The validation results show that species-specific characteristics of the LiDAR waveforms can be accurately reproduced with MCRT and the vegetation models used. Also, the mean signal levels (peak amplitude) were reasonably close to real data (max. 19% difference). If absolute accuracy is required, more detailed measurements on vegetation parameters (e.g. leaf area, leaf angle distribution, reflectance properties) as well as reflectance characteristics of the calibration targets are needed. In addition, validation of the scattering model against laboratory measurements is recommended. To design a best suitable sensor for seedling stand inventory, three sensor parameters (footprint size, pulse width, sampling frequency) were altered one at a time, and the classification accuracy of simulated LiDAR waveforms between the three selected species was evaluated. It was shown that classification accuracy increases with larger footprint size, but saturates at app. 0.35 m footprint. Effects of pulse width and sampling frequency were negligible. The computation times with our non-optimized algorithms and a normal desktop computer were 10–40 s per LiDAR pulse. We conclude that ray tracing simulator is a useful tool for developing new interpretation techniques, and testing hypotheses considering the interpretation of LiDAR data.

LITERATURE CITED

Lintunen, A., Sievänen, R., Kaitaniemi, P., Perttunen, J., 2011. Models of 3D crown structure for Scots pine (Pinus sylvestris) and silver birch (Betula pendula) grown in mixed forest. *Canadian Journal of Forest Research* **41**, 1779–1794.

Hancock, S., Lewis, P., Foster, M., Disney, M., Muller, J.-P., 2012. Measuring forests with dual wavelength lidar: A simulation study over topography. *Agricultural and Forest Meteorology* **161**, 123–133.

North, P. R. J., Rosette, J. A. B., Suarez, J. C., Los, S. O., 2010. A Monte Carlo radiative transfer model of satellite waveform LiDAR. *International Journal of Remote Sensing* **31**, 1343–1358.

Widlowski, J.-L., Robustelli, M., Disney, M., et al., 2008. The RAMI on-line model checker (ROMC): A web-based benchmarking facility for canopy reflectance models. *Remote Sensing of Environment* **112**, 1144–1150.

Proceedings of the 7th International Conference on Functional-Structural Plant Models, Saariselkä, Finland, 9 - 14 June 2013. Eds. Risto Sievänen, Eero Nikinmaa, Christophe Godin, Anna Lintunen & Pekka Nygren. http://www.metla.fi/fspm2013/proceedings. ISBN 978-951-651-408-9.

Between- and within-tree shading in mixed stands: shoot-level simulation

Anna Lintunen[1,*], **Pekka Kaitaniemi**[2], **Jari Perttunen**[3] and **Risto Sievänen**[3]
[1] *Dept. Forest Sciences, Univ. Helsinki, P.O. BOX 27, 00014 Univ. Helsinki, Finland,* [2]*Hyytiälä, Forestry Field Station, Dept. Forest Sciences, Univ. Helsinki, Hyytiäläntie 124, 35500 Korkeakoski, Finland,* [3]*Finnish Forest Research Institute, Vantaa Res. Ctr, P.O. BOX 18, 01301 Vantaa, Finland*
**correspondence*: anna.lintunen@helsinki.fi

Highlights: Between- and within-tree light transmission is simulated with ray casting method in reconstructed mixed stands consisting of Scots pine and silver birch.

Keywords: crown architecture, light transmission, self-shading

Light interception of foliage is dependent on between- and within-tree shading. The more light is transmitted through the neighbours, the more the light conditions in a tree crown are determined by the structure of the tree itself. We analysed light transmission in reconstructed mixed stands with varying age and density with ray casting method using the LIGNUM model (Sievänen et al. 2008). To reconstruct the stands consisting of Scots pine (*Pinus sylvestris* L.) and silver birch (*Betula pendula* Roth.) with 50% mixture, we used LIGNUM to reproduce 3D structural tree models that correspond to shoot level configurations of real individual trees grown in mixed forest stands (Lintunen et al. 2011). Radiation calculations were based on incoming radiation (direct and diffuse PAR) from 161 sky sectors, whose relative brightness was derived from standard overcast sky. Radiation transmission to the shoots of the target pine at different heights was analysed separately for transmission through the surrounding stand and through the target tree itself. Results show that self-shading reduces the amount of incoming light more than the neighbours apart from the sparse crown bottom of trees (visible as "L"-shaped self-transmission curve in Fig. 1). In sparse stands, self-shading has larger role than in the dense stands as expected.

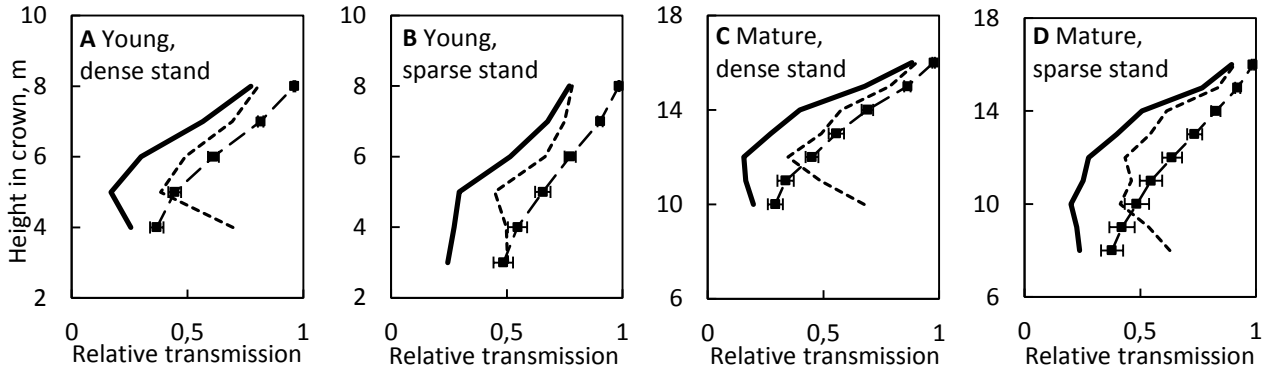

Figure 1. Transmission of radiation through the neighbors (average and 95% CI of ten repetitions; squares with vertical bars), through the target pine (dashed line) and both together (solid line) at different stands. The stands consist of a circular plot (r = 20m) surrounded by a homogeneous border forest. Inside the circular plot, reconstructed trees are situated randomly.

LITERATURE CITED

Lintunen A, Sievänen R, Kaitaniemi P, Perttunen J. 2011. Models of 3D crown structure for Scots pine (*Pinus sylvestris*) and silver birch (*Betula pendula*) grown in mixed forest. *Canadian Journal of Forest Research* **41**: 1779-1794.

Sievänen R, Perttunen J, Nikinmaa E, Kaitaniemi, P. 2008. Toward extension of a single tree functional structural model of Scots pine to stand level: effect of the canopy of randomly distributed, identical trees on development of tree structure. *Functional Plant Biology* **35**: 964-975.

Proceedings of the 7th International Conference on Functional-Structural Plant Models, Saariselkä, Finland, 9 - 14 June 2013.
Eds. Risto Sievänen, Eero Nikinmaa, Christophe Godin, Anna Lintunen & Pekka Nygren.
http://www.metla.fi/fspm2013/proceedings. ISBN 978-951-651-408-9.

A modeling approach to simulate the whole-plant leaf expansion responses to light in three annual dicotyledonous species

Benoit Pallas[1,4], Jérémie Lecoeur[2], Karine Chenu[3], Hervé Rey[1], Frédéric Gay[1] and Angélique Christophe[4]*
[1]CIRAD - Montpellier – France, [2]Syngenta CP Muenchwilen AG, Stein – Switzerland, [3]The University of Queensland, Toowoomba – Australia, [4] INRA LEPSE, 2 Place Viala, 34060 Montpellier cedex 2 - France
* *correspondence:* christop@supagro.inra.fr

Highlights: A generic leaf area growth model based on the simulation of leaf growth dynamics in response to light microclimate was built, calibrated and validated for three dicotyledonous species.

Keywords: leaf area, temperature, radiation, relative elongation rate, development.

Plant leaf area plasticity is a key adaptive process to fluctuating environmental resources. Modeling and simulating leaf area is necessary to analyze and explore plant agronomic performances under various environments. The purpose of this work was to propose a generic plant model simulating leaf area dynamics. The model simulates plant leaf area dynamics according to temperature and light conditions. Three dicot species with different patterns of vegetative growth were selected: *Arabidopsis thaliana* L., *Helianthus annuus* L. and *Lactuca sativa* L. First, the model simulates organ and plant development on the basis of an organogenetic body plan, driven by intrinsic organ growth and production rhythms. These rhythms are modeled according to temperature through thermal time. This organogenetic body plan allows estimating for each leaf its potential time of (i) initiation, of (ii) end of exponential growth and of (iii) end of expansion (Fig. 1A). Response curves between development rate and the amount of intercepted radiation are used to simulate the impact of light conditions on these developmental timings (Chenu et al. 2005). The model computes the potential relative elongation rates (RER) of each leaf according to its insertion rank and according to its age (Fig. 1B). Each day, the RER during the exponential phase of leaf expansion is computed as the product of potential relative elongation rates and of a stress coefficient calculated according to the amount of absorbed radiation by the plant. Lastly, individual leaf area is computed and whole plant leaf area is obtained by summing the area of individual leaves. This growth model is coupled with a phylloclimate model estimating on a daily basis the amount of absorbed radiation by leaves using 3D reconstructions of plants and a radiative balance. Model parameterization was derived from experiments conducted for the three species in field, greenhouse and growth chambers. For each species, an independent data set was used to validate the model under different light conditions. According to the quality of the simulations (Fig. 1C), the model appears to be promising to simulate the dynamics of leaf area in response to light and temperature for the three different species. Sensitivity analyses were performed to analyze the relative contributions to plant leaf area of plant development rate, duration of the exponential expansion phase and sensitivity to light conditions. Lastly, for the parameters related to these processes, a sensitivity analysis was carried out to identify optimal target parameter values that maximize whole plant leaf area development under different light regimes.

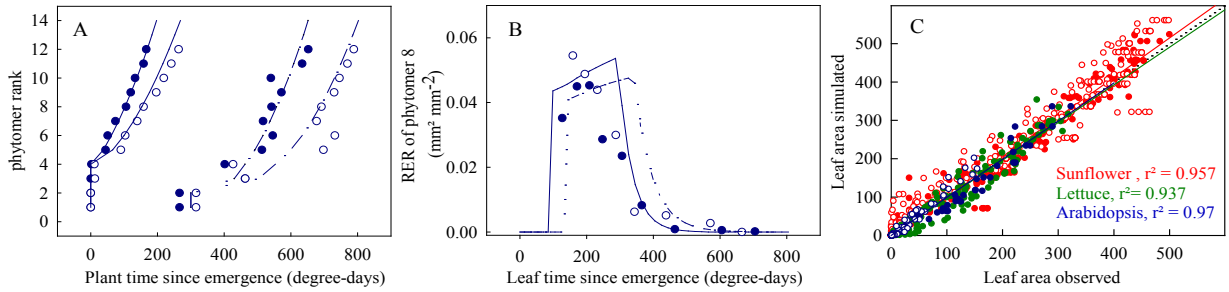

Fig. 1 Results of model simulations for two light regimes (9.3 mol m^{-2} day^{-1},color symbols and 3.7 mol m^{-2} day^{-1} empty symbols). Times of leaf initiation and end of leaf expansion for all phytomers of *Arabidopsis thaliana* plants (A), time-course of RER for phytomer 8 (B) and observed and simulated individual leaf area for sunflower (cm^2), lettuce (cm^2) and Arabidopsis Thaliana (mm^2) (C). Lines represent simulation results. Color symbols refer to high light conditions and empty symbols refer to low light conditions.

Chenu K, Franck N, Dauzat J, Barczi JF, Rey H, Lecoeur J. 2005. Integrated responses of rosette organogenesis, morphogenesis and architecture to reduced incident light in *Arabidopsis thaliana* results in higher efficiency of light interception. *Functional plant Biology* **32:** 1123-1134.

Proceedings of the 7th International Conference on Functional-Structural Plant Models, Saariselkä, Finland, 9 - 14 June 2013. Eds. Risto Sievänen, Eero Nikinmaa, Christophe Godin, Anna Lintunen & Pekka Nygren. http://www.metla.fi/fspm2013/proceedings. ISBN 978-951-651-408-9.

Characterization of the relationship between quantity and quality of solar radiation in canopy under contrasting sky conditions

Cailian Lao[1], Zhaoli Xu[2], Yan Guo[1], Yan Jin[2] and **Yuhong Yang[2*]**
[1] *China Agricultural University, Beijing 100083, PR China*
[2]*Yunnan Academy of Tobacco Agricultural Sciences, Kunming 650021, PR China*
**correspondence:* toyyred@263.net

Highlights: Spatial radiation distribution in tobacco canopy was measured and analyzed according to spectral composition under clear and overcast sky conditions.

Keywords: light quality and quantity, light environment, radiation, three-dimensional canopy

The light environment of a canopy is substantially affected by plant architecture and sky condition (Escobar-Gutierrez *et al*. 2009). The objective of this study was to reveal the relationship between quality and quantity of radiation in canopy under different sky conditions. Measurement was conducted in a tobacco (*Nicotiana tabacum,* cultivar 'K326') field (24°18′N, 102°29′E, Altitude: 1642 m) in Yunnan, China. Incoming spectral irradiation was measured at the three-dimensional grids around a plant located at the center of tobacco canopy (Fig.1) using FieldSpec3 field spectroradiometer (ASD Inc., USA) equipped with a Remote Cosine Receptor (model A124505, ASD Inc.), and the photosynthetic photon flux density above canopy was measured instantaneously using AccuPAR (model LP-80, Decagon Devices inc., USA) on July 22 (overcast) and July 30 (clear), respectively. The fraction of PAR (fPAR) and the spectral ratios between red (R), blue (B), green (G) and far-red (FR) measured at these sampling points were examined. The results (Tab.1) illustrated that R/FR had very high correlation with fPAR, while that for B/R was the lowest, and their relationship could be characterized as quadratic functions of log(fPAR). These relationships were more significant under overcast sky condition. This study indicated that certain relationships existed between light quantity and quality within plant canopy, and their relationships varied with spectral ratios and were affected by sky conditions.

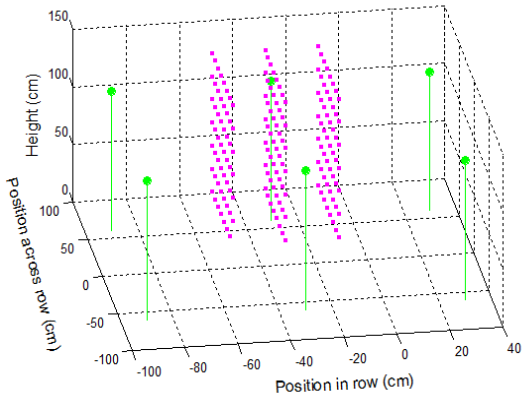

Fig.1 Measurement points (magenta) in the tobacco canopy (green)

Tab.1 Relationships between spectral ratios and faction of PAR (fPAR) in light environment of tobacco canopy

Spectral ratio	Sky condition	Function of log(fPAR)	R^2
R/FR	Overcast	$0.062x^2+0.57x+1.36$	0.99
	Clear	$0.065x^2+0.69x+1.85$	0.97
B/G	Overcast	$-0.048x^2+0.0058x+0.94$	0.92
	Clear	$-0.028x^2$ -1.1E-5x+0.91	0.71
B/R	Overcast	$-0.070x^2-0.11x+1.11$	0.79
	Clear	$-0.077x^2-0.35x+0.69$	0.32

R, B, G and FR refer to red, blue, green, far-red, respectively.

ACKNOWLEDGEMENTS

This research was supported by China National Tobacco Corporation (110201102008).

LITERATURE CITED

Escobar-Gutierrez AJ, Combes D, Rakocevic M, de Berranger C, Eprinchard-Ciesla A, Sinoquet H, Varlet-Grancher C. 2009. Functional relationships to estimate Morphogenetically Active Radiation (MAR) from PAR and solar broadband irradiance measurements: The case of a sorghum crop. *Agric For Meteorol* **149:** 1244–1253.

Proceedings of the 7th International Conference on Functional-Structural Plant Models, Saariselkä, Finland, 9 - 14 June 2013. Eds. Risto Sievänen, Eero Nikinmaa, Christophe Godin, Anna Lintunen & Pekka Nygren. http://www.metla.fi/fspm2013/proceedings. ISBN 978-951-651-408-9.

Artificial neural networks in modeling of environmental time series for yerba-mate growth dynamics

Fabio Takeshi Matsunaga[1,2], **Miroslava Rakocevic**[1] and **Jacques Duílio Brancher**[2]
[1]*Agronomical Institute of Paraná - IAPAR, P.O. Box 481, CEP 86047-902, Londrina, PR, Brazil,* [2]*State University of Londrina - UEL, P.O. Box 6001, CEP 86044-290, Londrina, PR, Brazil*
ftakematsu@gmail.com

Highlights: The artificial neural networks (ANN) are a solution to model the nonlinear systems. The monthly mean values of environmental and morphological data were used to build time series related to yerba-mate growth. Time series and data relative to rhythmic growth were used for ANN training. The final results of this FSPM are yerba-mate mock-ups, related to two particular environmental conditions.

Keywords: backpropagation algorithm, multilayer perceptron, shoot elongation, temperature

INTRODUCTION

InterpolMateS1 software allows the 3D reconstructions during a biennial yerba-mate growth (Matsunaga et al. 2012) considering male (MA) and female (FE) individuals in two distinct light environments - forest understory (FUS) and cultivation under open area - in monoculture (MO). The growth flushes and pauses of yerba-mate rhythmic growth are controlled endogenously and modified by environment (Rakocevic and Martim, 2011). The representations of leaf and shoot dynamics are the central components of this specific yerba-mate FSPM, based on cubic splines interpolation, which considers a biennial period between two subsequent prunings coupled with VPlants for 3D reconstructions.

Many mathematical and computational modeling principles were performed in modeling of plant growth dynamics related to environmental conditions. The multiple regression models can be used for this purpose, but their performance could be low, especially when the nonlinear relationships were established, which is very common in ecology (Lek et al. 1996). The uses of differential equations (Zhang et al. 2007), or predefined equations (Laaboudi et al. 2012), give better performance and accuracy, but require a larger number of not always available ecological parameters.

Methodologically advanced solution in nonlinear system modeling is the use of artificial neural networks (ANN). ANN requires only some input parameters, even when some are unknown. Han and Fan (2006) used ANN and principle component analysis to solve multivariate time series prediction problems. Bayesian generalized associative functional networks were applied to model the dynamical plant growth process of greenhouse crops and predict their dry matter production (Qu and Hu, 2009).

Our actual interest in yerba-mate FSPM development is focused on the inclusion of the environmental impacts on yerba-mate growth responses and synchronization of growth variables. Time series analysis permitted the emphasizing of growth degree days and night/day length as principal environmental factors affecting yerba-mate shoot elongation and the number of green leaves (Rakocevic and Martim, 2011) in two light environments. It was hypothesized that correlations between environmental and growth time series could be recognized by ANN. The aim of this work was to improve the InterpolMateS1 software using the ANN training for: 1/correlation between the environmental impacts relative to two particular growth environments and the morphological responses of yerba-mate males and females, and 2/ synchronization of morphological responses.

APPLICATION OF ANN TO MODEL TIME SERIES IN YERBA-MATE GROWTH AND STRUCTURE

Data sets for yerba-mate (*Ilex paraguariensis*) growth were built from measurements differencing plant growth environment (MO and FUS) and gender (MA and FE). The plant architecture (Rakocevic et al. 2011) and growth were reconstructed from morphological parameters followed on 90 branches of thirty plants, considering: rate of shoot elongation, metamer number increase, leaf number increase, leaf shed and leaf area increase per shoot. The morphogenetic parameters were followed monthly at three branches for each individual, during a biennial period (June 2003 – June 2005), resulting in 25 observations. Those responses represent the intrinsic plant program modified by environmental conditions, where the average minimum (minT) and maximum temperatures (maxT), sum of growing degree days (GDD), average rainfalls (RF) and night length (NL) were observed. The monthly mean values of morphological and environmental data were applied to build plant growth and environmental time series. Those time series, information about periods of rhythmic growth and respective growth pauses, were used for ANN training.

The perceptron multilayer ANN was chosen to model time series in yerba-mate growth because of its facilities of interpretation and ability to solve non-linear problems (Jantzen, 1998). It generates a mathematical-computational model of morphological responses to input variables (environmental inputs and yerba-mate growth cycle definition). The developed ANN for yerba-mate growth uses the supervised machine learning, which consists of: 1/ backpropagation algorithm and 2/ rules for morphological parameters synchronization within ANN training. The backpropagation algorithm extends the analysis that underpins the delta rule to neural nets with hidden nodes formulae. The delta rule algorithm always makes a change in weights of connections, and is based on activation of nodes opposed to output (Hecht-Nielsen, 1989). The synchronization is performed by logical functions, centralizing the rate of metamer appearance and defining its interrelations with other parameters during the periods of growth flushes and pauses.

The architecture of yerba-mate ANN (Fig. 1) consists of three layers: 1/ an input layer containing six nodes to receive input variables, 2/ a hidden layer with $2n+1$ nodes (Hecht-Nielsen, 1989), where n is the number of input variables and 3/ an output layer that computes the simulated data and back-propagates the errors to the hidden layer. The training phase of the ANN consists on the feed-forward phase and the back-propagation phase. During the feed-forward phase, the nodes compute the outputs using an activation sigmoid function in the hidden layer, and pass the results of the function to the nodes in the output layer.

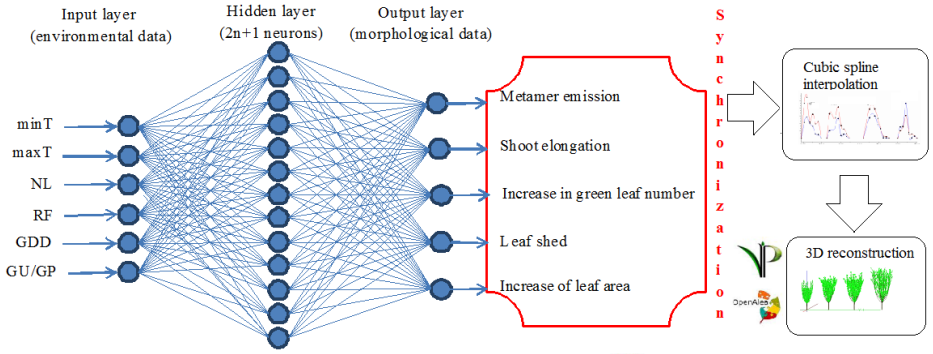

Fig. 1. Schema of ANN used for modeling the yerba-mate time series, and growth parameter synchronization. The network input variables are average minimum and maximum temperatures (minT and maxT), night length (NL), rainfalls (RF), growth degree days (GDD), and periods of growth flushes and pauses (GU/GP). The output consists of morphological responses that are synchronized by logical functions. Cubic splines interpolation helps the 3D reconstruction in VPlants.

After the synchronization of the morphological outputs, those values are interpolated using the cubic splines interpolation method (Matsunaga *et al.*, 2012), permitting the daily-step reconstructions of yerba-mate structure in 3D (Fig. 1, right side).

RESULTS AND DISCUSSION

ANN training was able to detect the correlations between yerba-mate growth and environmental variables in two growth environments. The empirical tests of yerba-mate ANN were resulted in 10^5 as the maximum iterations for a stable network functioning. The root mean square error (RMSE, fitted to 1), and bias were used for ANN validation (Tab. 1). The correlations between yerba-mate environmental and growth variables in FUS were less recognized by ANN than those in MO. The leaf area increase was the response with the lowest adjustments for both genders, when time series were modeled for yerba-mate growth under a forest shade. In a future work, it is possible to improve those outputs by adding momentum constant on delta rule in ANN (Jantzen, 1998).

Tab. 1. Bias and RMSE calculated for artificial neural network outputs obtained after 100,000 iterations, and adjusted to measured shoot parameters for yerba-mate male and female plants grown in two contrasted light environments (open areas and forest understory).

Growth parameters	**Females**				**Males**			
Environment	Monoculture		Forest understory		Open area		Forest understory	
	RMSE	bias	RMSE	bias	RMSE	bias	RMSE	bias
Shoot elongation	1	**-0.005**	0.480	**0.177**	1	**-0.241**	1.860	**-0.119**
Metamer emission	1	**-0.005**	0.819	**-0.177**	1	**0.116**	0.706	**-0.006**
Leaf number increase	1	**-0.058**	0.037	**0.039**	1	**0.040**	1.067	**-0.028**
Leaf shed	1	**-0.280**	1	**0.027**	1	**-0.030**	1	**0.053**
Increase of leaf area	1	**-1.641**	0.631	**0.910**	1	**0.519**	7.628	**-0.848**

The ANN training performed more precise 3D reconstruction outputs (Fig. 2), due to accurate definition relative to periods of growth flushes and variable synchronization (Fig. 1). The metamer emission, branching and leaf shed respected the environmental conditions and logical rules (Fig. 2A *versus* Fig. 2B), permitting the leaf area distribution according to the most probable occurrence.

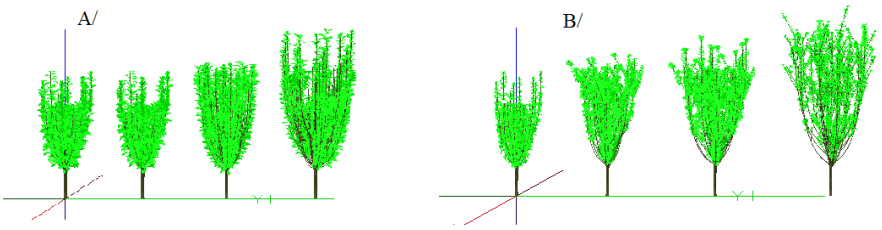

Fig. 2. Reconstructions of one female cultivated in monoculture relative to four growth unit formations A/ before and B/ after the ANN training.

ANNs use the supervised learning and are precise only for established conditions according to known and expected outputs (Zhang et al. 2007). This modeling approach could permit the accuracy for simulations using different environmental conditions and variety of morphological definitions for yerba-mate shoot architecture, but would require the additional training.

ACKNOWLEDGMENTS

The study was supported by grants for the invited researcher [M.R.] offered by Consórcio Pesquisa Café, and for the master formation [F.T.M.] offered by CAPES.

LITERATURE CITED

Han, M, Fan, M. 2006. Application of neural networks on multivariate time series modeling and prediction. *Proceedings of the American Control Conference*, Minneapolis, Minnesota, USA: 3698-3703.

Hecht-Nielsen, R. 1989. Theory of the backpropagation neural network. *Proceedings of the International Joint Conference on Neural Networks:* 593-605.

Jantzen, J. 1998. *Introduction To Perceptron Networks*, Technical University of Denmark, Department of Automation, Lyngby, Technical report n° 98-H 873: 1-32.

Laaboudi, A, Mouhouche, B, Draoui B. 2012. Neural network approach to reference evapotranspiration modeling from limited climatic data in arid regions, *International Journal of Biometeorology* **56**: 831–841.

Lek, S, Delacoste, M, Baran, Ph, Dimopoulos, I, Lauga, J, Aulagnier, S. 1996. Application of neural networks to modelling nonlinear relationships in ecology. *Ecological Modelling* **90**:39-52.

Matsunaga, FT, Rakocevic, M, Brancher, JD. 2012. InterpolMateS1- the Module for interpolation of growth and production of yerba-mate. *IEEE PMA'12*: 367-370.

Qu, H-B, Hu, B-G. 2009. Variational learning for generalized associative functional networks in modeling dynamic process of plant growth. *Ecological Informatics* **4**:163–176.

Rakocevic, M, Costes, E, Assad, ED. 2011. Structural and physiological sexual dimorphism estimated from 3D virtual trees of yerba-mate (*Ilex paraguariensis* St. Hil.) is modified by cultivation environment. *Annals of Applied Biology* **156(6)**:178-191.

Rakocevic, M, Martim SF. 2011. Time series in analysis of yerba-mate biennial growth modified by environment. *International Journal of Biometeorology* **55(2)**:161-171.

Zhang, W, Bai, C, Liu, G. 2007. Neural network modeling of ecosystems: a case study on cabbage growth system. *Ecological Modelling* **201**:317-325.

Proceedings of the 7th International Conference on Functional-Structural Plant Models, Saariselkä, Finland, 9 - 14 June 2013. Eds. Risto Sievänen, Eero Nikinmaa, Christophe Godin, Anna Lintunen & Pekka Nygren.
http://www.metla.fi/fspm2013/proceedings. ISBN 978-951-651-408-9.

Building the foundations of a *Coffea arabica* FSPM

Jean Dauzat[1], Sébastien Griffon[1], Olivier Roupsard[2], Philippe Vaast[2] and Gustavo Rodrigues[3]
[1]*Cirad, UMR AMAP, F-34000, Montpellier, France,* [2]*Cirad, UMR Eco&Sol, Montpellier,* [3]*Embrapa-CNPTIA, Campinas, Brazil*
**correspondence:* dauzat@cirad.fr

Highlights: Several data sets are being gathered to build a functional-structural model for *Coffea arabica*. The one pitfall in this integration process is the difficulty of calibrating a large number of parameters. A step by step procedure is thus necessary to validate the sub-models. The focus is put here on the backward reconstruction of the plant structure from its description at a given times as a way to decrease the degrees of freedom of the model before addressing the carbon acquisition and allocation.

Keywords: *Coffea Arabica*, plant structure, AMAPstudio, light capture

INTRODUCTION

Coffee is the most valuable product worldwide after oil. A quite large literature is dedicated to the agronomy and physiology of coffee tree (DaMatta et al. 2007) but there have been few attempts to model plant growth and production on functional bases. The most integrative process-based model was recently proposed by Rodriguez et al. (2011). This model combines phenology, shoot and root dynamics, light interception, photosynthesis and carbon allocation. However it works with cohorts of branches and leaves and doesn't explicitly consider the plant geometry and topology. Our purpose is thus to lay the foundations of coffee FSPM using information obtained in different experiments.

FSPMs mostly lie on four cornerstones: plant topology, plant geometry, carbon acquisition and carbon allocation. Putting together these different components leads to complex models with numerous parameters and, as far as many parameters need to be calibrated, there is then no insurance that proper parameter values can be obtained through automatic optimization methods. A step by step procedure is thus necessary for calibrating and validating the components of the integrated model.

Plant topology is the first step to address when aiming to develop a functional growth model with an explicit 3D structure. Basically the plant structure is the result of bud activity (growth, dormancy, death and ramification processes) over time. Unfortunately the functional bases of organogenesis are complex and poorly understood. A way to overcome this problem is to force the plant structure against field observations. This procedure is not straightforward since the plant structure cannot be reasonably measured all along its development and in coffee trees and there is no growth marker that can be used for inferring the age of the elements of a plant structure (Taugourdeau et al. 2012). Dating the elements of a coffee tree therefore needs a precise knowledge of the growth rates of plant sub-structures. Fortunately the growth rates of the main stem and branches are closely related in coffee trees (deReffye, 1990), making possible to retrieve back in time the plant structure in former stages. This procedure is illustrated here for arabica coffee plants at six growth stages from DAP 156 to 797. The experience acquired on modeling the carbon acquisition and the 3D plant structure is also briefly presented.

MATERIAL AND METHODS

Available information comes from several studies on Arabica coffee in Costa Rica –mainly the ICAFE experiment (Vaast et al. 2004) and the Orosi experiment (Franck et al. 2006)- and in Brazil (Rodrigues et al. 2011). The Costa Rica experiments were conducted for plants grown under different natural or artificial shade (Franck and Vaast, 2009). The effect of fruit load and ring braking was studied (Vaast et al. 2002 & 2004). These studies allowed to parameterize Farquhar's model for the different growth irradiances Dauzat et al. 2006). In both experiments 3D digitizing was performed on several plants along a row.

The Brazilian experiment was set up in the Embrapa Cerrado experimental field near Brasilia to compare the response of two cultivars (Iapar, drought tolerant and Rubi, drought sensitive) to temporary water shortage in terms of plant architecture, shoot and root biomass, physiology and gene expression. The experiment was conducted during two years with subplots irrigated or not during the dry season for each cultivar. Three treatments were applied as illustrated in Fig. 1. Three times a year, before, during and after

the dry season, plants were taken from the field to the laboratory for a comprehensive description of plant architecture including the measurement of leaves and internodes length, the stem and branch diameter and the branching angles. The total dry matter of stem and branches was then measured as well as the dry matter of roots. The dry matter of leaves was measured separately for each branch.

Data were coded under the MTG format (Godin & Caraglio, 1998) and loaded as an ArchiTree in the AMAPstudio-Xplo software (Griffon and Coligny, 2012) for performing simple analyses or for exporting data to dedicated statistical software such as R. XPLO was also used for creating 3D plant models under the AMAPstudio "OPF" format. The AMAPstudio-Simeo software (ibid.) was then used to create virtual plots and to run the simulation of light interception. The light model is an adaptation of the MMR model (Dauzat et al. 2008) that calculates the irradiance of individual plant organs.

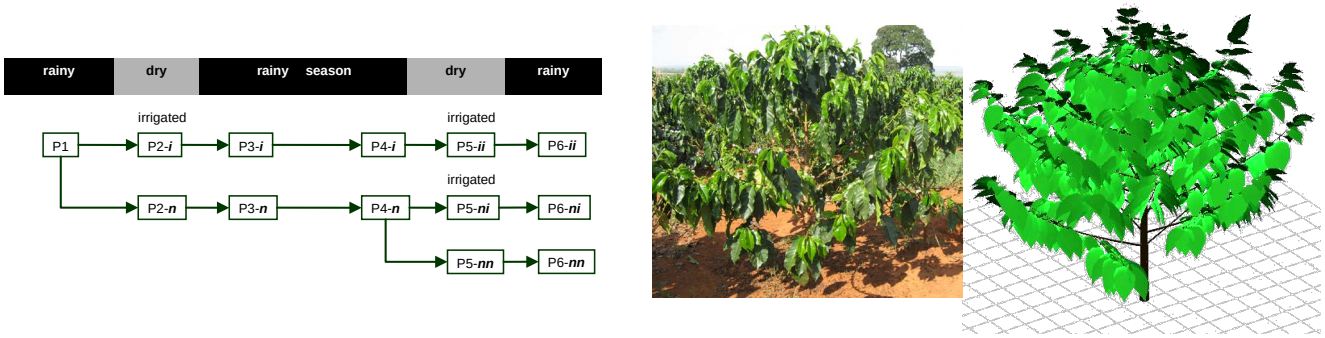

Fig. 1. A: Treatments applied on the different plots P in the Brazilian experiment. The plot were irrigated (i) or non irrigated (n) during the first and the second dry season. B: view of a plant in P5. C: example of simulated plant.

RESULTS AND DISCUSSIONS

Coffea arabica seedlings develop an orthotropic stem bearing systematically two plagiotropic branches on each node with the exception of some very basal nodes. These first order branches are sylleptic, i.e. they start their development with no delay. Branches may themselves develop two plagiotropic ramifications (second order branches) on each node and these ramifications may also develop two third order ramifications and so on. However these ramifications develop with delays and are set up at uneven node positions. Because plants are generally coppiced every 2 or 3 years in order to keep them short and facilitate fruit collection, the plant architecture remains rather simple with branch orders limited to 3 or 4.

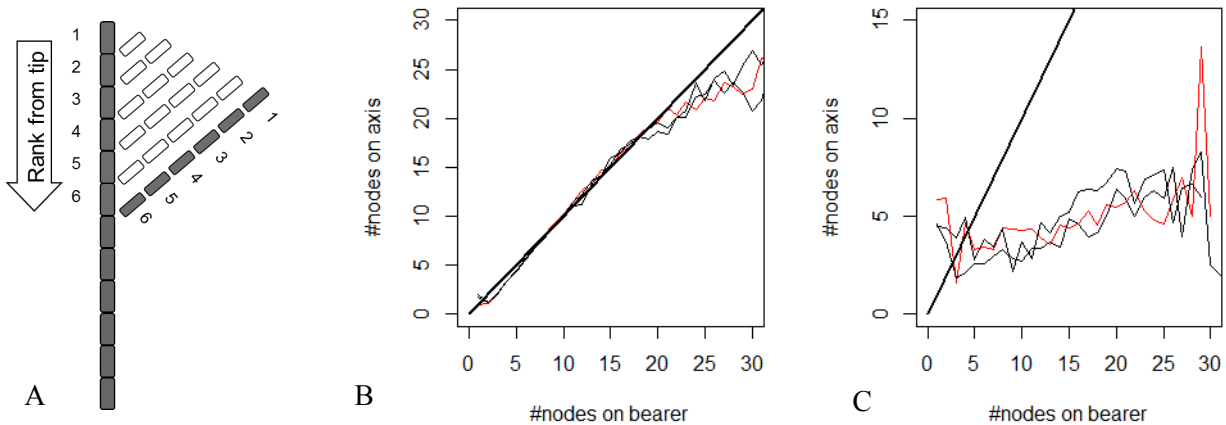

Fig. 2. A: comparison of the number of nodes on branches vs. the number of nodes on their bearing axis. B: results obtained for 1st order branches vs. main stem. C: results obtained for 2nd order branches vs. 1st branches. (Results obtained for the Iapar cultivar). The 3 lines in B and C correspond to the 3 treatment (ii, ni and nn).

The main stem phyllochron was found to be about constant over the two years for irrigated plants but was slightly increased during the dry seasons for non-irrigated plants. In order to analyze the phyllochron of branches we compared their number of metamers to the number of metamers of the distal portion of their bearer axis (Fig. 2A). Results show that the first order branches have the same growth rate as the main stem except for older branches in which the growth rate progressively decreases (Fig. 2B). The same trends are observed for the two cultivars in all treatments. Likewise second or third order branches have a growth rate

similar to their bearer. However their set up is spread out in time, leading to ramifications of about 1/3 the size of the distal portion of their bearer on average (Fig. 2B). Second and third order branches are more or less randomly located on "mature" nodes (nodes of rank >15) whatever the size and position of their bearer.

Different responses to water shortage were found for the two cultivars in terms of biomass acquisition. The main explanation is that the sensitive cultivar has a poor stomatal regulation and therefore rapidly exhausts the soil water reserves. However the analyses revealed no clear response of plant architecture to drought.

Virtual plants were simulated based on the above mentioned organogenetic rules and compared to actual plants in terms of biometric data and light capture. This step was achieved owing to a plant builder in which bud events -i.e. initiation of new metamers- are triggered by a scheduler. By doing so the complete plant structure is automatically updated at any time.

Simulations fairly reproduced the plant structure on average (Fig. 1B & C) but failed to render the inter-plant variability. Given that plants were sampled to cover the spectrum of plant height at the setting of the experiment, it was therefore necessary to initialize the plant development in young stages before running the simulations. This was achieved by applying the organogenetic rules to associate an initiation date to each plant component and finally get the plant state at any date. Likewise the number of leaves was interpolated from field observations for each branch order.

Ongoing steps using previous results from Costa Rica experiments are (i) the evaluation of light capture vs. the geometrical parameters by comparing simulated plants to digitized plants and performing sensitivity analyses of light interception vs. leaves angles, (ii) the integration and re-parameterization of the carbon acquisition model (Dauzat et al. 2006) and (iii) checking the consistency between the simulated carbon acquisition and the biomass accumulation over time. A major question mark for steps ii and iii is the negative feedback from sinks to carbon sources (Franck et al. 2006 & 2009; Vaast et al. 2002 & 2004) suggesting that the growth of coffee trees can be sink driven in case of a low fruit load.

LITERATURE CITED

DaMatta F, Ronchi CP, Maestri M, Barros RS. 2007. Ecophysiology of coffee growth and production. *Braz. J. Plant Physiol.* **vol.19 no.4**

Dauzat J, Franck N, Rapidel B, Luquet D, Vaast P. 2006. Simulation of Ecophysiological Processes on 3D Virtual Stands with the ARCHIMED Simulation Platform. Plant Growth Modeling and Applications, 2006. PMA '06. IEEE press: 101-108.

Dauzat J, Clouvel P, Luquet D, Martin P. 2008. Using virtual plants to analyse the light-foraging efficiency of a low-density cotton crop. *Annals of Botany*, **101**: 1153-1166.

Franck N, Vaast P, Génard M, Dauzat J. 2006. Soluble sugars mediate sink feedback down-regulation of leaf photosynthesis in field-grown Coffea arabica. *Tree Physiology* **26**: 517–525

Franck N, Vaast P. 2009. Limitation of coffee leaf photosynthesis by stomatal conductance and light availability under different shade levels. Trees **23**:761–769.

Godin C, Caraglio Y. 1998. A multiscale model of plant topological structures. *J. of Theoretical Biology* **191**: 1–46.

Griffon S, de Coligny F 2012. AMAPstudio: a Software Suite for Plants Architecture Modelling. In: Kang M, Dumont Y, Guo Y, eds. Plant Growth Modeling, Simulation, Vizualization and Applications. IEEE press: 141-147.

Rodrigues GC, Rojas JSD., Roupsard O, Leroy T, Pot D, Moreira MZ, Verdeil JL, Dauzat J, Jourdan C, Andrade AC, Marraccini P. 2011. Preliminary results on phenotypic plasticity of coffee (*Coffea arabica* cv. Rubi and Iapar59) plants in response to water constraint under field conditions**.** In: 23rd International Conference on Coffee Science.ASIC. Int. Conference on Coffee Science (ASIC). 23, 2010/10/03-08, Bali, Indonesia 698-703.

Rodríguez D, Cure JR, Cotes JM, Gutierrez AP, Cantor F. 2011. A coffee agroecosystem model: I. Growth and development of the coffee plant. *Ecological Modelling* **222**: 3626– 3639.

Taugourdeau O, Dauzat J, Griffon S, Sabatier S, Caraglio Y, Barthélémy D. 2012. Retrospective analysis of tree architecture in silver fir (*Abies alba* Mill.): ontogenetic trends and responses to environmental variability. *Annals of Forest Science* **69**:713–721

Reffye (de) P, Snoeck J, Jaeger M. 1990. Modélisation et simulation de la croissance et de l'architecture du Caféier. Proceedings of 13ème Colloque International sur le Café. Paipa, Colombie : 523-546.13ème Colloque International sur le Café, 21-25/08/1989, Paipa, Colombie.

Vaast P, Génard M, Dauzat J. 2002. Modeling the effects of fruit load, shade and plant water status on coffee berry growth and carbon partitioning at the branch level**.** *Acta horticulturae.* **584:** 57-62.

Vaast P, Angrand J, Franck N, Dauzat J, Génard M. **2004**. Fruit load and branch ring-barking affect carbon allocation and photosynthesis of leaf and fruit of *Coffea arabica* in the field. *Tree Physiology* **25**: 753–760

Proceedings of the 7th International Conference on Functional-Structural Plant Models, Saariselkä, Finland, 9 - 14 June 2013. Eds. Risto Sievänen, Eero Nikinmaa, Christophe Godin, Anna Lintunen & Pekka Nygren. http://www.metla.fi/fspm2013/proceedings. ISBN 978-951-651-408-9.

Evaluation of a photon tracing model and virtual plants to simulate light distribution within a canopy in a growth chamber

Julien Le Gall[1], Hervé Autret[1], Didier Combes[2], Christophe Renaud[3], Jessica Berthloot[1], Nathalie Leduc[4], Bruno Andrieu[5], Vincent Guérin[1], Michael Chelle†[5], Sabine Demotes-Mainard[1]†[*]

[1]INRA, UMR 1345 IRHS, SFR 4207 QUASAV, F-49071 Beaucouzé, France. [2]INRA, UR4 P3F, F-86600 Lusignan, France. [3]Université du Littoral Côte d'Opale, LISIC EA4491, F-62228 Calais, France. [4]Université d'Angers, UMR 1345 IRHS, SFR 4207 QUASAV, F-49045 Angers, France. [5]INRA, UMR 1091 EGC, F-78850 Thiverval-Grignon, France.

† M. Chelle and S. Demotes-Mainard contributed equally to this work.

**correspondence:* sabine.demotes@angers.inra.fr

Highlights: Radiance distribution in a growth chamber is anisotropic. Our objective is to evaluate the accuracy of light simulations in a rose canopy grown in a growth chamber using virtual plants and a photon tracing model dedicated to growth chambers. The question of the scale at which the system reproduces the observed variability is specifically addressed.

Keywords: photon tracing model, growth chamber, light phylloclimate, plant architecture

Growth chambers are frequently used to study plant physiology. Yet, in growth chambers, in addition to light variations due to plant architecture there is a strong anisotropic distribution of radiance due to the characteristics of the chamber itself. A photon tracing model was developed to simulate light distribution in growth chambers (SEC2, Chelle et al. 2007). Our objective is to evaluate SEC2 ability to simulate accurately light distribution in a canopy using virtual plants.

In a first step the virtual representation of the growth chamber included the geometry and the optical properties of the surfaces, as well as a representation of the light sources. This virtual growth chamber was used to simulate the 3D radiative field using the SEC2 model. In absence of plants, the simulation predicted well the light distribution in a 40 cm thick horizontal layer corresponding to usual canopy occupation (RMSEP=6.2%). A second step consisted in the evaluation of the model for light simulated within five canopies of rose bushes differing in individual plants architecture. Spectral irradiance was measured with different sensor orientations and at different locations within the canopy. Some locations were very close to each other to study the micro-local variability, whereas other locations were chosen to assess light vertical and horizontal (border effect) penetration in the canopy. Measurements show that the light variability was high, *e.g.*: the differences in photon flux density in the red waveband was up to 159% at the same position between two canopies, and up to 91% at 1 cm of distance within a canopy. The plants constituting the canopies were digitized (Polhemus Fastrack, Colchester, USA) and the reconstitution of the virtual canopies in the virtual growth chamber are in progress. The comparison of the simulations with the measurements will assess the ability of the whole system (photon tracing model, in silico reconstruction of growth chamber and plants) to simulate light distribution in a canopy in a growth chamber for PAR, red:far red ratio and blue light. We will specifically address the question of the scale at which light variability is correctly accounted for: are the general tendencies as vertical/horizontal light penetration simulated? the micro-local variations?

In the system evaluated here all interactions among light sources, materials and plants were modelled, as in Buck-Sorlin et al. (2011) for glasshouses, which is an alternative to Chenu et al. (2008) who characterized the radiative system by measurements. These results will assess the ability of the system to be further used to investigate plant response to phylloclimate.

LITERATURE CITED

Buck-Sorlin G, De Visser PHB, Henke M, Sarlikioti V, Van der Heijden GWM., Marcelis LFM, Vos J, 2011. Towards a functional-structural plant model of cut-rose: simulation of light environment, light absorption, photosynthesis and interference with the plant structure. *Annals of Botany* **108***:* 1121-1134.

Chelle M, Renaud C, Delepoulle S and Combes D, 2007. Modeling light phylloclimate within growth chambers, In: Prusinkiewicz P, Hanan J, Lane B eds. *Functional-Structural Plant Models. 5th International Workshop.* Napier (NZ), 571-574.

Chenu K, Rey H, Dauzat J, Lydie G, Lecoeur J, 2008. Estimation of light interception in research environments: a joint approach using directional light sensors and 3D virtual plants applied to sunflower (*Helianthus annuus*) and *Arabidopsis thaliana* in natural and artificial conditions*. Functional Plant Biology* **35** : 850-866.

Proceedings of the 7th International Conference on Functional-Structural Plant Models, Saariselkä, Finland, 9 - 14 June 2013. Eds. Risto Sievänen, Eero Nikinmaa, Christophe Godin, Anna Lintunen & Pekka Nygren. http://www.metla.fi/fspm2013/proceedings. ISBN 978-951-651-408-9.

Simulating maize plasticity in leaf appearance and size using regulation rules

Junqi Zhu*[1], Bruno Andrieu[2,3], Vos Jan[1], Wopke van der Werf[1], Christian Fournier[4,5] and Jochem B. Evers[1]

[1] Centre for Crop Systems Analysis,Wageningen University, 6708 PB Wageningen, The Netherlands,
[2]INRA, UMR 1091 EGC, F-78850 Thiverval-Grignon, France
[3]AgroParisTech, UMR 1091 EGC, F-78850 Thiverval-Grignon, France
[4]INRA, UMR 759 LEPSE, F-34060 Montpellier, France
[5]SupAgro, UMR 759 LEPSE, F-34060 Montpellier, France
**correspondence:* junqi.zhu@wur.nl

Highlights: Plants regulate their architecture in response to the growth environment, which challenges us to design models capable of performing well in different conditions. By using self-regulating rules, we reproduced blade and collar emergence time, and organ size distribution along phytomer rank in maize under varying growing conditions. The role of emergence events, e.g. blade tip emergence, collar emergence, in controlling growth phase and elongation duration of different components of one phytomer (blade, sheath and internode) are confirmed.

Keywords: growth regulation, plasticity, blade tip emergence, collar emergence, organ size distribution

INTRODUCTION

Plants react plastically to their environment and to management interventions by adjusting their structure and physiological functions (Sultan, 2010). At the plant level, the main plastic traits are the number of phytomers produced, the size of their organs, the number of branches produced, phyllotaxis, leaf inclination angle, and developmental characteristics such as plastochron (thermal time interval between initiation of successive leaf primordia), phyllochron (time interval between appearance of successive leaves), and leaf elongation rate (Nelson, 2000).

Phyllochron is determined by both timing of leaf initiation at the shoot apical meristem and leaf elongation through the whorl of leaves (Skinner & Nelson, 1995). A stable phyllochron is usually found in most grasses (Fournier *et al.*, 2005; Fournier *et al.*, 2007). Additionally, typical patterns of blade, sheath and internode final size against phytomer rank are found for most Gramineae (Fournier *et al.*, 2007).

However, phyllochron and final organ sizes of an individual plant may change depending on environmental conditions during development (Birch *et al.*, 1998);(Dornbusch *et al.*, 2011). Regulation rules linking organ development within and between phytomers have been reported. For example, there is evidence for a coordination mechanism in which tip emergence, defined as when tip exceeds the highest ligule, of the blade itself controls blade elongation, resulting in a stable phyllochron (Fournier *et al.*, 2005; Verdenal *et al.*, 2008). This idea can also be applied to sheath and internode elongation in which sheath initiation is related to blade tip emergence and fast elongation of internode is related to collar emergence, defined as when collar exceeds the highest ligule (Fournier & Andrieu, 2000; Andrieu *et al.*, 2006). However plant modelers have as yet not succeeded to predict how plant structure and function respond to their environment using such rules.

The aim of this work is (i) to understand how a regular phyllochron emerges from coordination of the dynamic processes of leaf initiation, leaf elongation and whorl construction, as well as (ii) to explain plasticity in leaf appearance in different planting patterns, based on coordination rules between phytomers. Ultimately, we want to predict how phyllochron responds to changes in environment, based on a quantitative model of the regulation rules that govern coordination between the processes of initiation, growth and appearance of plant organs. To this end, we constructed a functional-structural plant model to quantitatively characterize plant responses to growth interaction with neighbors. The model also allows us to simulate plasticity in the patterns of size of blades, sheaths and internodes along the stem, and we expect that it will be useful in understanding the competition for light resources between plants.

HYPOTHESES AND SIMULATIONS

Our model is based on Fournier & Andrieu (2000) and Andrieu et al. (2006), and extends these works with a holistic system view on regulation of whole plant development. The basic hypotheses are as follows:

a. The growth rate of a blade depends on the length of its growing zone, which in turn depends on the length of the sheath tube from which the blade tip emerges.
b. Before tassel initiation, sheath initiation is synchronized with blade tip emergence of the same rank; after tassel initiation, sheaths are initiated at a regular thermal time interval (Andrieu et al., 2006).
c. After ear initiation, collar emergence triggers rapid elongation of the internode of the same rank (Fournier & Andrieu, 2000).
d. Number of initiated leaves and the number of appeared leaves are coordinated with 0.63 appeared leaves per initiated primordia after leaf appearance of rank 3 (Padilla & Otegui, 2005).

The growth scheme of one phytomer, including blade, sheath, internode, is shown in in Fig.1.

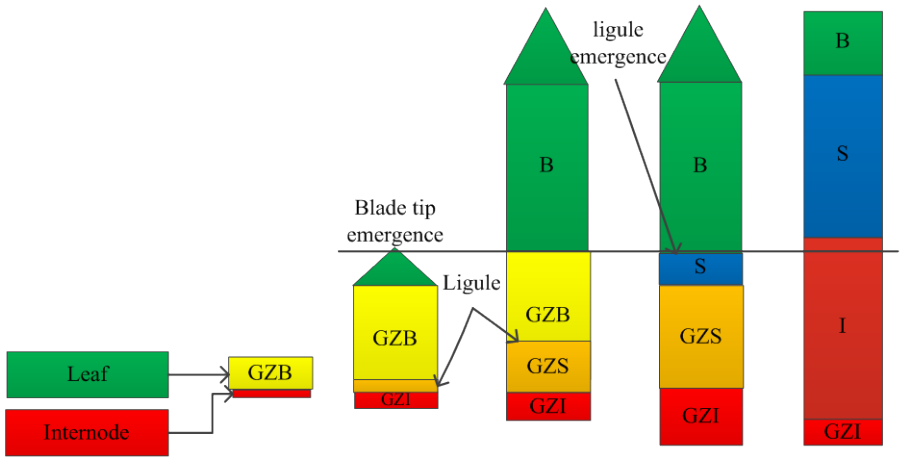

Fig.1. Growth scheme of one phytomer. GZ is growing zone where cells divide and elongate. B, S and I represent blade, sheath and internode, respectively. Internode initiation occurs half a plastochron after blade initiation. Before tassel initiation, the ligule appears at the bottom of the growing zone, synchronized with the time of blade tip emergence. After tassel initiation, ligule appears in GZB with a regular thermal time interval (Andrieu et al., 2006). The length of the GZB is linked with time when ligule appears in it, and growth activity gradually shifts from blade to sheath after this. Ligule emergence triggers the growth activity transition between sheath and internode.

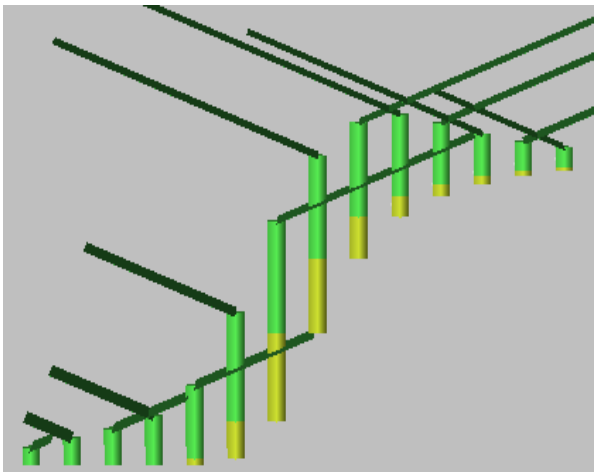

Fig.2 Snapshot of simulation of internode (light green), sheath (green), blade (dark green) extension of different phytomers (count from left right: 1 to 14) at collar emergence of rank 10 in GroIMP

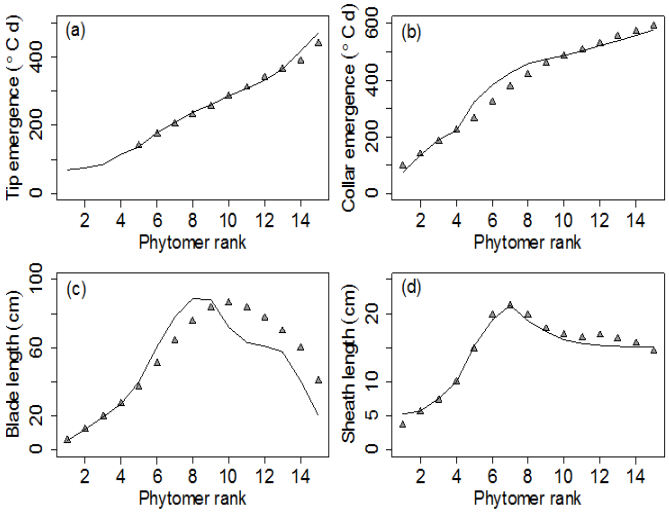

Fig.3: (a) tip emergence, (b) collar emergence, (c) final blade length, (d) final sheath length versus phytomer rank, observed (triangle) and simulated (line). Observed data: Andrieu et al., 2006.

We implemented the model using the GroIMP platform based on Java language and L-system (Hemmerling *et al.*, 2008). The whole plant growth was simulated at phytomer level (Fig. 2). Each element of the phytomer (blade, sheath, and internode) was characterized by several state variables: length and growth phase, e.g. has tip (collar) emerged. The length and growth phase together determine the growth rate of each component. Summed length of blade, sheath and internode determines tip emergence and collar emergence time by comparing with the sheath length with highest ligule. Subsequently, such events trigger the growth transition from blade to sheath and from sheath to internode.

The relative growth rate at normal population density for blade and sheath of maize (cultivar 'Déa') from Andrieu et al. (2006) and for internode from Fournier and Andrieu (2000) were used to parameterize the model. The growth phases, growth rates, and growth durations were controlled by the regulation rules as mentioned above. Properties of phytomers 1 to 4 were forced as an input.

RESULTS AND DISCUSSION

Simulated tip and collar emergence were consistent with obervations in Andrieu et al (2006) (Fig. 3a). Collar emergence was slightly overestimated for ranks 5-8 (Fig. 3b) The model underestimated final blade length for high ranks (Fig. 3c). Overall, the model reproduced organ emergence and organ size distribution well, based on simple regulation rules that control the growth shift between blade, sheath and internode. The role of emergence events, e.g. blade tip emergence and collar emergence, in controlling growth phase and elongation duration of different components of one phytomer (blade, sheath and internode) are confirmed.

This method enables complex features of architectural development to emerge from a small number of parameters and interactions between different phytomers, which makes it easy to predict correctly how a plant responds to a change in morphology. Therefore, we will use this model to study the shade avoidance response of maize at high population density and in wheat-maize intercropping condtions, aiming at better understanding the performance of maize in competitive environments such as crop species mixtures.

LITERATURE CITED

Andrieu B, Hillier J, Birch C. 2006. Onset of Sheath Extension and Duration of Lamina Extension are Major Determinants of the Response of Maize Lamina Length to Plant Density. *Annals of Botany* **98**(5): 1005-1016.

Birch CJ, Vos J, Kiniry J, Bos HJ, Elings A. 1998. Phyllochron responds to acclimation to temperature and irradiance in maize. *Field Crops Research* **59**(3): 187-200.

Dornbusch T, Baccar R, Watt J, Hillier J, Bertheloot J, Fournier C, Andrieu B. 2011. Plasticity of winter wheat modulated by sowing date, plant population density and nitrogen fertilisation: Dimensions and size of leaf blades, sheaths and internodes in relation to their position on a stem. *Field Crops Research* **121**(1): 116-124.

Fournier C, Andrieu B. 2000. Dynamics of the Elongation of Internodes in Maize (Zea mays L.): Analysis of Phases of Elongation and their Relationships to Phytomer Development. *Annals of Botany* **86**(3): 551-563.

Fournier C, Andrieu B, Buck-Sorlin G, Evers JB, Drouet JL, Escobar-Gutierrez AJ, Vos J 2007. Functional-structural modelling of gramineae.In J. Vos LFMM, P.H.B. de Visser, P.C. Struik and J.B. Evers *Functional-Structural Plant Modelling in Crop Production*. Dordrecht: Springer. 175-186.

Fournier C, Durand JL, Ljutovac S, Schaufele R, Gastal F, Andrieu B. 2005. A functional-structural model of elongation of the grass leaf and its relationships with the phyllochron. *New Phytologist* **166**(3): 881-894.

Hemmerling R, Kniemeyer O, Lanwert D, Kurth W, Buck-Sorlin G. 2008. The rule-based language XL and the modelling environment GroIMP illustrated with simulated tree competition. *Functional Plant Biology* **35**(10): 739-750.

Nelson CJ 2000. Shoot morphological plasticity of grasses: leaf growth vs. tillering.In Lemaire G, Hodgson, J., De Moraes, A., C. Nabinger, P.C. de F. Carvalho. *Grassland ecophysiology and grazing ecology*. Wallingford: CABI 101-126.

Padilla JM, Otegui ME. 2005. Co-ordination between leaf initiation and leaf appearance in field-grown maize (Zea mays): Genotypic differences in response of rates to temperature. *Annals of Botany* **96**(6): 997-1007.

Skinner RH, Nelson CJ. 1995. Elongation of the Grass Leaf and its Relationship to the Phyllochron. *Crop Sci.* **35**(1): 4-10.

Sultan SE. 2010. Plant developmental responses to the environment: eco-devo insights. *Current Opinion in Plant Biology* **13**(1): 96-101.

Verdenal A, Combes D, Escobar-Gutiérrez AJ. 2008. A study of ryegrass architecture as a self-regulated system, using functional–structural plant modelling. *Functional Plant Biology* **35**(10): 911-924.

Proceedings of the 7th International Conference on Functional-Structural Plant Models, Saariselkä, Finland, 9 - 14 June 2013. Eds. Risto Sievänen, Eero Nikinmaa, Christophe Godin, Anna Lintunen & Pekka Nygren. http://www.metla.fi/fspm2013/proceedings. ISBN 978-951-651-408-9.

How petiole flexibility changes light interception at the tree scale.

Loïc Tadrist[1,2,*], Emmanuel de Langre[1] and Marc Saudreau[2]
[1]Department of Mechanics, *LadHyX, École Polytechnique, CNRS, 91128 Palaiseau, France*
[2]*INRA, UMR 547 PIAF, 63100 Clermont-Ferrand, France*
**correspondence:* loic.tadrist@ladhyx.polytechnique.fr

Highlights: Leaf inclination angle plays a key role for light interception of a tree. However existing models for this quantity are empirical, not predictive and do not take into account the fact that leaves are flexible. Based on a petiole deformation model and a multi-scale approach we propose a model of leaf inclination angle distribution. As an example, we quantify how much leaf flexibility may change light interception of a tree.

Keywords: light interception, leaf mechanics, leaf inclination angle distribution

INTRODUCTION

Light transmission within a canopy is commonly described by a Beer-Lambert like law (Chartier, 1966). The transmission coefficient of the Beer-Lambert law mainly depends on two parameters: the leaf area local density and the leaf inclination angle distribution (LIAD). LIAD corresponds to the probability that a leaf taken randomly on the tree has a certain inclination angle, ϕ defined as the angle between the leaf midrib and the vertical axis. Usually, these distributions are measured experimentally and fitted with spherical or ellipsoidal functions (Campbell, 1986) without taking explicitly into account neither the mechanical behavior of the leaves nor the tree structure. However leaves are known to be flexible objects which bend under their own weight or because of wind. Such flexibility can vary among species and with time, affecting LIAD, and thus affecting the direct light interception and plant functions (Parveaud et al., 2008).

LIADs commonly used in functional-structural plant models (FSPM) remain purely empirical and do not account for physiological, structural or mechanical properties of the plant and for abiotic interactions with its environment. The main objective of this work is to build up a model of LIAD of a plant by coupling a single mechanistic model of the system compounded of a flexible simple leaf model with a tree structure model.

For simplicity, we do not take into account growth history, phototropism, gravitropism. The analysis is focused on the effect of petiole flexibility on LIAD. After introducing the model and comparing simulated LIAD with observed LIAD, we quantify the direct effect of leaf flexibility on light transmission within a canopy. To emphasize the necessity of a leaf flexibility model in FSPMs, we also expose a case where the leaf flexibility changes according to the tree physiology: the protective gain of flexibility of anisohydric tree leaves during drought period in summer. At last we conclude giving other applications of our model concerning possible calculation of wind drag, water retention or leaf temperature.

LEAF INCLINATION ANGLE DISTRIBUTION MODELIZATION

The mechanical behavior of a single leaf has been investigated and some models have been already proposed (Niklas, 1999). But for plants, and especially for trees, interesting physiological traits are integrated values at the plant scale such as photosynthesis, global transpiration, or wind drag. Thus beyond the leaf flexibility modeling, the challenge is also to be able to account for the two different scales: leaf scale and whole foliage. As the number of leaves on a tree is large (up to 10^5), we propose to link these two scales through a statistical analysis of the tree structure which holds the leaves.

Leaf mechanics

Leaf mechanical description is based on the model of Niklas (1999) in which we take into account geometrical non-linearities. For the sake of simplicity we describe only simple leaves, not compounded leaves nor sessile leaves. The leaves we consider have only one flexible petiole and one rigid lamina. The petiole is considered to be an elastic beam without mass whereas the lamina is a weighting and rigid plate. Let us consider the deformation of the petiole due to the weight of the lamina. In the non-dimensional equation the number of gravity G appears:

$$G = \frac{mgL^2}{EI}$$

where *m* is the mass of the lamina, *L* the length of the petiole and *EI* the bending modulus of the petiole. This number defines two regimes of deformation. If G << 1, the mass of the leaf is not important enough to bend the petiole, this is the rigid regime. If G > 1, the petiole bend and the inclination angle of the leaf changes because of the weight of the lamina, this is the flexible regime.

Tree structure

The tree structure is simply rendered by an iterative model for a sympodial tree (Rodriguez, 2008). The iteration starts from a vertical trunk. At each iteration, a mother branch gives two daughter branches. These two branches are separated from the mother axis by a branching angle, θ_0. For trees, typical number of iteration is 8 up to 10. We compute the distribution of shoots bearing leaves for a tridimensional tree. Results show that the distribution is a normal distribution which depends only on the branching angle. Expressions of the mean, μ, and the standard deviation, σ, are:

$$\mu = \frac{\pi}{2}\sin\frac{3\theta_0}{2} \qquad \sigma = \frac{\pi}{4}\sin\frac{3\theta_0}{2}$$

Tree structure model was assessed on a digitized walnut tree (fig.2. a,b). Petiole deformation model has proved efficiency on idealized leaves and real leaves (Apricot tree, cherry tree, apple tree and ficus, data not show).

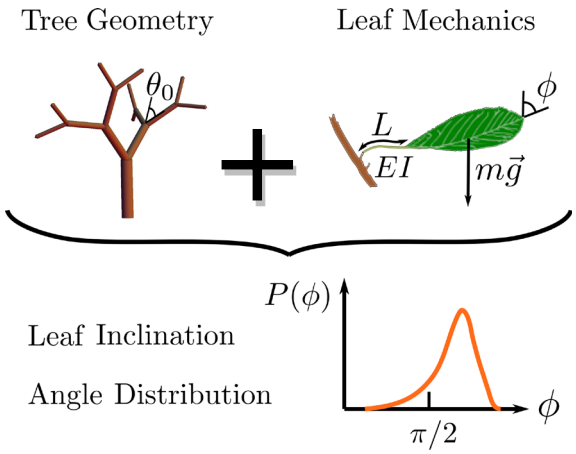

Fig. 1. Schematic view of the methodology used for obtaining leaf inclination angle distribution. Definition of the geometrical and mechanical parameters.

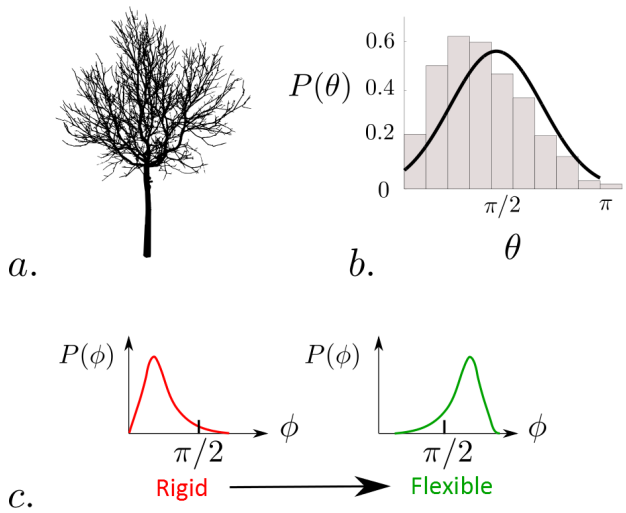

Fig. 2. (a) Digitalized walnut of which the branch inclination angle is plotted in (b). (c) Example of two different leaf inclination angle distribution (red correspond to rigid leaves and green to flexible ones).

Leaf inclination angle distribution

Leaf inclination angle distribution is computed from the branch inclination angle assuming that leaves grow with a branching angle θ_0 with the holding branch and that the leaf can bend because of gravity (fig.1). In this manner, we obtain an analytical expression of the peak of the LIAD taking into account both tree structure and leaf mechanics. We show in figure 2.c the evolution of LIADs between the rigid case and the flexible case. The model predictions compare well several LIADs measured on different trees (apple tree) give satisfactory tendencies.

RESULTS AND DISCUSSION

Effect of flexibility on light interception

Since we know explicitly the dependence of the LIAD on the leaf flexibility, we can predict the position of the mean value, the peak of the distribution and its width. If the leaves are rigid, the peak position is only due to the tree structure. Contrary, when leaves are flexible, the peak is shifted towards π, meaning that the leaves bend down, (fig.2 c, fig.4 insets a,b).

With this LIAD expression, we compare light interception ($I(G)$) for different leaf rigidity. For a sun at zenith, direct light interception calculation was done numerically thanks to the Beer-Lambert law:

$$\frac{I(G)}{I(0)} = \frac{1 - e^{-A\int P_G(\varphi)\cos\varphi\, d\varphi}}{1 - e^{-A\int P_0(\varphi)\cos\varphi\, d\varphi}}$$

where A is a constant depending on the leaf foliage density, P_G the LIAD at a given G and P_0 the LIAD when the petioles are completely rigid.

Clearly, flexibility changes the light interception capacity of trees. The graph below shows the variation of the light interception at noon for a tree of branching angle, $\theta_0 = \pi/3$ (fig.3) when varying *G*.

When the flexibility is increasing, light interception of the tree decreases. Accordingly, light interception is higher when flexibility is low. This result is not general and may change depending on the latitude and the day of year.

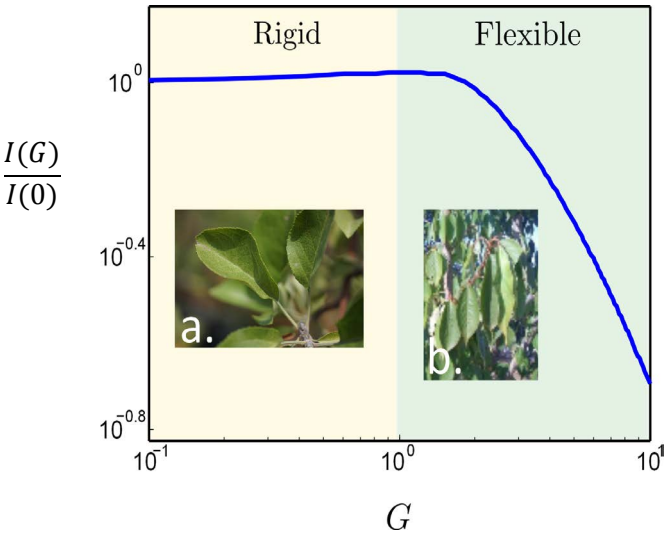

Fig. 3. Evolution of light interception in function of flexibility. G=1 separates the yellow domain where leaves are rigid (b) from the green domain where leaves are flexible (a). Light interception is lower for flexible leaves.

An example of excess radiation protection varying flexibility

As an example of change of leaf flexibility, some anisohydric trees can change their flexibility during the day thanks to a change in their turgor pressure, Faisal et al. (2010). This phenomenon appears when the tree is in water stress, mainly in summer. It decreases its internal turgor pressure in order to close its stomata and avoid evaporating to much water. Without stomata sweating, the leaf temperature is given by the balance of light radiation and air convection. If the leaf stops sweating but receives as much radiation energy as before, its temperature will increase. This can result on photo-inhibition and even leaf necrosis. For this kind of trees, increase of flexibility make them sure not to intercept as much light as before and favor air convection, thus protecting their leaves without sweating. Our model allows to understand and to quantify this physical phenomenon taking into account the loss of rigidity of the petiole due to a decrease of turgor pressure onto the LIAD

CONCLUSION

We developed a simple model of leaf inclination angle distribution in order to understand the effect of leaf flexibility on light interception on a tree. This model is based on a multiscale approach, from the mechanics of a single leaf to the entire foliage properties through the tree structure. This work shows that: (i) the LIAD changes strongly due to leaf flexibility; and (ii) the direct light interception depends highly on flexibility of leaves. Our approach of tree foliage properties remains general. It proved to be an efficient model to understand the effect of leaf flexibility on light interception. However, much more can be deduced from such a model like leaves temperature, wind drag due to leaves on a tree or water/snow retention.

LITERATURE CITED

Chartier P. 1966. Étude du microclimat lumineux dans la végétation, *Annales d'agronomie* **17**, 571–602.

Campbell G. 1986. Extinction coefficients for radiation in plant canopies calculated using an ellipsoidal inclination angle distribution, *Agricultural and forest meteorology* **36**, 317–321.

Niklas K. 1999. A mechanical perspective on foliage leaf form and function. *New phytologist* **143**, 19–31.

Parvaud C-E, Chopard J, Dauzat J, Courbaud B, Auclair D. 2007. Modelling foliage characteristics in 3D tree crowns: influence on light interception and leaf irradiance. *Trees* **22,** 87-104.

Rodriguez M, de Langre E, Moulia B, 2008. A scaling law for the effects of architecture and allometry on tree vibration modes suggests a biological tuning to modal compartmentalization. *American Journal of Botany,* **95**, 1523–1537.

Faisal T, Abad E K, Hristozov N, Pasini D. 2010. The Impact of Tissue Morphology, Cross-Section and Turgor Pressure on the Mechanical Properties of the Leaf Petiole in Plants. *Journal of Bionic Engineering* **7 Suppl.**, S11 – S23.

Proceedings of the 7th International Conference on Functional-Structural Plant Models, Saariselkä, Finland, 9 - 14 June 2013. Eds. Risto Sievänen, Eero Nikinmaa, Christophe Godin, Anna Lintunen & Pekka Nygren.
http://www.metla.fi/fspm2013/proceedings. ISBN 978-951-651-408-9.

Concept and Calibration of Virtual Wheat Including Stochastic Tillering

Feng Lu[1], Rey Herve[2], Mailhol Jean-Claude[3], Kang Mengzhen[1], de Reffye Philippe[2]
[1] *CPlant, LIAMA, Institute of Automation, Chinese Academy of Science, Beijing, China,* [2] *CIRAD-UMR AMAP, Montpellier, France,* [3] *Irstea, UMR G-eau, F-34096, Montpellier, France*
**correspondence:* fyafeng@gmail.com

Highlights: Present study has introduced a comprehensive theoretical architecture to note probability of phytomer occurrence to describe wheat structural development. This provided an intermediary to compute the overall level of growth functions. The model then was calibrated on observation of variform individuals.

Keywords: Functional structure plant models (FSPM), GreenLab model, stochastic architecture, plant model calibration, durum wheat (*Triticum turgidum* L. *var Dakter*)

INTRODUCTION

Plastic tillering of wheat delivers growth adaptation to its environment, depending on various internal and external factors (Evers et al. 2011). Modeling studies devote to approach the essential drive of architecture variation, for a better understanding of interaction with internal functions (Evers et al. 2007; 2010). However, stochastic architecture makes research on growth function particularly difficult to link real plants. Present work aims to combine growth functions with a stochastic tillering development modeling to achieve the model calibration on the field observation.

EXPERIMENT AND MEASUREMENTS

An experiment was conducted in 2009 on the loamy soil of the experimental site of the IRSTEA Institute (43°40' N, 3°50' E) in Montpellier, France. Durum wheat (Dakter variety) was sown on 2008/11/9 at 150 kg/ha. Owing to rainfall events during spring (736 mm on the cropping cycle), irrigation was not necessary. The soil was enriched with fertilizer (230 kg/ha of N) in three applications on the basis of the initial soil N content in order to achieve the potential yield (9.0 Mg/ha). Appropriate herbicides were sprayed to ensure a non-limited development. Meteorological data including precipitation, global radiation and air temperature were fully recorded at the station.

Nine harvests have been conducted about every two weeks since the seventh blade was visible till the final crop mature. Eight plants per harvest were sampled destructively. Leaf blades, sheaths, internodes, spikes and roots were dissected. Organ fresh masses were measured along the main stem and in the compartment per each tiller. Four plants were dried and weighed for evaluation of the dry mass.

IMPROVED STOCHASTIC GREENLAB MODEL

GreenLab (Yan et al., 2004) is an FSPM dedicated to capturing the sink-source relationship underlying plant growth. The stochastic GreenLab (GL2) introduces probabilities to account for bud dynamics of growth, death and branching, so architectures with variation can be processed. Instead of computing the mean and variance of biomass production of plant from the mean and variance of the number of organs (Kang et al., 2008a), improved method simulates the sink-source function according to theoretical architecture.

If buds branching, growth and survival are certain events, plant architecture will develop all potential phytomers and tillers. Theoretical architecture is built from the potential architecture but with occurrence probability of each phytomer explicitly indicated.

Supposing all buds of a plant share the same probability a, b and c of branching, growth and survival, the probability of each phytomer presents in the potential architecture can be accurately estimated, and therefore the theoretical architecture can be built (Fig.1 a). This architecture is essentially a comprehensive view of the architecture of a species. The estimated probability of existence can be regarded as the right "number" of the corresponding organs of the theoretical average plant. Therefrom, theoretical demand and function can be represented accurately with the theoretical number of organs. The rest principles are common to the classical GreenLab model.

MODEL CALIBRATION

Topology and PA definition

In the current study, mainstem of wheat carries a maximum number of 12 internodes, with one branching order tillers emerging from the first four to five phytomers. We used three physiological ages (PA) (Barthélémy and Caraglio, 2007) to distinguish gradients of organs properties. PA1 represented mainstem under top flower, PA2 indicated first-order tillers under top flower, and PA3 stood for all top flowers, consisting of an internode with a spike. Maximum numbers of phytomer were 11, 8 and 1 respectively.

Probabilities estimation

Branching probability of an axillary bud used the percentage of tiller counts in sample numbers. The estimation of Growth probabilities was by the mean and variance of phytomer number (renewal process, see de Reffye et al., 2012) for the mainstem and by the mean and variance of "summed phytomer number" (Kang et al., 2008b) for tillers. Survival probability for the mainstem was set to 1 since all main stems reproductive. For tillers, they were estimated as constant values for each tiller position (Tab. 1). The theoretical architecture of durum wheat was then derived (Fig.1b).

Tab. 1 Estimated bud probabilities according to *PA* and tiller rank on mainstem (*Rk*)

	Branching Probability (a)					*Growth Probability (b)*			*Survival Probability (c)*						
PA	*1*					*1*	*2*	*3*	*1*	*2*					*3*
Rk	1	*2*	*3*	*4*	*5*					*1*	*2*	*3*	*4*	*5*	
Value	0.87	0.91	0.50	0.13	0.20	0.99	0.91	1	1	0.95	0.94	0.86	0.74	0.52	1

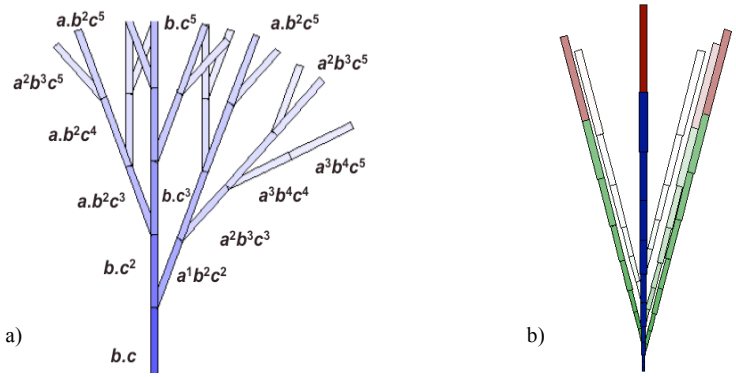

Fig. 1 Theoretical architecture schematic (a) and the example of durum wheat (b). Products of *a*, *b* and *c* indicate occurrence probability of the phytomer, corresponding to the color depth.

Target data and calibration of sink-source function

GreenLab model has been calibrated on both phytomers and compartments grouped by PA. To sum up measurements from variform individuals, phytomers and compartments were processed in bottom-up or top-down alignment. Therefore aligned phytomers or tillers were a mixture of different ages. Analogue simulation was necessary to make modeling output matchable to the observation. We used binomial distribution (B(k, p)) to simulate mixture of phytomers at rank k from the bottom, and negative binomial distribution (NB(k, p)) to simulate the mixture of phytomers at rank k from top.

For PA 1 organs were averaged with top-down alignment. For PA2 and PA3, tillers and top flowers were treated as substructure attached to mainstem, and their compartments were averaged with bottom-up alignment.

A target file was built with 32 plants from four harvests, one single set of sink-source parameters (Tab. 2) were estimated by non-linear least square method (Zhan et al., 2003) to minimize the root mean square error between the target and model output. Calibrated model provides simulation close to the measurements (Fig.2).

Tab. 2 Calibrated parameters of sink-source function, their value and coefficient of variation (*)

Parameter	R	S_p	B_b	B_p	B_i	B_f	P_{b2}	P_{p1}	P_{p2}	P_{i1}	P_{i2}	P_{i3}	P_{f3}
Value	65.76	92.25	1.66	2.54	2.75	1.07	1.56	1.21	0.26	0.83	0.57	1.16	2.13
*	9.89	18.39	0.26	0.6	0.44	0.34	0.73	0.11	0.74	0.09	0.08	0.25	1.21

R - Empirical parameter of assimilate function; S_p - Theoretical projective area (cm^2);
P - Sink factor; B - Parameter of beta function describing the sink variation;
Subscript 1, 2, 3 - PA 1, 2 and 3; Subscript b, p, i, f - indicate organ blade, sheath, internode and spike

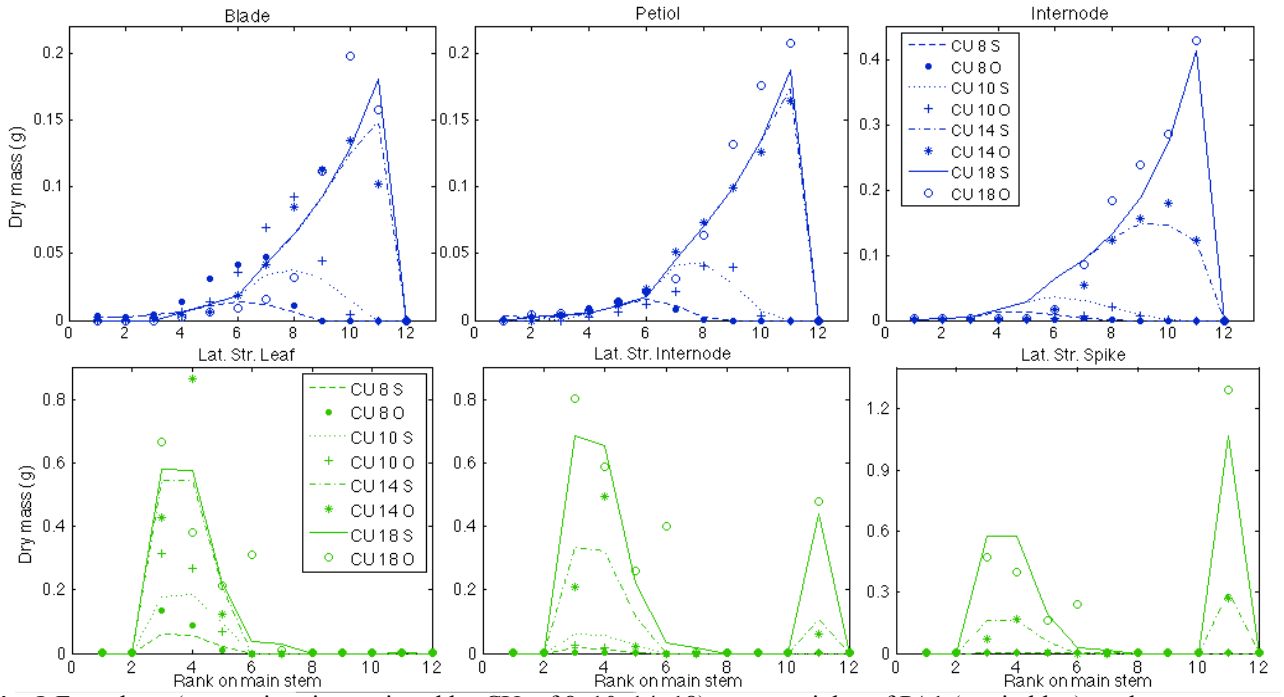

Fig. 2 Four dates (computing time units, abbr. CU, of 8, 10, 14, 18) organ weights of PA1 (up, in blue), and compartment weights per each tillers and top flowers of PA2 and PA3 (bottom, in green). Measurements (O) in symbols and simulation (S) in lines.

CONCLUSION

The improved stochastic GreenLab model applied theoretical architecture as an intermediary to simulate growth functions of wheat from an overall level. Binomial distribution and negative binomial distribution were employed to simulate mixture of phytomers picked in bottom-up or top-down from variform individuals. Therefore, observations and modeling output could be comparable, and the virtual wheat was then calibrated.

ACKNOWLEDGEMENT

The fieldwork was conducted in the PhD project of the first author, funded by China Scholarship Council and supported by CIRAD. Thanks are due to two anonymous reviewers for their constructive comments.

REFERENCES

Barthélémy D, Caraglio Y. 2007. Plant architecture: a dynamic, multilevel and comprehensive approach to plant form, structure and ontogeny. *Annals of botany*, **99**(3), 375–407

De Reffye P, Edelin C, Françon J, Jaeger M and Puech C. 1988. Plant models faithful to botanical structure and development. *Computer graphics*, **22**(4), 151–158.

De Reffye P, Kang M, Hua J and Auclair D. 2011. Stochastic modelling of tree annual shoot dynamics. *Annals of Forest Science*, **69**(2), 153–165

Evers J, Vos J, Chelle M, Andrieu B, Fournier C, Struik P. 2007. Simulating the effects of localized red:far-red ratio on tillering in spring wheat (Triticum aestivum) using a three-dimensional virtual plant model. *New Phytologist*, 176(2), 325–36

Evers J, Vos J, Yin X, Romero P, van der Putten P and Struik P. 2010. Simulation of wheat growth and development based on organ-level photosynthesis and assimilate allocation. *Journal of Experimental Botany*, **61**(8), 2203–2216

Evers J, van der Krol A, Vos J and Struik P. 2011. Understanding shoot branching by modelling form and function. *Trends in plant science*, **16**(9), 464–7

Kang M, Cournède P, de Reffye P, Auclair D, Hu, B. 2008a. Analytical study of a stochastic plant growth model: Application to the GreenLab model. *Mathematics and Computers in Simulation*, **78**(1), 57–75.

Kang M, Evers, J, Vos J, De Reffye P. 2008b. The derivation of sink functions of wheat organs using the GREENLAB model. *Annals of botany*, **101**(8), 1099–1108

Yan H, Kang M, de Reffye P and Dingkuhn M. 2004. A dynamic, architectural plant model simulating resource-dependent growth. *Annals of botany*, **93**(5), 591–602

Zhan Z, de Reffye P, Houllier F and Hu B. 2003. Fitting a Functional-Structural growth model with plant architectural data. In B Hu and M Jaeger (Eds.), *Proceedings of 1st International Symposium on Plant Growth Modeling, Simulation, Visualization and Applications* (PMA03), 108–117

Proceedings of the 7th International Conference on Functional-Structural Plant Models, Saariselkä, Finland, 9 - 14 June 2013. Eds. Risto Sievänen, Eero Nikinmaa, Christophe Godin, Anna Lintunen & Pekka Nygren. http://www.metla.fi/fspm2013/proceedings. ISBN 978-951-651-408-9.

The effect of canopy structure on photochemical reflectance signal

Matti Mõttus[1] and **Miina Rautiainen**[2]
[1]*Department of Geosciences and Geography, PO BOX 64, FI-00014 University of Helsinki,*
[2]*Department of Forest Sciences, PO BOX 27, FI-00014 University of Helsinki, Finland*
**correspondence:* matti.mottus@helsinki.fi

Highlights: We measured the angular distribution of spectral scattering properties of Scots pine shoots. We were able to scale the photochemical reflectance index (PRI) between two canopy structural levels using photon recollision probability. We found non-negligible anisotropy in shoot PRI possibly caused by reflectance of the needle wax coating.

Keywords: photon recollision probability, canopy structure, PRI, Scots pine

Leaf-level photosynthetic efficiency can be estimated by measuring leaf reflectance at 531 nm. This spectral region reveals physiological adaptations aimed at coping with excess photosynthetically active radiation: interconversion of the xanthophyll cycle pigments, and reversible chloroplast conformation changes. Thus, including for reference an additional wavelength (570 nm) where the interconversion should have no effect as a reference, Gamon et al. (1992) proposed the photochemical reflectance index (PRI) to monitor plant functioning. Unfortunately, at the level of a vegetation canopy, the PRI signal conveying information on leaf photochemical processes is distorted by multiple interactions within the canopy and variations in illumination and viewing geometry. Only canopy structural models which can account for multiple photon-vegetation interactions and take into account angular effects in radiation scattering can provide a means of retrieving leaf-level PRI from canopy-level remote sensing data.

We present a mathematical model for scaling normalized difference vegetation indices (such as PRI) between different vegetation structural levels. The model is based on the novel concept of photon recollision probability which allows for a physical and robust parameterization of the structure of a vegetation canopy. To validate the model, we used spectral measurements of ten Scots pine (*Pinus sylvestris* L.) shoots made from many viewing directions. Next, we scaled the needle-level PRI values to the level of a shoot using the photon recollision probability value calculated from measurements of shoot geometric properties. Finally, we analyzed the angular dependence of PRI and compared it with the shoot scattering directionality model proposed by Mõttus et al. (2012).

We found that the approach based on photon recollision probability can reasonably well scale PRI between the two structural levels. However, this model cannot predict the considerable angular variation in shoot-level PRI. Using previous knowledge on the general scattering properties of pine shoots, we found indication that the angular variation in PRI signal can be attributed to specular scattering of the wax coating on needles. These results provide a strong basis for further development of accurate models for coping with dependence of canopy-level PRI on view and illumination conditions as well as scaling the measured signal between different levels of canopy structure.

LITERATURE CITED

Gamon JA, Peñuelas J, Field CB. 1992. A narrow-waveband spectral index that tracks diurnal changes in photosynthetic efficiency. *Remote Sensing of Environment* **41**:35-44.

Mõttus M, Rautiainen M, Schaepman ME. 2012. Shoot scattering phase function for Scots pine and its effect on canopy reflectance. *Agricultural and Forest Meteorology* **154-155**:67-74.

Proceedings of the 7th International Conference on Functional-Structural Plant Models, Saariselkä, Finland, 9 - 14 June 2013. Eds. Risto Sievänen, Eero Nikinmaa, Christophe Godin, Anna Lintunen & Pekka Nygren. http://www.metla.fi/fspm2013/proceedings. ISBN 978-951-651-408-9.

A geometric model for scaling between needle and shoot spectral albedos

Miina Rautiainen[1], **Matti Mõttus**[2], **Lucia Yáñez-Rausell**[3,4], **Lucie Homolová**[3,4], **Zbyněk Malenovský**[5] and **Michael E. Schaepman**[3]

[1]*Department of Forest Sciences, PO Box 27, 00014 Univ. of Helsinki, Finland* ,[2]*Department of Geosciences and Geography, PO Box 64, 00014 Univ. of Helsinki, Finland,* [3] *Department of Geography, Univ. of Zurich, Winterthurerstrasse 190, CH-8057 Zurich, Switzerland,* [4] *Laboratory of Geo-Information Science and Remote Sensing, Wageningen Univ., PO BOX 47, 6700 AA Wageningen, The Netherlands,* [5]*School of Geography and Environmental Studies, Univ. of Tasmania, Hobart 7001, Australia*

**correspondence:* miina.rautiainen@helsinki.fi

Highlights: The spherically averaged shoot silhouette to total needle area ratio (STAR) can be used as a scaling parameter to link needle- and shoot-level spectral albedos in coniferous canopies.

Keywords: scaling, spectra, *Pinus sylvestris*

Spectral data convey information about the physiological processes and biochemical properties of plant leaves and canopies. Up- and downscaling spectral data between different plant architectural levels, such as from leaf-level to shoot- and canopy-levels, would allow to link spectral remote sensing data with leaf-level physiological processes. Such scaling has long been a challenge, especially in conifers. As the amount of data acquired through imaging spectroscopy, or hyperspectral remote sensing, is rapidly increasing, models for linking spectra measured at different scales are crucially needed in global modeling of plant productivity.

A key property of any scaling model is that the input parameters should have a physical interpretation – preferably an intuitive one –, and it should be possible to measure the parameters in the field or in a laboratory. The link between canopy structure and spectra can be modeled using a relatively recent development in canopy radiation physics: the spectral invariants theory. So far, the spectral invariant that has gained the most attention is the photon recollision probability, the probability by which a photon scattered from a leaf or needle in the canopy will interact within the canopy again. It is directly linked to the geometric structure of a canopy. Spectral invariants may prove useful in developing scaling methods which are as realistic as 3D models but as simple as 1D models, i.e., they offer an efficient way to describe the hierarchical structure of vegetation. Even though theoretical studies on the spectral invariants theory offer promising prospects, empirical observations are needed to validate the performance of these parameters.

In this study (Rautiainen et al. 2012), we tested empirically if it is possible to scale between the spectra of different plant structural levels using one of the spectral invariants, the recollision probability. We focused on two coniferous structures, needles and shoots, using Scots pine as our study species. The recollision probability was calculated directly from a plant structural parameter: the spherically averaged shoot silhouette to total needle area ratio (STAR). We measured both structural and spectral properties of the shoots and needles in laboratory conditions in the Remote Sensing Laboratories of University of Zurich. The hemispherical-bidirectional reflectance distribution functions of each shoot were measured using the LAGOS goniometer and an attached ASD spectroradiometer (350-2500 nm). The spectral albedos for needles were measured in a calibration laboratory using another spectroradiometer and an integrating sphere. The STAR of the shoots was calculated from digital photographs of shoot silhouettes.

We showed that it is possible to scale from needle albedo to shoot albedo using a model based on only one structural characteristic of the shoot, STAR. The upscaling model performed best in the visible and shortwave infrared wavelengths. From the perspective of further applications, we would like to investigate whether the spectral albedo of a whole tree crown (and furthermore, a stand) can be linked to the crown spherically averaged silhouette area through a simple relationship. In other words, can we upscale crown spectral albedo from shoot spectral albedo similarly?

LITERATURE CITED

Rautiainen, M., Mõttus, M., Yáñez-Rausell, L., Homolová, L., Malenovský, Z., Schaepman, ME. 2012. A note on upscaling coniferous needle spectra to shoot spectral albedo. *Remote Sensing of Environment* **17**: 469-474.

Proceedings of the 7th International Conference on Functional-Structural Plant Models, Saariselkä, Finland, 9 - 14 June 2013. Eds. Risto Sievänen, Eero Nikinmaa, Christophe Godin, Anna Lintunen & Pekka Nygren. http://www.metla.fi/fspm2013/proceedings. ISBN 978-951-651-408-9.

Protocol for foliage modeling and light partitioning in *Coffea arabica*

Miroslava Rakocevic[1], **Fabio Takeshi Matsunaga**[1,2], **Evelyne Costes**[3], **Jonas Barbosa Tosti**[1,2], **Yann Guédon**[4], **Letícia de Cássia Santin**[1,2] and **André Luiz Johann**[1]

[1]Agronomical Institute of Paraná - IAPAR, P.O. Box 481, CEP 86047-902, Londrina, PR, Brazil; [2]State University of Londrina - UEL, P.O. Box 6001, CEP 86044-290, Londrina, PR, Brazil; [3]INRA, UMR AGAP, Avenue Agropolis, TA A-96/03, 34398 Montpellier, France; [4]CIRAD, UMR AGAP & Inria, Virtual Plants, F-34095 Montpellier, France

miroslava@iapar.br

Highlights: Virtual coffee trees were reconstructed using partial morphological data, newly developed modules, AmostraCafe3D and VirtualCafe3D, and VPlants software. Leaf area size, STAR and transmitted PAR in different horizontal layers were computed on the virtual coffee plants and confronted to measurements.

Keywords: 3D reconstructions, STAR, tree layer samples, VPlants

INTRODUCTION

The architecture of *Coffea arabica* L. is described by Roux's model and characterized by continuous growth and branch dimorphism. The main axis (first order axis) is orthotropic, composed of internodes of relatively regular length with opposite and decussate leaves. This orthotropic axis bears plagiotropic branches of 2nd to 5th orders that are responsible for berry production. The leaves of plagiotropic branches follow decussate phyllotaxy, but both internode torsion and petiole angle reorient leaves, resulting in dorsiventral shoots (Dengler 1999). The lowest order plagiotropic branches are of great longevity. The highest branching orders appear in three- to four-year-old coffee plants, so that the structure becomes complex in the early tree life. Each year foliage formation precedes the intensive investments in berry ripening. The foliage light interception and shading could induce important impacts on final coffee quality (Vaast et al. 2006).

Functional-structural plant models offer the way to study the crown and tree development on the basis of a structurally accurate description that combines resource capture at the same level of detail (Sievänen et al. 2010). The aims of this study were to (a) reconstruct a 3D structure of whole *C. arabica* trees using detailed or partial morphological information collected on whole plants and (b) use these virtual coffee trees to estimate leaf area distribution and light interception partitioning between horizontal layers.

TREE MEASUREMENTS, ABSTRACTION AND CODIFICATION

Coffee mock-ups were reconstructed using VPlants software (http://www-sop.inria.fr/virtualplants/wiki/doku.php?id=software#software) on the basis of tree coding using multiscale tree graph - MTG (Godin and Caraglio 1998) with three scales of description (plant, axe and metamer). The main axes were always described at metamer scale and numerous variables were collected: length of each internode; length/width/elevation angle/cardinal orientation of leaves, and position/orientation/total length of borne plagiotropic branches. When young plants were measured, the same variables plus the flower and berry number and positions were collected for 2nd order plagiotropic branches. On adult plants, four 2nd order plagiotropic branches were sampled (each oriented to one cardinal point), to represent each 40 cm-thick layer along the vertical tree profile. These sampled 2nd order plagiotropic branches were described at metamer scale plus the detailed description of their lateral plagiotropic branches of 3rd to 5th order. All other 2nd order plagiotropic branches were described by their position along the orthotropic axis, total branch length, berry number and the cardinal orientation.

For this study four three-years-old adult plants and five ten-month-old seedlings of cv. IAPAR 59 (popular cultivar in Paraná coffee-culture) were measured in the experimental field (IAPAR, Londrina, Brazil - 23° 18' 37" S, 51° 09' 46" W, 585 m altitude). The adult ones were planted in a distance 0.5 m in line and 2.5 m between lines in 2009, and the seedlings in 2012. They were grown under non-limited water and nutrition conditions. The adult plants were considered at two periods, one relative to berry ripening (April 2012) and second to berry harvesting (July 2012).

AMOSTRACAFE3D – MODULE FOR INCLUSION OF MISSED DATA TO PARTIALLY MEASURED BRANCHES

A module (called AmostraCafe3D), aiming at reconstructing the whole coffee plants based on branch sampling data, was developed in Python. The output MTG are the input MTG containing the collected data augmented with calculated information for plant reconstruction. The first step considers the reconstruction of 2nd order partially measured branches, based on point wise average lengths of the internodes obtained from the completely described branches situated on the same layer and approximately similar cardinal orientation (actually the orientation is not always clear, due to internode torsion) of four plants. The following steps treat the leaf and fruit number, and 3rd to 5th order plagiotropic branch reconstructions based on estimated probability of leaf, branching and berry occurrences. The estimated probabilities were calculated from occurrences built for measured 2nd order plagiotropic shoots, considering the metamer index and layer/orientation/ period of sampling. 'Random' Python library was applied to randomly display leaves, berries and lateral branches along the 2nd order shoots that were partially measured, based on previously estimated probabilities. The adapted leaf area index calculated from these reconstructed plants (Fig. 1B) is considered for the validation of foliage size produced by AmostraCafe3D.

VIRTUALCAFE3D – MODULE FOR GEOMETRICAL ADJUSTMENTS

The coffee plant reconstructions were constrained by attributed phyllotaxis of 90° and 180° inducing errors in leaf and branch positions and orientations. Also, the leaf attributes were not assigned to a specific leaf within each pair in the MTG. Thus, a module named VirtualCafe3D was developed under the NetBeans IDE platform (Java Standard Edition), to overcome these shortcomings. The algorithm consists of: 1) spatial settings of leaves originated on plagiotropics (from 2nd to 5th branching order), 2) spatial settings of leaves originated on orthotropic axis and 3) correction of the branch orientation. The general solution for leaf and branch orientation corrections consists of the replacement of a node with two leaves by two successive nodes, each with one leaf, separated by a very short "virtual" internode (Matsunaga and Rakocevic, 2011). The algorithmic steps vary for each solved adjustment. The validation was performed by reconstructing the 3D mock-ups using PlantFrame function and by visually checking the branch and leaf orientation in PlantGLViewer in the VPlants software (Pradal et al. 2008).

LEAF AREA ADJUSTMENTS AND LIGHT INTERCEPTION COMPUTATION

Virtual trees were then constructed using PlantFrame function of VPlants and visualized using PlantGLViewer. A coffee leaf was constructed using 16 triangles in GEOM module and transposed into the Cartesian coordinate system by the adjustments for 1 cm length-L x 1 cm width-W in VegeSTAR software (Adam et al. 2006). To set the allometry, the adapted coefficients for LW leaf shape model (Antunes et al. 2008) were introduced. Two measurement methods were performed to assess the foliage reconstructions, one direct and one indirect (Fig. 1).

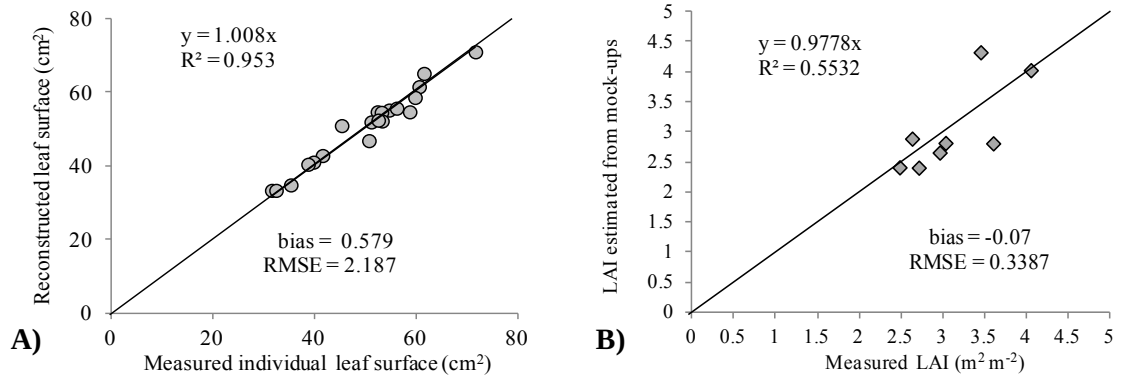

Fig. 1. Adjustments of measured leaf areas to reconstructed ones - R^2, bias, RMSE, and 1:1 line are indicated. **A**) Individual leaf surfaces measured with LICOR 3000 and **B**) Adapted leaf area index (LAI) for coffee plants measured with LICOR 2000.

The direct method considered the individual leaf surface measurements. Ten leaves were measured (LICOR 3000) at each period of observation and their surface was compared to outputs of individual leaf reconstructions from VegeSTAR (Fig. 1A). The indirect method considered the leaf area index (LAI) measurements with LICOR 2000 (Fig. 1B). It was adapted for coffee plants by a set of ten measurements: the first and the last one shot above the canopy, while eight measurements correspond to 5 cm and 35 cm distance of the trunk

points below the plant crown and oriented to four cardinal points. LAI outputs correspond to the crown projected on soil (calculated from x- and y-axis projections). LAI of eight mock-ups fitted well to measured plants (bias = -0.07 and RMSE=0.338 at Fig. 1B). The measurements with LICOR 2000 were accepted when over- or underestimation was about 10% for coffee plants (Angelocci et al. 2008).

Fig. 2. Visualisations of juvenile and adult coffee plant mock-ups.

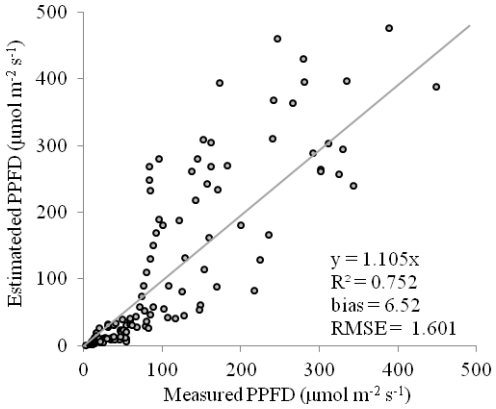

Fig. 3. Measured *versus* estimated transmitted radiation calculated in VegeSTAR from mock-ups.

The visualisation of mock-ups built for one seedling (from detailed description at metamer scale), and one adult plant (from sampling) is shown on Fig. 2. Silhouette to Total Area Ratio (STAR) was computed with VegeSTAR. Directional light interception for 16 directions and STAR sky-integrated indexes of light interception were estimated under Standard Over Cast (SOC) sky radiance distribution. Those STAR values were calculated within 40 cm-thick layers on coffee crown. The transmitted PAR was calculated for the representative plants based on the estimated interception. STAR outputs were calculated for each 15 minutes, over two particular days (14 April and 19 August, 2012) during which morphogenetic and light measurements were performed (Fig. 3). The relative high bias observed between estimated and measured values could result from estimation performed on isolated plants whereas measurements performed in field were affected by distances between plants in the stand. This protocol will be further improved and applied to estimate the light interception efficiency of foliage positioned in diverse layers along vertical coffee tree profiles, cardinal point orientation and stages of development, aiming at better understanding the local shading impacts on final coffee quality.

ACKNOWLEDGMENTS

The study was supported by Consórcio Brasileiro de Cafés (project n° 02.09.20.008.00.03).

LITERATURE CITED

Adam, B, Dones, N, Sinoquet, H. 2006. *VegeSTAR*: *software qui calcule l'interception lumineuse et la photosynthèse*. Version 3.2. Clermont-Ferrand: INRA.

Angelocci, LR, Marin, FR., Pilau, FG., Righi, EZ, Favarin, JL. 2008. Radiation balance of coffee hedgerows. *Revista Brasileira de Engenharia Agrícola e Ambiental* **12(3)**: 274–281.

Antunes, WC, Pompelli, MF, Carretero, DM, daMatta, FM. 2008. Allometric models for non-destructive leaf area estimation in coffee (*Coffea arabica* and *Coffea canephora*). *Annals of Applied Biology* **153**:33–40.

Dengler, NG. 1999. Anisophylly and dorsiventral shoot symmetry. *International Journal of Plant Sciences* **160 (S6)**: 67-80.

Godin, C, Caraglio, Y. 1998. A multiscale model of plant topological structures. *Journal of Theoretical Biology* **191**: 1-46.

Matsunaga, FT, Rakocevic, M. 2011. Software para ajuste da geometria na reconstrução de cafeeiros em 3D. *Proceedings* of VII Simpósio de Pesquisa dos Cafés do Brasil, Araxá, Brazil: 1-5.

Pradal, C, Dufour-Kowalski, S, Boudon, F, Godin, C. 2008. OpenAlea: a visual programming and component-based software platform for plant modeling. *Functional Plant Biology* **35(9-10)**: 71-760.

Sievänen, R, Perttunen, J, Nikinmaa, E, Kaitaniemi P. 2010. Radiation conditions and competition in a tree stand simulated with a shoot-based model *Proceedings* of the 6th FSPM 2010, Davis, USA: 64-66.

Vaast, Ph, Bertrand, B, Perriot, J-J, Guyot, B, Génard, M. 2006. Fruit thinning and shade improve bean characteristics and beverage quality of coffee (*Coffea arabica* L.) under optimal conditions. *Journal of the Science of Food and Agriculture* **86(1)**: 197-204.

Proceedings of the 7th International Conference on Functional-Structural Plant Models, Saariselkä, Finland, 9 - 14 June 2013. Eds. Risto Sievänen, Eero Nikinmaa, Christophe Godin, Anna Lintunen & Pekka Nygren. http://www.metla.fi/fspm2013/proceedings. ISBN 978-951-651-408-9.

A self-organising model of Macadamia with application to pruning in orchards

Neil A White[1] and **Jim Hanan**[2]
[1]*Agri-Science Queensland, Department of Agriculture, Fisheries and Forestry, Toowomba, Qld 4350, Australia,* [2] *The University of Queensland, Queensland Alliance for Agriculture and Food Innovation, St. Lucia, Qld 4072, Australia j.hanan@uq.edu.au*
**correspondence:* neil.white@qld.gov.au

Highlights: A self-organising model of a macadamia that responds to pruning was created using the L-system-based language Lpfg. QuasiMC was used to determine light distribution within the canopy and reaching the orchard floor. Macadamia is an evergreen sub-tropical tree in the family *Proteaceae* and presents modelling challenges because of the abundance of leaves and multiple axillary buds.

Keywords: Macadamia; self-organising; pruning; light distribution; high throughput computing.

The self-organising model (Palubicki et al., 2009) expressed using Lpfg (Karwowski and Prusinkiewicz, 2003) was used as the basis for a model of macadamia (*Macadamia integrifolia* Maiden & Betche) that could be used to explore canopy management options. The model was modified to include three leaves at each node and potentially multiple axial buds at each leaf. Sensing of the light environment to guide new growth was done by buds in the original implementation, but this was likely to cause difficulties during subsequent model development as macadamia are thought to have as many as five axillary buds (Bennell, 1984). Instead, leaves were added, using their midpoint to cause shadowing. The amount of light available for growth was sensed at the leaf level and used to represent vigour, which was then accumulated acropetally. Buds also sensed the light environment but only to provide demand in the subsequent redistribution phase. Tree models were initiated by reading in an initial structure digitised from a small tree and then allowed to develop for a number of years. Empirical relationships were derived from a set of 24 digitised trees after conversion to multiscale tree graphs (MTG) and analysis with the OpenAlea software library (Godin et al., 1999, Pradal et al., 2008). The ability to write MTG files was embedded within the model so that various tree statistics could be exported for each run of the model. To explore the parameter space a series of runs was completed using a high-throughput computing platform, HTCondor, (Thain et al., 2005). While this was run on a single machine, essentially in batch mode, it could be adapted to large collections of distributed computer resources. When combined with MTG generation and analysis with OpenAlea it provided a convenient way in which hundreds of simulations could be explored. We allowed the model trees to develop using self-organisation and simulated cultural practices such as hedging, topping, removal of the leader and limb removal. Using QuasiMC (Cieslak et al., 2008) we were able to assess changes in light distribution within the canopy and the light available at the orchard floor. The lessons learnt from this will be applied to other evergreen, tropical fruit and nut trees.

LITERATURE CITED

Bennell MR. 1984. *Aspects of the biology and culture of the Macadamia*, PhD Thesis, University of Sydney, Australia.

Cieslak M, Lemieux C, Hanan J, Prusinkiewicz P. 2008. Quasi-Monte Carlo simulation of the light environment of plants. *Functional Plant Biology*, **35**: 837-849.

Godin C, Costes E, Sinoquet H. 1999. A Method for Describing Plant Architecture which Integrates Topology and Geometry. *Annals Of Botany*, **84**: 343-357.

Karwowski R, Prusinkiewicz P. 2003. Design and Implementation of the L+C Modeling Language. *Electronic Notes in Theoretical Computer Science*, **86**: 134-152.

Palubicki W, Horel K, Longay S, Runions A, Lane B, Měch R, Prusinkiewicz P. 2009. Self-organizing tree models for image synthesis. *ACM Transactions on Graphics*, **28**: doi: 10.1145/1576246.1531364.

Pradal C, Dufour-Kowalski S, Boudon F, Fournier C, Godin C. 2008. OpenAlea: a visual programming and component-based software platform for plant modelling. *Functional plant biology*, **35**: 751-760.

Thain D, Tannenbaum T, Livny M. 2005. Distributed computing in practice: the Condor experience. *Concurrency and Computation: Practice and Experience*, **17**: 323-356: 10.1002/cpe.938.

Proceedings of the 7th International Conference on Functional-Structural Plant Models, Saariselkä, Finland, 9 - 14 June 2013. Eds. Risto Sievänen, Eero Nikinmaa, Christophe Godin, Anna Lintunen & Pekka Nygren.
http://www.metla.fi/fspm2013/proceedings. ISBN 978-951-651-408-9.

Simulating the effect of extreme climatic events on tree architecture with a minimal FSPM

Olivier Taugourdeau [1-2] and **Jean-Francois Barczi** [3]
[1]UM2-UMR AMAP, F34000 Montpellier France. [2]CEF-UQAM-Chaire CRSNG/Hydro-Québec H2X1Y4 Montréal Québec Canada; [3]: CIRAD-UMR AMAP, F34000 Montpellier France.
**correspondence: barczi@cirad.fr*

Highlights: Tree response to extreme climate events is a hot topic. Minimal mathematical modelling of the interaction between tree growth and climate variation may help better understand how trees cope with extreme climatic events.

Keywords: Plant architecture, DRAFt model, Plant growth, Functional-Structural model, minimal mathematical modelling.

INTRODUCTION

Empirical studies and climate predictions highlight that climate change is associated with increasing occurrences of extreme climatic events (e.g. drought, heat wave and spring frost, Girard *et al.* 2012).

As trees develop a perennial structure, two hypotheses can be made: (i) the structure records past climatic events and thus may be affected for several years after a single extreme event and (ii) the same tree at different age may be affected differently by extreme climatic events.

The aim of this study is to test *in silico* these two hypotheses with a functional-structural tree model. This requires a model that can be analytically studied, and in which plant functions (organ size, carbon capture) and development (organ number per type) are emergent properties of the simulations. For instance the GREENLAB model (de Reffye & Hu, 2003) has many useful properties for analytical study, but the development sub-model remains relatively complex (i.e. high realism), in particular, the number of axes types is set by parameters. On the other hand, the model LIGNUM (Perttunen *et al.* 1996, 1998) contains a simple development sub-model, but the sub-model for plant function is complex. It depends on simulations of light interception that prevent analytical study and also require complex parameter calibration (e.g. organs shapes, morphogenetic responses to incident light).

DRAFt model (Taugourdeau *et al.* 2012) is a compromise between the two modeling approaches. In DRAFt, the approach to modeling plant functions is similar to GREENLAB when the developmental modelling is similar to LIGNUM. In summary, DRAFt is based on simple developmental and functional rules, but is expected to be less realistic than GREENLAB or LIGNUM. Moreover, DRAFt includes just 6 parameters, including a parameter that can be linked with the effect of climate. Finally, crown complexity is truly an emergent property of simulations.

MODEL: DRAFt

DRAFt (Demande, Répartition, Architecture & Fonctionnement with discrete time) is a recent FSPM model presented by Taugourdeau, Barczi & Caraglio (2012). This model provides interesting properties for *in silico* experiments as simulated crown complexity emerges from modelled processes and its equation system can be analytically studied.

DRAFt is an iterative, discrete time, growth cycle model that decomposes each successive growth cycle, typically a year, into 6 sequential substeps:

1. Growth Unit (GU) primary growth based on previous iteration carbon allocation (or taken from a seed at first iteration)
2. Branching on new GUs (bud production)
3. Carbon assimilation by new GUs
4. Carbon allocation to primary and secondary growth (compartment scale)
5. Secondary growth at GU scale from carbon allocated to secondary growth compartment
6. Carbon allocation to each bud from carbon allocated to primary growth compartment

Details about hypothesis and equations can be found in Taugourdeau *et al.* (2012). Among the 6 parameters, two parameters are critical for the present study:

- a set the among of biomass assimilated by a unit of GU length. Q_t the among of biomass assimilated at time t is the product of a and the sum of new GU lengths: $Q_t = a.\sum_i \ GUlength_{t,i}$.

• *cf* is the ratio between GU length and initial diameter and is assumed constant. It allows to compute GU length and initial diameter based on its initial volume, Vinit (i.e. its biomass): $GUlength_i = \sqrt[3]{\frac{4*cf^2}{\pi}.Vinit_i}$.

An implementation of DRAFt was achieved using Xplo software from the AMAPstudio free-to-use package (Griffon and de Coligny, 2012; http://amapstudio.cirad.fr). It is written in Java and generates the corresponding ArchiTree topology and allows simple shaping geometry for 3D rendering purpose. Another implementation of DRAFt was achieved using R software.

ANALYTICAL STUDY

Effect of climate variations on shoot lengths

Thanks to the DRAFt formalism, the first consequences of an extreme event can be analytically studied. Let assume that *a* may vary along the simulation:$Q_t = a_t.\sum_i \quad GUlength_{t,i}$and may remain constant except for a given time step:$a_{t=T} = V_a.a_{t\neq T}$with V_a the relative variation of biomass assimilation efficiency at year T. Let$GUlength_{t=T+1,i}$be the length of a GU the year that follows T. According to DRAFt assumptions it can be demonstrated that (*cf.* Taugourdeau *et al.* 2012 for variables and parameters descriptions):

$$GUlength_{t=T+1,i} = \sqrt[3]{\frac{4.\mathrm{cf}}{\pi}.db_i.\frac{V_a.a_{t\neq T}.\sum_i \quad GUlength_{t,i}}{D_{t=T+1}}},$$

$$GUlength_{t=T+1,i} = \sqrt[3]{V_a}.C_{t=T+1}$$

with$C_{t=T+1}$the length of the same GU if the extreme event do not occurs (i.e. V_a=1). As cube-root function is a function with decreasing slope, it implies an asymmetric response of GU lengths to opposite extreme events: for example, +20% of biomass assimilation efficiency, implies +6.3% of shoot lengths ($\sqrt[3]{1.2}$), when -20% of biomass assimilation efficiency, implies -7.2% of shoot lengths ($\sqrt[3]{0.8}$). This is a key result as assimilation is proportional to lengths of GUs in DRAFt and drives following cycle assimilation.

The asymmetric response is mainly the consequence of two model assumptions: (i) the amount of assimilated biomass is proportional to GU lengths and (ii) the GU length:initial diameter ratio is constant and implies a cubic root relationship between GU length and allocated biomass (i.e. GU volume, see Taugourdeau *et al.* 2012 for details).

Naturally this analytical demonstration only deals with the following year and avoids more complex responses during the rest of the simulation linked with threshold effect on branching.

NUMERICAL STUDY

Effect of tree architecture on tree responses to extreme climatic events

3 simulations were run with the same set of parameters (*Q0*=0.2, *dc*=.01, *cf*=30, *a*=5, *vb*=25, *da*=0.65), except for parameter *a*. In the first case, *a* remained constant along the whole simulation, in the two others cases *a* remained constant along the whole simulation except for the 4th or the 15th growth cycle (i.e. year) when *a* was reduced by 70% (i.e. a reduction of 70% of the carbon assimilated at this particular growth cycle) and returned to the original value after this extreme event.

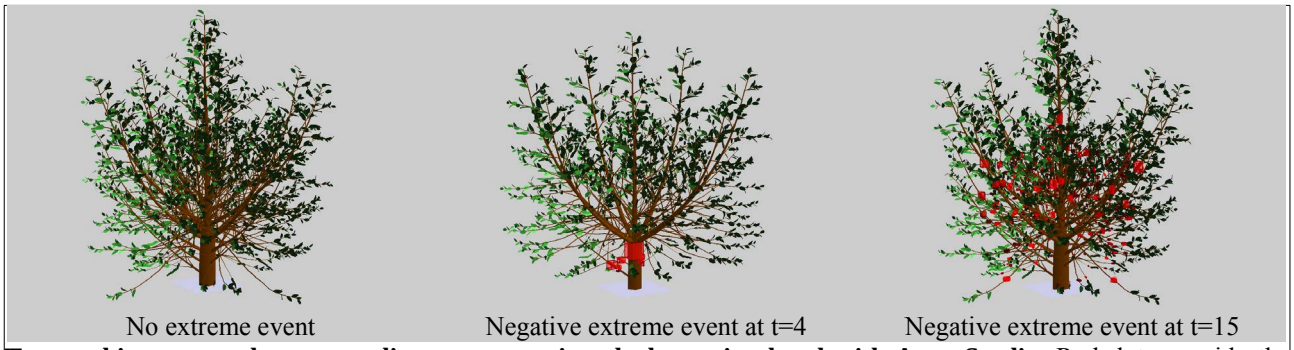

No extreme event | Negative extreme event at t=4 | Negative extreme event at t=15

Tree architecture and extreme climate event: virtual plants simulated with AmapStudio. Red dots provide the location of GUs that were produced during the year that follows the extreme event.

Thanks to DRAFt emerging properties, most of the studied architectural output variables are affected for several years after the extreme event. But, the system is, at least partially, resilient: after 3 years main axis shoot length trends return to the "regular" trend which is consistent with empirical results on the effect of

2003 extreme summer drought on mediterranean *Pinus halepensis* tree architecture (Girard *et al.* 2012). The analytical results of the previous part also predict this resilience: a decrease of 20% only implies a decrease of -7.2% of following year assimilation.

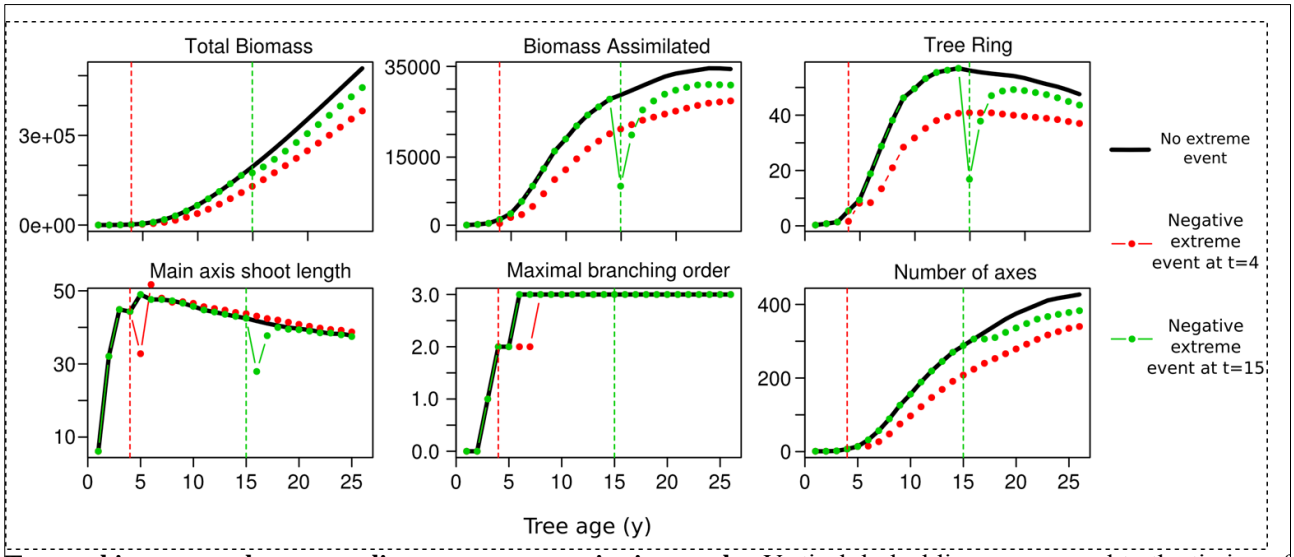

Tree architecture and extreme climate event: quantitative results. Vertical dashed lines correspond to the timing of the negative extreme event (see main text for details).

It is evident that for the later extreme event, the maximal branching order shows no shift compared to the reference which may be related to the absence of any mortality rules in the model.

Results also show the critical importance of the timing of the extreme event on tree responses: the late extreme event has a lower impact on tree growth and architecture.

CONCUSION

The analytical analysis highlights the central role played by GU constant allometry assumptions in DRAFt. It opens new perspectives for empirical studies on tree. For instance, does trees change their shoot shape in response to extreme climate events to reduce their consequences?

From the numerical simulations, we can conclude that an extreme event affects simulated tree architecture for several years and that younger trees appear more sensitive to an extreme event than older ones. We also suspect that the DRAFt model may be improved with some additional features (flexible shoot allometry, mortality and reserve capabilities) to better react to extreme events. This hypothesis must be reinforced by comparison to empirical data.

Similar analytical and/or numerical studies should be made on other Tree FSPMs (e.g. GREENLAB and LIGNUM) to characterize their behavior in response to extreme climate events.

ACKNOWLEDGMENTS

OT was funded by a PhD grant of the French research ministry and by a postdoctoral grant of the Chaire de recherche CRSNG/Hydro-Québec. Y. Caraglio and C. Nock provided useful comments on the manuscript.

LITERATURE CITED

Girard F, Vennetier M, Guibal F, Corona C, Ouarmim S, Herrero A. 2012. Pinus halepensis Mill. crown development and fruiting declined with repeated drought in Mediterranean France. *European Journal of Forest Research* **131**: 919–931.

Griffon S, de Coligny F. 2012. AMAPstudio: a Software Suite for Plants Architecture Modelling. In: Kang M, Dumont Y, Guo Y, eds. Plant Growth Modeling, Simulation, Vizualization and Applications. IEEE press, 2012; 141-147.

Perttunen J, Sievänen R, Nikinmaa E. 1998. LIGNUM: a model combining the structure and the functioning of trees. *Ecological Modelling* **108**: 189–198.

Perttunen J, Sievänen R, Nikinmaa E, Salminen H, Saarenmaa H, Väkevä J. 1996. LIGNUM: a tree model based on simple structural units. *Annals of Botany* **77**: 87.

De Reffye P, Hu B. 2003. Invited talk. Relevant qualitative and quantitative choices for building an efficient dynamic plant growth model: GreenLab case. *Plant Growth Modeling and Applications, Proceedings*: 87–107.

Taugourdeau O, Barczi JF, Caraglio Y. 2012. Simulation of Morphogenetical Gradients Using a Minimal Functional-Structural Plant Model (FSPM) . *In: Kang M, Dumont Y, Guo Y, eds. Plant Growth Modeling, Simulation, Vizualization and Applications. IEEE press, 2012;* 379-387

Proceedings of the 7th International Conference on Functional-Structural Plant Models, Saariselkä, Finland, 9 - 14 June 2013. Eds. Risto Sievänen, Eero Nikinmaa, Christophe Godin, Anna Lintunen & Pekka Nygren. http://www.metla.fi/fspm2013/proceedings. ISBN 978-951-651-408-9.

Testing a radiation transmission model for stands consisting of individual 3D Scots pine and silver birch trees

Pekka Kaitaniemi[1,*], **Risto Sievänen**[2], **Anna Lintunen**[3], and **Jari Perttunen**[2]

[1]*Hyytiälä Forestry Field Station, Dept. Forest Sciences, Univ. Helsinki, Hyytiäläntie 124, 35500 Korkeakoski, Finland*, [2]*Finnish Forest Research Institute, Vantaa Res. Ctr, P.O. BOX 18, 01301 Vantaa, Finland*, [3]*Dept. Forest Sciences, Univ. Helsinki, P.O. BOX 27, 00014 Univ.Helsinki, Finland*
**correspondence*: pekka.J.kaitaniemi@helsinki.fi

Highlights: Model-based estimation of light transmission showed acceptable precision in stands, which were reconstructed in 3D using basic tree-level forest inventory variables as input. It appears possible to limit the time costs of computation by restricting the number of sky sectors for ray tracing of light in the model.

Keywords: boreal forest, crown architecture, light transmission, mixed stand, tree structure

We have earlier designed models to reconstruct the 3D crown structure for Scots pine and silver birch using basic tree level input variables: tree height, crown height, diameter at breast height, and the degree of competition estimated with simple indices (Lintunen et al. 2011). Here we assessed the precision of estimating the transmission of photosynthetically active radiation (PAR) within mixed stands constructed in the LIGNUM-system using the 3D trees generated with the models. We measured PAR in field plots on fully overcast days and then estimated the corresponding levels of PAR using equivalent model-generated plots (Fig. 1). In total, 26 field measured 3D plots consisting of 3m to 15m tall tree individuals were reconstructed within 5m around the plot centre. The border forest surrounding the reconstructed plot was modelled as a homogeneous stand with its species-specific LAI and crown layer depth adopted from the reconstructed 3D trees. PAR reaching the measurement point was calculated using a range of 12 to 360 sky sectors with their brightness derived from the radiation distribution of the standard overcast sky. Shading was calculated by backward ray tracing of light paths from the sample position towards each sky sector. Light transmission in the border forest was calculated with the Beer-Lambert law. The results were analysed using the amount of PAR standardized with respect to PAR at an open site. The maximum fit with model-predicted PAR (r^2 = 0.63) was obtained when only 12 light paths were used (Fig. 2). The fit was poorer (r^2 = 0.54) if a fully homogeneous stand was used instead of including 3D trees. Good fit with only 12 light paths shows potential to restrict the time costs of computation required to estimate light transmission in spatially explicit stand models where short-term PAR on overcast days can serve as a surrogate variable to drive growth.

LITERATURE CITED

Lintunen A, Sievänen R, Kaitaniemi P, Perttunen J. 2011. Models of 3D crown structure for Scots pine (*Pinus sylvestris*) and silver birch (*Betula pendula*) grown in mixed forest. *Canadian Journal of Forest Research* **41**: 1779-1794.

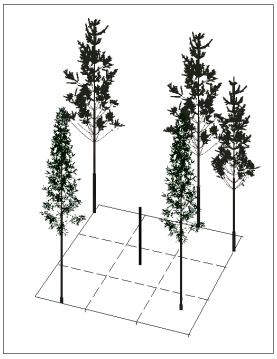

Fig. 1. The model was used to predict PAR measured on the top of the black bar in the middle.

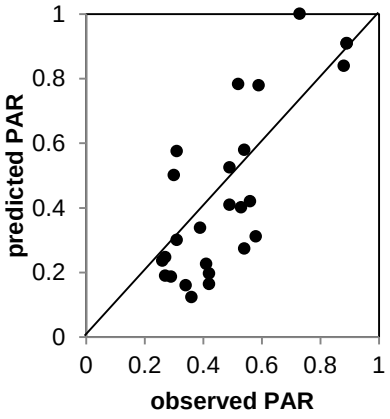

Fig. 2. Comparison of predicted and field-measured PAR.

Proceedings of the 7th International Conference on Functional-Structural Plant Models, Saariselkä, Finland, 9 - 14 June 2013. Eds. Risto Sievänen, Eero Nikinmaa, Christophe Godin, Anna Lintunen & Pekka Nygren. http://www.metla.fi/fspm2013/proceedings. ISBN 978-951-651-408-9.

Variation in structural and optical properties of sun exposed and shaded leaves: A model based approach

Petr Lukeš[1*], **Pauline Stenberg**[1], **Miina Rautiainen**[1], **Matti Mõttus**[2] and **Kalle M. Vanhatalo**[1]
[1] *Department of Forest Sciences, PO Box 27, 00014 University of Helsinki, Finland,* [2] *Department of Geosciences and Geography, PO Box 64, 00014 University of Helsinki, Finland*
**correspondence:* petr.lukes@helsinki.fi

Highlights: A database of optical, structural and biochemical properties of leaves of boreal species was established. The database was used to validate simulations of leaf spectra with the PROSPECT model. The relationships between leaf spectra and structure were similar for all species but the strongest for birch. The spectra of coniferous needles were more dependent on canopy position than birch spectra.

Keywords: leaf optical properties, structure, leaf radiative transfer model, boreal forest, PROSPECT

Leaf and needle (further commonly referred to as leaves) reflectance and transmittance convey information about the structure and biochemical constituents of leaf tissues (e.g. chlorophylls, carotenoids) and can be directly linked to the photosynthetic processes of plants via the light use efficiency. Both leaf structure and biochemical composition respond to decreasing light levels at deeper canopy positions and depend thus directly on canopy structure. Reliable information on leaf pigment and nutrient content and its variation, obtainable from reflectance and transmittance spectra, is required in detailed models of canopy functioning, estimation of canopy light absorption, as well as the interpretation of remote sensing data. Both structural and biochemical properties of leaves respond to decreasing light levels reaching deeper canopy positions and also to plant phenological stages.

We measured the reflectance and transmittance spectra of leaves of typical tree species in boreal Europe – Scots pine (*Pinus sylvestris* L.), Norway spruce (*Picea abies* (L.) Karsten) and Silver birch (*Betula pendula* Roth) – using a spectroradiometer coupled with an integration sphere. Measurements were calculated to hemispherically integrated reflectance and transmittance factors. Simultaneously, we measured leaf biochemical composition, water content and specific leaf area. Two different canopy positions (sunlit and shaded) were sampled. To generalize our measurements, we used the leaf-level radiative transfer model PROSPECT (Jacquemoud and Baret, 1990). The model requires only few input parameters of leaf biochemistry (e.g. chlorophyll a+b content, dry matter content, equivalent water thickness) and structure (leaf structure parameter) to simulate leaf reflectance and transmittance from 400 to 2500 nm in 1 nm step. When run in inverse mode, the model can be used to retrieve leaf structural and biochemical parameters from leaf spectra. The model allowed us to parameterize relationships between leaf spectra, biochemistry and structure for different irradiance conditions and canopy structures.

For both coniferous species transmittance was lower than reflectance whereas for birch it was similar. The relationships between the optical and structural properties of leaves and needles were similar for all species but the strongest for birch. The coniferous species, in turn, showed higher dependency of transmittance and reflectance spectra on canopy position. The results presented in this study will be part of the database of optical, structural and biochemical properties of tree species in the European boreal zone.

LITERATURE CITED

Jacquemoud S, Baret F. 1990. PROSPECT: A model of leaf optical properties spectra. *Remote Sensing of Environment* **34**: 75-91.

Proceedings of the 7th International Conference on Functional-Structural Plant Models, Saariselkä, Finland, 9 - 14 June 2013. Eds. Risto Sievänen, Eero Nikinmaa, Christophe Godin, Anna Lintunen & Pekka Nygren. http://www.metla.fi/fspm2013/proceedings. ISBN 978-951-651-408-9.

Influence of Morphological Traits on Wood Litter Production

Konrad Abramowicz[1], **Åke Brännström**[1,2], **Daniel Falster**[3] and **Raffaele Rani***[1]
[1]*IceLab, Department of Mathematics and Mathematical Statistics, Umeå University, 901 87 Umeå , Sweden,* [2]*Evolution and Ecology Program, International Institute for Applied Systems Analysis, 2361 Laxenburg, Austria,* [3]*Department of Biological Sciences, Faculty of Science, Macquarie University NSW 2109, Australia*
**correspondence:* raffaele.rani@math.umu.se

Highlights: We study the effect of variation of morphological traits on the wood litter production using an L-systems based model.

Keywords: L-systems, wood litter production, architectural traits, morphological traits, physiological traits.

Wood-litterfall is among the principal factors determining carbon accumulation in soil. Understanding the mechanisms that give rise to this process is therefore an important task for the estimation of carbon balances of forests and to develop management practices which balance timber production with carbon sequestration (Franklin et al., 2012). In fire-prone areas, wood litterfall is an important facilitator of forest fires, but a predictive theory of fire risk based on the rate of wood litterfall, branch diameter distributions have yet to be developed.

In this study, we investigate how morphological traits (e.g. branching angle, metamer length and branching frequency) affect the wood litter production. Similar questions have been studied theoretically using continuous population dynamics models, e.g., Falster et al. (2011) and the dependence of ecosystem processes on traits has long been investigated (Eviner, 2004). We use an L-systems (Lindenmayer and Prusinkiewicz, 1990) based model introduced by Sterck and Schieving (2007). The model respects fundamental physiological principles of plant growth, accounts for the age and weight of a plant's constituent parts. The model provided promising results when investigating the effects of size, shading, carbon economy, meristem population and reproductive allocation on the ontogenetic patterns in 3-D growth and structure.

The project, currently in its initial phase, aims to elucidate how differences in architectural and physiological traits between species affect the rate of biomass loss due to branch turnover. In addition, as various architectural strategies show different patterns in the size-dependence of biomass loss, we hypothesize that growth efficiency (fraction of biomass lost due to branch turnover) is inversely proportional to crown width.

REFERENCES

Eviner, V. 2004. Plant traits that influence ecosystem processes vary independently among species. *Ecology* 85(8): 2215–2229

Falster D.S., Bränsström, Å, Dieckmann, U, Westoby, M. 2011. Influence of four major plant traits on average height, leaf-area cover, net primary productivity, and biomass density in single-species forests: a theoretical investigation. *Journal of Ecology* 99: 148-164

Franklin, O., Johansson, J., Dewar, R.C., Dieckmann, U., McMurtrie, R.E., Brännström, Å., Dybzinski, R. 2012. Modeling carbon allocation in trees: a search for principles. *Tree Physiology* 32(6): 648-66.

Lindenmayer A., Prusinkiewicz P., 1990. The algorithmic beauty of plants, 4th edn. Springer-Verlag, New York

Sterck, F.J., Schieving, F. 2007. 3-D growth patterns of trees: effects of carbon economy, meristem activity, and selection. *Ecologival Monographs* 77(3): 405-420

Proceedings of the 7th International Conference on Functional-Structural Plant Models, Saariselkä, Finland, 9 - 14 June 2013. Eds. Risto Sievänen, Eero Nikinmaa, Christophe Godin, Anna Lintunen & Pekka Nygren. http://www.metla.fi/fspm2013/proceedings. ISBN 978-951-651-408-9.

L-Pea: an architectural model of pea (*Pisum sativum*) development

Romain Barillot[1], **Pierre Huynh**[1], **Abraham J Escobar-Gutiérrez**[2] and **Didier Combes**[2*]
[1]*LUNAM Université, Groupe Ecole Supérieure d'Agriculture, UPSP Laboratoire d'Ecophysiologie Végétale & Agroécologie, 55 rue Rabelais, BP 30748, F-49007 Angers cedex 01, France.*
[2] *INRA, UR4 P3F, Equipe Ecophysiologie des plantes fourragères, Le Chêne - RD 150, BP 6, F-86600 Lusignan, France.*
**correspondence:* didier.combes@lusignan.inra.fr

Highlights: an architectural model of pea, called L-Pea, was developped based on the L-System formalism. The input data account for the development of branches and phytomers as well as the kinetics of the vegetative organs growth.

Keywords: architectural model, morphogenesis, *Pisum sativum*, plant architecture.

Currently, pea (*Pisum sativum*) is the principle source of vegetable proteins. However, the productivity of pea crop is still under its potential. Studying pea architecture (*e.g.* Leaf Area Index (LAI), plant height, foliar inclination) enables to analyze its interactions with abiotic (light, nirtogen, water) and biotic factors (foliar diseases). Architectural models therefore appear as suitable tools for studying the functioning of pea (Barillot *et al.*, 2012). The aim of the present work was therefore to develop an architectural model of pea growth, hereafter called L-Pea (Fig. 1).

The model is based on the L-system formalism and implemented on the L-Py platform (Boudon *et al.*, 2012). Pea morphogenesis was modelled as being driven by thermal time which can be incremented from meteorological data at each time step. The above ground architecture is represented as a succession of phytomers that compose main stems and branches. Kinetics of phytomer and branch production are described in a *vegetative module*. Phytomers are considered as a collection of organs encoded as modules that support their state *i.e.* age, length, topology and geometry. The elongation and coordination of the organs generated in the *vegetative module* are then handled by a *growth module*. The initial parameters of phytomer production and organ growth were mainly based on measurements performed on a field-grown crop of winter pea, *cv.* Lucy.

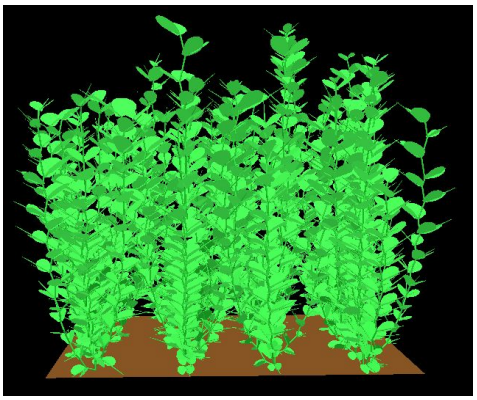

Fig.1: side view of a canopy of 3D pea plants generated from L-Pea model

In a companion study, the L-Pea model was interfaced with a dynamic model of wheat development (Fournier *et al.*, 2003) in order to generate virtual wheat-pea mixtures. This allowed us to study the relations between the architecture of the component species and the level of light partitioning. Detailed methods and results are given in Barillot *et al.* (2013). To our kwonoledge L-Pea is the first architectural model of pea available in the literature. This model can therefore provide a suitable framework for studying the behaviour of contrasted pea architecture towards light interception or foliar disease dispersion.

LITERATURE CITED

Barillot R, Combes D, Chevalier V, Fournier C, Escobar-Gutiérrez AJ. **2012**. How does pea architecture influence light sharing in virtual wheat-pea mixtures? A simulation study based on pea genotypes with contrasting architectures. *AoB Plants* **pls038**.

Boudon F, Pradal C, Cokelaer T, Prusinkiewicz P, Godin C. **2012**. L-Py: an L-System simulation framework for modeling plant development based on a dynamic language. *Frontiers in Plant Science* **3**.

Fournier C, Andrieu B, Ljutovac S, Saint-Jean S. **2003**. ADEL-wheat: A 3D architectural model of wheat development. *Proceedings of the 2003 Plant Growth Modeling, Simulation, Visualization, and Applications*. Beijing, China: IEEE Computer Society, 54–63.

Barillot R, Fournier C, Huynh P, Escobar-Gutiérrez AJ, Combes D. 2013. How do variations of architectural parameters affect light partitioning within wheat pea mixtures? A simulation study based on a virtual plant approach. *7th International Workshop on Functional-Structural Plant Models.* Saariselkä, Finland.

Proceedings of the 7th International Conference on Functional-Structural Plant Models, Saariselkä, Finland, 9 - 14 June 2013. Eds. Risto Sievänen, Eero Nikinmaa, Christophe Godin, Anna Lintunen & Pekka Nygren.
http://www.metla.fi/fspm2013/proceedings. ISBN 978-951-651-408-9.

Modeled and measured fPAR in a boreal forest

Titta Majasalmi[1], **Miina Rautiainen**[1]and **Pauline Stenberg**[1]
[1]*Department of Forest Sciences, PO BOX 27, FI-00014 University of Helsinki, Finland*
**correspondence:* titta.majasalmi@helsinki.fi

Highlights: A new model was developed for the estimation of fPAR based on the spectral invariants theory. Good agreement was found between modeled and measured fPAR in boreal forests. The model was applied to study the effect of canopy structure and sky conditions on fPAR.

Keywords: fPAR, canopy structure, photosynthesis, spectral invariants, canopy radiation

The fraction of absorbed Photosynthetically Active Radiation (fPAR) plays a critical role in carbon balance studies and is one of the Essential Climate Variables (ECV). fPAR can be used to monitor CO_2 assimilation by vegetation both seasonally and inter-annually. Temporal courses of fPAR cannot be directly measured but need to be estimated based on models which quantify the dependency of absorbed radiation on canopy structure. The aim of this study was to develop a physically-based canopy absorption model and to compare modelled and measured fPAR in structurally different forest stands.

We extended a previously developed model (Rautiainen & Stenberg 2005) for the estimation of fPAR based on the spectral invariants theory (Knyazikhin et al. 2011). The model uses leaf area index (LAI), canopy gap fractions and spectra of foliage and understory as input data. For validation of the model, measurements of instantaneous fPAR were performed using the TRAC instrument (Leblanc et al. 2002) in nine Scots pine, Norway spruce and Silver birch stands at Hyytiälä Forestry Field Station in June 2012. Continuous data on incoming radiation were obtained from the SMEAR flux tower. In addition, extensive stand inventory, LAI and canopy gap fraction data were acquired for all stands. Good agreement (RMSE ~0.05) was found between modeled and measured fPAR. Next, we applied the model to estimate temporal courses of fPAR. Polynomial functions were fitted to the measured canopy gap fractions to create a hemispherical gap fraction distribution for each stand. These hemispherical gap fraction distributions were used together with the sky irradiance models by Grant et al. (1996) to simulate incoming radiation fields. We show diurnal and seasonal courses of fPAR and how they are linked to forest structure.

LITERATURE CITED

Grant RH, Heisler GM, Gao W. 1996. Photosynthetically-active radiation: sky radiance distributions under clear and overcast conditions. *Agricultural and Forest Meteorology* **82**:267-292.

Knyazikhin Y, Schull MA, Xu L, Myneni RB, Samanta A. 2011. Canopy spectral invariants. Part 1: A new concept in remote sensing of vegetation. *Journal of Quantitative Spectroscopy & Radiative Transfer* **112:**727–735.

Rautiainen M, Stenberg, P. 2005. Application of photon recollision probability in coniferous canopy reflectance simulations. *Remote Sensing of Environment* **96:** 98-107.

Leblanc SG, Chen JM, Kwong M. 2002. Tracing Radiation and Architecture of Canopies. TRAC MANUAL Version 2.1.3. Available: http://faculty.geog.utoronto.ca/Chen/Chen's%20homepage/PDFfiles/tracmanu.pdf. [Cited: 10 Jan 2013].

Proceedings of the 7th International Conference on Functional-Structural Plant Models, Saariselkä, Finland, 9 - 14 June 2013. Eds. Risto Sievänen, Eero Nikinmaa, Christophe Godin, Anna Lintunen & Pekka Nygren.
http://www.metla.fi/fspm2013/proceedings. ISBN 978-951-651-408-9.

Real-time calculation of total light interception in crop canopy

Weiliang Wen[1,2,3], Xinyu Guo*[1,2,3], Boxiang Xiao[1,2,3] and Shenglian Lu[1,2,3]

[1]Beijing Research Center for Information Technology in Agriculture, Beijing Academy of Agriculture and Forestry Sciences, Beijing, 100097, China, [2]National Engineering Research Center for Information Technology in Agriculture, Beijing, 100097, China, [3]Key Laboratory for Information Technology in Agriculture, Ministry of Agriculture, Beijing 100097, China.

**correspondence:* guoxy@nercita.org.cn

Highlights: Daily total PAR interception is divided into three scales: organ, plant and canopy, and the core is organ scale calculation. Calculation of total intercepted PAR could be combined with photosynthetic rate parameter to study the relation between photosynthesis efficiency and production of specified canopy, after that, further analysis of agricultural production decisions may be carried out.

Key words: Total light interception, real-time calculation, sky visible rate

INTRODUCTION

Simulation of distribution of photosynthetically active radiation (PAR) in crop canopy is a key factor of quantitative photosynthesis simulation in precise agricultural model. Most current light interception research focused on simulation algorithms of spatial light distribution within the canopy (Chenu et al, 2008; Wang et al, 2008). The development of computer hardware and 3D scanner now helps to generate more accurate geometric model of crop canopy, which leads to a better geometric basis for light distribution calculation. The calculation is developed into a more accurate surface element scale instead of simple statistical model.

Generally, daily total PAR interception is divided into three scales: organ, plant and canopy, and the core part is organ-scale calculation. Calculation of total intercepted PAR could be combined with photosynthetic rate parameters to investigate the relation between photosynthesis efficiency and production rate of specified canopy, and then further analysis of agricultural production decisions may be carried out.

There are three components of light intercepted into canopies, i.e. direct solar radiation, sky diffuse radiation, multi-reflected and scattered radiation. The third component may be omitted in the estimation of total PAR into canopies (Alados et al, 2002). The speed of light interception calculation has beenone of the bottlenecks of this research. In fact, direct light calculation is much faster and can be calculated in real-time for every time step, however, diffuse light calculation is very time consuming and limits speed from real-time. In this paper, a robust algorithm of real-time calculation of total light interception in crop canopy is proposed to estimate total light interception in different scales along with the time changing.

MATERIALS AND METHODS

The field experiment was carried out at the experimental field of Beijing Academy of Agriculture and Forestry Sciences (39°94'N, 116°29'E), China. Maize (*Zea mays* L. variety 'XY335') canopy architecture and intensity of PAR were measured in sub-plots located in the middle of the canopy on September 23 and September 25 of 2010 respectively. A 5 plants × 3 rows geometric model containing 195576 facets (Fig.1) was constructed using measured morphology data acquired by 3D digitizer (Xiao et al, 2011). Geometric organs are composed of basic facets, and blades require double-sided facets. It's assumed that the 3D structure of the canopy kept unchanged during the calculating procedure. Continuous intercepted PAR with a

3-second time interval was measured for the ear leaf on the plant in the middle of the canopy using a self-developed light interception device which contains 11 sensors uniformly distributed on the leaf. This measurement process begins at 10:11 and ends at 15:25.

For each facet in the canopy, the sky visible rate (SVR) was calculated through projecting all the facets on a hemisphere which located on the calculating facet (Wang et al, 2005). In this method, proportion of unoccluded area of the hemisphere was calculated to acquire the facet's SVR. For all the facets in the canopy, this calculation is time-consuming. We adopted a multi-resolution subdivision hemisphere method here to calculate SVR of a given canopy, also applied multi-core parallel computing to speed up. A canopy with 150000 facets took 30 minutes to calculate SVR by multi-core parallel computing on an 8-core processor workstation. Since SVR of each facet doesn't change when the geometric canopy is still, this proposed method pre-computed SVR to make total calculation real-time.

Suppose T is the total time of the calculation and it is divided into N sections, i.e. N+1 time node and the length of each time section is *T/N*. Actual external light data including total radiation R_i and the proportion of direct light was measured at each time node *i, i=0,…,N*. Therefore, initial external direct light R_i^{direct} and diffuse light $R_i^{diffuse}$ were calculated at each time node.

Direct light interception within the canopy was calculated by Z-Buffer projection. Diffuse light intercepted on each facet was obtained by multiplying external diffuse light and SVR on the facet. Finally, total light intercepted by an organ in time length *T* is:

$$R = \frac{T}{N}\sum_{i=1}^{N}\sum_{k=1}^{M}(R_i^{direct}\cos\theta + R_i^{diffuse} r_k)s_k$$

Where s_k is the area of facet k, r_k is the SVR of facet k, *M* is the total facet number of a organ or a plant or canopy, $\cos\theta$ indicates the cosine value of the angle between *k*-th facet's normal and the direct light direction. The total intercepted light calculation of an organ in *T* is complete. Because of the direct light distribution is using Z-Buffer projection in real-time, with a finite number of productions and summations, the entire calculation could achieve real-time.

RESULTS AND DISCUSSION

We selected intercepted PAR from the measured data at 20 time points from 10:30to 15:15per 15minutes and meanwhile intercepted PAR on the same blade was simulated on the same 20 time points. Fig.2 shows the relation between the measured data and simulation. These results show that the general trend and data distributed range are almost same between the simulation and measured data. The main reason of the errors can be attributed to 2 factors: (1) Error from artificial digitized geometric model. (2) Breeze leads to instability of the upper leaves in the experiment. Fig.3 provides a visualization result at 12:00.

As a result, the proposed method could calculate the total light interception among a specified period of time at different scales including organ scale, plant scale and canopy scale. Furthermore, this method could be combined with actual field equipments to achieve real-time calculation of situational awareness and also could be used for real-time rendering of the light distribution animation of crop canopy.

ACKNOWLEDGEMENTS

This work is supported by the National Natural Science Foundation of China (Grant No. 31171454) and National Science and Technology Support Program (Grant No. 2012BAD35B01).

LITERATURE CITED

Alados I, Foyo-Moreno I, Olmo FJ, Alados-Arboledas L, 2002. Improved estimation of diffuse photosynthetically active radiation using two spectral models. *Agric For Meteorol* 111:1–12.

Chenu K, Rey H, Dauzat J, Lydie G, Lecoeur J, 2008. Estimation of light interception in research environments: a joint approach using directional light sensors and 3D virtual plants applied to sunflower (Helianthus annuus) and

Arabidopsis thaliana in natural and artificial conditions. *Functional Plant Biology*, 35: 850-688.

Wang XP, Guo Y, Wang XY, Ma YT, Li BG, 2008. Estimating photosynthetically active radiation distribution in maize canopies by a three-dimensional incident radiation model. *Functional Plant Biology*, 35: 867-875.

Wang XP, Guo Y, Li BG, Wang XY, Ma YT, 2005. Evaluating a three dimensional model of diffuse photosynthetically active radiation in maize canopies. *Ini J Biometeorol,* 50: 349-357.

Xiao BX, Wen WL, Guo XY, Lu SL, 2011. Digital plant colony modeling based on 3D digitization. *ICIC Express Letters Part B: Applications*, 2(6): 2185-2766.

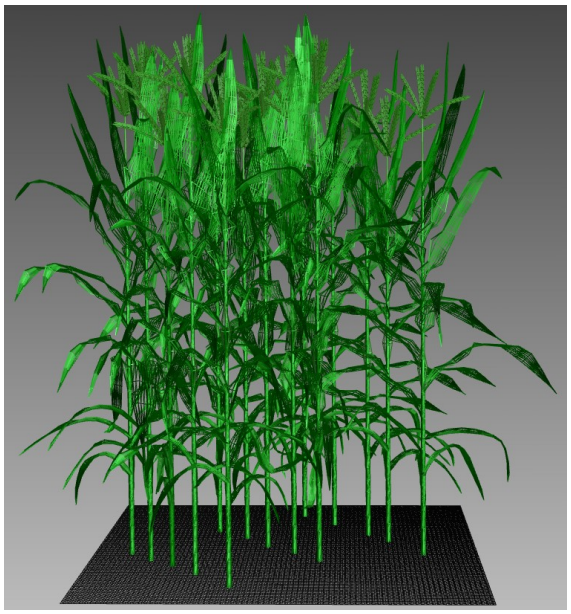

Figure 1: Geometric model of the canopy.

Figure 3: Visualization of the simulated interception at 12:00.

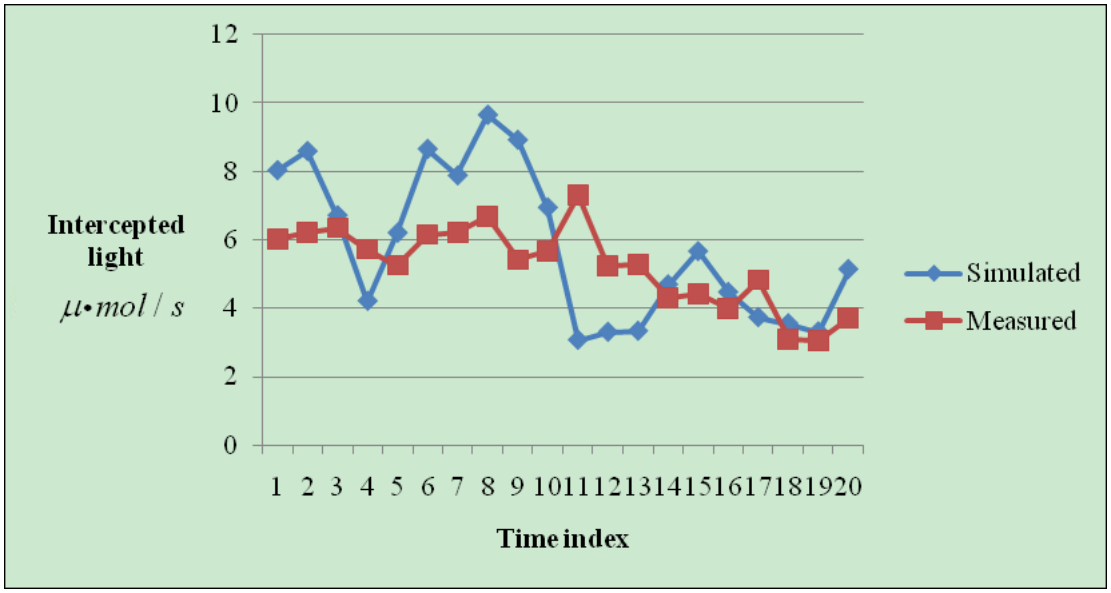

Figure 2: Contrast between simulation and measured data.

FUNCTIONAL-STRUCTURAL PLANT MODELS FOR PROBLEM SOLVING IN VEGETATION MANAGEMENT

Proceedings of the 7th International Conference on Functional-Structural Plant Models, Saariselkä, Finland, 9 - 14 June 2013. Eds. Risto Sievänen, Eero Nikinmaa, Christophe Godin, Anna Lintunen & Pekka Nygren.
http://www.metla.fi/fspm2013/proceedings. ISBN 978-951-651-408-9.

A generic model of interactions between FSPM, foliar pathogens and microclimate

Guillaume Garin[1], Christophe Pradal[2], Bruno Andrieu[3], Vianney Houlès[1], Corinne Robert[3] and **Christian Fournier[4]**

[1] ITK, avenue de l'Europe, F-34830 Clapiers, France, [2] CIRAD, UMR AGAP and INRIA, Virtual Plants, F-34398 Montpellier, France, [3] INRA, UMR 1091 EGC, F-78850 Thiverval-Grignon, France, [4] INRA, UMR 759 LEPSE, F-34060 Montpellier, France

**correspondence:* guillaume.garin@itkweb.com

Highlights: A framework was defined to model the interactions between FSPM, foliar fungal pathogens and microclimate, with the concern of interoperability of the components and extensibility. The framework was applied on two existing models of pathosystems (powdery mildew on grapevine and septoria on wheat) to make them more modular and extensible. It will facilitate the design of new disease models on FSPMs.

Keywords: generic modeling, crop architecture, foliar pathogens, powdery mildew, septoria

INTRODUCTION

Functional–structural plant models (FSPMs) are used for the development of increasingly complex simulation models (Cieslak et al. 2011). This reinforces the need to share and reuse submodels in the form of software components (Pradal et al. 2008) and entails standardizing the protocols of communication between them (Fournier et al. 2010). These issues are particularly encountered in epidemiology. The complexity arising from coupling FSPMs with models of fungal foliar pathogens motivated the development of more generic approaches (Mammeri et al. 2010).

Our goal is to design a modular and extensible plant-pathogen model. Two models available on the OpenAlea platform were reviewed: wheat septoria (Robert et al. 2008) and grapevine powdery mildew (Calonnec et al. 2008). The following questions were addressed: What information must the FSPM and pathogen models exchange? Can we identify processes that are common to most foliar pathogens? What levels of detail of plant representation are relevant to model diseases? How to manage different spatial and temporal scales between plant and pathogen?

Beyond demonstrating a practical application of our model, focusing on these contrasted pathosystems aims to prove its adaptability.

DESIGN OF THE MODEL

A pathosystem comprises three main entities: the functional-structural crop, the pathogen population and the physical environment. Each model operating on these entities has its own temporal and spatial scales, while models share a number of variables. For the sake of modularity, we first ensured that each component of the system could be modified independently, without altering the functioning of the others. To do so, we based our model on the generic principles proposed in OpenAlea for exchanging information between components (Fournier et al. 2010). A central data structure representing the canopy at different scales: the Multiscale Tree Graph (MTG: Godin and Caraglio, 1998) is used to circulate variables computed between models (Fig. 1 – See legend). This makes it possible to simulate plant-pathogen interactions such as the competition for a common resource.

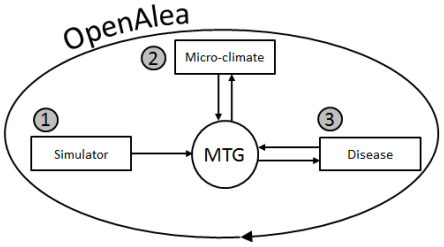

Fig. 1. Schematic of the protocol of communication between pathogen – FSPM – climate through a central data structure representing the canopy (i.e. MTG). At each time step, plant related models update properties of the MTG. Physical models, compute the micro-environment and store it as new MTG properties. These variables are read in the MTG by the fungal model which, in turn, writes new information to the MTG. This information is then used by the plant or physical models to complete their computation.

Consistency of spatial scales

The multi-scale structure of the MTGs is used to access plant and environmental variables at both very fine and coarse scales. The discretization of the plant in our model (phyto-element) is flexible depending on the processes that are modeled and the significance of differences in local values. It is relevant to identify zones on the plant that are homogeneous for variables of interest, and associate the pathogen model at this scale in the MTG. For powdery mildew, a phyto-element was a whole vine leaf; for septoria, a phyto-element was a short (2 cm) sector of wheat leaf.

Definition of generic protocols for disease models interacting with the FSPM

The model for the fungal system can be broken down into the following generic submodels (Fig. 2): initiation of the disease, lesion growth and update, coordination of surface distribution in case of competition, dispersal of spores, and management of nutrients in the phyto-element as a function of fungal uptake. Even if considerable variation exists in the modeling of such processes, it is believed that most foliar pathogens can be modeled by a combination of these submodels. Standardized protocols have been designed for each of them and will not change when passing from one fungus to another or from a complex to a simpler model.

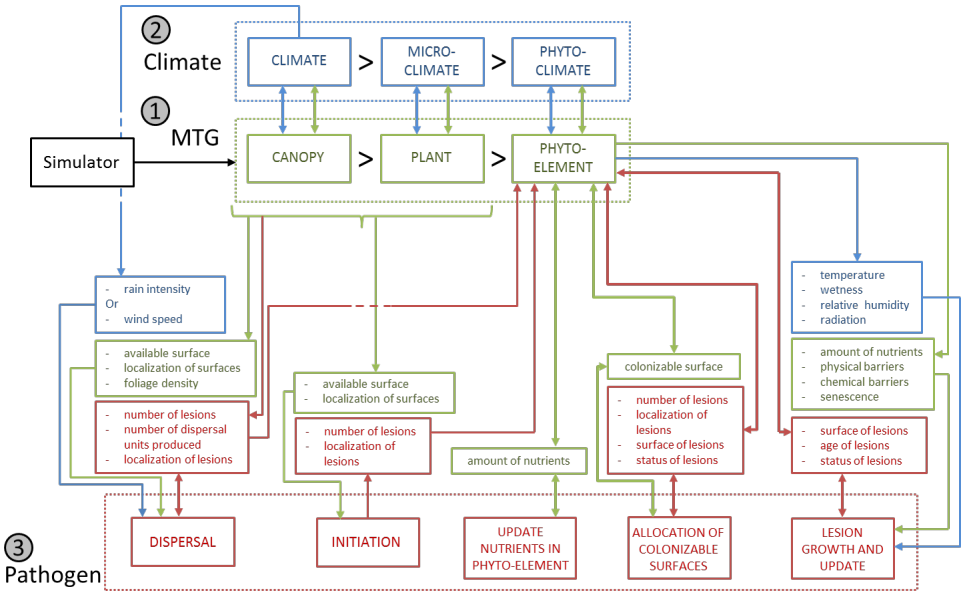

Fig. 2. Relationships between the MTG (green), the pathogen (red) and climate (blue) in the model

Definition of template classes for the disease

Foliar pathogens share common structural features for which a common scheme can be proposed. Diseases are spread by dispersal units and generic symptoms are lesions on leaves. In the model, all lesions on a given phyto-element share the same environmental variables, yet each lesion is treated individually. '*DispersalUnit*' and '*Lesion*' have been defined as virtual classes whose interfaces include methods and properties shared by all foliar pathogens. This still leaves great latitude to specialize methods representing a specific disease within the class.

Management of temporal scales

In our study cases, the progress of an individual lesion in physiological age (i.e. cumulation of favorable conditions) and surface is modeled by a continuous growth curve. This curve is modulated by external conditions. Three different temporal scales thus intermingle in our model: the continuous time of plant growth, the continuous time of lesion development and the discrete time of dispersal events. OpenAlea provides tools to coordinate and schedule the different components. Computations for updating plants and lesions are performed on a regular basis, and the intervals are interrupted if necessary when a discrete dispersal event occurs.

IMPLEMENTATION OF TWO PATHOSYSTEM MODELS

The models of Robert et al. (2008) for wheat septoria and Calonnec et al. (2008) for grapevine powdery mildew were re-implemented within the framework described above. Besides demonstrating the applicability

of our approach, this work initiated the development of a library in which formalisms can be picked up for the construction of future models.

In the case of wheat, plant is simulated using Adel-wheat (Fournier et al. 2003) whereas grapevine is simulated by an Lsystem based on TopVine (Louarn et al. 2008). L-Py is used for the generic generation of a MTG from an Lsystem string. Microclimate is simulated using Caribu and RATP.

Adel-Septo and the powdery mildew models were broken down into reusable components:

- The protocol of initiation consists of instantiating primary lesions on leaves (artificial or natural inoculation).
- Each lesion inherits from the class '*Lesion*' with its interface. The surface, the development stage and the rate of production of new dispersal units evolve with the physiological age of the lesion according to pathogen-dependent rules. Each fungus is described by a set of parameters, and specific methods were designed into the classes '*Septoria(Lesion)*' and '*PowderyMildew(Lesion)*' to account for different development mechanisms.
- For both diseases, an additional module coordinates the growth of lesions as a function of healthy surface on leaves that can still be colonized.
- Dispersal is very different between the two chosen pathogens but always occurs in 3 phases: liberation of dispersal units, transport and deposit. Septoria dispersal is a vertical phenomenon triggered by rain splash. The 1D dispersal model from AdelSepto was retrieved and wrapped to comply with the new generic protocol. Dispersal units are rain droplets containing spores. In contrast, powdery mildew dispersal is horizontal according to wind direction. A PlantGL algorithm computes the intersection of a cone with the scene and estimates individual spore deposits. In both cases, each deposited '*DispersalUnit*' will potentially give rise to a new instantiation of a '*Lesion*'.

The outputs of the new wheat model were compared to those of Septo3D giving consistent results. The interoperability of the system components was demonstrated by the instantiation and development of powdery lesions on wheat.

DISCUSSION

With our methodology, two existing models of foliar pathogens have been made more modular and extensible. Reusable disease components were identified and they can be modified without having to change the plant model. We expect the design of new disease models to be accelerated within our framework. The integration of other pathosystems will be necessary to confirm the choices made or to detect limits in the genericity of our approach.

LITERATURE CITED

Calonnec A, Cartolaro P, Naulin J-M, Bailey D, Langlais M. 2008. A host-pathogen simulation model: Powdery Mildew of grapevine. *Plant Pathology* **57**:493-508.

Cieslak M, Seleznyova A-N, Prusinkiewicz P, Hanan J. 2011. Towards aspect-oriented functional-structural plant modeling. *Annals of Botany* **108**(6): 1025-1041.

Fournier C, Pradal C, Louarn G, Combes D, Soulié J-C, Luquet D, Boudon F, Chelle M. 2010. Building modular FSPM under OpenAlea: concepts and applications. In: DeJong T. and Da Silva D. (Editors), 6th International Workshop on Functional-Structural Plant Models, Davis, pp. 97-100.

Godin C, Caraglio Y. 1998. A multiscale model of plant topological structures. *Journal of theoretical Biology* **191**:1-46.

Louarn G, Lecoeur J, Lebon E. 2008. A three-dimensional statistical reconstruction model of grapevine (*Vitis vinifera*) simulating canopy structure variability within and between cultivar/training system pairs. *Annals of Botany* **101**(8):1167-1184.

Mammeri Y, Burie J-B, Calonnec A, Cokelaer T. 2010. Modelling of the airborne dispersal of a pathogen over a structured vegetal cover. In: DeJong T. and Da Silva D. (Editors), 6th International Workshop on Functional-Structural Plant Models, Davis, pp. 50-52.

Pradal C, Dufour-Kowalski S, Boudon F, Fournier C, Godin C. 2008 OpenAlea: a visual programming and component-based software platform for plant modelling. *Functional Plant Biology* **35**:751-760.

Robert C, Fournier C, Andrieu B, Ney, B. 2008. Coupling a 3D virtual wheat plant model with a Septoria tritici epidemic model (Septo3D): a new approach to investigate plant-pathogen interactions linked to canopy architecture. *Functional Plant Biology* **35**:997-1013.

Proceedings of the 7th International Conference on Functional-Structural Plant Models, Saariselkä, Finland, 9 - 14 June 2013. Eds. Risto Sievänen, Eero Nikinmaa, Christophe Godin, Anna Lintunen & Pekka Nygren. http://www.metla.fi/fspm2013/proceedings. ISBN 978-951-651-408-9.

Using 3D virtual plants to evaluate the canopy role in the progression of a splash-dispersed crop disease: a case study based on wheat cultivar mixtures

Christophe Gigot[1,2,4], Claude de Vallavieille-Pope[3], Marc Leconte[3],Claude Maumené[4], Laurent Huber[1,2] and **Sébastien Saint-Jean[2,1,*]**

[1]INRA, UMR1091 Environnement et Grandes Cultures, F78850 Thiverval-Grignon, France, [2]AgroParisTech, UMR Environnement et Grandes Cultures, F78850 Thiverval-Grignon, France,[3]INRA, UR1290 BIOGER CPP, F78850 Thiverval-Grignon, Franc,[4]ARVALIS—Institut du Végétal, Station Expérimentale de Boigneville , F91720 Boigneville, France

**correspondence:* Sebastien.Saint-Jean@AgroParisTech.fr

Highlights: A model taking into account physical mechanisms involved in splash dispersal of pathogens and host cultivar quantitative resistance has been developed to study the potential of heterogeneous three-dimensional crop canopies such as cultivar mixtures to prevent disease progression. We investigated different spatial organizations, proportions and resistance levels of wheat cultivars mixtures to allow better control of septoria tritici blotch.

Keywords: cultivar mixture, splash dispersal, septoria tritici blotch, wheat, modelling, heterogeneous canopy

INTRODUCTION

Increasing plant diversity within a crop by the use of cultivar mixtures is a strategy, that reduces severity of wind-borne diseases (Wolfe 1985; Finckh and Mundt 1992; Hau and de Vallavieille-Pope 2006). The interest of cultivar mixture practice for the case of rain-borne diseases was controversial. Depending on the study, results are inconsistent, for example previous studies showed rather significantly benefits for reducing splash dispersed diseases (Jeger et al. 1981; Mundt et al. 1995; Mille and Jouan 1997; Mille et al. 2006) or rather non-significant effects (Cowger and Mundt 2002). Septoria tritici blotch (STB), is one of the predominant foliar rain-born diseases on wheat crops caused by the fungus *Mycosphaerella graminicola*, and is regularly responsible for substantial yield losses up to 40% (Oste et al. 2000). Findings of Mille et al. (2006), show the interest of using wheat cultivar mixture to control STB. Recently Gigot et al. (2013) confirmed consistent reduction depending on disease pressure of STB disease severity by the use of cultivar mixture over four years. In this last study, it is also discussed that better control of STB should occur for specific proportions and resistance differences of wheat cultivar mixture of susceptible and resistant components. Newton et al. (1997) also confirmed that for the splash-dispersed *Rhynchosporium secalis* on barley, increasing the number of components brought more benefits on disease control. Therefore, to take full advantage of cultivar mixtures, the design of cultivar mixture needs improvement. Relying only on experimental knowledge can be tedious and time-consuming, for example Mille et al. (2006) had to test experimentally two component mixtures two by two for providing an optimal four components mixture.

We propose here to rely on modelling, to enhance and speeding up the process of designing efficient wheat cultivar mixtures on the control of STB. We investigated different mixture compositions such as spatial organizations, proportions and resistance levels. To do so, such model should at least take into account splash dispersal of spores and the inherently heterogeneous canopy properties of the cultivar mixtures (Calonnec et al. 2013). Because the spores are dispersed at short distances, due to the splashing mechanism from 0 to 20 cm (Fitt et al. 1989; Huber et al. 2006), and plant organs of different resistant types, are spatially heterogeneous, it leads to consider a spatial scale less than 1 cm for modelling dispersal. To reach such requirement, one solution is to describe the physical scene with the help of virtual three dimensional plants (Fournier et al. 2003), as it has been used for light interception computations (e.g. Chelle and Andrieu 1998).

MODEL DESCRIPTION

Here, we propose to focus on physical mechanisms involved in splash dispersal of a non-specialised pathogen within heterogeneous canopies of cultivar mixtures. For this purpose, we developed a framework

that takes into account different mechanistic and stochastic models (Saint-Jean et al. 2008; Gigot 2013), including (i) the 3D spatial localization of wheat plant organs of at least two cultivars (periodic boundary conditions have been applied to simulate an infinite canopy); (ii) the calculation of droplet population dispersal based on Monte Carlo integration (Saint-Jean et al. 2004) within a 3D virtual scene; (iii) from this set of trajectories, the potential progression pattern of septoria tritici blotch is assessed on the whole canopy under several assumptions of cultivar resistance levels of the intercepted surfaces; (iv) the polycyclic nature of epidemics, forced by the rainfall occurrences, is modelled by iterating the previous calculations.

RESULTS AND DISCUSSION

Disease progression was computed for different wheat canopies. Highly susceptible pure stand, a moderately resistant pure stand, highly resistant pure stand and an equi-proportion mixture of the previous components have been tested. For those sets of canopies, initial inoculum was set at the fourth leaf (from the top) to 10% of leaf surface diseased. Three cycles of disease progression, *i.e.* pathogen generations or rain events, were computed. Evolution of disease severity (*i.e.* proportion of diseased surface over total leaf surface) was calculated on each leaf depending on their localisation in the canopy, level of resistance and the amount of the disease at the previous cycle. Here, we summed the disease of all the leaf levels of a plant to compute the progression of the disease at the canopy scale (Fig. 1). As it is expected, the more susceptible the cultivar is, the faster the disease progression is (Fig. 1). Comparatively to the mean of the pure stands, the progression of disease potential within the mixture was globally reduced by 35% after three dispersal cycles (Fig. 1). Such order of magnitude of disease reduction has been confirmed in field experiments (Gigot et al. 2013). Increasing both differences between resistance levels and proportion of the more resistant cultivar resulted generally in a higher expected protective effect against the pathogen. Nevertheless, this rule was not observed for very high proportions of a rather resistant cultivar.

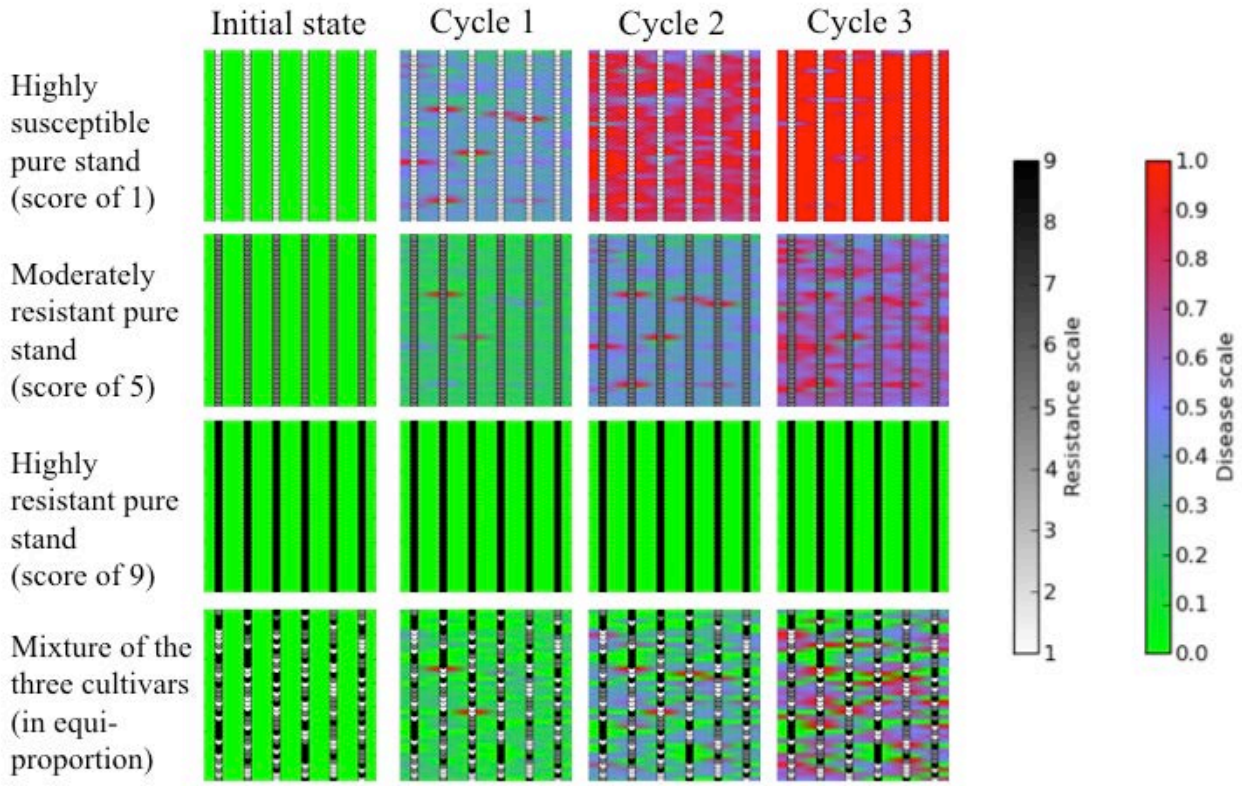

Fig. 1. Disease progression within a wheat cultivar mixture for 4 wheat canopy types (from top to bottom, highly susceptible pure cultivar; moderately resistant pure cultivar; highly resistant pure cultivar and three cultivar mixture in equi-proportion of the previous cultivars). Grey scale represents from light to darker the resistance scale. Colour scale (from green to red) represents the increasing potential of disease severity.

Our results illustrate that (i) mixture efficiency against a splash dispersed fungus may evolve differently across the successive pathogen generations, and (ii) optimal cultivar proportions can be established depending on resistance levels. Mixture component characteristics have to be precisely considered to find a compromise in terms of diversity within the field. Therefore such modelling approaches could be used for the design of cultivar mixture in order to find optimal and complementary properties of the mixture in order to integrate protective effects against splash-dispersed diseases among other beneficial properties of cultivar mixtures.

ACKNOWLEDGMENTS

This work received financial support from the French Ministry of Agriculture (contract CTPS C032010) and from "Fondation pour la Recherche sur la Biodiversité–LU" ("Les Champs de Biodiversité"). Managed by the ANRT (Association Nationale de la Recherche Technique), the PhD grant of Christophe Gigot was cofinanced by ARVALIS – Institut du Végétal and the French Ministry of Research and Education.

LITERATURE CITED

Calonnec A, Burie J-B, Langlais M, Guyader S, Saint-Jean S, Sache I, Tivoli B. **2013**. Impacts of plant growth and architecture on pathogen processes and their consequences for epidemic behaviour. *European Journal of Plant Pathology* **135**: 479–497.

Chelle M, Andrieu B. **1998**. The Nested radiosity model for the distribution of light within plant canopies. *Ecological Modelling* **111**: 75–91.

Cowger C, Mundt CC. **2002**. Effects of Wheat Cultivar Mixtures on Epidemic Progression of Septoria Tritici Blotch and Pathogenicity of Mycosphaerella graminicola. *Phytopathology* **92**: 617–623.

Finckh MR, Mundt CC. **1992**. Plant competition and disease in genetically diverse wheat populations. *Oecologia* **91**: 82–92.

Fitt BDL, McCartney HA, Walklate PJ. **1989**. The role of rain in dispersal of pathogen inoculum. *Annual Review of Phytopathology* **27**: 241–270.

Fournier C, Andrieu B, Ljutovac S, Saint-Jean S. **2003**. ADEL-Wheat: a 3D Architectural Model of wheat development. In: Hu B-G, Jaeger M, eds. *Plant Growth Modeling and Applications*. Springer Verlag, 54–63.

Gigot C. **2013**. Potentialités des associations de variétés pour limiter la progression épidémique de la septoriose du blé : rôle des mécanismes de dispersion des spores par la pluie dans un couvert végétal hétérogène. PhD Thesis, L'Institut des Sciences et Industries du Vivant et de l'Environnement (AgroParisTech), Paris France.

Gigot C, Saint-Jean S, Huber L, Maumené C, Leconte M, Kerhornou B, de Vallavieille-Pope C. **2013**. Protective effects of a wheat cultivar mixture against splash-dispersed septoria tritici blotch epidemics. *Plant Pathology* **in press (10.1111/ppa.12012)**.

Hau B, de Vallavieille-Pope C. **2006**. Wind-dispersed diseases. In: COOKE BM, JONES DG, KAYE B, eds. *The Epidemiology of Plant Diseases*. Springer Netherlands, 387–416.

Huber L, Madden LV, Fitt BDL. **2006**. Environmental biophysics applied to the dispersal of fungal spores by rain-splash. In: Cooke BM, Gareth DG, Kaye B, eds. *The epidemiology of plant diseases*. Springer, 348–370.

Jeger MJ, Griffiths E, Jones DG. **1981**. Disease progress of non- specialised fungal pathogens in intraspecific mixed stands of cereal cultivars. I. Models. *Annals of Applied Biology* **98**: 187–198.

Mille B, Belhaj Fraj B, Monod H, de Vallavieille-Pope C. **2006**. Assessing Four-Way Mixtures of Winter Wheat Cultivars from the Performances of their Two-Way and Individual Components. *European Journal of Plant Pathology* **114**: 163–173.

Mille B, Jouan B. **1997**. Influence of varietal associations on the development of leaf and glume blotch and brown leaf rust in winter bread wheat. *Agronomie* **17**: 247–251.

Mundt CC, Brophy LS, Schmitt MS. **1995**. Choosing crop cultivars and cultivar mixtures under low versus high disease pressure: A case study with wheat. *Crop Protection* **14**: 509–515.

Newton AC, Ellis RP, Hackett CA, Guy DC. **1997**. The effect of component number on Rhynchosporium secalis infection and yield in mixtures of winter barley cultivars. *Plant Pathology* **46**: 930–938.

Oste B, Huguerot G, Delos M, Freydier M, Henaff GL, Gatellet J, Pillon O, Feurprier B, Vergnaud A. **2000**. Bilan phyto-sanitaire de la campagne 1998/99. *Phytoma, la défense des végétaux* **523**: 12–16.

Saint-Jean S, Chelle M, Huber L. **2004**. Modelling water transfer by rain-splash in a 3D canopy using Monte Carlo integration. *Agricultural and Forest Meteorology* **121**: 183–196.

Saint-Jean S, Kerhornou B, Derbali F, Leconte M, de Vallavieille-Pope C, Huber L. **2008**. Role of rain-splash in the progress of Septoria leaf blotch within a winter wheat variety mixture. *Aspects of Applied Biology* **89**: 49–54.

Wolfe MS. **1985**. The current status and prospects of multiline cultivars and variety mixtures for disease resistance. *Annual Review of Phytopathology* **23**: 251–273.

Proceedings of the 7th International Conference on Functional-Structural Plant Models, Saariselkä, Finland, 9 - 14 June 2013. Eds. Risto Sievänen, Eero Nikinmaa, Christophe Godin, Anna Lintunen & Pekka Nygren. http://www.metla.fi/fspm2013/proceedings. ISBN 978-951-651-408-9.

An integrated and modular model for simulating and evaluating how canopy architecture can help reduce fungicide applications

Christian Fournier[1,2], **Christophe Pradal** [2], **Mariem Abichou**[3], **Bruno Andrieu**[3], **Marie-Odile Bancal**[3], **Carole Bedos**[3], **Pierre Benoit**[3], **Camille Chambon**[3], **Romain Chapuis** [1,3], **Eric Cotteux**[4], **Laure Mamy**[5], **Neil Paveley**[6], **Valérie Pot**[3], **Sebastien Saint-Jean**[3], **Claire Richard**[7], **Carole Sinfort**[4], **Alexandra Ter Halle**[7], **Eric Van Den Berg**[8], **Anne Sophie Walker**[9] and **Corinne Robert**[3]

[1]*INRA-SupAgro UMR 759 LEPSE F-34090 Montpellier, France,* [2]*CIRAD, UMR AGAP and INRIA, Virtual Plants, F-34398 Montpellier, France,* [3] *INRA-AgroParisTech UMR 1091 EGC F-78850 Thiverval-Grignon, France,* [4]*IRSTEA-SupAgro UMR ITAP, F-34090 Montpellier, France,* [5]*INRA UR 251 PESSAC F-78000 Versailles, France,*[6]*ADAS High Mowthorpe, Duggleby, North Yorkshire YO17 8BP United Kingdom,*[7]*CNRS-Université Blaise Pascal UMR 6505 LPMM F-63177Aubière France ,* [8]*ALTERRA, Research Institute for the Green World, Postbus 47-6700AA, Wageningen, NetherLands,* [9]*INRA-AgroParisTech UMR 1290 BIOGER F-78850 Thiverval-Grignon, France.*

**correspondence:* Christian.Fournier@supagro.inra.fr

Highlights: An integrated model coupling architectural canopy development, disease dynamics, pesticide application, pesticide decay and effect of pesticide on disease dynamics has been developed. It allows simulation of the dynamics of epidemics overall a growth season, together with the evaluation of impacts on environment, yield reduction and erosion of pesticide efficiency. This tool allows for a multi-criteria evaluation of different fungicide applications strategies and for designing new strategies that reduce pesticide applications by increasing natural resistance linked to canopy architecture.

Keywords: Pesticide, architecture, simulation, disease escape, Septoria, Wheat.

INTRODUCTION

European countries are moving towards the promotion of a sustainable agriculture that balances production and profitability with product quality and environmental protection. To reduce the use of chemical protection, it is possible to optimize fungicide applications, use resistant or tolerant varieties and improve the control of pests by an appropriate management of the dynamic of crop canopy architecture.

The canopy architecture determines the life environment of the pathogen: it is responsible for the amount and location of its substrate (healthy leaf surfaces), and for the distances to travel to colonize healthy tissues from infected areas. Focusing on wheat, a number of studies showed that canopy architecture significantly modulates Septoria epidemics (Eyal, 1971, Bahat et al. , 1980, Lovell et al. 1997 and 2004, Shaw and Royle, 1993), and that it is a relevant target for improving disease escape (Lovell et al., 2004; Ando et al. 2005) . Such effects however vary with climatic condition and are not easy to disentangle experimentally. The recent developments of models that couple a 3D model of the development of architecture and epidemics (Calonnec et al. 2008, Robert et al. 2008,Pangga et al., 2011) makes it possible to better understand the conditions of success of such strategies.

The canopy architecture also influences the interception of the fungicide and its distribution on the plants. This directly determines the fraction of pesticide that actually reaches pathogens, therefore the efficacy of the treatment. When spraying, the pesticide interception by the canopy and the fraction reaching the ground are often estimated empirically or by an expert judgment, although it is possible to asses it by modeling when canopy architecture is known.

Finally, the architecture determines the microclimatic conditions on leaves, and thus the environmental fate of the applied products. The environmental fate of a fungicide depends on its ability to penetrate the plant to degrade, to volatilize to the atmosphere or to be washed-off by rain (Willis et al., 1987). Volatilization from the canopy may represent more than 10% of the applied dose in a few days or weeks depending on the physicochemical nature of the compound, application method, surface properties and climatic conditions (van den Berg et al., 1999). Leaching by rain is a potentially significant source of dissemination of pesticides to soil and water. Its importance depends on the pesticide, the time between treatments, the intensity and duration of rainfall (Aubertot et al. 2005). Photodegradation also involves radiative transfer to the leaf surface (Katagi, 2004). Models recommended for the pesticide registration on

national or EU levels, such as PEARL (Leistra et al., 2001) describe this overall behavior but still face the limits of knowledge about certain processes taking place on the foliage (Scholtz et al., 2002; Leistra et al., 2005) and of simplifications in the representation of canopy architecture.

An integrated assessment of the sustainability of a pesticide reduction strategy must also take into account the erosion of efficacy of chemicals.

The objective of this work is to build an integrated model for simulating the effects of architecture on the dynamics of the epidemics, its interactions with pesticide interception and consequences on the efficacy and the environmental fate of the products. The ultimate goal is to optimize the strategies of fungicide application and to use disease escape linked to architecture in order to reduce the amounts of applied fungicides. In this perspective, we also aimed at providing post-processing utilities for a multi-criteria evaluation of reduction strategies including agronomic criteria (yields), environmental impacts and erosion of efficacy of fungicides, which depends on frequency of treatments.

The model is developed for the pathosystem wheat-Septoria, which is the major disease for wheat in France and Western Europe. This choice is also motivated by the facts that the control of Septoria is based mainly on chemical control that Septoria epidemics are influenced by canopy architecture and that architectural models already exists (Robert et al. 2008).

MODEL DESCRIPTION

The model is mostly based on the coupling of a series of already existing models. We use the OpenAlea platform (Pradal et al, 2008) to perform the coupling. This platform allows for importing models written in different languages, and to wrap them as python software components. One or several integrated models could then be built by chaining the execution of these components in a dataflow. The integrated model is also designed to avoid implicit dependences between components. To do so, all the communication between components is made through data reading/writing on a central structure representing the canopy.

Two main applications were built. A first application allows for the simulation, at an hourly time step of the development of wheat architecture, of Septoria epidemics dynamics, of fungicide application, of fungicide effect on Septoria infectious cycle and of the fate of fungicide on the leaves. It involves six main sub-models, each being divided in several components and connected together in a repeated hourly loop.

The principal sub-models were:

- ADEL-Wheat (Fournier et al., 2003). This model is based on the OpenAlea version of Adel-Wheat (Fournier et al. 2010) that allows for simulating 3D architectural wheat development at different stages. Two main improvements have been added: a new parameterization protocol that allows an automated fit from experimental data (Abichou et al., this volume) and (ii) a new simulation frame that allow for updating a canopy from a given existing state. This module creates or modifies an MTG representing the canopy at different scales, from organ to canopy.
- Septo3D-Cycle: This model simulates the growth of a lesion of Septoria. It has been extracted as an individual component from the Septo3D model (Robert et al., 2008). The model was extended to take into account the effect of fungicide, as described below
- A model of fungicide effect on disease dynamics, adapted from the model of Milne et al. (2007). This model allows for computing the global effect of a mixture of product, given their doses and parameters describing dose-response curve for each product. Dose-response curves describe two effects of a product on fungus: a protectant effect that decrease infection efficiency, and an eradicant effect that reduce the rate of development of the lesions.
- Septo3D-Dispersion: this model originates from Septo3D model (Robert et al. 2008), and was implemented as an independent component using the generic frame defined by Garin et al. (unpublished). It allows for simulating spores dispersal by rain, using a 1D multilayered approach.
- A model simulating fungicide interception. We use the projection algorithm included in the Caribu light model (Chelle et al., 1998) to simulate the surfaces reached by fungicide, together with the quantity of product hitting the surfaces. A physical model (Saint-Jean et al., 2006) is then used to predict the fraction of product that will effectively be fixed on the surface, splashed or leached. This model uses an experimental measurement of droplets size and velocity emitted from the nozzle of the application device.
- A model simulating the persistence of the fungicide on the leaf. We use a special version of the PEARL model (van den Berg, 2008) to estimate dynamically the fraction of product that remains active on the

surface, or that is lost due to penetration into the plant, volatilization or washing by rain. This model is called for every leaf elements in the canopy, using local micro-environment for light distribution and for rain intensity. These two variables were estimated using the Caribu model (Chelle et al, 1998).

A second application evaluates impacts based on the simulation results of the first application. Three impacts were considered:

- Impact on crop performance (yield) is estimated using a model, based on empirical laws established for wheat (Bancal et al., 2007).
- Environmental impacts are computed using standard versions of PEARL (van den Berg 2008) and PRZM (Carsel et al, 1998) models.
- Erosion of fungicide efficacy is estimated as a function of the number of selection events encountered by fungus exposed to products.

RESULTS AND DISCUSSION

This study allowed building an integrated application that can be used for assessing several strategies of reduction of fungicide application, with an emphasis on canopy architecture effects. The model results from an assembly of several sources, developed in different laboratories for different uses. OpenAlea plateform was particularly suited to achieve such collaborative integration, with support for coupling, documenting and testing. Our first objective was to get an operational integrated model, and this will be demonstrated with simulations of simple scenarios. In a future study, the model will be used for assessing different application strategies. Here, we rather tried to perform partial validation and calibration of each sub models. Occasionally this required an assembly of components slightly different from the integrated model. Partial validations were done by comparing simulation results with experimental data, or by qualitative assessments of model behavior by experts. These validation results include a comparison of the simulated canopy with photographs, a comparison of simulated fungicide interception in the canopy with experimental data, and an overall assessment of the behavior of the models regarding epidemic dynamics as a function of the date of application

LITERATURE CITED

Ando K, R. Grumet, K. Terpstra and J. D. Kelly. 2005. Manipulation of plant architecture to enhance crop disease control. *CAB Reviews: Perspectives in Agriculture, Veterinary Science, Nutrition and Natural Resources 2007* **2**: No. 026

Aubertot, J.N., J.M. Barbier, A. Carpentier, J.J. Gril, L. Guichard, P. Lucas, S. Savary, I. Savini, and M. Voltz. 2005. Pesticides, agriculture et environnement. Réduire l'utilisation des pesticides et limiter leurs impacts environnementaux.. Expertise Scientifique Collective INRA/CEMAGREF.

Bahat, A., I Gelernter, M.B. Brown and Z. Eyal 1980 Factors affecting the vertical progression of Septoria Leaf Blotch in Short-Statured Wheats. *Phytopathology* **70** (3): 179-184

Bancal, M-O., Robert, C., Ney. B 2007. Modelling wheat growth and yield losses from late epidemics of foliar diseases using loss of green leaf area per layer and pre-anthesis reserves. Annals of Botany. 2007 : 777-789.

Calonnec, A., P. Cartolaro, J. M. Naulin, D. Bailey, and M. Langlais. 2008. A host pathogen simulation model: powdery mildew of grapevine. *Plant Pathology* **57**:493-508

Carsel R.F., Imhoff J.C., Hummel P.R., Cheplick J.M., Donigian A.S.Jr., 1998. PRZM 3, a model for predicting pesticide and nitrogen fate in the crop root and unsaturated soil zones: Users manual for release 3.12. *National Exposure Research Laboratory*, Office of Research and Development, US Environment Protection Agency.

Chelle M., Andrieu B., Bouatouch K. – 1998 - Nested radiosity for plant canopies. The Visual Computer, 14:109-125

Eyal, Z. 1971. The kinetics of pycnidiospore liberation in Septoria tritici. *Canadian Journal of Boany*., **49**: 1095-1099.

Fournier C., Andrieu B., Ljutovac S. & Saint-Jean S. 2003. ADEL-wheat: a 3D architectural model of wheat development. In: Plant Growth Modeling and Applications (eds B.-G. Hu & M. Jaeger), pp. 54-66. Tsinghua University Press and Springer, Beijing, China

Fournier C., Pradal C., Louarn G., Combes D., Soulié J.-C., Luquet D., Boudon F. & Chelle M. 2010 Building modular FSPM under OpenAlea: concepts and applications. In: FSPM 2010. Proceedings of the 6th International Workshop on Functional-Structural Plant Models (eds T. DeJong & D.D. Silva), pp. 97-100. Plant Science Department,University of California, Davis

Katagi T 2004 Photodegradation of pesticides on plant and soil surfaces. *Rev Environ Contam Toxicol* **182**: 1-189.

Leistra, M., van der Linden, A.M.A., Boesten, J.J.T.I., Tiktak, A. and ven den Berg, F., 2001. PEARL model pesticide behaviour and emissions in soil-plant systems; Descriptions of the processes in FOCUS PEARL v 1.1.1. Alterra- report 013, ISSN 1566-7197, RIVM report 711401 009, Alterra RIVM, Wageningen, 115p.

Leistra, M. 2005. Estimating input data for computations on the voplatilisation of pestiides from plant canopies and competing processes. *Aterra repport 1256*

Lovell, D.J., Parker, S.R., Hunter, T., Royle, D.J. and Coker, R.R., 1997. Influence of crop growth and structure on the risk of epidemics by Mycosphaerella graminicola (*Septoria tritici*) in winter wheat. . *Plant Pathology*, **46**(1): 126-138.

Lovell, D.J., Parker, S.R., Hunter, T., Welham, S.J. and Nichols, A.R., 2004. Position of inoculum in the canopy affects the risk of septoria tritici blotch epidemics in winter wheat. *Plant Pathology*, **53**(1): 11-21

Milne A., Paveley N., Audsley E. and Parsons D. 2007. A model of the effect of fungicides on disease-induced yield loss, for use in wheat disease management decision support system**.** *Annals of Applied Biology*. **151**, p.113-125

Pangga, I.B., J. Hanan, and S. Chakraborty. 2011. Pathogen dynamics in a crop canopy and their evolution under changing climate. *Plant Pathology* **60**:70-81.

Pradal C., Dufour-Kowalski S., Boudon F., Fournier C. & Godin C. 2008 OpenAlea: a visual programming and component-based software platform for plant modelling. *Functional Plant Biology*, **35**, 751-760

Robert C., Fournier C., Andrieu B., Ney B. 2008. Coupling a 3D virtual wheat (Triticum aestivum) plant model with a Septoria tritici epidemic model (Septo3D): a new approach to investigate plant-pathogen interactions linked to canopy architecture. Functional Plant Biology, 35 (10) p 997-1013.

Saint-Jean S., A. Testa, L. V. Madden, et L. Huber. **2006**. Relationship between pathogen splash dispersal gradient and Weber number of impacting drop. *Agricultural and Forest Meteorology*, **141**(2-4):257-26.

Scholtz, M.T., Voldner, E., McMillan, A.C. and Van Heyst, B.J., 2002. A pesticide emission model (PEM) Part I: model development. *Atmospheric Environment* **36**, 5005-5013.

Shaw, M.W. and D.J. Royle. 1993. Factors determining the severity of epidemics of Mycosphaerella graminicola on winter wheat in the UK. *Plant Pathol*ogy, **42**:882-899

van den Berg, F., Kubiak, R., Benjey, W.G., Majewski, M.S., Yates, S.R., Reeves, G.L., Smelt, J.H. and van der Linden, A.M.A., 1999. Emission of pesticides into the air. *Water, Air, and Soil Pollution* **115**, 195-218.

van den Berg, F., Bedos, C. and Leistra, M. 2008. Volatilisation of pesticides computed with the PEARL model for different initial distributions within the crop canopy, *International Advances in Pesticide Application*. Association of Applied Biology, Cambridge (UK), 131-138.

Willis and McDowell, 1987. Pesticide persistence on foliage. *Reviews Environ. Contam. Toxicol*. **100** : 23-73

Proceedings of the 7th International Conference on Functional-Structural Plant Models, Saariselkä, Finland, 9 - 14 June 2013. Eds. Risto Sievänen, Eero Nikinmaa, Christophe Godin, Anna Lintunen & Pekka Nygren. http://www.metla.fi/fspm2013/proceedings. ISBN 978-951-651-408-9.

Weeds In Space – field-level epidemiology of herbicide resistance

David Thornby[1]
[1]*Department of Agriculture, Fisheries and Forestry, Queensland. PO Box 2282, Toowoomba, QLD, Australia*
**correspondence:* david.thornby@daff.qld.gov.au

Highlights: Spatial epidemiology of herbicide resistance is insufficiently understood at present to allow us to provide quantified strategies for farmers attempting to contain or eradicate patches of resistance. SHeRA, a spatially-explicit model of herbicide-resistant weeds in patches, is a useful new tool for developing efficient strategies using a zonal management approach.

Keywords: Herbicide resistance, glyphosate, *Echinochloa colona*, patch dynamics, eradication, modelling

INTRODUCTION

Across the world, wherever industrialised production of food and fibre plants occurs, weeds have evolved to become resistant to commonly-used herbicides (Heap, 2013). At first, weeds became resistant to specialised, high-risk herbicides such as ACCase and ALS inhibitors, but changes in usage patterns over the last 20 years have seen the widespread development of populations resistant to even lower risk herbicides like glyphosate.

In Australian agriculture, the emphasis on dealing with resistance (to glyphosate in particular) is shifting from prevention to management. Enough farmers and land managers are now confronted with a population of resistant weeds that it makes sense to investigate and promote strategies for dealing with resistant biotypes that are present, rather than resistance as it evolves. Resistance management recommendations to date include useful tactics, but package them in non-quantified, generic ways, and are not aimed at eradication.

Through modelling, biochemistry and molecular biology, science has developed a good understanding of how, why, and when resistance occurs. This knowledge led to, underpins and validates current management recommendations. However, questions remain about the epidemiology of resistance: where it occurs in space, how patches grow, move, and spawn new patches, and at what rate these processes occur for different species. Understanding resistance epidemiology better at a field level could help us decide whether, and under what conditions, local eradication of resistant biotypes is a feasible goal, and to identify cost-effective zonal management approaches that could be used to achieve it.

MODEL DEVELOPMENT

In order to examine the spatial dynamics of herbicide resistance in an agricultural situation, we developed SHeRA, the **S**patial **He**rbicide **R**esistance **A**nalyser. SHeRA is a stochastic integer-based model of weed life cycles and gene flow, implemented in Python 3.2 and numpy 1.7. Sub-populations of weeds of 1 m^2 each, arranged in a grid, are subjected to a set of management tactics and, through flowering and seed set, communicate with each other through short- and long-distance movement of pollen and seeds.

Patch dynamics in an agricultural weed are a function of the pressure for expansion and propagation exhibited by the patch, and the manager's pressure for containment and eradication (see Cousens & Mortimer, 1995). In the case of resistance, patch expansion occurs both through seed dispersal and through pollen flow from resistant patches to the surrounding conspecific population. The presence of non-resistant conspecific plants causes a complex balance of competing non-resistant pollen (Baker & Preston, 2008) and the presence of potential seed parents for the creation of new, relatively distant heterozygous offspring. In the case of species that are self-fertile, like *E. colona*, questions remain over how important rare outcrossing events are in the propagation and expansion of resistance patches. Since successful outcrossing mainly occurs with close neighbours, and less frequently at longer distances that are limited by wind speed and pollen lifespan, SHeRA includes processes for both. Short-distance movement is simulated through sharing of pollen clouds and seeds proportionally with neighbours within a pre-defined distance. Long-distance movement is simplified as a random allocation of a random number of propagules with randomly-chosen distant cells.

SHeRA runs on a yearly timestep. The events in one step are as follows:

1. Germinate weed cohort one
2. Apply control measures to cohort one
3. Germinate cohort two
4. Apply control measures to cohort one survivors and cohort two
5. Germinate cohort three
6. Apply control measures to cohort one and two survivors and cohort three
7. Apply control measures to mature survivors of all cohorts
8. Determine potential seed production
9. Produce and move pollen between neighbouring cells and at long distance
10. Determine progeny genotypes
11. Move progeny (seed) between neighbouring cells
12. Process end-of-year mortality of new seeds prior to entering seed bank, and between-seasons mortality of old seeds in seed bank
13. Seed rain enters seed bank – return to start

Integer modelling is used in determining the survivorship of plants under self-thinning processes and simulated control tactics. As each cohort germinates, a number of plants (proportional to the cell's current seed bank density, rounded down) are entered into a Python list either as a 0 (no resistance alleles), 1 (one resistance allele, heterozygous) or 2 (homozygous resistant). Separate lists are maintained for each cohort. SHeRA simulates populations with a single-gene resistance mechanism, though that mechanism may be dominant, recessive, or in-between. For most currently-known glyphosate resistant populations, this is a reasonable simplification.

Cohort member lists are tested for survivorship against predetermined estimates of herbicide efficacy relative to genotype and plant age, with as many tests performed in series as necessary to determine the number and genotypes of individuals that survive a whole season of management tactics.

Seed production per plant is affected by plant density according to Cousens' hyperbolic yield penalty model (Cousens, 1985), potentially reduced to account for fitness penalties due to resistance. We developed parameters and mechanisms to test the patch dynamics of glyphosate-resistant awnless barnyard grass (*Echinochloa colona* L. Link) in a glyphosate-resistant cotton farming situation, using a variety of published and unpublished data. Key parameter estimates for the *E. colona* implementation of SHeRA are given in Table 1.

Table 1. Parameter values for SHeRA simulating patches of glyphosate resistance in *Echinochloa colona*

Parameter	**Value**
Cohort 1 germination proportion (of total seed bank)	0.05
Cohort 2 germination proportion	0.05
Cohort 3 germination proportion	0.01
Carrying capacity	3000 plants/m^2
Initial seed bank density	400 seeds/m^2
Initial resistance patch size	4 m^2
Proportion of pollen shared with nearby cells	0.4
Pollen spread distance	2 cells
Chance of long distance pollination, per cell	0.01
Proportion of pollen spread at long distance	0.001
Mortality of seeds prior to entering seed bank	0.1
Annual seed mortality	0.5
Proportion of seed shared with nearby cells	0.2
Seed spread distance	1 cell
Self-fertilisation proportion	0.95
Maximum seed production	15 000 per plant

RESULTS

SHeRA provides outputs for total and per-cell values of seed bank density (separated by genotype) and resistance proportion, per step. This output can be used to analyse the rate of expansion of resistance patches and the success of any given strategy at controlling weed numbers across the whole field.

A simple test of patch dynamics is shown in Figs 1-3. We simulated three scenarios: glyphosate used alone after the emergence of every cohort (Fig 1); the glyphosate strategy plus paraquat applied to every cell in a containment zone 15m^2 in diameter around the original resistance patch (Fig 2); and the glyphosate strategy plus paraquat applied only to cells in the original patch zone (Fig 3). As expected, glyphosate alone allows the patch to spread. The addition of paraquat was only successful at severely limiting spread when applied in a zone outside the original patch; applications to the patch area alone were soon overtaken by survivors spreading seed and pollen outside the original patch zone.

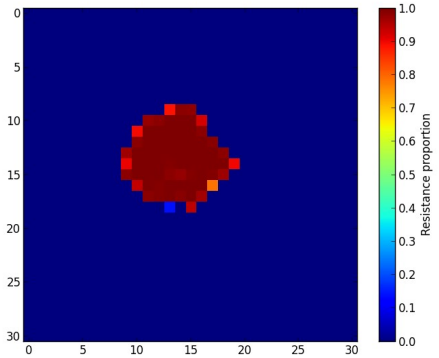

Fig 1. Resistance proportion in each cell of a test field after five years of glyphosate applied after emergence of every cohort

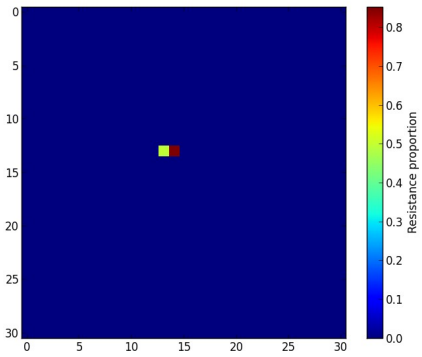

Fig 2. Resistance proportion in each cell of a test field after five years of glyphosate applied to every cohort plus paraquat applied to every cohort in a zone 12m^2 in diameter around the original resistance patch

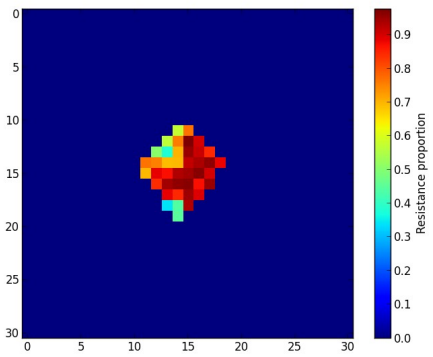

Fig 3. Resistance proportion in each cell of a test field after five years of glyphosate applied to every cohort plus paraquat applied to every cohort in the 4m^2 diameter of the original resistance patch

FURTHER WORK: ZONAL MANAGEMENT AND PATCH ERADICATION

When a patch of herbicide-resistant plants is identified, the manager of the land in which the patch occurs could choose to either manage the whole area as if it were herbicide-resistant, or to isolate the patch and perhaps some surrounding zone, and treat them differently from the rest of the area. In SHeRA, we nominate the original patch as the eradication zone, an area immediately outside the patch as the containment zone, and the rest of the field as the background zone. The eradication zone should receive highly intensive management aimed at preventing all seed set on all emerged plants, for as long as necessary to exhaust the supply of resistant seeds. The containment zone should receive sufficiently robust management to ensure that recruits from short-distance gene flow are likely to be controlled. The background zone receives some version of 'business as usual' management, which in a best-management-practice case would consist of glyphosate plus a range of options used in rotation, which would be of use in preventing the successful establishment of satellite patches of resistance.

We intend to use SHeRA to investigate the potential for eradicating glyphosate-resistant patches of *E. colona* in Australian non-irrigated cotton farming, and to optimise management tactics used in each zone such that the least intensive, effective strategies can be identified. This will require the development of a set of scenarios for weed management in glyphosate-tolerant cotton crops. We hope to develop quantified strategy recommendations for on-farm use where early identification of glyphosate-resistant *E. colona* occurs. The development and implementation of such strategies will be critical in determining the medium- to long-term sustainability of glyphosate-tolerant cotton farming in Australia.

LITERATURE CITED

Heap I 2013. *The International Survey of Herbicide Resistant Weeds*. Online. Internet. January 11, 2013 . Available www.weedscience.com

Cousens R, Mortimer M 1995. *The Dynamics of Weed Populations*. Chapter 7. Cambridge University Press, UK.

Baker J, Preston C 2008. The influence of pollen competition on gene flow in small patches of Lolium rigidum Gaud. (annual ryegrass). In: RD van Klinken, VA Osten, FD Panetta and JC Scanlan **(eds);** *Proceedings of the 16th Australasian Weeds Conference*. Weed Society of Queensland, Australia.

Cousens R 1985. An empirical model relating crop yield to weed and crop density and a statistical comparison with other models. *Journal of Agricultural Science* **105**: 513–521.

Proceedings of the 7th International Conference on Functional-Structural Plant Models, Saariselkä, Finland, 9 - 14 June 2013. Eds. Risto Sievänen, Eero Nikinmaa, Christophe Godin, Anna Lintunen & Pekka Nygren.
http://www.metla.fi/fspm2013/proceedings. ISBN 978-951-651-408-9.

Using functional-structural plant modeling to explore the response of cotton to mepiquat chloride application and plant population density

Shenghao Gu[1], Jochem B. Evers[2], Lizhen Zhang[1]*, Lili Mao[3], Jan Vos[2], Zhaohu Li[3]
[1]College of Resources and Environmental Sciences, China Agricultural University, Beijing 100193, China, [2]Centre for Crop Systems Analysis, Wageningen University, PO Box 430, 6700 AK, Wageningen, the Netherlands, [3]College of Agronomy and Biotechnology, China Agricultural University, Beijing 100193, China
**correspondence: zhanglizhen@cau.edu.cn*

Highlights: The crop growth regulator Mepiquat Chloride (MC) is widely used in cotton production to optimize the canopy structure in order to maximize the yield and fiber quality. Cotton plasticity in relation to MC and other agronomical practice was quantified using a functional-structural plant model of cotton development, ultimately aiming at helping cotton farmers to manage their crops optimally.

Keywords: Cotton (*Gossypium hirsutum* L.), canopy growth, light interception, morphology, pruning, simulation model

INTRODUCTION

In contrast to other crops, cotton (*Gossypium hirsutum* L.) the crop growth must be regulated and eventually terminated by chemical means. The crop growth regulator Mepiquat Chloride (MC) is commonly used in cotton production in China and other places in the world to maximize cotton yield and fiber quality (Oosterhuis and Egilla, 1996). Cotton canopy structure is often determined not only by MC control but also by planting density (Gwathmey and Clement, 2010) and other practices, which influences crop light interception and fruit formation and thereby biomass growth and yield. However, it is a great challenge to manage canopy structure due to the complexity and plasticity of cotton plant architecture.

Cotton has an indeterminate fruiting habit, and produces new foliage event on two different types of branches (vegetative and fruiting branches) (Zhao and Oosterhuis, 2000) with their own particular growth habit, which further complicates crop management. Because of the structural complexity and also the dynamics of leaf senescence, modeling cotton is difficult to realize. New techniques for collection, analysis, and concise representation of topological and geometric data have been applied to create a model of cotton morphogenesis and architecture based on L-systems by Room and Hanan (1995). Furthermore De Reffye et al. (1999) described a hydraulic model of cotton, focussing on vegetative growth. Jallas et al. (1999) added a visualization component to a mechanistic crop-level simulation of cotton. Hanan and Hearn (2003) established well-performed linked models between physiology and architecture of cotton. Functional-structural plant modelling (FSPM) (Vos et al, 2010) has become a promising tool to explore divergent management strategies in cotton.

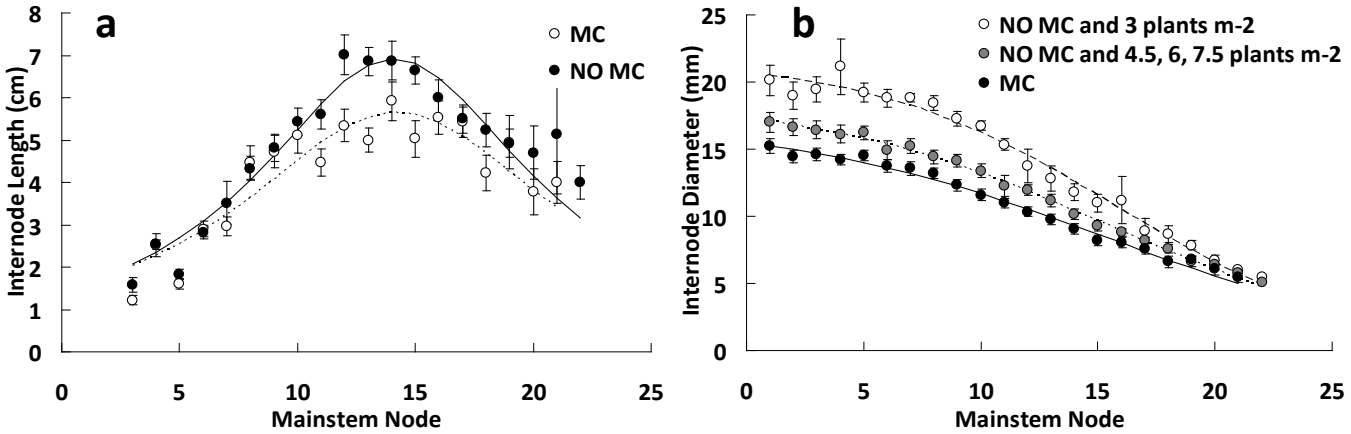

Fig. 1. Experimental data on internode length distribution along the main stem with and without MC (a); internode diameter at different population densities with and without MC (b)

The objective of this study was to optimize plant and crop structure by using a cotton FSPM, particularly to quantify cotton plasticity in relation to agronomical practices, and therefore to help farmers manage their crop optimally in given environmental conditions. Here we present the first results pertaining to leaf expansion and fruit numbers.

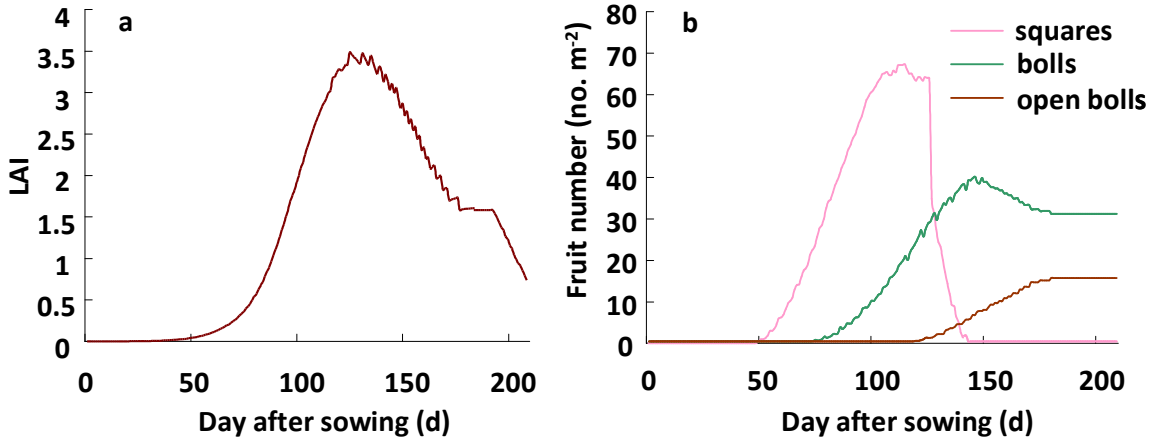

Fig. 2. Time-course changes in leaf area index (a), fruits number (b). The scenario shown here is for Anyang (eastern China) in 2002, MC applied, top cut-out at 30 July and side cut-out at 30 August, at a population density of 3.6 plants m^{-2}

SIMULATIONS

Field experiments were conducted that included treatments of plant with and without MC at four populations densities (3.0, 4.5, 6 and 7.5 plants m^{-2}) in 2011 and 2012 in the Yellow River region of China. The measured data on plant structure (as an example internode length and diameter with or without MC application at different population densities is shown in Fig. 1), were used to calibrate an FSPM of cotton, CottonXL, based on the simulation modeling platform GroIMP. The model simulates cotton leaf area expansion, and fruit number dynamics in terms of square, flower and boll development (exemplified in Fig. 2), plant height, vegetative/fruiting branch pattern and overall plant geometry (Fig.3), light interception and fiber quality. Input variables are daily temperature, planting density, MC application, cut-out time (termination of shoot tips of main stem and/or branches to prevent further phytomer development)

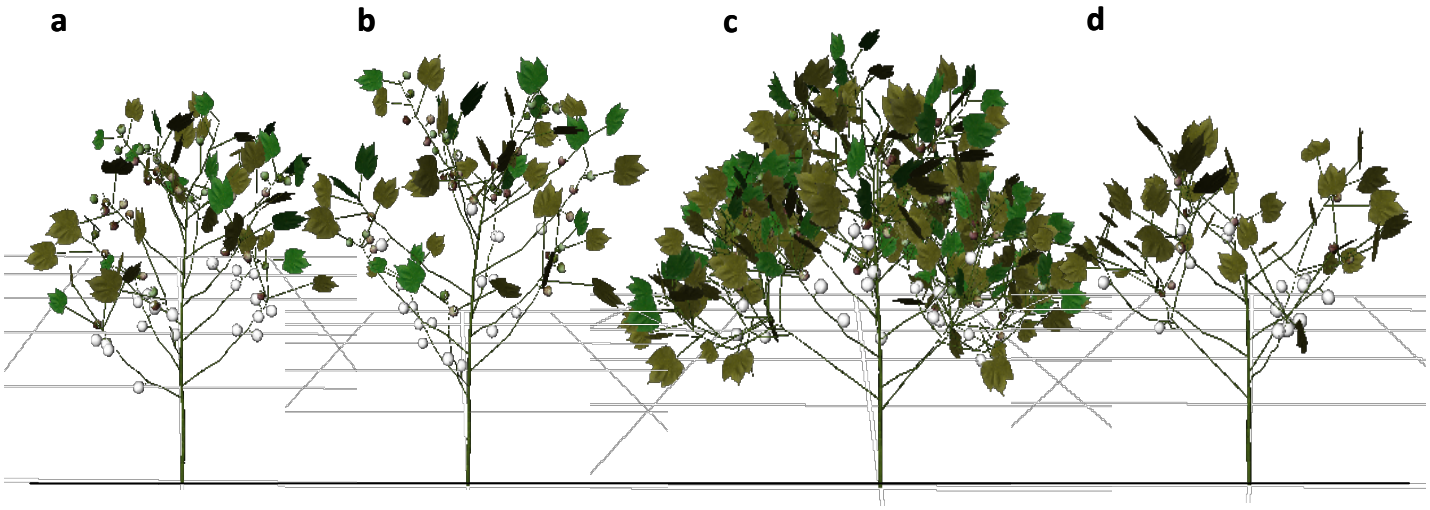

Fig. 3. Visual comparison between MC (a) and no MC application (b), without vegetative branches at a population density of 4.5 plants m^{-2}; between normal (c) and earlier (d) cut-out time with vegetative branches at a population density of 3 plants m^{-2}.

RESULTS AND DISCUSSION

MC application resulted in more compact plants, which is evident from the reduced internode length (Fig.1a). Internodes were also thinner under MC application, as well as at high population densities (Fig. 1b). The model simulated leaf area development and fruit numbers satisfactorily, although proper validation still needs to be performed. Plant compactness as a result of MC application can be observed from the visual output of the model (Fig. 3a, b), as well as the effect of early top and side cutting (Fig. 3c, d).

From these preliminary results we conclude that the model well simulates development of cotton structure as affected by sowing time and agronomical practices. Validation based on independent data will be done. The model can be applied as a systematic tool to explore the interaction between crop structure and functioning, and to optimize agronomic managements related to the morphology and productivity. However, to properly address such questions the FSPM still requires further development, taking partitioning of dry matter and further agronomical practices into consideration.

LITERATURE CITED

de Reffye, P, Blaise, F, Chemouny, S, Jaffuel, S, Fourcaud, T, Houllier, F. 1999. Calibration of hydraulic growth model on the architecture of cotton plants. *Agronomie: Agriculture & Environment* **19**: 265-280.

Gwathmey CO, Clement JD. 2010. Alteration of cotton source–sink relations with plant population density and mepiquat chloride. *Feid Crops Research* **116**: 101-107.

Jallas, E, Cretenet, M, Martin, P, Turner, S, Sequira, R. COTONS, A new approach in crop simulation modelling. In: Donatelli, M., Stockle, C., Villalobos, F., Villar Mir, J.M. (Eds.) Proc. Internat. Symposium Modelling Cropping Systems, 21-23 June 1999, Catalonia, Spain; pp. 85-86.

Oosterhuis DM, Egilla JN 1996. Field evaluation of plant growth regulators for effect on the growth and yield of cotton. In: Dugger P, Richter D, editors. Proc. Beltwide Cotton Conf.Memphis, TN: National Cotton Council. pp. 1213–1215.

Room, PM, Hanan, JS. 1995. Virtual cotton: a new tool for research, management and training. In: Constable, G.A., Forrester, N.W. (Eds.), Challenging the Future: Proceedings of the World Cotton Research Conference—1; Brisbane. CSIRO Publishing, Melbourne, pp. 40-44.

Vos J, Evers JB, Buck-Sorlin GB, Andrieu B, Chelle M and de Visser PHB. 2010. Functional–structural plant modeling: a new versatile tool in crop science. *Journal of Experimental Botany* **61**:2101-2115.

Zhao D, Oosterhuis DM. 2000. Pix Plus and Mepiquat Chloride Effects on Physiology, Growth, and Yield of Field-Grown Cotton. *Journal of Plant Growth Regulation* **19**: 415-422.

Proceedings of the 7th International Conference on Functional-Structural Plant Models, Saariselkä, Finland, 9 - 14 June 2013. Eds. Risto Sievänen, Eero Nikinmaa, Christophe Godin, Anna Lintunen & Pekka Nygren. http://www.metla.fi/fspm2013/proceedings. ISBN 978-951-651-408-9.

Model assisted phenotyping of the source-sink relationships underlying the genetic diversity of sugarcane productivity

Delphine Luquet[1*], Matthieu Gouy[2], Lauriane Rouan[1], Jean Francois Martiné[3], Eric Gozé[3], Audrey Thong-Chane[2], Jean-Christophe Soulié[1]

[1] *CIRAD, UMR AGAP, Avenue d'Agropolis, F-34398 Montpellier cedex 5*

[2] *eRcane - BP315 -97494 Ste-Clotilde - La Réunion – France*

[3] *CIRAD, UR102, Avenue d'Agropolis F-34398 Montpellier cedex 5*

**correspondance:* luquet@cirad.fr

Highlights: Ecomeristem, FSPM simulating sugarcane morphogenesis and plasticity depending on its nutritional status (C, H20), was used to analyze the genetic diversity of source-sink related traits controlling structural vs. non structural carbohydrate accumulation and thus sugar production. Results are discussed with respect to the challenge of FSPM assisted phenotyping and breeding.

Keywords: Model assisted phenotyping; complex traits; sugarcane production

Sugarcane productivity depends on its capacity to produce big plants that accumulate high quantity of sucrose per unit of stem volume. Accordingly sugar production is a complex trait resulting from dynamic C source-to-sink relationships and trade-offs within the plant. Up to now, sugarcane breeding largely focused on the observation of stem sweetness and size at harvest, without considering the processes that dynamically determine both structural and non structural carbohydrate accumulation.

FSPM are particularly relevant to formalize such complex source-sink relations. They can be useful to simulate and apprehend the diversity of phenotypes emerging from such hidden trade-offs among traits, depending on the genotype and its environment. Up to now the usefulness of model assisted phenotyping in the context of genetic studies was demonstrated only for models dealing with simple traits (Reymond *et al.* 2003). The application of complex trait models is reported as more challenging but crucial for two reasons (Luquet *et al.* 2012; Quilot *et al.* 2005): (i) complex trait phenotyping requires not only their dissection in simpler traits but also the identification of linkage(s) among them; (ii) similarly the subsequent exploration of plant ideotypes (combining traits to optimize plant behavior in a given environment) implies that such (genetic, physiological) linkages are accounted for.

Recently, *Ecomeristem*, a FSPM simulating rice plant vegetative morphogenesis (topology, biomass allocation, C storage/mobilization) and its plasticity depending on its nutritional status (C, H20), was used to analyze the genetic diversity of traits controlling rice early vigor. Model parameters controlling plant morphogenesis and source-sink relations were used to cluster and understand the behaviors met in the studied rice diversity panel and explore ideotypes (Luquet *et al.* 2012). In the context of DELICAS, project aimed to identify the genetic bases of sugarcane production, *Ecomeristem* was adapted to sugarcane. The present study aims at presenting this model version and its application for exploring the genetic diversity of the source-sink processes controlling sugarcane productivity. Once validated and tested on a panel of 20 genotypes, the model was used for phenotyping a diversity panel of 200 genotypes contrasting for morphology (leaf and internode size, tillering) and sweetness. The results highlight the opportunity and limits of the approach toward applications in a breeding context.

REFERENCES

Luquet D, Soulié JC, Rebolledo MC, Rouan L, Clément-Vidal A, Dingkuhn M. 2012. Developmental dynamics and early growth vigour in rice 2. Modelling genetic diversity using Ecomeristem. *Journal of Agronomy and Crop Science*, 14pp.

Quilot B, Kervella J, Genard M, Lescourret F. 2005. Analysing the genetic control of peach fruit quality through an ecophysiological model combined with a QTL approach. *Journal of Experimental Botany* **56**: 3083–3092.

Reymond M, Muller B, Leonardi A, Charcosset A, Tardieu F. 2003. Combining Quantitative Trait Loci analysis and an ecophysiological model to analyse the genetic variability of the responses of maize leaf growth to temperature and water deficit. *Plant Physiology* **131**: 664-675.

Proceedings of the 7th International Conference on Functional-Structural Plant Models, Saariselkä, Finland, 9 - 14 June 2013. Eds. Risto Sievänen, Eero Nikinmaa, Christophe Godin, Anna Lintunen & Pekka Nygren. http://www.metla.fi/fspm2013/proceedings. ISBN 978-951-651-408-9.

Modelling the colonization of the decay fungus *Heterobasidion annosum* in Scots pine (*Pinus sylvestris* L.) root system

Jari Perttunen[1*], Risto Sievänen[1], Tuula Piri[1], Tuomo Kalliokoski[1]
[1]*Finnish Forest Research Institute, Vantaa Res. Ctr, P.O. BOX 18, 01301 Vantaa, Finland*
**correspondence*: jari.perttunen@metla.fi

Highlights: We have constructed a three dimensional model that gives us structural information about the Scots pine root systems in a forest stand and the spatial distribution of roots in that stand. The model allows us to make predictions how fast *Heterobasidion annosum sensu stricto* colonises the pine roots, transmits from one root system to another and to recreate the distribution patterns of the pathogen in time and space.

Keywords: boreal forest, root architecture, *Pinus sylvestris*, *Heterobasidion annosum*

Heterobasidion species are economically the most destructive forest pathogens of conifers in Finland. It is estimated that annual losses caused by *H. parviporum* and *H. annosum s. str.* are about 50 million euros of which 90% are damages on Norway spruce (*Picea abies* L. Karst.) and 10% on Scots pine. The primary infection happens in summer, when the basidiospores of *Heterobasidion spp*. are released. The airborne spores infect freshly cut stumps when falling on them. The fungal mycelium then colonises the stump and spreads into root system. In pine roots, the fungus may spread up to 2.0 m per year. The fungus cannot grow freely in soil. Instead, it relies on root contacts and grafts to infect adjacent trees. Spreading of the fungus in pine stands results first in infection of individual trees and later groups of trees. Severe infection leads to the death of the trees (Risbeth 1950, 1951).

In this work we utilize a three dimensional structural model for woody root system for Scots pine (Kalliokoski et.al. 2010). This model describes the root system as a branching structure and it has been implemented as a part of the LIGNUM model (Fig. 1.). The model needs as input the characteristics of the main roots connected to the stump: diameter, length to the first branching point and spatial orientation. We have added geometrical algorithms to calculate the distance between any two root segments (Fig. 2.) and the existence of root contacts. In addition, the root model has a new module that describes the spread of the fungus in an infected root system. Furthermore the new module implements the transfer of the fungus to another root system in case of root contacts or if two root segments are close enough. With these new modelling components it is possible assess the colonization dynamics of *H. annosum* both in a single Scots pine root system and in a forest stand.

LITERATURE CITED

Kalliokoski, T, Sievänen, R, Nygren P. 2010. Tree roots as self-similar branching structures; Axis differentiation and segment tapering in coarse roots of three boreal forest tree species. *Trees* **24**: 219-236.

Rishbeth, J. 1950. Observations on the biology of *Fomes annosus*, with particular reference to East Anglian pine plantations. I The outbreaks of disease and ecological status of the fungus. Annals of Botany **14**: 365-383.

Rishbeth, J. 1951. Observations on the biology of *Fomes annosus*, with particular reference to East Anglian pine plantations. II Spore production, stump infection, and saprophytic activity in stumps. Annals of Botany **15**: 1-21

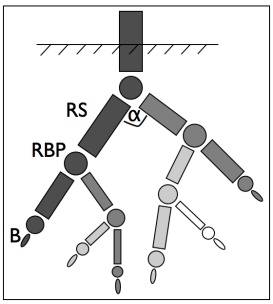

Fig. 1. Schematic presentation of the bifurcating root system: RS=root segment, RBP= root branching point, B=bud, α=branching angle. Shades of grey denote branching orders.

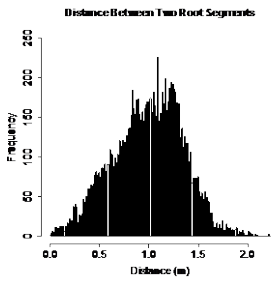

Fig. 2. Distance between two root segments in a set of two root systems. The transfer of *H. annosum* between them is possible but unlikely: segments must be connected or no more than few millimetres apart.

Proceedings of the 7th International Conference on Functional-Structural Plant Models, Saariselkä, Finland, 9 - 14 June 2013. Eds. Risto Sievänen, Eero Nikinmaa, Christophe Godin, Anna Lintunen & Pekka Nygren. http://www.metla.fi/fspm2013/proceedings. ISBN 978-951-651-408-9.

StressMaster: a web application for dynamic modelling of the environment to assist in crop improvement for drought adaptation

Karine Chenu[1], Al Doherty[2], Greg J. Rebetzke[3], Scott C. Chapman[3]
[1] *The University of Queensland, QAAFI, 203 Tor Street, Toowoomba, 4350 Queensland, Australia*
[2] *Agri-Science Queensland, DAFF, QPI&F, APSRU, 203 Tor Street, Toowoomba, 4350, Australia.*
[3] *CSIRO Plant Industry, PO Box 160, Canberra, ACT 2601*
[4] *CSIRO Plant Industry, QBP, 306 Carmody Road, St. Lucia, 4067 Queensland, Australia*
**correspondence:* karine.chenu@uq.edu.au

Highlights: Drought frequently limits crop production. A modelling approach was used to characterise the water deficit that wheat plants experience over the cropping season in targeted environments. Using this insight, the StressMaster application assists in decision-making in managed environment trials to increase the probability of attaining a seasonal drought pattern that represents the targeted environments.

Keywords: Environment characterisation, drought, water deficit, mega-environment, wheat, APSIM model, StressMaster.

INTRODUCTION

While a multitude of studies are proclaiming the identification of new genes or QTL for improved abiotic-stress tolerance, a significant contribution from these findings to released varieties is yet to be realised (e.g. Richards et al., 2010). Phenomics platforms are being developed to provide new insights into gene function and environmental responses (e.g. Granier et al., 2006) but the number of genotype x environment combinations to be tested is beyond the capacity of any platform. Drought affects gene expression and physiological processes to a different extent depending on the timing and the intensity of the stress (e.g. Fischer et al., 2011). As a consequence, genes and traits can have positive or negative effect on yield, depending on the environment (e.g. Chenu et al., 2009; Tardieu, 2012), highlighting the need to phenotype in the target environments whenever possible. Within a limited geographic area, spatial and temporal variations in rainfall occurring over diverse soil types gives rise to an almost unlimited number of drought patterns that crops might experience. There is thus a need to characterise the environment of the 'target populations of environments' (TPE) to identify major stress patterns and provide focus to research and breeding experiments (e.g. Chapman et al., 2000).

In the case of complex abiotic stress(es) such as drought, environment characterisation is difficult given that (i) plants are sensitive to a water deficit during most of their growth cycle, with different processes involved at different stages, so that a characterisation over time is required; (ii) the stress is influenced by the crop itself (i.e. by plant growth and transpiration, and by any factors that may affect them), the soil characteristics and water supply (rainfall, irrigation), which makes the stress pattern difficult to quantify (timing and intensity) even at a local scale; and (iii) both soil characteristics (e.g. available soil water) and rainfall patterns vary spatially and over time, which makes characterisation challenging over long-term periods and large geographic areas.

Modelling tools open opportunities to resolve this challenge, as they can be applied to multi-site long-term characterisation, thus leading to more comprehensive environmental sampling than conventional field studies (e.g. Hammer and Jordan, 2007). Secondly, they allow the simulation of the stress *per se* by accounting for the interactions between the plants and their environments (*e.g.* Chelle et al., 2005; Chenu et al., 2007 and 2008). By capturing the feedback between plant growth and soil water depletion, a functional modelling approach has been shown to characterise water deficits better than standard indices based on climatic data (Muchow et al., 1996).

The aim of this study was to analyse the drought patterns of wheat crops across the large and contrasting Australian wheatbelt TPE over 123 years. The goals were to (i) identify the nature of the main water deficits (timing, duration, intensity), (ii) analyse the spatial and seasonal variation in frequency of occurrence of the main water-deficit patterns, and (iii) develop an application to assist in-season water management and target representative stress in field trials.

SIMULATIONS

The APSIM crop model (e.g. Keating *et al.*, 2003) was used to simulate crop drought patterns for the check variety 'Hartog' across the Australian wheatbelt over 123 years. To represent the Australian wheat cropping system, the major production area was divided into 22 regions and 60 locations, each representing between 130 000 and 230 000 hectares of planted wheat (averaged data from 1975-2000, 2005 and 2006; source: Australian Bureau of Statistics). The simulations used weather records for 1889-2011 (SILO Patched Point Dataset; http://www.longpaddock.qld.gov.au/silo/).

The daily drought pattern was calculated for each crop based on a water-deficit index ("water supply/demand ratio") which indicates the degree to which the soil water extractable by the roots ("water supply") is able to match the potential transpiration ("water demand"). For each environment (site x year x sowing date x initial soil water x climatic scenario), this daily index was centred around flowering and averaged over 100°Cd from emergence to 450°Cd after flowering. A statistical analysis was used to cluster the seasonal water-deficit patterns into a few environment types.

Developed to allow water-management at irrigated trials, the APSIM-based web-application 'StressMaster' simulates the drought pattern that wheat crops have experienced in a specific trial up to the current date and predicts the likely future drought pattern for the remainder of the season based on historical climatic records. Different irrigation and fertilisation scenarios can be tested in the application to assess their influence on future drought events. The crop-cycle stress patterns for each scenario are classified based on which environment type they were most similar to, i.e. based on the minimum sum of squared differences between the water-deficit pattern under consideration compared to the water-deficit pattern of the environment types. Users can then decide which management scenario to apply to their trial to increase their chance to obtain the desired experimental environment type.

RESULTS AND DISCUSSION

In characterising the target population of environments, four main drought-environment types that contrasted in the timing and intensity of the stress were identified across the wheatbelt (Fig. 1). The frequency of these environment types was subject to spatial (Fig. 2) and temporal variation (data not shown), with a tendency for higher frequency of severe stresses during the last decade (Chenu et al., 2013).

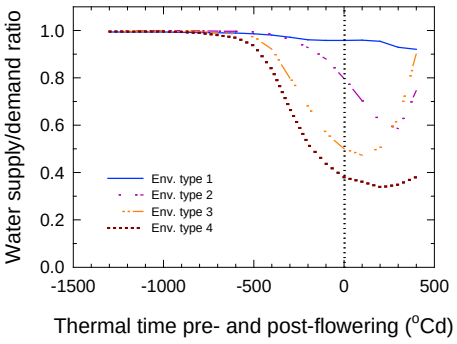

Fig. 1. Simulated water-stress index for the four environment types identified across the Australian wheatbelt. The stress index corresponds to the ratio of soil water supply to crop water demand and is represented. Adapted from Chenu et al. (2013).

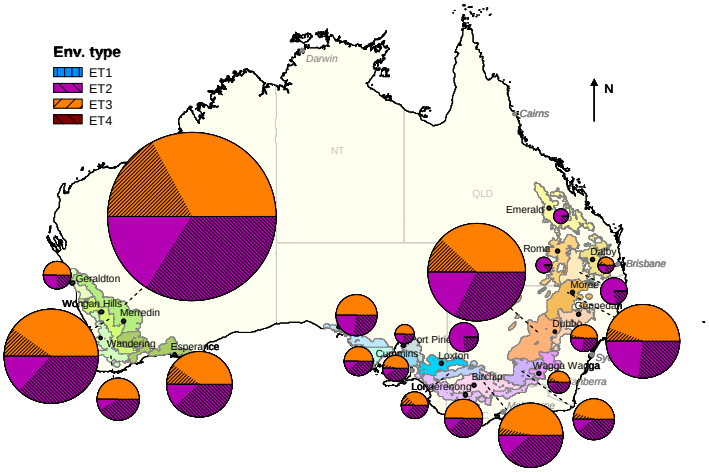

Fig. 2. Map of the frequencies of each environment type (pie charts) across the Australian wheatbelt. Data simulated for the check variety Hartog over 123 years for the different regions of the wheatbelt. The size of the pie charts is proportional to the wheat-planted area in the associated region. Adapted from Chenu et al. (2013).

High spatial and temporal variations in rainfall in Australia present a risk for plant breeders, who typically select germplasm based on 3-5 years of multi-site trials, i.e. based on environment conditions which may differ greatly to the conditions that newly released cultivars will experience during the 5-20 years of their commercial life. Environmental characterisation can help reduce this risk by assisting in (i) selecting trial locations (e.g. Trethowan et al., 2003; Rebetzke et al., 2013); (ii) weighting genotype performance by the

representativeness of their growing environment with respect to the TPE; (iii) unravelling genotype-environment interactions to better interpret genotype performance in the main environment types (e.g. Löffler et al., 2005; Chenu et al., 2011).

In order to quantify the value of genes, traits and germplasms in target environments, modelling can also help design managed drought environments within breeding programs or physiology/genetics based research projects (*e.g.* Bänziger et al., 2006; Rebetzke et al., 2013). The StressMaster application has been implemented to assist management decision-making and increase the probability of attaining the desired environment types (Fig. 3). Based on information concerning the soil, the climate (weather station in the field or nearby), the genotype, and the management used (*e.g.* sowing date, depth, fertilisation), StressMaster simulates in "real time" the drought pattern that plants have experienced up to "today", and predicts their future drought pattern based on historical climatic records used for the rest of the season. The application is being used to define irrigation regimes at the national (GRDC funded) Managed Environment Facilities in Australia, where wheat benchmarking germplasm and diverse populations varying for potential adaptive traits are currently phenotyped (Rebetzke et al., 2013).

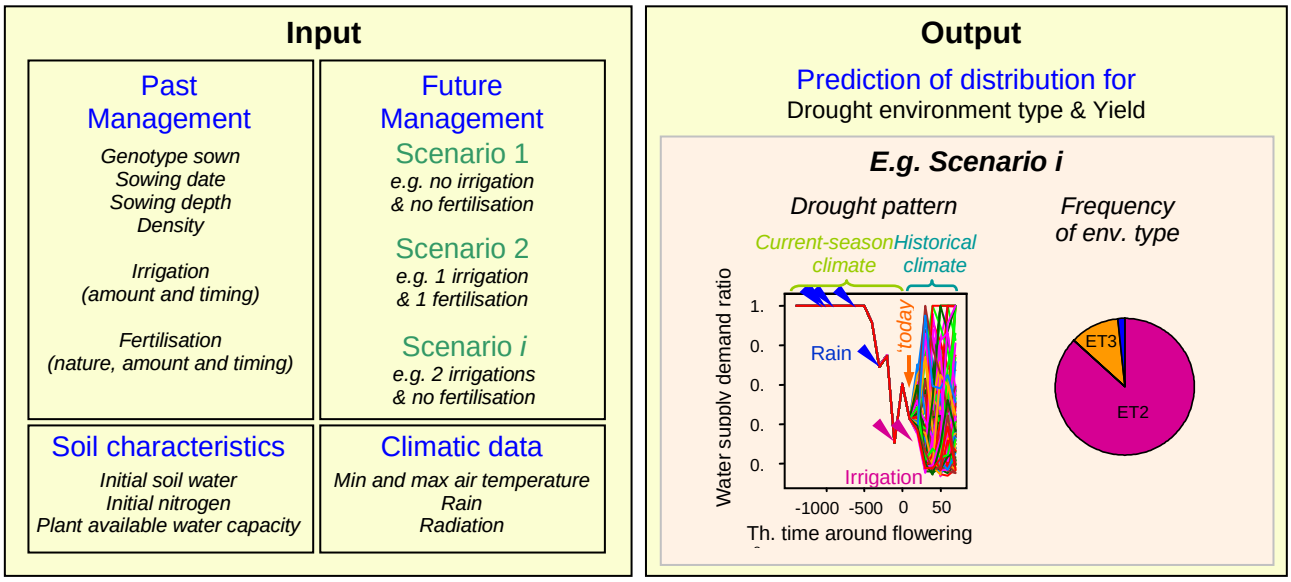

Fig. 3. Schematic view of the StressMaster application where soil, climatic and management information are input to simulate in 'real time' the frequency of drought-environment type and the yield distribution for various irrigation-fertilisation scenarios.

LITERATURE CITED

Bänziger M, Setimela PS, Hodson D, Vivek B. 2006. *Agricultural Water Management* **80**: 212-224.

Chapman SC, Cooper M, Hammer GL, Butler DG. 2000. *Australian Journal of Agricultural Research* **51**: 209-221.

Chelle M. 2005. *New Phytologist* **166**: 781-790.

Chenu K, Chapman SC, Tardieu F, McLean G, Welcker C, Hammer GL. 2009. *Genetics* **183**: 1507-1523.

Chenu K, Cooper M, Hammer GL, Mathews KL, Dreccer MF, Chapman SC. 2011. *Journal of Experimental Botany* **62**: 1743-1755.

Chenu K, Deihimfard R, Chapman SC. 2013. *New Phytologist* doi: 10.1111/nph.12192.

Chenu K, Franck N, Lecoeur J. 2007. *New Phytologist* **175**: 472-481.

Chenu K, Rey H, Dauzat J, Lydie G, Lecoeur J. 2008. *Functional Plant Biology* **35**: 850-866.

Fischer RA. 2011. *Crop & Pasture Science* **62**: 95-114.

Granier C, Aguirrezabal L, Chenu K, Cookson SJ, Dauzat M, et al. 2006. *New Phytologist* **169**: 623-635.

Hammer GL, Jordan DR. 2007. In: Spiertz JHJ, Struikc PC, van Laar HH, eds. *Scale and complexity in plant systems research: gene-plant-crop relations.* Wageningen UR-Frontis Series No. 21. Dordecht, The Netherlands: Springer: 45-61.

Keating BA, Carberry PS, Hammer GL, Probert ME, Robertson MJ, et al. 2003. *European Journal of Agronomy* **18**: 267-288.

Löffler CM, Wei J, Fast T, Gogerty J, Langton S, et al. 2005. *Crop Science* **45**: 1708-1716.

Muchow RC, Cooper M, Hammer GL. 1996. In: Cooper M, Hammer GL, eds. *Plant adaptation and crop improvement*: CAB International, Wallingford, 349-364.

Rebetzke GJ, Chenu K, Biddulph B, Deery DM, Moeller C, et al. 2013. *Functional Plant Biology*. 40: 1-13.

Richards RA, Rebetzke GJ, Watt M, Condon AG et al. 2010. *Functional Plant Biology* **37**: 85-97.

Tardieu F. 2012. *Journal of Experimental Botany* **63**: 25-31.

Proceedings of the 7th International Conference on Functional-Structural Plant Models, Saariselkä, Finland, 9 - 14 June 2013. Eds. Risto Sievänen, Eero Nikinmaa, Christophe Godin, Anna Lintunen & Pekka Nygren. http://www.metla.fi/fspm2013/proceedings. ISBN 978-951-651-408-9.

Arbuscular mycorrhizal fungi (AMF) diversity obtained from gooseberry plantations (*Physalis peruviana*) in the Colombian Andean region

Ramírez-Gómez Margarita[1], Oehl Fritz[2], Pérez Adrian [1] and **Rodríguez Alia[3]**
[1]Colombian Corporation of Agricultural Research, CBB. Mosquera, Cundinamarca, [2]Agroscope Reckenholz-Tänikon ART, 3 Universidad Nacional de Colombia, Bogotá
**correspondence:* mramirezgomez@gmail.com

Highlights: This research focused on determining the relationship between arbuscular mycorrhizal fungal diversity and soil physical -chemical properties, in gooseberry plantations in Andean Mountains from 1500 to 2700 m.a.s.l. The spore abundance, spore morphotype and diversity index were determined and analyzed through multiple regression. It was possible determine that some soil conditions affect the abundance and diversity of AMF.

Keywords: Arbuscular mycorrhizal fungi, ecotype diversity, spore abundance, Andean soils,

Arbuscular mycorrhizal fungi (AMF) are able to establish association with 80% of plants which are components of most terrestrial ecosystems and agro-ecosystems (Smith and Read, 2008). Knowledge regarding the diversity and variability of AMF in specific ecosystems is the basis for pre-selection in application programmes to optimize the symbiosis (Hector *et al*., 2001; Kogel **,** 2008). The objective of the present work was to evaluate the diversity of AMF in soils below gooseberry, in a transect from 1500 to 2700 m above sea level, in the Andean area where the edaphic-climatic differences are quite high. A total of 10 pooled soil samples were collected from gooseberry plantations during dry and rainy seasons. Chemical and physical soil analysis, were performed in order to establish the relationship between soil characteristics and AMF diversity. In addition, spore abundance, diversity index, presence of morphotypes (Noss, 1990), and arbuscular mycorrhizal genus or species were recorded. Spores morphology was used for taxonomic identification. The results showed natural colonization by AMF in all of the soils evaluated. Forty eight AMF species and 22 morphotypes were identified from the area of study, reflecting high diversity present in tropical mountain areas. Spore abundance ranged between 20 and 120 g^{-1} of soil, in wet season and between 387 and 1531 spores g^{-1} soil in dry season. In rainy season 15 morphotypes and 33 species of AMF were identified, while in dry season 22 morphotypes and 48 species of AMF were found. Multiple regression showed, for rainy season, that spore abundance was reduced significantly with altitude (by-56.4%), soil clay content (by-12,7%) and soil compaction at 10 cm deep (by-15%) and that it was increased significantly in soils with high Ca and Mg content (by + 8%) and S content (by +3.8%). By contrast, for dry season, spore abundance only shows a negative relation with soil cation exchange capacity (by -37%), soil compaction at 5 cm depth (by -33.6%) and soil pH (by -8%) as reported by Horn and Lebert, 1994, Nadian *et al*., 1997 and Serralde and Ramírez, 2004. Diversity indexes (Shannon, Simpson Index) were affected by Ca, Mg and K content in soils (by 30%). Results allow us to confirm that there is a clear effect of some physical and chemical soil characteristics, in the composition of the community of AMF associated to gooseberry plantation in the Andean Mountains of Colombia.

LITERATURE CITED

Hector A, Joshi J, Lawler SP, *et.al* , 2001. Conservation implications of the link between biodiversity and ecosystem functioning. *Oecologia* **129**, 624–628.

Kogel KH, 2008. Compatible host–microbe interactions: Mechanistic studies enabling future agronomical solutions *Journal of Plant Physiology* **165**, 1-8

Horn R, Lebert M. 1994. Soil compactability and compressibility. In: Soon, S.D., Ouwerkerk, C.van. Eds., Soil Compaction in Crop Production. Elsevier Publishers, Amsterdam, The Netherlands, pp. 45-69

Nadian H, Smith S, Alston A, *et.al,* 1997. Effects of soil compaction on plant growth, phosphorus uptake and morphological characteristics of AMF colonization of *T. subterraneum*. *New Phytol*. **135**, 303-311.

Noss RF, 1990. Indicators for monitoring biodiversity: a hierarchical approach. *Conserv. Biol*. **4**, 355–364.

Smith SE, Read DJ. 2008. Mycorrhizal symbiosis. Academic Press, London.

Serralde AM, Ramírez M. 2004. Análisis de poblaciones de micorrizas en maíz *(Zea mays)* cultivado en suelos ácidos bajo diferentes tratamientos agronómicos. *Revista Corpoica* **5**,1: 31-40.

Proceedings of the 7th International Conference on Functional-Structural Plant Models, Saariselkä, Finland, 9 - 14 June 2013. Eds. Risto Sievänen, Eero Nikinmaa, Christophe Godin, Anna Lintunen & Pekka Nygren. http://www.metla.fi/fspm2013/proceedings. ISBN 978-951-651-408-9.

Adaptation of timber plantations (*Gmelina arborea* and *Pachira quinata*) with Arbuscular Mycorrhizal Fungi in the Caribbean region, Colombia

Ramírez-Gómez Margarita[1], Roveda-Hoyos Gabriel[2], Baquero-Maestre Cesar[1], Martinez-Atencia Judith[1], Gutiérrez Braulio[2] and Rodríguez Miguel[3]

[1]Colombian Corporation of Agricultural Research, CBB. Mosquera, Cundinamarca. [2]Department of Agronomy, PO Box 14490, National University of Colombia, Bogotá. [3] Pizano S.A.

**correspondence:* mramirezgomez@gmail.com

Highlights: The objective was select for timber plantations, the best interaction with arbuscular mycorrhizal fungi (AMF) considering both, agronomic and economic aspects, in order to get forest systems well adapted to the Caribbean Region. Four AMF genera (*Glomus, Acaulospora, Scutellospora* and *Gigaspora*) and 20 ecotypes were identified from the area of study, reflecting the high diversity present in tropical area.

Keywords: Arbuscular mycorrhizal fungi, ecotypes diversity, Caribbean soils, *Gmelina arborea, Pachira quinata*.

SUMMARY

The adaptation of timber plantations in the tropical Caribbean region is a good alternative for reforestation and land recovery for reducing pressure on natural forests, improving timber availability and the profitability for producers (Habte, *et. al,* 2001, Kogel, 2008, Kuypert. *et.al.,* 2004, Kernaghan,2005). This research consider both, agronomic and economics aspects in order to select the best AMF-plant association, adapted to the Caribbean area. For the evaluation the diversity of AMF in soils with *Gmelina arborea and Pachira quinata* plantations, almost 100 soil and root samples were collected during dry and rainy seasons. Chemical and physical soil analyses were performed in order to establish the relationships between soil characteristics and AMF diversity. Four AMF genera (*Glomus, Acaulospora, Scutellospora* and *Gigaspora*) and 20 ecotypes were identified from the area of study, reflecting the high diversity present in tropical forest, as was reported previously (Habte *et al*., 2001). There was high variation in spore count, between 1 to 121/g of soil, with a predominance of the *Glomus spp* not only in terms of abundance, but also in diversity. This result confirms *Glomus* plasticity and adaptability to different environments. In order to evaluate the effects of association between *Gmelina arborea* and *Pachira quinata* with 6 mixed isolates of AMF (4 native and 2 introduced + 50% of fertilizers), compared with controls with different doses of fertilization, 10, 50 and 100%, in a randomized complete blocks design, with three repetitions. Forest species showed high dependency of association with AMF and differential response linked with specific type of AMF isolated (Habte et al, 2001, Cardoso and Kuyper, 2006, Bainarda *et al*, 2010). The AMF association showed several benefits for timber plantations, expressed in improving plant growth and reduction in chemical fertilizers application (up to 50%) and in the cost of seedling production in 19%, for both plantation *G. arborea* and *P. quinata*, as consequence of the reduction of 37 days for the seedling under greenhouse. The biofertilization with native AMF in timber plantation should be included in the establishment model for improving to wood access and the profitability for producers.

REFERENCES

Bainarda L, Klironomos BJ, Gordon A. 2010. Arbuscular mycorrhizal fungi in tree-based intercropping systems: A review of their abundance and diversity. Pedobiología- Journal Homepage: www.elsevier.de/pedobi

Cardoso I, Kuyper T. 2006. Mycorrhizas and tropical soil fertility. *Agriculture, Ecosystems and Environment* **116**: 72–84

Habte M, Miyasaka SC, Matsuyama DT. 2001. Arbuscular mycorrizal fungi improve early forest -tree establisment. In. Horst et al (ed). *Plant nutrition - Food security and sustainability of agro - ecosystems*. 644-645. Kluwer Academia Publishers. Netherlands.

Kernaghan G. 2005. Mycorrhizal diversity: Cause and effect? *Pedobiologia* **49**: 511-520

Kogel KH. 2008 Compatible host-microbe interactions: Mechanistic studies enabling future agronomical solutions *Journal of Plant Physiology* **165**: 1-8.

Kuypert W, Cardoso I, Onguene NA., *et.al.* 2004. Managing Mycorrhiza in tropical Multispecies Agroecosystems. In: *Below -ground Interactions in tropical Agroecosystems: Concepts and models with Multiple Plant Components*. CABI Publishing (ICRAF). Van Noordwijk M, Cadish C and Ong C.K. (ed) pag 243-261.

Proceedings of the 7th International Conference on Functional-Structural Plant Models, Saariselkä, Finland, 9 - 14 June 2013. Eds. Risto Sievänen, Eero Nikinmaa, Christophe Godin, Anna Lintunen & Pekka Nygren. http://www.metla.fi/fspm2013/proceedings. ISBN 978-951-651-408-9.

CyberPlantS: a European initiative towards collaborative plant modeling

Michaël Chelle[1], **Christophe Godin**[2], **Risto Sievänen**[3], **Jan Vos**[4], **Mathieu Javaux**[5], **Gerhard Buck-Sorlin**[6], **Hartmut Stützel**[7], **Ana Maria Tarquis**[8] *et al.**

[1]*INRA, France,* [2]*INRIA Virtual Plants, 34000 Montpellier, France,* [3]*Finnish Forest Research Institute, Vantaa, Finland,* [4]*Wageningen University, 6700 AK Wageningen, the Netherlands,* [5]*Université Catholique de Louvain, 1348 Louvain-la-Neuve, Belgium,* [6]*Agrocampus Ouest, 49000 Angers, France,* [7]*Leibniz Universität Hannover, 30419 Hannover, Germany,* [8]*Technical University of Madrid, 28040 Madrid, Spain*

** other contributing partners: U. of Göttingen (G), ECP (F), Forrest Research (UK), KeyGene N.V. (NL), Agralis (F), Simosol Oy (FI), CIRAD (F), IRTA (SP), Phillips Research (NL), U. of Reading (UK).*

Correspondence: chelle@grignon.inra.fr

Highlights: The current European research landscape of 3D plant modeling shows fragmentation and critically lacks coordination. The CyberPlantS initiative aims at creating the first European network on advanced plant simulation systems and associated e-infrastructure. The network will aim at innovation in computational plant modeling with a focus on plant architecture and plant-environment interactions. It is focused on the development of a new paradigm, namely cyberplants. Cyberplants refers to cybernetic systems, as biological and environmental components of vegetation exchange signals to achieve specific goals. Cyberplants also refers to cyberspace, which designates a collaborative approach based on a network community relying on a cyberinfrastructure.

Keywords: collaborative approach, modeling cyber-infrastructure

Vegetation management faces challenges arising from a shift in perception of the roles of agriculture and forestry. It is expected to ensure food security, preserve the environment (diminish pollution, preserve biodiversity), provide materials for bio-economy, improve quality of life, and substitute fossil resources. To face these challenges in an increasingly complex and rapidly changing context (climate, land use, world economy, etc), new vegetation management strategies have to be developed. In parallel to field trials, modeling and simulation tools are necessary to address such a complexity. Models have already been used for vegetation management and have proven their potential benefit. However, the development of vegetation management in the changing context of a sustainable future, where plant canopies will become spatially more heterogeneous (providing low inputs to vegetation, preserving biodiversity, developing new cropping/forestry systems like intercropping, etc) and where current statistical correlations linking the plant functioning and environment may become erroneous, will impose new constrains on vegetation models. Future models should thus be able to explicitly deal with feedback loops between individual plants and their local environment (where environment consists of the physical surrounding above and below ground, but also the biotic environment including neighboring plants).

In the 1990's, pioneering scientists recognized the importance of developing models of plant growth, which explicitly represented plant architecture in three dimensions. They started to design Functional-Structural Plant Models and associated software platforms. Emphasis on combining plant function with plant structure, irrespective of the target of the application (agriculture, horticulture, forestry), has been a cohesive force. Different modeling approaches and systems have been developed, but inter-operability among them is just beginning to emerge. The current European research on 3D plant modeling shows fragmentation and lacks coordination. Developing a European strategy in the domain of 3D plant simulations is becoming an urgent necessity. The CyberPlantS initiative aims at creating a European network on advanced plant simulation systems and associated cyber-infrastructure. This initiative gathers scientists in ecophysiology, agronomy, and forestry as well as in physics, mathematics, and computer science, for the development of a new paradigm, namely *cyberplants*. This term is intended to highlight three key aspects of the new concept: i) the term "cyberplants " refers to the cybernetics approach, which aims at studying complex, dynamical, goal-oriented systems. A cyberplant therefore consists of modular, fully interoperable and interchangeable computational components. ii) "cyberplants " refers to cyber-space, as it is intended to create a collaborative framework based on a network community and relying on an e-infrastructure. (iii) It finally refers to the future generation of students and scientists who are subjected to live in an increasing digital world.

Proceedings of the 7th International Conference on Functional-Structural Plant Models, Saariselkä, Finland, 9 - 14 June 2013. Eds. Risto Sievänen, Eero Nikinmaa, Christophe Godin, Anna Lintunen & Pekka Nygren. http://www.metla.fi/fspm2013/proceedings. ISBN 978-951-651-408-9.

Modeling parthenium weed early canopy architecture in response to environmental factors and the impacts on biological control activity of the summer rust

Ruey Toh[1], **Kunjithapatham Dhileepan**[3], **Roger G. Shivas**[3], **Steve W. Adkins**[1] and **Jim Hanan**[2]
[1] *The University of Queensland, Tropical and Subtropical Weeds Research Unit, School of Agriculture and Food Sciences, St Lucia, QLD 4072, Australia,* [2] *The University of Queensland, Queensland Alliance for Agriculture and Food Innovation, Biological Information Technology, St Lucia, QLD 4072, Australia,* [3] *Biosecurity Queensland, Department of Agriculture, Fisheries and Forestry, 41 Boggo Road, Dutton Park, QLD 4102, Australia*
**correspondence:* ruey.toh@uqconnect.edu.au

Highlights: An L-systems based 3D canopy architecture model is created for simulating and visualising the early growth of parthenium weed in response to four environmental factors (temperature, CO_2, soil moisture and plant density) and the activity of the summer rust. The outcomes provide a tool to help study the interaction between an invasive weed, a biological control agent and the environment.

Keywords: L-systems, 3D model, canopy architecture, Parthenium hysterophorus, Puccinia xanthii var. parthenii-hysterophorae, environment

INTRODUCTION

Parthenium weed (*Parthenium hysterophorus* L., Asteraceae) is an annual invasive species found across five continents with the potential to invade many more regions (McConnachie et al., 2011). With its characteristics of strong suppression and allergy, parthenium weed affects agriculture, natural ecosystems, and human and animal health (Navie et al., 1996). Management of parthenium weed is most effective if undertaken on young plants. Due to the ability of parthenium weed to adapt to environmental changes through alterations in its physiology, morphology and life cycle, it is becoming more vigorous and prolific (Nguyen, 2011; Shabbir, 2012) and difficult to control. Biological control agents are an important component of the current management strategy for parthenium weed. However these organisms are also affected by environmental changes. Research into the interaction between parthenium weed, biological control agents and the environment has been undertaken for certain insects but not for fungal pathogens, specifically the summer rust (*Puccinia xanthii* var. *parthenii-hysterophorae* Seier, H.C. Evans & Á. Romero). A changed plant architecture is suggested to in turn change the activities of a pathogen (Pangga et al., 2011), but this is yet to be confirmed for the case of parthenium weed. In order to determine how the early canopy architecture of parthenium weed responds to environmental factors and how this affects activity of the summer rust, a modeling study on parthenium weed early canopy architectural development in response to a number of abiotic (temperature, CO_2, and soil moisture) and biotic (plant density) factors was conducted by creating a three-dimensional (3D) model using Lindenmayer-systems (L-systems, Lindenmayer, 1968a, b).

PARTHENIUM WEED MODEL

The impacts of four abiotic and biotic environmental factors, i.e. temperature regime (day/night 22/15, 27/20, and 32/25 ± 1 °C), CO_2 concentration (350 and 550 ppm), soil moisture level (100 and 75 % of field capacity), and plant density (one and five plants pot^{-1}) on young parthenium weed plants (up to 28 days old) were studied using controlled environment rooms (CER) at Ecosciences Precinct, Brisbane. During the experimental period, the development of the parthenium weed plant canopy architecture was tracked with a sonic digitizer. Digitized points were used to calculate the parameter inputs (i.e. leaf length and width, petiole length, and internode length) for modeling the early growth and canopy architecture of parthenium weed in response to different environmental factors. At the end of experiment, all leaves were harvested and divided into four silhouette groups according to leaf age and lobing. Visualization of each leaf was modeled using this silhouette classification and image digitization of leaves, together with a texture mapping approach using a color scanner and Adobe® Photoshop® CS3, Gimp version 2.8.2 and L-studio software. Plant development was modeled using the thermal time concept in L-systems, where cumulative degree-days and

node number were the parameters used to control maximum growth of parthenium weed plant. The initiation of a new metamer by an apex (A) forming an internode (I), a leaf (L) and a new apex repeated was activated by an L-system decomposition rule when cumulative degree-days (dd) was greater than the defined plastochron (PLASTOCHRON) in the time step:

A(treatment,dd,node):dd>PLASTOCHRON -->
I(treatment,dd-PLASTOCHRON,node)[L(treatment,dd-PLASTOCHRON,node)]
/(137.5)A(treatment,dd-PLASTOCHRON,node+1)

The correlation of plant growth to thermal time under each factor was studied by analysing the calculated plant height and total leaf area using an ANOVA General Linear Model (Minitab® 15) and a Polynomial Regression Analysis (SigmaPlot® 11.0). Three key findings were then obtained, *viz*. i) plant height and total leaf area were highly correlated with thermal time; ii) plant height was reduced under elevated CO_2 concentration ($F = 34.27$; d.f. = 1; $P < 0.01$), reduced soil moisture level ($F = 61.80$; d.f. = 1; $P < 0.01$) and an increased plant density ($F = 8.26$; d.f. = 1; $P < 0.01$) and iii) total leaf area was reduced under an increased plant density ($F = 19.23$; d.f. = 1; $P < 0.01$). As an example, a simulation and visualization of the effect of temperature regime on parthenium weed canopy architecture is shown in Fig. 1.

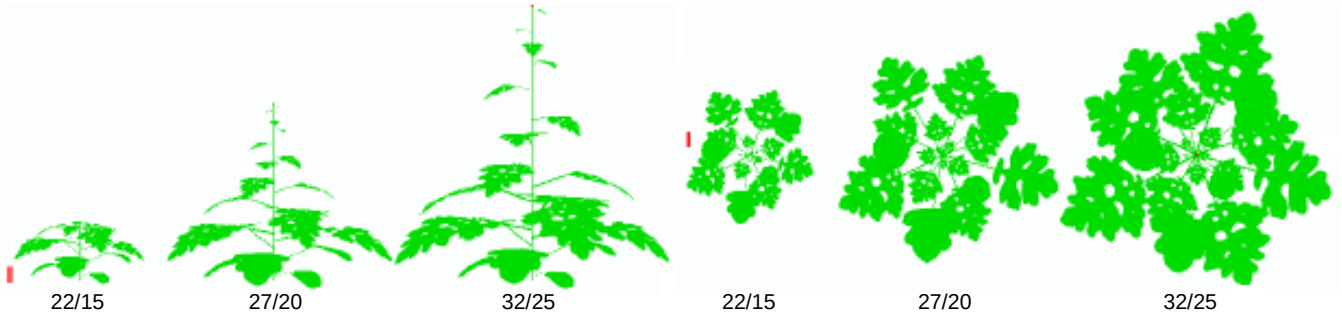

Fig. 1. Side- and top- views of the early parthenium weed canopy architecture in response to three different temperature regimes 28 days after germination. The red dot indicates the first flower formed on the plant. Red scale bar = 1 cm.

PARTHENIUM WEED MODEL INCORPORATED WITH THE SUMMER RUST DISTRIBUTION

A study of the impact of canopy architecture on the distribution of the summer rust was undertaken by spraying spore suspensions onto parthenium weed plants with different canopy architecture. At the end of experiment (*ca*. 15 days after inoculation), all leaves were carefully harvested for image digitization processing and analysis. Disease severity was calculated for each leaf as follows:

disease severity = (disease area/leaf area) * 100 %

disease area = (captured $pixels_{DA}$/pixels of the image file) * dimensions of the image file

leaf area = (captured $pixels_{LA}$/pixels of the image file) * dimensions of the image file

where 'captured $pixels_{DA}$' defined the brownish colour of pustule-like telia of the summer rust using a colour threshold with hue ranging from 10 to 25 and saturation ranging from 0 to 100, while 'captured $pixels_{LA}$' defined the green colour of parthenium weed leaves using a colour threshold with hue ranging from 40 to 110 and saturation from 0 to 100. The impact of each environmental factor on disease severity was determined using an ANOVA General Linear Model (Minitab® 15). Two key findings were then obtained, *viz*. i) similar disease severities were found similar throughout temperature regimes ($F = 1.21$; d.f. = 2; $P = 0.32$), CO_2 concentrations ($F = 0.27$; d.f. = 1; $P = 0.61$), soil moisture levels ($F = 0.52$; d.f. = 1; $P = 0.48$) and plant densities ($F = 3.77$; d.f. = 1; $P = 0.07$) and ii) size of telia was observed variable across all factors. Fig. 2 shows the outcome of incorporation of the summer rust distribution on the model shown in Fig. 1.

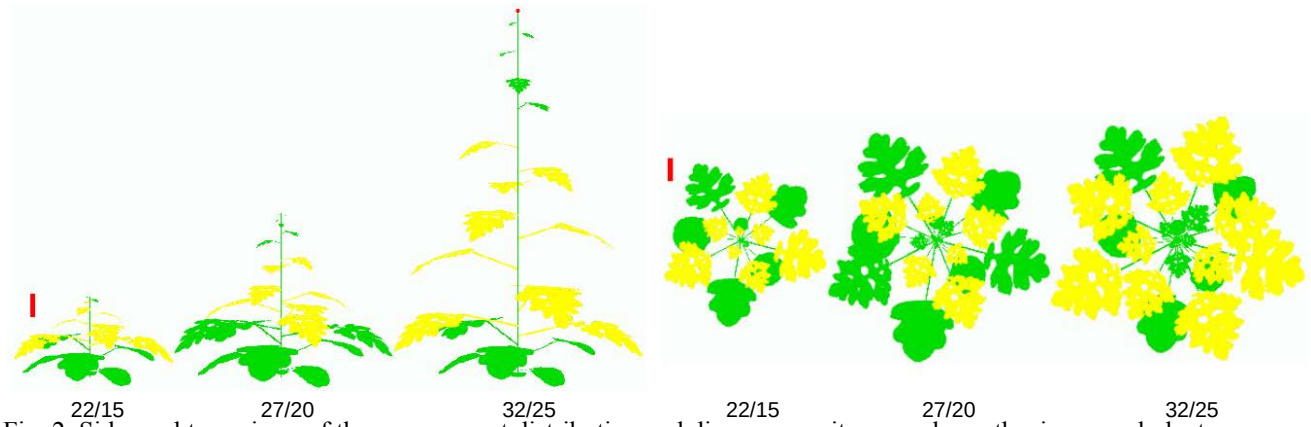

Fig. 2. Side- and top- views of the summer rust distribution and disease severity on early parthenium weed plant canopy grown at three different temperature regimes. The red dot indicates the first flower formed on the plant. Red scale bar = 1 cm. Leaves in green and yellow indicate 0 and ≤ 3 % disease severity respectively.

PERSPECTIVES

A 3D L-system based model of parthenium weed canopy architectural development has been created to provide a tool for simulation and visualization of the growth of young parthenium weed plants in response to four environmental factors (i.e. temperature, CO_2, soil moisture and plant density). The possibility of adapting this model for study of a biological control agent has also been demonstrated. Two aspects may be considered for future work in parthenium weed modeling, *viz*. i) a validation with an expanded range of environmental factors to refine the current model and ii) further modeling to simulate the development of inflorescence structures and flower and seed production. With these extensions, a better prediction may be made for not only the individual growth of parthenium weed but also the dynamic trend of its population in response to the environment over time, and thereby assist weed managers or ecologists to evaluate the risk of local parthenium weed population. In addition, two research gaps may be investigated for the summer rust, *viz*. i) modeling the spatial movement of spore and ii) modeling the epidemics and its impact on parthenium weed population over time. With these models, a better understanding in its activity of biological control will be provided. Furthermore, all these concepts can be applied to incorporate other biological control agents thereby developing a comprehensive model that simulates and predicts the interactions between parthenium weed and multiple biological control agents under a defined environment, allowing easier estimation of the effect of weed management.

LITERATURE CITED

Lindenmayer A. 1968a. Mathematical models for cellular interactions in development I. Filaments with one-sided inputs. *Journal of Theoretical Biology* **18**: 280-299.

Lindenmayer A. 1968b. Mathematical models for cellular interactions in development II. Simple and branching filaments with two-sided inputs. *Journal of Theoretical Biology* **18**: 300-315.

McConnachie AJ, Strathie LW, Mersie W, Gebrehiwot L, Zewdie K, Abdurehim A, Abrha B, Araya T, Asaregew F, Assefa F, Gebre-Tsadik R, Nigatu L, Tadesse B, Tana T. 2011. Current and potential geographical distribution of the invasive plant *Parthenium hysterophorus* (Asteraceae) in eastern and southern Africa. *Weed Research* **51**: 71-84.

Navie SC, McFadyen RE, Panetta FD, Adkins SW. 1996. The biology of Australian weeds 27. *Parthenium hysterophorus* L. *Plant Protection Quarterly* **11**: 76-88.

Nguyen TLT. 2011. *The invasive potential of parthenium weed (Parthenium hysterophorus L.) in Australia*. PhD Thesis, University of Queensland, Australia.

Pangga IB, Hanan J, Chakraborty S. 2011. Pathogen dynamics in a crop canopy and their evolution under changing climate. *Plant Pathology* **60**: 70-81.

Shabbir A. 2012. *Towards the improved management of parthenium weed: complementing biological control with plant suppression*. PhD Thesis, University of Queensland, Australia.

Proceedings of the 7th International Conference on Functional-Structural Plant Models, Saariselkä, Finland, 9 - 14 June 2013. Eds. Risto Sievänen, Eero Nikinmaa, Christophe Godin, Anna Lintunen & Pekka Nygren.
http://www.metla.fi/fspm2013/proceedings. ISBN 978-951-651-408-9.

Cotton fiber quality determined by fruit position, temperature and management

Xuejiao Wang[1], Jochem B. Evers[2], Lizhen Zhang[1]*, Lili Mao[3], Xuebiao Pan[1], Zhaohu Li[3]
[1]*College of Resources and Environmental Sciences, PO Box 10,0193 China Agricultural University, China*
[2]*Centre for Crop Systems Analysis, PO Box 430 Wageningen University, The Netherlands*
[3]*College of Agronomy and Biotechnology, PO Box 10,0193 China Agricultural University, China*
**correspondence: zhanglizhen@cau.edu.cn*

Highlights: CottonXL is a tool to explore cotton fiber quality in relation to fruit position, to improve cotton quality by optimizing cotton plant structure, as well as to help farmers understand how the structure of the cotton plant determines crop growth and quality.

Keywords: Cotton development, fiber length, fiber strength, micronaire, simulation model

INTRODUCTION

Cotton fiber quality is a critical factor determining fiber price and the quality of textile products. Fiber quality is measured mainly as fiber length, strength and micronaire (fineness). The textile industry has a preference for longer, stronger and moderate micronaire for producing high quality yards (Mishra et al. 2001). The quality of cotton fiber results from an interaction between environmental (Yeates et al. 2010), genetic (Richard et al. 2006) and management factors (Girma et al. 2007), determined by the position of and the resources obtained by each fruit. Cotton fiber quality shows a significant spatial distribution in China.

Fiber growth and development of single fruits is informative. However cotton fiber quality for all fruits depending on their position in the plant in relation to environmental factors (e.g. temperature, sowing date, pruning management, and the interaction with genetics) have not been addressed well quantitatively, due to the structural complexity of the cotton plant. The objective of this study was to quantify cotton fiber quality in response to sowing date, cut-out (removal of the shoot tip), and environment, using a functional-structural plant model (FSPM) of cotton development.

SIMULATIONS

Simulation of cotton fiber quality was implemented in CottonXL (Gu et al. 2013, this conference) by extending fruit development with routines for fiber length, strength and micronaire of each fruit. For simulation of fiber quality, the potential increase of fiber length, strength and micronaire was developed and calibrated based on field experiments. The effects of environmental factors such as daily average temperature, and the difference between maximum and minimum temperature was derived from literature.

Field experiments were conducted in 2005, 2007 and 2009 in Yangtze River region of China with different sowing dates. Potential fiber quality of cotton for single fruits was developed by using above field experiments (Fig.1). The actual increase of fiber quality was calculated by multiplying with effects of temperature.

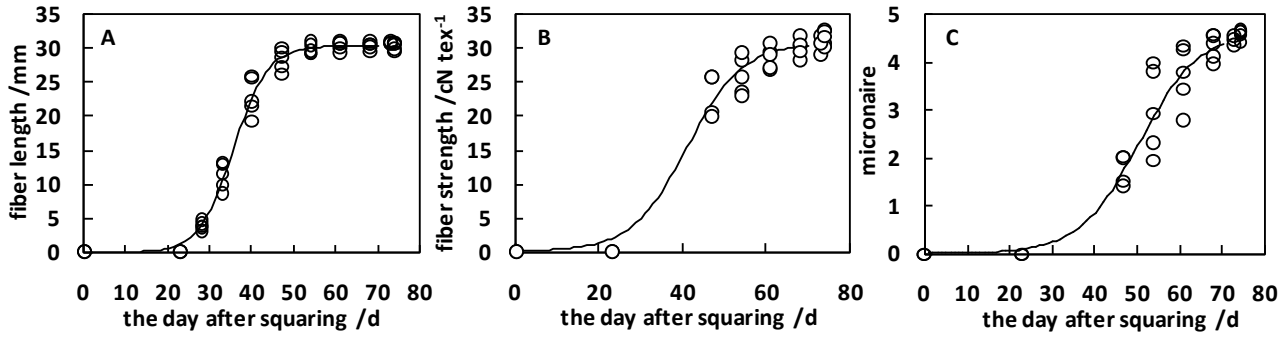

Fig.1 Relationship between fiber length (A), strength (B), micronaire (C) and fruit age in cotton

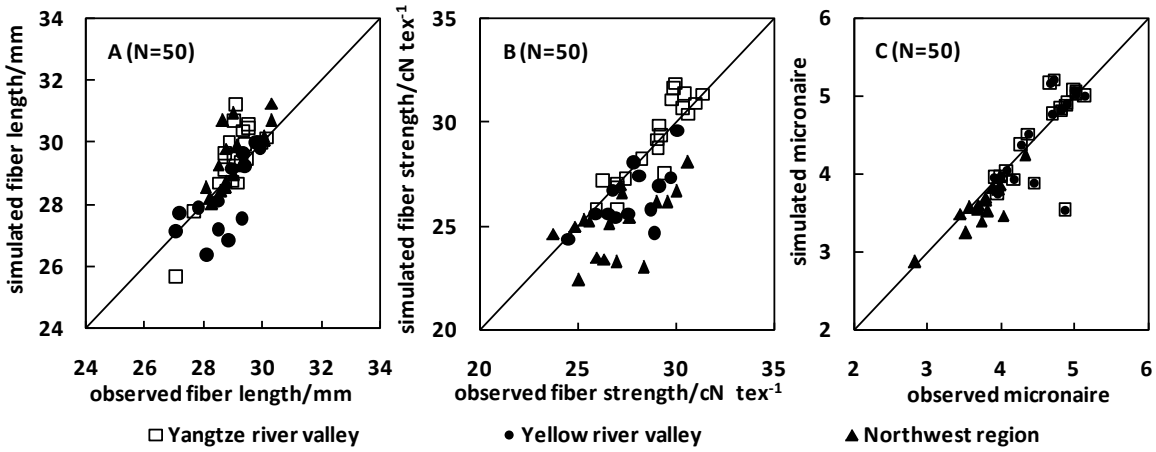

Fig.2 Comparison of observed and simulated cotton fiber length (A), strength (B) and micronaire (C)

The national-wide survey of cotton fiber quality in three cotton producing regions in China were used for model validation (Fig.2). The RMSEs between the simulated and observed values of fiber length, strength and micronaire were 1.26 mm, 2.18cN tex^{-1}, and 0.28. The REs between the simulated and observed values of fiber length, strength and micronaire were 4.45%, 7.78% and 6.8%.

The scenarios used to address the objectives included three locations at Xinjiang, Yellow River region and Yangtze River region, five sowing dates, six cut-out dates, removal versus maintenance of vegetative branches. Distribution of fiber length, strength and micronaire within the cotton crop was expressed visually as well as against cumulative phytomer rank (CPN), which is the phytomer rank of a fruit counted from the bottom of the plant.

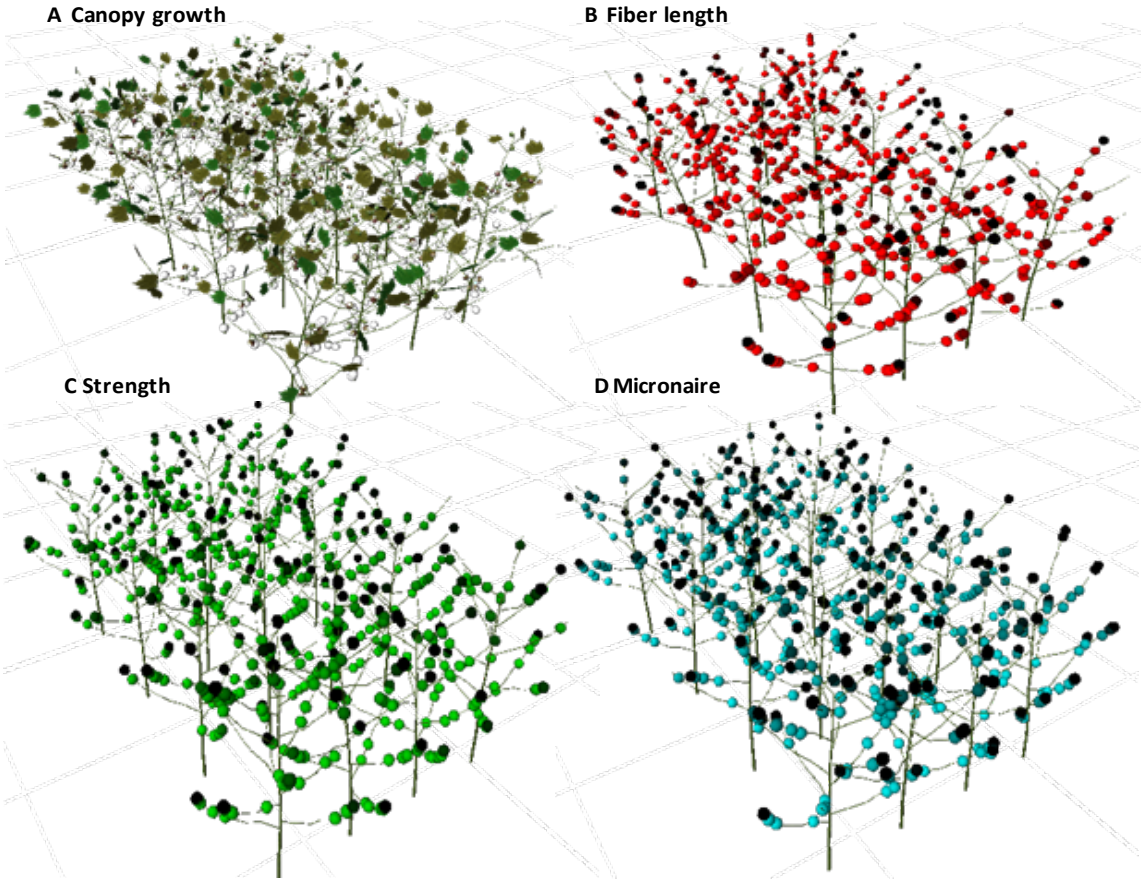

Fig.3 Output of CottonXL for canopy development (A), fiber length (B), strength (C) and micronaire (D). The scenario shown here is fort Anyang in 2002, mepiquat chloride applied, top cut at 30 July and side cut at 30 August, at a population density of 3.6 plants m^{-2}

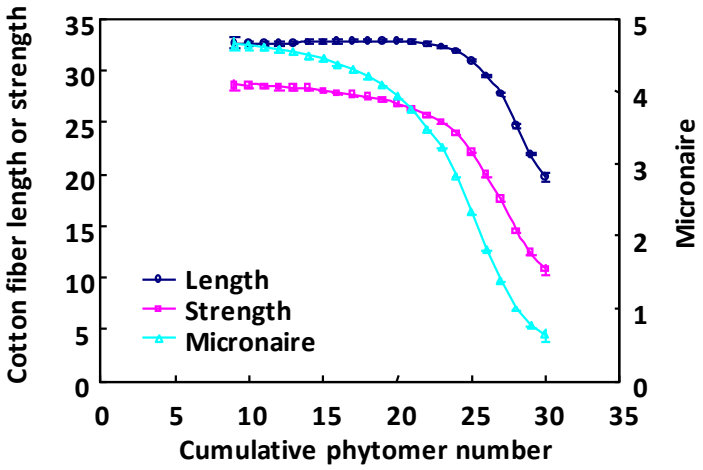

Fig.4 Cotton fiber length (mm), strength (cN tex^{-1}) and micronaire versus different cumulative phytomer number

RESULTS AND DISCUSSION

The model simulated the 3D distribution of fiber length, strength and micronaire according to their age, position in the canopy and prevailing temperature during development (Fig. 3). Fruits at CPN lower than 20 had similar values for fiber quality. Fruits developed at higher ranks, especially above CPN values of 25, had very low fiber quality (Fig. 4).

Cotton fiber quality responded to ecological zone, temperature and agronomical practices (not shown), e.g. sowing date and pruning time (cut-out date). CottonXL is a useful tool to explore cotton fiber quality related to fruit positions and improve cotton quality by optimizing plant structure, as well as to help farmers understand how the plant structure determines crop growth and quality. Forthcoming publications will present model validation and detailed scenario analyses.

LITERATURE CITED

Campbell B T, Jones M A. 2005. Assessment of genotype × environment interactions for yield and fiber quality in cotton performance trials. *Euphytica,* **144:** 69-78.

Girma K, Teal R K, Freeman K W, Boman R K, Raun W R. 2007. Cotton lint yield and quality as affected by applications of N, P, and K fertilizers. *The Journal of Cotton Science,* **11:** 12-19.

Mishra R, Yadav N R, Wilkin T A. 2001. Manipulation of fiber quality in transgenic cotton via ectopic expression of fibre gene. *In, Proceedings of Beltwide Cotton Conference,* 1437-1439.

Richard G P, Roy G C, Jinfa Z. 2006. Genetic variation for agronomic and fiber properties in an introgressed recombinant inbred population of cotton. *Crop Science,* **46:** 1311-1317.

Yeates S J, Constable G A, McCumstie T. 2010. Irrigated cotton in the tropical dry season. III: Impact of temperature, cultivar and sowing date on fibre quality. *Field Crops Research,* **116:** 300-307.

Proceedings of the 7th International Conference on Functional-Structural Plant Models, Saariselkä, Finland, 9 - 14 June 2013. Eds. Risto Sievänen, Eero Nikinmaa, Christophe Godin, Anna Lintunen & Pekka Nygren.
http://www.metla.fi/fspm2013/proceedings. ISBN 978-951-651-408-9.

Mathematical Modelling of the biocontrol of *Rubus alceifolius*, an invasive plant in Réunion Island.

Yves Dumont[1], **Alexandre Mathieu**[2], **Serge Quilici**[2]
[1]*CIRAD, Umr AMAP, Montpellier, France*
[2]*CIRAD, Umr PVBMT, Saint Pierre, Ile de la Réunion, France*
**correspondence:* yves.dumont@cirad.fr

Highlights: Invasive plants have become a major threat throughout the world, in particular in islands where the biodiversity is important and even unique. Since the 17th century, many weeds or invasive plants have been introduced in Réunion Island. Among them *Rubus alceifolius*, a giant bramble, is the most invasive and threatening to the endemic vegetation. After years of unsuccessful and even detrimental controls with herbicide applications and/or mechanical removal, a new biological control program has been launched, based on the release of a biocontrol agent, *Cibdela janthina*, a sawfly. Modelling Rubus-Cibdela interactions is not only helpfull to formalize knowledges but also to guide control strategies and decision-making, in particular before field releases. The aim of this talk, is to present a minimal mathematical model and some results based on ongoing experiments in Réunion Island.

Keywords: invasive plant, weed, biocontrol agent, plant-herbivore interaction, mathematical modelling, integro-differential equation, delay differential equation, qualitative analysis, simulation.

INTRODUCTION

Biological invasions, be they accidental or deliberate, currently constitute one of the main threat to biodiversity after habitat destruction and fragmentation. In particular invasive alien plants, like weeds, do not only impact biodiversity conservation, but can also reduce the quality and the quantity of agricultural products, with economic consequences. Thus, their control is an absolute necessity. Since the mid of the nineteenth century, classical biological control has proved to be a viable ecological solution to provide long-term control of invasive plants (Julien and Griffiths 1998). It is based on the importation and release of host-specific natural enemies (the biological agents). Weeds biological control is mainly used in Australia, New Zealand, Canada, South Africa and in the USA (Cruttwell McFadyen 1998), with relative good successes. Surprisingly, no biological control agents against alien plants have been released in Europe. One drawback of Control programs is that they need to be conducted over a period from ten to twenty years. Indeed, the effects of the control are not immediate and this may explain why biological control programs are declared failures or left. Mathematical modelling and, in particular, the qualitative study of the models, can be very helpful to hightligths all possible long-term dynamics according to weed-agent interactions, but also to the parameter values related to the weeds and the biocontrol agent. Moreover, it can also help to improve control strategies, using numerical simulations (Dumont et al. 2010, 2012).

Since human settlement in Réunion island (a volcanic island in the Indian Ocean) during the 17th century, various invasive plants have been introduced, but one is particularly invasive: the giant bramble, *Rubus alceifolius* Poir. (Rosaceae) (see Fig 1), which has been accidentalty introduced in the nineteenth century (and later in Queensland, Australia) and has spread throughout the island, from the Sea level to 1700 m. altitudes, due to its high plasticity and well adapted growth strategies (Baret 2002, Baret et al. 2004). Since the last thirty years, the main tools to control this weed have been pesticide applications and mechanical control or cutting control. However, Réunion island having a chaotic relief, it is not possible to treat all invaded areas. Moreover these control tools are not only inefficient but also costly. Thus, biological control is the only option that could reduce the impacts of this invasive alien plant. That is why a research program has been launched in 1997 to consider the so-called classical biocontrol: a biocontrol agent is released only once, assuming that it will establish and further releases will not be necessary. For *Rubus alceifolius* , after several studies, the selected biocontrol agent was *Cibdela janthina*. It is multivoltin sawfly, with 6 to 7 generations per year without diapause periods. The females lay eggs in batches, inside the main veins of young leaves at the apex of the plant. Only the larvae are phytopagous and can severaly defoliate R. alceifolius by consuming all leaves, except the thick middle veins and the petiole. Larvae have between five and seven feeding instars, depending on their sex and environmental parameters, but only the two last are big

consumers of leaves (see Fig. 2).

After some preliminary studies between 2001 and 2007, *Cibdela janthina* has been selected and released in 2008 in the South-East part of la Réunion. Since then the Cibdela population has spread through the island. The first objective has also been reached: *Rubus alceifolius* has completely disappeared in some places (in particular at low altitudes), while in other places an equilibrium between Rubus and Cibdela has apparently been reached . Altogether, some unexpected situations appeared, and that is why new biological and ecological investigations have began two years ago. Field experiments are ongoing to provide parameters and study the impact of the altitude on the interaction between rubus and cibdela. In this context, and because we are first mainly interested in the long term behavior of the bramble biomass, when attacked by sawfly, at different altitudes, we start with a minimal (in the sense "less parameters as possible") Mathematical model. From our point of view, this is a first step towards more complex and detailed models, like Functional and Structural models, that require more precise knowledge on plant-pest interactions.

MINIMAL MATHEMATICAL MODELLING

Models related to the control of pest invasions by biocontrol agent are not numerous. For instance, in Chalak et al. (2011), the authors developed *discrete* deterministic and stochastic models to compare biocontrol made by two different agents: weevils and mycoherbicides. See also Stuart et al. (2002).

Here, since we are in mainly interested in the long term interactions between rubus and cibdela, we apply mathematical *continuous* modelling to model the biocontrol of *rubus alcefolius* or the Rubus-Cibdela interactions. We consider two main variables: B, the rubus biomass on a given surface, L the density of rubus density larvae. At this stage of our study, this two compartments model is « sufficient » in the case where we consider only rubus-cibdela interactions in a single domain, like a massif.

Our model is build as follows. Without biocontrol, rubus biomass is assumed to follow a logistic law, where r_0 is the net growth rate without cibdela, and B_{max} is related to the maximal biomass capacity of the massif. In the presence of cibdela, $r_1(L)$ becomes a nonlinear bounded and positive function, following the « Herbivory Optimization Hypothesis ». The damages caused by the larvae are modeled using a Holling functional response, $p(B)$. We assume that the time needed from feeding to newborns may vary from individual to individual, such that the larvae recruitment is $b\int_0^\infty e^{-m_L s}K(s)p\big(B(t-s)\big)L(t-s)\,ds$. b is the birth-rate, K(s) is a nonnegative probability distribution function representing the likelihood of taking time s to have offsprings, and $\int_0^\infty K(s)ds = 1$. m_L is the larvae death-rate, $e^{-m_L s}$ is the probability of an individual which starts to eat at time $t-s$ to be still alive at time t. Altogether, we derive the following system of integro-differential equations

$$\begin{cases} \frac{dB}{dt} = r_0 B(r_1(L)B_{max} - B) - p(B)L, \\ \frac{dL}{dt} = b\int_0^\infty e^{-m_L s}K(s)p\big(B(t-s)\big)L(t-s)\,ds - m_L L. \end{cases} \quad (1)$$

When $r_1(L) = 1$, and $K(s) = \delta_\tau(s)$, Model (1) reduces to a delay-differential equation that is well posed and has a unique positive solution (Gourley et al. 2005). Set $\mathcal{R} = \frac{f e^{-\eta m_L p(B_{max})}}{m} \leq 1$. If $\mathcal{R} \leq 1$, then system (1) will converge to $(B_{max}, 0)$. If $\mathcal{R} > 1$, then a positive equilibrium, (B^*, L^*), can exist. In the general case, depending on the values taken by τ and b, we show that system (1) can either develop a sustainable periodic behavior, or converge to (B^*, L^*), or even have a chaotic behavior, according to the parameter values.

Finally, based on recent results on cibdela biology (Mathieu et al., 2013), it may be possible to consider temperature (time) dependant parameters in model (1).

CONCLUSION

Despite their apparent simplicity, the previous models have complex dynamics that are able to reproduce various observed behaviors of rubus-cibdela interactions at different altitudes in Réunion Island: at low altitudes (below 350-400m), massif of rubus has almost disappeared, while above, rubus and cibdela populations seem to co-exist with various amplitudes, depending on the altitudes and the season. However numerous questions are still open: if other ressources for cibdela are available, how would the rubus-cibdela dynamic be affected. When attacked by cibdela, rubus consider several defenses mechanisms, like tolerance,

using reserve biomass and/or increasing the production of seeds playing a great role in the renewal of rubus massif. Patch modelling may be also important to consider in order to connect rubus massifs at different altitudes. Another next stage in our study would be to refine plant-insect interactions, and then, using previous architectural studies (Fig. 1, Baret 2003), to derive a Plant-Insect FSPM model. If a rubus FSPM model seems to be feasible, taking into account knowledge on the bramble, additional studies are necessary to understand precisely the interactions between rubus and cibdela, in order to model them efficiently (see Lebon et al. 2013 for further investigations on plant defences and plant responses to (insect) herbivore attacks).

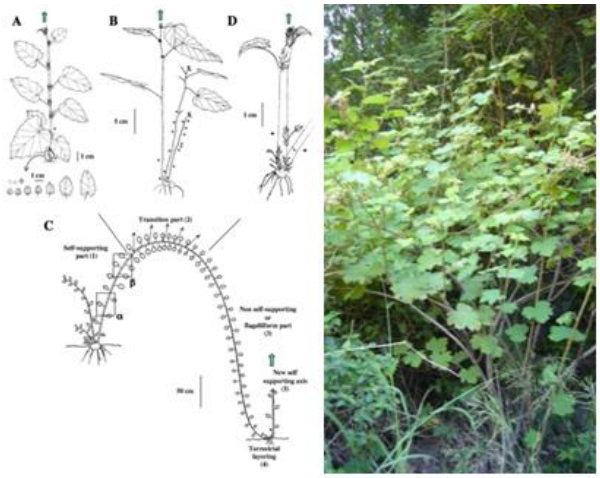

Fig. 1. *Rubus alceifolius* (Baret 2002; Baret et al. 2004)

Fig. 2. Larvae of *Cibdela janthina*… at work! (Mathieu et al., 2013)

LITERATURE CITED

Julien M.H., Griffiths M.W. 1998. Biological Control of Weeds: a world catalogue of agents and their target weeds. 4th ed., CABI, Wallingford (UK): 223 pp.

Cruttwell McFadyen RE, 1998. Biological Control of Weeds, *Annual Rev. of Entomology*, **43**: 369 -393.

Dumont Y, Russel JC, Lecomte V, Le Corre M, 2010. Conservation of endangered endemic seabirds within a multi-predator context: the Barau's Petrel in Réunion Island, *Natural Res. Mod*. **23**(3): 381-436.

Dumont Y, Tchuenche JM, 2012. Mathematical Studies on the Sterile Insect Technique for the Chikungunya Disease and Aedes albopictus, *Journal of Mathematical Biology*, **65**(5): 809-854.

Mathieu A, Quilici S, 2013. Development and Life History Traits of *Cibdela janthina* (Hymenoptera: Argidae) Larval Stage, submitted.

Baret S, Maurice S, Le Bourgeois T, Strasberg D, 2004. Altitudinal variation in fertility and vegetative growth in the invasive plant Rubus alceifolius Poiret (Rosaceae), on Réunion island. *Plant Ecology*, **172**(2): 265–273.

Baret S, Nicolini E, Le Bourgeois T, Strasberg D, 2003. Developmental patterns of the invasive bramble (Rubus alceifolius Poiret, Rosaceae) in Réunion Island : an architectural and morphometric analysis. *Annals of Botany*, **91**(1) :39–48.

Buckley YM, Rees M, Sheppard AW, Smyth MJ, 2005. Stable coexistence of an invasive plant and biocontrol agent: a parameterized coupled plant-herbivore model, *J. Applied Ecology*, **42**: 70-79.

Stuart RM, Kriticos DJ, Ash JE, 2002. Modelling the biological control of bitou bush (*Chrysanthemoides monilifera*: Asteraceae) by *Mesoclanis polana* (Tephritidae), 13th Australian Weeds Conference: weeds "threats now and forever?", Western Australia, 8-13: 591-594.

Chalak M, Ruijs A, Van Ierland EC, 2011. Biological control of invasive plant species: A stochastic analysis. *Weed Biology and Management*, **11**: 137–151.

Gourley S-A, Kuang Y, 2004. A Stage Structured Predator-Prey model and Its Dependence on Maturation Delay and Death Rate, *Journal of Mathematical Biology*, **49**: 188-200.

Lebon A, Mailleret L, Dumont Y, Grognard F, 2013. Modelling the combined effects of plant tolerance and resistance in plant-herbivore systems, submitted to *Ecological Modelling*.